Polymer materials for roll coated solar cells: strategies tom improve performance and stability

Heckler, Ilona Maria; Bundgaard, Eva

Publication date:
2016

Document Version
Publisher's PDF, also known as Version of record

POLYMER MATERIALS FOR ROLL COATED SOLAR CELLS:

STRATEGIES TO IMPROVE PERFORMANCE AND STABILITY

Ph.D. Thesis

Ilona Maria Heckler

Technical University of Denmark

December 2016

Author:

Ilona Heckler

Supervisor:

Senior scientist Dr. Eva Bundgaard

Sponsorship:

The Villum Foundation's Young Investigator Program (Project: Materials for Energy Production)

Assessment committee:

Professor Jens Wenzel Andreasen, Technical University of Denmark

Professor David M. Tanenbaum, Pomona College, CA, USA

Associate Professor Ergang Wang, Chalmers University of Technology, Sweden

Technical University of Denmark

Department of Energy Conversion and Storage

Organic Energy Material Section

Frederiksborgvej 399

4000 Roskilde

Denmark

ISBN: 978-87-92986-59-7

December 2016

To my grandma Gertrud who always believed in me and my ability.

"*You must never be fearful of what you are doing when it is right*."

Marie Skłodowska-Curie

Preface

This PhD thesis contains the main results of three years of research and studying at the Technical University of Denmark carried out between January 2014 and December 2016. The experiments were performed at the section of Organic Energy Materials (OEM), Department of Energy Conversion and Storage under the supervision of Dr. Eva Bundgaard and during a six months research stay at Hasselt University, Belgium under the supervision of Professor Dr. Wouter Maes and in collaboration with his group. This led to five peer-reviewed publications (including one review) with major contribution in four of them. The publication with a detailed description of my contribution can be found in Appendix C. Another publication is currently in progress.

The work was financially supported by the Villum Foundation Young Investigator Program and was part of the project "*Materials for Energy Production*".

Structure of the thesis

The thesis is structured in six different chapters. **Chapter 1** gives an introduction to the background, history and definitions of polymer solar cells and their stability. This chapter includes some parts of a review with my contribution (Gevorgyan *et al.* 2017 in the Journal of Physics D: Applied Physics) and a detailed motivation for each chapter.

Chapter 2 deals with a screening of polymers for roll-coated polymer solar cells to find the right candidates for upscaling. Polymers need to fulfil different requirements to be in the range of these candidates. The polymers were compared in terms of their feasibility of synthesis and coating as well as on the performance and stability of the resulting device. This chapter is based on the publication Bundgaard *et al.* from 2015 in Advanced Energy Matererials. My personal contribution was the roll-coating and testing of a significant number of different polymers in polymer solar cells.

Chapter 3 is about a backbone screening of polymers based on benzothiadiazole and thiophene with different incorporation of these monomers and their influence on photovoltaic characteristics including comparison with similar polymers reported in literature. This chapter is not published yet, but the publication is in progress. Here I performed synthesis, analysis and application in roll-coated devices.

Chapter 4 is about the chemical modification of three different polymers which are suitable for roll-coated polymer solar cell to improve the stability. The influence on the stability of the materials and the devices was investigated by exchanging partly some of the side chains with known stabilizing side chains from the literature. The side chains were investigated in their influence in different polymers as well as different positions within one of the polymers. This chapter is based on two publications (Heckler *et al.* 2016 in Materials and Heckler *et al.* 2016 in the Journal of Materials Chemistry A). The work reported in this chapter was mostly performed during my research stay at Hasselt University, where most of the syntheis was perfromed. In Denmark, I prepared the roll-coated devices and analyzed them.

Chapter 5 analyses two different polythiophenes with removable side chains to improve their stability and surveys their possibility to be applied in polymer solar cells. This chapter is based on a publication with minor contribution (Toušek *et al.* 2016 in Solid-State Electronics) and on unpublished results.

The **final chapter** concludes this work. For additional information, there are three appendices.

Appendix A shows a detailed description of the methods and materials used in this thesis including ananlysis of the produced molecules.

Appendix B contains all experimental details including different characterization and additional graphs.

Appendix C contains the publications and detailed personal contribution.

Acknowledgement

First of all, I would like to thank Eva for giving me, 3 years ago, the opportunity to start my PhD study with her. In the course of this time she was a supervisor who always had an open door for questions and discussions. With her guidance I always had the freedom of organizing my work according to my own knowledge. *Eva, jeg er meget glad, at du var min supervisor i de tre år.*

Next I would like to thank Wouter, who was my supervisor during my external stay at Hasselt University in Belgium. He was always open for discussions. I would also like to thank Jurgen who did a lot of spin-coating and their measuring of the materials I made there. In the end I would like to thank both groups DSOS and PRD, I was surrounded by during my stay.

I would like to thank the whole group in OEM. First I would like to thank the chemistry team: Martin, Jon, Ole, and Francesco L. I thank Martin and Jon for answering questions about synthesis problems, and for

some nice discussions; and for correcting part of my thesis. I would like to thank Ole who helped me often looking for chemicals and for measuring my polymers with SEC. I would like to thank Francesco L. He was always open for discussions, a nice company during the long hours of work and good to joke around with.

Next, I would like to thank Suren and Morten, who helped me both with stability measurements and advices. I would like to thank also Mikkel and Roar who were always open for questions and help. Special thanks go to Frederik who was leading the group most of my time there. He had always an open door for everybody. *Jeg vil også gerne sige tak til June som altid rensede glasvarer fra laboratoriet og Henrik for kemikaliebestilling. Jeg vil også gerne sige tak til Birgit, som rettede altid tekster på dansk (også Resuméet her). Til sidst vil jeg gerne sige tusind tak til Bente. Hun var allerede meget sød da jeg kom til jobsamtale for mere end tre år siden. Hun hjalp mig meget med alle problemer som skulle blive løst i de tre år.* I also would like to thank Rafa, Francesco, Thue, Lea, Markus, Tiago, Giovanni and Mariana, and everyone else who I forgot or already left the group for making the three years to a very enjoyable time. *Außerdem möchte ich natürlich auch Markus danken für den Austausch und die Hilfe bei der Korrektur der deutschen Zusammenfassung der Dissertation.*

Last I would like to thank Gisele. She was the one who started her PhD at the same time, and now we will finish together which also makes me happy. We did not just only share an office but became very good friends during this time. We talked about positive results we got, but also discussed our problems. I think the time was very enjoyable, and we had a lot of fun together at work, but also outside work.

The time as a PhD student was also successful because of all my friends who supported and believed in me. First of all I would like to thank Dechan, Neomy and Soheila, who all read part of my thesis and gave me good suggestions, especially Neomy, who was always there for me and read most of it. I also would like to thank KaRa who believed in me and supported me every day. I would like to thank my flat mates Luciano, Sonya and Tomek who made living in Denmark fun. *Natürlich möchte ich auch meinen Freunden in Deutschland danken, speziell Katrin und Claudi, die stolz auf mich sind weil ich es so weit gebracht habe und das Ganze bis zum Schluss durchgezogen habe.*

Als letztes möchte ich meiner Familie danken. Sie haben mich immer unterstützt und mich motiviert hat. Deshalb habe ich diese Arbeit auch meiner Großmutter Gertrud gewidmet, die immer an mich geglaubt hat und sehr stolz auf mich ist.

Risø, 31st December 2016

Ilona Heckler

Abstract

Solar cells are among the renewable energy technologies with a large potential in terms of solar energy availability. The solar cells based on conjugated polymers belong to the third generation of this technology and their attractive features include a fast and cheap solution-processed production. At DTU Energy the focus is the roll-to-roll coating process of these materials in order to reach large area devices, as the processability and scalability of the technology is an important factor. The processability using roll-coating techniques and the stability of the used materials can be crucial. Therefore this project focuses on the synthesis of conjugated polymers and their application in roll-coated polymer solar cells.

The first part of this project aims at using a screening strategy to find suitable polymer candidates for well performing solution processed polymer solar cells. A large number of polymers was screened by applying them in roll-coated solar cells and their performance, stability and number of synthetic steps was compared, to find promissing candidates. In the end seven polymers with a sufficient efficiency were found to behave in a higher or in similar manner as poly(3-hexylthiophene). Further polymers were prepared based on well-performing benzothiadiazole and thiophene based polymers with different incorporation ratios of these monomers. The incorporation ratio has different effects on the polymer properties and the performance and stability of the corresponding roll-coated devices. The best efficiency was achieved with a polymer by using an incorporation of four thiophenes in the repeating unit.

The second part of the work aims at using a known strategy to improve the solar cells stability. Three of the polymers from the polymer screening were therefore partly modified with stabilizing side chains, 2-phenetyl and 2-ethanol, respectively, to influence especially the device stability but also the performance. For most modifications a decrease of the solar cell efficiency was observed. The incorporation of 10% of these side chains show improvements of the stability of devices in a minor degree with a variation in the photo- and thermal stability. In addition to the use of different side chains, the impact of different positioning of one side chain was investigated, showing that the incorporation onto the acceptor or donor unit of the polymer showed a degradation or improvement of the resulting properties. In addition, the approach of side chain removable on polythiophene was compared in terms of optical properties and morphologies of two polymers with different (thermal or acidic) cleavage processes. It was found that their properties were not the same and therefore different results from the corresponding solar cells can be expected.

Resumé

Solcellerne har et stort potentiale blandt de vedvarende energiteknologier. Solceller baseret på konjugerede polymerer tilhører tredje generations solcelleteknologi. Denne teknologis attraktive egenskab omfatter en hurtig og billig produktion gennem rulle-til-rulle forarbejdning af polymeropløsinger. På DTU Energi er en stor del af fokus især på rulle-til-rulle fremstillede polymersolceller for at opnå produktionen i stor skala, og her er procceseringen med rulle-til-rulle fremstillingsteknikken og stabiliteten af de anvendte materialer af afgørende betydning. Derfor er dette projekt fokuseret på syntesen af konjugerede polymere og deres anvendelse i rulle-til-rulle fremstillede polymersolceller.

I første del af projektet var formålet at finde effektive organiske solceller, som er baseret på egnede polymererkandidater. Et stort antal polymerer blev screenet ved at anvende dem i rulle-coatede solceller og sammenligner deres effektivitet, stabilitet og antal af syntese trin for at finde egnede kandidater. Til sidste blev der fundet syv polymerer, som virkede bedre end eller på tilsvarende måde som poly(3-hexylthiophen). Yderligere polymerer blev fremstillet med udgangspunkt i velfungerende benzothiadiazol-thiophenpolymerer med forskellige forhold mellem disse monomerer. Bladningsforholdet indvirkede på polymerernes egenskaber og på effektiviteten og stabiliteten i de tilsvarende rullefremstillede solceller. Den bedste effektivitet blev opnået for en polymer med fire thiophener i gentagelsesenheden.

Formålet med anden del af projektet var at anvende en kendt strategi til forbedring af solcellestabilitet. Tre af polymererne fra polymerscreeningen blev derfor delvis modificeret med stabiliserende sidekæder, henholdsvis 2-phenetyl og 2-ethanol. Modificering skulle forbedre især solcellestabilitet, men også effektiviteten. For de fleste modificerede polymerer blev der observeret et fald i solcelleeffektiviteten. Anvendelsen af 10% af de nye sidekæder viser forbedringer af solcellestabiliteten inklusiv en variation i den foto- og termiske stabilitet. Desuden blev virkningen af forskellige positioner af én sidekæde undersøgt. Resultaterne viser, at sidekæden på acceptor- eller donorenheden af polymeren bevirker en nedbrydning eller forbedring af de resulterende egenskaber. Til sidst blev anvendelsen af forskellige kløvbare sidekæder på polythiophen sammenlignet med hensyn til optiske egenskaber og morfologier af to polymerer med forskellige (termisk eller sure) spaltningsprocesser.

Zusammenfassung

Solarzellen gehören zu den erneuerbaren Energietechnologien, die ein großes Potenzial in Bezug auf die Solarenergieverfügbarkeit besitzen. Die organischen Solarzellen, die auf konjugierten Polymeren basiert sind, gehören zu der dritten Generation dieser Technologie. Ihre attraktiven Eigenschaften sind u.a. eine schnelle und kostengünstige Fertigung unter Verwendung dieser Polymere in Lösungen. Im Institut für Energie an der DTU liegt der Schwerpunkt der Forschung auf Rolle-zu-Rolle-Fertigungsprozessen dieser Materialien zur Herstellung von großflächigen organischen Solarzellen, da die Verarbeitbarkeit und Skalierbarkeit der Technologie ein wichtiger Faktor ist. Die Verarbeitbarkeit durch industrielle Fertigungsverfahren und die Stabilität der verwendeten Materialien ist entscheidend für deren Erfolg. Deshalb ist dieses Projekt auf die Synthese konjugierter Polymere und deren Anwendung in flüssigprozessierten Polymer-Solarzellen fokussiert.

Diese Promotion erforschte u.a. eine Screening-Strategie um geeignete Polymerkandidaten für organische Solarzellen mit einem hohen Wirkungsgrad zu finden. Eine riesige Menge an Polymeren wurde gescannt, indem sie in Solarzellen mittels Schlitzdüsenbeschichtung aus den Polymerlösungen hergestellt wurden. Der Wirkungsgrad, die Stabilität und die Anzahl der Syntheseschritte wurden verglichen, um geeignete Kandidaten zu finden. Am Ende kristallisierten sich sieben Polymere mit verbesserten oder ähnlichen Eigenschaften als Poly(3-hexylthiophen) heraus. Weitere Polymere, die auf effizienten Benzothiadiazol-Thiophenpolymeren basieren, wurden hergestellt mit einem unterschiedlichen Einbauverhältnis der Monomere. Das Einbauverhältnis hatte unterschiedliche Auswirkungen auf die Polymereigenschaften und den Wirkungsgrad, sowie der Stabilität der entsprechenden Solarzellen. Der beste Wirkungsgrad wurde durch ein Polymer mit einem Einbau von vier Thiophenen in der Wiederholungseinheit erreicht.

Der zweite Teil der Arbeit zielte darauf ab, eine bekannte Strategie zur Verbesserung der Solarzellenstabilität zu verwenden. Drei der Polymere aus dem vorrausgegangenen Screeining wurden daher teilweise mit stabilisierenden Seitenketten wie 2-Phenetyl und 2-Ethanol modifiziert, um insbesondere die Solarzellenstabilität, aber auch den Wirkungsgrad zu beeinflussen. Durch die meisten Modifikationen wurde eine Abnahme des Solarzellenwirkungsgrades beobachtet. Der Einbau von 10% der stabilisierenden Seitenketten zeigte Verbesserungen in der Solarzellenstabilität in geringem Maße einschließlich einer Variation an Licht- und thermischer Stabilität. Neben der Verwendung verschiedener Seitenketten zur Stabilitätsverbesserung, wurde der Einfluss unterschiedlicher Seitenkettenpositionen untersucht. Diese Untersuchung zeigte, dass der Einbau an den Akzeptoren- oder Donatoreneinheit des Polymers eine Verschlechterung bzw. Verbesserung der resultierenden Eigenschaften zeigte. Zusätzlich zu

dem Ansatz mit stabilisierenden Seitenketten wurden zwei Polythiophene mit unterschiedlichen entfernbaren (über einen thermischen oder sauren Spaltungsprozess) Seitenketten über ihre optischen Eigenschaften und Oberflächenstruktur verglichen und festgestellt, dass sie nicht übereinstimmen und somit auch Solarzellen mit unterschiedlichen Eigenschaften ergeben würden.

List of Abbreviations

A	Acceptor
A_M	Monomer acceptor
AM	Air mass
BDT	Benzo[1,2-*b*:4,5-*b'*]dithiophene
BHJ	Bulk heterojunction
BT	Benzo[*c*][1,2,5]thiadiazole
CB	Chlorobenzene
CF	Chloroform
CV	Cyclic voltammetry
D	Donor
Đ	polydispersity
D_M	Monomer donor
E_0	Value where 80% of the initial value is left
E_{50}	Value where 50% of the initial value is left
E_g	Optical band gap
$E_{g,ec}$	Electrochemical band gap
EtOH	2-ethanol
EtPh	2-phenethyl
EQE	External quantum efficiency
ETL	Electron transport layer
FF	Fill factor
HD	2-hexyldecyl
HTL	Hole transport layer
HOMO	Highest occupied molecular orbital
ISOS	International summit on OPV stability
ITO	Indium tin oxide
J	Current density
J_{SC}	Short circuit current density
$\lambda_{(max)}$	Wavelength (with maximal absorption)
LUMO	Lowest unoccupied molecular orbital
M_n	Numerous molecular weight in Da (Dalton)
M_x	Monomer number x
NMR	Nuclear magnetic resonance
OD	2-octyldodecyl

ODCB	*Ortho*-dichlorobenzene
OPV	Organic photovoltaic
$PC_{61}BM$	[6,6]-Phenyl C_{61} butyric acid methyl ester
$PC_{71}BM$	[6,6]-Phenyl C_{71} butyric acid methyl ester
PCE	Power conversion efficiency
PEDOT	Poly(3,4-ethylenedioxythiophene)
PPV	Poly[1,4-phenylenevinylene]
PS	polystyrene
PSC	Polymer solar cell
PSS	Poly(4-styrenesulfonate)
PT	Polythiophene
PV	photovoltaic
P3HT	Poly[3-hexylthiophene]
P_x	Polymer number x
RC	Roll-coating/-coated
R_d	Degradation rate
RHC	Rapid-heat-cool calorimetry
SC	Spin-coating/-coated
SEC	Size exclusion chromatography
Si	Silicon
SWV	Square wave voltammetry
T_{80}	Time where 80% of the initial value is left
T_{50}	Time where 50% of the initial value is left
TEM	Transmission electron microscope
T_g	Glass transition temperature
Th	Thiophene
TzTz	Thiazolo[5,4-d]thiazole
UV-vis	Ultraviolet-visible light
V	Voltage
V_{OC}	Open circuit voltage

Table of Contents

Preface v

Abstract ix

Resumé x

Zusammenfassung xi

Abbreviation xiii

Table of Contents xv

Chapter 1 Introduction 1

1.1 Background and Technology 1

1.2 Polymer Materials 3

1.2.1 Polymers in History 3

1.2.2. Conjugated Polymers 4

1.2.3 Synthesis of Conjugated Polymers 6

1.3. Polymer Solar Cells 7

1.3.1. Device Structure and Working Principle 7

1.3.2. Device Preparation 10

1.3.3. Characterization 11

1.4. Stability of Polymer Solar Cells 12

1.4.1. Chemical Modifications to Improve the Stability 13

1.4.2. Stability Investigation 16

1.5. Motivation of the Project 17

1.6. References 17

Chapter 2 Screening of Polymers for Polymer Solar Cells 23

2.1. Introduction 23

2.2. Donor-Acceptor-Polymers 25

2.2.1. Synthesis 25

2.2.2. Characterization 27

2.3. Polymer Solar Cells 28

2.3.1. Preparation 28

2.3.2. *J-V* Characteristics 29

2.4. Evaluation of the Polymer Screening 32

2.5. Conclusion 35
2.6. References 36
Chapter 3 The Impact of the Thiophene –Benzothiadiazole – Ratio in Conjugated Polymers 39
3.1. Introduction 39
3.2. Polymers based on Thiophene and Benzothiadiazole from the Polymer Screening 41
3.3. Polymers based on Thiophene and Benzothiadiazole 43
3.3.1. Synthesis 43
3.3.2. Characterization 45
3.3.3. Polymer Stability 47
3.4. Polymer Solar Cells 48
3.4.1. Preparation and Characterization 48
3.4.2. Solar Cell Stability 50
3.5. Conclusion 52
3.6. References 52
Chapter 4 Side Chain Modification in Polymers to Influence the Solar Cells Stability 55
4.1. Introduction 55
4.2. Synthesis 57
4.2.1. Monomer Synthesis 57
4.2.2. Polymer Synthesis 60
4.3. Comparison of 2-Phenethyl Side Chain Modification in Different Polymer Backbones 60
4.3.1. Polymer Properties 60
4.3.2. Polymer Solar Cells 63
4.3.3. Device Stability Analysis 67
4.4. Comparison of 2-Ethanol Side Chain Modifications in Different Positions in the Same Polymer Backbone 71
4.4.1. Polymer Characterization 71
4.4.2. Polymer Solar Cells 74
4.4.3. Device Stability Analysis 77
4.5. Comparison of the Different Side Chain Modifications with a Focus on their Degradation Behaviour 79
4.5.1. Photostability of the Polymer Films 79
4.5.2. Lifetime of the Roll-Coated Devices 81
4.5.3. Thermal Stability of the Spin-Coated Device 82
4.6. Conclusion 83
4.7. References 83

Chapter 5 Comparison of Side Chain Removable Polymers 87

5.1. Introduction 87

5.2. Thermo- *vs.* acid cleavage 89

5.3. Conclusion 92

5.4. References 92

Chapter 6 Conclusion and Outlook 95

Appendix A 97

Appendix B 129

Appendix C 137

Chapter 1.

Introduction

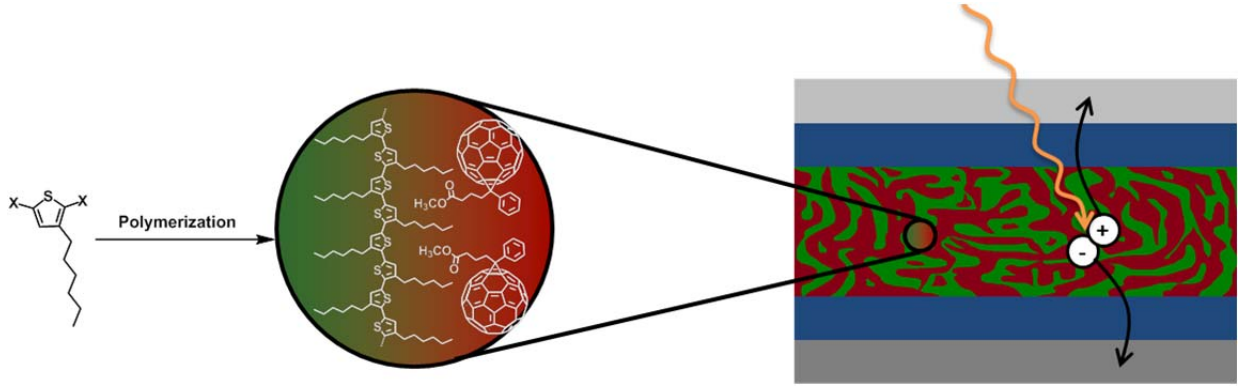

1.1. Background and Technology

Nowadays, people living in the 21st century face environmental challenges like the greenhouse effect and global warming. These effects make us think about the impact of modern society on human life as we know it now and even in the future. In order to sustain the life we have, the use of fossil fuel for energy production needs to be reduced significantly. As fossil fuels are a limited resource, there is a driving force to invest in alternative "*renewable*" energy sources (e.g. wind, water, geothermal heat and sun light). In 2015 about 23.7% of the electricity was based on renewable sources. While wind and water energy add a large amount to the global electricity production in 2015, only 1.2% of global electricity production was from solar energy [1]. In comparison, solar energy is available all over the world in large amounts (~23,000 TWy/y) while there is only ~130 TWy/y wind energy [2]. This makes the use of photovoltaic (PV) technologies to a large interest for our society.

The PV technology is classified in three different generations (Figure 1.1. bottom):

I. The first generation is a wafer-based technology based on crystalline silicon (Si) or gallium arsenide.
II. The second generation is based on thin films of hydrogenated amorphous Si, cadmium telluride or copper indium gallium diselenide.
III. The third generation includes different thin film devices like organic photovoltaic (OPV), dye-sensitized solar cells, colloidal quantum dot photovoltaics and perovskite solar cells as well as a variety of exotic concepts like multi-junction cells.

Recently Jean *et al.* proposed a new classification of the PV technology based on the material complexity (Figure 1.1), which can be defined as the number of atoms in a unit cell/molecule/repeating unit [3] and which is dependent on the crystallinity of the material.

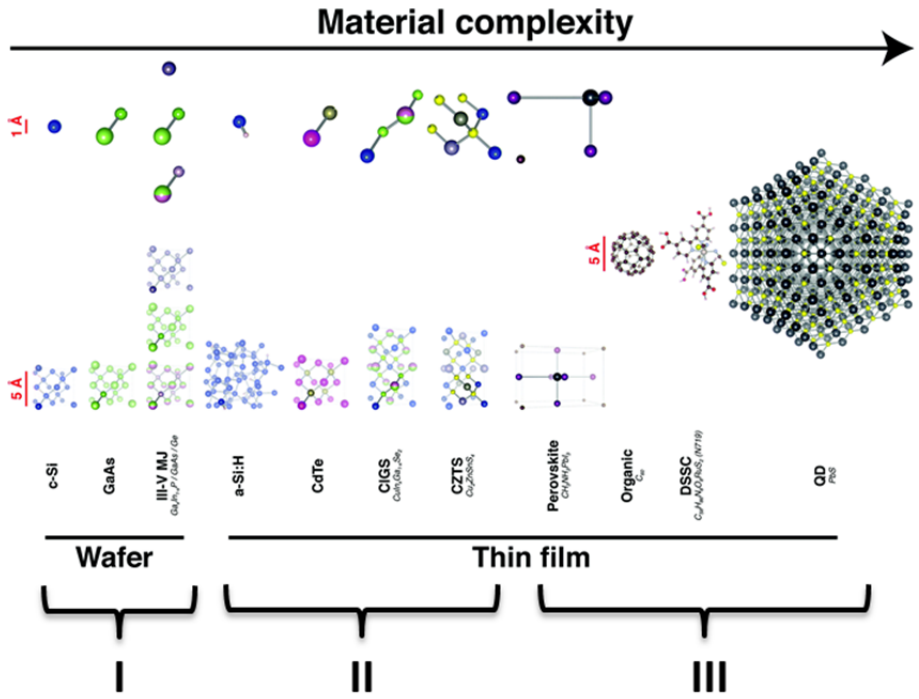

Figure 1.1. *PV technology classifications based on material complexity (top) and generations (I, II and III) (bottom). [3] – Adapted with permission of The Royal Society of Chemistry, ©2015.*

Figure 1.2. *The critical triangle for solar technologies* [4].

In order to produce electricity of low cost, there are a few important requirements within the solar cell technology which need to be fulfilled and these can be found in the critical triangle (Figure 1.2). In here, a high stability and performance of the technology as well as low costs to produce it is depicted.

OPV is a third generation solar cell. It has many attractive features which include the potential to be semi-transparent and flexible. OPV can be solution processed which enables the production of large area devices *via* a fast continuous process and thus, low production and material costs [4]. In addition, the materials

properties used in OPV can be easily engineered by chemical tailoring of the materials [5]. Polymer solar cells (PSCs) are one class within the field of OPV. They form an attractive charge generation component for a use in a low cost PV technology [6].

1.2. Polymer Materials

1.2.1. Polymers in History

"*A molecule of high relative molecular mass, the structure of which essentially comprises the multiple repetition of units derived, actually or conceptually, from molecules of low relative molecular mass.*" [7] – is the definition of the term "*polymer*" as defined by the International Union of Pure and Applied Chemistry (IUPAC). In the 19th century different discoveries, e.g. the vulcanization of natural rubber by C. Goodyear, are the basis of the polymer field [8]. A revolutionary milestone in the area of polymer and macromolecular chemistry was set in 1920s by H. Staudinger by his concepts (e.g. polymer chains are based on a large number of monomers), definitions (macromolecules, polymerization process and products) and research (e.g. the polymerization of isoprene) in this field, which was then awarded the Nobel Prize in Chemistry in 1953 [8,9]. The discovery of conducting polymers and the ability to dope these polymers in the range from metal to insulator in the 1980s was rewarded the Nobel Prize in Chemistry in 2000 to A. Heeger, A. MacDiarmid and H. Shirakawa. This discovery offered a new *"generation of polymeric materials"*, which features the optical and electrical properties of metals or semiconductors, but keeps the material properties and processing advantages of polymers [10]. Some examples of polymer structures with conjugated systems are shown in Figure 1.3.

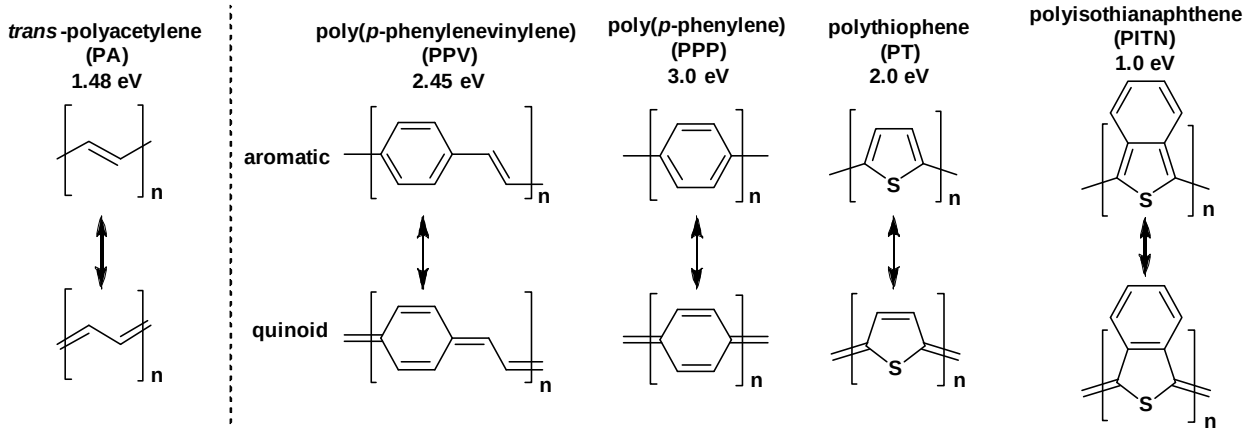

Figure 1.3. *Chemical structures in their aromatic and the quionid state and band gaps of some selected conjugated polymers* [5,10–14].

1.2.2. Conjugated Polymers

According to the definition of IUPAC, "*a conjugated system is a molecular entity whose structure may be represented as a system of alternating single and multiple bonds*" [15]. *Trans*-polyacetylene (PA; Figure 1.3) is the simplest conjugated polymer system. The linear structure is unstable towards delocalization of the double bonds [14].

As a result a conjugated system has one essential property which is the existence of π-electrons which can jump between the π-orbitals of the carbon atoms leading to distinct optical properties (light absorption and emission and charge generation and transport) [5]. This bond-length alternation due to a gain in electronic energy is called the Peierls effect and is a major characteristic of conjugated polymers [10,14]. When the length of the conjugated system increases to be macromolecular, the electronic properties can be described in terms of a semiconductor [5]. A conductor is classified according to their band gap (E_g) which is defined as the energy between the highest occupied molecular orbital (HOMO, valence band) and the lowest unoccupied molecular orbital (LUMO, conductive band). While conductors have no E_g and insulators have a very high E_g, semiconductors is in between a conductor and insulator. The interaction of the π-orbitals of monomer units within a polymer chain results in a structure of the energy bands with E_g of a semiconductor. As an example, the calculated energy levels of oligo- and polythiophene (PT) are shown in Figure 1.4 (left) which shows E_g decreases with an increased number of thiophenes. The final E_g of a PT is ~2 eV [14].

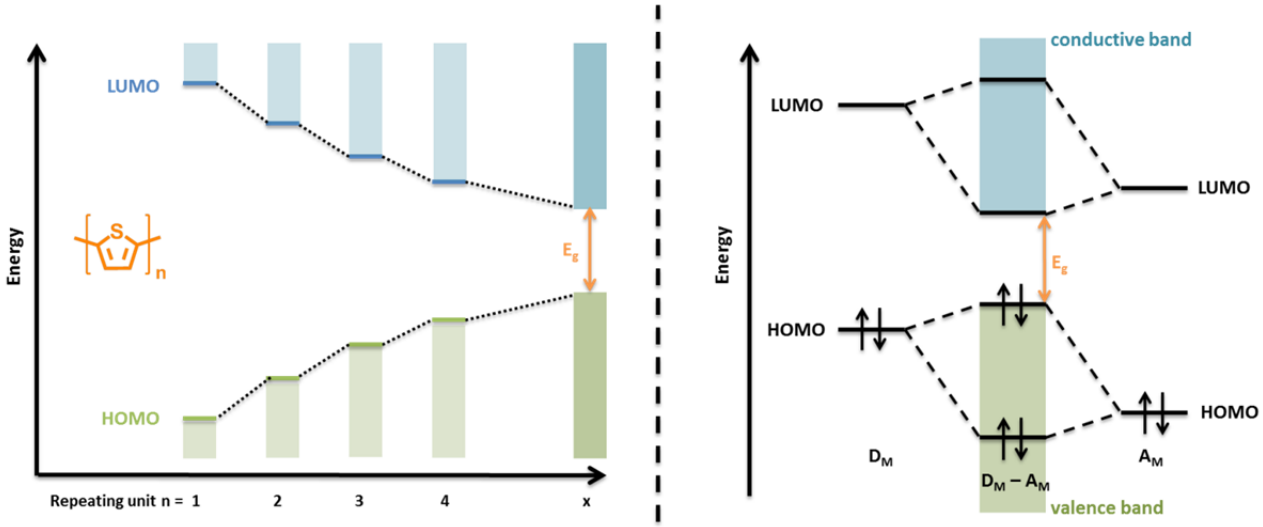

Figure 1.4. *Energy levels (calculated) of oligothiophenes and PT. Adapted with permission from Elsevier ©1998* [12] *(left) and energy level diagrams of the donor and acceptor units and of a donor-acceptor type semiconducting polymer* [14] *(right).*

The E_g value for PT is higher than the one for PA (1.48 eV). The reason for a higher value for PT and other conjugated polymers like poly(phenylenevinylene) (PPV) and poly(*p*-phenylene) (PPP) (2.45 eV and 3.0 eV) than originates from the two possible resonance structures, the aromatic and the quionid state, with

different energetic levels (Figure 1.3). In comparison to this, PA has two resonance structures which are energetically identical, as the structures are identical. In PPV, PPP and PT the aromatic structures are energetically preferred, as the aromaticity maintains within the phenylene and thiophene unit, respectively. In comparison to this state, the quinoid resonance structure where the π-electrons are delocalized along the conjugated chain by converting the double bond into single bonds and *vice versa* (Figure 1.3) results in the loss of aromaticity of the aromatic unit. This pronounces the single bond character of the connecting bond between two thiophenes. To increase the double bond character of this bond, the quinoidal structure needs to be more energetically preferred and stabilized. The loss of aromaticity needs to be compensated with higher resonance energy from another aromatic system. This can be achieved by the fusion of a second ring onto the monomer unit; [16] e.g. the loss of aromaticity in polyisothianaphthene (PITN) (Figure 1.3) is small upon going from the aromatic to the quinoid state, because the fused phenyl ring gains aromaticity in the other resonance structure. This results in an E_g of 1.0 eV for PITN [14]. E_g plays an important role for the optical properties of the conjugated polymers.

In 1992 a new class of small band gap polymers was introduced with the possibility of band gap engineering [17]. Here the interaction between a coupled donor (D_M; electron releasing unit) and acceptor (A_M, electron withdrawing unit) unit influences the double bond character of a linkage between two units as the charges can be moved around (D_M–A_M ↔ D_M^+=A_M^-). [14] An alternating D_M–A_M sequence within a conjugated polymer increases, therefore the double-bond character of the single bonds between the D_M–A_M monomer units results in a modification of the energy level and E_g of these so-called D_M-A_M or "push-pull" copolymers (Figure 1.5). One characteristic is that the energy levels (LUMO and HOMO) of the polymer are mostly determined by the LUMO of the A_M and the HOMO of the D_M unit, respectively [18]. This means that the HOMO is mostly located on the D_M while the LUMO is on the A_M. Orbital mixing (Figure 1.4 right) of the D_M and A_M units leads to a narrow HOMO-LUMO energy separation [19]. Tuning E_g even further is possible by engineering of the D_M and A_M using e.g. electron withdrawing/donating groups on the A_M/D_M unit [18].

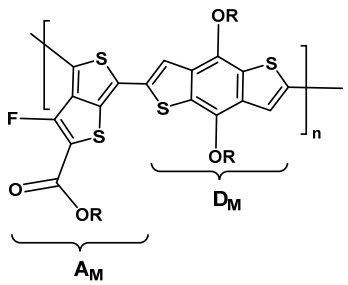

Figure 1.5. *Example of a push-pull polymer with monomer acceptor (A_M) and monomer donor (D_M).*

1.2.3. Synthesis of Conjugated Polymers

Within the field of organic synthesis, Migita-Kosugi-Stille cross-coupling (commonly called Stille cross-coupling) is a popular palladium-catalyzed reaction to form a C–C bond. The reaction is a step growth polymerization where a high molecular weight can only be achieved by high reaction conversion. The polymer chain formation occurs in a sequence of independent reaction events forming dimers, short and longer oligomers until at high conversion long chains are formed. Therefore a 1:1 equivalence of the two monomers is necessary [20].

The cross-coupling is the reaction of organotin reagents (R'–SnR''$_3$) with organic electrophiles (R–X) (Scheme 1.1). In 1993 Yu *et al.* adapted this reaction for the synthesis of conjugated polymers [21] to improve their properties (e.g. solubility issue) [22]. The advantages of this polymerization are mild reaction conditions and toleration of many functional groups (amines, aldehydes, esters, ethers and nitro groups) in the reactants with a high reaction yield. It also opens the possibility of the synthesis of polymers with variable E_g's, depending on the structure of the backbone and the electronic effects of the substituents. Disadvantage of this method is the use of highly toxic organotin materials [23]. The mechanism of the reaction (simplified version seen in Scheme 1.1) was studied by Stille [21] and other groups [24–26]. The first step is the oxidative addition of a R–X species to Pd^0, followed by the transmetalation including an insertion of the R'–SnR''$_3$ forming the activated complex. The last step consists of the reductive elimination of R–R' including a newly formed C–C single bond.

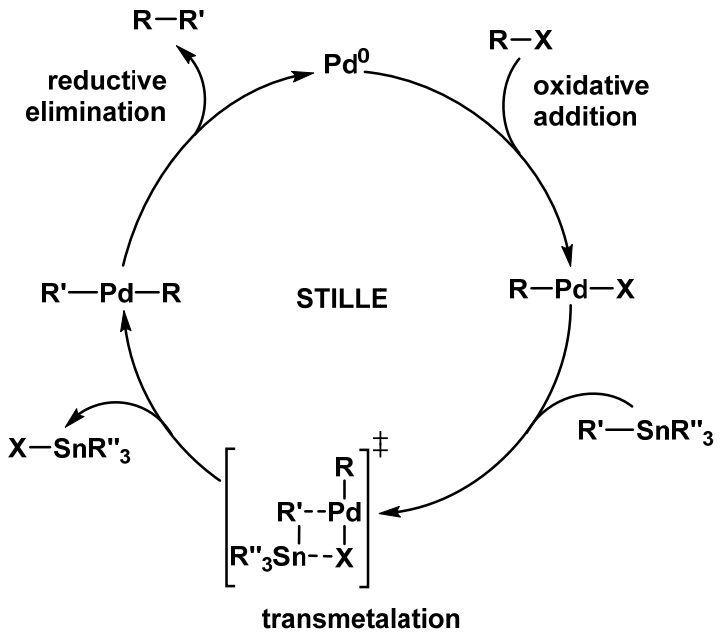

Scheme 1.1. *The catalytic cycle for the Stille cross-coupling* [21,25,26].

1.3. Polymer Solar Cells

The area of PSCs is a large part of the research within the field of OPV growing exponentially since discovering their potential for the solar energy field. The research was addressing different areas within the field (efficiency, stability, processability, device architecture, etc.), leading to a variety of milestones reached by large efforts on engineering D_M-A_M copolymer materials and PSC architecture. The most significant one was set in 2015, when the efficiency mark of 10% [27,28] was reached and exceeded even 11% in 2016 [29] for small area (in mm^2 scale) PSCs. In addition, a shift from spin coating (SC) towards roll coating (RC) process within the last 8 years was seen, in order to reach large area PSCs [30]. Specifically this goal was reached by building the first solar park based on roll-to-roll coated PSCs [31]. In the following sections the principle of operation, the device structure and the PSC preparation are explained in detail.

1.3.1. Device Structure and Working Principle

The simplest organic semiconductor device – a single layered PSC – consists of an active electron donor (D) material, a conjugated polymer between two electrodes, which can absorb light and transfer electricity. The single layered device (Figure 1.6, left), which was poor in performance due to a lack of charge separation, [32,33] was soon replaced by a bilayer structure (Figure 1.6. middle) of organic thin films. In this system the charge generation does not depend on the electric field [34]. The bilayer consists of the D material and an electron acceptor (A) with different electron affinities to trigger exciton dissociation [35]. For the electron acceptor, a fullerene was found to be suitable for accepting electrons [36] and be used as a photovoltaic junction, where a photoinduced electron transfer occurs [37]. Improved properties of the devices were achieved *via* a network of internal D-A heterojunctions [38,39]. This so-called bulk heterojunction (BHJ) (Figure 1.6. right) is formed by a blend of the D-A material and is nowadays the most used type of active layer in a PSCs.

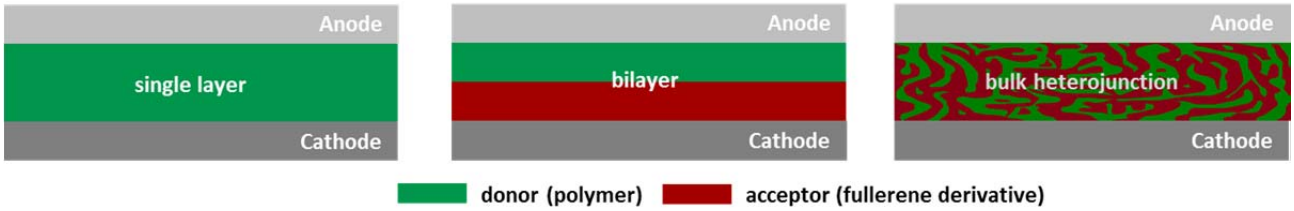

Figure 1.6. *Examples of active layer structures (single-, bilayer and bulk heterojunction) of PSCs.*

A well investigated system in a BHJ is poly(3-hexylthiophene) (P3HT) and [6,6]-phenyl C_{61} butyric acid methyl ester ($PC_{61}BM$) as D and A, respectively (Figure 1.7). Electricity generation mechanism in a PSC occurs in three steps (Figure 1.7, right) [40]:

1. Light absorption
2. Charge separation
3. Charge transport

The process between the first and second step is described by a photo induced charge transfer in the following [37,41]:

a. Excitation on the donor $D + A \rightleftharpoons D^* + A$

b. Delocalization of the excitation $D^* + A \rightleftharpoons [D + A]^*$

c. Partial charge transfer $[D + A]^* \rightleftharpoons [D^{\delta+} + A^{\delta-}]^*$

d. Formation of the ion radical $[D^{\delta+} + A^{\delta-}]^* \rightleftharpoons [D^{+\bullet} + A^{-\bullet}]$

e. Charge separation $[D^{+\bullet} + A^{-\bullet}] \rightleftharpoons D^{+\bullet} + A^{-\bullet}$

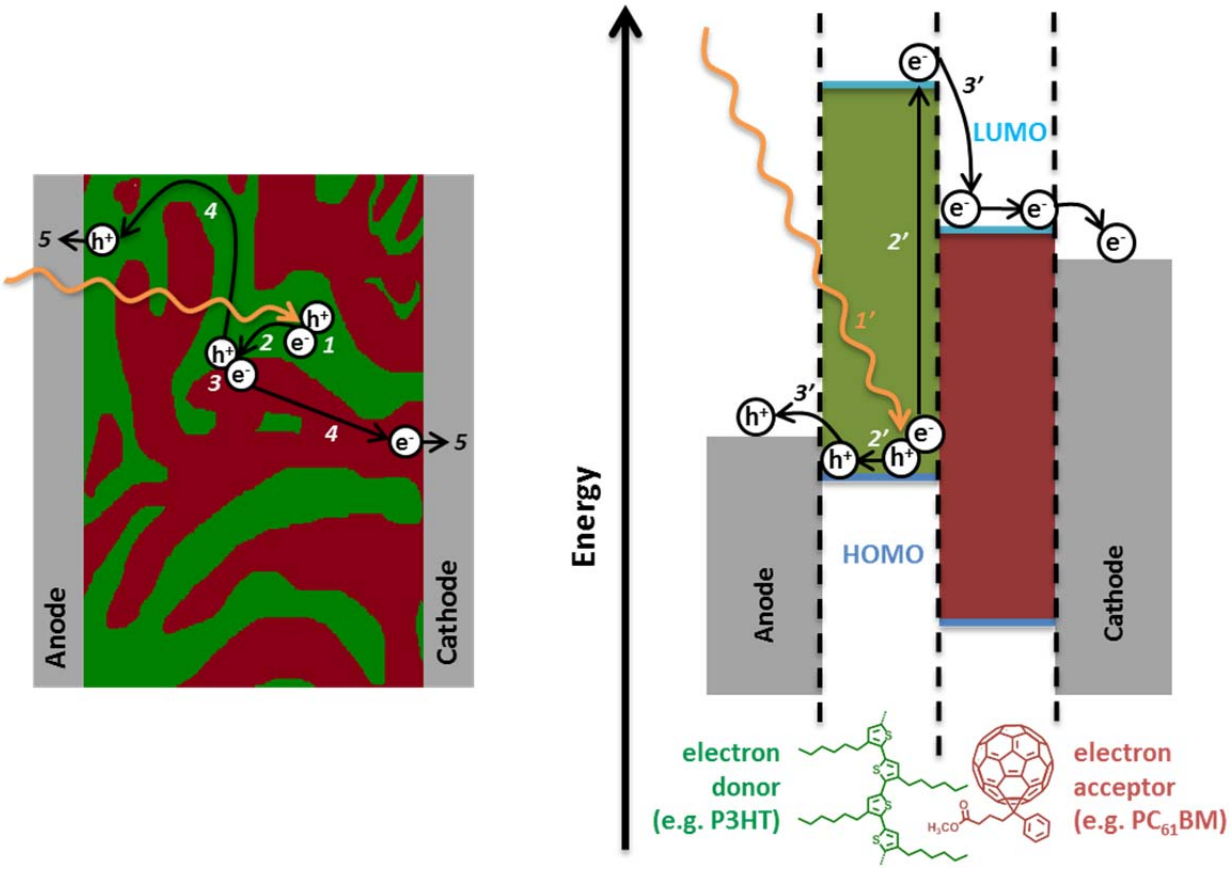

Figure 1.7. *Solar cell working principle within the active layer (left) of a heterojunction PSC and in the energy level diagram (right) including the structures of P3HT and $PC_{61}BM$* [40].

The process (Figure 1.7, left) starts with the absorption of photons of the D material (polymer) in the active layer of the PSC. This generates excitons (electron-hole pair) (**1**) which can then diffuse through the donor phase to a charge transfer region in the cell (**2**). This process is in competition with the recombination of the

charges which brings the excited system back to the ground state [5,42]. The excited system can relax back to the ground state at any time by releasing energy in form of heat or emitting light [37]. At the interface between the D-A material in the PSC the charges separate (**3**), thereafter the hole in the D material and the electron in the A material are transported towards (**4**) and then transferred (**5**) onto the respective electrodes to produce the photocurrent. Interaction with other charges or atoms can slow down the travel speed or even lead to recombination and thereby limit the photocurrent [5,42].

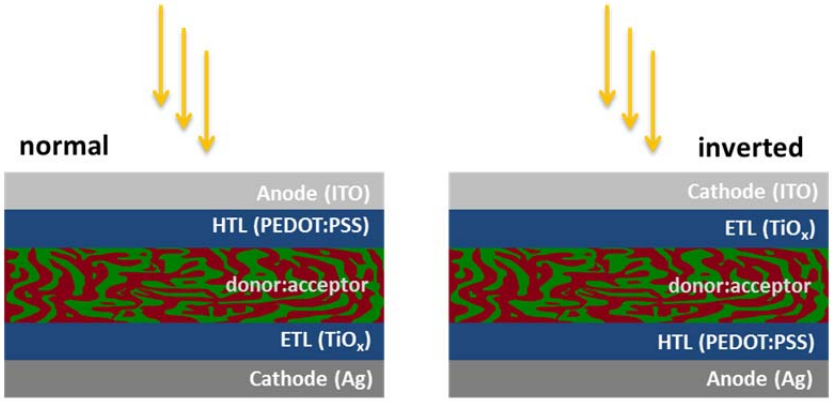

Figure 1.8. *The normal (left) and inverted (right) device geometry of BHJ PSCs consisting of anode, cathode, hole transport layer (HTL), electron transport layer (ETL) and photoactive layer (donor:acceptor) with examples for the materials* [43].

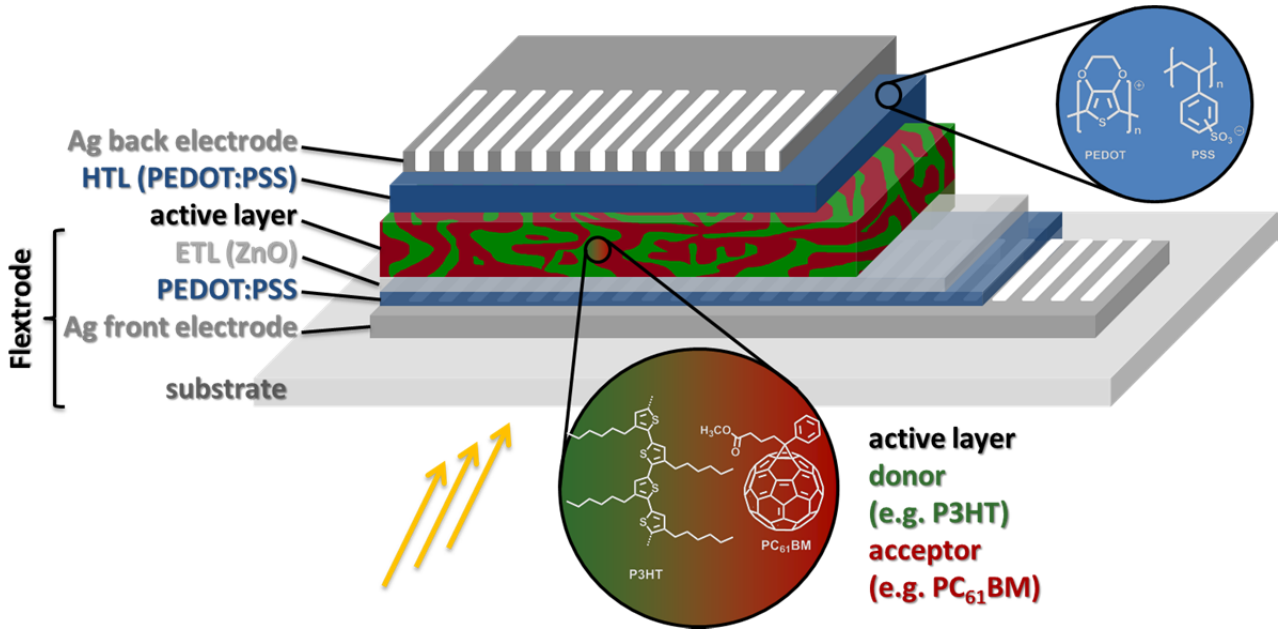

Figure 1.9. *Schematic drawing of the inverted PSC produced via RC: on the flextrode was coated a conductive layer of PEDOT:PSS, an electron transport layer (ETL), an active layer blend (of P3HT and $PC_{61}BM$), a hole transport layer (HTL) and a silver back electrode.*

The device structures of the PSCs are shown in Figure 1.8. The architecture in most common devices consists of multiple layers. The two different geometries reported in literature are the normal (conventional) and the inverted device structure [43–45]. The differences of the architectures are whether the semitransparent electrode is formed by the anode or cathode; so the inverted structure is a reversed normal device. A PSC device normally consists also of some interfacial layers; a hole transport layer (HTL) between anode and active layer and an electron transport layer (ETL) between the cathode and the active layer. In the normal geometry, the anode is mostly a semitransparent indium tin oxide layer (ITO) followed by a HTL (e.g.poly(3,4-ethylenedioxythiophene):poly(styrene sulfonate) (PEDOT:PSS)) (Figure 1.9), the active layer, an ETL (e.g. TiO_x, LiF/Al, Ca) and the anode (e.g. Al, Ag). In the inverted geometry, the cathode and anode materials are exchanged [43–45].

1.3.2. Device Preparation

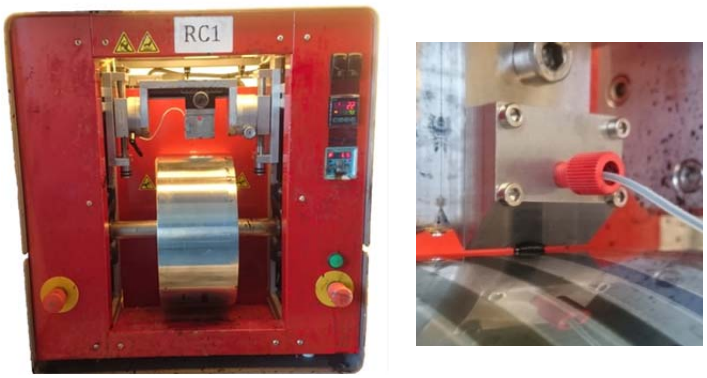

Figure 1.10. *Mini roll-coater (left) and the slot-die coating of the active layer (right) [46,47][46,47].*

PSCs are processed from solutions in different ways. In laboratories, where the cells are prepared in small quantity with a small active area (mm^2 scale), a SC process is mostly used for preparation. The normal architecture with the specific materials (ITO, metal oxides and Al) is often used in SC PSCs. The advantages of this process are that the film thickness can be regulated easily, while it becomes uniform during the coating process. It is also a fast operating and low cost process. The disadvantages of this technique are the large material waste during the process and the difficulties of coating on larger substrates [48], which makes the process not scalable. Therefore the coating process shifted to different techniques (e.g. slot die coating) [49]. At DTU Energy/Risø the production of large area PSCs is performed using RC techniques. A mini roll-coater (100 x 1 cm^2) (Figure 1.10 left) [50] or a roll-to-roll printing machine (m^2 range) [51] is used for applying polymers in PSCs. The coating process on the mini roll-coater is performed in ambient environment in a standard laboratory making the printing a fast and easy process. The architecture for the RC PSCs (Figure 1.9) is mostly an inverted geometry and the production is ITO and Al free, which means that no toxic and easily processed materials (no vacuum necessary) are used. The front electrode (cathode) is Ag on a

polyethylene terephthalate foil (substrate), followed by a conductive layer of PEDOT:PSS and an ETL of ZnO forming the so-called *flextrode*, which is produced in a fast inline roll-to-roll automated printing [51]. These layers are followed by slot-die coating of the active layer consisting of a BHJ of a polymer – $PC_{61}BM$ mixture, another PEDOT:PSS layer (HTL), followed by flexographic printing of the Ag electrode [46,47].

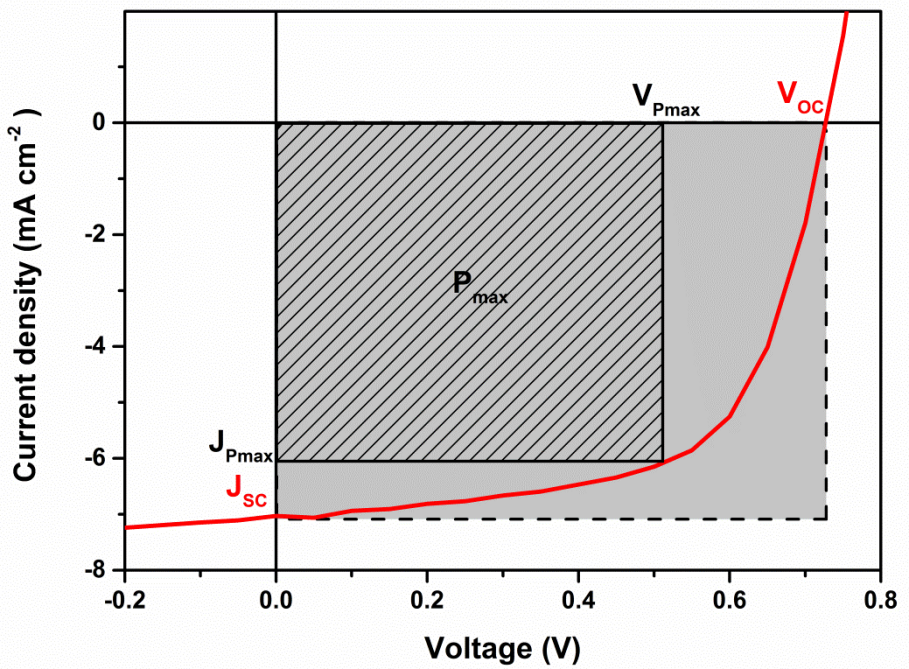

Figure 1.11. *Typical current density-voltage curve of an illuminated PSC including the maximum power point (P_{max}) the open circuit voltage (V_{OC}) and the short circuit current density (J_{SC}).*

1.3.3. Characterization

The main characteristic of an illuminated PSC is the current density (*J*) –voltage (*V*) curve (Figure 1.11), including the key parameters short-circuit current density (J_{SC} in mA cm^{-2}), the open-circuit voltage (V_{OC} in V) and the fill factor (FF in %). The curve is obtained by applying a range of voltage on the cell and measuring the photocurrent. The device generates power under illumination when $J_{SC}<J$ and $V<V_{OC}$ (in Figure 1.11, the part of the red curve in the grey box). At the maximum power point (P_{max} = V_{Pmax} x J_{Pmax}) the product of voltage (V_{Pmax}) and current density (J_{Pmax}) is the largest. From the V_{OC} and J_{SC} the power conversion efficiency (PCE), which is defined as the ratio of the produced power (P_{out}) and the power input (power of the incident light) (P_{light}), can be calculated according to [6,35,52,53]:

$$PCE = \frac{P_{out}}{P_{light}} = \frac{J_{SC} \times V_{OC} \times FF}{P_{light}} \quad (1.1)$$

where the light intensity is standardized at 1000 W m^{-1} with a spectral distribution on the earth's surface at an angle of impact of 48.2° of the sunray, defined as Air Mass (AM) 1.5 [54]. FF gives information about the

charge transport through the layer, which is in competition with charge recombination, and the quality of charge extraction. Furthermore, the series and shunt resistances influence the FF. The FF is defined as [6,35]:

$$FF = \frac{J_{Pmax} \times V_{Pmax}}{J_{SC} \times V_{OC}} \quad (1.2)$$

The V_{OC} is independent of the illumination intensity [55], but affected by the morphology of the active layer [56], the strength of the electron acceptor [57] and is linear dependent on the HOMO of the donor and the LUMO of the acceptor [55,58]:

$$V_{OC} = \frac{1}{e}\left(\left|HOMO_{polymer}\right| - \left|LUMO_{acceptor}\right|\right) - 0.3\ V \quad (1.3)$$

The J_{SC} is determined by the external quantum efficiency (EQE), which depends on all basic mechanisms of a solar cell (light absorption, charge separation, charge transport and charge collection). The measurement is performed by shining monochromatic light of the absorption spectrum range on a device. The EQE is defined as a fraction of absorbed photons (power input) which are converted to charges (current) [6,35]:

$$EQE = \frac{1240 \times J_{SC}}{\lambda \times P_{light}} \quad (1.4)$$

and the EQE of a solar cell is measured and plotted against the wavelengths.

1.4. Stability of Polymer Solar Cells

One major criterion for commercializing a technology like PSCs is to achieve a long lifetime, which means that the stability needs to be high. This topic has been addressed in many articles [59–64] and reviews [35,44,65–67] which focused on factors that affect the stability of a PSC. Different external [68,69] and internal factors [70] are summarized in Figure 1.12 [71].

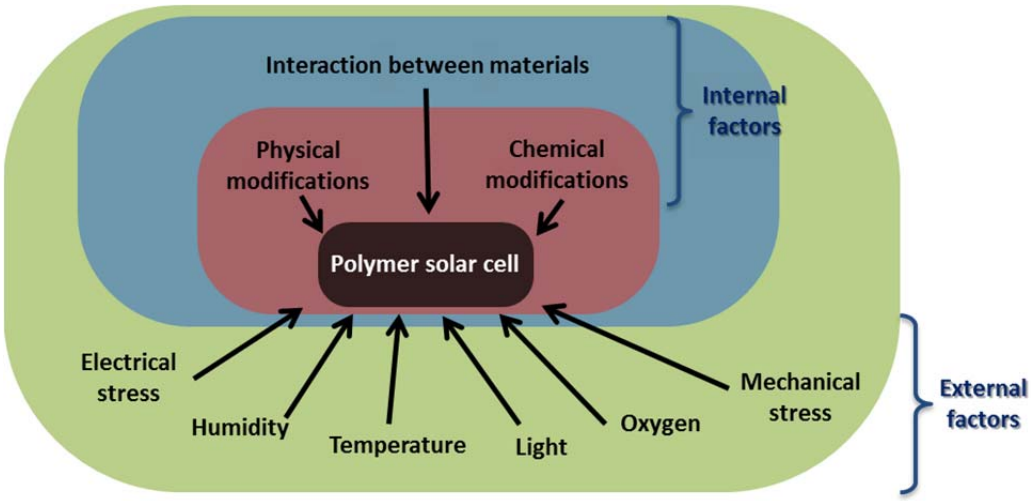

Figure 1.12. *A diagram summarizing the factors influencing the stability of a PSC* [71].

Stability improvements of PSCs can be physically (e.g. better encapsulation) or chemically. All material within the PSC can be exchanged by new materials or chemically modified to increase the stability. The fullerene based electron acceptor can be modified with stabilizing [72,73] or cross-linkable [74] groups or exchanged by fullerene free materials to prevent fullerene crystallization [75–77]. In the same way the HTL (PEDOT:PSS) can be modified [78] or exchanged by other materials [79,80] to improve the stability.

1.4.1. Chemical Modifications to Improve the Stability

The active layer of a PSC is also vulnerable to external factors (light, temperature, humidity) leading to the degradation of the D-A material. The physical ways would be to remove e.g. organic impurities [81], to use specific solvent mixtures [82] or to add (aluminium) nanoparticles [83] to create an optimal defined PAL morphology with a great stability. To avoid degradation through the chemical modification of the conjugated polymers, different research groups have focused on this. Some of the strategies are described in the following. These chemical modifications are based on different strategies (Figure 1.13).

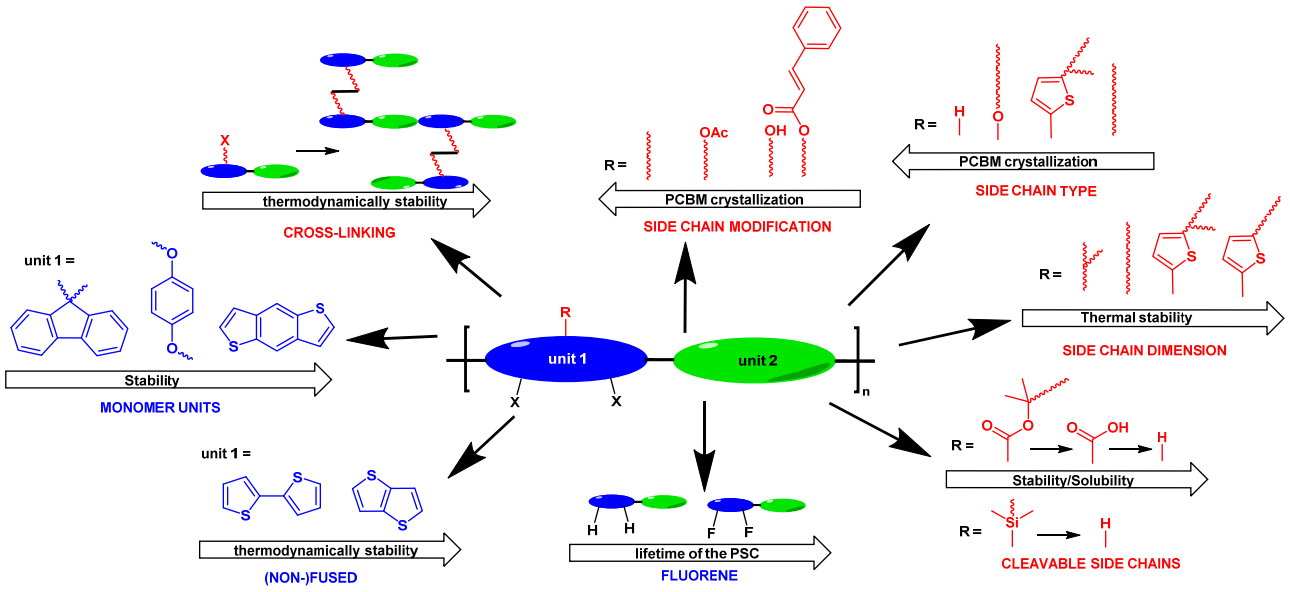

Figure 1.13. *Stability strategies on the polymer backbone (blue) or the polymer side chains (red) to improve the stability of the active layer in PSCs.*

Two pathways can be followed with different approaches in how to increase the stability:

1. Backbone modification
    - ❖ Molecule fusion of e.g. thiophene within the backbone for a more rigid [84] and more linear [85] backbone for a thermodynamically more stable polymer.
    - ❖ Increasing amount of fluorine on the backbone (e.g. on benzothiadiazole) increases the stability [86–88].

- ❖ Monomer units have different stabilities, e.g. fluorene < benzodithiophene [89,90].

2. Side chain modification

- ❖ Cross-linking of functionalized side chain to give an insoluble network with a stabilized morphology [91,92].
- ❖ Side chain removal after film formation in a thermal or acidic step for a highly insoluble polymer [93–98].
- ❖ Side chain type and dimensionality leads to different morphological stabilities [99–101].
- ❖ Side chain modification by introducing different stability groups [102–105] or reduction of the side chain density [106].

The advantage of PSCs is their processability from solution due to the presence of solubility side chains in the polymer. However, this is also a major weak point of the active layer of a PSC. Tierney *et al.* [101] investigated which impact different side chain have on the photochemical and morphological stability of D_M-A_M copolymer based PSCs (Figure 1.15). The stability of the investigated polymers decreased from linear alkyl > no chain > alkoxy > thienyl/branched. The morphological stability of a BHJ is controlled by two processes: the fullerene derivative dimerization and crystallization, so the stability depends on the crystallization rate. The thienyl/branched chains cause steric hindrance in polymer films, locking the chain in place and reducing possible paths in the 3D space for fullerene diffusion. An increase of the rotational freedom and steric hindrance are seen for the alkoxy and thienyl/branced chains. Most stable are polymers with linear side chains due to an even distribution along the backbone and dense packed aggregates (Figure 1.14) [101].

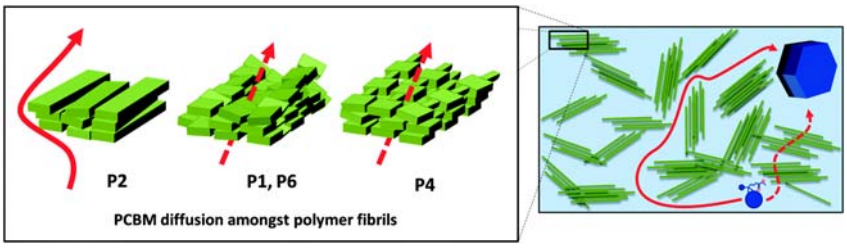

Figure 1.14. *Polymer (P1/P2/P4/P6 with an alkyl/alkoxy/alkylthienyl/proton as side chain) aggregate formations based on the side chain distribution and rotation, which regulate the transport of fullerene derivatives either pass around the aggregates or through them* [101]*. - Reproduced with permission of Royal Society of Chemistry and the PCCP Owner Societies.*

On the molecular level, $PC_{61}BM$ dimerization by a [2+2] photo-cycloaddition during illumination and in the absence of oxygen has been reported as a degradation mechanism for PSCs. For different types of fullerenes (C_{60}, $PC_{61}BM$ and bis-$PC_{61}BM$ which contains two ester groups), it was shown that with increasing amount of

ester groups, the stability can already be increased due to an increased steric hindrance [107]. In another study, devices based on an indene-C_{60} bisadduct and **P3HT** were less stable than devices based on $PC_{61}BM$ and **P3HT**. The low surface energy of indene-C_{60} bisadduct makes molecules migrate more easily than the higher energy of the $PC_{61}BM$. Building a more stable and interpenetrating D-A blend would therefore be more difficult [108]. This shows that the immutability of the morphology to have an optimal function of the PSC is addressed by many research papers.

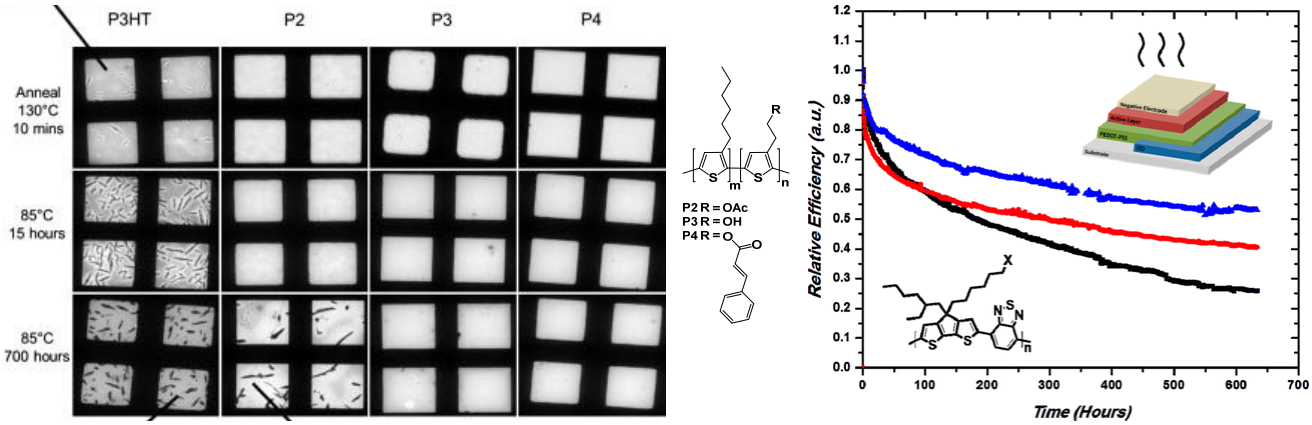

Figure 1.15. *TEM images (left) of PT based (structure in the middle):$PC_{61}BM$ blends (1:1) degraded at 85°C* [102] *(Adapted with permission from Elsevier ©2014) and the efficiency of thermal degradation PSCs of polymers with different side groups (X = OH - blue, ester - red, CH_3 - black, right). Reprinted with permission from* [103]*. ©2015, American Chemical Society.*

Maes *et al.* reduced the side chain density in a D_M-A_M copolymer leading to a PSC with an increased efficiency and device stability under thermal stress due to an optimized morphology of the active layer [106]. Furthermore several articles have been reported where the side chain of the polymers were exchanged (partly) by a stabilizing group. This specific focus on the chemical manipulation of the materials used in PSCs is to improve the thermal and morphological stability of PSCs [18,44,66,90,91,109]. This approach was introduced by Friend *et al.* [110] and Vanderzande *et al.* [111] previously where phenyl and phenethyl, respectively, groups were introduced in PPV. This side chain introduction prevents the photooxidation and thermal degradation, respectively, of the active layer. As glass transition temperature (T_g) of conjugated polymers has a critical impact on the thermal stability and the morphology, [112] the main purpose of a new side chain was to increase the T_g and thus the thermal stability. This approach was investigated further by using different functional groups (alcohol or ester and cinnamoyl) in a polythiophene [102,104,109,113] and a D_M-A_M conjugated polymer [103], resulting in an enhanced thermal stability without a focus on the T_g (Figure 1.15). In case of PT the specific functional groups were introduced in a small ratio (10%) into a random poly(3-alkylthiophene) to improve the thermal stability through a decay in crystallization of the fullerene derivative in the active layer [102,104,109,113]. This phase separation is shown in transmission

electron microscope (TEM) images in Figure 1.15 (left) [102]. In case of the D_M-A_M copolymer the specific functional moiety is corporated onto one side chain of the polymer. Under thermal stress the active layer shows no phase separation and fullerene crystallization, and thus an enhanced long-term stability of the PSC parameters (efficiency, Figure 1.15 right) [103].

1.4.2. Stability Investigation

For a better understanding of the stability of polymers and PSCs, it is important to measure the stability/degradation accurately in different conditions. Samples of the material/devices can be exposed to different controlled external factors (Figure 1.12.). The investigation can be e.g. under thermal stress, light exposure or in oxygen environment.

The polymers can be investigated with thermogravimetric analysis (TGA), where the decomposition of a material in an inert atmosphere is investigated with increasing heat according to a weight loss of the material. The photochemical degradation of a polymer material or active layer can be investigated by constant illumination (1000 W m^{-2}, AM 1.5) of the sample. The ultraviolet-visible light (UV-vis) absorption of the film can be monitored during this time [89,114]. The illumination results in the photodegradation of the material triggered by different photochemical reactions with an impact on the polymer backbone, the polymer side chains and the fullerene molecules, which can lead to the loss of the π-conjugation in the polymer backbone [115–118].

The PSC itself can be investigated on its stability by the influence of different controlled external factors. In 2011 an article [119] was published by participants of the international summit on OPV stability (ISOS) about consensus stability testing protocols for OPV materials, including outdoor and laboratory testing under different conditions. The laboratory conditions depend on the influence of light, temperature and humidity. Two examples of laboratory testing are the ISOS-D-2 and ISOS-L-1. The ISOS-D-2 is a dark test under high temperature (65/85°C) with ambient relative humidity, while ISOS-L-1 is a weathering test under a solar simulator under ambient temperature and relative humidity. Furthermore some guidelines to report the data was provided. As such lifetime parameters were introduced: T_{80} the time where a device retains 80% of its initial value (e.g. PCE) and its corresponding (PCE) value E_0. These values describe also the initial degradation phase.

1.5. Motivation of the Project

Nowadays the focus of research in the OPV field shifts from a small to large scale technology. Even though a lot of research is still based on the small scale, as there is still an ongoing research in increasing the maximum efficiency, it is a goal for many researchers to bring OPV to the market. Therefore the cost, performance and stability are important factors. Other important factors include the processability and scalability of the materials in OPV. My PhD project has been mainly focused on the processability (*via* RC) and stability of the polymer materials. Specifically the project was focused on the synthesis of conjugated polymers and their application in RC PSCs. The monomer and polymer materials were synthesized, characterized and tested in their ability to be applied in PSCs. The two main topics were

1. finding optimal candidates for devices processed *via* RC techniques
2. using stabilizing strategies to influence the thermal and photostability of the final devices.

With this approach it could be possible to take the final steps and bring the PSC technology closer towards the market.

1.6. References

1. Renewables 2016 Global Status Report: http://www.ren21.net/wp-content/uploads/2016/06/GSR_2016_Full_Report_REN21.pdf (19/09/2016).

2. Perez, R.; Perez, M. *A Fundamental Look At Supply Side Energy Reserves For The Planet*; 2015; Vol. 62.

3. Jean, J.; Brown, P. R.; Jaffe, R. L.; Buonassisi, T.; Bulovic, V. Pathways for Solar Photovoltaics. *Energy Environ. Sci.* **2015**, *8*, 1200–1219.

4. Brabec, C. J. Organic photovoltaics: technology and market. *Sol. Energy Mater. Sol. Cells* **2004**, *83*, 273–292.

5. Nunzi, J.-M. Organic photovoltaic materials and devices. *C. R. Phys.* **2002**, *3*, 523–542.

6. Günes, S.; Neugebauer, H.; Sariciftci, N. S. Conjugated polymer-based organic solar cells. *Chem. Rev.* **2007**, *107*, 1324–1338.

7. Jenkins, A. D.; Kratochvíl, P.; Stepto, R. F. T.; Suter, U. W. Glossary of Basic Terms in Polymer Science. *Pure Appl. Chem.* **1996**, *68*, 2287–2311.

8. Mülhaupt, R. Hermann Staudinger and the Origin of Macromolecular Chemistry. *Angew. Chemie - Int. Ed.* **2004**, *43*, 1054–1063.

9. Staudinger, H. Über Polymerisation. *Berichte der Dtsch. Chem. Gesellschaft* **1920**, *53*, 1073–1085.

10. Heeger, A. J. Nobel Lecture: Simuconducting and Metallic Polymers: The Fourth Generation of Polymeric Materials. *Rev. Mod. Phys.* **2001**, *73*, 681–700.

11. Hall, N. Twenty-five years of conducting polymers. *Chem. Commun.* **2003**, 1–4.

12. Salzner, U.; Lagowski, J. B.; Pickup, P. G.; Poirier, R. A. Comparison of geometries and electronic structures of polyacetylene, polyborole, polycyclopentadiene, polypyrrole, polyfuran, polysilole, polyphosphole, polythiophene, polyselenophene and polytellurophene. **1998**, *96*, 177–189.

13. Holt, A. L.; Leger, J. M.; Carter, S. A. Electrochemical and optical characterization of p- and n-doped poly[2-methoxy-5-(2-ethylhexyloxy)-1,4-phenylenevinylene]. *J. Chem. Phys.* **2005**, *123*, 044704(1-7).

14. Van Mullekom, H. A. M.; Vekemans, J. A. J. M.; Havinga, E. E.; Meijer, E. W. Developments in the chemistry and band gap engineering of donor-acceptor substituted conjugated polymers. *Mater. Sci. Eng.* **2001**, *32*, 1–40.

15. Cited from http://goldbook.iupac.org/ search: ”conjugated systems” from 28. October 2016.

16. Chochos, C. L.; Choulis, S. a. How the structural deviations on the backbone of conjugated polymers influence their optoelectronic properties and photovoltaic performance. *Prog. Polym. Sci.* **2011**, *36*, 1326–1414.

17. Havinga, E. E.; Ten, H. W.; Wynberg, H. A new class of small band gap organic polymer conductors. *Polym. Bull.* **1992**, *29*, 119–126.

18. Lu, L.; Zheng, T.; Wu, Q.; Schneider, A. M.; Zhao, D.; Yu, L. Recent Advances in Bulk Heterojunction Polymer Solar Cells. *Chem. Rev.* **2015**, *115*, 12666–12731.

19. Kularatne, R. S.; Magurudeniya, H. D.; Sista, P.; Biewer, M. C.; Stefan, M. C. Donor-acceptor semiconducting polymers for organic solar cells. *J. Polym. Sci. Part A Polym. Chem.* **2013**, *51*, 743–768.

20. Braun, D.; Cherdron, H.; Rehahn, M.; Ritter, H.; Voit, B. *Polymer Synthesis: Theory and Practice*; 5th ed.; Springer Verlag: Berlin, 2013.

21. Stille, B. J. K. The Palladium-Catalyzed Cross-Coupling Reactions of Organotin Reagents with Organic Electrophiles. *Angew. Chemie - Int. Ed.* **1986**, *25*, 508–524.

22. Bao, Z.; Chan, W.; Yu, L. Synthesis of Conjugated Polymer by the Stille Coupling Reaction. *Chem. Mater.* **1993**, *5*, 2–3.

23. Marzano, G.; Ciasca, C. V; Babudri, F.; Bianchi, G.; Pellegrino, A.; Po, R.; Farinola, G. M. Organometallic Approaches to Conjugated Polymers for Plastic Solar Cells: From Laboratory Synthesis to Industrial Production. *European J. Org. Chem.* **2014**, 6583–6614.

24. Casado, A. L.; Espinet, P. Mechanism of the Stille Reaction. 1. The Transmetalation Step. *J. Am. Chem. Soc.* **1998**, *120*, 8978–8985.

25. Casado, A. L.; Espinet, P.; Gallego, A. M. Mechanism of the stille reaction. 2. Couplings of aryl triflates with vinyltributyltin. Observation of intermediates. A more comprehensive scheme. *J. Am. Chem. Soc.* **2000**, *122*, 11771–11782.

26. Espinet, P.; Echavarren, A. M. The mechanisms of the Stille reaction. *Angew. Chemie - Int. Ed.* **2004**, *43*, 4704–4734.

27. Liu, Y.; Zhao, J.; Li, Z.; Mu, C.; Ma, W.; Hu, H.; Jiang, K.; Lin, H.; Ade, H.; Yan, H. Aggregation and morphology control enables multiple cases of high-efficiency polymer solar cells. *Nat. Commun.* **2014**, *5*, 5293 (1-8).

28. Yue, W.; Ashraf, R. S.; Nielsen, C. B.; Collado-Fregoso, E.; Niazi, M. R.; Yousaf, S. A.; Kirkus, M.; Chen, H.-Y.; Amassian, A.; Durrant, J. R.; McCulloch, I. A Thieno[3,2-b][1]benzothiophene Isoindigo Building Block for Additive- and Annealing-Free High-Performance Polymer Solar Cells. *Adv. Mater.* **2015**, *27*, 4702–4707.

29. Zhao, J.; Li, Y.; Yang, G.; Jiang, K.; Lin, H.; Ade, H.; Ma, W.; Yan, H. Efficient organic solar cells processed from hydrocarbon solvents. *Nat. Energy* **2016**, *1*, 15027 (1-7).

30. Krebs, F.; Gevorgyan, S.; Alstrup, J. A roll-to-roll process to flexible polymer solar cells: model studies, manufacture and operational stability studies. *J. Mater. Chem.* **2009**, 5442–5451.

31. Krebs, F. C.; Espinosa, N.; Hösel, M.; Søndergaard, R. R.; Jørgensen, M. 25th anniversary article: Rise to power - OPV-based solar parks. *Adv. Mater.* **2014**, *26*, 29–39.

32. Wöhrle, D.; Meissner, D. Organic Solar Cells. *Adv. Mater.* **1991**, *3*, 129–138.

33. Chamberlain, G. A. Organic solar cells: A review. *Sol. Cells* **1983**, *8*, 47–83.

34. Tang, C. W. Two-layer organic photovoltaic cell. *Appl. Phys. Lett.* **1986**, *48*, 183–185.

35. Grossiord, N.; Kroon, J. M.; Andriessen, R.; Blom, P. W. M. Degradation mechanisms in organic photovoltaic devices. *Org. Electron.* **2012**, *13*, 432–456.

36. Allemand, P.-M.; Koch, A.; Wudl, F. Two Different Fullerenes Have the Same Cyclic Voltammetry. *J. Am. Chem. Soc.* **1991**, *113*, 1050–1051.

37. Sariciftci, N. S.; Smilowitz, L.; Heeger, A. J.; Wudl, F. Photoinduced Electron Transfer from a Conducting Polymer to Buckminsterfullerene. *Adv. Sci.* **1992**, *258*, 1474–1476.

38. Halls, J. J. M.; Walsh, C. A.; Greenham, N. C.; Marseglia, E. A.; Friend, R. H.; Moratti, S. C.; Holmes, A. B. Efficient photodiodes from interpendetrating polymer networks. *Lett. to Nat.* **1995**, *376*, 498–500.

39. Yu, G.; Gao, J.; Hummelen, J. C.; Wudl, F.; Heeger, A. J. Polymer Photovoltaic Cells: Enhanced Efficiencies via a Network of Internal Donor-Acceptor Heterojunctions. *Science (80-.).* **1995**, *270*, 1789–1791.

40. Abdulrazzaq, O. a.; Saini, V.; Bourdo, S.; Dervishi, E.; Biris, A. S. Organic Solar Cells: A Review of Materials, Limitations, and Possibilities for Improvement. *Part. Sci. Technol.* **2013**, *31*, 427–442.

41. Koeppe, R.; Sariciftci, N. S. Photoinduced charge and energy transfer involving fullerene derivatives. *Photochem. Photobiol. Sci. ciences* **2006**, *5*, 1122–1131.

42. Kaur, N.; Singh, M.; Pathak, D.; Wagner, T.; Nunzi, J. M. Organic materials for photovoltaic applications: Review and mechanism. *Synth. Met.* **2014**, *190*, 20–26.

43. Steim, R.; Kogler, F. R.; Brabec, C. J. Interface materials for organic solar cells. *J. Mater. Chem.* **2010**, *20*, 2499–2512.

44. Jørgensen, M.; Norrman, K.; Gevorgyan, S. a.; Tromholt, T.; Andreasen, B.; Krebs, F. C. Stability of polymer solar cells. *Adv. Mater.* **2012**, *24*, 580–612.

45. Su, Y.-W.; Lan, S.-C.; Wei, K.-H. Organic photovoltaics. *Mater. Today* **2012**, *15*, 554–562.

46. Carlé, J. E.; Andersen, T. R.; Helgesen, M.; Bundgaard, E.; Jørgensen, M.; Krebs, F. C. A laboratory scale approach to polymer solar cells using one coating/printing machine, flexible substrates, no ITO, no vacuum and no spincoating. *Sol. Energy Mater. Sol. Cells* **2013**, *108*, 126–128.

47. Helgesen, M.; Carlé, J. E.; Krebs, F. C. Slot-Die Coating of a High Performance Copolymer in a Readily Scalable Roll Process for Polymer Solar Cells. *Adv. Energy Mater.* **2013**, *3*, 1664–1669.

48. Sahu, N.; Parija, B.; Panigrahi, S. Fundamental understanding and modeling of spin coating process: A review. *Indian J. Phys.* **2009**, *83*, 493–502.

49. Burgues-Ceballos, I.; Stella, M.; Lacharmoise, P.; Martinez-Ferrero, E. Towards industrialization of polymer solar cells: material processing for upscaling. *J. Mater. Chem. A* **2014**, *2*, 17711–17722.

50. Dam, H. F.; Krebs, F. C. Simple roll coater with variable coating and temperature control for printed polymer solar cells. *Sol. Energy Mater. Sol. Cells* **2012**, *97*, 191–196.

51. Hösel, M.; Søndergaard, R. R.; Jørgensen, M.; Krebs, F. C. Fast Inline Roll-to-Roll Printing for Indium-Tin-Oxide-Free Polymer Solar Cells Using Automatic Registration. *Energy Technol.* **2013**, *1*, 102–107.

52. Brunetti, F. G.; Kumar, R.; Wudl, F. Organic electronics from perylene to organic photovoltaics: painting a brief history with a broad brush. *J. Mater. Chem.* **2010**, *20*, 2934–2948.

53. Kularatne, R. S.; Sista, P.; Nguyen, H. Q.; Bhatt, M. P.; Biewer, M. C.; Stefan, M. C. Donor–Acceptor Semiconducting Polymers Containing Benzodithiophene with Bithienyl Substituents. *Macromolecules* **2012**, *45*, 7855–7862.

54. Rostalski, J.; Meissner, D. Monochromatic versus solar efficiencies of organic solar cells. *Sol. Energy Mater. Sol. Cells* **2000**, *61*, 87–95.

55. Widmer, J.; Tietze, M.; Leo, K.; Riede, M. Open-Circuit Voltage and Effective Gap of Organic Solar Cells. *Adv. Funct. Mater.* **2013**, *23*, 5814–5821.

56. Liu, J.; Shi, Y.; Yang, Y. Solvation Induced Morphology Effects on the Performance of Polymer Based Photovoltaic Devices. *Adv. Funct. Mater.* **2001**, *11*, 420–424.

57. Brabec, C. J.; Cravino, a.; Meissner, D.; Sariciftci, N. S.; Fromherz, T.; Rispens, M. T.; Sanchez, L.; Hummelen, J. C. Origin of the Open Circuit Voltage of Plastic Solar Cells. *Adv. Funct. Mater.* **2001**, *11*, 374–380.

58. Scharber, M. C.; Mühlbacher, D.; Koppe, M.; Denk, P.; Waldauf, C.; Heeger, A. J.; Brabec, C. J. Design Rules for Donors in Bulk-Heterojunction Solar Cells - Towards 10 % Energy-Conversion Efficiency. *Adv. Mater.* **2006**, *18*, 789–794.

59. Neugebauer, H.; Brabec, C.; Hummelen, J. C.; Sariciftci, N. S. Stability and photodegradation mechanisms of conjugated polymer/ fullerene plastic solar cells. *Sol. Energy Mater. Sol. Cells* **2000**, *61*, 35–42.

60. Rivaton, A.; Chambon, S.; Manceau, M.; Gardette, J. L.; Lemaître, N.; Guillerez, S. Light-induced degradation of the active layer of polymer-based solar cells. *Polym. Degrad. Stab.* **2010**, *95*, 278–284.

61. Manceau, M.; Rivaton, A.; Gardette, J. L.; Guillerez, S.; Lemaître, N. The mechanism of photo- and thermooxidation of poly(3-hexylthiophene) (P3HT) reconsidered. *Polym. Degrad. Stab.* **2009**, *94*, 898–907.

62. Tournebize, A.; Gardette, J.-L.; Taviot-Guého, C.; Bégué, D.; Arnaud, M. A.; Dagron-Lartigau, C.; Medlej, H.; Hiorns, R. C.; Beaupré, S.; Leclerc, M.; Rivaton, A. Is there a photostable conjugated polymer for efficient solar cells? *Polym. Degrad. Stab.* **2015**, *112*, 175–184.

63. Chambon, S.; Manceau, M.; Firon, M.; Cros, S.; Rivaton, A.; Gardette, J. L. Photo-oxidation in an 18O2 atmosphere: A powerful tool to elucidate the mechanism of UV-visible light oxidation of polymers - Application to the photodegradation of MDMO-PPV. *Polymer (Guildf).* **2008**, *49*, 3288–3294.

64. Norrman, K.; Madsen, M. V.; Gevorgyan, S. a.; Krebs, F. C. Degradation Patterns in Water and Oxygen of an Inverted Polymer Solar Cell. *J. Am. Chem. Soc.* **2010**, *132*, 16883–16892.

65. Jørgensen, M.; Norrman, K.; Krebs, F. C. Stability/degradation of polymer solar cells. *Sol. Energy Mater. Sol. Cells* **2008**, *92*, 686–714.

66. Lee, J. U.; Jung, J. W.; Jo, J. W.; Jo, W. H. Degradation and stability of polymer-based solar cells. *J. Mater. Chem.* **2012**, 24265–24283.

67. Madogni, V. I.; Kounouhéwa, B.; Akpo, A.; Agbomahéna, M.; Hounkpatin, S. A.; Awanou, C. N. Comparison of degradation mechanisms in organic photovoltaic devices upon exposure to a temperate and a subequatorial climate. *Chem. Phys. Lett.* **2015**, *640*, 201–214.

68. Savagatrup, S.; Printz, A. D.; O'Connor, T. F.; Zaretski, A. V.; Rodriquez, D.; Sawyer, E. J.; Rajan, K. M.; Acosta, R. I.; Root, S. E.; Lipomi, D. J. Mechanical degradation and stability of organic solar cells: molecular and microstructural determinants. *Energy Environ. Sci.* **2014**, *8*, 55–80.

69. Turkovic, V.; Engmann, S.; Egbe, D. a. M.; Himmerlich, M.; Krischok, S.; Gobsch, G.; Hoppe, H. Multiple stress degradation analysis of the active layer in organic photovoltaics. *Sol. Energy Mater. Sol. Cells* **2014**, *120*, 654–668.

70. Waters, H.; Bristow, N.; Moudam, O.; Chang, S. W.; Su, C. J.; Wu, W. R.; Jeng, U. S.; Horie, M.; Kettle, J. Effect of processing additive 1,8-octanedithiol on the lifetime of PCPDTBT based Organic Photovoltaics. *Org. Electron. physics, Mater. Appl.* **2014**, *15*, 2433–2438.

71. Gevorgyan, S. A.; Heckler, I. M.; Bundgaard, E.; Corazza, M.; Hösel, M.; Søndergaard, R.; Benatto, G. A.; Jørgensen, M.; Krebs, F. C. Improving , characterizing and predicting the lifetime of organic photovoltaics. *J. Phys. D. Appl. Phys.* **2017**, *50*, 103001 (1-35).

72. George, Z.; Xia, Y.; Sharma, A.; Lindqvist, C.; Andersson, G. G.; Inganäs, O.; Moons, E.; Müller, C.; Andersson, M. R. Two-in-one: cathode modification and improved solar cell blend stability through addition of modified fullerenes. *J. Mater. Chem. A* **2016**, 2663–2669.

73. Chen, L.; Tian, S.; Chen, Y. Enhanced performance for organic bulk heterojunction solar cells by cooperative assembly of ter(ethylene oxide) pendants. *Polym. Chem.* **2014**, *5*, 4480.

74. Chen, C.-P.; Huang, C.-Y.; Chuang, S.-C. Highly Thermal Stable and Efficient Organic Photovoltaic Cells with Crosslinked Networks Appending Open-Cage Fullerenes as Additives. *Adv. Funct. Mater.* **2014**, n/a-n/a.

75. Wang, S.; Qu, Y.; Li, S.; Ye, F.; Chen, Z.; Yang, X. Improved Thermal Stability of Polymer Solar Cells by Incorporating Porphyrins. *Adv. Funct. Mater.* **2015**, *25*, 748–757.

76. Wang, S.; Wang, M.; Chen, Z.; Yang, X. Selection strategy of porphyrins for achieving thermally stable polymer solar cells. *J. Mater. Chem. A* **2015**, *3*, 21051–21059.

77. Li, S.; Liu, W.; Shi, M.; Mai, J.; Lau, T.-K.; Wan, J.-H.; Lu, X.; Li, C.-Z.; Chen, H. A spirobifluorene and diketopyrrolopyrrole moieties based non-fullerene acceptor for efficient and thermally stable polymer solar cells with high open-circuit voltage. *energy* **2016**, *9*, 604–610.

78. Lee, J. J.; Lee, S. H.; Kim, F. S.; Choi, H. H.; Kim, J. H. Simultaneous enhancement of the efficiency and stability of organic solar cells using PEDOT:PSS grafted with a PEGME buffer layer. *Org. Electron. physics, Mater. Appl.* **2015**, *26*, 191–199.

79. Shi, Y.; Tan, L.; Chen, L.; Chen, Y. Self-assembled buffer layer from conjugated diblock copolymers with ethyleneoxide side chains for high efficiency polymer solar cells. *J. Mater. Chem. C* **2014**, *2*, 8054–8064.

80. Hou, X.; Li, Q.; Cheng, T.; Yu, L.; Wang, F.; Lin, J.; Dai, S.; Li, Y.; Tan, Z. Improvement of the power conversion efficiency and long term stability of polymer solar cells by incorporation of amphiphilic Nafion doped PEDOT-PSS as a hole extraction layer. *J. Mater. Chem. A* **2015**, *3*, 18727–18734.

81. Mateker, W. R.; Douglas, J. D.; Cabanetos, C.; Sachs-Quintana, I. T.; Bartelt, J. a.; Hoke, E. T.; El Labban, A.; Beaujuge, P. M.; Fréchet, J. M. J.; McGehee, M. D. Improving the long-term stability of PBDTTPD polymer solar cells through material purification aimed at removing organic impurities. *Energy Environ. Sci.* **2013**, *6*, 2529.

82. Li, L.; Jacobs, D. L.; Che, Y.; Huang, H.; Bunes, B. R.; Yang, X.; Zang, L. Poly(3-hexylthiophene) nanofiber networks for enhancing the morphology stability of polymer solar cells. *Org. Electron. physics, Mater. Appl.* **2013**, *14*, 1383–1390.

83. Sygletou, M.; Kakavelakis, G.; Paci, B.; Generosi, A.; Kymakis, E.; Stratakis, E. Enhanced Stability of Aluminum Nanoparticle-Doped Organic Solar Cells. *ACS Appl. Mater. Interfaces* **2015**, *7*, 17756–17764.

84. Zhang, S.; Yang, B.; Liu, D.; Zhang, H.; Zhao, W.; Wang, Q.; He, C.; Hou, J. Correlations among Chemical Structure, Backbone Conformation, and Morphology in Two Highly Efficient Photovoltaic Polymer Materials. *Macromolecules* **2016**, *49*, 120–126.

85. Wu, Y.; Li, Z.; Ma, W.; Huang, Y.; Huo, L.; Guo, X.; Zhang, M.; Ade, H.; Hou, J. PDT-S-T: A new polymer with optimized molecular conformation for controlled aggregation and π-π Stacking and its application in efficient photovoltaic devices. *Adv. Mater.* **2013**, *25*, 3449–3455.

86. Carlé, J. E.; Helgesen, M.; Zawacka, N. K.; Madsen, M. V.; Bundgaard, E.; Krebs, F. C. A comparative study of fluorine substituents for enhanced stability of flexible and ITO-free high-performance polymer solar cells. *J. Polym. Sci. Part B Polym. Phys.* **2014**, *52*, 893–899.

87. Nguyen, T. L.; Choi, H.; Ko, S.-J.; Uddin, M. a.; Walker, B.; Yum, S.; Jeong, J.-E.; Yun, M. H.; Shin, T. J.; Hwang, S.; Kim, J. Y.; Woo, H. Y. Semi-crystalline photovoltaic polymers with efficiency exceeding 9% in a ~300 nm thick conventional single-cell device. *Energy Environ. Sci.* **2014**, *7*, 3040–3051.

88. Livi, F.; Zawacka, N. K.; Angmo, D.; Jørgensen, M.; Krebs, F. C.; Bundgaard, E. Influence of Side Chain Position on the Electrical Properties of Organic Solar Cells Based on Dithienylbenzothiadiazole- alt -phenylene Conjugated Polymers. *Macromolecules* **2015**, *48*, 3481–3492.

89. Manceau, M.; Bundgaard, E.; Carlé, J. E.; Hagemann, O.; Helgesen, M.; Søndergaard, R.; Jørgensen, M.; Krebs, F. C. Photochemical stability of π-conjugated polymers for polymer solar cells: a rule of thumb. *J. Mater. Chem.* **2011**, *21*, 4132–4141.

90. Bundgaard, E.; Helgesen, M.; Carlé, J. E.; Krebs, F. C.; Jørgensen, M. Advanced functional polymers for increasing the stability of organic photovoltaics. *Macromol. Chem. Phys.* **2013**, *214*, 1546–1558.

91. Rumer, J. W.; McCulloch, I. Organic photovoltaics: Crosslinking for optimal morphology and stability. *Mater. Today* **2015**, *18*, 425–435.

92. Nam, C.-Y.; Qin, Y.; Park, Y. S.; Hlaing, H.; Lu, X.; Ocko, B. M.; Black, C. T.; Grubbs, R. B. Photo-Cross-Linkable Azide-Functionalized Polythiophene for Thermally Stable Bulk Heterojunction Solar Cells. *Macromolecules* **2012**, *45*, 2338–2347.

93. Helgesen, M.; Madsen, M. V.; Andreasen, B.; Tromholt, T.; Andreasen, J. W.; Krebs, F. C. Thermally reactive Thiazolo[5,4-d]thiazole based copolymers for high photochemical stability in polymer solar cells. *Polym. Chem.* **2011**, *2*, 2536–2542.

94. Helgesen, M.; Carlé, J. E.; Andreasen, B.; Hösel, M.; Norrman, K.; Søndergaard, R.; Krebs, F. C. Rapid flash annealing of thermally reactive copolymers in a roll-to-roll process for polymer solar cells. *Polym. Chem.* **2012**, *3*, 2649–2655.

95. Bundgaard, E.; Hagemann, O.; Bjerring, M.; Nielsen, N. C.; Andreasen, J. W.; Andreasen, B.; Krebs, F. C. Removal of Solubilizing Side Chains at Low Temperature: A New Route to Native Poly(thiophene). *Macromolecules* **2012**, *45*, 3644–3646.

96. Gevorgyan, S. A.; Krebs, F. C. Bulk Heterojunctions Based on Native Polythiophene. *Chem. Mater.* **2008**, *20*, 4386–4390.

97. Helgesen, M.; Krebs, F. C. Photovoltaic Performance of Polymers Based on Dithienylthienopyrazines Bearing Thermocleavable Benzoate Esters. *Macromolecules* **2010**, *43*, 1253–1260.

98. Krebs, F. C.; Spanggaard, H. Significant Improvement of Polymer Solar Cell Stability. *Chem. Mater.* **2005**, *17*, 5235–5237.

99. Xu, X.; Wu, Y.; Fang, J.; Li, Z.; Wang, Z.; Li, Y.; Peng, Q. Side-chain engineering of benzodithiophene-fluorinated quinoxaline low-band-gap co-polymers for high-performance polymer solar cells. *Chem. - A Eur. J.* **2014**, *20*, 13259–13271.

100. Li, Z.; Wu, F.; Lv, H.; Yang, D.; Chen, Z.; Zhao, X.; Yang, X. Side-Chain Engineering for Enhancing the Thermal Stability of Polymer Solar Cells. *Adv. Mater.* **2015**, *27*, 6999–7003.

101. Morse, G. E.; Tournebize, A.; Rivaton, A.; Chassé, T.; Taviot-Gueho, C.; Blouin, N.; Lozman, O. R.; Tierney, S. The effect of polymer solubilizing side-chains on solar cell stability. *Phys. Chem. Chem. Phys.* **2015**, *17*, 11884–11897.

102. Kesters, J.; Kudret, S.; Bertho, S.; Van den Brande, N.; Defour, M.; Van Mele, B.; Penxten, H.; Lutsen, L.; Manca, J.; Vanderzande, D.; Maes, W. Enhanced intrinsic stability of the bulk heterojunction active layer blend of polymer solar cells by varying the polymer side chain pattern. *Org. Electron.* **2014**, *15*, 549–562.

103. Kesters, J.; Verstappen, P.; Raymakers, J.; Vanormelingen, W.; Drijkoningen, J.; D'Haen, J.; Manca, J.; Lutsen, L.; Vanderzande, D.; Maes, W. Enhanced Organic Solar Cell Stability by Polymer (PCPDTBT) Side Chain Functionalization. *Chem. Mater.* **2015**, *27*, 1332–1341.

104. Bertho, S.; Campo, B.; Piersimoni, F.; Spoltore, D.; D'Haen, J.; Lutsen, L.; Maes, W.; Vanderzande, D.; Manca, J.

Improved thermal stability of bulk heterojunctions based on side-chain functionalized poly(3-alkylthiophene) copolymers and PCBM. *Sol. Energy Mater. Sol. Cells* **2013**, *110*, 69–76.

105. Campo, B. J.; Bevk, D.; Kesters, J.; Gilot, J.; Bolink, H. J.; Zhao, J.; Bolsée, J.-C.; Oosterbaan, W. D.; Bertho, S.; D ’haen, J.; Manca, J.; Lutsen, L.; Assche, G. Van; Maes, W.; Janssen, R. A. J.; Vanderzande, D. Ester-functionalized poly(3-alkylthiophene) copolymers: Synthesis, physicochemical characterization and performance in bulk heterojunction organic solar cells. *Org. Electron.* **2013**, *14*, 523–534.

106. Verstappen, P.; Kesters, J.; D’Olieslaeger, L.; Drijkoningen, J.; Cardinaletti, I.; Vangerven, T.; Bruijnaers, B. J.; Willems, R. E. M.; D’Haen, J.; Manca, J. V.; Lutsen, L.; Vanderzande, D. J. M.; Maes, W. Simultaneous Enhancement of Solar Cell Efficiency and Stability by Reducing the Side Chain Density on Fluorinated PCPDTQx Copolymers. *Macromolecules* **2015**, *48*, 3873–3882.

107. Distler, A.; Sauermann, T.; Egelhaaf, H. J.; Rodman, S.; Waller, D.; Cheon, K. S.; Lee, M.; Guldi, D. M. The effect of PCBM dimerization on the performance of bulk heterojunction solar cells. *Adv. Energy Mater.* **2014**, *4*, 1300693 (1-6).

108. Guo, M.-N.; Liu, S.-W.; Guo, N.; Yang, L.-Y.; Qin, W.-J.; Yin, S.-G. Performance and Stability of Polymer Solar Cells Based on the Blends of Poly(3-Hexylthiophene) and Indene-C60 Bis-Adduct. *Chinese Phys. Lett.* **2016**, *33*, 3–7.

109. Cardinaletti, I.; Kesters, J.; Bertho, S.; Conings, B.; Piersimoni, F.; D’Haen, J.; Lutsen, L.; Nesladek, M.; Van Mele, B.; Van Assche, G.; Vandewal, K.; Salleo, A.; Vanderzande, D.; Maes, W.; Manca, J. V. Toward bulk heterojunction polymer solar cells with thermally stable active layer morphology. *J. Photonics Energy* **2014**, *4*, 040997 (1-12).

110. Koch, A. T. H.; Harrison, N. T.; Haylett, N.; Daik, R.; Feast, W. J.; Friend, R. H. Enhanced photostability of poly (1,3-phenylene diphenylvinylene)-derivatives by diphenyl-substitution. *Synth. Met.* **1999**, *100*, 113–122.

111. Vandenbergh, J.; Conings, B.; Bertho, S.; Kesters, J.; Spoltore, D.; Esiner, S.; Zhao, J.; Van Assche, G.; Wienk, M. M.; Maes, W.; Lutsen, L.; Van Mele, B.; Janssen, R. A. J.; Manca, J.; Vanderzande, D. J. M. Thermal Stability of Poly[2-methoxy-5-(2’-phenylethoxy)-1,4-phenylenevinylene] (MPE-PPV): Fullerene Bulk Heterojunction Solar Cells. *Macromolecules* **2011**, *44*, 8470–8478.

112. Müller, C. On the glass transition of polymer semiconductors and its impact on polymer solar cell stability. *Chem. Mater.* **2015**, *27*, 2740–2754.

113. Campo, B. J.; Bevk, D.; Kesters, J.; Gilot, J.; Bolink, H. J.; Zhao, J.; Bolsée, J.-C.; Oosterbaan, W. D.; Bertho, S.; D’Haen, J.; Manca, J.; Lutsen, L.; Van Assche, G.; Maes, W.; Janssen, R. A. J.; Vanderzande, D. Ester-functionalized poly(3-alkylthiophene) copolymers: Synthesis, physicochemical characterization and performance in bulk heterojunction organic solar cells. *Org. Electron.* **2013**, *14*, 523–534.

114. Tromholt, T.; Madsen, M. V.; Carlé, J. E.; Helgesen, M.; Krebs, F. C. Photochemical stability of conjugated polymers, electron acceptors and blends for polymer solar cells resolved in terms of film thickness and absorbance. *J. Mater. Chem.* **2012**, *22*, 7592–7601.

115. Schweitzer, C.; Schmidt, R. Physical mechanisms of generation and deactivation of singlet oxygen. *Chem. Rev.* **2003**, *103*, 1685–1757.

116. Abdou, A.; Holdcroft, S. Mechanisms of Photodegradation of Poly(3-alkylthiophenes) in Solution. *Macromolecules* **1993**, *26*, 2954–2962.

117. Wasserman, H. H.; Scheffer, J. R.; Cooperb, J. L. Singlet Oxygen Reactions with 9,10-Diphenylanthracene Peroxide. *J. Am. Chem. Soc.* **1972**, *94*, 4991–4996.

118. Krebs, F. C. *Stability and Degradation of Organic and Polymer Solar Cells*; Krebs, F. C., Ed.; 1st ed.; John Wiley & Sons, Ltd: West Sussez, United Kingdom, 2012.

119. Reese, M. O.; Gevorgyan, S. A.; Jørgensen, M.; Bundgaard, E.; Kurtz, S. R.; Ginley, D. S.; Olson, D. C.; Lloyd, M. T.; Morvillo, P.; Katz, E. A.; Elschner, A.; Haillant, O.; Currier, T. R.; Shrotriya, V.; Hermenau, M.; Riede, M.; Kirov, K. R.; Trimmel, G.; Rath, T.; Inganäs, O.; Zhang, F.; Andersson, M.; Tvingstedt, K.; Lira-Cantu, M.; Laird, D.; McGuiness, C.; Gowrisanker, S.; Pannone, M.; Xiao, M.; Hauch, J.; Steim, R.; Delongchamp, D. M.; Rösch, R.; Hoppe, H.; Espinosa, N.; Urbina, A.; Yaman-Uzunoglu, G.; Bonekamp, J.-B.; van Breemen, A. J. J. M.; Girotto, C.; Voroshazi, E.; Krebs, F. C. Consensus stability testing protocols for organic photovoltaic materials and devices. *Sol. Energy Mater. Sol. Cells* **2011**, *95*, 1253–1267.

Chapter 2.

Screening of Polymers for Polymer Solar Cells

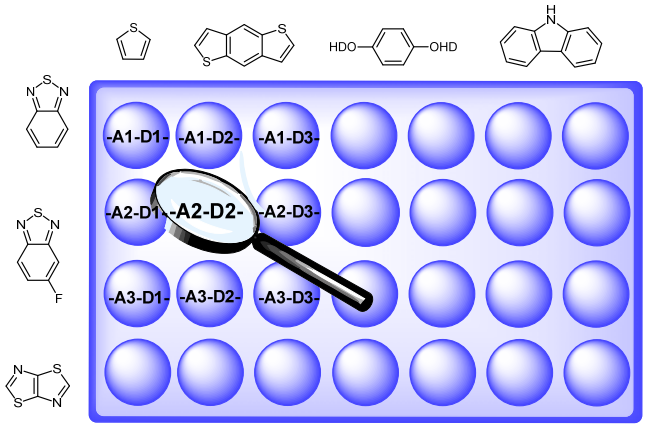

2.1. Introduction

The research in PSCs was increased exponentially over the last years; in particular more complex polymers were synthesized in order to obtain high performing PSCs. The performance is compared within the PSC research area with an ongoing competition to reach the highest efficiencies. High efficiencies of 10% have been obtained for small area devices (mm^2 scale) [1]. The efficiencies for large area PSCs are significant lower as demonstrated in Figure 2.1 [2]. The PCE is plotted as a function of the active area, showing a drop in efficiency with an increased active area. For the large scale process different criteria may need to be fulfilled. Most devices are produced via SC on glass substrates, often using ITO as a transparent electrode. For larger devices, however, flexible substrates, no rare or non-toxic materials (e.g. no ITO) and RC processes are desirable and the focus should shift more towards the production and final applications. In the laboratories at DTU Energy, the main interest of research is on the production of large area PSCs by applying the roll-to-roll technology.

A large amount of polymer materials are described in literature and makes them to suitable candidates for light absorbing materials in the active layer based on promising D_M or A_M monomers like benzo[*c*][1,2,5]thiadiazole (BT) or thiophene (Th) [3,4]. These advanced conjugated polymers have been successful applied and optimized in small laboratory-scale SC devices to improve the PCE continuously [5]. In

a perspective Po *et al.* [6] surveyed and analyzed the polymer synthesis and application in PSCs, which were published in 2013, in terms of their synthetic complexity and high efficiency. The synthetic complexity describes the ability for a large scale production of the polymers. The group evaluated different polymers with efficiencies over 6% in their scalability potential addressing the problems of upscaling the synthesis by taking different parameters into account (e.g. the synthetic steps and yields). They also addressed the importance of four requirements for a light absorbing polymer material when applied in PSC: performance (high efficiency), stability (high photochemical stability of the polymer/device and morphological stability of the active layer), cost (material production: synthetic and purification steps and cost of the raw materials) and process (printability of the layers in PSCs). The *golden triangle* introduced in Chapter 1 can in this context be modified to be a *golden square* (Figure 2.2.) with these four critical areas for solar technologies.

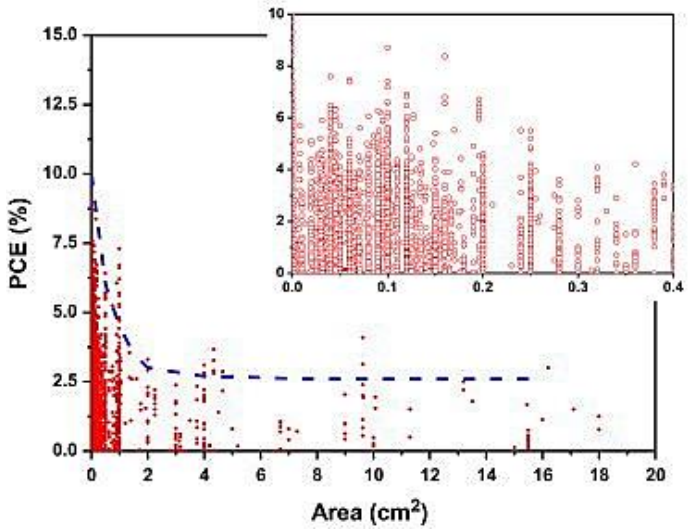

Figure 2.1. *A plot of the PCE as a function of the active area. Reprinted from* [2] *with permission from Elsevier ©2013.*

The main focus in this chapter is to build a library of light absorbing polymers used in RC PSC to show the polymers potential in fulfilling the above described criteria. One could argue that many polymer materials have already been compared in reviews [7–9], however each laboratory is using different methods (spin speed, light source) and do not always fulfill all criteria. Therefore similar devices can result in different performances, which can than lead to a wrong impression of their potential. Studies have also shown that not only the production but also the PSC testing of the same devices in different laboratories gives a diversity of the results [10].

Hence a large amount of polymers were applied in RC PSCs and the work was carried out in a 2 year project in a team of many researchers. The main focus of my contribution was the RC production of the PSCs and their analysis. However, the project is presented herein as a whole. A total amount of 14 acceptor and 8 donor monomers were combinatorial paired resulting in 104 different polymers with different optical,

electrical and PV properties. In the course of the chapter the polymers were eliminated. The elimination started during the synthesis of the polymers, continued with the coating process and was finalized by the device analysis. Only some of the polymers could be applied in PSC with different efficiencies among the different devices. In the end a few leading polymer candidates were identified to be suitable for PSCs prepared *via* RC techniques. This was done by the introduction of a merit factor which is based on the four criteria from the critical areas (Figure 2.2). The factor will be described in detail in Chapter 2.4.

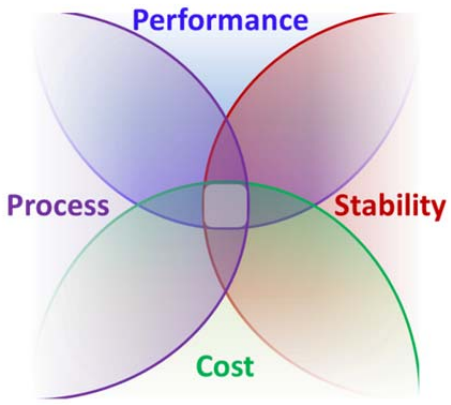

Figure 2.2. *Adapted critical areas for solar technologies.*

2.2. Donor-Acceptor-Polymers

2.2.1. Synthesis

104 polymers were synthesized *via* combinatorial pairing of the monomers **M1**-**M13** (A_M) with **M14**-**M21** (D_M). The monomers (Figure 2.3) were chosen based on high efficient devices previously reported in the literature [11–13]. One example is **M6** which was chosen as an A_M for polymers with reported efficiencies of up to 5.6% [11–13]. To ensure good solubility of the polymer, each monomer was bearing a sufficient side chain. Therefore some monomers were used with a variation in their side chains (**M2**, **M6**, **M14**, **M18** and **M21**). However, for some structures a shorter side chain could improve the results. For example the polymers from the combination **M6M20** with a dodecyl side chain on the Th's next to the thiazolo[5,4-d]thiazole (TzTz) group were not as promising (PCE = 0.3%) [14] as for **P8** where the Th's are bearing a hexyl side chain (PCE = 1.8%) [15].

The polymers were mainly prepared *via* Stille cross-coupling polymerization of a dibrominated A_M and distannylated D_M. Some selected polymers (**P1**-**P9**) are shown in Figure 2.4. The selection was carried out by elimination of failing polymers during synthesis and analysis of the 104 polymers. The 9 selected polymers

are in good agreement with the *golden square* (high performance, stability, processing and synthetic steps (=cost) in comparison to **P3HT**). These 9 polymers are described in more detail on the following pages.

14 of the polymers (hereof 8 based on **M19**) could not be synthesized due to steric hindrance and low reactivity of the monomers. These polymers are indicated by **x** in Table 2.2 (page 30).

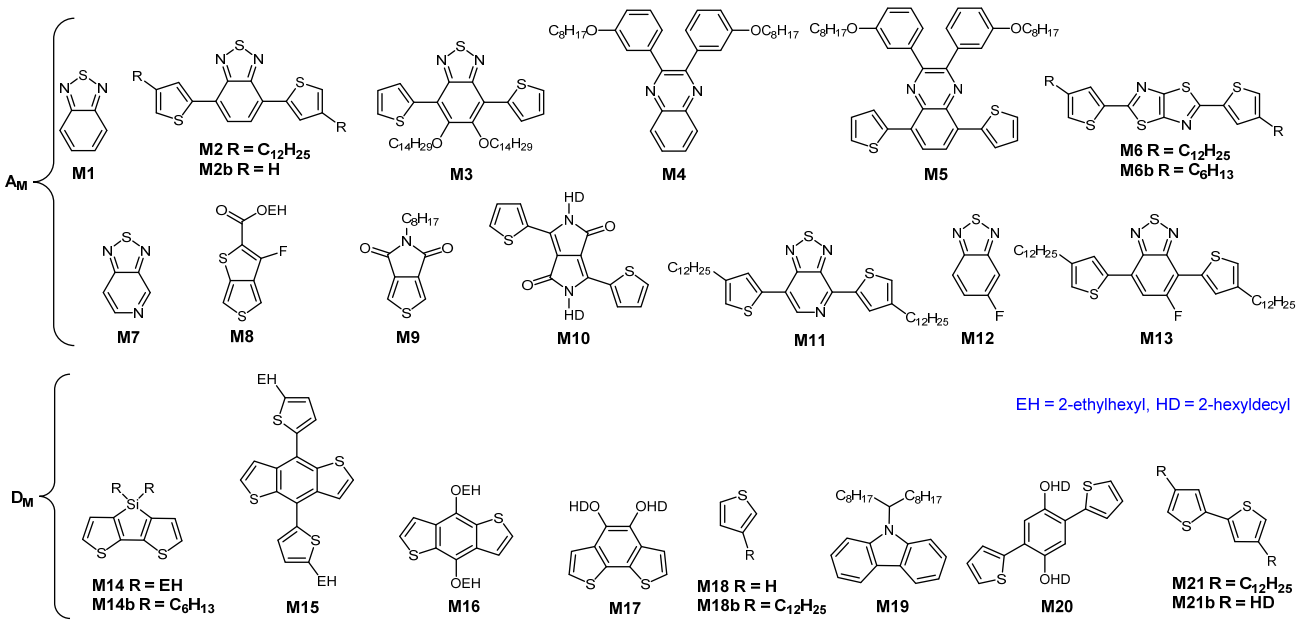

Figure 2.3. *Monomer units used for polymerization.*

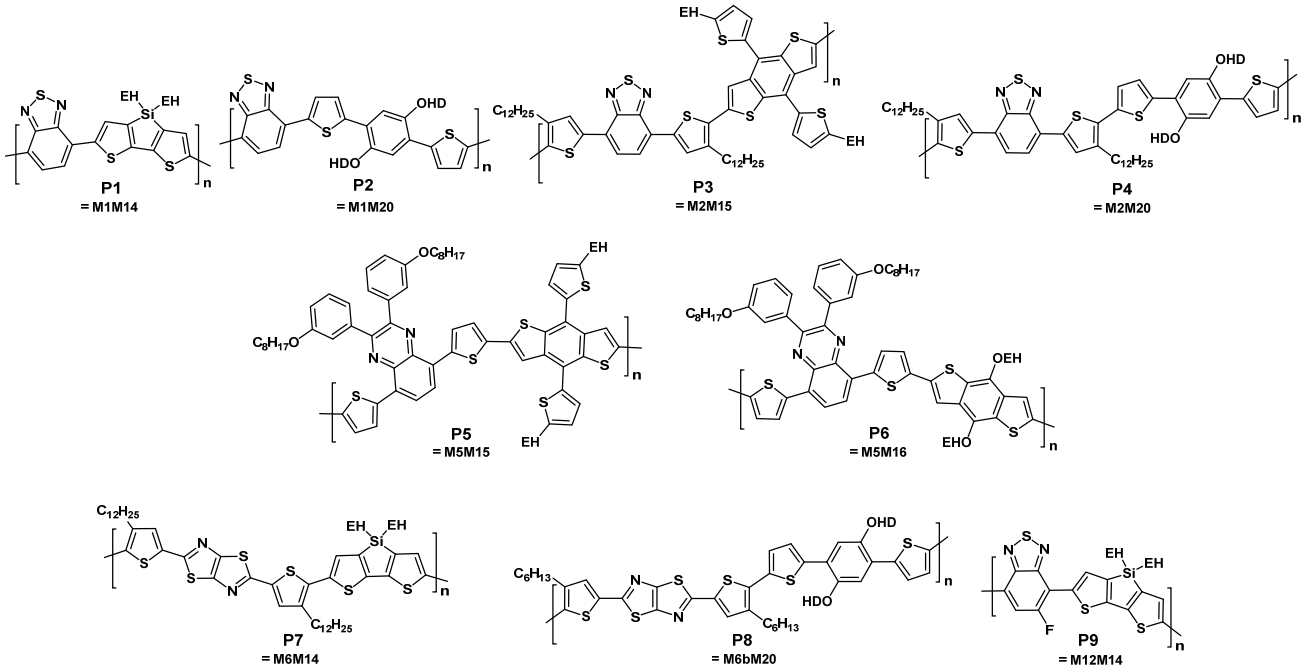

Figure 2.4. *Selected polymers **P1**-**P9**.*

2.2.2. Characterization

The 90 successfully synthesized polymers were analyzed by size exclusion chromatography (SEC), revealing a large variation in the numerous molecular weight (M_n) (seen for selected polymers in Table 2.1). Low molecular weight polymers can be a result of low reactivity, steric hindrance and poor solubility of the polymer. Lower M_n for polymers based on **M20** may be ascribed to impurities in the stannylated monomer, as an easy recrystallization was not possible due to a liquid monomer.

Table 2.1. *Optical and electronic properties of the selected polymers.*

	M_n[a] (kDa)	Đ[a]	E_g[b] (eV)	HOMO[c] (eV)	LUMO[d] (eV)	R_d[e] (%/h)
P1	96.0	9.9	1.47	-5.00	-3.53	1.11
P2	13.0	2.1	1.73	-5.07	-3.34	1.48
P3	12.4	11.4	1.61	-4.95	-3.34	0.54
P4	7.5	3.2	1.65	-5.07	-3.42	0.83
P5	100.7	3.1	1.73	-4.90	-3.17	0.33
P6	50.0	1.3	1.59	-5.01	-3.42	5.71
P7	9.6	2.0	1.77	-5.13	-3.36	10.8
P8[f]	44.0	1.9	1.91	-5.24	-3.33	2.82
P9	6.8	1.9	1.50	-5.12	-3.62	0.52

[a] Molecular weight (M_n) and polydispersity (Đ) determined from SEC against polystyrene (PS) standard, [b] optical band gap (E_g) calculated from the onset of the UV-vis absorption spectrum of the polymer film, [c] highest occupied molecular orbital (HOMO) estimated from SWV curves, [d] lowest unoccupied molecular orbital (LUMO) calculated from the HOMO and E_g, [e] the degradation rate (R_d) was calculated from the degradation of the UV-vis absorption of a polymer film, [f] the result for **P8** were taken from Chapter 4.

UV-vis absorption spectra of the polymer films were recorded and are shown in Figure 2.5. E_g (Table 2.1) were estimated from the spectra of the polymer *via* an onset of the absorption curve [16]. The values were within the range of 1.47 to 1.77 eV of the selected polymers **P1**-**P9**. **P1** and **P9** absorbed in a higher nm range than the other polymers (**P2**-**P8**), therefore their E_g was much lower. On the other side **P8** absorbed in a lower nm range, yielding in a higher E_g. The absorption profiles of **P2** and **P5** as well as the ones of **P3** and **P4** deviated very similar. E_g of **P3HT** was with 1.9 eV a bit lower than the reference value (2.0 eV) [17].

Square wave voltammetry (SWV) curves were recorded for all polymers including **P3HT** using ferrocene as reference. The HOMO levels (in Table 2.1) were estimated from the curves, while the LUMO levels (in Table 2.1) were calculated from the HOMO levels and the corresponding E_g. The HOMO level of **P3HT** was estimated to be -4.9 eV, which is higher than the value (-5.2 eV) in literature [18], while the LUMO level of $PC_{61}BM$ was -3.85 eV, which is lower than the value (-3.75 eV) in literature [18].

The photochemical stabilities of the polymer films were measured with an automated setup described in literature and Appendix A, where the UV-vis absorption of the polymer was measured as a function of time under sun irradiation (AM 1.5) [19]. The stability within the group of selected polymers **P1**-**P9** was highest for polymers based on BT-based (**M2**, **M12**) or benzo [1,2-*b*:4,5:*b'*]dithiophene (BDT)-based (**M15**) units. This is in agreement with a literature study about the photochemical stability of different D_M-A_M copolymers, where the BT and Th units are reported to be among the more photochemically stable monomer units [20].

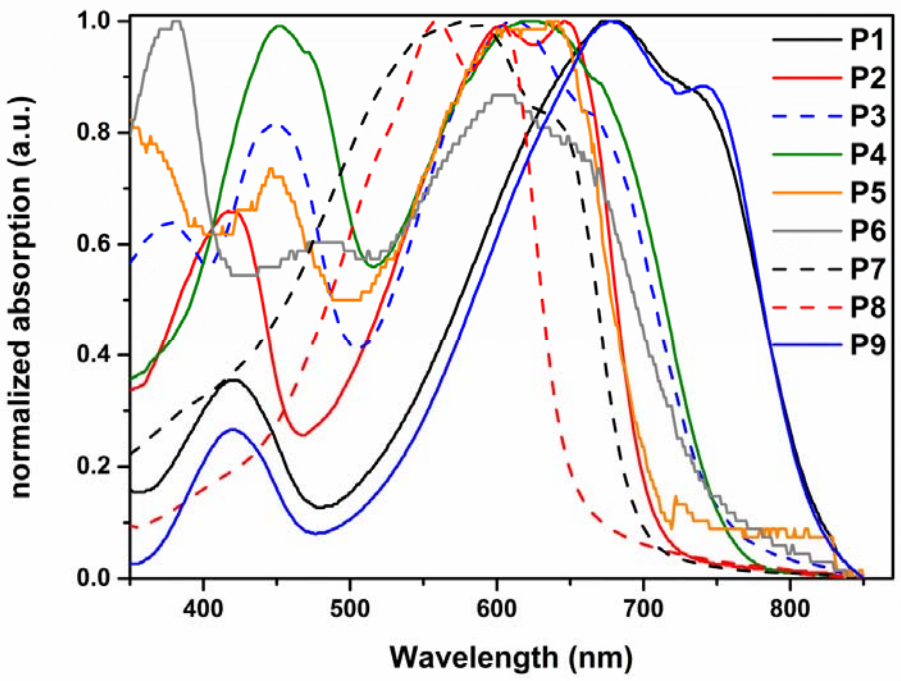

Figure 2.5. *UV-vis spectra of the films of the polymers* ***P1***-***P9****.*

2.3. Polymer Solar Cells

2.3.1. Preparation

The successfully synthesized polymers were applied in RC PSCs using the *flextrode* substrate on the mini roll-coater. For all polymers several parameters were varied and studied during the screening, e.g. solvent (chloroform (CF) and *ortho*-dichlorobenzene (ODCB)), ratio between polymer and $PC_{61}BM$ (1:1 and 1:2) and the active layer thickness (315 nm, 400 nm and 475 nm), however, it was impossible to vary more parameters like the coating temperature or solvent additives due to this large numbers of polymers. So the coating temperature was kept at 70 °C, while no additives were used. The choice of a low and a high boiling solvent would affect the morphologies of the polymers in the active layers. Figure 2.6 shows, that the best solvent for applying the polymers in PSCs is ODCB with a polymer to $PC_{61}BM$ ratio of 1:2. The active layer

thickness depends on the polymer and cannot be specifically defined. As mentioned previously, **x** in Table 2.2 indicates the polymers which could not be synthesized. Many polymers, however, failed also to result in working PSCs due to coating defects (insufficient solubility of the polymer or de-wetting of the active layer on the substrate) or device defects (electrical shorts due to defects or destruction/no switching of the device during the switching process). This is shown in Table 2.2. by NA and 0/<0.1, respectively.

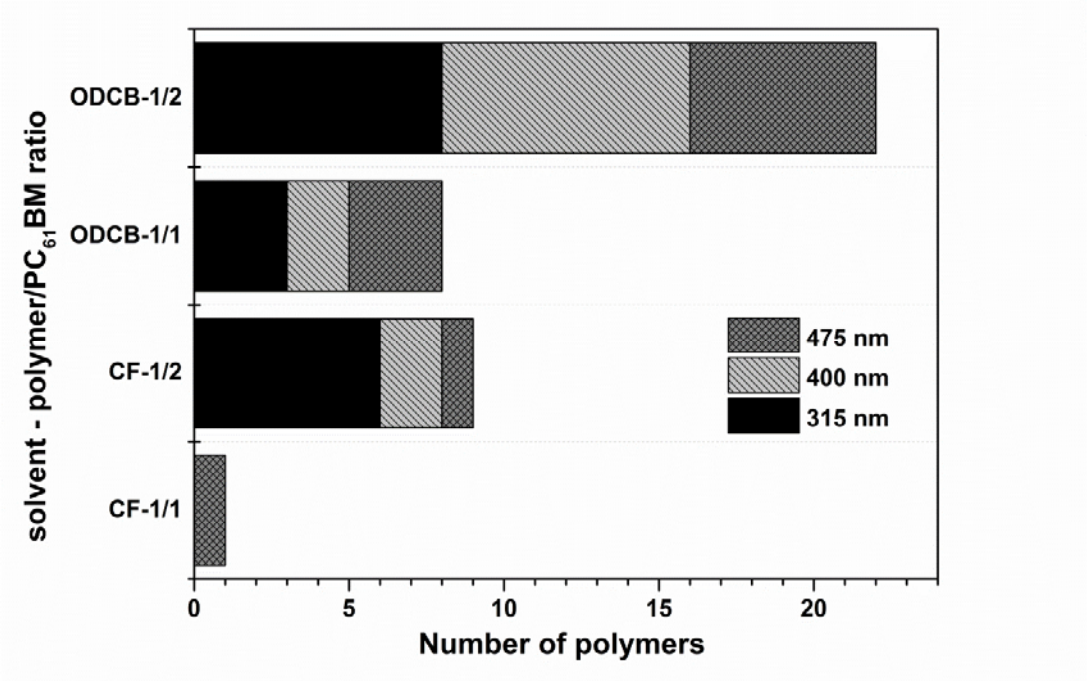

Figure 2.6. *Illustration of the number of polymers that gave the best PCE with the selected solvent (CF or ODCB) with a specific polymer to $PC_{61}BM$ ratio (1:1 or 1:2) and a defined active layer thickness of all monomer combinations from Table 2.2.*

2.3.2. *J-V* Characterization

The average PCE including the standard deviation for the PSCs which were prepared with their best coating parameters (see Figure 2.6) are presented in Table 2.2. As mentioned previously **x**, NA or 0/<0.1 are failures on the way to working PSCs. Many of the polymers which failed in this study, performed well in SC devices from literature, e.g. the **M10M15** polymer has a reported performance of 6.17% [21], while it failed to result in any device in this study. Other examples are the **M8M15** and **M8M16** polymer with reported PCE of 9.35% and 8.21%, respectively, [5] while it had a very low performance herein (0.46% and 0.10 %).

The efficiencies (Table 2.2) represent working devices. The green highlighted polymers (the selected polymers (**P1**-**P9**) in Figure 2.4) have PCE's > 1%. In comparison to **P3HT** there are only two polymers, which perform better (**P2** and **P8**).

The 9 selected and well-performing polymers are described below in more detail. The polymers are based on the A_M **M1**, **M2**, **M5**, **M6** and **M12** and the D_M **M14**, **M15**, **M16** and **M20**. All monomers and 45 of the polymers (whereof 4 were not applied in PSCs) were reported in literature before. The references of some selected polymers (**P1**, **P2**, **P6** and **P7**) including the efficiencies of the devices are listed in Table 2.3. The small devices described in literature were prepared in normal geometry devices *via* SC, with ITO and under vacuum. In the active layer, the polymers were combined with [6,6]-Phenyl C_{71} butyric acid methyl ester ($PC_{71}BM$) yielding high efficiency of above 5% (except for **P6**). However, the efficiencies from literature cannot be directly compared to **P6** and **P7** as the polymers from literature bear slightly different side chains. This was shown in a previous study [22], where the **P2** backbone was investigated in detail in the impact on the efficiency by the type and the length of the side chains. It was shown that **P2** bearing a 2-hexyldecyl (HD) side chain had an efficiency of 1.2% whereas the polymer with a dodecyl chain had a PCE of 0.1%. So changing the side chain will change the properties of the resulting PSCs [22].

Table 2.2. *PCE of all polymers synthesized via combinatorial pairing of the monomers* ***M1-M13*** *with* ***M14-M21****.*[a]

	M14	M15	M16	M17	M18	M19	M20	M21
M1	1.28±0.11	0.34±0.09	**x**	0	<0.1	**x**	1.75±0.29	0
M2	0.16±0.04	1.03±0.19	0.48±0.07	0	<0.1	NA	1.24±0.14	0
M3	0.21±0.06	NA	0.53±0.11	0.23±0.04	0.48±0.09	0.18±0.02	0.37±0.04	0.27±0.04
M4	<0.1	0.16±0.03	<0.1	0	0.49±0.11	**x**	0	**x**
M5	0.24±0.05	1.30±0.21	1.13±0.01	0	0.14±0.05	<0.1	0.55±0.08	<0.1
M6	1.05±0.10	0.76±0.17	0.60±0.09	0.58±0.15	0	**x**	1.80±0.28	**x**
M7	<0.1	NA	0	NA	NA	**x**	<0.1	**x**
M8	0.17±0.05	0.46±0.10	0.10±0.03	0	<0.1	**x**	<0.1	0
M9	0.20±0.08	0.56±0.15	0.42±0.13	0	0	**x**	0	NA
M10	0	0	0	0	NA	0	0	NA
M11	0.21±0.07	0.34±0.05	**x**	0	<0.1	**x**	0.18±0.02	<0.1
M12	1.19±0.08	0.13±0.04	**x**	0.21±0.07	0	**x**	0.54±0.13	0
M13	0.49±0.14	0	NA	NA	NA	<0.1	0	NA

[a] Double underlined numbers: polymers prepared from **M2b** or **M6b** single underlined numbers: polymers prepared from **M14b**, **M18b** or **M21b**. The (failed) processes in the table are marked with: **x** = no synthesis of the polymer could be performed, NA = polymer could not be applied in PSCs, 0 or <0.1 = measurement of the PSCs failed. The green highlighted values are the selected polymers with efficiencies of >1%.

Table 2.3. *Averaged J-V characteristics of devices prepared via RC from the selected polymers **P1**-**P9**.*[a]

	PCE (%)	V_{OC} (V)	J_{sc} (mA cm^{-2})	FF	$PCE_{literature}$ (%)	Literature
P1[b]	1.28 (1.37)	0.55 (0.56)	2.92 (2.99)	0.42 (0.43)	5.6[g]	[23]
P2[c]	1.75 (2.21)	0.72 (0.75)	2.43 (2.92)	0.52 (0.53)	5.08[g]	[24]
P3[d]	1.03 (1.30)	0.59 (0.56)	2.62 (2.96)	0.35 (0.41)	no reference	-
P4[d]	1.24 (1.38)	0.63 (0.63)	2.16 (2.39)	0.48 (0.48)	no reference	-
P5[e]	1.30 (1.48)	0.61 (0.61)	2.85 (2.99)	0.39 (0.42)	no reference	-
P6[e]	1.13 (1.13)	0.56 (0.56)	2.62 (2.64)	0.41 (0.40)	1.68[g] (R in para in **M5**)	[25]
P7[e]	1.05 (1.14)	0.63 (0.63)	1.83 (1.93)	0.47 (0.49)	5.59[g] (R = hexyl in **M6**)	[11]
P8[f]	1.80 (2.26)	0.63 (0.64)	2.99 (3.50)	0.50 (0.53)	no reference	-
P9[e]	1.19 (1.25)	0.64 (0.65)	2.35 (2.40)	0.42 (0.42)	no reference	-

[a] *J-V* characteristics of the best performing device are shown in brackets, [b] device prepared from CF, a polymer-to-$PC_{61}BM$ ratio of 1:1 and a layer thickness of 475 nm, [c] device prepared from CF, a polymer-to-$PC_{61}BM$ ratio of 1:2 and a layer thickness of 400 nm, [d] device prepared from ODCB, a polymer-to-$PC_{61}BM$ ratio of 1:2 and a layer thickness of 315 nm, [e] device prepared from ODCB, a polymer-to-$PC_{61}BM$ ratio of 1:2 and a layer thickness of 400 nm, [f] device prepared from ODCB, a polymer-to-$PC_{61}BM$ ratio of 1:2 and a layer thickness of 475 nm, the result for **P8** were taken from Chapter 4, [g] SC devices prepared using $PC_{71}BM$, ITO and vacuum.

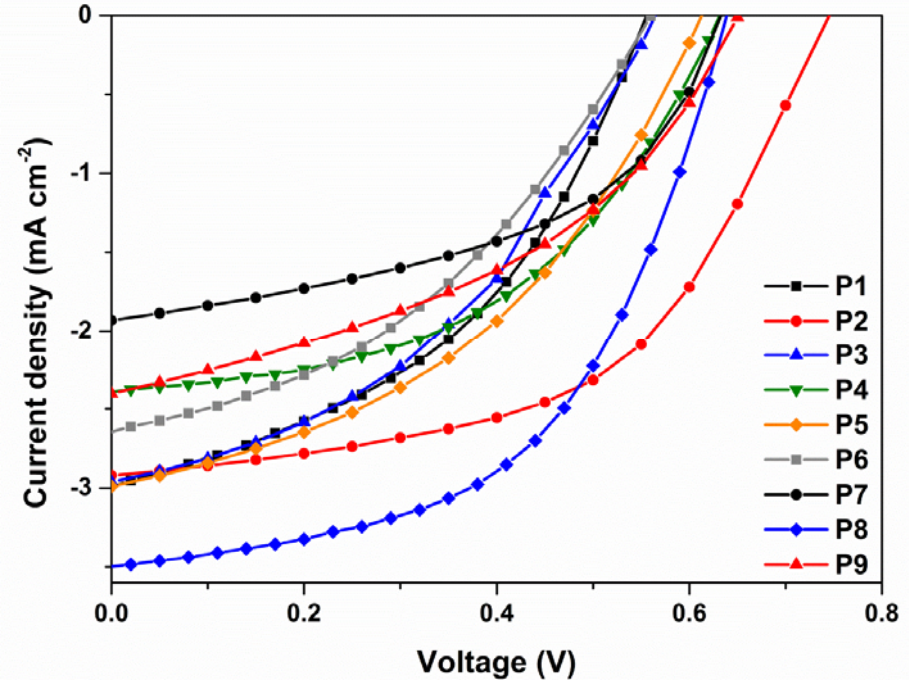

Figure 2.7. *J-V curves of the best PSCs from the selected polymers **P1**-**P9**.*

The *J-V* characteristics (average and best) of the selected polymers are shown in Table 2.3 and Figure 2.7. **P2** and **P8** have the highest (best) PCE of around 2.1%. The high PCE of **P2** is the result of a high V_{oc} (0.75 V) and a high FF (53%), while **P8** has a high J_{sc} (3.50 mA cm^{-2}). As the V_{OC} and the HOMO level of the polymers

(relatively to the LUMO of $PC_{61}BM$) are proportionally related, an increase or decrease of the HOMO level of the polymer should result in a decrease and increase the V_{OC}, respectively [26].

2.4. Evaluation of the Polymer Screening

The data collection of 104 polymers filled a large data base, as for each polymer 12 different PSC coatings were prepared (different solvent, polymer-to-$PC_{61}BM$ ratio and active layer thickness) whereof at least 5 cells were characterized. Further, all optical, electrochemical and photochemical stability measurements were collected in a data base. A large amount of resources (manpower and material) was needed to perform this project lasting about 2 years.

First the polymers can be evaluated over their number of synthetic steps, as this step adds a large part to the amount of energy which is needed to produce the PSC in large scale and thus to the cost of the devices [27]. If a high performing polymer is applied in PSCs in a large-scaled roll-to-roll process, in an industrial context the first step is the production of the polymer in large amounts. Therefore a low number of synthetic steps including a high yield, easy purification of the materials and low costs of the starting materials is a demand [6,28]. As an example the synthesis of **P3HT** (3 steps) and **P7** (11 steps) are shown in Scheme 2.1. With more than double the steps as for **P3HT**, it is clear that the synthesis of **P7** will use more energy which will be reflected in higher costs for the production of the polymer in large scale. The number of synthetic steps of the corresponding starting materials [28] for each selected polymer is shown in Table 2.4.

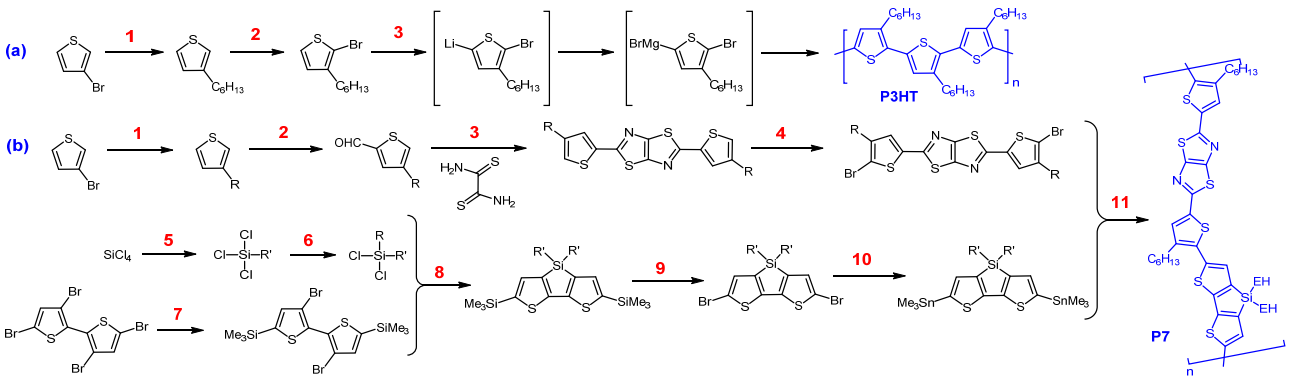

Scheme 2.1. *Schematic drawing of (a)* ***P3HT*** [29] *and (b)* ***P7*** [30,31] *synthesis to reveal their synthetic steps.*

Second, the polymers were eliminated during the screening according to their failure (Figure 2.8 step 1-3) in these areas, which is indicated by **x**, NA 0 or <0.1 in Table 2.2:

- Infeasibility of synthesis, purification and characterization (e.g. steric hindrance of the side chains and because of low solubility of the polymer) (**x**)
- Infeasibility of coating (e.g. dewetting of the active layer or PEDOT-PSS layer on top of it) (NA)

- ❖ Infeasibility of switching of the device (resistor) or shunting of the device (0 or <0.1)

These reasons of failure, seen in Figure 2.8 for all 104 polymers, show the challenge of this study, to find suitable candidates for RC fabrication of PSCs. 40 of the polymers finally resulted in working PSCs (Figure 2.8 step 4+5), while 66 polymers were eliminated (Figure 2.8 step 1-3).

Table 2.4. *Calculation of the merit factor (χ) of the selected polymers* ***P1****-****P9*** *and* ***P3HT****.*

	PCE[a]	V_{OC}[a]	$V_{OC,calc}$[b]	synthetic steps	E_g[a]	R_d[a]	χ[c]	χ_{rel}[c]
P1	1.28	0.55	0.55	#11	1.47	1.11	208	1.20
P2	1.75	0.72	0.62	#6	1.73	1.48	512	2.97
P3	1.03	0.59	0.50	#12	1.61	0.54	363	2.11
P4	1.24	0.63	0.62	#9	1.65	0.83	303	1.76
P5	1.30	0.61	0.45	#15	1.73	0.33	512	2.97
P6	1.13	0.56	0.56	#15	1.59	5.71	22	0.13
P7	1.05	0.63	0.68	#11	1.77	10.8	17	0.10
P8[6]	1.80	0.63	0.79	#6	1.91	2.82	218	1.26
P9	1.19	0.64	0.67	#11	1.50	0.52	464	2.69
P3HT	1.57	0.50	-	#3	1.90	4.00	173	-

[a] PCE (in %), V_{OC} (in V) E_g (in eV) and R_d (in %) taken from Table 2.1, [b] $V_{OC,calc}$ calculated with formula 2.5, [c] χ calculated with formula 2.1 and χ_{rel} (relative merit factor) calculated with formula 2.3.

At last, the polymers with a low performance (<1%) were eliminated too (Figure 2.8 step 4), so that 9 polymers (**P1**-**P9**) were left with an (non-optimized) efficiency of >1 %. For further evaluation of the 9 polymers, other parameters (V_{OC}, stability, band gap, synthetic steps) were also important to be suitable for the RC of PSCs, so that the other critical areas in the *golden square* were fulfilled. The important factors were combined in a merit factor (χ):

$$\chi = \frac{PCE \times V_{oc} \times relative\ stability \times band\ gap\ (nm)}{synthetic\ steps} = \frac{PCE \times V_{oc} \times \frac{R_d(P3HT)}{R_d(polymer)} \times \frac{1240}{E_g}}{synthetic\ steps} \quad (2.1)$$

The *PCE* needs to be as high as possible. The photochemical stability was shown to vary amongst the polymers, [20] so it must be taken into consideration in χ as it is one major criterion. For χ, degradation rate (R_d) of the polymer was normalized to R_d(P3HT) at an equal absorption value to give a *stability* value (reciprocal value). A high V_{OC} is also desirable to be incorporated into χ. As the absorption of the polymer

should cover the higher wavelength areas, the (reciprocal) *band gap* (in nm) which is the onset in the absorption spectrum of the polymer film, should be as high as possible. In the end, the number of *synthetic steps* is considered as well, as it is connected to the energy consumption during the synthesis and has an influence on the cost of the material production and thus of the PSC. The main focus was to show the ability to apply these polymers in RC PSCs, while other publications are more addressed on the upscaling of the synthesis [6].

Instead of comparing the merit factor for each polymer, they were compared relative to the merit factor of **P3HT**:$PC_{61}BM$ device. The results are shown in Table 2.4.

$$\chi_{rel} = \frac{\chi_{polymer}}{\chi_{P3HT}} \quad (2.2)$$

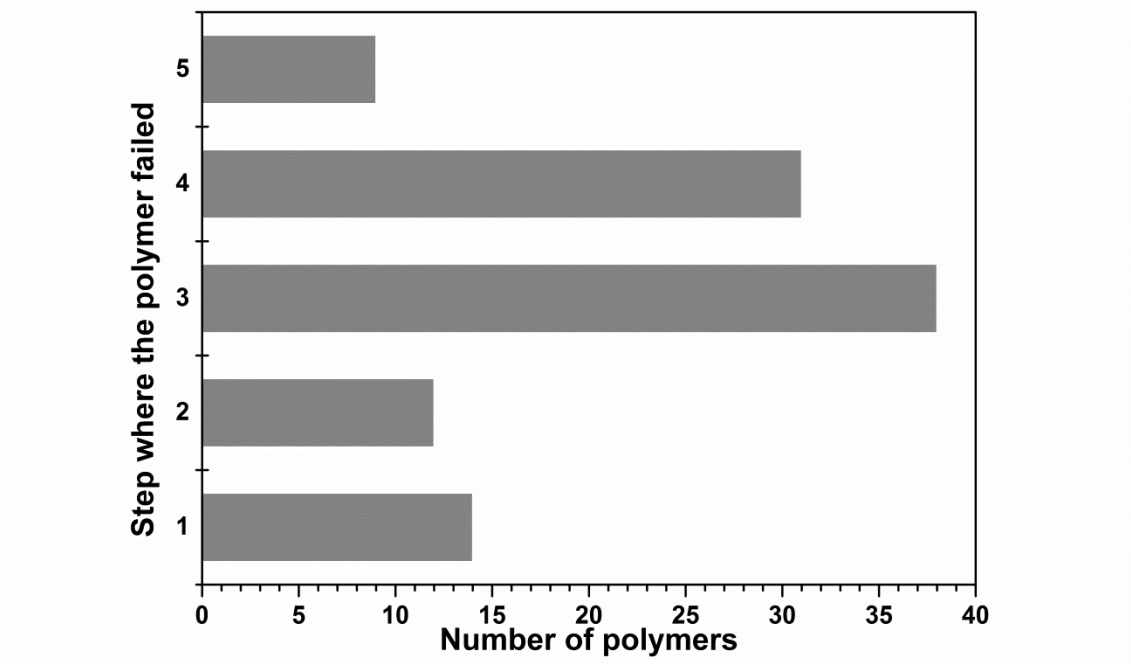

Figure 2.8. *Illustration of the number of polymers that were eliminated during the screening process: (1) synthesis and characterization, (2) coating of the device, (3) device switching process, (4) performance < 1% and (5) > 1%.*

From this calculation 7 out of 9 polymers with efficiencies >1% have a similar or better χ in comparison to **P3HT**. Comparing the whole library of 104 polymers with the 7 suitable candidate for application in RC PSCs, demonstrates that the success rate is low and all requirements for RC techniques seem to be much higher than for SC one. For all prepared polymers a variation of different properties can be achieved, showing the strength of the combinatorial approach, as almost any number for V_{OC}, HOMO energy level and E_g can be matched. Herein, the selected polymers (**P1**-**P9**) reveal V_{OC} values within a range of 0.55 to 0.77 V, HOMO energy levels within a range of -4.90 to -5.24 eV, and the E_g's within a range of 1.47 to 1.91 eV.

The relationship between V_{OC} and HOMO is known to be

$$V_{OC} = \frac{1}{e}\left(\left|HOMO_{polymer}\right| - \left|LUMO_{acceptor}\right|\right) - 0.3\,V \quad (2.3)\ [26]$$

including *e* as elementary charge and the LUMO of the $PC_{61}BM$ acceptor as -3.85 eV.

In this study we found that to some extend the polymers followed this trend, though there was a little higher loss for the devices (~ 0.6 V),

$$V_{OC} = \frac{1}{e}\left(\left|HOMO_{polymer}\right| - \left|LUMO_{acceptor}\right|\right) - 0.6\,V \quad (2.4)$$

so the V_{OC} for the selected polymers was calculated in Table 2.4. The higher loss could be a result of using the RC instead of SC technique.

2.5. Conclusion

From this study it is clear that a large effort is required to successfully develop a library of polymers and apply them in (RC) PSCs. Especially finding the right candidate meeting all requirements is difficult. The main requirements are

- a successful and easy synthesis and purification of the polymer
- RC of the polymer in devices
- yielding a fully working PSC with a preferable high performance

Herein, we prepared a library of 104 polymers *via* combinatorial pairing of 8 donor and 13 acceptor monomers illustrating the huge challenge in forming such a library to find the right candidate with a high performance to fulfilling all criterias in the best way. 14 polymers failded at the first step and could not be synthesized due to steric hinderance. In the further steps, coating and switching of the devices, other 52 polymers were eliminated, due to coating problems (insolubility of the polymer, dewetting of the active layer). Finally 40 polymers resulted in working PSCs. After the elimination of another 31 polymers due to their low performance, 9 polymer candidates had rather high efficiencies of >1%,

For a better understanding of these candidates and to relate them to the *golden square*, a merit factor was introduced, including the power conversion efficiency, open circuit voltage, stability, band gap and synthetic steps. In combination with the applied RC technology it covers all critical areas of the solar technology. The merit factors of the candidates were compared to the one of **P3HT**, revealing 7 optimal candidates to be similar or better than **P3HT**.

The present study showed that 7 out of 104 polymers (corresponding to 6.7% of the polymers) with efficiencies of minimum 1% are performing similar or better than the prototypical reference **P3HT** and are therefore suitable for further development. The other materials fail along the way, but for some of them there might be potential to overcome the problem by suitable modifications.

The first attempt could be to repeat the synthesis of the polymers, which failed to be synthesized, by using the same backbone, but different side chains. Failures during the coating and testing of the devices could be solved by using different device structures, increasing of the active layer thickness or a change in the coating solvent.

Further progress on the suitable candidates could be to do specific side chain engineering as already shown for **P2** previously [22]. Improving the *J-V* characteristics could be realized through further optimization of the coating parameters (solvent, polymer-$PC_{61}BM$ ratio, etc.) or of the use of even another acceptor. Therefore, this study can be seen as *a drop in the ocean* for raw candidates that can be expected to be suitable to be developed further.

2.6. References

1. Liu, Y.; Zhao, J.; Li, Z.; Mu, C.; Ma, W.; Hu, H.; Jiang, K.; Lin, H.; Ade, H.; Yan, H. Aggregation and morphology control enables multiple cases of high-efficiency polymer solar cells. *Nat. Commun.* **2014**, *5*, 5293 (1-8).

2. Jørgensen, M.; Carlé, J. E.; Søndergaard, R. R.; Lauritzen, M.; Dagnæs-Hansen, N. A.; Byskov, S. L.; Andersen, T. R.; Larsen-Olsen, T. T.; Böttiger, A. P. L.; Andreasen, B.; Fu, L.; Zuo, L.; Liu, Y.; Bundgaard, E.; Zhan, X.; Chen, H.; Krebs, F. C. The state of organic solar cells—A meta analysis. *Sol. Energy Mater. Sol. Cells* **2013**, *119*, 84–93.

3. Liang, F.; Lu, J.; Ding, J.; Movileanu, R.; Tao, Y. Design and synthesis of alternating regioregular oligothiophenes/ benzothiadiazole copolymers for organic solar cells. *Macromolecules* **2009**, *42*, 6107–6114.

4. Bundgaard, E.; Shaheen, S. E.; Krebs, F. C.; Ginley, D. S. Bulk heterojunctions based on a low band gap copolymer of thiophene and benzothiadiazole. *Sol. Energy Mater. Sol. Cells* **2007**, *91*, 1631–1637.

5. Liao, S. H.; Jhuo, H. J.; Cheng, Y. S.; Chen, S. A. Fullerene derivative-doped zinc oxide nanofilm as the cathode of inverted polymer solar cells with low-bandgap polymer (PTB7-Th) for high performance. *Adv. Mater.* **2013**, *25*, 4766–4771.

6. Po, R.; Bianchi, G.; Carbonera, C.; Pellegrino, A. "All That Glisters Is Not Gold": An Analysis of the Synthetic Complexity of Efficient Polymer Donors for Polymer Solar Cells. *Macromolecules* **2015**, *48*, 453–461.

7. Bian, L.; Zhu, E.; Tang, J.; Tang, W.; Zhang, F. Recent progress in the design of narrow bandgap conjugated polymers for high-efficiency organic solar cells. *Prog. Polym. Sci.* **2012**, *37*, 1292–1331.

8. Zhou, H.; Yang, L.; You, W. Rational Design of High Performance Conjugated Polymers for Organic Solar Cells. *Macromolecules* **2012**, *45*, 607–632.

9. Facchetti, A. π-Conjugated polymers for organic electronics and photovoltaic cell applications. *Chem. Mater.* **2011**, *23*, 733–758.

10. Livi, F.; Søndergaard, R. R.; Andersen, T. R.; Roth, B.; Gevorgyan, S. Round-Robin Studies on Roll-Processed ITO-free Organic Tandem Solar Cells Combined with Inter-Laboratory Stability Studies. *Energy Technol.* **2015**, *3*, 423–427.

11. Zhang, M.; Guo, X.; Li, Y. Synthesis and Characterization of a Copolymer Based on Thiazolothiazole and Dithienosilole for Polymer Solar Cells. *Adv. Energy Mater.* **2011**, *1*, 557–560.

12. Huo, L.; Guo, X.; Zhang, S.; Li, Y.; Hou, J. PBDTTTZ : A Broad Band Gap Conjugated Polymer with High. *Macromolecules* **2011**, *44*, 4035–4037.

13. Carlé, J. E.; Helgesen, M.; Madsen, M. V.; Bundgaard, E.; Krebs, F. C. Upscaling from single cells to modules – fabrication of vacuum- and ITO-free polymer solar cells on flexible substrates with long lifetime. *J. Mater. Chem. C* **2014**, *2*, 1290–1297.

14. Bundgaard, E.; Livi, F.; Hagemann, O.; Carlé, J. E.; Helgesen, M.; Heckler, I. M.; Zawacka, N. K.; Angmo, D.; Larsen-Olsen, T. T.; dos Reis Benatto, G. A.; Roth, B.; Madsen, M. V.; Andersson, M. R.; Jørgensen, M.; Søndergaard, R. R.; Krebs, F. C. Matrix Organization and Merit Factor Evaluation as a Method to Address the Challenge of Finding a Polymer

Material for Roll Coated Polymer Solar Cells. *Adv. Energy Mater.* **2015**, *5*, 1402186 (1-16).

15. Heckler, I.; Kesters, J.; Defour, M.; Madsen, M.; Penxten, H.; D'Haen, J.; Van Mele, B.; Maes, W.; Bundgaard, E. The Influence of Conjugated Polymer Side Chain Manipulation on the Efficiency and Stability of Polymer Solar Cells. *Materials (Basel).* **2016**, *9*, 181 (1-18).

16. Bundgaard, E.; Krebs, F. C. Low-Band-Gap Conjugated Polymers Based on Thiophene , Benzothiadiazole , and Benzobis (thiadiazole). *Macromolecules* **2006**, *39*, 2823–2831.

17. Salzner, U.; Lagowski, J. B.; Pickup, P. G.; Poirier, R. A. Comparison of geometries and electronic structures of polyacetylene, polyborole, polycyclopentadiene, polypyrrole, polyfuran, polysilole, polyphosphole, polythiophene, polyselenophene and polytellurophene. **1998**, *96*, 177–189.

18. Al-Ibrahim, M.; Roth, H. K.; Zhokhavets, U.; Gobsch, G.; Sensfuss, S. Flexible large area polymer solar cells based on poly(3-hexylthiophene)/ fullerene. *Sol. Energy Mater. Sol. Cells* **2005**, *85*, 13–20.

19. Tromholt, T.; Madsen, M. V.; Carlé, J. E.; Helgesen, M.; Krebs, F. C. Photochemical stability of conjugated polymers, electron acceptors and blends for polymer solar cells resolved in terms of film thickness and absorbance. *J. Mater. Chem.* **2012**, *22*, 7592–7601.

20. Manceau, M.; Bundgaard, E.; Carlé, J. E.; Hagemann, O.; Helgesen, M.; Søndergaard, R.; Jørgensen, M.; Krebs, F. C. Photochemical stability of π-conjugated polymers for polymer solar cells: a rule of thumb. *J. Mater. Chem.* **2011**, *21*, 4132–4141.

21. Yuan, J.; Zhai, Z.; Dong, H.; Li, J.; Jiang, Z.; Li, Y.; Ma, W. Efficient Polymer Solar Cells with a High Open Circuit Voltage of 1 Volt. *Adv. Funct. Mater.* **2013**, *23*, 885–892.

22. Livi, F.; Zawacka, N. K.; Angmo, D.; Jørgensen, M.; Krebs, F. C.; Bundgaard, E. Influence of Side Chain Position on the Electrical Properties of Organic Solar Cells Based on Dithienylbenzothiadiazole- alt -phenylene Conjugated Polymers. *Macromolecules* **2015**, *48*, 3481–3492.

23. Chen, H.-Y.; Hou, J.; Hayden, A. E.; Yang, H.; Houk, K. N.; Yang, Y. Silicon atom substitution enhances interchain packing in a thiophene-based polymer system. *Adv. Mater.* **2010**, *22*, 371–375.

24. Nguyen, T. L.; Choi, H.; Ko, S.-J.; Uddin, M. a.; Walker, B.; Yum, S.; Jeong, J.-E.; Yun, M. H.; Shin, T. J.; Hwang, S.; Kim, J. Y.; Woo, H. Y. Semi-crystalline photovoltaic polymers with efficiency exceeding 9% in a ~300 nm thick conventional single-cell device. *Energy Environ. Sci.* **2014**, *7*, 3040–3051.

25. Bathula, C.; Song, C. E.; Lee, W.-H.; Lee, J.; Badgujar, S.; Koti, R.; Kang, I.-N.; Shin, W. S.; Ahn, T.; Lee, J.-C.; Moon, S.-J.; Lee, S. K. Synthesis and characterization of quinoxaline-based polymers for bulk-heterojunction polymer solar cells. *Thin Solid Films* **2013**, *537*, 231–238.

26. Scharber, M. C.; Mühlbacher, D.; Koppe, M.; Denk, P.; Waldauf, C.; Heeger, A. J.; Brabec, C. J. Design Rules for Donors in Bulk-Heterojunction Solar Cells - Towards 10 % Energy-Conversion Efficiency. *Adv. Mater.* **2006**, *18*, 789–794.

27. García-Valverde, R.; Cherni, J. A.; Urbina, A. Life cycle analysis of organic photovoltaic technologies. *Prog. Photovoltaics Res. Appl.* **2010**, *18*, 535–558.

28. Marzano, G.; Ciasca, C. V; Babudri, F.; Bianchi, G.; Pellegrino, A.; Po, R.; Farinola, G. M. Organometallic Approaches to Conjugated Polymers for Plastic Solar Cells: From Laboratory Synthesis to Industrial Production. *European J. Org. Chem.* **2014**, 6583–6614.

29. McCullough, R. D.; Williams, S. P.; Tristram-Nagle, S.; Jayaraman, M.; Ewbank, P. C.; Miller, L. The First Synthesis and New Properties of Regioregular, Head-To-Tail Coupled Polythiophenes. *Synth. Met.* **1995**, *69*, 279–282.

30. Hou, J.; Chen, H.-Y.; Zhang, S.; Li, G.; Yang, Y. Synthesis, characterization, and photovoltaic properties of a low band gap polymer based on silole-containing polythiophenes and 2,1,3-benzothiadiazole. *J. Am. Chem. Soc.* **2008**, *130*, 16144–16145.

31. Helgesen, M.; Carlé, J. E.; Krebs, F. C. Slot-Die Coating of a High Performance Copolymer in a Readily Scalable Roll Process for Polymer Solar Cells. *Adv. Energy Mater.* **2013**, *3*, 1664–1669.

Chapter 3.

The Impact of the Thiophene – Benzothiadiazole – Ratio in Conjugated Polymers

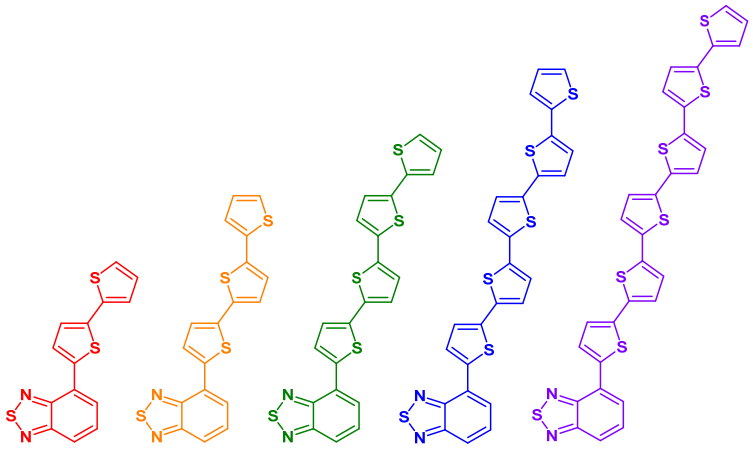

3.1. Introduction

The conjugated polymers with different backbones for PSCs has been studied in order to achieve high PCEs. Some groups focus on the polymerization of highly advanced conjugated monomers yielding in a highly efficient polymer with a ridged backbone structure (Figure 3.1. **PTBTIT**); e.g. Yue et al. reported an isoindigo based polymer applied in PSCs with efficiencies of up to 9.7 % [1]. The disadvantage of these polymers is the number of synthetic steps to prepare them. To decrease the number of synthetic steps the focus should be on the synthesis of polymers based on simple monomers, and benzo[c][1,2,5]thiadiazole (BT) and thiophene (Th) seem to be attractive towards this goal. The group of Yan could apply such a polymer (Figure 3.1, **PBTff4T**) in PSCs reaching efficiencies of 10.8% [2] and 11.3% [3], respectively, in small area devices. Furthermore, they studied the influence of the number of Th's in these polymers [4]. Prior to their results other groups [5–7] studied the influence of the number of Th's in these polymers based on Th and non-fluorinated BT.

However, the polymers based on Th and BT (Table 3.1.) had only been applied in SC PSCs. An overview of the synthesized polymers in literature with different numbers (m) of Th's is shown in Table 3.1. The number varied up to 8 Th's per BT. The efficiencies were up to 11.3% depending on the electron acceptor ($PC_{61}BM$ or $PC_{71}BM$) in the active layer, the kind of solvent or the use of possible additives. It was seen that the incorporation of 4 units resulted in efficiencies >10% [2–4].

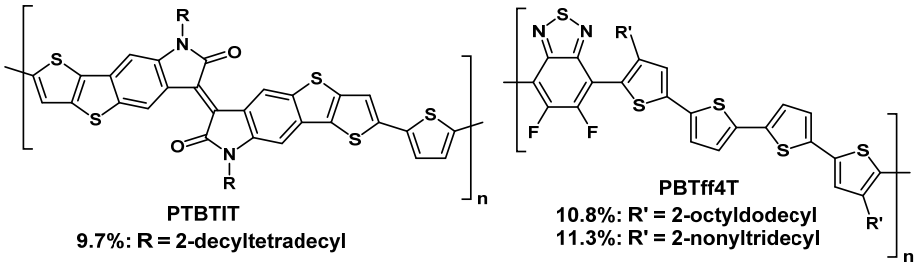

Figure 3.1. *High efficient polymers which were studied in literature [1–3] for PSCs.*

Table 3.1. *Polymers based on Th and BT studied in literature.*

Polymer structure	m	Side chain	Polymer[a]	PCE[d] (%)	Reference
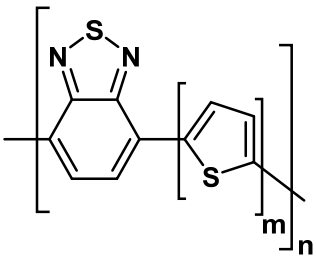	**1-4**	3,7,11-trimethyldodecyl	(**P10**- **P13**)[b]	NA	[5]
	4	2-ethylhexyl	**P13**[b]	NA	[5]
	2-6	n-$C_{12}H_{25}$	NA, **P14**, **P16**[b], **P19**/**P20**[b], **P21**	1.23, 0.93, 1.62, 1.91, 2.23[e]	[6]
	6, 8	n-C_8H_{17}	**P21**, NA	1.39, 1.73[e]	[7]
	4	2-octyldodecyl	**P16**[c]	10.8[f]	[2]
	2	2-tetradecylhexadecyl	**P17**[c]	4.3[g]	[4]
	3-4	2-hexyldecyl	**P14**[c], **P16**[c]	3.7, 7.0[g]	[4]
	3	2-hexyldecyl	**P18**[c]	9.7[g]	[4]
	3	2-hexyldecyl/2-hexylnonyl	**P18**[c]	10.5[g]	[4]
	4	2-octyldodecyl	**P16**[c]	10.2[g]	[4]
	4	2-nonyltridecyl	**P16**[c]	11.3[g]	[3]

[a] polymers from literature similar to the polymers studied in this work shown in Figure 3.3, [b] side chain positions are different, [c] polymers in reference with 5,6-difluoro-BT, [d] PCE from SC PSCs, [e] active layer consists of polymer:$PC_{61}BM$, [f] active layer consists of polymer: modified-$PC_{71}BM$, [h] active layer consists of polymer:$PC_{61}BM$.

The E_g of some of these polymers [5,6] was plotted as a function of the numbers of Th per BT units. (Figure 3.2) It can be seen, that in both cases with increasing amounts of Th, E_g decreased. Other studies showed

that with an increase of the number of Th per repeating unit in a polymer or per comonomer (other than BT), E_g decreased while the PCE also decreased [8]. As already described in Chapter 2, the high efficiencies in these studies are misguiding due to a small active area and the production process of the devices. In the future, the laboratory scale devices should shift to RC techniques to be able to produce devices in large scale.

This chapter focuses on the synthesis of polymers based on Th and BT and their application in RC PSCs, to investigate the influence of the Th content on the optical properties as well as on the *J-V* characteristics of the resulting RC PSCs. This leads to suitable polymers for RC PSCs containing the preferred number of Th's per BT unit.

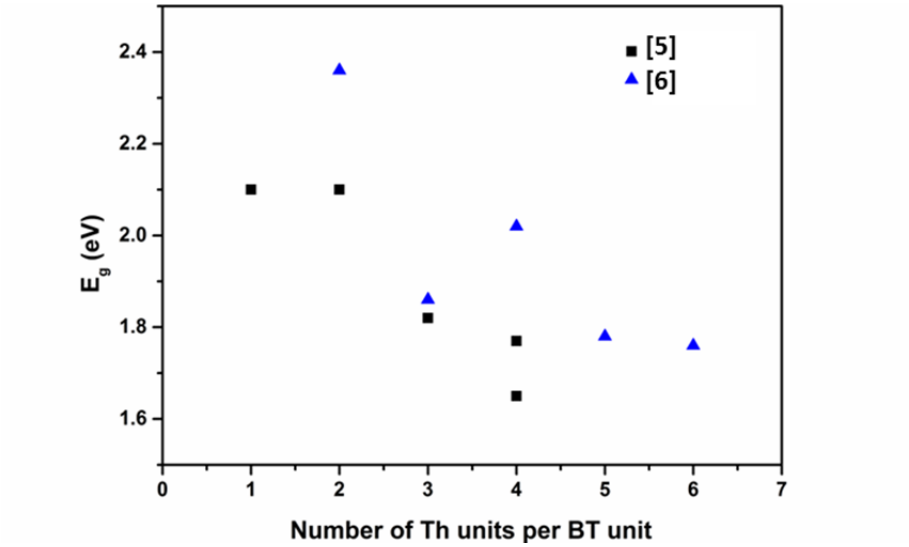

Figure 3.2. *Band gap (E_g) of polymers from reference* [5] *and* [6] *plotted as a function of the number of thiophene (Th) units per benzothiadiazole (BT) unit.*

3.2. Polymers based on Thiophene and Benzothiadiazole from the Polymer Screening (Chapter 2)

Prior to this chapter the screening of polymers *via* combinatorial pairing of monomers from Chapter 2 included also four monomers based on Th and BT (**M1**, **M2**, **M18** and **M21**) which resulted in four different polymers (Figure 3.3: **P10** - **P13**). In this chapter these polymers are described closer. The optical and electronic properties of the selected polymers, as well as their application in PSCs are presented in Table 3.2. It should be noticed that only **P12** was a high M_n polymer, while the other three polymers had a M_n of below 10 kDa. Their E_g, extrapolated from the corresponding UV-vis spectrum, varied from 1.58 to 2.05 eV. The photochemical R_d of the polymer film, calculated from periodical UV-vis measurements while exposed to

light (1.5 AM) was low for **P10** and **P12**, while **P11** and **P13** degraded fast. A reason for a faster degradation could be due to the low M_n of the polymers. All polymers were thereafter applied in RC PSCs with an inverted structure as described in Chapter 2. However, none of them resulted in working devices. The results give a negative perspective in the beginning of this chapter, but knowing from the previous studies, a change in the length or position of the side chain can affect the outcome of the *J-V* characteristics [9].

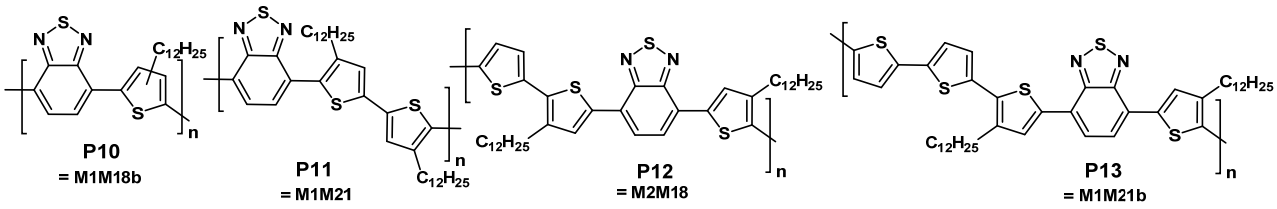

Figure 3.3. *Polymers **P10-P13** based on Th and BT from Chapter 2.*

Table 3.2. *Optical and electronic properties of **P10-P13** and their PSCs application from Chapter 2.*

Polymer	M_n[a] (kDa)	Đ[a]	E_g[b] (eV)	HOMO[c] (eV)	LUMO[d] (eV)	R_d[e] (%/h)	PCE[f] (%)
P10	9.3	2.2	1.79	-5.50	-3.71	2.46	0
P11	4.7	1.7	1.89	-5.39	-3.50	30.88	0
P12	540.0	4.2	1.58	-4.92	-3.34	0.45	0
P13	8.6	1.5	2.05	-5.17	-3.12	20.22	0

[a] Molecular weight (M_n) and polydispersity (Đ) determined from SEC against PS standard, [b] optical band gap (E_g) calculated from the onset of the UV-vis absorption spectrum of the polymer film, [c] highest occupied molecular orbital (HOMO) estimated from SWV curves, [d] lowest unoccupied molecular orbital (LUMO) calculated from the HOMO and E_g, [e] the degradation rate (R_d) was calculated from the degradation of the UV-vis absorption of a polymer film, [f] no PSCs could be obtained.

Due to a strong influence of the side chain position, it is important to review the knowledge within literature on where to place the side chain within Th-BT based polymers. In 1990, Wudl *et al.* investigated in a comparative study the influence of the side chain position in PT derivatives revealing the best absorption for head-to-tail PTs (Figure 3.4, I). Regiospecific head-to-tail polymers have a blue shifted absorption, which must be due to a dominant intrachain sulfur-alkyl steric repulsion forcing the backbone out of the co-planarity and π-conjugation [10]. This shows that the side chains should not be attached on the polymer backbone towards each other, so that they overlap, as the steric hindrance should be minimalized. This means that a side chain positioning as shown in Figure 3.4 I and II are possible. Cho *et al.* investigated the side chain position in Th next to a BT (Figure 3.4, III) of cyclopentadithiophene based copolymers. PSCs based on a copolymer with side chains towards BT resulted in suppressed performance due to its aggregated morphology, while the copolymer with the side chains away from BT had a low performance due to inefficient harvesting of the solar spectrum and a low mobility. The copolymer without side chain was most efficient with a PCE of 3.8%. These results give an idea of how solubility chains can affect the properties of

the conjugated polymers, and that these side chains also influence the morphological properties of a polymer film [11]. In contrast, You *et al.* investigated the same variation in a BDT based copolymer with similar results. However, with the side chain away from BT the device had a higher efficiency (2.17%) with a similar E_g of the polymer in comparison to the polymer without side chains (0.72%). This polymer has less steric hindrance and a better control over the morphology due to a good solubility [12]. In another investigation by Troshin *et al.* the position of the side chain on Th was investigated in a BT, Th and carbazole based polymer [13]. The best polymer and *J-V* characteristics were provided by the side chain on the second Th towards the BT, while the polymers with side chain on the first Th towards the BT (Figure 3.4, IV) were less promising (efficiency is 5.1% vs. 0.6%) [13]. The side chain position in **P2** was investigated by Livi *et al.* to find the optimal positioning in this promising polymer for RC PSC. The polymer with no side chain on the Th revealed the best polymer and solar cell characteristics [9]. All these examples justify that it is of great importance where on the polymer backbone the side chain is attached.

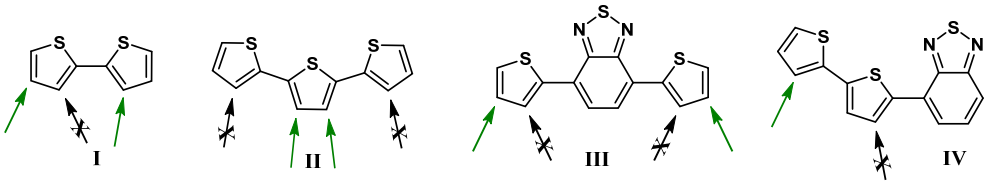

Figure 3.4. *Design rules for Th and BT based polymers.*

3.3. Polymers based on Thiophene and Benzothiadiazole

3.3.1. Synthesis

In this chapter, 8 conjugated copolymers (**P14**-**P21**, Figure 3.5.) were synthesized based on different ratios of Th and BT. In some of the polymers the position of the side chains were varied as well. In general, the side chain positioning of these polymers followed the rules from Chapter 3.1 including a relative balance of the side chain and backbone size. The side chains were kept as HD and in a few polymers a 2-octyldodecyl (OD) side chain was used. The polymers are based on the monomer units **M2**, **M18**, **M21** and **M22** (Scheme 3.1., blue structures) and were combined so that different ratios of Th and BT within the polymers were achieved. **P17** had a ratio of Th:BT of 2:1, **P14**, **P15** and **P18** of 3:1, **P16** of 4:1, **P19** and **P20** of 5:1 and **P21** of 6:1. The attempts to achieve higher ratios were limited by purification methods as it was already difficult to purify e.g. **M22b**.

The monomers (**M2**, **M18c**, **M21** and **M22**) and their activated (stannylated or brominated) derivatives (**3.7**-**3.9**, **3.10**-**3.15**) were synthesized by adapting literature procedures (see experimental details in Appendix A

and Scheme 3.1), except for **M18** which was received commercially. The synthesis of the monomers included 4 different methods: attaching of the side chains, stannylation with trimethyltin chloride, bromination with N-bromosuccinimid (NBS) and Stille cross-coupling. **M21b** was synthesized by the standard Stille cross-coupling of two commercial reagents. **M2b** and **M2c** were synthesized by Stille-cross coupling of the dibrominated BT and a commercially available mono-stannylated Th (**3.6**) or an alkylated and mono-stannylated Th (**3.3**). **M22**, **M22b** and **M22c** were also synthesized via Stille cross-coupling using activated **M2b** (distannylated or dibrominated) and **M2c** (dibrominated), respectively, and different mono-stannylated Th without or with an HD or OD side chain. The final **M18**, **M18c**, **M21b** and **M2b** were activated by forming the bis-stannylated compound, while **M2b**, **M2c**, **M22**, **M22b** and **M22c** were dibrominated with NBS to activate the monomers. The monomers were purified using different methods: recrystallization and column chromatography. The **M22b** and **M22c** and their activated derivative were difficult to purify by column chromatography due to an increase in formed byproducts with similar structure (e.g. mono- or tribrominated molecules). Standard Stille cross-coupling polymerizations of the stannyl-activated monomers with the bromo-activated monomers were prepared for **P14**-**P21** (Figure 3.5). The polymerizations of **P19** and **P20** were rather unsuccessful, due to a low solubility of the BT based monomers, and were received in small yields after purification of the polymers by Soxhlet extraction.

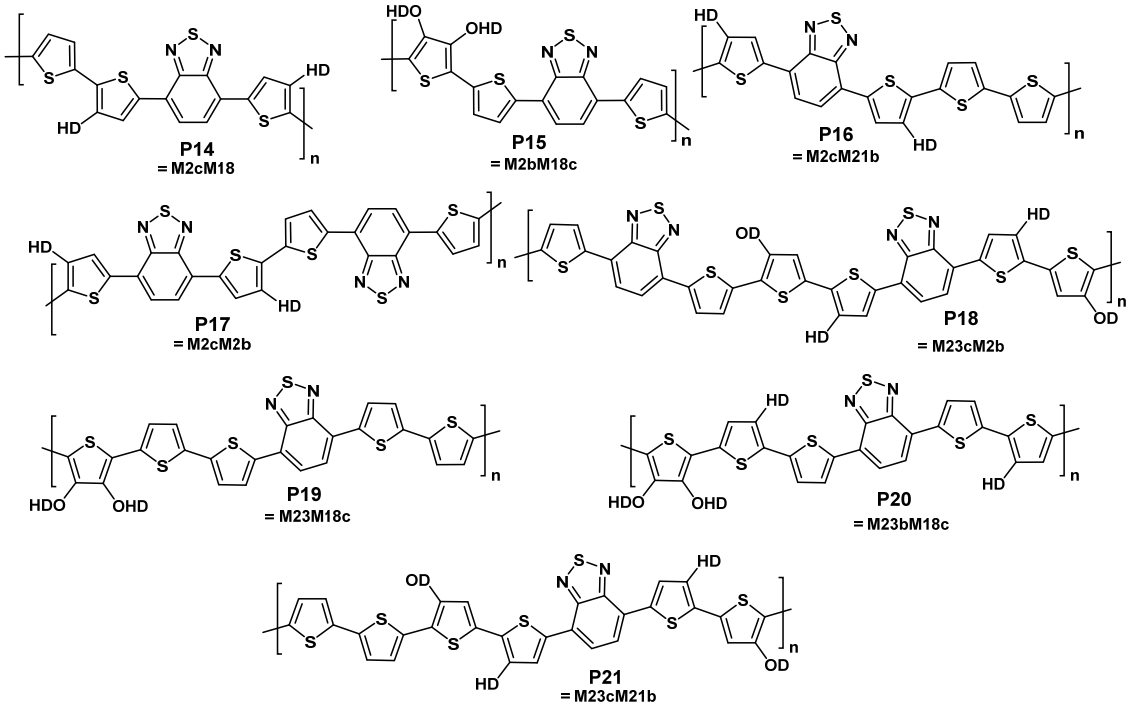

Figure 3.5. *Polymers based on Th and BT prepared in this chapter.*

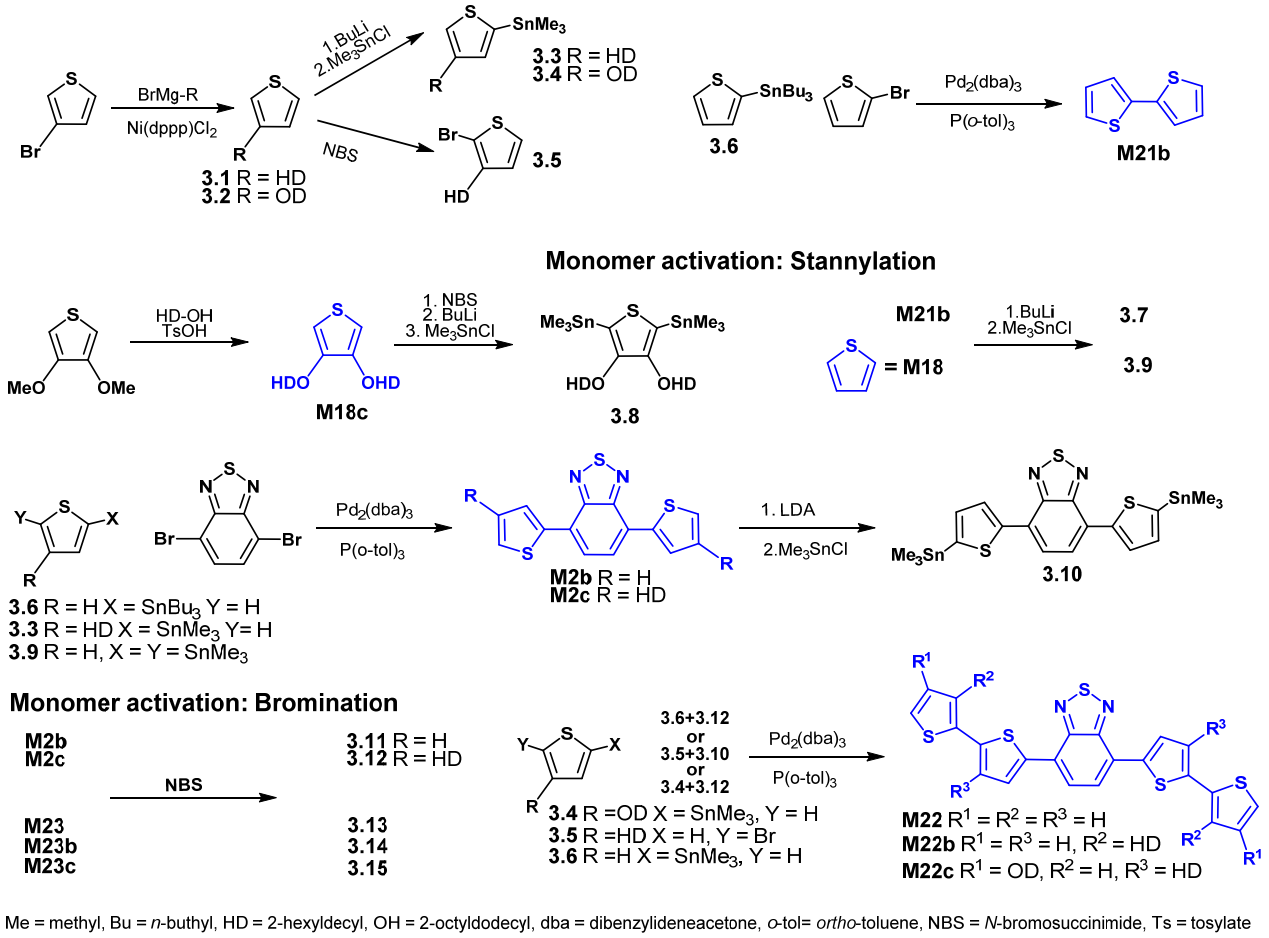

Me = methyl, Bu = *n*-buthyl, HD = 2-hexyldecyl, OH = 2-octyldodecyl, dba = dibenzylideneacetone, *o*-tol= *ortho*-toluene, NBS = *N*-bromosuccinimide, Ts = tosylate

Scheme 3.1. *Synthetic routs yielding monomers based on Th and BT.*

3.3.2. Characterization

The polymers **P14**-**P21** were characterized using standard techniques and ^{1}H NMR (nuclear magnetic resonance) spectra were recorded of the copolymers in chloroform-d_1 or *ortho*-dichlorobenzene-d_4 (details in Appendix A and Appendix B Figure B.3.1). The spectra of **P14, P16, P21** and **P18** showed high M_n polymers with small end groups of the CH_2 of the HD side chain on the Th group around 2.5 ppm. The spectra of **P15** and **P20** showed low M_n polymers with clear aromatic signals around 7-8 ppm. The spectra of **P17** and **P19** revealed no clear answer to the M_n of the polymers due to low solubility in the corresponding solvent.

M_n (Table 3.3) could be determined by SEC only for **P14** and **P16** to be around 22 kDa and for **P21** and **P18** to be around 43 kDa. **P20** had a low molecular weight. **P15** and **P19** aggregated and **P17** was insoluble in chlorobenzene (CB), so no measurements could be performed to determine M_n.

UV-vis spectra of the polymers were recorded in CF solution (except for **P17** which was in ODCB solution) and of the films on glass substrates (Figure 3.6.), and details from the spectra are listed in Table 3.3. The absorption of **P15** solution was in a higher wavelength range (787 nm for λ_{onset}) than the other polymers with a rather broad λ_{max} (659 nm). **P14** and **P16** had very similar absorption profile, which was shifted a bit towards lower wavelength for the absorption of the **P14** solution. Therefore, their E_g (1.64 eV) was also the same even though the polymers contain different amounts of Th's. **P17** had a rather different absorption profile. The absorption of the polymer solution had a λ_{max} of 608 nm with a local maximum in the higher wavelength range (~740 nm). These two maxima appeared again in the spectrum of the polymer film with λ_{max} at 734 nm and a smaller one around 650 nm. This resulted in a low E_g (1.56 eV). **P18, P19** and **P20** had similar but slightly shifted absorption profiles than **P14** and **P16**, respectively, especially in the polymer film spectra. The absorption of **P21** with a high incorporation of the Th show a shift for both the solution and film based spectrum with the highest E_g (1.73 eV) measured among the polymers. For comparison the UV-vis absorption spectrum of a **P3HT** film is also shown. It was clear that the more Th incorporated in BT-Th based polymers the closer the properties lean towards PT (/**P3HT**).

Table 3.3. *Optical and electronic properties of* **P14**-**P21**.

Polymer	Th:BT ratio	SEC[a]		UV-vis solution[b]		UV-vis film[b]		
		M_n (kDa)	Đ	λ_{max}	λ_{onset}	λ_{max}	λ_{onset}	E_g (eV)
P14	3:1	21.4	1.6	565	680	639	755	1.64
P15	3:1	aggregate	-	659	787	696	798	1.55
P16	4:1	24.9	1.8	584	713	642	755	1.64
P17	2:1 (4:2)	insoluble	-	608[c]	790[c]	724	795	1.56
P18	3:1 (6:2)	43.7	1.9	591	712	669	760	1.63
P19	5:1	aggregated	-	576	734	623	751	1.65
P20	5:1	low	-	555	655	610	739	1.68
P21	6:1	42.1	1.8	540	637	595	716	1.73

[a] Molecular weight (M_n) and polydispersity (Đ) determined from SEC against PS standard, [b] optical band gap (E_g) calculated from the onset of the UV-vis absorption spectrum of the polymer solution in CF or of the polymer film, [c] polymer solution in ODCB.

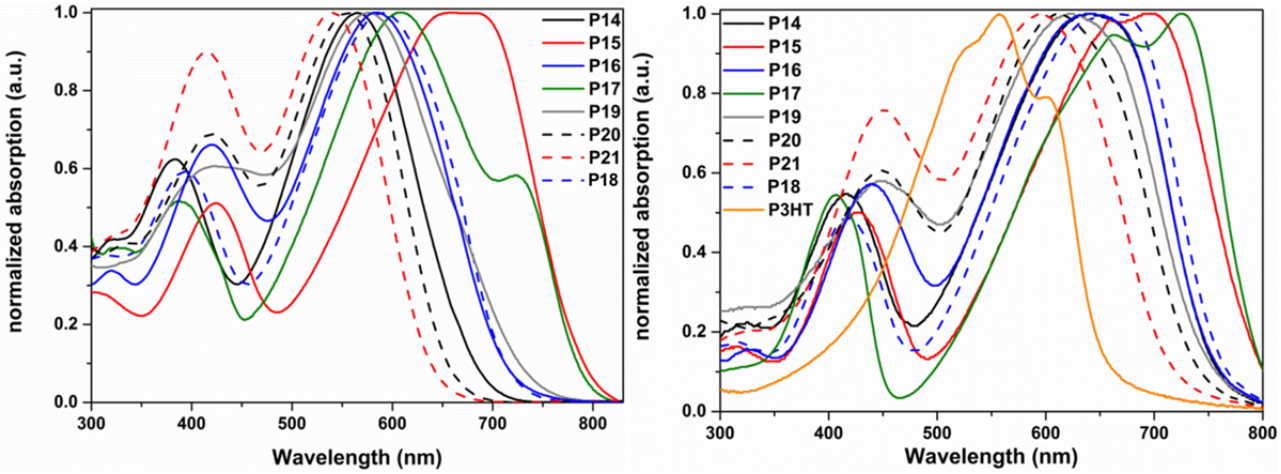

Figure 3.6. *UV-vis absorption spectrum of the polymer solution (left) in CF or ODCB and of the polymer film (right) on a glass substrate.*

The E_g's of all the polymers were estimated from the films according to a literature procedure [15] by fitting a tangent onto the onset of the curve and converting the read off wavelength to eV, to be between 1.55 eV-1.73 eV. E_g's from this work (Chapter 2 and 3) and publications [4,7] were plotted against the number of Th per BT unit (Figure 3.7). The result shows that the E_g increases with an increase of Th units in a polymer based on BT and Th. This is the opposite of the trend, which was seen in Figure 3.2, where the E_g values from reference [5,6] decreased with increasing amounts of Th. However, in this case E_g as well as the absorption spectrum approximate the value (2.0 eV [16]) and the absorption curve of **P3HT** (Figure 3.6, orange), respectively. An increase of Th's per BT unit in the polymer also approximates the polymer to be almost a PT derivative. This means that there is also a shift from a low band gap D_M-A_M polymer towards a simple conjugated polymer. The change in bond-length alternation of the Th-BT based polymers, with higher density of Th will decrease the double bond character between the units in the backbone again (in comparison to a low band gap D_M-A_M polymer) resulting in an increase of the E_g [17]. An exception to this trend was seen for three polymers of Chapter 2. This variation of E_g could be due to the side chains in the polymer which also influence the morphology of the film. This effect of different side chains length, nature and positions on the same polymer backbone was shown by Livi *et al.* on **P2** [9].

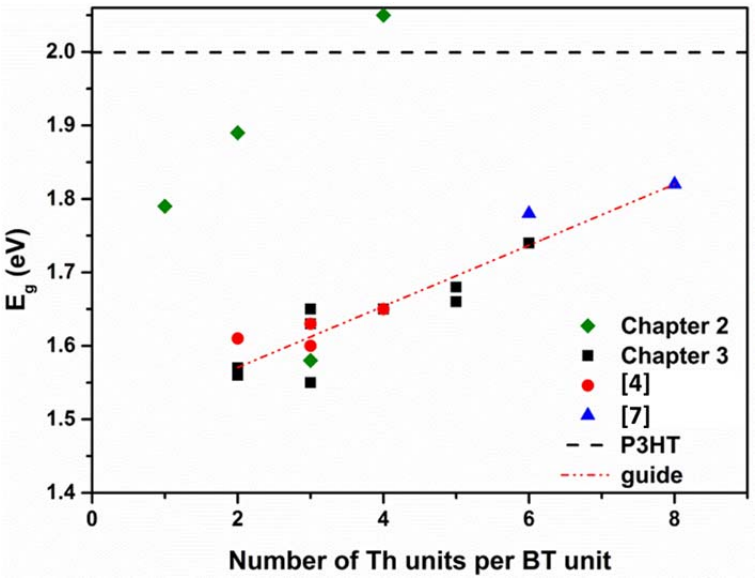

Figure 3.7. *E_g of polymers from the current work and two references [4] and [7] plotted as a function of the number of Th's per BT unit.*

3.3.3. Polymer Stability

Photochemical stabilities of the pristine polymer films of **P14**-**P18** and **P21** were investigated by measuring the UV-vis absorption under constant solar irradiance (AM 1.5) within a frequent time interval. **P19** and **P20** were not investigated further as the yields of the polymers were low with low solubility in common solvents and low M_n. Exposure of the films to light resulted in a slight blue shift of the absorption maximum and a clear loss of the polymer film colour. From the normalized degradation curves (Figure 3.8) which are based on the absorption maxima, different degradation rate were present. It is clearly seen that **P14**-**P16** and **P18** degraded very similar and showed no absorption after ~75 h for **P14** and **P18** and ~85 h for **P15** and **P16**, whereas the film of **P17** degraded very slowly, even after 300 h there was still ~50% of the initial absorption left. The degradation of the absorption curve of **P21** degraded in a different trend. The absorption of the polymer film decreased rapidly to be vanished after ~25 h. This is again an approximation towards the degradation of **P3HT** UV-vis absorption, which is shown in Figure 3.8 as a dashed line.

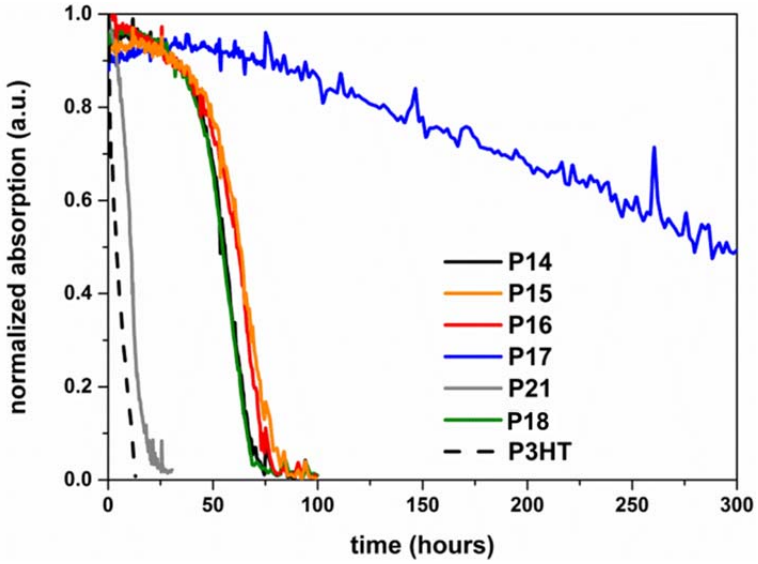

Figure 3.8. *Stability tests under solar irradiance of* ***P14-P18, P21*** *and* ***P3HT*** *showing the degradation of the UV-vis absorption.*

3.4. Polymer Solar Cells

3.4.1. Preparation and Characterization

The BT-Th based polymers **P14-P18**, and **P21** were applied in BHJ PSCs to investigate the influence of different ratios of Th and BT on the PV properties as well as the stabilities of the PSC. The devices had an inverted architecture (Chapter 1.3.1) of PET/Ag grid/PEDOT:PSS/ ZnO/polymer:$PC_{61}BM$/PEDOT:PSS/Ag grid with device areas of around 1 cm^2. The active layer of the synthesized polymers was coated on a commercially available *flextrode* substrate using a mini roll-coater. The solvent and the active layer thickness were adapted from the ones used in Chapter 2 to yield possible high efficiencies, while the polymer-to-$PC_{61}BM$ ratio was 1:2. The *J-V* characteristics of the devices were measured under a solar simulator (1000 W m^{-1}, AM 1.5) and are summarized in Table 3.4.

Table 3.4. *J-V characteristics*[a] *(V_{OC}, J_{SC}, FF and PCE) for the PSCs based on* ***P14-P18*** *and* ***P21****.*

Polymer	Th:BT ratio[g]	PCE (%)	V_{OC} (V)	J_{sc} (mA m^{-2})	FF	$PCE_{ref.}$ (%)	Reference
P14[b]	3:1	1.30 (1.56)	0.73	3.86	0.46	0.93[h] 3.7[i,j]	[6] [4]
P15[c]	3:1	0.09 (0.10)	0.55	0.44	0.37	-	-

P16[c]	4:1	2.00 (2.35)	0.68	6.53	0.45	7.0[i]	[4]
P17[d]	2:1 (4:2)	1.59 (1.68)	0.62	5.40	0.49	4.3[i,j]	[4]
P18[e]	3:1 (6:2)	0.74 (0.84)	0.74	2.16	0.47	10.7[i,j]	[4]
P21[f]	6:1	0.08 (0.09)	0.57	0.44	0.30	1.39[h] 2.23[h]	[7] [6]

[a] *J-V* parameters are averaged over at least 3 devices, devices prepared with a polymer:$PC_{61}BM$ of 1:2, [b] device prepared from ODCB:CB=1:2 and a layer thickness of 600 nm, [c] device prepared from ODCB and a layer thickness of 450 nm, [d] device prepared from ODCB and a layer thickness of 400 nm, [e] device prepared from ODCB:CB=1:2 and a layer thickness of 500 nm, [f] device prepared from ODCB and a layer thickness of 550 nm, [g] thiophene-benzothiadiazole ratio in the polymer, [h] active layer consists of polymer: modified-$PC_{71}BM$, [i] active layer consists of polymer:$PC_{61}BM$, [j] difluorinated on BT.

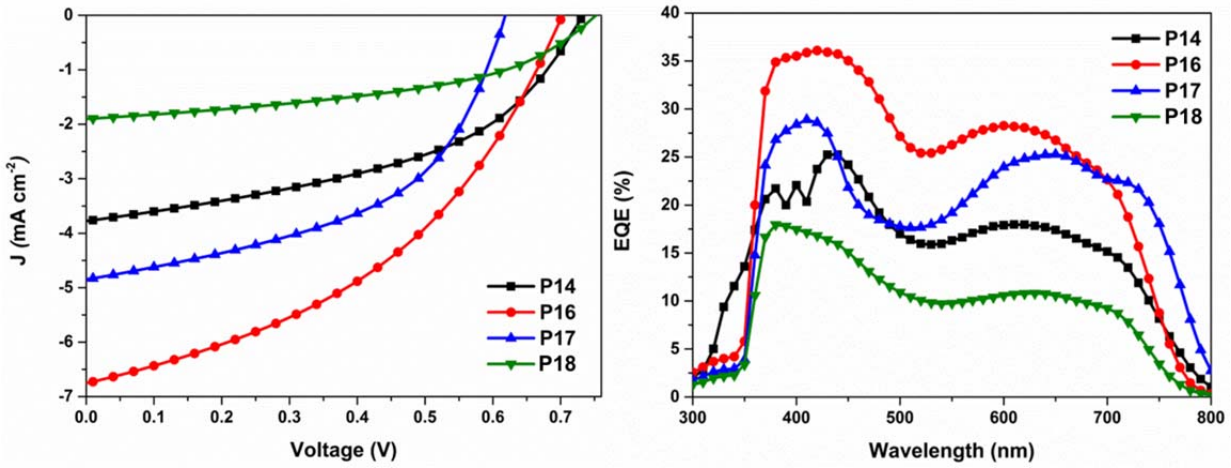

Figure 3.9. *J-V curves (left) and EQE spectra (right) of the best PSCs based on* ***P14***, ***P16***, ***P17*** *and* ***P18****.*

For **P14**, **P16**, **P17** and **P18** the *J-V* curves are also shown in Figure 3.9 (left). **P15** and **P21** are not shown because they did not result in working PV devices mainly due to a low J_{SC}. **P16** had the best working devices with the highest efficiency of 2.35%, mainly due to a high J_{SC}. This polymer had a Th-BT ratio of 4:1. This is in agreement with the results from literature where the incorporation of four Th units in a Th-BDT based polymer resulted in the highest efficiencies in these studies of >10 [2–4]. **P17** had a similar *J-V* curve progression as **P16** but with a lower J_{SC} and V_{OC} resulting in 1.59% PCE. **P14** and **P18** had similar curve progressions with higher V_{OC} than the other two device types. However, again a reduced J_{SC} was visible, leading to 1.30% and 0.74% PCE of **P14** and **P18**, respectively. This gives the assumption that incorporation of an even number of Th (a 4:1- or 2:1-ratio for **P16** and **P17**) could have a positive effect on the efficiency while an odd number (a 3:1-ratio for **P14** and **P18**) revealed a lower efficiency. The FF's of all devices were around 47%. In comparison the efficiencies of the RC PSCs from polymers in this work were as expected lower than the SC devices from literature (Table 3.4). The most efficient device from literature work (PCE = 10.7%) [4] is correlating to **P18** of this work. Even though this polymer could be applied here in RC PSCs, it resulted in a

rather low efficiency (0.74%). However, **P16** was here the most efficient polymer in PSCs (2.0%), while it was also quite high in SC devices (7.0%) [4].

The intensities of the EQE spectra (Figure 3.9.) of the PSCs reflect the results of the *J-V* characteristics. The maxima for all devices were around 400 nm. The local maximum in the higher wavelength region was for **P14**, **P16** and **P18** around 620 nm, while it was shifted for **P17** to be around 650 nm.

3.4.2. Solar Cell Stability

The PSCs were additionally investigated by a lifetime study under ISOS-L-1 standards [18] using three different PSCs per polymer. All devices were exposed to solar illumination (approximately AM 1.5, 1000 W m^{-2}) for around 20 days. The devices were handled the same way (coated, encapsulated), so similar effects of the illumination can be expected [19]. *J-V* curves were measured within specific time intervals, smaller ones (1 min) in the beginning of the experiments and then larger intervals (30 min) after ~24 h. Averages of all *J-V* characteristics over time were taken from the values of each device. The normalized average PCEs were plotted against the time for each polymer and is shown in Figure 3.10. Cell failures (cell failed but recovered again) occurred for some devices, but data was in this case left out in the graphs. The efficiency of all PSCs decreased quickly for all cells in the first phase (0 – 8 h) of the study. **P18** based devices degraded very fast, already after 12 h they were degraded by 50% and after 100 h the devices showed a performance close to zero. The fast degradation could be due to the large amount of side chains in comparison to the other polymers, so the polymer film had a different morphology due to a different packing of the polymer chains.

Further, **P14** and **P16** based devices showed similar degradation in the beginning of the study. After ~20 h the degradation of the **P14** based devices was, however, slower than the **P16** based devices retaining ~25% and ~20% of the initial PCE after a study time of 450 h, whereas **P17** based devices degraded much slower compared to other devices in the beginning of the study. After ~20 h the degradation continued to be faster than the **P14** and **P16** based, after 450 h only ~10% of the initial PCE was left. Due to different starting values (Figure 3.10 right) of **P14** and **P16**, the degradation curve slope degraded to the same PCE value (0.3% efficiency of the devices), while **P17** had a final PCE of 0.1%, so the high starting value could not compensate the fast degradation. **P18** had a small initial value as well as the fastest degradation; therefore the measurements were already stopped after ~150 h.

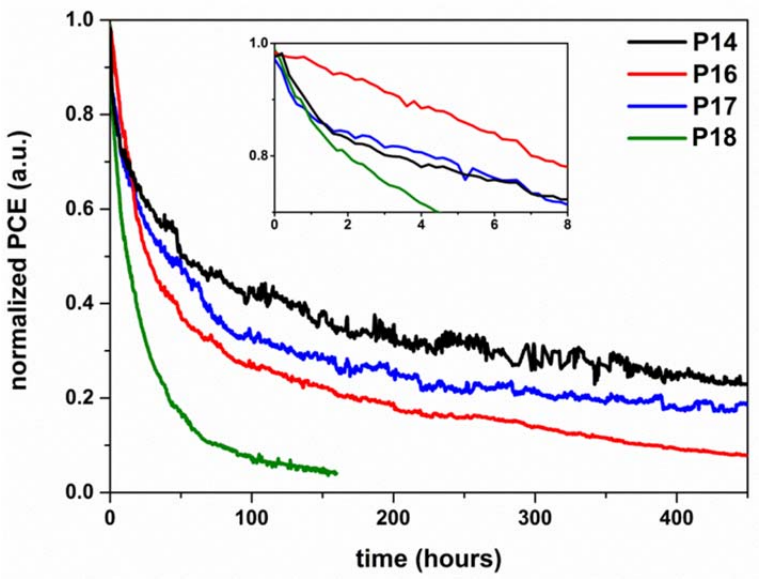

Figure 3.10. *Stability tests under solar irradiance of the PSCs showing the degradation of the normalized PCE.*

The V_{OC} of **P14**, **P16** and **P17** stayed constant while the J_{SC} degraded similar to the PCE. The degradation of the FF of the **P14** and **P16** devices had a similar slope, while the one for **P17** stabilized to be ~80% of the initial FF after ~100 h. The other *J-V* characteristics of the **P18** devices degraded fast similar to the PCE (Appendix Figure B.3.2).

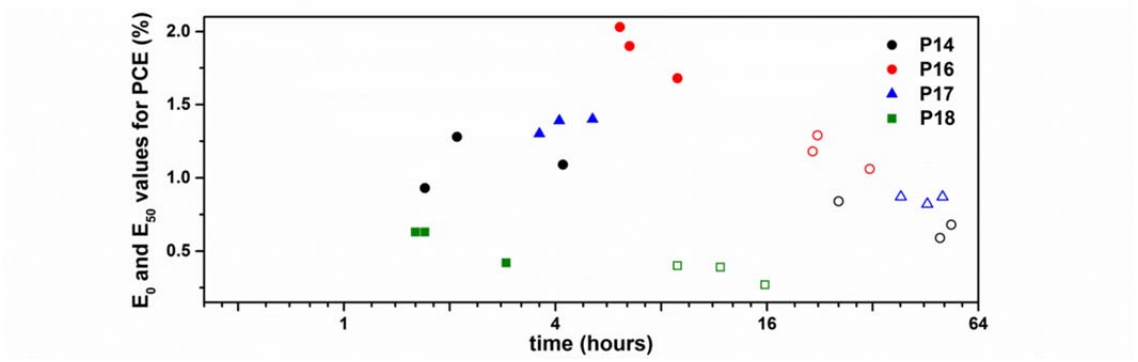

Figure 3.11. *The diagram shows T_{80}/E_0 (solid) and T_{50}/E_{50} (open) of the lifetime measurements (ISOS-L-1) of all cells from PSCs based on **P14**, **P16**, **P17** and **P18**.*

It is clearly seen in Figure 3.11, where the PCE values (E_0 and E_{50}) of 80% and 50% of the initial values of the devices were plotted against the corresponding degradation times (T_{80} and T_{50}), that **P18** degraded the fastest (low T_{80} and T_{50}) with small corresponding PCE values (E_0 and E_{50}). **P16** seemed to be most stable in the beginning of the experiment, with a high T_{80} and E_0 value. **P14** and **P17** degraded in a similar manner. It seems that the incorporation of **M22b**, and thus a higher density of Th in the repeating unit had a negative effect on the stability as well. The smaller differences of **P14**, **P16** and **P17** are affecting the lifetime stability

slightly, especially in a longer time frame. The same differences were seen in the Chapter 3.3.1 for smaller differences in efficiencies.

3.5. Conclusion

In this chapter eight polymers **P14**-**P21** based on benzo[c][1,2,5]thiadiazole (BT) and thiophene (Th) were synthesized. The polymers contained different ratios of Th-BT with different positioning of the side chains. Three of the polymers showed low M_n in SEC, two aggregated during the measurement and one was insoluble in the used solvent. Thereby, four polymers showed M_n's of ~20 kDa and ~40 kDa, respectively. The UV-vis spectra of the polymer films revealed different E_g's for different Th-BT ratios. These values and E_g values from literature [4,7] showed that with an increasing amount of Th in the polymer they increase and approximate the E_g value of **P3HT**. This increase is due to a change in the bond-length alteration of the polymers. The polymers were also investigated in terms of their photo degradation, where it is shown again, that **P21** with a high incorporation of Th (6:1 ratio to BT) has a fast degradation rate, which is again closer to the one for **P3HT**. **P17** with a low incorporation of Th (2:1 ratio to BT) showed a much slower degradation rate than **P14**-**P16** and **P18**, which are in the center span. The other polymers were not included in further studies, due to their low M_n and a low yield.

The polymers were applied in RC PSCs showing efficiencies of >1% for **P14**, **P16** and **P17**. **P18** had a maximum efficiency of 0.83%, while **P15** and **P21** failed during the *J-V* measurements. **P16** revealed the highest efficiency of 2.35% with a Th-BT ratio of 4:1. Lifetime stability measurements of the PSCs showed the fastest degradation for **P18** beside its low efficiency. The high value of the device efficiency is overlapped with a faster degradation of the **P16** devices in comparison to **P17** and **P14**.

The results show different effects of different Th densities within a BT-Th based polymer. For future work it would be interesting to know what exact role the side chains play in this arrangement. Especially on polymers with a 2:1, 3:1 and 4:1 ratio, but also on polymers with odd and even numbers of Th units in the polymer backbone. It is then also important to improve the RC parameters (D-A ratio, solvent, active layer thickness, etc.) of the PSCs production.

3.6. References

1. Yue, W.; Ashraf, R. S.; Nielsen, C. B.; Collado-Fregoso, E.; Niazi, M. R.; Yousaf, S. A.; Kirkus, M.; Chen, H.-Y.; Amassian, A.; Durrant, J. R.; McCulloch, I. A Thieno[3,2-b][1]benzothiophene Isoindigo Building Block for Additive- and Annealing-Free High-Performance Polymer Solar Cells. *Adv. Mater.* **2015**, *27*, 4702–4707.

2. Liu, Y.; Zhao, J.; Li, Z.; Mu, C.; Ma, W.; Hu, H.; Jiang, K.; Lin, H.; Ade, H.; Yan, H. Aggregation and morphology control enables multiple cases of high-efficiency polymer solar cells. *Nat. Commun.* **2014**, *5*, 5293 (1-8).

3. Zhao, J.; Li, Y.; Yang, G.; Jiang, K.; Lin, H.; Ade, H.; Ma, W.; Yan, H. Efficient organic solar cells processed from hydrocarbon solvents. *Nat. Energy* **2016**, *1*, 15027 (1-7).

4. Hu, H.; Jiang, K.; Yang, G.; Liu, J.; Li, Z.; Lin, H.; Liu, Y.; Zhao, J.; Zhang, J.; Huang, F.; Qu, Y.; Ma, W.; Yan, H. Terthiophene-Based D-A Polymer with an Asymmetric Arrangement of Alkyl Chains That Enables Efficient Polymer Solar Cells. *J. Am. Chem. Soc.* **2015**, *137*, 14149–14157.

5. Bundgaard, E.; Krebs, F. C. Low-Band-Gap Conjugated Polymers Based on Thiophene , Benzothiadiazole , and Benzobis (thiadiazole). *Macromolecules* **2006**, *39*, 2823–2831.

6. Yue, W.; Zhao, Y.; Song, D.; Tian, H.; Xie, Z.; Yan, D.; Geng, Y.; Wang, F. Poly(oligothiophene-alt-benzothiadiazole)s: Tuning the structures of oligothiophene units toward high-mobility "black" conjugated polymers. *Macromolecules* **2009**, *42*, 6510–6518.

7. Liang, F.; Lu, J.; Ding, J.; Movileanu, R.; Tao, Y. Design and synthesis of alternating regioregular oligothiophenes/ benzothiadiazole copolymers for organic solar cells. *Macromolecules* **2009**, *42*, 6107–6114.

8. Liu, X.; Cai, P.; Chen, Z.; Zhang, L.; Zhang, X.; Sun, J.; Wang, H.; Chen, J.; Peng, J.; Chen, H.; Cao, Y. D-A copolymers based on 5,6-difluorobenzotriazole and oligothiophenes: Synthesis, field effect transistors, and polymer solar cells. *Polym. (United Kingdom)* **2014**, *55*, 1707–1715.

9. Livi, F.; Zawacka, N. K.; Angmo, D.; Jørgensen, M.; Krebs, F. C.; Bundgaard, E. Influence of Side Chain Position on the Electrical Properties of Organic Solar Cells Based on Dithienylbenzothiadiazole- alt -phenylene Conjugated Polymers. *Macromolecules* **2015**, *48*, 3481–3492.

10. Maior, R. M. S.; Hinkelmann, K.; Eckert, H.; Wudl, F. Synthesis and characterization of two regiochemically defined poly(dialkylbithiophenes): a comparative study. *Macromolecules* **1990**, *23*, 1268–1279.

11. Lee, S. K.; Seo, J. H.; Cho, N. S.; Cho, S. Effect of side chain position on solar cell performance in cyclopentadithiophene-based copolymers. *Thin Solid Films* **2012**, *520*, 5438–5441.

12. Zhou, H.; Yang, L.; Xiao, S.; Liu, S.; You, W. Donor-acceptor polymers incorporating alkylated dithienylbenzothiadiazole for bulk heterojunction solar cells: Pronounced effect of positioning alkyl Chains. *Macromolecules* **2010**, *43*, 811–820.

13. Akkuratov, A. V.; Susarova, D. K.; Moskvin, Y. L.; Anokhin, D. V.; Chernyak, A. V.; Prudnov, F. A.; Novikov, D. V.; Babenko, S. D.; Troshin, P. A. A strong influence of the positions of solubilizing alkyl side chains on optoelectronic and photovoltaic properties of TTBTBTT-based conjugated polymers. *J. Mater. Chem. C* **2015**, *3*, 1497–1506.

14. Akkuratov, A. V.; Susarova, D. K.; Kozlov, O. V.; Chernyak, A. V.; Moskvin, Y. L.; Frolova, L. A.; Pshenichnikov, M. S.; Troshin, P. A. Design of (X-DADAD) n Type Copolymers for Efficient Bulk Heterojunction Organic Solar Cells. *Macromolecules* **2015**, *48*, 2013–2021.

15. Bundgaard, E.; Krebs, F. C. Low-Band-Gap Conjugated Polymers Based on Thiophene , Benzothiadiazole , and Benzobis (thiadiazole). *Macromolecules* **2006**, *39*, 2823–2831.

16. Salzner, U.; Lagowski, J. B.; Pickup, P. G.; Poirier, R. A. Comparison of geometries and electronic structures of polyacetylene, polyborole, polycyclopentadiene, polypyrrole, polyfuran, polysilole, polyphosphole, polythiophene, polyselenophene and polytellurophene. **1998**, *96*, 177–189.

17. Van Mullekom, H. A. M.; Vekemans, J. A. J. M.; Havinga, E. E.; Meijer, E. W. Developments in the chemistry and band gap engineering of donor-acceptor substituted conjugated polymers. *Mater. Sci. Eng.* **2001**, *32*, 1–40.

18. Reese, M. O.; Gevorgyan, S. A.; Jørgensen, M.; Bundgaard, E.; Kurtz, S. R.; Ginley, D. S.; Olson, D. C.; Lloyd, M. T.; Morvillo, P.; Katz, E. A.; Elschner, A.; Haillant, O.; Currier, T. R.; Shrotriya, V.; Hermenau, M.; Riede, M.; Kirov, K. R.; Trimmel, G.; Rath, T.; Inganäs, O.; Zhang, F.; Andersson, M.; Tvingstedt, K.; Lira-Cantu, M.; Laird, D.; McGuiness, C.; Gowrisanker, S.; Pannone, M.; Xiao, M.; Hauch, J.; Steim, R.; Delongchamp, D. M.; Rösch, R.; Hoppe, H.; Espinosa, N.; Urbina, A.; Yaman-Uzunoglu, G.; Bonekamp, J.-B.; van Breemen, A. J. J. M.; Girotto, C.; Voroshazi, E.; Krebs, F. C. Consensus stability testing protocols for organic photovoltaic materials and devices. *Sol. Energy Mater. Sol. Cells* **2011**, *95*, 1253–1267.

19. Jeong, J.; Seo, J.; Nam, S.; Han, H.; Kim, H.; Anthopoulos, T. D.; Bradley, D. D. C.; Kim, Y. Significant Stability Enhancement in High-Efficiency Polymer:Fullerene Bulk Heterojunction Solar Cells by Blocking Ultraviolet Photons from Solar Light. *Adv. Sci.* **2015**, 1500269 (1-10).

Chapter 4.

Side Chain Modification in Polymers to Influence the Solar Cells Stability

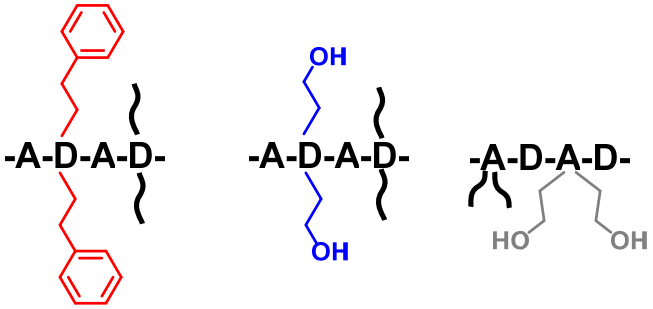

4.1. Introduction

The challenges of applying polymers in PSCs are focused on four different areas; the cost, performance, processability and stability as displayed in the *golden square*, which were all addressed in Chapter 2. However, the main focus was on the performance (>1% efficiency) and polymer processability (application in RC PSCs). In this chapter the focus will be on the stability of the PSCs.

The side chains of the polymers are known to have a large impact on the stability of the material and on the D-A blend formation, but are needed due to solubility reasons [1,2] to be able to apply them in fully solution processed PSCs. Over time an instability of the BHJ morphology can occur upon applying external stress (light, temperature, etc.), leading to a phase separation/demixing of the polymer and fullerene (crystallization of the fullerene), which appears as one of the main problems in BHJ PSCs [3]. To prevent the crystallization of fullerenes within the active layer, the use of non-crystallizing polymer-fullerene blends [4], nucleation agents [5], cross-linkable functional groups [6] and the removal of the side chains [7,8] after deposition were proposed, to 'freeze' the morphology of the active layer and increase the lifetime of the devices prepared from these materials by preventing phase separation. In another approach the side chain density of a low band gap copolymer was reduced enhancing the efficiency and thermal stability [9]. This shows that the

modification of the donor material in the active layer blend is a possibility to improve its stability. The introduction of a stabilizing side chain in different conjugated polymers is another example of modification of the donor material. This resulted in a significant enhancement of the stability of the corresponding PSCs. Vanderzande *et al.* demonstrated that for a poly(phenylenevinylene) derivative the introduction of a 2-phenethyl (EtPh) group increased the T_g and therefore improved the thermal stability by reducing the phase separation when exposed to stress [10]. Similar side chain modifications were performed to increase the stability of a PT derivative and of a D_M-A_M copolymer based PSCs using small amounts (5-10%) of an alcohol, ester or cinnamoyl group [11,12].

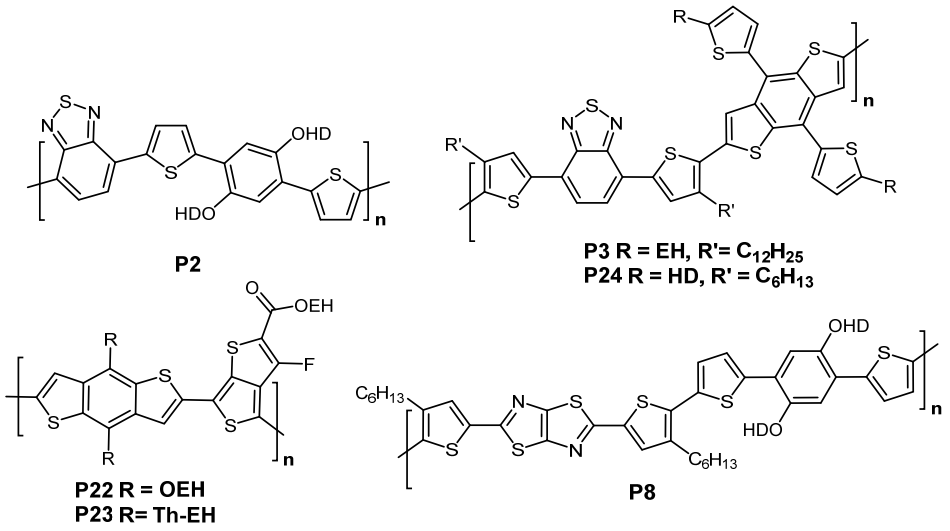

Figure 4.1. *Chemical structures of high performing polymers in literature (**P22** and **P23**) and of some selected polymers suitable for RC PSCs (**P2**, **P3**, **P8** and **P24**).*

The highly investigated [13–16] polymer **P22** and **P23** (Figure 4.1, **M8M16** and **M8M15** from Chapter 2) in terms of PSC efficiency and stability could not be translated to RC processing in Chapter 2. However, **P2**, **P3** and **P8** were identified to be suitable for RC PSCs. In this chapter the previous mentioned strategy to improve the stability of PSCs by modifying the side chain, was translated onto the three different promising conjugated polymers (**P2**, **P3**, and **P8**). In previous work, the impact of the nature, length and positioning of side chains on the polymer backbone and their electrical properties was demonstrated [15]. Therefore, the side chains in **P3** were changed to be HD and hexyl (**P24**) to enhance the efficiency of the resulting PSCs [17]. The side chains were modified by partially exchanging the solubilizing HD or hexyl chains by different known stabilizing groups to increase the stability of the resulting PV devices.

Chapter 4 is divided into three further subchapters. After discussing the synthesis, Chapter 4.3 deals with the influence of the EtPh side chain, where it was investigated in terms of a partial incorporation in different backbones (**P2**, **P8** and **P24**) to elevate the T_g and thereby the thermal

stability. In Chapter 4.4 the attempt of another side chain (2-ethanol (EtOH)) also in comparison to the EtPh side chain was investigated in terms of its influence in the stability on the polymer and PSCs. The EtOH side chain was thereby positioned on the D_M and A_M unit using the polymer backbone based on **P24**. Last, Chapter 4.5 compares the two attempts with approaches and mechanisms from the literature.

4.2. Synthesis

In this chapter, 13 low band gap copolymers (Figure 4.1 and Figure 4.2) were synthesized based on phenylene, Th, BT, TzTz and BDT building blocks (Scheme 4.1). **P2**, **P8** and **P24**, bearing a HD and/or hexyl side chain, were adapted from Chapter 2 or reported previously [17,18]. **P25a,b** were derived from **P2** and were prepared with a partial substitution (5%, 10%) of the HD by the EtPh side chain. **P26a,b** have the same backbone as **P8**, but also with a partial substitution (5%, 10%) of the HD by the EtPh side chain. Whereas **P24** was manipulated by partial substitution (5%, 10%) of the HD chain by EtPh in **P27a,b**, of the HD chain by EtOH in **P28a,b** and of the hexyl chain by EtOH in **P29a,b**.

4.2.1. Monomer Synthesis

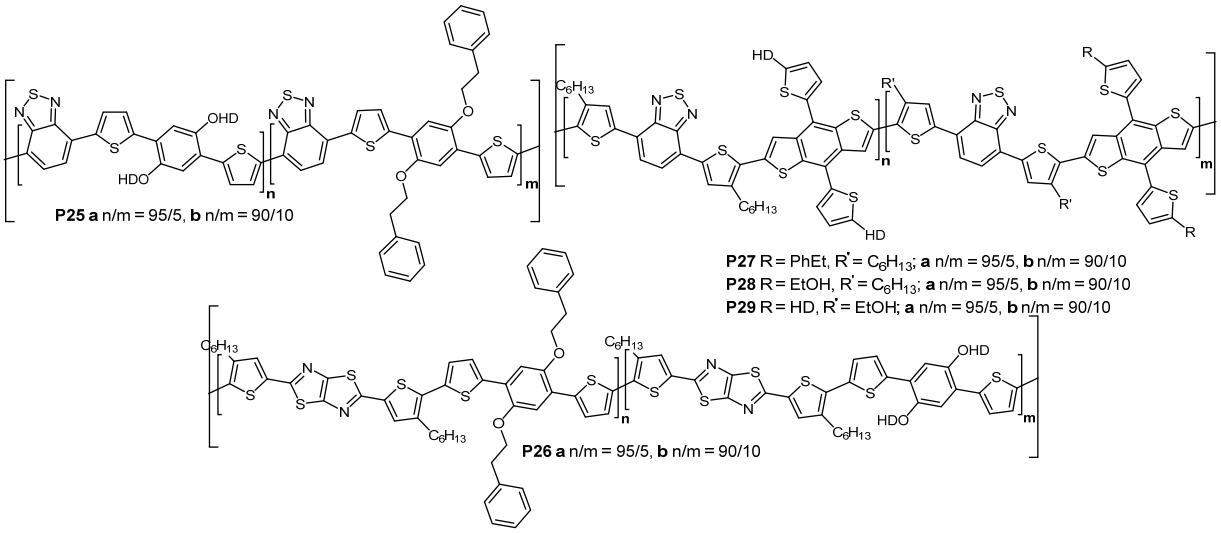

Figure 4.2. *Chemical structures of the investigated statistical copolymers **P25** - **P29**.*

The monomers (**M24**-**M32**, Scheme 4.1 blue structures) and their activated (stannylated or brominated) derivatives (**DTP-HD**, **DTP-Ph**, **BDT-HD**, **BDT-Ph**, **BDT-OH**, **BT-hex**, **BT-OH** and **TzTz-hex**) were synthesized by adapting literature procedures (see experimental details in Appendix A and Scheme 4.1), except for **M29** which was commercially available. **M24** and **M25** were prepared according to a procedure consisting of four steps starting from hydroquinone [15]. The first two steps (bromination and alkylation of hydroquinone) of the **M25** synthesis resulted in a mixture of

mono- and di-alkylated product in low yields (25% and 32%, respectively) under the standard conditions used for **M24**, so an alternative Williamson ether reaction was performed [10] and 47% of the di-alkylated product was collected. However, there was still 29% of the mono-alkylated side product which was removed through recrystallization from ethanol. Thereafter, a Stille cross-coupling with 2-(tributylstannyl)thiophene was performed resulting in **M25**.

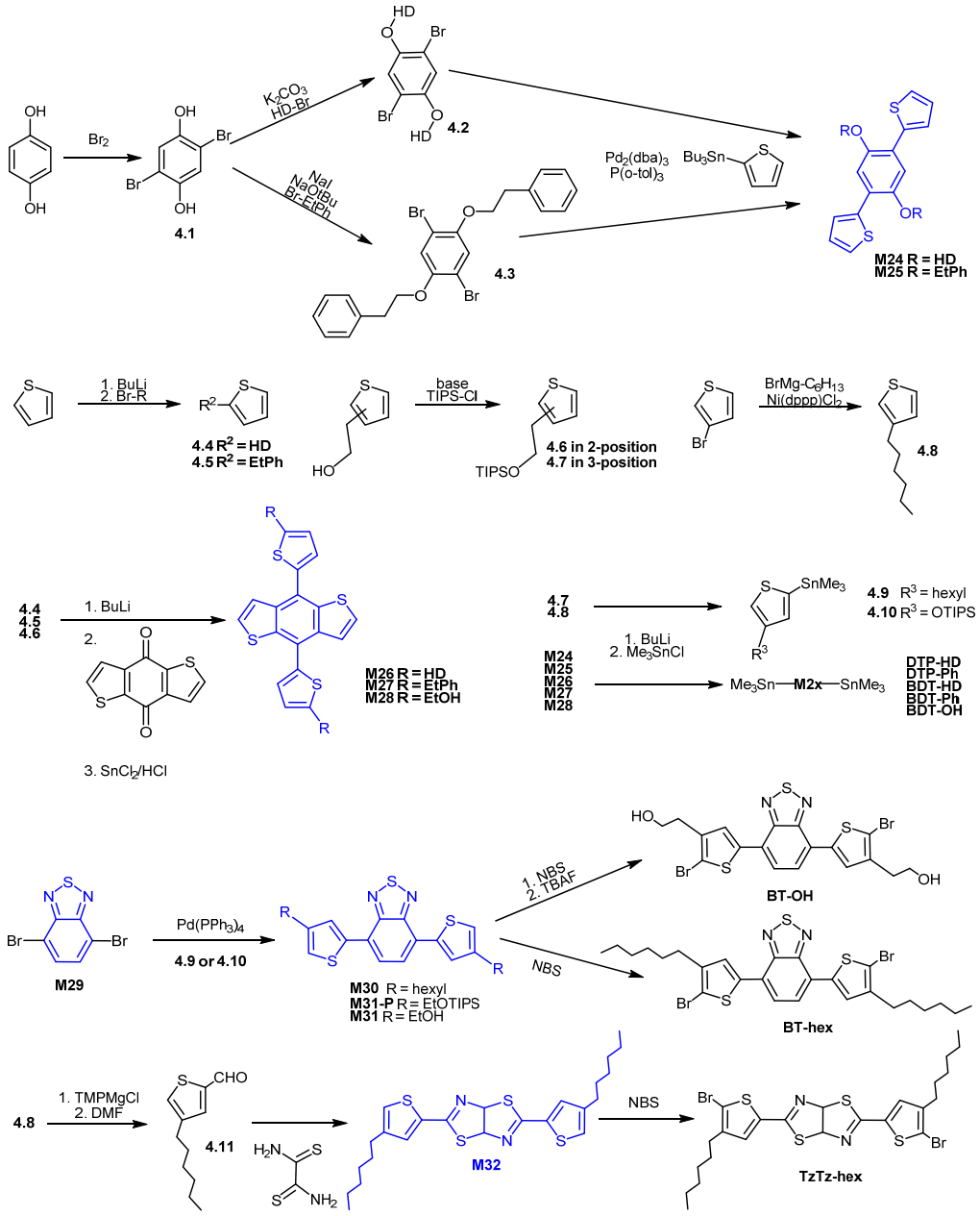

HD = 2-hexyldecyl, EtPh = 2-phenylethyl, EtOH = 2-ethanol, NBS = *N*-bromosuccinimide, TBAF = tetra-*N*-butylammonium fluoride, TIPS = triisopropylsilyl

Scheme 4.1. *Synthetic routes yielding monomers based on* ***DTP, BDT, BT*** *and* ***TzTz****.*

M26 was synthesized *via* a standard three-step synthesis [19,20] starting from benzo[1,2-*b*;4,5-*b'*]dithiophene-4,8-dione (dione) and Th. The alkylation of Th in 2-position followed a lithiation with

n-buthyl lithium (BuLi) in 5-position, before it was reacted with the dione and the product reduced with tin(II)chloride ($SnCl_2$) in acidic environment yielding **M26**.

M27 and **M28** were synthesized in a similar manner using the same reaction conditions, but for the synthesis of **M28**, 2-(thiophen-2'yl)ethanol was used as starting material instead of Th. As a first step, the alcohol group was protected with a triisopropylsilyl (TIPS) group. This group was removed again in the third step by $SnCl_2$ in acidic environment. During the workup of **M28**, the acidic ester was partly formed beside the alcohol while using ethyl acetate as solvent. The product mixture was saponified using a sodium hydroxide solution to yield the product. The final step of **M24-M28** was their activation by a bis-stannylation yielding **DTP-HD**, **DTP-Ph**, **BDT-HD**, **BDT-Ph** and **BDT-OH**. For **M28** a large excess (7 equivalent) of BuLi was used to obtain a fully lithiated compound.

M30 was synthesized *via* a standard four-step synthesis [21] starting from 4,7-dibromobenzo[*c*][1,2,5] thiadiazole (**M29**) and 3-bromothiophene. The alkylation of the Th in 3-position followed by a stannylation in 5-position, before it was reacted with **M29** in a Stille cross-coupling yielding **M30**.

M31 was synthesized in a similar manner using the same reaction steps, but 2-(thiophen-3'yl)ethanol was used as starting material. As a first step, the alcohol group was again protected with a TIPS group before it was stannylated and coupled with **M29** in a Stille cross-coupling yielding **M31-P**, which was still protected on the alcohol group. **M32** was synthesized according to a literature procedure [22]. The final step of **M29**-**M32** was their activation by dibromination yielding **BT-hex** and **TzTz-hex**. For **M31-P** a subsequent step after dibromination removed the TIPS group with tetra-n-butylammonium fluoride (TBAF) yielding **BT-OH** (the activated **M31**).

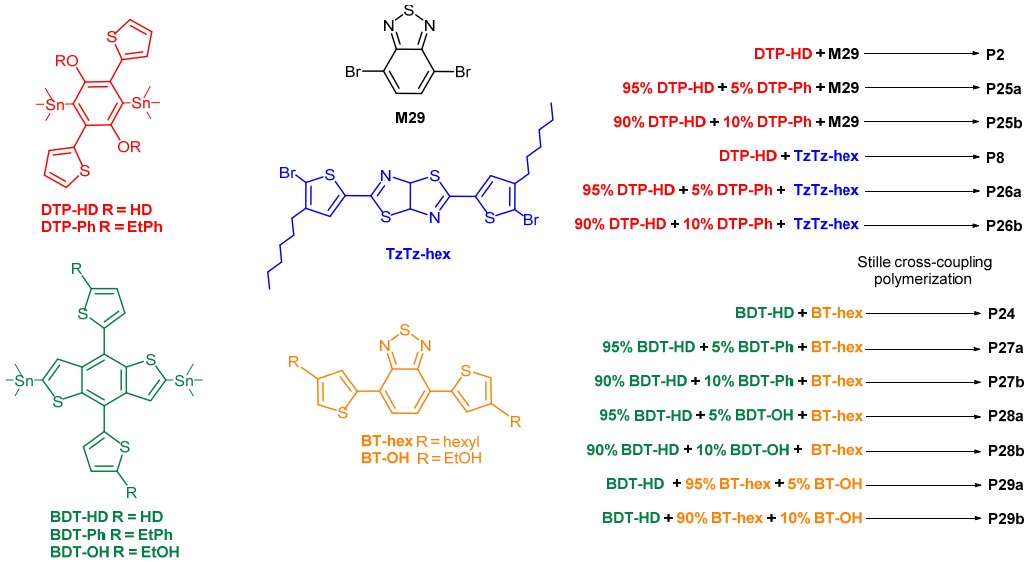

Scheme 4.2. *Stille cross-coupling polymerization yielding* ***P2, P8*** *and* ***P24*** *-* ***P28****.*

4.2.2. Polymer Synthesis

Standard Stille cross-coupling polymerization of the bis-stannyl monomers (**DTP-HD**, **DTP-Ph**, **BDT-HD**, **BDT-Ph** and **BDT-OH**) with the dibromo monomers (**M29**, **BT-hex**, **BT-OH** and **TzTz-hex**) (Scheme 4.2) yielded **P2**, **P8** and **P24**-**P29** (Figure 4.1 and Figure 4.2). **P2**, **P8** and **P24** were obtained as standard alternating copolymers only containing solubility side chains (HD and hexyl). The synthesis of **P25**-**P29** targeted statistical copolymers based on these standard copolymers, but with partial exchange (5% or 10%) of the HD or hexyl side chain. Complete substitution of the solubilizing side chain was attempted for the backbone based on **P2** coupling **M25** and **M29**. However, the obtained alternating polymer could not be characterized due to a lack of solubility. Therefore a partial substitution of 5% and 10% was chosen to be incorporated in these kinds of polymers according to previous studies [11]. The results of the characterization of all polymers are described in detail in the Chapters 4.3.1 and 4.4.1.

4.3. Comparison of 2-Phenethyl Side Chain Modification in Different Polymer Backbones

4.3.1. Polymer Properties

Polymer Characterization

The polymers **P2** and **P25a,b** (BT based), **P8** and **P26a,b** (TzTz based) and **P24** and **P27a,b** (BDT based) were characterized using standard techniques. ^{1}H NMR spectra were recorded of the BT and BDT based polymers in chloroform-d_1 (details in Appendix B Figure B.4.1). The spectra of **P25a,b** showed small broad signals around 4.33 ppm and 3.34 ppm for the CH_2 groups of the new side chain. The integration of the high field signal (3.34 ppm) is compared with the signal for the O-CH_2 group of the HD side chain. For **P25a** the ratio is 4.9/95.0 while for **P25a** the ratio is 9.4/90.0 showing a successful incorporation of the stabilizing EtPh side chain. The spectra of the **P24** and **P27a,b** show the main signals of the polymer backbone as well as of the solubility side chain HD. **P27a,b** show also a small signal of the ethyl group of the CH_2 of the EtPh side chain. But the signals are not seen clearly due to overlapping with the α-CH_2 signal of the HD side chain, with small signals at 3.1 and 3.2 ppm. Due to a low solubility of the TzTz based polymers in chloroform-d_1 and chlorobenzene-d_5 no spectra could be obtained.

M_n (Table 4.1.) of the polymers were determined by SEC to be around 40 kDa for the BT, between 30-80 kDa for the TzTz and around 20 kDa for the BDT based polymers.

UV-vis spectra were recorded in CF for the BT and BDT based polymers and in CB for the TzTz based polymers and of the polymer films on glass slides (Figure 4.3, left). The onset and the absorption maximum

(λ_{max}) in the UV-vis spectra of the BT based polymer solution shifted slightly to lower wavelength with increasing amounts of EtPh. Minor differences were seen in the spectra of the films. The TzTz based polymers showed with increasing amount of EtPh a shift towards higher wavelength of the absorption curve of the polymer solution with an additional shoulder in the higher wavelength area. The spectra of the polymer film, is again very similar. The BDT based polymer solutions show minor differences in their absorption spectra. However, the curves flatten out at higher wavelength with increasing amount of EtPh. The absorption spectra of the polymer film show a different behaviour. The absorption curve of **P24** has a maximum around 680 nm and a shoulder around 630 nm. **P27a,b** show the opposite behaviour, with a clear maximum around 630 nm and a shoulder around 680 nm for both polymers with incorporated EtPh side chain. However, their absorption curve is broader in comparison to the polymer without this new side chain. E_g of all the polymers were estimated from the films according to a literature procedure [25] to be 1.73 eV for the BT based polymers, 1.91 eV for the TzTz based polymers and 1.66 eV for the BDT based polymers.

Table 4.1. *Optical and electronic properties of the polymers (**P2**, **P25a,b**, **P8**, **P26a,b**, **P24** and **P27a,b**) involved in the manipulated side chain investigation with 2-phenethyl. Data from* [23,24].

Polymer	side chain[a]	M_n[b] (kDa)	Đ[b]	E_g[c] (eV)	$E_{g,ec}$[d] (eV)	HOMO[d] (eV)	LUMO[d] (eV)	R_d[e] (%/h)
P2	0%	42	1.9	1.73	2.07	-5.37	-3.30	1.66
P25a	5%	39	2.1	1.73	2.03	-5.34	-3.31	1.63
P25b	10%	43	2.1	1.73	1.99	-5.31	-3.32	1.69
P8	0%	44	1.9	1.91	2.24	-5.24	-3.01	2.82
P26a	5%	30	3.1	1.91	2.21	-5.20	-2.99	2.60
P26b	10%	78	1.5	1.91	2.22	-5.21	-2.99	2.13
P24	0%	23	3.9	1.66	1.85	-5.28	-3.43	1.15
P27a	5%	19	4.1	1.65	1.88	-5.27	-3.39	1.17
P27b	10%	18	3.7	1.66	1.87	-5.27	-3.40	1.16

[a] Percentage of EtPh side chains in the polymer, [b] Molecular weight (M_n) and polydispersity (Đ) determined from SEC against PS standard, [c] optical band gap (E_g) calculated from the onset of the UV-vis absorption spectrum of the polymer film, [d] $E_{g,ec}$, HOMO and LUMO were estimated from the CV curves, [e] the degradation rate (R_d) was calculated from the degradation of the UV-vis absorption of a polymer film.

Cyclic voltammetry (CV) revealed the electrochemical band gap ($E_{g,ec}$) for the polymers. For the BT based polymers it decreased slightly (2.07 eV → 1.99 eV) with an increasing amount of EtPh due to a small increase of the HOMO level (Table 4.1.), for the BDT based polymers $E_{g,ec}$ was around 1.87 eV, while there was also no significant changes of the $E_{g,ec}$ (~2.22 eV) of the TzTz polymer series upon incorporation of the EtPh group.

Polymer Stability

The thermal properties of the polymers were investigated by rapid-heat-cool calorimetry (RHC) (Appendix B Figure B.4.2). It was chosen over regular different scanning calorimetry as lower amounts of polymers are required and there is a higher sensitivity to thermal transitions [26,27]. The analysis showed semicrystalline

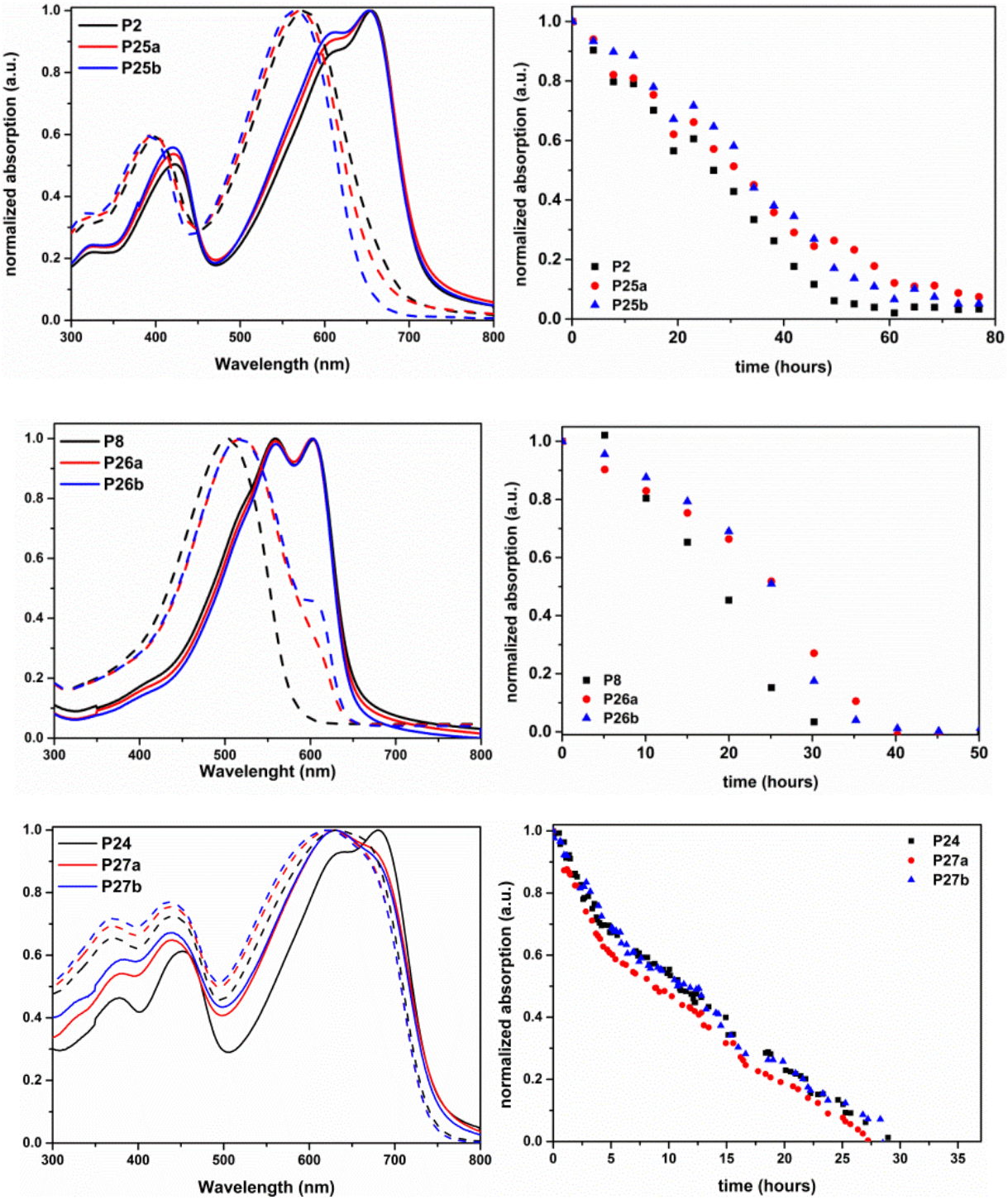

Figure 4.3. *Normalized UV-vis absorption spectra (left) of the polymer solutions (dashed) and films (solid) and degradation of the maximum values of the normalized UV-Vis absorption as a function of time during sun irradiance of the polymer films (right) for the BT (top), TzTz (middle) and BDT (bottom) based polymers* ***P2****,* ***P8****,* ***P24****-****P27****. Adapted from* [23] *(MDPI, Creative Commons Attribution License) and from* [24] *with permission from The Royal Society of Chemistry ©2016.*

materials of the BT polymer group. **P2** showed a sharp peak at 254°C, while the melting temperature of the polymers with modified side chains was increased (260°C for **P25a** and 265°C for **P25b**) and a broadened curve progression, but with similar melting enthalpy (12.0 J g^{-1} for **P2** and 11.5 J g^{-1} for **P25a,b**). However, the crystallinity of the manipulated materials might be slightly suppressed due to a random incorporation of the Th-phenylene-Th units. The T_g of the polymers were not detectable.

The analysis of **P8**, **P24** and **P26**-**P27** showed no melting peaks and complete amorphous materials. In case of the TzTz based polymers, an increasing T_g could be detected between 148°C and 156°C with increasing amount of the EtPh side chain. In case of the BDT based polymers, T_g's between 140°C and 150°C were detected with no conclusion on the influence of the EtPh side chain. However, the BT and TzTz based polymers showed slightly increased thermal properties with an increasing EtPh content.

Photochemical stabilities of the polymers were investigated of the pristine polymer films measuring the UV-vis absorption under a solar simulator in a frequent time interval [28]. Exposure of the films to light resulted in a slight blue shift with decreasing of the maximum of the absorption curve and a clear loss of the colour of the polymer film. From the normalized degradation curves (Figure 4.3, right) which are based on the absorption maxima, R_d could be detected (Table 4.1). The BT and BDT based polymers revealed R_d of around 1.66% h^{-1} and 1.16% h^{-1}, respectively, whereas the rate for the TzTz based polymers improved from 2.82% h^{-1} to 2.13% h^{-1} with an increase of the new side chain. The absorption of the BT based polymer films were nearly gone after 60 h of light exposure, while **P2** and the BDT based polymers degraded after 30 h. **P26a,b** showed no absorption after 40 h of light exposure. The side chain modifications improved the stability of the TzTz based polymer, while the BT and BDT based polymers revealed the same.

4.3.2. Polymer Solar Cells

These polymers were applied in BHJ PSCs *via* RC and SC techniques to investigate the influence of the partially exchanged HD side chains with EtPh side chains on the PV properties as well as the stabilities of the devices.

Roll coated devices

The RC devices had an inverted architecture (Chapter 1.3.1) of PET/Ag grid/PEDOT:PSS/ ZnO/polymer:$PC_{61}BM$/PEDOT:PSS/Ag grid with device areas of around 1 cm^2. The active layer of the synthesized polymers was coated on the pre-prepared substrate *flextrode* using a mini roll-coater. The polymers were coated differently depending on the polymer. **P2** was coated according to procedures similar to Chapter 2, while **P8** and **P24** were additionally optimized. The devices were then finalized with a layer of PEDOT:PSS and Ag grid. The finished devices were encapsulated between glass slides with UV-curing

adhesive. The solar cell characteristics were measured under a solar simulator (1000 W m^{-1}, AM1.5) and are summarized in Table 4.2 and Figure 4.4 (left).

The active layers based on the BT based polymer were produced from ODCB with a total concentration of 40 mg mL^{-1} of a polymer:$PC_{61}BM$ solution with a ratio of 1:2. The coating was performed at 80°C with an active layer thickness of 360 nm, 450 nm and 540 nm. The final devices were measured and the maximum PCE of 3.05% was achieved by **P2** at a layer thickness of 450 nm. **P25a,b** achieved their highest performance (2.65% and 2.16%, respectively) at an active layer thickness of 360 nm. This shows that a decrease in PCE, mainly due to a decrease in J_{SC}, was observed upon increasing the amount of the EtPh chain.

Table 4.2. *J-V parameters*[a] *(V_{OC}, J_{SC}, FF and PCE) for the polymer:$PC_{61}BM$ RC and SC PSCs based on **P2**, **P25a**,**b**, **P8**, **P26a**,**b**, **P24** and **P27a**,**b**. Data from* [23,24].

Polymer	Method[b]	V_{OC} [V]	J_{SC} [mA cm^{-2}]	FF	PCE (best) [%]
P2	RC [c]	0.75	7.83	0.47	2.81 (3.05)
	SC [d]	0.74	10.38	0.56	4.31 (4.42)
P25a	RC [c]	0.74	6.52	0.52	2.51 (2.65)
	SC [d]	0.72	10.22	0.56	4.15 (4.54)
P25b	RC [c]	0.73	5.76	0.50	2.10 (2.17)
	SC [d]	0.71	9.41	0.55	3.68 (4.09)
P8	RC [e]	0.69	6.69	0.61	2.67 (2.73)
	SC [e]	0.72	6.60	0.58	2.76 (2.92)
P26a	RC [e]	0.68	6.95	0.59	2.59 (2.72)
	SC [e]	0.65	8.57	0.55	3.06 (3.06)
P26b	RC [e]	0.69	7.00	0.60	2.66 (2.76)
	SC [e]	0.61	8.15	0.63	3.13 (3.21)
P24	RC [e]	0.73	7.79	0.60	3.43 (3.60)
	SC [f]	0.75	9.74	0.61	4.50 (5.27)
P27a	RC [e]	0.73	7.73	0.59	3.35 (3.47)
	SC [f]	0.76	9.79	0.62	4.58 (4.73)
P27b	RC [e]	0.73	7.79	0.57	3.25 (3.43)
	SC [f]	0.76	9.23	0.61	4.31 (4.49)

[a] *J-V* parameters are averaged over 5 devices for RC and 2–8 devices for SC, [b] RC: RC in air with an inverted device geometry of ~1 cm^2 (PET substrate/Ag grid/PEDOT- PSS/ZnO/polymer:$PC_{61}BM$/ PEDOT-PSS/Ag grid), SC: SC under inert atmosphere with a device geometry of 3 mm^2 (glass/ITO/ PEDOT-PSS/polymer:$PC_{61}BM$/Ca/Al). [c] in a 1:2 ratio processed from ODCB, [d] in a 1:1.5 ratio processed from ODCB, [e] in a 1:1.5 ratio processed from ODCB/CB = 4/1, [f] 1:2 ratio processed from CF.

The active layer based on **P8** was first optimized by a variation of the solvent (ODCB, CF, ODCB:CB and CB:CN), the active layer thickness (520 nm and 600 nm) and the polymer:$PC_{61}BM$ ratio (1:1.5, 1:2; 40 mg mL^{-1}) (Table 4.3). The highest PCE (2.73%) was reached from a solvent mixture of ODCB:CB (4:1), a ratio of polymer:$PC_{61}BM$ of 1:1.5 and an active layer thickness of 520 nm. These parameters were used for all three polymers yielding efficiencies within the same range (2.73%, 2.72% and 2.76% for **P8** and **P26a**,**b**,

respectively; Table 4.2). The modification of the polymers had no influence on the performance of the devices; the progression of the *J-V* curve is similar for all three polymers (Figure 4.4, left).

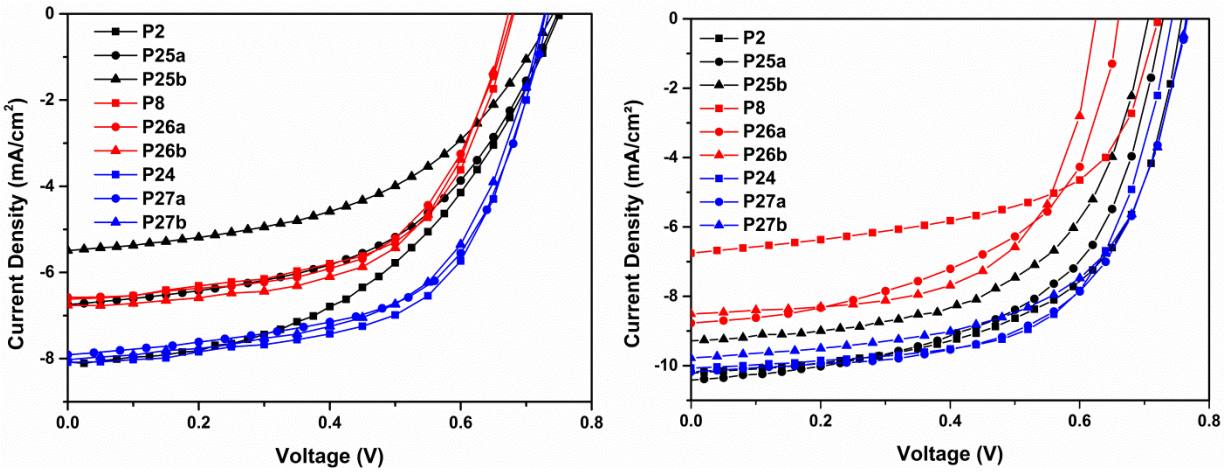

Figure 4.4. *J-V curves for the best PSCs prepared via RC (left) and SC (right) using the BT (black), TzTz (red) and BDT (blue) based polymer series. Adapted from* [23] *(MDPI, Creative Commons Attribution License) and from* [24] *with permission from The Royal Society of Chemistry ©2016.*

Table 4.3. *Averaged J-V parameters for PSCs based on P8 (top) or P24 (bottom), RC from different solvents and using different polymer:$PC_{61}BM$ ratios. Data partly from* [23].

Solvent[a]	P8:$PC_{61}BM$[b]	d [c] (nm)	V_{OC} [d] (V)	J_{SC} [d] (mA cm^{-2}d)	FF[d]	PCE [d] (best) (%)
ODCB	1:2	520	0.70	7.05	0.50	2.42 (2.51)
CF	1:2	520	0.64	4.23	0.50	1.30 (1.59)
CB/3%CN	1:2	520	0.67	5.86	0.54	2.09 (2.25)
ODCB/CB 4/1	1:2	520	0.66	6.79	0.52	2.28 (2.54)
ODCB/CB 4/1	**1:1.5**	**520**	**0.69**	**6.69**	**0.61**	**2.67 (2.73)**
ODCB/CB 4/1	1:1.5	600	0.66	6.76	0.52	2.30 (2.57)
ODCB	1:2	450	0.71	7.59	0.61	3.07 (3.31)
ODCB	1:1.5	450	0.71	7.22	0.62	2.95 (3.15)
ODCB	1:1	450	0.69	6.68	0.56	2.34 (2.59)
CF	1:2	450	-[e]	-[e]	-[e]	-[e]
CB/3%CN	1:2	450	0.72	5.71	0.61	2.46 (2.51)
ODCB/CB 4/1	**1:2**	**450**	**0.73**	**7.79**	**0.60**	**3.43 (3.60)**
ODCB/CB 4/1	1:2	390	0.72	7.46	0.62	3.34 (3.49)

[a] *Ortho*-dichlorobenzene (ODCB), chloroform (CF), chlorobenzene (CB), 2-chloronaphthalene (CN), [b] polymer:$PC_{61}BM$ ratio of the active layer blend, [c] active layer thickness, [d] average over 5-6 devices, [e] no *J-V* characteristics could be obtained due to an inhomogeneous active layer.

The coating of the active layers based on **P24** was first optimized by a variation of the solvent (ODCB, CF, ODCB:CB and CB:CN), temperature (60, 70 and 80 °C), the active layer thickness (390 nm and 450 nm) and

the polymer:$PC_{61}BM$ ratio (1:1, 1:1.5, 1:2; 40 mg mL^{-1}). The results (Table 4.3) show the best *J-V* characteristics for a polymer:$PC_{61}BM$ ratio of 1:2 coated from ODCB:CB = 4:1 at 80°C with a layer thickness of 450 nm. For consistency the parameters were maintained for **P27a,b**. The *J-V* characteristics show, that modification of the polymers had only a small influence, revealing a maximal PCE of 3.60% of **P24** and with a highest PCE of 3.47% and 3.43% for **P27a** and **P27b**, respectively. The *J-V* curve progression is once again similar for all three polymers (Figure 4.4, left).

The EQE spectra (Appendix B Figure B.4.3) of the BT and BDT based RC PSCs showed local maxima in the higher wavelength region around 600 nm. The maxima of both devices decreased with increasing amount of EtPh side chain. For the TzTz based PSCs there are no distinct differences on the EQE among the different EtPh contents.

Spin coated devices

The SC devices had a traditional geometry (Chapter 1.3.1) of glass/ITO/PEDOT:PSS/ polymer:$PC_{61}BM$/Ca/Al with device areas of around 3 mm^2 (Table 4.2 and Figure 4.4, right). The SC devices were coated under similar conditions as the RC devices.

The active layer of the BT based polymer blends were coated from a ODCB solution with polymer:$PC_{61}BM$ ratio of 1:1.5 (40 mg mL^{-1}). Efficiencies of the devices (Table 4.2 and Figure 4.4 right) of around 4%, so as expected, higher values than the RC devices were obtained with again a decrease in efficiencies with an increasing amount of the EtPh side chain. The decrease of the PCE is due to a small decrease of the J_{SC} and V_{OC}.

Table 4.4. *Averaged J-V parameters for the solvent and fullerene screening of the SC PSCs based on* ***P24****.*

Active layer[a]	Solvent	V_{OC} (V)[c]	J_{SC} (mA cm^{-2})[c]	FF[c]	PCE (best) (%)[c]
P24:$PC_{61}BM$	ODCB[b]	0.76	8.90	0.53	3.59 (3.84)
P24:$PC_{61}BM$	CF[b]	0.75	9.74	0.61	**4.50 (5.27)**
P24:$PC_{71}BM$	ODCB[b]	0.74	10.70	0.56	4.45 (4.60)
P24:$PC_{71}BM$	CF[b]	0.75	9.59	0.56	3.98 (4.26)

[a] PSCs prepared by SC with a polymer:fullerene ratio of 1:2, [b] *o*-dichlorobenzene (OD), chloroform (CF), [c] average over 4 devices.

The active layers based on the TzTz based polymer were, as the RC devices, produced from a solvent mixture of ODCB:CB (4:1), a ratio of polymer:$PC_{61}BM$ of 1:1.5 (40 mg mL^{-1} for **P8** and **P26a**; 50 mg mL^{-1} for **P26b**) with the efficiencies for all three polymers in the same range as the RC devices. The higher concentration of the **P26b** solution was employed for an optimal active layer thickness. For these devices an increase of the performance from 2.92% to 3.21% was seen for an increase in the EtPh content due to an increase of J_{SC}, which could balance out the decrease in V_{OC} (Table 4.2 and Figure 4.4 right).

The coating of the active layers based on **P24** was optimized by a variation of the solvent (ODCB and CF) and of the acceptor ($PC_{61}BM$ and $PC_{71}BM$). The results (Table 4.4) show the best *J-V* characteristics for a polymer:$PC_{61}BM$ ratio of 1:2 with a total concentration of 15 mg mL^{-1} coated from CF with a layer thickness of 110 nm. The low blend concentration was used due to a faster evaporation of the CF in comparison to ODCB. **P27a,b** were coated using the same parameters. The *J-V* characteristics, which are summarized in Table 4.2 and Figure 4.4 (right), are also decreasing with an increasing amount of EtPh side chain (5.27%, 4.73% and 4.49% for **P24** and **P27a**,**b**, Table 4.2).

4.3.3. Device Stability Analysis

Lifetime testing

The RC devices were investigated by a lifetime study under ISOS-L-1 [29] standards using at least three different PSCs of the best efficiencies for each polymer. All cells were exposed to light (AM 1.5, 1000 W m^{-2}) for maximum 80 days. The devices were handled the same way (coated, encapsulated), so similar effects of the illumination can be expected [30]. *J-V* curves were measured in specific time intervals, smaller ones (1 min) in the beginning of the experiments and larger in the end (30 min). Averages of all *J-V* characteristics over time were taken from the values of each cell. The normalized average values were plotted against the time for each polymer type (BT, TzTz and BDT) as seen in Figure 4.5. Measurement failures (error in the system) or cell failures (a cell failed but recovered again to the initial value) occurred for all polymer types and this data was not displayed. The efficiency of all PSCs decreased quickly for all cells in first phase (0 – 5 h) of the study.

For the BT based polymers the first phase was more apparent for **P2** than for **P25a,b**. The new side chains seem to have a positive effect on this initial degradation phase. The devices reached 80% of their initial values after 5 h, 29 h and 111 h (T_{80}) for **P2** and **P25a,b**, respectively. Hereafter, the efficiencies decreased linear. The slope for **P25b** is larger than for **P25a** and **P2**, respectively, showing for all a finial PCE of 25% of the initial values after 80 days of exposure to light. The higher stability of the PCE from the PSCs based on polymer with a high content of EtPh in the beginning of the study was counteracted in the linear phase of the study. The V_{OC}, J_{SC} and FF decays are shown in Appendix B Figure B.4.4. The V_{OC}s of **P2** and **P25a** had a similar stability, while the one of **P25b** degraded faster after 20 days. J_{SC} decay curves proceeded for all similar to the efficiency decay curves, as did the FF.

In the initial phase (2 h) of the PSCs based on the TzTz based polymers a rapid reduction to 65% and 70% of the initial PCE value was observed for **P8** and **P26a**, respectively, while the one based on **P26b** took a steeper decay to 35% of the initial PCE. The PCE of **P8** and **P26a** based PSCs hereafter stayed rather constant until

day 10. Thereafter, **P26b** recovered again to 60% of the initial PCE value. The recovery process and the constant values could be a result of slow photo-annealing [31] overlapped with the standard degradation. For **P26b** the increase of the PCE by photo-annealing seemed to be higher than the decrease *via* standard degradation. Hereafter, the PCEs decrease continuously with a smaller slope for **P26b** than for **P8** and **P26a**. As such, **P26a** showed 20%, while **P8** and **P26b** showed 30% of the initial PCE values after 70 days of exposure to light. The influence on the stability of the PCE from the PSCs based on polymers with a high content of EtPh side chain seemed positive in the second stage of the study. The V_{OC}, J_{SC} and FF decays are shown in Appendix B Figure B.4.4. The V_{OC}s of all PSCs had a similar stability. The J_{SC} and FF decay curves proceeded similar to the efficiency decay curves for all devices.

In the first phase (6 h) the PSCs based on **P27a** (BDT based polymer) decreased relatively fast to 65% of its initial values, while **P24** and **P27b** degraded a bit slower to 70% of the initial value. After 20 days of constant sun irradiation, the PSCs of **P24** started to degrade faster than the ones of **P27b**. During the final stage of the degradation, the PCE curves had a quite linear decay resulting in 20%, 23% and 30% of their initial performance of **P27a**, **P24** and **P27b**, respectively, based PSCs. These results gave the assumption that 5% incorporation of the EtPh side chain did not result in an improvement of the stability; however, 10% of the EtPh chain increased the stability slightly. The V_{OC}, J_{SC} and FF decays are shown in Appendix B Figure B.4.6. The V_{OC} curves of all PSCs had a similar trend. The J_{SC} decay curves of **P27a** degraded faster than the other two, while there was an improvement of FF decay curves of the PSCs based on **P27b** in comparison to the ones based on **P24** and **P27a**.

Thermal degradation testing

The SC devices were investigated by a thermal degradation study similar to ISOS-D-2 [29] standards. All cells were exposed in a nitrogen-containing glovebox at 85°C for around 400 hours (~17 days). *J-V* curves were measured in specific time intervals using an automated setup (BT and TzTz based) or measured manually (BDT based). Averages of all *J-V* characteristics over time were taken from the values of each cell. The normalized average PCEs were plotted against the time for each polymer type (BT, TzTz and BDT) in Figure 4.5.

The average degradation curve of the devices based on **P2** was linear. After around 350 h the degradation levelled out to retain a value which correlated to 30% of the initial PCE. For the PSCs based on the modified polymers **P25a,b**, the PCE increased slightly in the beginning of the test. This was followed by a rapid decay of the PCE to 50% and 40% of the initial value until 150 hours of exposure to heat. Thereafter, the PCE stayed constant. The V_{OC}, J_{SC} and FF decays are shown in Appendix B Figure B.4.5. The V_{OC}s of the polymers remained constant, while the J_{SC}s and FF proceeded similar to the corresponding PCEs for all devices.

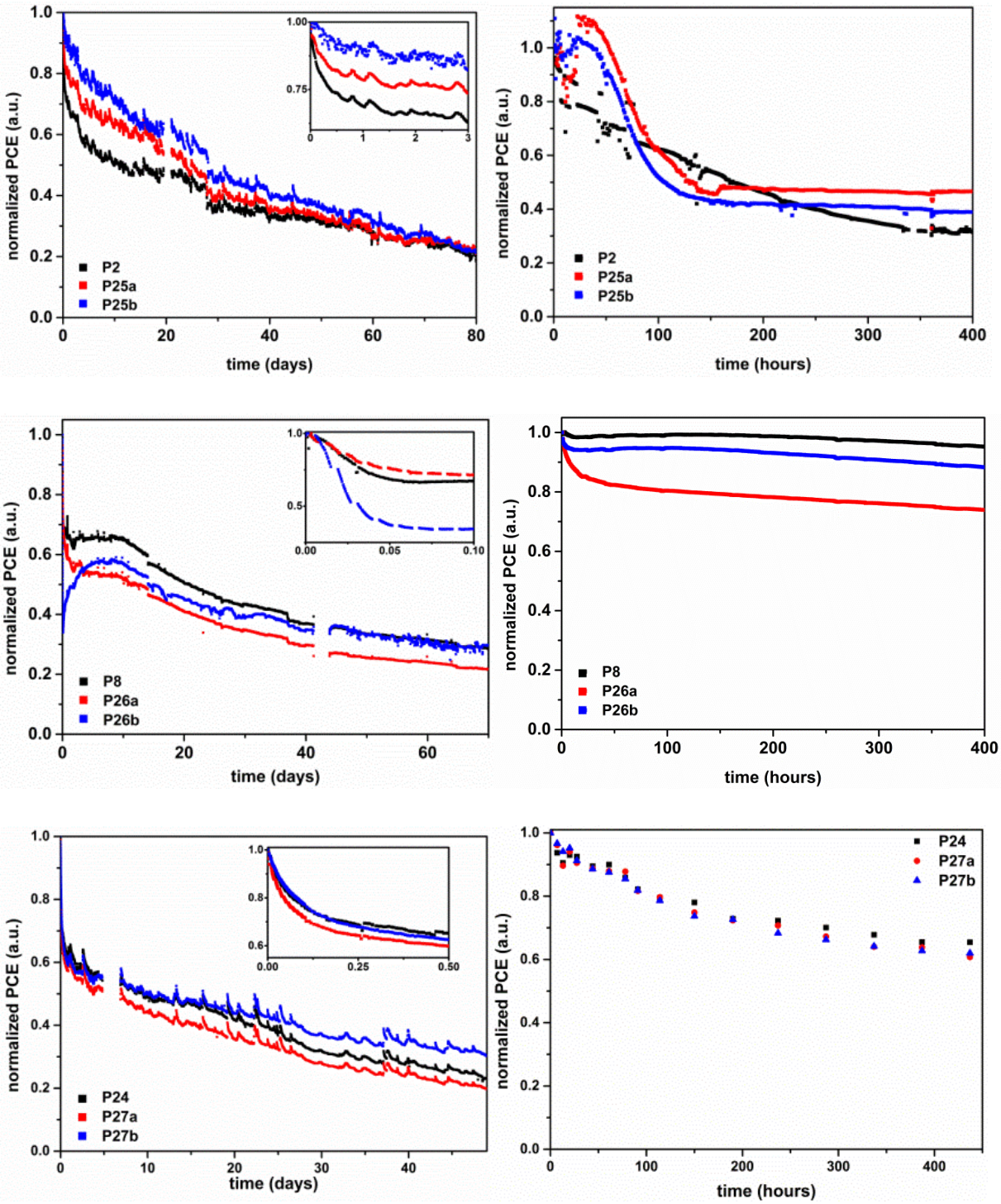

Figure 4.5. *Normalized PCE of the average lifetime measurements (ISOS-L-1) of the PSCs (left), and thermal degradation test (ISOS-D-2) of the PSCs (right) for the BT (top), TzTz (middle) and BDT (bottom) based polymer series. Adapted from* [23] *(MDPI, Creative Commons Attribution License) and from* [24] *with permission from The Royal Society of Chemistry ©2016.*

The thermal degradation of the TzTz based polymers showed a different trend. The parent polymer **P8** showed a high stability during the whole study, with around 95% of the initial PCE after 400 h. In comparison

an initial degradation phase was observed for the PSCs with modified side chain revealing 85% and 90% of the initial value. During the progress of the experiment, the PCE decreased by another 10% through a linear decay. The V_{OC}, J_{SC} and FF decays are shown in Appendix B Figure B.4.5. The V_{OC}s of all PSCs remained nearly constant. The J_{SC} for **P8** and **P26a** had a small decay in the curve, which is especially levelled out by an increase in FF for **P8**.

The thermal degradation of the BDT based PSCs had a similar behaviour for all devices and the PCE degraded to 60-70% of the initial value. The V_{OC} and J_{SC} decays are shown in Appendix B Figure B.4.7 and FF in Figure 4.11. The V_{OC} of all PSCs decay curves were similar and the J_{SC} degraded similar to the PCE.

To elaborate the different results of the thermal degradation, the active layer of the PSCs based on BT and TzTz based polymers were investigated with microscopic techniques after thermal exposure. The BDT series was not included as there was no difference within the thermal degradation among the different amount of EtPh side chain within the polymers (Figure 4.5). The non-encapsulated RC PSCs were heated at 85°C and optical microscope images were taken. The BT based devices showed images (Figure 4.6. top, left) with no differences within the first 5 h of thermal exposure (not shown). However, after 24 h particles started to form, which resulted in strong phase separation of all films after four days due to degradation during the long time exposure to thermal stress. For further assessment of the thermal degradation and phase separation, the active layers of the SC PSCs were investigated by transmission electron microscopy (TEM) before and after exposure to thermal stress (Figure 4.6. bottom, left). The active layers showed no distinctive features before the exposure to heat. After applying thermal stress, once again large phase separation appeared within all active layers with different contents of EtPh side chain. The formation of these domains are most likely fullerene crystals and responsible for the loss in J_{SC} as observed previously. [32] The large domains of **P25b** have a softer shape than the domains of **P2**, which can be related to the different amount of EtPh side chains and are possible a hint for the different trends of the thermal degradation curves in Figure 4.5. The T_g, which were related with the degradation in previous studies [10], could, however, not be correlated with this phase separation, as it could not be detected for this polymer series.

The TzTz based devices show optical microscope images (Figure 4.6. top, right) of the RC active layer before and after seven days of exposure to thermal stress. However, even after this long stress test, no particular changes were seen in the morphology. This could be correlated with the minor efficiency loss during the thermal stress test (Figure 4.5). As expected no phase separation appeared due to T_g's higher than the stress test temperature (85°C) leading to a higher thermal stability of the whole series in comparison to the BT series. However, there was no difference or even improvement of the stability of the active layer with modified polymers. For further investigation of the degradation and phase separation, the active layers of the SC PSCs before and after exposure to thermal stress were assessed by TEM (Figure 4.6. bottom, right).

The layers showed a rather smooth morphology before the exposure to heat, but after applying thermal stress for 400 h, phase separation appeared within all active layers. The domains were less than the domains of the BT based active layer, however, with different sizes. The sizes can be correlated with the loss of PCE during the thermal stress test, e.g. **P26a** had the largest loss in efficiency as well as the largest presumable formed fullerene crystals.

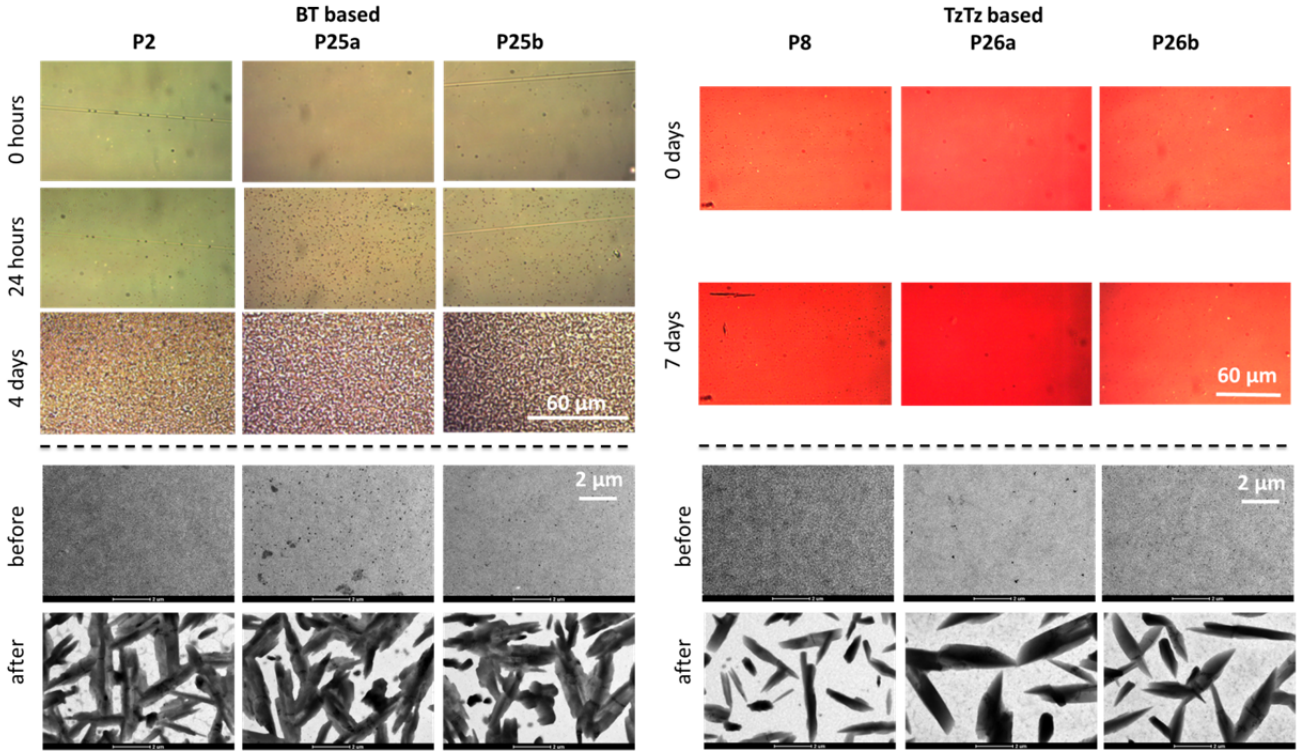

Figure 4.6. *Optical microscope images of the active layers of RC PSCs based on **P2**, **P25a** and **P25b** after exposure to 85 °C for 0 h, 24 h and 4 days (top, left) and **P8**, **P26a** and **P26b** after exposure to 85 °C for 0 days and 7 days (top, right); TEM images of the active layers of SC PSCs based on **P2**, **P25a** and **P25b** (bottom, left) and **P8**, **P26a** and **P26b** (bottom, right) before and after exposure to 85 °C for 400 hours. Adapted from* [23] *(MDPI, Creative Commons Attribution License).*

4.4. Comparison of 2-Ethanol Side Chain Modifications in Different Positions in the Same Polymer Backbone

4.4.1. Polymer Characterization

The polymers **P28a,b** and **P29a,b** were characterized using standard techniques and compared to the results of similar polymers (**P24** and **P27a,b**) described in the Chapter 4.3 and seen in Figure 4.7. ^{1}H NMR spectra were recorded in chloroform-d_1 (details in Appendix B Figure B.4.1). The spectra of the **P28a,b** and **P29a,b** show the main signals of the backbone as well as of the HD side chain. The two small signals (3.1 and 3.2

ppm) of the ethyl group of the EtPh side chains are not seen clearly due to an overlapping with the α-CH_2 signal of the HD side chain.

M_n (Table 4.5.) of all polymers were determined by SEC affording a M_n of around 20 kDa.

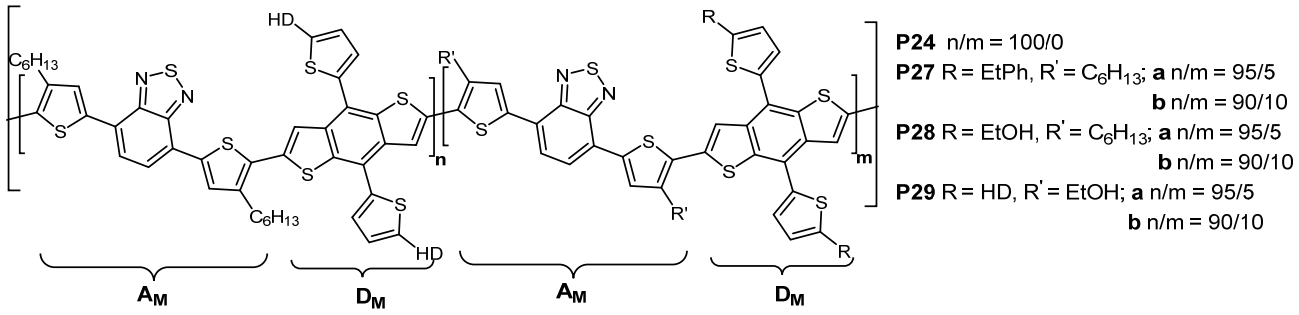

Figure 4.7. *Chemical structures of the BDT based polymers copolymers* ***P27*** *and* ***P27*** *-* ***P29****.*

UV-vis spectra were recorded of the polymers in CF solutions (Figure 4.8 dashed lines) showing minor absorption differences among the seven polymers with absorption maximum of ~ 670 nm. The UV-vis curves for **P27a,b**, **P28a** and **P29a,b** flattens out slightly in the higher wavelength range. **P28b**, however, had a similar curve progression with a broad absorption curve. The absorption spectra of the polymer films on glass slides (Figure 4.8 solid lines) showed for **P24** an absorption maximum around 680 nm and an absorption shoulder at higher energy around 630 nm. **P27a,b** and **P29a,b** showed the opposite behaviour, with a clear maximum around 630 nm and a shoulder around 680 nm. However **P28a,b** showed similar curve progression to the parent polymer and the other polymers with new side chain, showing two (local) maxima in the range of 630 nm and 680 nm. The shoulders in the UV-vis spectra can be related to the incorporation of the different new side chains. E_g of all polymers were estimated from the absorption profile of the films according to a literature procedure [25] to be 1.66 eV.

Table 4.5. *Optical and electronic properties of the polymers (****P24, P27a,b, P28a,b*** *and* ***P29a,b****) involved the investigation of different substituted side chains. Data from* [24].

Polymer	side chain[a]	M_n[b] (kDa)	Đ[b]	E_g[c] (eV)	$\Delta E_{g,ec}$[d] (eV)	HOMO[d] (eV)	LUMO[d] (eV)	R_d[e] (% h^{-1})
P24	-	22.5	3.9	1.66	1.85	-5.28	-3.43	1.15
P27a	D_M-EtPh	19.3	4.1	1.65	1.88	-5.27	-3.39	1.17
P27b	D_M-EtPh	18.3	3.7	1.66	1.87	-5.27	-3.40	1.16
P28a	D_M-EtOH	23.1	4.5	1.65	1.87	-5.26	-3.39	1.04
P28b	D_M-EtOH	25.4	7.9	1.66	1.82	-5.20	-3.38	0.83
P29a	A_M-EtOH	16.2	3.8	1.66	1.92	-5.29	-3.37	1.14
P29b	A_M-EtOH	13.3	3.2	1.66	1.90	-5.28	-3.38	1.46

[a] side chain modification in D_M or A_M unit of the polymer using EtPh or EtOH, [b] Molecular weight (M_n) and polydispersity (Đ) determined from SEC against PS standard, [c] optical band gap (E_g) calculated from the onset of the UV-vis absorption spectrum of the polymer film, [d] HOMO, LUMO and $E_{g,ec}$ estimated from CV measurements, [e] the degradation rate (R_d) was calculated from the degradation of the UV-vis absorption of a polymer film.

CV measurement was performed to estimate the HOMO and LUMO level of the polymers (Table 4.5). For **P24** the $E_{g,ec}$ was calculated to be 1.85 eV. The substitutions of the side chain increased $E_{g,ec}$ slightly; e.g. 1.90 eV for **P29a,b**. An exception was **P28b** with a lower $E_{g,ec}$ of 1.82 eV and the highest HOMO level of -5.20 eV. The HOMO levels of the other copolymers were similar to the one of the parent polymer **P24** (around -5.28 eV). In comparison to **P24** the LUMO levels of the modified copolymers increased slightly. A comparison between the modification on the D_M and A_M moieties showed that the HOMO level is lower for the polymers with modification on the A_M moiety.

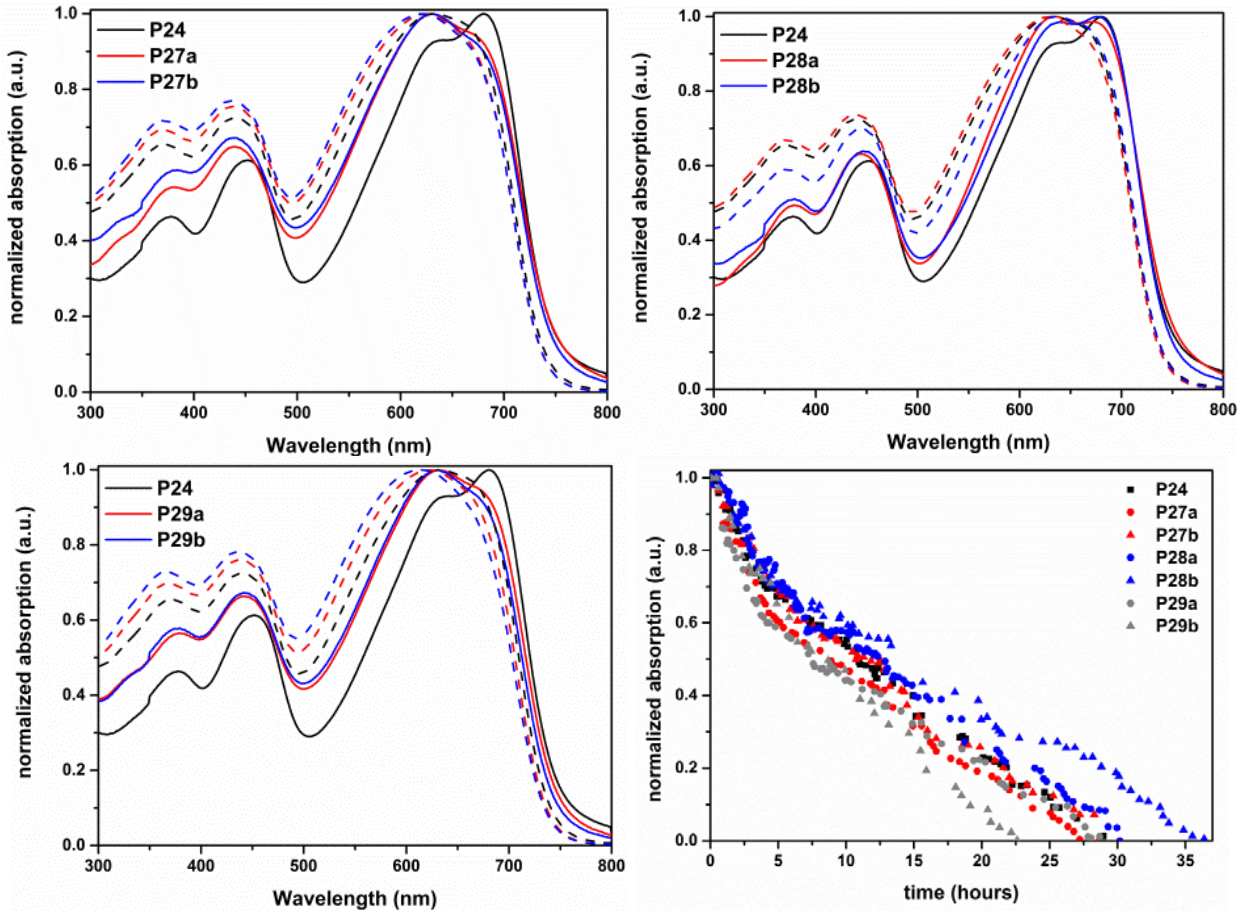

Figure 4.8. *Normalized UV-vis absorption spectra for the* ***P27a,b*** *(top, left),* ***P28a,b*** *(top, right) and* ***P29a,b*** *(bottom, left) polymer solutions (dashed) and films (solid) and normalized UV-vis absorption maximum evolution of the polymer films under constant sun irradiance (bottom, right). Adapted from* [24] *with permission from The Royal Society of Chemistry ©2016.*

Polymer Stability

The thermal properties of the polymers were investigated by RHC. The analysis showed amorphous materials with a broad T_g in the range of 135°C -150°C for all polymers (Appendix B Figure B.4.2).

The thermal stability of the polymers was investigated by thermogravimetric analysis (TGA; Appendix B Figure B.4.2). In this analysis the decomposition of all polymers starts around 400°C. The parent polymer **P24** decomposed slightly faster than the modified copolymers, which can be again related with the incorporation of these new side chains. An exception was **P28b** where the decomposition is more rapid in the beginning, but changes to a slower one in the end.

Photochemical stabilities of the polymers were investigated of the pristine polymer films measuring the UV-vis absorption under constant illumination in a specific time interval (5 min). The exposure to light resulted in a slight blue shift and decrease of the absorption maximum and a colour loss of the polymer films. R_d could be detected from the normalized degradation curves (Table 4.5). **P24**, **P27a,b** and **P29a** polymer films revealed R_ds of around 1.16% h^{-1}, whereas R_d for **P29b** increased to 1.46% h^{-1} showing a negative effect of the EtOH side chain in the A_M unit. However, the incorporation of the EtOH side chain onto the D_M unit improved R_d to 1.04% h^{-1} for **P28a** (5% content) and even further to 0.83% h^{-1} for **P28b** (10% content) and thus increased the stability. Further analysis of the degradation curve of the absorption maxima (Figure 4.8) revealed a visible improved stability of **P28b** after already 10 h, while the curve for **P29b** decreased at a stronger rate. No distinct absorption maximum could be detected after ~23 h for **P29b**, 27-31 h for **P24**, **P27a,b**, **P28a** and **P29a** and ~37 h for **P28b**.

4.4.2. Polymer Solar Cells

The polymers were applied in BHJ PSCs *via* RC and SC techniques to investigate the influence of the side chain modification with EtOH group in different positions of the same polymer backbone on the PV properties as well as the stabilities of the devices. It was also compared to the parent copolymer and the polymer with the EtPh side chain modification.

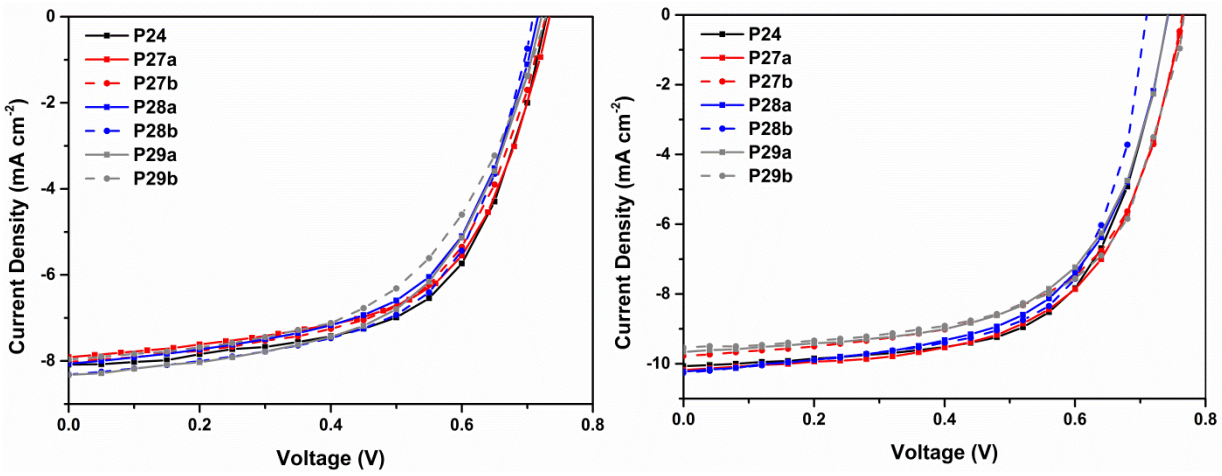

Figure 4.9. *J-V curves for the best PSCs prepared via RC (left) and SC (right) using* ***P24, P27-P29****. Adapted from* [24] *with permission from The Royal Society of Chemistry ©2016.*

Roll coated devices

The RC devices were prepared as described previously in Chapter 4.3. The *J-V* characteristics were measured of the final devices under a solar simulator (1000 W m^{-1}, AM 1.5) and are summarized in Table 4.6 and Figure 4.9 (left). The coating parameters used for the active layer of **P24** (polymer: $PC_{61}BM$ ratio of 1:2; ODCB:CB ratio of 4:1; coated with an active layer thickness of 450 nm at 80°C) were maintained for the processing of the PSCs based on **P28a** and **P29a**. However, the active layers showed poor properties in comparison to **P24** and **P27a,b**, by the formation of pinholes (Figure 4.10). Changing the solvent ratio to 3:2 of the ODCB:CB solvent mixtures resulted in a better film morphology by improving the PCEs (best) from 3.25% to 3.38% and from 3.11% to 3.41% for **P28a** and **P29a**, respectively, due to an increase in J_{SC} and FF. The *J-V* characteristics revealed minor effects on the efficiency upon incorporation of different side chains. A reduction of the efficiency was obtained for **P29b** of 3.16% in comparison to **P24** (3.60%). The efficiency values for the other polymers are in between. J_{SC} and V_{OC} were similar for the entire polymer series, while small differences in efficiency appeared due to a small variation in FF (0.60% for **P24** and 0.55% for **P29a,b**).

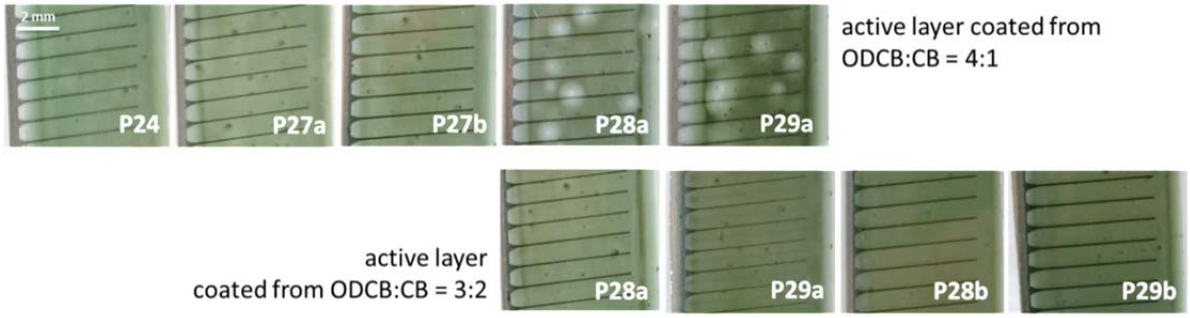

Figure 4.10. *Images of different RC active layers based on* ***P24*** *and* ***P27-P29*** *using a ratio of 4:1 (top) and 3:1 (bottom) of ODCB:CB. Adapted from* [24] *with permission from The Royal Society of Chemistry ©2016.*

The EQE spectra of the RC PSCs (Appendix B Figure B.4.3) showed local maxima ~600 nm. The maxima of devices with the EtPh modification on D_M and EtOH modification on A_M decreased slightly with increasing amount of EtPh and EtOH side chain. The maximum of devices with the EtOH modification on D_M showed no decrease with 10% incorporation.

Spin coated devices

The SC devices were prepared as described previously in Chapter 4.3. The coating parameters used for the active layer of **P24** (polymer: $PC_{61}BM$ ratio of 1:2; coated from CF) were maintained again for the PSCs based on among incorporation of the different side chains.

Table 4.6. *J-V parameters[a] (V_{OC}, J_{SC}, FF and PCE) for the polymer:$PC_{61}BM$ solar cells based on (**P24**, **P27a,b**, **P28a,b** and **P29a,b**). Adapted from* [24] *with permission from The Royal Society of Chemistry ©2016.*

Polymer	Method[b]	V_{OC} (V)	J_{SC} (mA cm^{-2})	FF	PCE (best) (%)
P24	RC[c]	0.73	7.79	0.60	3.43 (3.60)
	SC[d]	0.75	9.74	0.61	4.50 (5.27)
P27a	RC[c]	0.73	7.73	0.59	3.35 (3.47)
	SC[d]	0.76	9.79	0.62	4.58 (4.73)
P27b	RC[c]	0.73	7.79	0.57	3.25 (3.43)
	SC[d]	0.76	9.23	0.61	4.31 (4.49)
P28a	RC[e]	0.72	7.63	058	3.17 (3.38)
	SC[d]	0.76	10.80	0.60	4.89 (5.55)
P28b	RC[e]	0.71	7.76	0.60	3.27 (3.54)
	SC[d]	0.72	10.48	0.67	5.03 (5.33)
P29a	RC[e]	0.72	7.99	0.55	3.16 (3.42)
	SC[d]	0.76	9.93	0.60	4.50 (4.74)
P29b	RC[e]	0.73	7.76	0.54	3.04 (3.16)
	SC[d]	0.76	9.30	0.61	4.34 (4.54)

[a] *J-V* parameters averaged over 5 devices for RC and 4–8 devices for SC. [b] SC: spin-coated under inert atmosphere with a normal device geometry (glass/ITO/PEDOT:PSS/polymer:$PC_{61}BM$/Ca/Al) for 3 mm^2 active area. RC: roll-coated in air at 80 °C, 1:2 ratio for polymer:$PC_{61}BM$, an active layer thickness of 450 nm and an inverted device geometry for ~1 cm^2 (PET substrate/Ag-grid/PEDOT:PSS/ZnO/polymer:$PC_{61}BM$/PEDOT:PSS/Ag-grid)). [c] Processed from ODCB/CB = 4/1. [d] 1:2 ratio processed from CF. [e] Processed from ODCB/CB = 3/2.

Averaged efficiencies of the devices were of around 4.5-5%, as expected higher than the RC devices. As described previous, the incorporation of the EtPh side chain on the D_M unit decreased the (best) efficiency (5.27%, 4.73% and 4.49% for **P24** and **P27a**,**b**, Table 4.6). However, the incorporation of the EtOH side chain in the D_M unit increased the efficiency slightly to be up to 5.55% and 5.33% for **P28a,b**. On the counter side, the incorporation of the EtOH side chain on the A_M unit decreased the efficiency (4.74% and 4.54% for **P29a**,**b**) as already seen for the RC devices. The values of the PCE were also reflected in the values of J_{SC}. The devices with 10% of the EtOH on the A_M and EtPh on the D_M unit (**P27b** and **P29b**) was ~9.3 mA and thus lower than the reference **P24** and as **P27a** and **P29a** (~9.8 mA). The positive effect of the EtOH group on the D_M (**P28a,b**) unit was also reflected in an increase of the J_{SC} of the devices (>10 mA). However, the V_{OC} of **P28b** was lower than of the other devices (0.72 V *vs.* ~0.76 V), which was counteracted by a higher FF of **P28b** (67% *vs.* ~61%).

4.4.3. Device Stability Analysis

Lifetime testing

The RC devices were also analysed by a lifetime study for 50 days, handling the devices the same way as previous. The normalized average values were plotted against the time for each polymer with different side chains in Figure 4.11. The efficiency of all PSCs decreased quickly for all cells in the first phase of the study.

In the first phase (6 h) of the PSCs based on **P27a** the PCE decreased relatively fast to 65% of its initial values, while **P24** and **P27b** degraded slower to 70% of the initial PCE (EtPh based polymers). In the second stage of the degradation, the PCE curves had a relative linear decay resulting in 20% and 30% of the initial performances of the **P27a**,**b** based PSCs. (Figure 4.5)

Within the first 6 h of the lifetime experiments of the PSCs based on EtOH side chain incorporation on D_M unit, **P28a** decreased in the same manner as **P24** to 70% of the initial PCE, while **P28b** decreased a bit slower to 72% of the initial value. In the second rather linear step, **P28a** and **P24** degrade relative similar, while the efficiency of **P28b** was more stable, resulting in 23% and 25% of the initial performances of **P28a**,**b** based PSCs (Figure 4.11 left). In the first degradation stage of the third group, where the EtOH is on the A_M unit, **P29a,b** decreased slightly slower than **P24**. In the second step, **P29a** and **P24** degrade relative similar, while the efficiency of **P29b** was degrading faster, and after ~35 h slower than **P24**, resulting in 23% and 26% of the initial performances of **P29a**,**b** based PSCs (Figure 4.11 right).

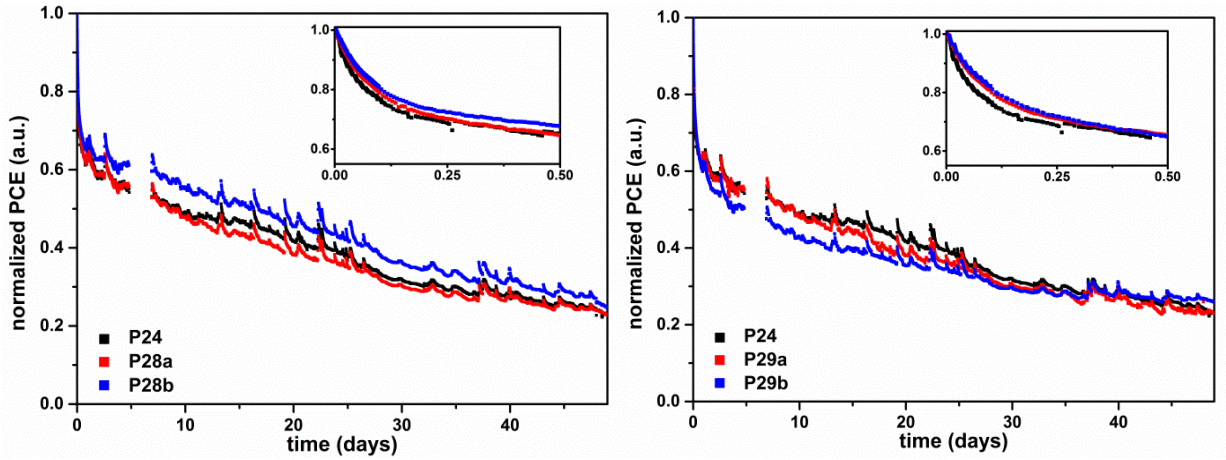

Figure 4.11. *Stability measurements of RC PSCs based on* ***P28a,b*** *(left) and* ***P29a,b*** *(right) in comparison to* ***P24*** *under constant sun irradiance (AM 1.5) according to ISOS L-1 standards in terms of normalized PCE. Adapted from* [24] *with permission from The Royal Society of Chemistry ©2016.*

The other *J-V* characteristics (V_{OC}, J_{SC}, FF; Appendix B Figure B.4.6) showed similar trends. The V_{OC} of the PSCs with 10% new side chain showed always similar (**P28b**, **P29b**) or increased (**P27b**) stability in comparison to the

V_{OC} stability from the PSCs based on **P24**. However, The V_{OC} of the polymers with 5% new side chain showed always lower stability. The J_{SC} showed a similar trend as the V_{OC}. The stability of the PSCs with 10% new side chain was similar to **P24**, while the ones with 5% have a lower stability. The stability of the FF was again improved for **P27b**, as well as, **P28a,b** and **P29a** in comparison to **P24**. The remaining samples (**P27a**, **P29b**) had a similar FF stability than the reference material. The negative trend of the substituted EtOH side chain on the A_M unit in **P29b** was reflected in a faster decrease of the J_{SC} and FF especially during the first stage. Surprisingly, these devices retained a higher V_{OC}. The positive influence of the EtPh side chain in **P27b** was seen throughout all *J-V* characteristics during the experiment with the highest retained values (0.62 V, 3.5 mA cm^{-2} and 45%). From the experiment could be concluded that an exchange of 5% of the side chains by different functional stabilizing moieties does not result in improved device stabilities.

Thermal degradation testing

The SC devices were also investigated by a thermal degradation for ~450 hours. The normalized average values for the PCE and FF were plotted against the time in Figure 4.12.

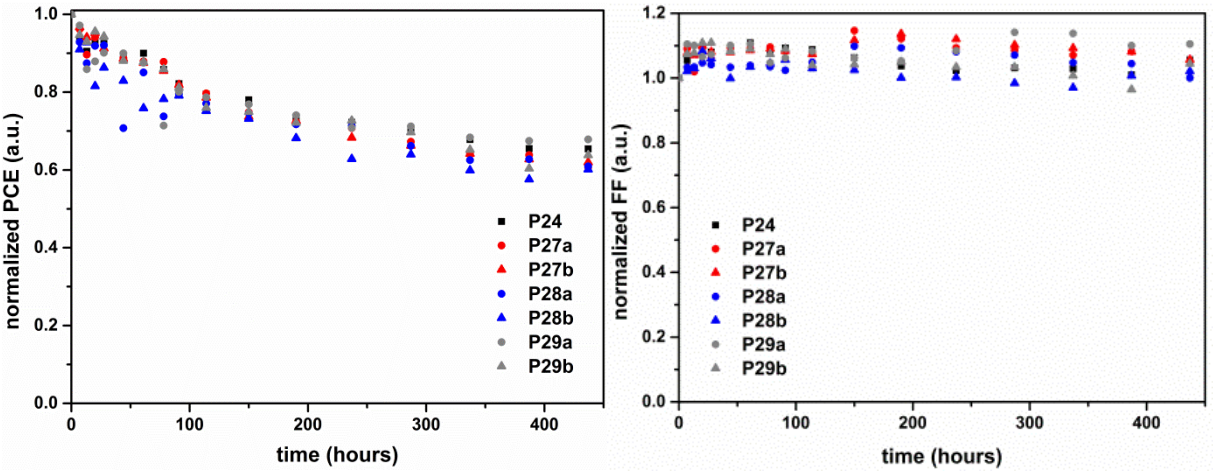

Figure 4.12. *Stability measurements of SC PSCs based on* ***P24, P27-P29*** *under thermal stress (85 °C) in terms of the averaged PCE (left) and FF (right). Adapted from* [24] *with permission from The Royal Society of Chemistry ©2016.*

All devices had relative similar behaviour and the PCE degraded to 60-70% of the initial value. The V_{OC} and J_{SC} decays are shown in Appendix B Figure B.4.7. The V_{OC} of all PSCs curves were similar with a minor decay and the J_{SC} degraded in a similar manner as the PCE. The FFs of all devices increase within the first 50 h to around 105-110% of the initial value. **P27a,b** and **P28a** continued with a constant value before the FFs increased further after around 150 h of thermal stress; the value of **P29a** increased after around 300 h again. The values of **P24**, **P28b** and **P29b** remained relative constant during the rest of the experiment. This similar degradation trend can be connected with the stress test temperature of 85°C, which is lower than the T_g's of

the polymers (~140°C) [33]. As such no phase separation is expected to be present in the active layer by crystallization of $PC_{61}BM$, which is a known degradation mechanism [3,10].

4.5. Comparison of the Different Side Chain Modifications with a Focus on their Degradation Behaviour

4.5.1. Photostability of the Polymer Films

The stability of the films was measured by tracking the absorption of the polymer films under solar illumination which resulted in colour loss for all films and no absorption was detected in the end. Similar degradation curves were seen within the BT and TzTz polymer series and partly within the BDT series (**P24**, **P27a,b**, **P28a**, **P29a**), which seemed to be due to a common photodegradation pathway for these polymers. Rivaton et al. proposed a degradation route where the alkoxy side chains on a phenyl building block in a PPV derivative are cleaved off via photolysis [34]. Since the observed degradation profiles looked very similar and the same type of alkoxy side chains are employed in the BT and TzTz based polymers, it is assumed a similar behaviour for these two polymer series, practically independent of the presence of the EtPh groups. The incorporation of these groups showed thereby no noticeable effects on the photochemical degradation curves (**P25a,b**, **P26a,b** and **P27a,b**), with slopes similar to the reference materials **P2**, **P8** and **P24**. The incorporation of different side chains and in different positions of the BDT based polymers, however, show clearly different photochemical degradation. 5% substitution of the EtOH side chains on A_M unit showed no influence (**P29a**). Unfortunately, a negative trend was observed for the 10% incorporated EtOH group in the A_M unit (**P29b**). The incorporation of the EtOH side chain within the D_M revealed a slower photodegradation, which was clearly visible for the 10% substituted polymer (**P28b**). One main difference of the polymers **P28a,b** and **P29a,b** is the group (D_M or A_M) where the new side chain is attached. Another main difference between the polymers with the EtOH side chains was, that in **P28a,b** the new side chain was not directly attached on the conjugated polymer backbone, while in **P29a,b** the side chain was attached on the Th which is part of the polymer backbone.

The degradation within the active layer can be caused by chemical reactions. Different degradation mechanisms are described in the literature. As light is one of the main triggers for the degradation, conjugated polymers degrade in different ways [35]:

1. Photobleaching (disruption of the conjugation)
2. Free radical attack/pyrolysis (chain scissoring/cross linking/side chain removal)
3. Photooxidation (disruption of the conjugation/side chain removal)
4. Photodoping (weak bound donor-acceptor charge transfer complex, reversible)

Photobleaching (Scheme 4.3./1) starts with the formation of singlet oxygen by absorbing light in a specific wavelength region [36]. In a Diels-Alder addition it reacts with e.g. Th in P3HT forming peroxide and subsequently leading to the disruption of the π-conjugation [35]. Furthermore, sulphur-containing conjugated polymers can be photooxidized forming a sulfoxide species at the Th unit and rupturing the aromatic system (Scheme 4.3 /2) [37,38]. In addition it has been reported that singlet oxygen is reacting with anthracene [39], so conjugated polymers should undergo similar reactions during photooxidation. A free radical pathway happens in another process where either the side chain or the backbone is scissored (Scheme 4.3 /3 and /4) [40].

The radical scissoring and the oxidation of the sulphur atom of Th were shown to be responsible for the loss of the π-conjugation, therefore resulting in vanishing of the polymer colour/material [41]. The EtOH side chain in **P29a,b** were anchored onto the Th within the A_M unit forming backbone, this degradation pathway might be induced more rapidly in comparison to the polymers with the other side chain or in different position. It is difficult to show the degradation mechanisms occurring within the polymer series. Especially balancing out the reasons for how the incorporation of different side chains influenced the slower and faster degradation of polymer films based on **P28b** and **P29b**, respectively.

A last degradation mechanism is the reversible p-doping of polymers by oxygen. Slow physical adsorption forms a weak charge-transfer complex, which is even accelerated by light influence [35].

As the *J-V* characteristics of devices based on conjugated polymers are dependent on the molecular weight [42–44] the different mechanisms (photoinduced oxidation, chain scission and disrupting of the π-conjugation) can lead to a variation of the chain lengths and therefore affect the PV and optical properties of the polymer [45]. These mechanisms might occur in the polymer during light exposure, but no specific investigation was performed under the stress test described in this chapter.

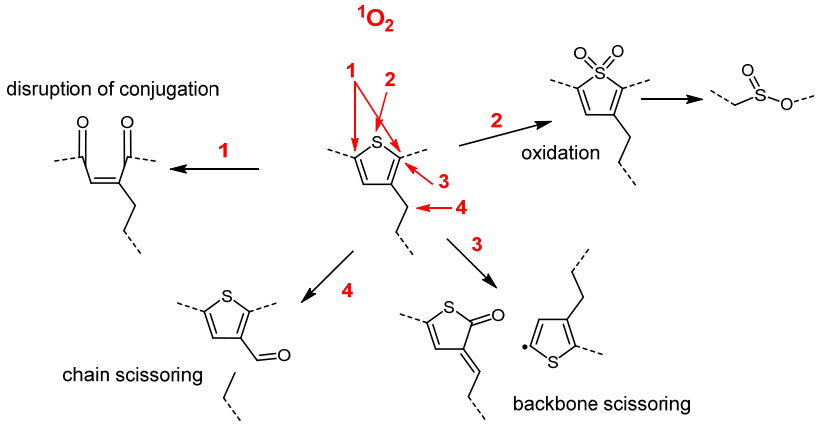

Scheme 4.3. *Chemical attack of thiophene containing polymer with an alkyl chain by singlet oxygen under illumination.* [38,40]

The polymer structure (amount/length of the side chains, nature of the backbone) could influence the photochemical stability of the polymers and therefore also of the resulting devices [46–49]. Manceau *et al*. showed that the use of different D_M or A_M units within the backbone changed the photochemical stability of the polymer. In addition, some general ranking for of D_M-A_M polymers for PSCs were proposed [50]. Andersson *et al.* reported a polymer series with different substituted BDT or unsubstituted thienothiophene units, to investigate the effect of structural modifications on the polymer film and the corresponding device stability [49]. Similar to the results in this chapter, a demonstration of different trends among the photochemical stability of the polymer films and the corresponding devices was proposed [49].

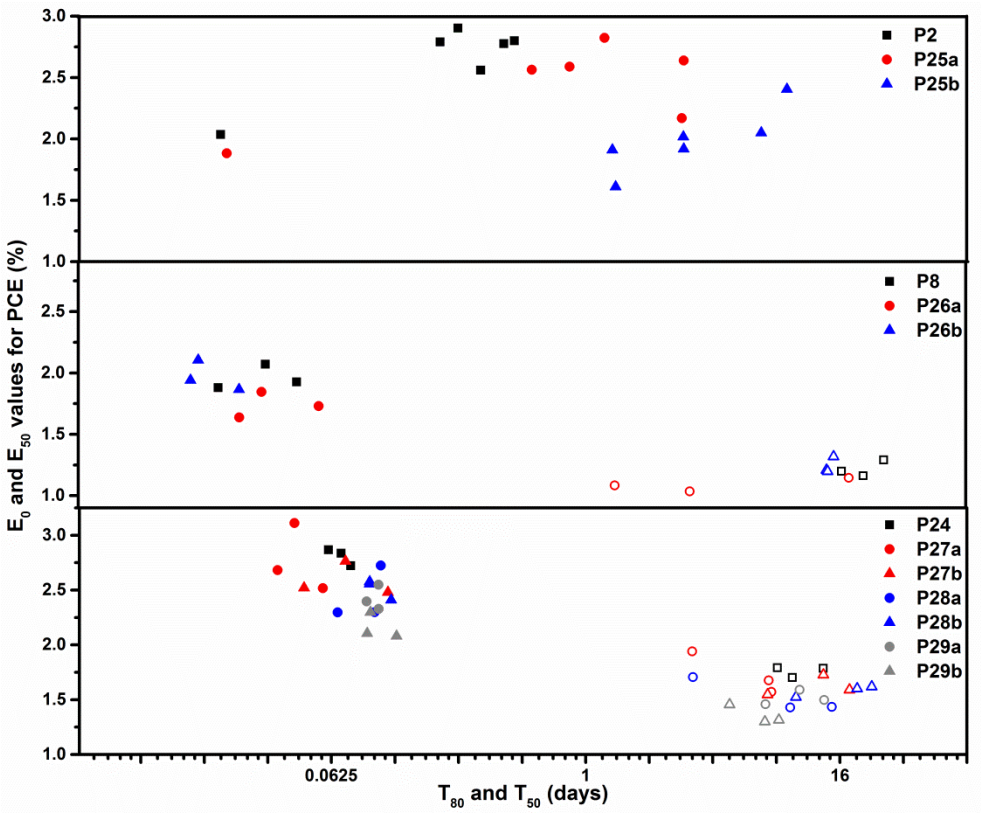

Figure 4.13. *The diagram presents T_{80}/E_0 (solid) and T_{50}/E_{50} (open) of the lifetime measurements (ISOS-L-1) of all cells from PSCs based on BT (top), TzTz (middle) and BDT (bottom) polymers.*

4.5.2. Lifetime of the Roll-Coated Devices

The stability of the RC devices was measured by scanning the *J-V* characteristics under constant solar illumination. Hereby all devices had a decay in their efficiency. Figure 4.13 shows 80% (E_0) and 50% (E_{50}) decay of the efficiencies with the corresponding degradation time (T_{80} and T_{50}). It shows an improved time (T_{80}) for the devices based on BT with increasing amount of the EtPh side chain, but with a lower PCE (E_0) due to a lower initial value. This part of the studies clearly shows that the incorporation of EtPh side chains could

have a positive effect on the stability. The second group of polymers (TzTz based) showed no improvement among the T_{80} and T_{50} values. In addition the efficiencies (slope of the curves) of the devices with new side chain degraded faster and with a different pattern. The incorporation of the EtPh chain in the third polymer series (BDT) did not improve the T_{80} and T_{50} values, however in even longer terms, the polymer with 10% new side chain seemed to degrade slower. This first part of the lifetime study showed different effects among the different polymer backbones and with incorporation of different HD/EtPh ratios.

The second part of the study was the comparison of the different side chains within different positions of the same backbone (BDT). The comparison of the lifetime analysis of the PSCs showed that the position of the side chains, either on D_M or A_M unit, influenced the stability of the resulting devices. The T_{80} and T_{50} values are similar to the one of the parent polymer **P24**, but mostly lower in terms of the E_0 and E_{50} values. For the degradation curve of the light-induced test, **P29b** (EtOH on A_M unit) showed the most rapid degradation. Applying the EtOH and EtPh on the D_M unit a slightly improved stability of the device was noticed. 5% incorporation of the side chain showed only minor improvements for the degradation curve of the device with the polymer based on EtPh (**P27a**). Even though 10% EtPh incorporation showed a stronger effect on the photochemical degradation of the solar cell an improved stability could be achieved.

4.5.3. Thermal Stability of the Spin-Coated Device

The stability of the SC devices was measured by scanning the *J-V* characteristics under constant thermal stress. Hereby all devices had different decays in their solar cell performance. All three polymer groups show very different results when the new side chains were incorporated. The modified BT-based (**P25a,b**) device showed a fast decrease in efficiency, followed by a stable value, whereas the parent device with **P2** was decreasing linear over the whole time frame. The second series (TzTz) showed a small loss of the PCE during the exposure of thermal stress for the modified polymers (**P26a,b**), whereas there was almost no decrease for the parent polymer **P8**. The thermal degradation of the devices based on the BDT polymer proceeded very similar for all devices containing the different side chains.

The comparison between the three different polymer backbones makes it clear that the modification of a side chain by EtPh or EtOH groups could have a notably different influence on the PV parameters of the resulting PSCs. The influence of stabilizing side chains was previously studied by Vanderzande *et al.* [10], which was adopted herein to improve the stability of the PSCs. In particular, the influence on the thermal stability and phase separation of the D-A blend was part of this study. Known mechanisms of the active layer degradation are the fullerene crystallization and dimerization [51–53]. Specifically the fullerene crystallization/phase separation of the active layer could be related in previous studies to the T_g of the

polymer [33]. In this work, however, the T_g's of the polymers could not clearly be related with the thermal degradation of the devices, due to e.g. undetectable T_g (TzTz and BDT).

4.6. Conclusion

In this chapter three reference polymers **P2**, **P8** and **P24** based on benzo[*c*][1,2,5]thiadiazole, thiazolo[4,5-*d*]thiazole and benzo[1,2-*b*:4,5-*b'*]dithiophene, respectively, which were adopted from Chapter 2, were successfully synthesized and adapted through a modification by partial exchange (5%, 10%) of some of the side chains (2-hexyldecyl and hexyl) with stabilizing side chains (2-phenethyl and 2-ethanol) to be **P25**-**P29**. The initial goal was to adapt successfully demonstrated side chain modification in the past [10–12] to elevate the T_g of the polymers and thus the (thermal) stability. As the polymers showed no destinct T_g's, they were additionally investigated to show the influence of these new functionalizations on the photostability of the polymers and polymer solar cells (PSCs).

The application of different stabilizing side chain on different polymer backbones demonstrated a variation of results on the PSC performance and stability. These results showed that a 10% side chain substitution can already improve the stability of the polymer films and the corresponding PSCs in a small degree. It was also seen that the incorporation of the new side chains had a different effect by using different backbones. It shows that for each backbone the incorporation of (different) stabilizing side chains can have a different impact. It clearly shows that the variation of side chains, especially in different positions (acceptor or donor unit of the polymer), has an influence on the stability. All in all, no clear design rules, significantly improved stabilities, nor general trends could be explored. The results show, however, that engineering of side chain can be a powerful tool to influence or optimize the efficiency, as well as stability of PSCs, and create basic ideas for future work.

Future work should include finding the right combination of solubility and stabilizing side chain in the right backbone. This can be seen as a challenge and should be approached by the method used in Chapter 2. Besides trying different types of stabilizing side chains, the ratios of side chains and their effect on different polymer backbones could be investigated as well. Furthermore, studies to reveal detailed degradation mechanisms for the different polymers could be an interesting research topic.

4.7. References

1. Yang, L.; Zhou, H.; You, W. Quantitatively analyzing the influence of side chains on photovoltaic properties of polymer-fullerene solar cells. *J. Phys. Chem. C* **2010**, *114*, 16793–16800.

2. Nguyen, T. L.; Song, S.; Ko, S.; Choi, H.; Jeong, J.; Kim, T.; Hwang, S.; Kim, J. Y.; Woo, H. Y. Benzodithiophene-Thiophene-Based Photovoltaic Polymers with Different Side-Chains. *J. Polym. Sci. Part A Polym. Chem.* **2015**, *53*, 854–862.

3. Cardinaletti, I.; Kesters, J.; Bertho, S.; Conings, B.; Piersimoni, F.; D'Haen, J.; Lutsen, L.; Nesladek, M.; Van Mele, B.; Van Assche, G.; Vandewal, K.; Salleo, A.; Vanderzande, D.; Maes, W.; Manca, J. V. Toward bulk heterojunction polymer solar cells with thermally stable active layer morphology. *J. Photonics Energy* **2014**, *4*, 040997 (1-12).

4. Lindqvist, C.; Bergqvist, J.; Bäcke, O.; Gustafsson, S.; Wang, E.; Olsson, E.; Inganäs, O.; Andersson, M. R.; Müller, C. Fullerene mixtures enhance the thermal stability of a non-crystalline polymer solar cell blend. *Appl. Phys. Lett.* **2014**, *104*, 153301(1-4).

5. Lindqvist, C.; Bergqvist, J.; Feng, C.-C.; Gustafsson, S.; Bäcke, O.; Treat, N. D.; Bounioux, C.; Henriksson, P.; Kroon, R.; Wang, E.; Sanz-Velasco, A.; Kristiansen, P. M.; Stingelin, N.; Olsson, E.; Inganäs, O.; Andersson, M. R.; Müller, C. Fullerene Nucleating Agents: A Route Towards Thermally Stable Photovoltaic Blends. *Adv. Energy Mater.* **2014**, *4*, 1301437 (1-10).

6. Rumer, J. W.; McCulloch, I. Organic photovoltaics: Crosslinking for optimal morphology and stability. *Mater. Today* **2015**, *18*, 425–435.

7. Gevorgyan, S. A.; Krebs, F. C. Bulk Heterojunctions Based on Native Polythiophene. *Chem. Mater.* **2008**, *20*, 4386–4390.

8. Bundgaard, E.; Hagemann, O.; Bjerring, M.; Nielsen, N. C.; Andreasen, J. W.; Andreasen, B.; Krebs, F. C. Removal of Solubilizing Side Chains at Low Temperature: A New Route to Native Poly(thiophene). *Macromolecules* **2012**, *45*, 3644–3646.

9. Verstappen, P.; Kesters, J.; D'Olieslaeger, L.; Drijkoningen, J.; Cardinaletti, I.; Vangerven, T.; Bruijnaers, B. J.; Willems, R. E. M.; D'Haen, J.; Manca, J. V.; Lutsen, L.; Vanderzande, D. J. M.; Maes, W. Simultaneous Enhancement of Solar Cell Efficiency and Stability by Reducing the Side Chain Density on Fluorinated PCPDTQx Copolymers. *Macromolecules* **2015**, *48*, 3873–3882.

10. Vandenbergh, J.; Conings, B.; Bertho, S.; Kesters, J.; Spoltore, D.; Esiner, S.; Zhao, J.; Van Assche, G.; Wienk, M. M.; Maes, W.; Lutsen, L.; Van Mele, B.; Janssen, R. A. J.; Manca, J.; Vanderzande, D. J. M. Thermal Stability of Poly[2-methoxy-5-(2'-phenylethoxy)-1,4-phenylenevinylene] (MPE-PPV): Fullerene Bulk Heterojunction Solar Cells. *Macromolecules* **2011**, *44*, 8470–8478.

11. Kesters, J.; Kudret, S.; Bertho, S.; Van den Brande, N.; Defour, M.; Van Mele, B.; Penxten, H.; Lutsen, L.; Manca, J.; Vanderzande, D.; Maes, W. Enhanced intrinsic stability of the bulk heterojunction active layer blend of polymer solar cells by varying the polymer side chain pattern. *Org. Electron.* **2014**, *15*, 549–562.

12. Kesters, J.; Verstappen, P.; Raymakers, J.; Vanormelingen, W.; Drijkoningen, J.; D'Haen, J.; Manca, J.; Lutsen, L.; Vanderzande, D.; Maes, W. Enhanced Organic Solar Cell Stability by Polymer (PCPDTBT) Side Chain Functionalization. *Chem. Mater.* **2015**, *27*, 1332–1341.

13. Carlé, J. E.; Jørgensen, M.; Krebs, F. C. Polymers for organic photovoltaics based on 1,5-bis(2-hexyldecyloxy)-naphthalene, thiophene, and benzothiadiazole. *J. Photonics Energy* **2011**, *1*, 011111 (1-10).

14. Helgesen, M.; Carlé, J. E.; dos Reis Benatto, G. A.; Søndergaard, R. R.; Jørgensen, M.; Bundgaard, E.; Krebs, F. C. Making Ends Meet: Flow Synthesis as the Answer to Reproducible High-Performance Conjugated Polymers on the Scale that Roll-to-Roll Processing Demands. *Adv. Energy Mater.* **2015**, *5*, 1401996 (1-7).

15. Livi, F.; Zawacka, N. K.; Angmo, D.; Jørgensen, M.; Krebs, F. C.; Bundgaard, E. Influence of Side Chain Position on the Electrical Properties of Organic Solar Cells Based on Dithienylbenzothiadiazole- alt -phenylene Conjugated Polymers. *Macromolecules* **2015**, *48*, 3481–3492.

16. Liao, S. H.; Jhuo, H. J.; Cheng, Y. S.; Chen, S. A. Fullerene derivative-doped zinc oxide nanofilm as the cathode of inverted polymer solar cells with low-bandgap polymer (PTB7-Th) for high performance. *Adv. Mater.* **2013**, *25*, 4766–4771.

17. Carlé, J. E.; Helgesen, M.; Zawacka, N. K.; Madsen, M. V.; Bundgaard, E.; Krebs, F. C. A comparative study of fluorine substituents for enhanced stability of flexible and ITO-free high-performance polymer solar cells. *J. Polym. Sci. Part B Polym. Phys.* **2014**, *52*, 893–899.

18. Carlé, J. E.; Andreasen, J. W.; Jørgensen, M.; Krebs, F. C. Low band gap polymers based on 1,4-dialkoxybenzene, thiophene, bithiophene donors and the benzothiadiazole acceptor. *Sol. Energy Mater. Sol. Cells* **2010**, *94*, 774–780.

19. Huo, L.; Zhang, S.; Guo, X.; Xu, F.; Li, Y.; Hou, J. Replacing alkoxy groups with alkylthienyl groups: a feasible approach to improve the properties of photovoltaic polymers. *Angew. Chemie Int. Ed.* **2011**, *50*, 9697–9702.

20. Ellinger, S.; Ziener, U.; Thewalt, U.; Landfester, K.; Möller, M. Synthesis and self-organization of α,ω-substituted oligothiophenes with long, branched alkyl substituents. *Chem. Mater.* **2007**, *19*, 1070–1075.

21. Hou, Q.; Zhou, Q.; Zhang, Y.; Yang, W.; Yang, R.; Cao, Y. Synthesis and electroluminescent properties of high-efficiency saturated red emitter based on copolymers from fluorene and 4,7-Di(4-hexylthien-2-yl)-2,1, 3-benzothiadiazole. *Macromolecules* **2004**, *37*, 6299–6305.

22. Helgesen, M.; Carlé, J. E.; Krebs, F. C. Slot-Die Coating of a High Performance Copolymer in a Readily Scalable Roll Process for Polymer Solar Cells. *Adv. Energy Mater.* **2013**, *3*, 1664–1669.

23. Heckler, I.; Kesters, J.; Defour, M.; Madsen, M.; Penxten, H.; D'Haen, J.; Van Mele, B.; Maes, W.; Bundgaard, E. The Influence of Conjugated Polymer Side Chain Manipulation on the Efficiency and Stability of Polymer Solar Cells. *Materials (Basel).* **2016**, *9*, 181 (1-18).

24. Heckler, I. M.; Kesters, J.; Defour, M.; Penxten, H.; Van Mele, B.; Maes, W.; Bundgaard, E. A stability study of polymer solar cells using conjugated polymers with di ff erent donor or acceptor side chain patterns. *J. Mater. Chem. A Mater. energy Sustain.* **2016**, *4*, 16677–16689.

25. Bundgaard, E.; Krebs, F. C. Low-Band-Gap Conjugated Polymers Based on Thiophene , Benzothiadiazole , and Benzobis (thiadiazole). *Macromolecules* **2006**, *39*, 2823–2831.

26. Danley, R. L.; Caulfield, P. A.; Aubuchon, S. R. Rapid-Scanning Differential Scanning Calorimeter. *Am. Lab.* **2008**, *40*, 9–11.

27. Ghoos, T.; Van Den Brande, N.; Defour, M.; Brassinne, J.; Fustin, C.-A.; Gohy, J.-F.; Hoeppener, S.; Schubert, U. S.; Vanormelingen, W.; Lutsen, L.; Vanderzande, D. J.; Van Mele, B.; Maes, W. Amphiphilic N-methylimidazole-functionalized diblock copolythiophenes. *Eur. Polym. J.* **2014**, *53*, 206–214.

28. Tromholt, T.; Madsen, M. V.; Carlé, J. E.; Helgesen, M.; Krebs, F. C. Photochemical stability of conjugated polymers, electron acceptors and blends for polymer solar cells resolved in terms of film thickness and absorbance. *J. Mater. Chem.* **2012**, *22*, 7592–7601.

29. Reese, M. O.; Gevorgyan, S. A.; Jørgensen, M.; Bundgaard, E.; Kurtz, S. R.; Ginley, D. S.; Olson, D. C.; Lloyd, M. T.; Morvillo, P.; Katz, E. A.; Elschner, A.; Haillant, O.; Currier, T. R.; Shrotriya, V.; Hermenau, M.; Riede, M.; Kirov, K. R.; Trimmel, G.; Rath, T.; Inganäs, O.; Zhang, F.; Andersson, M.; Tvingstedt, K.; Lira-Cantu, M.; Laird, D.; McGuiness, C.; Gowrisanker, S.; Pannone, M.; Xiao, M.; Hauch, J.; Steim, R.; Delongchamp, D. M.; Rösch, R.; Hoppe, H.; Espinosa, N.; Urbina, A.; Yaman-Uzunoglu, G.; Bonekamp, J.-B.; van Breemen, A. J. J. M.; Girotto, C.; Voroshazi, E.; Krebs, F. C. Consensus stability testing protocols for organic photovoltaic materials and devices. *Sol. Energy Mater. Sol. Cells* **2011**, *95*, 1253–1267.

30. Jeong, J.; Seo, J.; Nam, S.; Han, H.; Kim, H.; Anthopoulos, T. D.; Bradley, D. D. C.; Kim, Y. Significant Stability Enhancement in High-Efficiency Polymer:Fullerene Bulk Heterojunction Solar Cells by Blocking Ultraviolet Photons from Solar Light. *Adv. Sci.* **2015**, 1500269 (1-10).

31. Lilliedal, M. R.; Medford, A. J.; Madsen, M. V.; Norrman, K.; Krebs, F. C. The effect of post-processing treatments on inflection points in currentvoltage curves of roll-to-roll processed polymer photovoltaics. *Sol. Energy Mater. Sol. Cells* **2010**, *94*, 2018–2031.

32. Bertho, S.; Haeldermans, I.; Swinnen, A.; Moons, W.; Martens, T.; Lutsen, L.; Vanderzande, D.; Manca, J.; Senes, A.; Bonfiglio, A. Influence of thermal ageing on the stability of polymer bulk heterojunction solar cells. *Sol. Energy Mater. Sol. Cells* **2007**, *91*, 385–389.

33. Müller, C. On the glass transition of polymer semiconductors and its impact on polymer solar cell stability. *Chem. Mater.* **2015**, *27*, 2740–2754.

34. Rivaton, A.; Chambon, S.; Manceau, M.; Gardette, J. L.; Lemaître, N.; Guillerez, S. Light-induced degradation of the active layer of polymer-based solar cells. *Polym. Degrad. Stab.* **2010**, *95*, 278–284.

35. Grossiord, N.; Kroon, J. M.; Andriessen, R.; Blom, P. W. M. Degradation mechanisms in organic photovoltaic devices. *Org. Electron.* **2012**, *13*, 432–456.

36. Schweitzer, C.; Schmidt, R. Physical mechanisms of generation and deactivation of singlet oxygen. *Chem. Rev.* **2003**, *103*, 1685–1757.

37. Kettle, J.; Waters, H.; Ding, Z.; Horie, M.; Smith, G. C. Chemical changes in PCPDTBT:PCBM solar cells using XPS and TOF-SIMS and use of inverted device structure for improving lifetime performance. *Sol. Energy Mater. Sol. Cells* **2015**, *141*, 139–147.

38. Manceau, M.; Rivaton, A.; Gardette, J. L.; Guillerez, S.; Lemaître, N. The mechanism of photo- and thermooxidation of poly(3-hexylthiophene) (P3HT) reconsidered. *Polym. Degrad. Stab.* **2009**, *94*, 898–907.

39. Wasserman, H. H.; Scheffer, J. R.; Cooperb, J. L. Singlet Oxygen Reactions with 9,10-Diphenylanthracene Peroxide. *J.*

Am. Chem. Soc. **1972**, *94*, 4991–4996.

40. Abdou, A.; Holdcroft, S. Mechanisms of Photodegradation of Poly(3-alkylthiophenes) in Solution. *Macromolecules* **1993**, *26*, 2954–2962.

41. Krebs, F. C. *Stability and Degradation of Organic and Polymer Solar Cells*; Krebs, F. C., Ed.; 1st ed.; John Wiley & Sons, Ltd: West Sussez, United Kingdom, 2012.

42. Müller, C.; Wang, E.; Andersson, L. M.; Tvingstedt, K.; Zhou, Y.; Andersson, M. R.; Inganäs, O. Influence of molecular weight on the performance of organic solar cells based on a fluorene derivative. *Adv. Funct. Mater.* **2010**, *20*, 2124–2131.

43. Moet, D. J. D.; Lenes, M.; Kotlarski, J. D.; Veenstra, S. C.; Sweelssen, J.; Koetse, M. M.; de Boer, B.; Blom, P. W. M. Impact of molecular weight on charge carrier dissociation in solar cells from a polyfluorene derivative. *Org. Electron. physics, Mater. Appl.* **2009**, *10*, 1275–1281.

44. Vangerven, T.; Verstappen, P.; Drijkoningen, J.; Dierckx, W.; Himmelberger, S.; Salleo, A.; Vanderzande, D.; Maes, W.; Manca, J. V. Molar Mass versus Polymer Solar Cell Performance: Highlighting the Role of Homocouplings. *Chem. Mater.* **2015**, *27*, 3726–3732.

45. Rivaton, A.; Tournebize, A.; Gaume, J.; Bussière, P.-O.; Gardette, J.-L.; Therias, S. Photostability of organic materials used in polymer solar cells. *Polym. Int.* **2014**, *63*, 1335–1345.

46. Chambon, S.; Rivaton, A.; Gardette, J. L.; Firon, M. Photo- and thermal degradation of MDMO-PPV:PCBM blends. *Sol. Energy Mater. Sol. Cells* **2007**, *91*, 394–398.

47. Manceau, M.; Chambon, S.; Rivaton, A.; Gardette, J. L.; Guillerez, S.; Lematre, N. Effects of long-term UVvisible light irradiation in the absence of oxygen on P3HT and P3HT: PCBM blend. *Sol. Energy Mater. Sol. Cells* **2010**, *94*, 1572–1577.

48. Xu, X.; Wu, Y.; Fang, J.; Li, Z.; Wang, Z.; Li, Y.; Peng, Q. Side-chain engineering of benzodithiophene-fluorinated quinoxaline low-band-gap co-polymers for high-performance polymer solar cells. *Chem. - A Eur. J.* **2014**, *20*, 13259–13271.

49. Gedefaw, D.; Tessarolo, M.; Prosa, M.; Bolognesi, M.; Henriksson, P.; Zhuang, W.; Seri, M.; Muccini, M.; Andersson, M. R. Induced photodegradation of quinoxaline based copolymers for photovoltaic applications. *Sol. Energy Mater. Sol. Cells* **2016**, *144*, 150–158.

50. Manceau, M.; Bundgaard, E.; Carlé, J. E.; Hagemann, O.; Helgesen, M.; Søndergaard, R.; Jørgensen, M.; Krebs, F. C. Photochemical stability of π-conjugated polymers for polymer solar cells: a rule of thumb. *J. Mater. Chem.* **2011**, *21*, 4132–4141.

51. Distler, A.; Sauermann, T.; Egelhaaf, H. J.; Rodman, S.; Waller, D.; Cheon, K. S.; Lee, M.; Guldi, D. M. The effect of PCBM dimerization on the performance of bulk heterojunction solar cells. *Adv. Energy Mater.* **2014**, *4*, 1300693 (1-6).

52. Heumueller, T.; Mateker, W. R.; Distler, A.; Fritze, U. F.; Cheacharoen, R.; Nguyen, W. H.; Biele, M.; Salvador, M.; von Delius, M.; Egelhaaf, H.-J.; McGehee, M. D.; Brabec, C. J. Morphological and electrical control of fullerene dimerization determines organic photovoltaic stability. *Energy Environ. Sci.* **2016**, *9*, 247–256.

53. Piersimoni, F.; Degutis, G.; Bertho, S.; Vandewal, K.; Spoltore, D.; Vangerven, T.; Drijkoningen, J.; Van Bael, M. K.; Hardy, A.; D'Haen, J.; Maes, W.; Vanderzande, D.; Nesladek, M.; Manca, J. Influence of fullerene photodimerization on the PCBM crystallization in polymer: Fullerene bulk heterojunctions under thermal stress. *J. Polym. Sci. Part B Polym. Phys.* **2013**, *51*, 1209–1214.

Chapter 5.

Comparison of Side Chain Removable Polymers

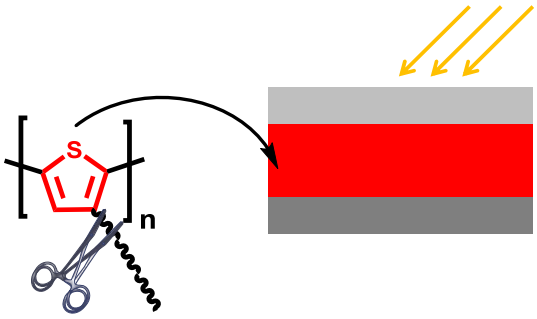

5.1. Introduction

The research in the area of conjugated polymers is mostly focused on reaching high efficiencies. A main problem is the stability of PSCs. This was also addressed closely in Chapter 4, where the side chains were partly modified to result in better stability of the polymer film and of the resulting PSCs. Another previously mentioned attempt was to build a rigid network of the polymer film by crosslinking of the polymers between the termini of the solubilizing side chains, which does neither interfere with the conjugated system, nor with the microstructure of the active layer blend [1]. In general, side chains are necessary to ensure good solubility of the polymer to be able to apply them in an all-solution coated (SC or RC) process of solar cells. However, once the film is formed, there is no need for these side chains. Therefore more than a decade ago, polymers with removable side chains for solar cell applications were introduced [2,3]. This was done by a removal post-film formation *via* thermal (Scheme 5.1 top) [4,5] and later *via* acid [6] treatment (Scheme 5.1 bottom) yielding a conjugated polymer material without side chains.

The thermo-cleavable polymers are studied quite intensively [5,7] especially on PT derivatives [2–4,8,9]. One example (Scheme 5.1.) is the cleavage of a PT containing a tertiary ester. The removal of the side chain happens at ~200°C, while the carboxylic acid in **PT-C** requires a temperature of ~300 °C. In a photochemical stability study these thermo-cleavable polymers were investigated to show the improved photostability (Figure 5.1. left) of the polymer without side chain [5]. The second, acid cleavable approach was performed to remove the side chains at room temperature, whereas temperature activated cleavage implies that the

reaction is only spontaneous at a certain temperature [6]. This allows a solution processed polymer film formation with subsequent removal of the side chain to result in insoluble material.

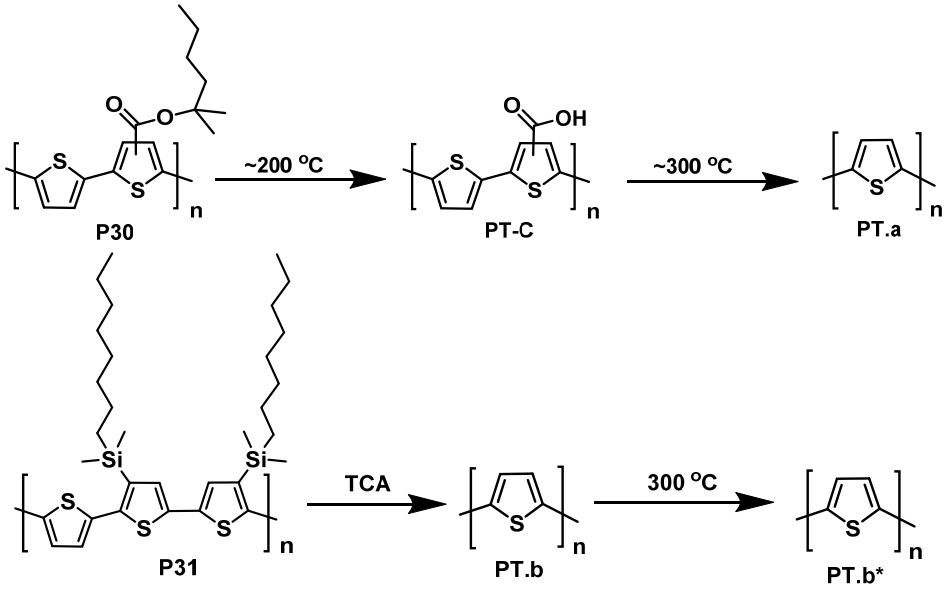

Scheme 5.1. *Chemical transition of the thermal cleavage of* ***P30*** *(PT based) [4] (top) and of the acid cleavage of* ***P31*** *(PT based) [6] (bottom).*

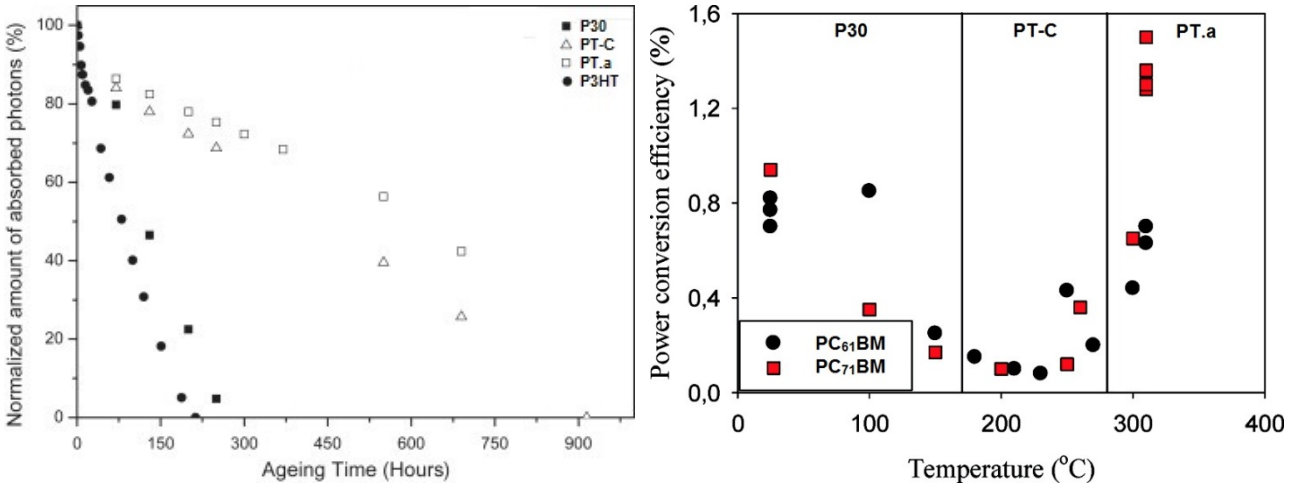

Figure 5.1. *Relative decay of the amount of absorbed photons of the photochemical degradation of* ***P30*** *(left).* [5] *Adapted with permission from Elsevier ©2010. The efficiency of the devices based on* ***P30*** *was plotted against the annealing temperature (right). Adapted with permission from* [9]*. ©2008 American Chemical Society.*

The application of the thermo-cleavable polymers in SC PSCs was successful for both **PT.a** based and low band gap D_M-A_M copolymers. [4,7,9] Hence, efficiencies of 0.6% for a **PT.a** blend with $PC_{61}BM$, 1.5% for a blend with $PC_{71}BM$ [9] and 0.25% for a D_M-A_M copolymer blend with $PC_{61}BM$ [7] were achieved. Figure 5.1.

(right) shows that during the first step of the side chain removal the efficiency decreased, while it increases again by removing the carboxylic acid. The application of these polymers in RC PSCs is not possible as the cleaving temperature is too high [10]. Especially when the coating occurs on flexible plastic foils, like poly(ethylene terephthalate) which has a melting point of 250°C, this method is not suitable. This leads to the question of applying the acid cleavable polymers in PSCs. However, prior to the project of this chapter the acid cleavable polymers were attempted to be applied in RC PSCs (further results in Appendix B). The devices failed due to *J-V* characteristics to be close to zero. Traces of the acid used for cleavage retained probably in the devices, even after evaporation attempts after coating of the active layer. But are the two PT layers based on different precursors actually the same? This question will be answered in this chapter, where a detailed comparison of the thermo- and acid-cleavable polymers was made.

5.2. Thermo- *vs.* Acid-Cleavage

The polymers **P30** and **P31** were adapted from literature procedures [2,6]. **P30** and **P31** were SC from a solution in ODCB and CF, respectively, on a glass or glass/ITO substrate of the polymer or polymer/$PC_{61}BM$ blend as described previously [6,9]. The side chains of **P31** were removed (Scheme 5.1 bottom) during the preparation of the polymer film by coating of the polymer solution in CF mixed with trichloroacetic acid (TCA) yielding an insoluble **PT.b** film [6]. Furthermore, the side chains of **P30** were eliminated by thermal treatment at 300°C leading to insoluble **PT.a** (Scheme 5.1 bottom) [6,9].

First the morphologies of the cleaved polymer blends on glass/ITO were analyzed by atomic force microscope (AFM) (Figure 5.2). The 10 µm x 10 µm AFM scans of the two types of PT were compared with a P3HT/ $PC_{61}BM$ blend. The root-mean-square roughness differed among the samples (Table 5.1.) and the lowest value was observed for **PT.a**, followed by **PT.b** and **P3HT**.

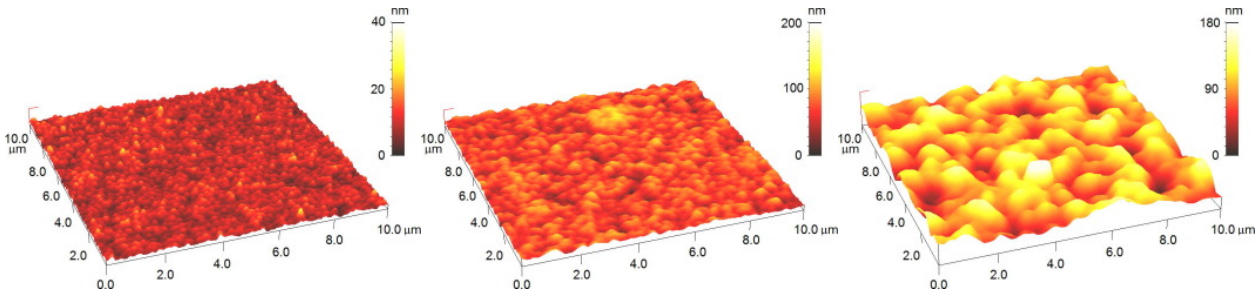

***Figure 5.2**. AFM image of **PT.a** (left), **PT.b** (middle) and P3HT (right) layers* [11]*. Reprinted with permission from Elsevier ©2016.*

UV-vis spectra were recorded of all untreated, cleaved and annealed polymer films on glass slights (Figure 5.3.). E_g and λ_{max} were extracted from the UV-vis spectra of the cleaved polymer films (Table 5.1). In the UV-

vis spectra it was seen that the untreated **P30, P31** and **P3HT** absorbed in different regions than the cleaved ones as expected. Thus **P31** absorbed in the higher energy area with a λ_{max} of approximately 400 nm. **P30** and **P3HT** absorbed, however, in higher wavelength region and had a λ_{max} of 536 nm and 557 nm, respectively. The absorption of the cleaved PT polymers shifted to lower wavelength with λ_{max} of 493 nm for **PT.a** and 504 nm for **PT.b**. In addition **PT.b** showed a small absorption shoulder around 580 nm. This showed as well that the polymer films are slightly different, even though the materials are the same. Annealing the **PT.b** polymer film at 300°C led to **PT.b***. The absorption spectrum of the annealed polymer film approximates the spectrum of **PT.a,** as the spectrum including λ_{max} moved to lower wavelength. In addition, the shoulder disappeared. The estimated E_g of the cleaved polymers are increased in comparison to **P3HT** (1.90 eV) to be 1.99 eV for **PT.a** and 1.94 eV for **PT.b**.

Table 5.1. *Surface parameters, optical and electronic properties of the cleaved polymers PT.a and PT.b and of P3HT. Data extracted from* [11].

	RMS[a] roughness (nm)	λ_{max}[b] (nm)	E_g[b] (eV)	HOMO[c] (eV)	LUMO[d] (eV)
PT.a	3	493	1.99	-5.14	-3.15
PT.b	15	504	1.94	-5.19	-3.25
P3HT	26	557	1.90	-5.14	-3.23

[a] root-mean-square (RMS) roughness determined by AFM, [b] λ_{max} and the optical band gap (E_g) determined from the UV-vis absorption spectrum of the polymer films, [c] highest occupied molecular orbital (HOMO) estimated from CV curves, [d] lowest unoccupied molecular orbital calculated from the HOMO and E_g.

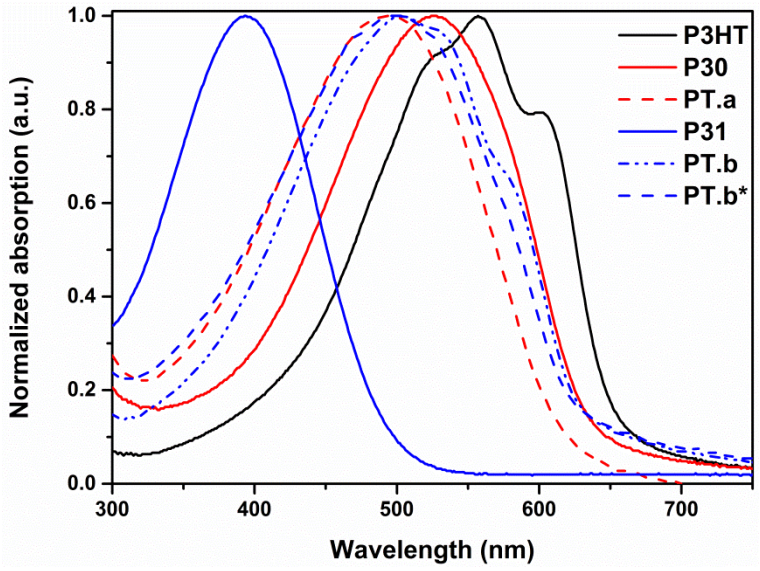

Figure 5.3. *UV-vis spectra of **P30** and **P31** films and their cleaved derivatives and **P3HT**.*

The photographs of the polymer films can be seen in Figure 5.4. **P3HT** has a purple colour and the film of **P30** is dark red, which changes to orange after cleavage. The film of **P31** is yellow and turns to light red after

cleavage. The colour change can be ascribed to the twisting of the thiophenes which is not the case when the side chains are removed. Thereafter, the polymer film is converted to orange during the thermal treatment of the polymer film. This results in the assumption that **PT.a** and **PT.b** have different nano-morphologies, also shown by different root-mean-square roughnesses. Heating **PT.b** at 300°C changed the morphology.

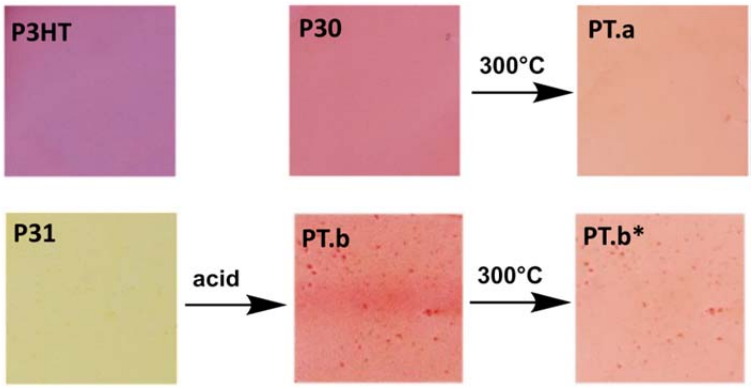

Figure 5.4. *Photographs of the polymer films of the untreated, cleaved and annealed polymer films based on* ***P30*** *and* ***P31*** *and of* ***P3HT****.*

CV measurements of the cleaved polymer films revealed the HOMO energy level of **PT.a** and **PT.b** (Table 5.1.) to be -5.14 eV for **PT.a** and -5.19 eV for **PT.b**. The HOMO level of **P3HT** was the same as for **PT.a**, but all similar to values from literature (5.20 eV) [12]. The LUMO levels were calculated using the values for the HOMO level and E_g [13].

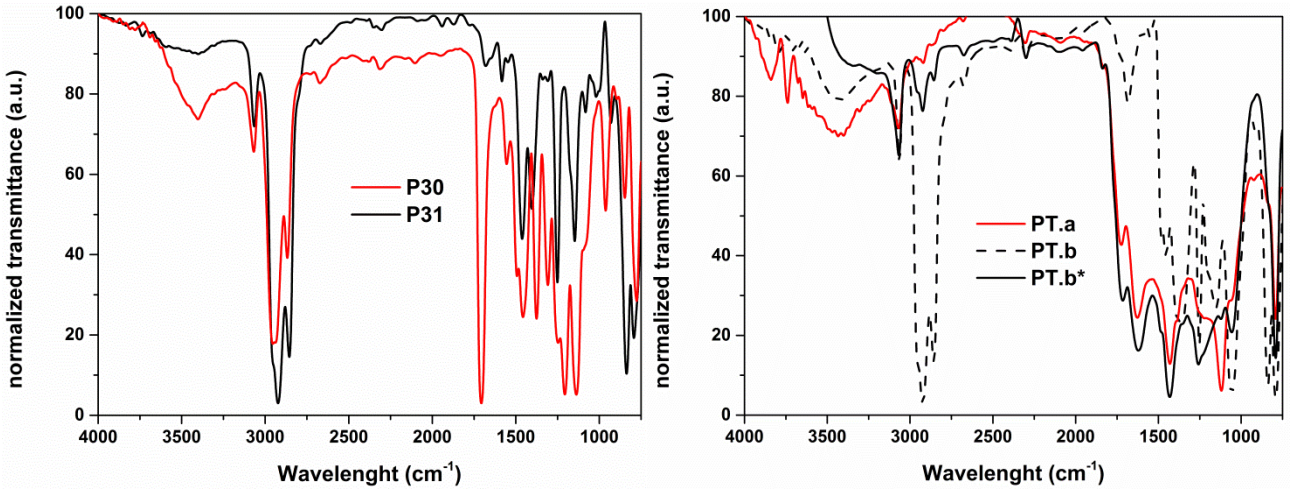

Figure 5.5. *FTIR spectra of* ***P30*** *and* ***P31*** *films (left) and their cleaved derivatives (right).*

In addition, to the previous results Fourier transform infrared (FTIR) spectra were recorded of the untreated and cleaved **P30** and **P31** on a KBr substrate (Figure 5.5). FTIR spectra of **P30** and **P31** show the characteristic bands for the C-H stretching vibration of the CH_2 chain remain still at 3000-2800 cm^{-1}. For **PT.a** the

characteristic absorption bands for ester moieties appeared at 1700 cm^{-1} for the C=O and at 1300 cm^{-1} for the C-O vibration. However, these C-H stretching vibration of the CH_2 chain disappear in the FTIR spectrum during the formation of **PT.a**. The two bands for the ester moieties decreased in their intensity after heating of the film at 300°C. During the thermal treatment the intensive broad band around 3500-3000 cm^{-1} intensified due to the formation of carboxylic acid which remained partly in the film upon complete cleavage. After treatment of **P31** with TCA an intensive broad band for Si-OH appeared around 3500-3000 cm^{-1}, this was ascribed to the presence of the TCA in the film. The characteristic bands for the C-H stretching vibration of the CH_2 chain remain still at 3000-2800 cm^{-1}. The removed side chains were retained in the polymer film, which is now clearly seen in the FTIR spectrum. However, after thermal annealing of the film at 300°C for 3h, the vibration band for CH_2 at 3000-2800 cm^{-1} and the intensive broad band for Si-OH around 3500-3000 cm^{-1} disappeared. The spectra of **PT.a** and **PT.b*** appeared now very similar.

5.3. Conclusion

In this chapter insoluble polythiophenes were prepared from different precursors and compared in terms of their properties. **P30** was cleaved by thermal treatment at 300°C yielding **PT.a**. **P31** was cleaved at room temperature by acid treatment pre-film formation in the polymer solution, yielding **PT.b**. AFM analysis showed different roughness of rather similar morphology of the cleaved polymer blends. The UV-vis absorption spectra of the two cleaved polymer films were slightly shifted, which changed by annealing of **PT.b**, to be similar to **PT.a**. FTIR measurments showed that the **PT.b** film retained the cleaved side chains which could be removed by thermal annealing at 300°C to result in a polymer film (**PT.b***) with similar FTIR transmission. Based on AFM scans, UV-vis and FTIR measurements, it was found that the two cleaved polymers were not identical. This was confirmed by simply comparing the images of the two polymer films. Annealing of **PT.b** at 300°C changed the properties to be similar to **PT.a**. These differences in morphology and remaining TCA and cleaved side chain could be reasons why acid cleavable polymers failed to be applied in (RC) PSCs. Once again a thermal treatment at high temperature does not make the polymers suitable for (RC) PSCs. The preliminary aim of the approach to use cleavable side chains was to improve the stability of the polymers and PSCs, respectively. These results show that this approach seems not suitable for RC PSCs in comparison to the potential of the approach described in Chapter 4, the modification of polymer side chains.

5.4. References

1. Rumer, J. W.; McCulloch, I. Organic photovoltaics: Crosslinking for optimal morphology and stability. *Mater. Today* **2015**, *18*, 425–435.

2. Liu, J.; Kadnikova, E. N.; Liu, Y.; McGehee, M. D.; Fréchet, J. M. J. Polythiophene containing thermally removable solubilizing groups enhances the interface and the performance of polymer-titania hybrid solar cells. *J. Am. Chem. Soc.*

2004, *126*, 9486–9487.

3. Krebs, F. C.; Spanggaard, H. Significant Improvement of Polymer Solar Cell Stability \dagger. *Chem. Mater.* **2005**, *17*, 5235–5237.

4. Tromholt, T.; Gevorgyan, S. a; Jørgensen, M.; Krebs, F. C.; Sylvester-Hvid, K. O. Thermocleavable materials for polymer solar cells with high open circuit voltage-a comparative study. *ACS Appl. Mater. Interfaces* **2009**, *1*, 2768–2777.

5. Manceau, M.; Helgesen, M.; Krebs, F. C. Thermo-cleavable polymers: Materials with enhanced photochemical stability. *Polym. Degrad. Stab.* **2010**, *95*, 2666–2669.

6. Bundgaard, E.; Hagemann, O.; Bjerring, M.; Nielsen, N. C.; Andreasen, J. W.; Andreasen, B.; Krebs, F. C. Removal of Solubilizing Side Chains at Low Temperature: A New Route to Native Poly(thiophene). *Macromolecules* **2012**, *45*, 3644–3646.

7. Petersen, M. H.; Gevorgyan, S. A.; Krebs, F. C. Thermocleavable Low Band Gap Polymers and Solar Cells Therefrom with Remarkable Stability toward Oxygen. *Macromolecules* **2008**, *41*, 8986–8994.

8. Brusso, J. L.; Lilliedal, M. R.; Holdcroft, S. π-Conjugated polymers with thermocleavable substituents for use as active layers in organic photovoltaics. *Polym. Chem.* **2011**, *2*, 175.

9. Gevorgyan, S. A.; Krebs, F. C. Bulk Heterojunctions Based on Native Polythiophene. *Chem. Mater.* **2008**, *20*, 4386–4390.

10. Helgesen, M.; Carlé, J. E.; Andreasen, B.; Hösel, M.; Norrman, K.; Søndergaard, R.; Krebs, F. C. Rapid flash annealing of thermally reactive copolymers in a roll-to-roll process for polymer solar cells. *Polym. Chem.* **2012**, *3*, 2649–2655.

11. Toušek, J.; Toušková, J.; Ludvík, J.; Liška, A.; Remeš, Z.; Kylián, O.; Kousal, J.; Chomutová, R.; Heckler, I. M.; Bundgaard, E.; Krebs, F. C. Comparison of the electron work function, hole concentration and exciton diffusion length for P3HT and PT prepared by thermal or acid cleavage. *Solid. State. Electron.* **2016**, *116*, 111–118.

12. Al-Ibrahim, M.; Roth, H. K.; Zhokhavets, U.; Gobsch, G.; Sensfuss, S. Flexible large area polymer solar cells based on poly(3-hexylthiophene)/ fullerene. *Sol. Energy Mater. Sol. Cells* **2005**, *85*, 13–20.

13. Carlé, J. E.; Helgesen, M.; Zawacka, N. K.; Madsen, M. V.; Bundgaard, E.; Krebs, F. C. A comparative study of fluorine substituents for enhanced stability of flexible and ITO-free high-performance polymer solar cells. *J. Polym. Sci. Part B Polym. Phys.* **2014**, *52*, 893–899.

Chapter 6.

Conclusion and Outlook

In this work different light absorbing polymers were synthezized and applied in fully solution processed polymer solar cells. 104 polymers were screened for their ability to be applied in roll-coated devices. The work illustrated the challenge to find candidates with a high performance. Elimination during the screening process using different criteria (synthetic steps, coating and efficiency) yielded a few candidates with efficiencies of >1%, which were found to be suitable for this technology.

In another attempt polymers based on benzo[*c*][1,2,5]thiadiazole and thiophene were synthezised and applied in polymer solar cells due to their high efficiencies in literature. The polymers showed that with an increasing amount of thiophenes, the band gaps as well as the photodegradation of these polymers approximate the ones of poly(3-hexylthiophene).

Hereafter three candidates from the polymer screening based on benzo[*c*][1,2,5]thiadiazole, thiazolo[4,5,*d*]thiazole and benzo[1,2-*b*:4,5-*b*']dithiophene, respectively, were adopted and partly modified with new stabilizing side chains to influence the solar cell performance and stability. As the modifications showed different influences on the efficiency and stability of the polymers and polymer solar cells, no clear design rules, can be proposed. However, engineering of the side chain can be a powerful tool to influence the properties and stability of solar cell devices.

In the last chapter, efforts using side chain cleavage to improve the solar cell stability were investigated further and surveyed for the use in roll-coated polymer solar cells. Insoluble polythiophenes were prepared from thermal and acid cleavable precursors. Different analysis showed that the two cleaved polymers were not identical. The acid cleaved polymer film showed the same results once it was also treated at the same temperature as the thermal cleaved film.

This thesis demonstrates that conjugated polymers can be crucial in terms of their application in roll-coated solar cells which requires additional considerations than when using common laboratory approach spin-coating. Finding a few candidates which seem to be suitable is just *one drop in the ocean*. Further improvements of these candidates by a side chain variation or even finding a better candidate by other polymer screenings could be a new challenge. Furthermore, specific optimization of the coating parameters or even the use of additives in the coating solution, are successful tools to further improve the device performance. This shows that it could be possible to find the right candidates with good performances to be used in large scale devices for different applications approaching the market. However, ongoing competition with similar technologies in the field makes the polymer solar cell technology more to be used in a niche market, as another limited factor is the stability and thus the lifetime of the devices. Therefore, one approach to improve the stability of polymer solar cells might be using the right combination of solubility and stabilizing side chain within the right backbone. This can lead to an increase of the photo- and thermal stability by trying different types of stabilizing side chains as well as different ratios of the side chains, whereas the approach of cleavable polymers for roll-coated devices seems not suitable.

Further investigations on the influence of the stability of the side chains in promising polymers could give a better understanding of the polymer degradation within a device to be able to foresee their upscaling opportunities in terms of their device lifetime.

Appendix A

Methods and Materials

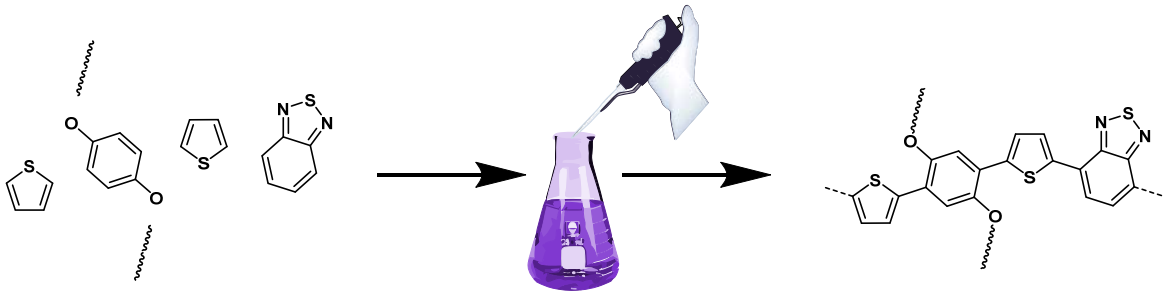

General

Unless stated otherwise, all reagents, chemicals and solvents were obtained from Sigma-Aldrich and used as received. N-bromosuccinimid (NBS) was recrystallized from water before usage. $PC_{61}BM$ (PV-A600) was purchased from Merck Chemicals (RC) and Sollenne (SC), while PEDOT:PSS (Orgacon EL-P 5010) was obtained from Agfa (RC, Chapter 2, 4) or CLEVIOS (RC, Chapter 3 and SC Chapter 4) from Heraeus. Thermally-curable Ag (PV-410) was received from DuPont, and UV-curable adhesive (DELO, Katiobond LP 655) was from DELO. Ca and Al were acquired from Alpha Aesar and Kurt J. Lesker, respectively. The flextrode substrate was produced in house according to literature [1] (Chapter 2 and 4) or received from infinityPV (Chapter 3). ITO coated glass substrates were received from Kintec (100 nm, 20 Ohm/sq). Column chromatography was carried out using silica gel in technical grades (60 Å, 70-230 mesh). *Preparative (recycling) size exclusion chromatography (recycling SEC)* was performed on a JAI LC-9110 NEXT system equipped with JAIGEL 1*H*, 2*H* and 3*H* columns (eluent CF, flow rate 3.5 mL min^{-1}).

Characterization Techniques

Monomer and Polymer Characterization

^{1}H and ^{13}C *NMR spectroscopy* (spectra see Appendix A) was performed on the samples in $CDCl_3$, dimethylsulfoxide (DMSO)-d_6 or ODCB-d_4 on a 500 MHz (Bruker) a 400 MHz (Varian Inova 400) or a 300 MHz (Varian Inova 300) spectrometer.

Analytical Size Exclusion Chromatography (SEC) was performed on a KNAUER chromatograph or on Spectra Series P100. The SEC using the KNAUER chromatograph was used in HPLC-grade CF or CB at room temperature employing 2 gel columns in succession with respective pore diameters of 104 Å and 105 Å. Both

gel columns had dimensions of 25 mm x 600 mm. A refractive index detector and two diode arrays UV-vis detectors (Smartline UV detector 2600) were used for analysis. The Spectra Series P100 (Spectra Physics) pump was equipped with two mixed-B columns (10 µm, 2 cm x 30 cm, Polymer Laboratories) and an Agilent 1100 DAD UV detector oparated at 60 °C. CB was used as the eluent at a flow rate of 1.0 mL min^{-1}. M_n were determined with a UV detection at λ_{max} of the polymer and relative to PS standards.

The UV-vis spectra were recorded on a Schimatzu UV-3600 Spectrophotometer or on an Agilent Technologies Cary 5000 UV-vis-NIR spectrophotometer. UV-vis spectra were obtained from CF or CB solutions and SC films on glass slides. The polymers with very low solubility (in Chapter 2 and 3) were dissolved in ODCB. Solutions of polymers were prepared and stirred at 70 ^oC overnight. The concentration of the solutions was 10 or 20 mg mL^{-1} in CF/CB/ODCB. A film was SC from the solutions and then diluted to a concentration of 0.01 or 0.02 mg mL^{-1}. The absorbance was plotted as a function of the wavelength. E_g was calculated from the offset in the absorbance spectra as described in the literature [2].

Fourier transform infra-red (FTIR) spectroscopy was performed on a Perkin Elmer Spectrum One FTIR Spectrometer of the polymer films (Chapter 5) on IR sample cards (KBr). A few drops of a solution of the to investigate polymer in CB was added with a pipet on the sample cards.

Atomic force microscopy (AFM) was measured of the morphology of the active layer (Chapter 5). Measurements were performed in the semi-contact mode using NSC-17 silicon cantilevers (Schaefer Technologie, GmbH) by means of Quesant Q-scope AFM (scan rate 2 Hz, resolution 512 X 512 points). The active layers were prepared by SC of polymer/$PC_{61}BM$ solution on ITO/glass substrates as described in literature including the cleavage of the side chain [3,4].

Cyclic Voltammetry (CV) and *Square Wave Voltammetry (SWV)* were either performed on CH Instruments Model 650A Potentiostat/Galvanostat Electrochemical Workstation or on an Autolab PGSTAT30 potentiostat from Metrohm using the GPES software (version 4.9). The measurements were carried out in a three electrode one compartment microcell at room temperature using a platinum wire working electrode, a platinum wire counter electrode, a $Ag/AgNO_3$ reference electrode (0.01 M $AgNO_3$) and 0.1 M NBu_4PF_6 in anhydrous acetonitrile as electrolyte. A constant flow of Argon allows purging and blanketing of the electrolyte prior to and during analysis. For solid state voltammetry of films, the polymer samples were dissolved in CF. The HOMO energy levels of the products were estimated using the onset potential of the first oxidation-reduction peak in the obtained CV curve. Ferrocene was used as an external standard and calculated according to literature [5,6].

Differential scanning calorimetry was performed on a prototype TA Instruments Rapid-Heat-Cool (RHC) instrument using a liquid nitrogen cooling system which was purged with helium (12 mL min^{-1}). The RHC cell

was heated by four quartz halogen lamps. The samples (~0.25 mg) were enclosed in dedicated non-hermetical aluminium crucibles and lids [7,8].

The photochemical stability of the polymer films were prepared by SC (and used for UV-vis measurements) on glass slides and analysed using the setup described in Figure A.1 [9], which uses a Steuernagel solar simulator with an Osram 1200-W metal halide arc lamp that approximately provides an AM 1.5 spectrum (1000 W/m^2). An optical fiber-based CCD spectrometer (Avantes AvaSpec 1024) and a UV–vis spectroscopic probe based on a halogen/deuterium light source (AvantesAvaLight-DHc) were used to measure the absorbance of the polymer films.

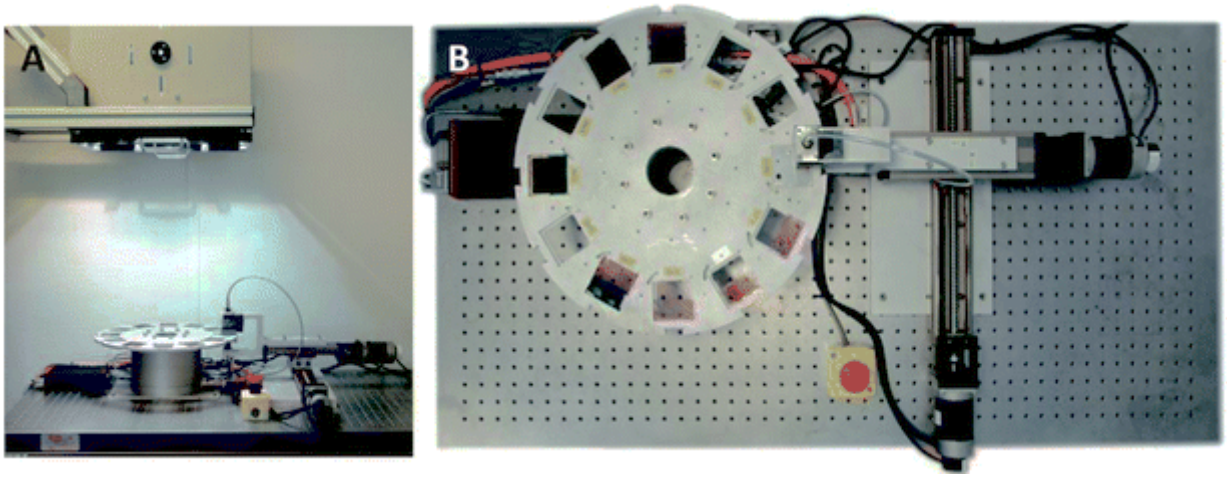

Figure A.1. *Side (left) and top (right) view of the photochemical degradation setup.* [9] - *Reproduced by permission of The Royal Society of Chemistry.*

Solar Cell Characterization

The *J-V characteristics* of the PSCs were analysed under a KHS 575 solar simulator with 1000 W/m^2 and AM 1.5 conditions using a Keithley (2400 SMU) source meter or under a Newport class A solar simulator (model 91195A), calibrated with a Si solar cell to give an AM 1.5 spectrum.

The area of the PSCs were studied using a *Light Beam Induced Current (LBIC)* technique described in literature [10] or on a LBIC Economy from infinityPV to estimate the correct area of the devices. However, for the large amount of polymers from Chapter 2 a mask with an area of 0.526 cm^2 was used for all measurements in order to have the same active area.

The *optical microscopy* images from the active layer (Chapter 4) were taken with an Axioskop from Zeiss.

The *external quantum efficiency (EQE)* measurements were carried out on a system from PV Measurements Inc. at 10 nm intervals between 300 and 800 nm. A calibrated Si cell was used before the experiment as a reference.

Transmission electron microscopy (TEM) measurements (Chapter 4) were performed on a FEI Tecnai Spirit using an accelerating voltage of 120 kV. TEM samples were prepared from pristine devices or from the devices utilized in the automated degradation chamber. By washing away the PEDOT:PSS layer with water, freestanding films were obtained.

ISOS-L-1 lifetime experiments [11] were performed using a solar simulator with AM 1.5 (1000 W/m^2) conditions. The *J-V* curve tracing of the PSCs was performed using an automated acquisition setup with a Keithley 2400 SMU.

ISOS-D-2 degradation experiments [11] were performed on PSCs positioned in an automated degradation chamber or on a hotplate (280 x 200 mm, type PZ28-2ET, Harry Gestigkeit GmbH, with a PR5 programmer controller) in nitrogen atmosphere (glovebox) at a constant temperature of 85 °C. In the automated setup the *J-V* characteristics were first measured every 30 minutes, and at a later stage every hour, using a White 5500 K LED (Lamina, with a maximum illumination of 0.53 sun). During the degradation tests on the hotplate, the *J-V* characteristics were measured manually at specific time intervals using a Newport class A solar simulator (model 91195A, calibrated with a Si cell, AM 1.5).

Synthesis

General Procedures

Bromination (with NBS)

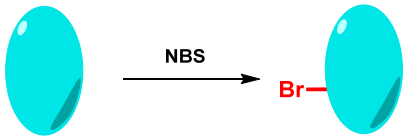

Scheme A.1. *Schematic drawing of the bromination with NBS.*

NBS was added to a solution of a compound in THF similar to literature procedure [2,12,13]. The mixture was stirred at room temperature. The reaction process was monitored by thin layer chromatography and stopped after complete conversion. To the reaction mixture was added water, and then the organic phase was washed twice with water. The organic phase was then dried with $MgSO_4$ and the solvent was removed under reduced pressure. The crude product was purified by column chromatography or recrystallization.

For the mono-bromination 1 equivalent (eq.) of the compound and 1 eq. of NBS were used.

For the di-bromination 1 eq. of the compound and 2.01 eq. of NBS were used.

Stannylation

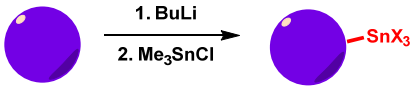

Scheme A.2. *Schematic drawing of the stannylation reaction.*

General procedure for the stannylation reactions [14–16]. To a solution of the non-stannylated compound in dry THF, BuLi (2.5 M in hexane) was added at -78 °C and the solution was stirred for 1 h. The temperature was slowly raised to room temperature and the solution was stirred for 20 min to 1 h. Afterwards, the reaction mixture was cooled down to -78°C again and Me_3SnCl (1.0 M in hexane or dissolved the corresponding amount in dry THF) was added. After the cooling bath was removed, the mixture was stirred for another 2 h. Water was added, the phases were separated and the organic phase was washed multiple times with water, dried over $MgSO_4$, filtered, and the solvent was removed under reduced pressure. The crude product was washed with MeOH to remove residual unreacted Sn-compounds.

For the mono-stannylation 1 eq. of the compound, 1.2-1.5 eq. of BuLi and 1.5-1.7 eq. of Me_3SnCl were used.

For the bis-stannylation 1 eq. of the compound, 3-4 eq. of BuLi and 3.5-5 eq. of Me_3SnCl were used.

Kumada Coupling

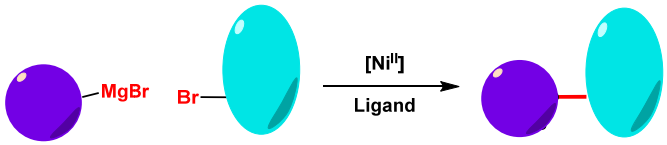

Scheme A.3*. Schematic drawing of the Kumada Coupling.*

A general Kumada coupling was performed in two steps [17]. In the first step the alkyl magnesium bromide (●–MgBr) was prepared in a Grignard reaction. To Mg (1.33 eq.) in a three-neck flask covered with diethyl ether was added dropwise the alkyl bromide (1.22 eq.) in diethyl ether with a speed that there was an ongoing reaction. To initiate the reaction, a few drops of 1,2-dibromoethane were used. If higher reaction temperature is needed (due to a slow reacting alkyl bromide) the solvent was changed to THF. After complete addition of the alkyl bromide, the reaction mixture was heated under reflux for 2h. In the second step, to [1,3-bis(diphenylphosphino)propane] dichloronickel(II) ($Ni(dppp)Cl_2$, 0.01 eq.) in a three-neck flask covered with an excess of diethyl ether was added dropwise a solution of an aromatic bromide (1 eq.).

Thereafter ●–MgBr solution from the first step was added *via* a cannula. The reaction mixture was heated under reflux overnight. At the next day the reaction mixture was cooled down and water was added. The water phase was first extracted twice with diethyl ether, and then the organic phase was washed twice with water and once with a 1 M sodium chloride solution. The combined organic phases were dried with $MgSO_4$ and the solvent was removed under reduced pressure. The crude product was purified by column chromatography.

Stille cross-coupling

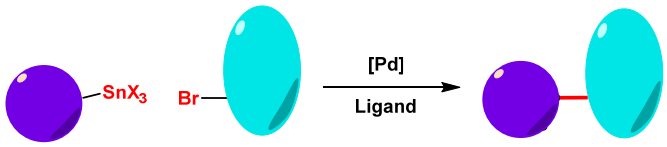

Scheme A.4. *Schematic drawing of the Stille cross-coupling.*

In a general procedure for the Stille cross-coupling [16,18] mono- or di-brominated reagent and mono- or bis-stannylated co-reagent were dissolved in anhydrous toluene in an 8 mL vial or a small round bottom flask connected to a reflux cooler under nitrogen. Then, 0.03-0.05 eq. of tris(dibenzylideneacetone)dipalladium(0) and 0.09-0.18 eq. of tris(o-tolyl)phosphine were added before the mixture was heated for at least 20 h at 110°C. The raw product solution was filtrated over celite using e.g. CF, the solvent was then removed under reduced pressure before the product was purified further.

For the mono-coupling 1-2.5 eq. of the di-brominated compound and 1 eq. of the mono-stannylated compound were used.

For the di-coupling 1 eq. of the di-brominated compound and 2.4-3 eq. of the mono-stannylated compound were used.

Chapter 2

All monomers (**M1-M21**) were prepared according to the literature procedures [2,19–39]. Exceptions are the monomers **M19** and **M21**, which were purchased from Lumtec, and **M1**, which was purchased from Sigma Aldrich. As the synthesis was not part of this work, it is therefore not described further.

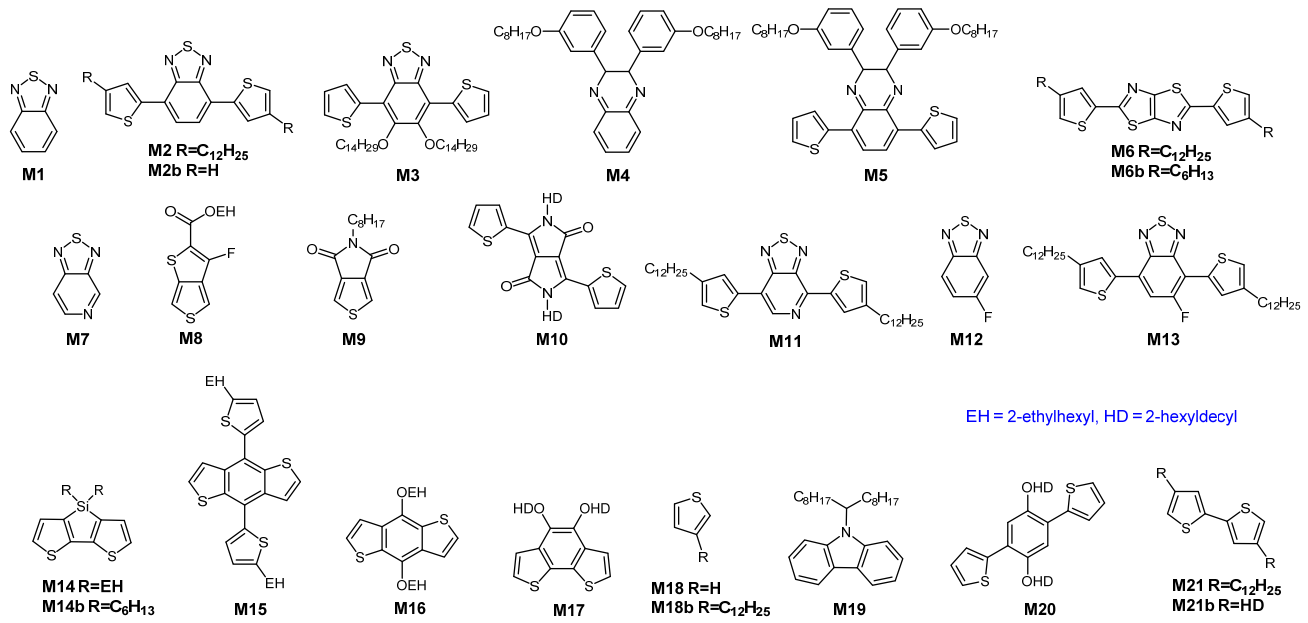

Figure A.2. *Molecule structures of* ***M1-M21****.*

Chapter 3

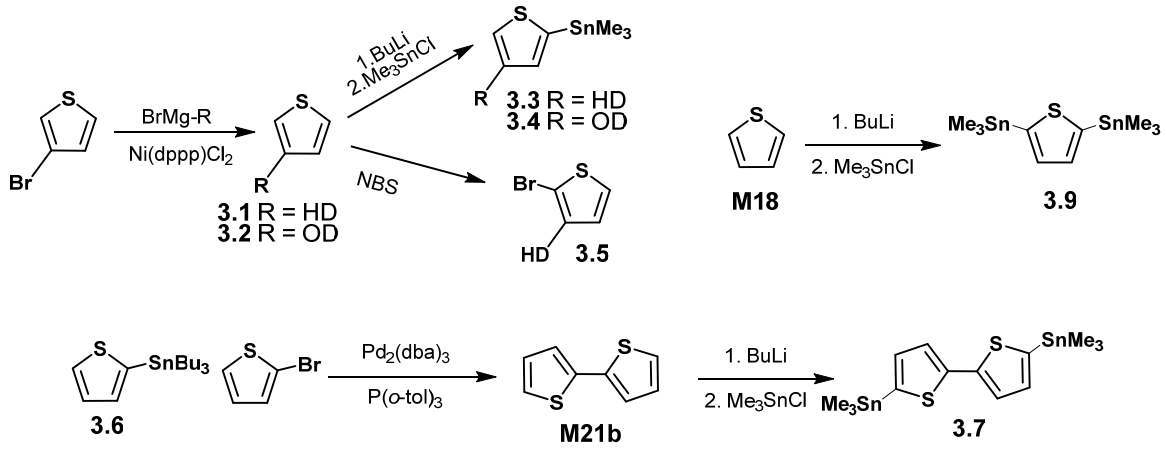

Scheme A.5*. Synthesis of* ***3.3-3.5, 3.7*** *and* ***3.9****.*

Trimethyl(4-(2-hexyldecyl)thiophen-2-yl)stannane (**3.3**), trimethyl(4-(2-octyldodecyl)thiophen-2-yl)stannane (**3.4**), 2-bromo-3-methylthiophene (**3.5**), 5,5'-Bis(trimethylstannyl)-2,2'-bithiophene (**3.7**) and 2,5-Bis(trimethylstannyl)thiophene (**3.9**) were synthesized adapted from various [13,17,40–43].

Trimethyl(4-(2-hexyldecyl)thiophen-2-yl)stannane (**3.3**): ^{1}H NMR ($CDCl_3$, 500 MHz) δ (ppm): 0.39 (s, 9H) 0.92-1.95 (m, 6H), 1.30-1.34 (m, 24H), 1.65-1.67 (m, 1H), 2.63 (d, *J* = 6.8 Hz, 2H), 7.00 (s, 1H), 7.18 (s, 1H),

Trimethyl(4-(2-octyldodecyl)thiophen-2-yl)stannane (**3.4**): ^{1}H NMR ($CDCl_3$, 500 MHz) δ (ppm): 0.37 (s, 9H), 0.90 (t, *J* = 6.9 Hz, 6H), 1.25 – 1.33 (m, 32H), 1.59 – 1.67 (m, 1H), 2.60 (d, *J* = 6.7 Hz, 2H), 6.97 (d, *J* = 1.0 Hz, 1H), 7.17 (d, *J* = 0.9 Hz, 1H).

2-Bromo-3-methylthiophene (**3.5**): ^{1}H NMR ($CDCl_3$, 500 MHz) δ (ppm): 0.87 – 0.90 (m, 12H), 1.22-1.31 (m, 24H), 1.63 (m, 1H), 2.49 (d, *J* = 7.1 Hz, 2H), 6.76 (d, *J* = 5.5 Hz, 1H), 7.17 (d, *J* = 5.6 Hz, 1H).

5,5'-Bis(trimethylstannyl)-2,2'-bithiophene (**3.7**): ^{1}H NMR ($CDCl_3$, 500 MHz) δ (ppm): 0.38 (s, 18H), 7.08 (d, *J* = 3.3 Hz, 2H), 7.27 (d, *J* = 3.3 Hz, 2H). ^{13}C NMR ($CDCl_3$, 126 MHz) δ: -8.0, 125.0, 136.0, 137.2, 143.2.

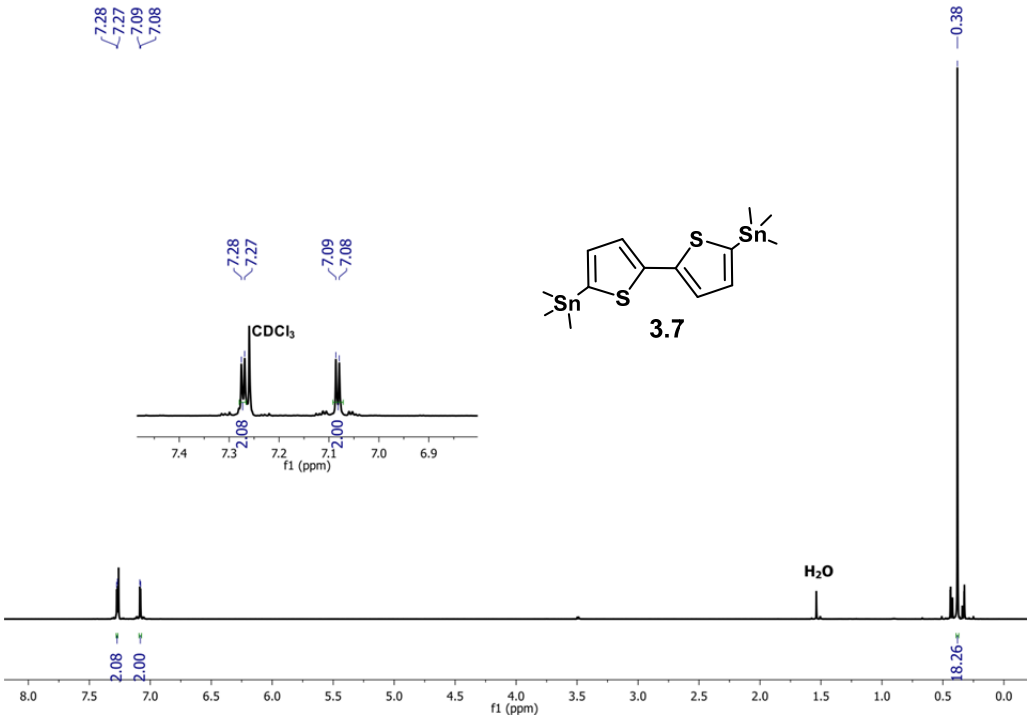

Figure A.3 *^{1}H NMR spectrum of compound **3.7** in $CDCl_3$.*

2,5-Bis(trimethylstannyl)thiophene (**3.9**). ^{1}H NMR ($CDCl_3$, 500 MHz) δ (ppm): 0.39 (s, 18H), 7.40 (s, 2H). ^{13}C NMR ($CDCl_3$, 126 MHz) δ: -8.0, 135.9, 143.1.

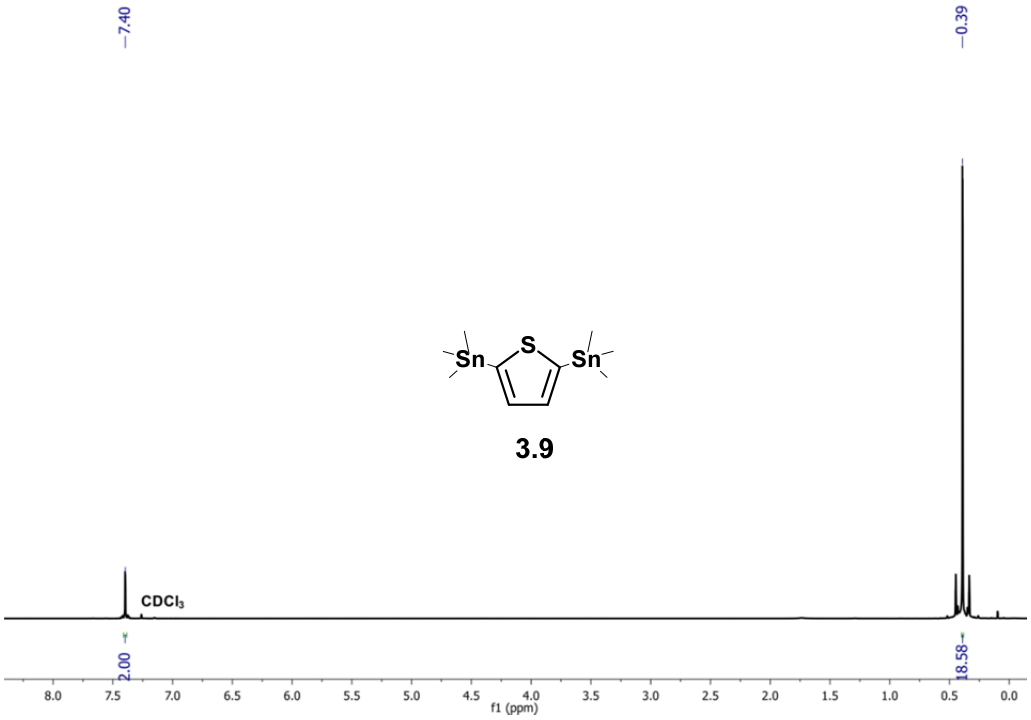

***Figure A.4**. [1]H NMR spectrum of compound **3.9** in $CDCl_3$.*

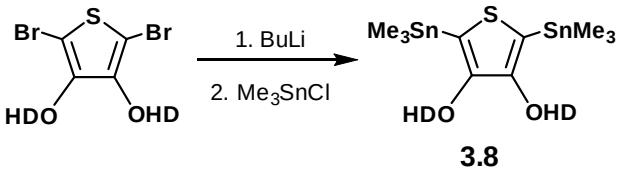

***Scheme A.6**. Synthesis of **3.8**.*

(3,4-di(2-hexyldecyloxy)thiophene-2,5-diyl)bis(trimethylstannane) (3.8): 2,5-dibromo-3,4-dimethoxy thiophene was synthesized first according to a literature procedure [44]. The bis-stannylation was performed according to the general procedure. Di-brominated compound (0.57 g, 1.0 mmol) in THF (30 mL), BuLi in hexane (2.0 mL, 5.0 mmol) and Me3SnCl (1.2 mL, 6.0 mmol): After washing the crude product with methanol, 3.8 was obtained (0.48 g, 54%). 1H NMR (CDCl3, 500 MHz) δ (ppm): 0.34 (s, 18H), 0.87–0.89 (m, 12H), 1.26–1.32 (m, 40H), 1.40–1.49 (m, 8H), 1.72–1.77 (m, 2H), 3.81 (d, J = 6.34 Hz, 2H). 13C NMR (CDCl3, 126 MHz) δ: -7.6, 14.3, 22.7, 22.9, 27.1, 27.2, 29.6, 29.8, 30.0, 30.3, 31.6, 32.1, 32.1, 39.2, 76.7, 123.1, 157.0.

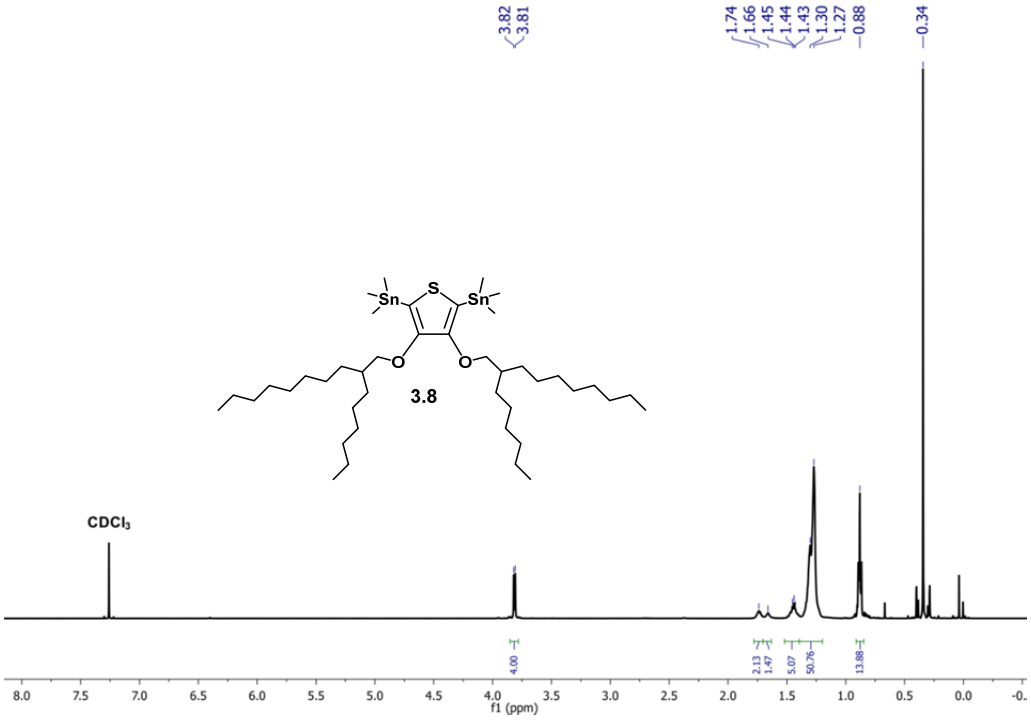

Figure A.5. *^{1}H NMR spectrum of compound **3.8** in $CDCl_3$.*

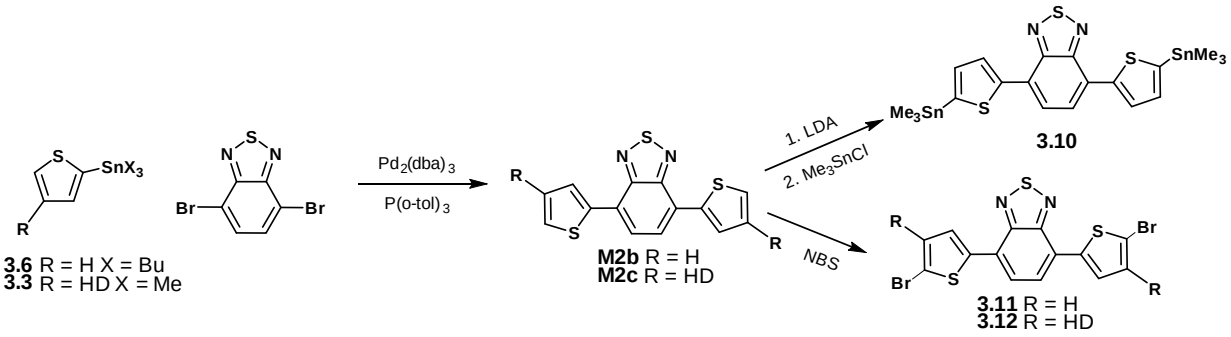

Scheme A.7. *Synthesis and stannylation/bromination of **M2b** and **M2c**.*

4,7-di(thiophen-2-yl)benzo[*c*][1,2,5]thiadiazole (**M2b**)*:* A general Stille cross-coupling reaction [26,45] was performed of the both commercially available **3.6** (3.2 mL. 10.0 mmol) and benzo[*c*][1,2,5]thiadiazole (1.2 g. 4.1 mmol) according to the general procedure. Recrystallization from ethanol yielded a dark orange solid (1.21 g, 98%). ^{1}H NMR ($CDCl_3$, 500 MHz) δ: 7.22 (dd, J = 5.1, 3.7 Hz, 2H), 7.46 (dd, J = 1.1, 5.1 Hz, 2H), 7.78 (s, 2H), 8.12 (dd, J = 1.1, 3.7 Hz, 2H). ^{13}C NMR ($CDCl_3$, 126 MHz) δ: 125.8, 126.0, 126.8, 127.5, 128.0, 139.4, 152.7.

4,7-bis(4-(2-hexyldecyl)thiophen-2-yl)benzo[*c*][1,2,5]thiadiazole (**M2c**)*:* A general Stille cross-coupling reaction [26,45] was performed of **3.3** (4.1 g. 10.0 mmol) and commercially available benzo[*c*][1,2,5]thiadiazole (1.22 g. 4.2 mmol) according to the general procedure in 50 mL toluene. The crude product was purified with column chromatography using hexane/CF (8.3/2) as an eluent yielding an

orange solid (1.5 g, 48%). ^{1}H NMR ($CDCl_3$, 500 MHz) δ: 0.85–0.89 (m, 12H), 1.26–1.31 (m, 48H), 1.68–1.72 (m, 2H), 2.63 (d, *J* = 6.76 Hz, 4H) 7.01 (d, J = 1.3 Hz, 2H), 7.83 (s, 2H), 7.95 (1.4 Hz, 2H). ^{13}C NMR ($CDCl_3$, 126 MHz) δ: 14.1, 22.7, 22.7, 26.6, 26.7, 29.4, 29. 7, 29.7, 30.1, 31.9, 33.4, 33.4, 35.1, 38.9, 122.5, 125.5, 126.0, 129.5, 138.8, 143.1, 152.7.

4,7-bis(5-(trimethylstannyl)thiophen-2-yl)benzo[c][1,2,5]thiadiazole (**3.10**). The bis-stannylation was performed similar to the general procedure [45]. **M2b** (1.8 g, 6.0 mmol) was dissolved in THF (100 mL). Lithium diisopropylamide in THF (3.0 eq., 18.0 mmol) and Me_3SnCl (4.2 g, 21 mmol) were added stepwise at -78°C according to the general procedure. The crude product was recrystallized from hexane/CF. ^{1}H NMR (CDCl3, 500 MHz) δ (ppm): 0.45 (s, 18H), 7.30 (d, J = 3.4 Hz, 2H), 7.86 (s, 2H), 8.19 (d, J = 3.5 Hz, 2H). ^{13}C NMR ($CDCl_3$, 126 MHz) δ: -8.0, 125.9, 126.0, 128.5, 136.2, 140.4, 145.2, 152.8.

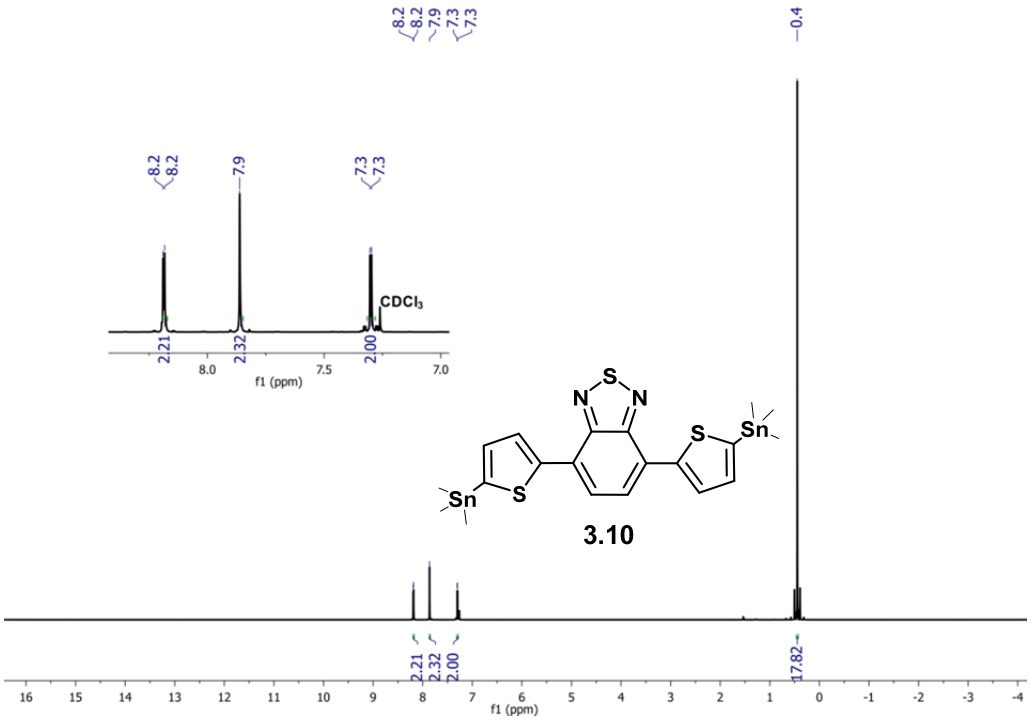

Figure A.6. *^{1}H NMR spectrum of compound **3.10** in $CDCl_3$.*

4,7-bis(5-bromothiophen-2-yl)benzo[*c*][1,2,5]thiadiazole (**3.11**). A general di-bromination was performed [26]. NBS (1.3 g, 7.2 mmol) was added to a solution of **M2b** (1.1 g, 3.6 mmol) in THF (20 mL) and stirred for 3h. A dark red solid precipitated, which was then recrystallized from CF (29.2 mg, 44%). ^{1}H NMR (ODCB-d_4, 400 MHz) δ (ppm): 7.21 (d, J = 4.0 Hz, 2H), 7.72 (s, 2H), 7.87 (d, J = 4.0 Hz, 2H). ^{13}C NMR (ODCB-d_4, 126 MHz) δ (ppm): 114.7, 124.6, 125.0, 130.6, 140.6, 151.8.

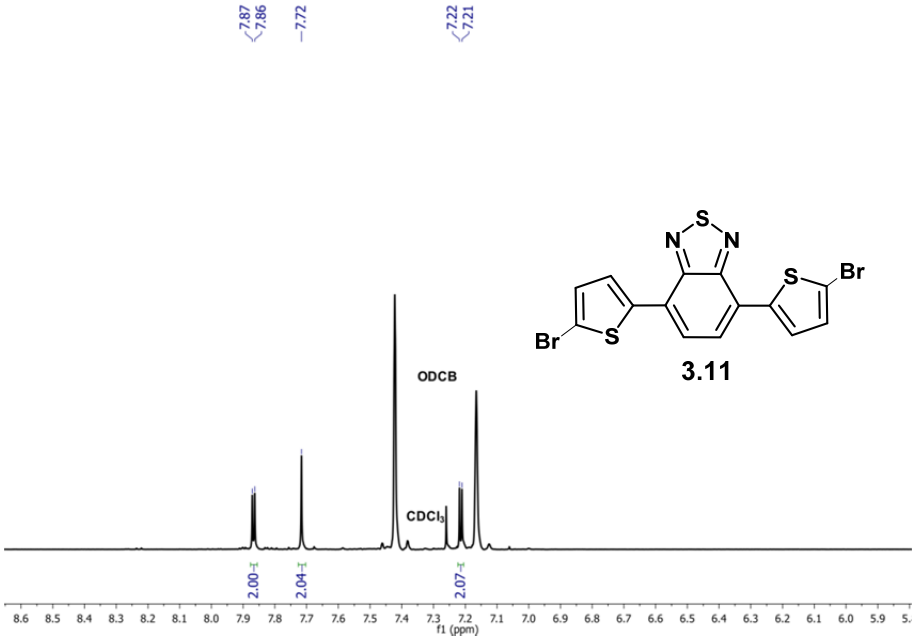

Figure A.7. *^{1}H NMR spectrum of compound **3.11** in ODCB-d_4.*

4,7-bis(5-bromo-4-(2-hexyldecyl)thiophen-2-yl)benzo[*c*][1,2,5]thiadiazole (**3.12**). A general di-bromination was performed [26]. NBS (0.93 g, 5.23 mmol) was added to a solution of **M2c** (1.95 g, 2.60 mmol) in THF (100 mL). The crude product was purified by recrystallization from hexane, affording a red solid (2.4 g, >99%). ^{1}H NMR ($CDCl_3$, 500 MHz) δ (ppm): 0.85–0.89 (m, 12H), 1.25–1.33 (m, 48H), 1.74–1.78 (m, 2H), 2.57 (d, *J* = 7.13 Hz, 4H), 7.78 (s, 2H), 7.78 (s, 2H). ^{13}C NMR ($CDCl_3$, 126 MHz) δ: 14.1, 22.7, 22.7, 26.6, 26.6, 29. 7, 29.7, 30.0, 31.9, 33.4, 33.5, 34.3, 38.6, 112.24, 124.85, 125.4, 128.71, 138.30,142.8, 152.3.

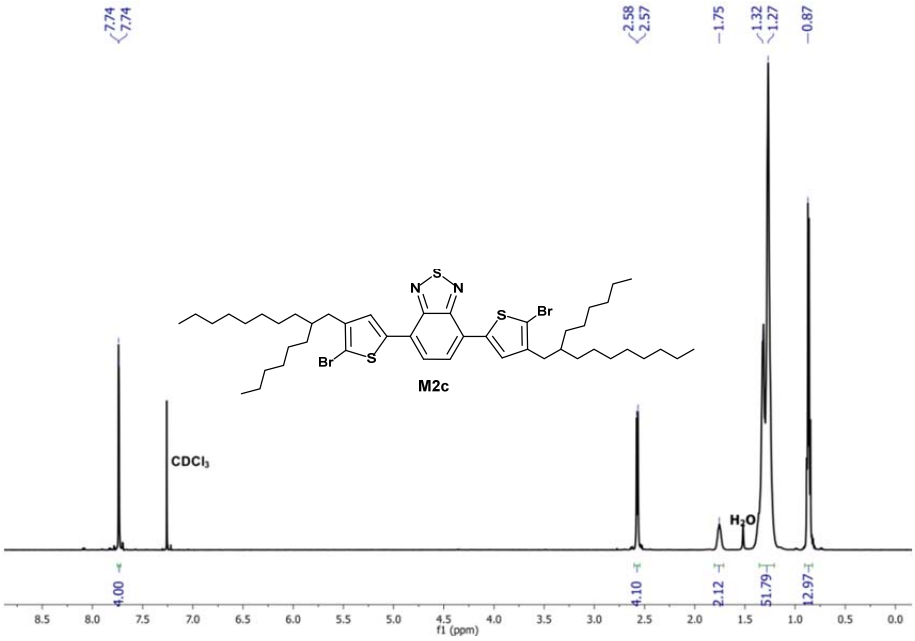

Figure A.8. *^{1}H NMR spectrum of compound **3.12** in $CDCl_3$.*

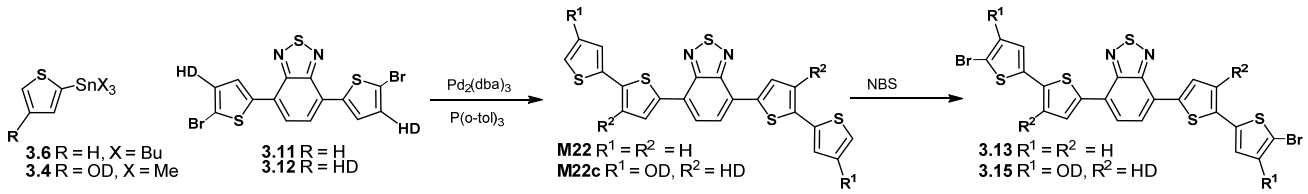

Scheme A.8**. Synthesis and bromination of **M22** and **M22c [13].

4,7-di(2,2'-bithiophen]-5-yl)benzo[*c*][1,2,5]thiadiazole (**M22**)*:* A general Stille cross-coupling reaction was performed [13] of **3.11** (0.59 g, 2.0 mmol) and **3.6** (1.6 mL, 4.6 mmol) according to the general procedure. Recrystallization from chloroform yielded a dark red solid (400 mg, 43%). ^{1}H NMR ($CDCl_3$, 500 MHz) δ: 7.06–7.08 (m, 2H), 7.27–7.31 (m, 2H), 7.87 (s, 2H), 8.06 (d, *J* = 3.9 Hz, 2H). ^{13}C NMR (ODCB-d_4, 126 MHz) δ: 124.2, 124.7, 125.0, 125.1, 125.6, 128.3, 128.8, 137.6, 138.4, 139.0, 152.6.

4,7-bis(4'-(2-octyldodecyl)-3-(2-hexyldecyl)-[2,2'-bithiophen]-5-yl)benzo[*c*][1,2,5]thiadiazole (**M22c**)*:* A general Stille cross-coupling reaction was performed [13] of **3.12** (0.45 g. 0.5 mmol) and **3.4** (0.92 g. 1.75 mmol) in toluene (~20 mL) according to the general procedure. Column chromatography using hexane as an eluent yielded a red oil (605 mg, 82%). ^{1}H NMR ($CDCl_3$, 500 MHz) δ (ppm): 0.85–0.90 (m, 24H), 1.24–1.32 (m, 112H), 1.62–1.67 (m, 2H), 1.77–1.85 (m, 2H), 2.56 (d, *J* = 6.8 Hz, 4H), 2.78 (d, *J* = 7.2 Hz, 4H), 6.90 (s, 2H), 7.03 (s, 2H), 7.82 (s, 2H), 7.96 (s, 2H). ^{13}C NMR ($CDCl_3$, 126 MHz) δ: 14.3, 22.7, 26.6, 26.7, 26.9, 29.5, 29.8, 29.9, 29.9, 29.9, 30.2, 30.3, 32.1, 33.6, 33.6, 33.7, 34.2, 35.2, 39.0, 39.1, 121.4, 125.3, 125.7, 128.4, 131.4, 133.6, 135.6, 136.7, 139.7, 142.5, 152.8.

4,7-bis(5'-bromo-[2,2'-bithiophen]-5-yl)benzo[*c*][1,2,5]thiadiazole (**3.13**)*:* A general bromination was performed [13]. NBS (308 mg, 1.73 mmol) was added to a solution of **M22** (392 mg, 0.86 mmol) in THF (20 mL). Recrystallization from toluene yielded a dark red solid (410 mg, 77%). ^{1}H NMR (ODCB-d_4, 500 MHz) δ: 7.08 (d, *J* = 4.3 Hz, 2H), 7.12 (d, *J* = 4.2 Hz, 2H), 7.33 (d, *J* = 4.3 Hz, 2H), 7.88 (s, 2H), 8.22 (d, *J* = 4.3 Hz, 2H). ^{13}C NMR (ODCB-d_4, 126 MHz) δ: 111.4, 123.9, 124.7, 124.9, 125.3, 128.5, 130.9, 137.6, 138.6, 139.0, 152.2.

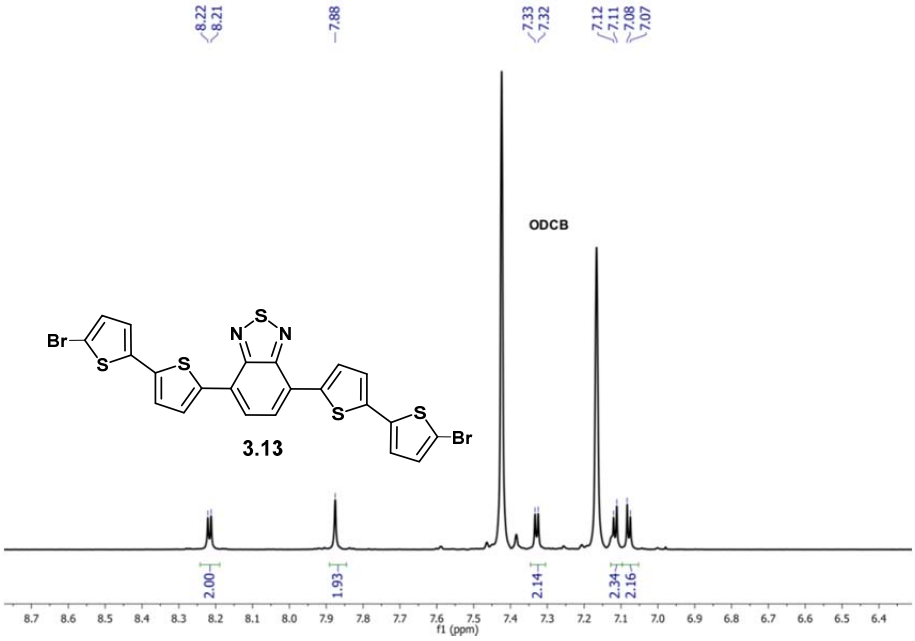

***Figure A.9**. [1]H NMR spectrum of compound **3.13** in ODCB-d_4.*

4,7-bis(5'-bromo-4'-(2-octyldodecyl)-3-(2-hexyldecyl)-[2,2'-bithiophen]-5-yl)benzo[*c*][1,2,5]thiadiazole (**3.15**)*:* A general bromination was performed [13]. NBS (147 mg, 0.82 mmol) was added to a solution of **M22c** (605 mg, 0.41 mmol) in THF (20 mL). Column chromatography using hexane as an eluent yielded a red oil (418.4 mg, 69%). ^{1}H NMR ($CDCl_3$, 500 MHz) δ (ppm): 0.84–0.89 (m, 24H), 1.24–1.31 (m, 112H), 1.67–1.73 (m, 2H), 1.75–1.79 (m, 2H), 2.51 (d, J = 7.1 Hz, 4H), 2.74 (d, J = 7.2 Hz, 4H), 6.88 (s, 2H), 7.82 (s, 2H), 7.94 (s, 2H), ^{13}C NMR ($CDCl_3$, 126 MHz) δ (ppm): 14.3, 14.3, 22.9, 26.7, 26.8, 29.5, 29.8, 29.8, 29.9, 29.9, 30.2, 30.2, 32.1, 33.6, 34.2, 34.4, 38.8, 39.1, 109.8, 125.4, 125.7, 128.0, 131.3, 132.6, 135.5, 137.2, 140.2, 141.9, 152.8.

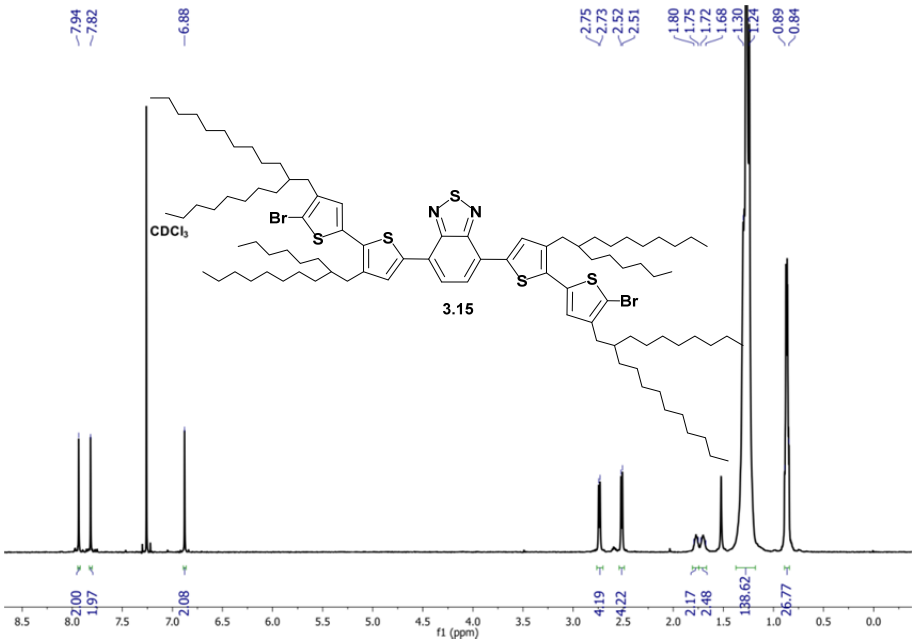

***Figure A.10**. [1]H NMR spectrum of compound **3.15** in $CDCl_3$.*

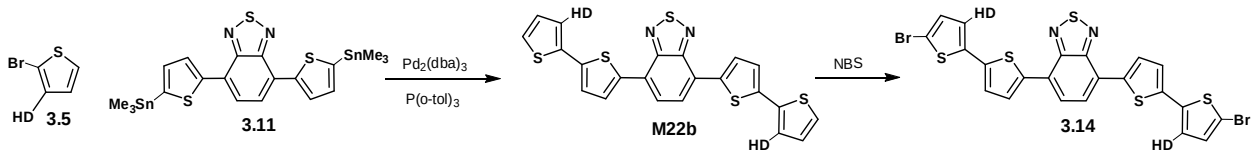

Scheme A.9. *Synthesis and bromination of* ***M22b****.*

4,7-Bis(3'-(2-hexyldecyl)[2,2'-bithiophen]-5-yl)benzo[*c*][1,2,5]thiadiazole (**M22b**)*:* A general Stille cross-coupling reaction was performed [13] of **3.5** (1.36 g, 3.5 mmol) and **3.10** (0.63 g, 1.0 mmol) according to the general procedure. Column chromatography from hexane/CH_2Cl_2 yielded a dark red solid (608.0 mg, 67%). ^{1}H NMR ($CDCl_3$, 500 MHz) δ: 0.84–0.88 (m, 12H), 1.24–1.31 (m, 48H), 1.72–1.78 (m, 2H), 2.80 (d, J = 7.2 Hz, 4H), 6.94 (d, J = 5.1 Hz, 2H), 7.23 – 7.20 (m, 4H), 7.83 (s, 2H), 8.11 (d, J = 3.8 Hz, 2H). ^{13}C NMR ($CDCl_3$, 126 MHz) δ: 14.2, 22.8, 26.7, 29.5, 29.8, 29.9, 30.2, 32.1, 33.7, 33.8, 34.1, 39.2, 124.1, 125.34, 125.8, 127.2, 128.1, 130.9, 131.2, 138.0, 139.2, 139.6, 152.7.

4,7-Bis(5'-bromo-3'-(2-hexyldecyl)[2,2'-bithiophen]-5-yl)benzo[*c*][1,2,5]thiadiazole (**3.14**)*:* A general bromination was performed [13]. NBS (155 mg, 0.87 mmol) was added to a solution of **M22b** (324 mg, 0.43 mmol) in THF (20 mL). Column chromatography using hexane as an eluent yielded a red oil (169 mg, 44%). ^{1}H NMR ($CDCl_3$, 500 MHz) δ (ppm): 0.85 (td, J = 7.0, 3.2 Hz, 12H), 1.32–1.16 (m, 48H), 1.66–1.71 (m, 2H), 2.72 (d, J = 7.2 Hz, 5H), 6.90 (s, 2H), 7.16 (d, J = 3.9 Hz, 2H), 7.86 (s, 2H), 8.09 (d, J = 3. 9 Hz, 2H). ^{13}C NMR ($CDCl_3$, 126 MHz) δ (ppm): 14.2, 22.8, 26.6, 29.5, 29.8, 29.9, 30.2, 32.1, 32.1, 33.6, 33.6, 34.1, 39.1, 111.0, 125.4, 125.7, 127.6, 128.0, 132.7, 133.4, 136.6, 139.6, 140.2, 152.6.

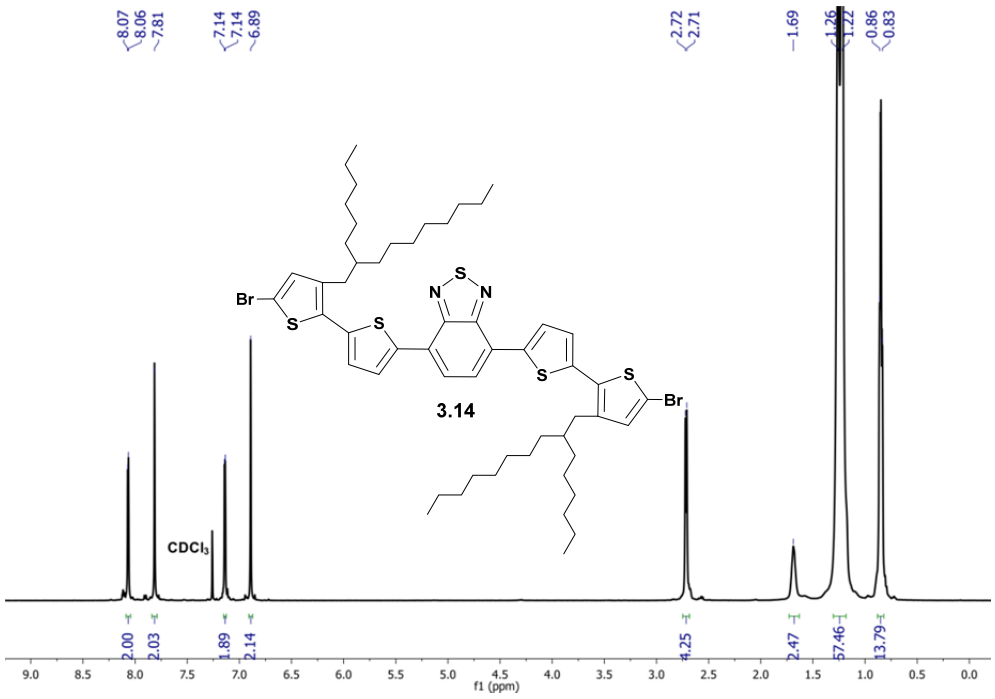

Figure A.11*. ^{1}H NMR spectrum of compound* ***3.9*** *in $CDCl_3$.*

Chapter 4

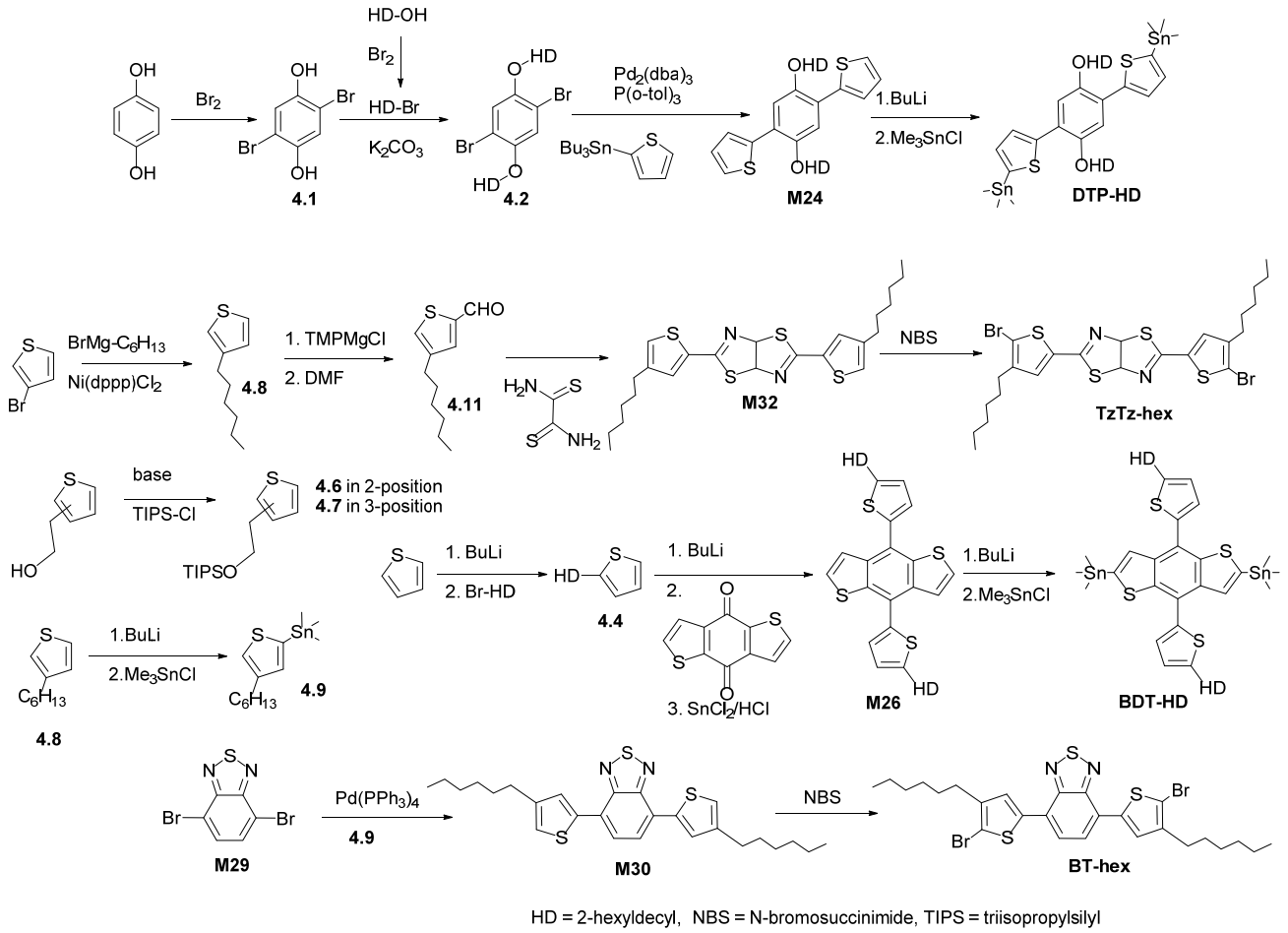

***Scheme A.10**. Monomer synthesis according to different literature procedures* [14–16,18,46–50].

2-Hexyldecylbromide (**HD-Br**), 2,5-dibromobenzene-1,4-diol (**4.1**), 1,4-dibromo-2,5-bis(2-hexyldecyl oxy)benzene (**4.2**), 2,2'-[2,5-bis(2-hexyldecyloxy)-1,4-phenylene]dithiophene (**M24**), {[2,5-bis (2-hexyldecyloxy)-1,4-phenylene]bis(thiophene-5,2-diyl)}bis(trimethylstannane) (**DTP-HD**), 2,5-bis (5-bromo-4-hexylthiophene-2-yl)thiazolo[5,4-d]thiazole (**TzTz-hex**), triisopropyl[2-(thiophen-2'-yl)ethoxy]silane (**4.6**), triisopropyl[2-(thiophen-3'-yl)ethoxy]silane (**4.7**), 4,8-Bis[5'-(2''-hexyldecyl)thiophene-2'-yl]benzo[1,2-*b*:4,5-*b*']dithiophene (**M26**), **BDT-HD** and **BT-hex** were synthesized according to various literature procedures [14–16,18,46–50] (Scheme A.12.).

2,2'-[2,5-bis(2-hexyldecyloxy)-1,4-phenylene]dithiophene (**M24**): ^{1}H NMR ($CDCl_3$, 500 MHz) δ: 0.87-0.91 (m, 12H), 1.37-1.36 (m, 48H), 1.89 (p, *J* = 6.1 Hz, 2H), 3.97 (d, *J* = 5.4 Hz, 4H), 7.10 (dd, *J* = 5.1, 3.7 Hz, 2H), 7.25 (s, 2H), 7.34 (dd, *J* = 5.3, 1.0 Hz, 2H), 7.53 (dd, *J* = 3.6, 0.9 Hz, 2H).

{[2,5-bis (2-hexyldecyloxy)-1,4-phenylene]bis(thiophene-5,2-diyl)}bis(trimethylstannane) (**DTP-HD**): ^{1}H NMR ($CDCl_3$, 500 MHz) δ: 0.39 (s, 18H), 0.87 (t7.23 (s, 2H),, *J* = 6.9 Hz, 12H), 1.27-1.36 (m, 48H), 1.88 (p, *J* = 6.1 Hz, 2H), 3.95 (d, *J* = 5.5 Hz, 4H), 7.18 (d, *J* = 3.4 Hz, 2H), 7.64 (d, *J* = 3.3 Hz, 2H).

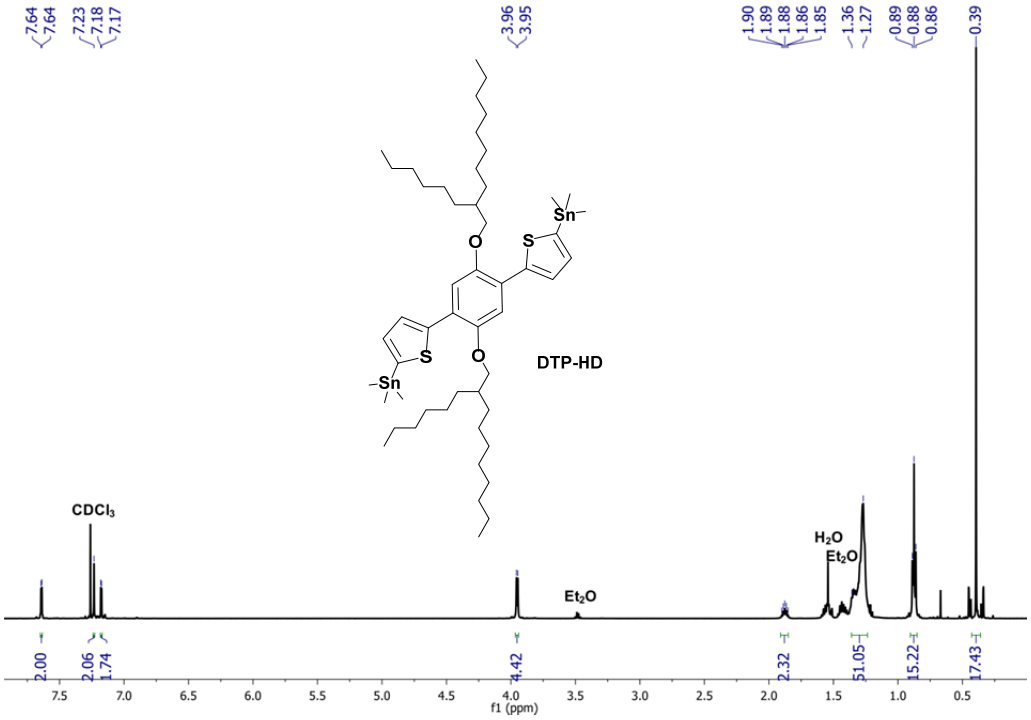

Figure A.12. *^{1}H NMR spectrum of compound **DTP-HD** in $CDCl_3$.*

2,5-Bis (5-bromo-4-hexylthiophene-2-yl)thiazolo[5,4-d]thiazole (**TzTz-hex**): ^{1}H NMR ($CDCl_3$, 500 MHz) δ: 0.91 (t, *J* = 6.9 Hz, 6H), 1.31-1.42 (m, 12H), 1.58-1.67 (m, 4H), 2.58 (t, *J* = 7.7 Hz, 4H), 7.27 (s, 2H).

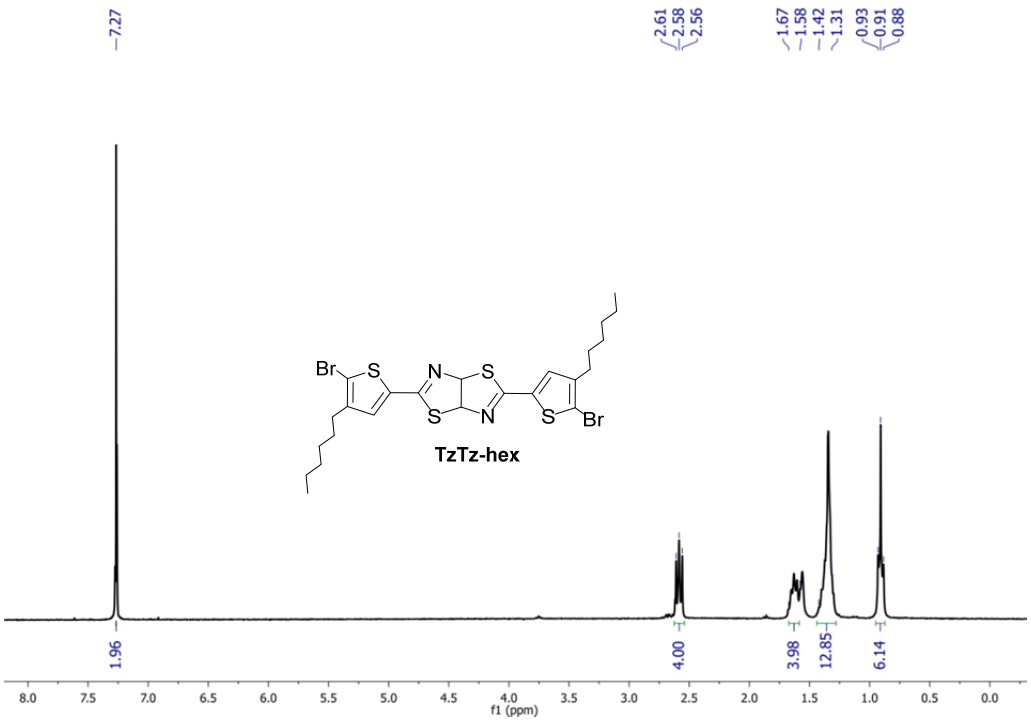

Figure A.13. *^{1}H NMR spectrum of compound **TzTz-hex** in $CDCl_3$.*

4,8-Bis[5'-(2''-hexyldecyl)thiophene-2'-yl]benzo[1,2-*b*:4,5-*b*']dithiophene (**M26**): ^{1}H NMR ($CDCl_3$, 500 MHz) δ: 0.83-0.90 (m, 12H), 1.29-1.35 (m, 48H), 1.68-1.76 (m, 2H), 2.85 (d, *J* = 6.7 Hz, 4H), 6.88 (d, *J* = 3.5 Hz, 2H), 7.29 (d, *J* = 3.5 Hz, 2H), 7.45 (d, *J* = 5.7 Hz, 2H), 7.64 (d, *J* = 5.7 Hz, 2H).

{4,8-Bis[5'-(2''-hexyldecyl)thiophen-2'-yl]benzo[1,2-*b*:4,5-*b*']dithiophene-2,6-diyl}bis(trimethylstannane) **BDT-HD**: ^{1}H NMR ($CDCl_3$, 500 MHz) δ: 0.39 (s, 18H), 0.85-0.90 (m, 12H), 1.26-1.37 (m, 48H), 1.67-1.79 (m, 2H), 2.86 (d, *J* = 6.7 Hz, 4H), 6.89 (d, *J* = 3.5 Hz, 2H), 7.31 (d, *J* = 3.5 Hz, 2H), 7.68 (s, 2H).

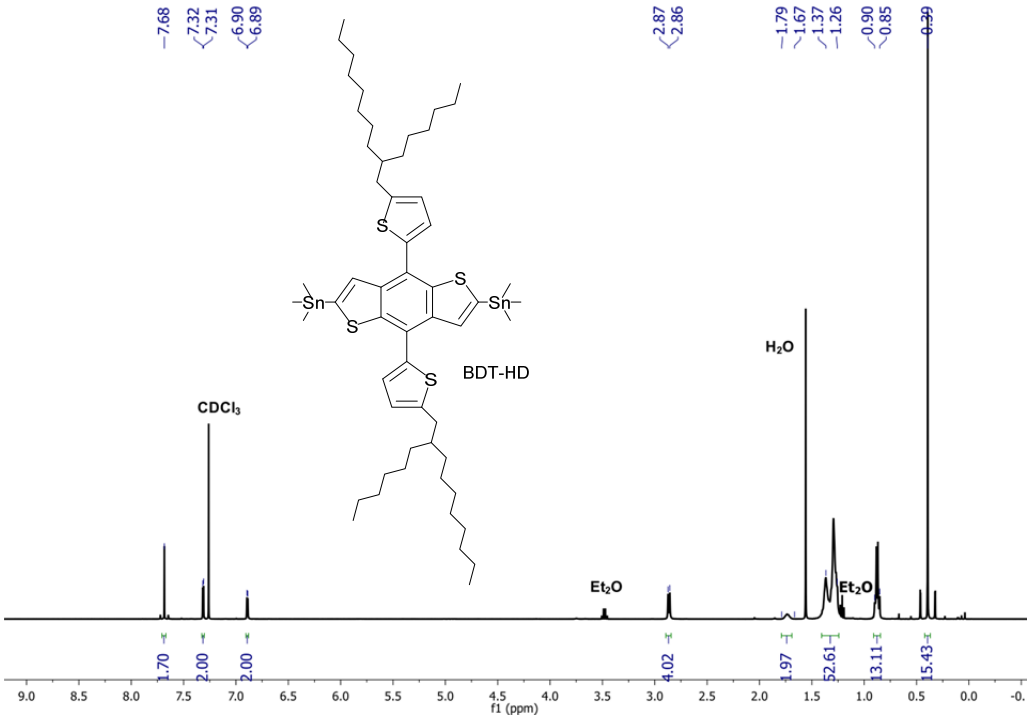

***Figure A.14**. ^{1}H NMR spectrum of compound **BDT-HD** in $CDCl_3$.*

4,7-Bis(4-hexylthiophen-2-yl)benzo[*c*][1,2,5]thiadiazole (**M30**): ^{1}H NMR ($CDCl_3$, 500 MHz) δ: 0.90 (t, *J* = 7.0 Hz, 6H), 1.31-1.43 (m, 12H), 1.70 (p, *J* = 7.5 Hz, 4H), 2.69 (d, *J* = 7.8 Hz, 4H), 7.04 (d, *J* = 1.2 Hz, 2H), 7.83 (s, 2H), 7.98 (d, *J* = 1.4 Hz, 2H).

4,7-bis(5-bromo-4-hexylthiophen-2-yl)benzo[*c*][1,2,5]thiadiazole (**BT-hex**): ^{1}H NMR ($CDCl_3$, 500 MHz) δ: 0.88-0.92 (m, 6H), 1.31-1.42 (m, 12H), 1.67 (p, *J* = 7.5 Hz, 1H),.2.64 (d, *J* = 7.7 Hz, 4H), 7.77 (s, 2H), 7.78 (s, 2H).

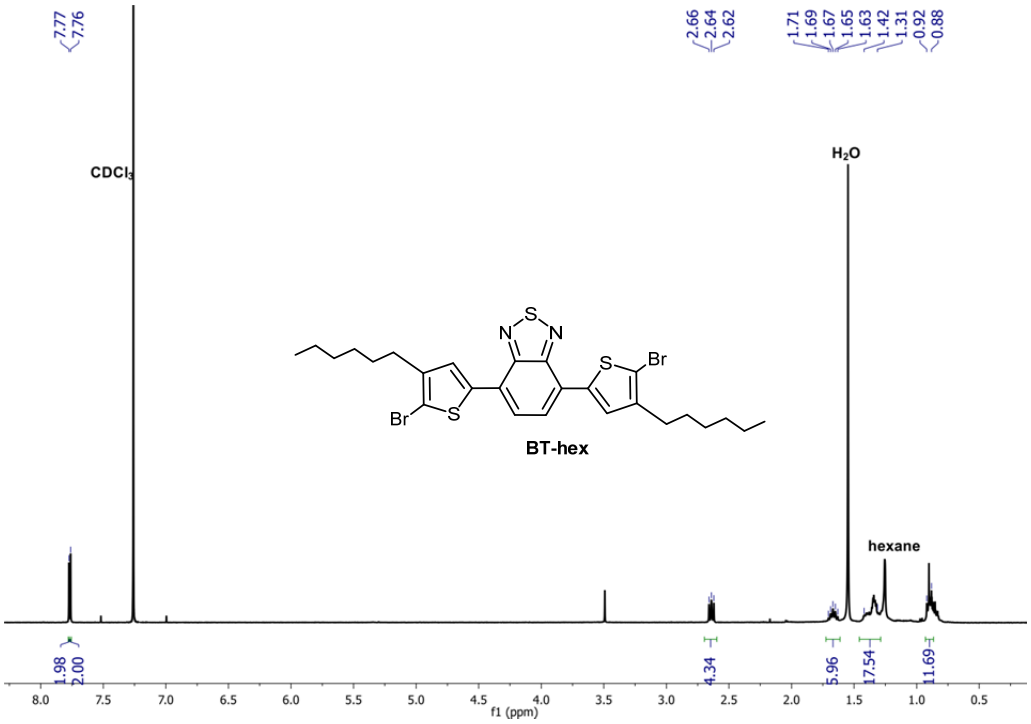

***Figure A.15**. [1]H NMR spectrum of compound **BT-hex** in $CDCl_3$.*

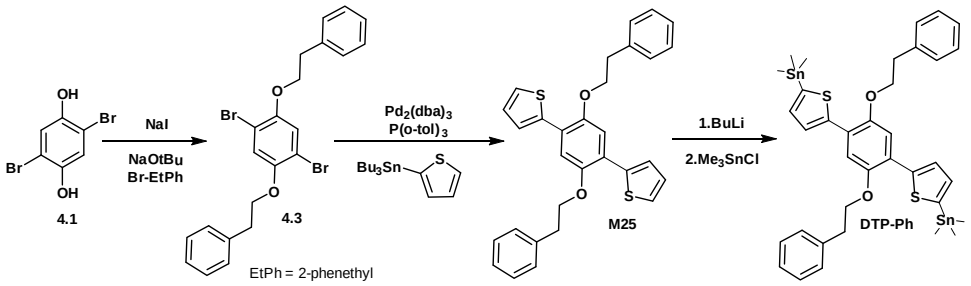

***Scheme A.11**. Synthesis and stannylation of **M25**.*

{[(2,5-Dibromo-1,4-phenylene)bis(oxy)]bis(ethane-2,1-diyl)}dibenzene (**4.3**) was synthesized using a similar reaction as reported in literature [51]. **4.1** (10.0 g, 37.3 mmol) and potassium tert-butanolate (10.0 g, 89.5 mmol) were dissolved in absolute ethanol (20 mL). The solution was degassed for 20 min with nitrogen. 2-Phenylethyl bromide (Br-EtPh, 11.5 mL, 82.1 mmol) was added dropwise. Thereafter sodium iodide (0.31 g, 2.1 mmol) was added in one go, followed by heating under reflux overnight. The next day, the organic solvent was removed after cooling down the reaction mixture. Then water was added to dissolve the inorganic salts. The water phase was extracted three times with CH_2Cl_2, followed by drying with $MgSO_4$. The product in organic solvent was filtrated and the solvent was removed. 8.42 g of **4.3** was obtained as a white powder by recrystallization from ethanol (yield: 47%). ^{1}H NMR ($CDCl_3$, 500 MHz) δ: 3.13 (t, J = 7.0 Hz, 4H), 4.83 (t, J = 7.0 Hz, 4H), 7.06 (s, 2H), 7.32-7.34 (m 10H). ^{13}C NMR ($CDCl_3$, 125 MHz) δ: 35.9, 71.1, 111.3, 118.6, 126.8, 128.6, 129.3, 138.0, 150.1.

2,2'-(2,5-Diphenethoxy-1,4-phenylene)dithiophene (**M25**)*:* A general Stille cross-coupling reaction was performed of **4.3** (4.0 g. 8.4 mmol) and commercially available mono-stannylated thiophene (9.4 g. 25.2 mmol) according to the general procedure. Recrystallization from CF

and methanol yielded a yellow solid (yield: 74%). ^{1}H NMR ($CDCl_3$, 500 MHz) δ: 3.23 (t, J = 7.2 Hz, 4H), 4.30 (t, J = 7.2 Hz, 4H), 7.06 (dd, J = 5.1, 3.7 Hz, 2H), 7.22 (s, 2H), 7.32-7.33 (m, 12H), 7.43 (dd, J = 3.7, 1.2 Hz, 2H). ^{13}C NMR ($CDCl_3$, 125 MHz) δ: 36.1, 70.8, 113.5, 123.4, 125.7, 125.8, 126.7, 127.0, 128.7, 129.2, 138.3, 139.1, 149.4.

[(2,5-Diphenethoxy-1,4-phenylene)bis(thiophene-5,2-diyl)]bis(trimethylstannane) (**DTP-Ph**) A general method was applied for the distannylation of **M25** [14]. A yellow solid was obtained, which was washed three times with methanol (yield: 73%). ^{1}H NMR ($CDCl_3$, 500 MHz) δ: 0.41 (s, 12H), 3.23 (t, J = 7.2 Hz, 4H), 4.31 (t, J = 7.2 Hz, 4H), 7.15 (d, J = 3.5 Hz, 2H), 7.22 (s, 2H), 7.33-7.34 (m, 10H), 7.56 (d, J = 3.5 Hz, 2H). ^{13}C NMR ($CDCl_3$, 125 MHz) δ: -8.1, 36.2, 70.6, 113.6, 123.3, 126.7, 127.1, 128.7, 129.2, 129.3, 135.4, 138.1, 138.4, 145.2, 149.2.

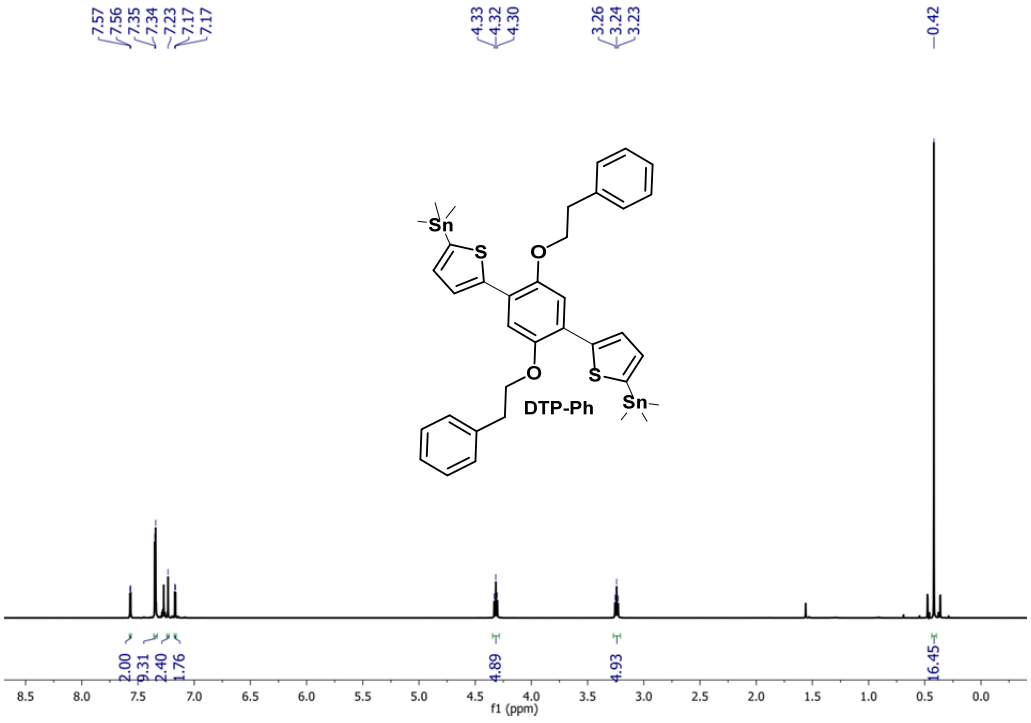

Figure A.16*. ^{1}H NMR spectrum of compound* ***DTP-Ph*** *in $CDCl_3$.*

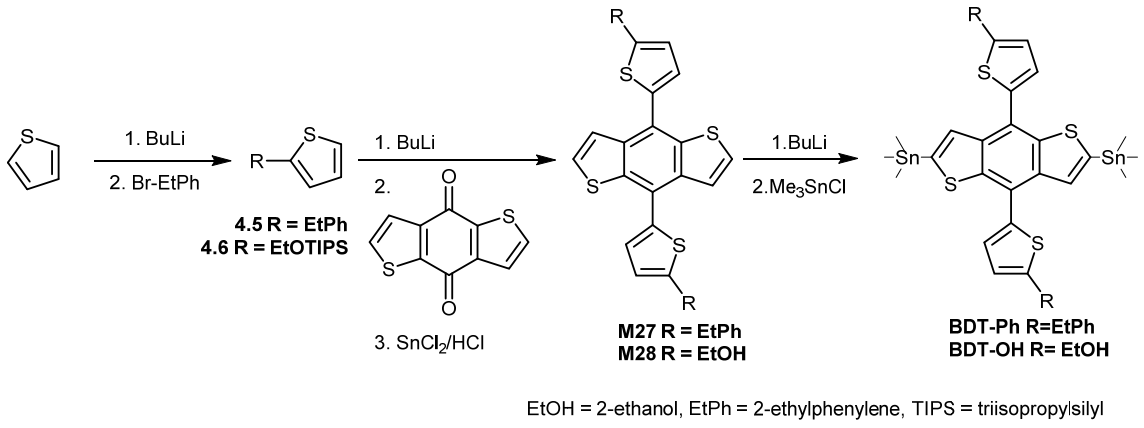

***Scheme A.12**. Synthesis and stannylation of **M27** and **M28**.*

2-(2'-Phenylethyl)thiophene (4.5). Synthesis according to the procedure for 4.4 [52]. Thiophene (1.6 mL, 20 mmol) was dissolved in dry THF (20 mL). BuLi (6.8 mL, 2.5 M in hexane, 17 mmol) was added dropwise at 0 °C. At room temperature, 2-phenylethyl bromide (2.9 mL, 21 mmol) was added in one go. The reaction mixture was then heated under reflux for 4 h. The crude product was purified by column chromatography using hexane as an eluent, affording a transparent liquid (1.2 g, 30%). ^{1}H NMR (CDCl3, 500 MHz) δ (ppm): 3.00 (t, J = 8.0 Hz, 2H), 3.15 (t, J = 8.0 Hz, 2H), 6.78 (dd, J = 3.4 Hz, 1.1 Hz, 1H), 6.92 (dd, J = 5.1 Hz, 3.4 Hz, 1H), 7.10 (dd, J = 5.1 Hz, 1.1 Hz, 1H), 7.20–7.32 (m, 5H). ^{13}C NMR (CDCl3, 126 MHz) δ (ppm): 31.9, 38.1, 123.1, 124.4, 126.2, 126.7, 128.3, 128.4, 141.2, 144.5.

General procedure for the synthesis of the benzodithiophene based compounds

The synthesis of **M27** and **M28** followed the procedure for **M26** [15]. BuLi (1.2 mL, 3.0 mmol, 2.5 M in hexane) was added dropwise to a solution of **4.5** (565 mg, 3.0 mmol) or **4.6** (797 mg, 2.8 mmol) in dry THF (20 mL) at 0 °C. The colour of the solution changed thereby from colourless to dark, whereafter the mixture was heated for 2 h at 50 °C. Then benzo[1,2-*b*:4,5-*b*']dithiophene-4,8-dione (220 mg, 1.0 mmol) was added and the mixture was heated for 1h. $SnCl_2$ (1.5 g, 8.0 mmol) in 12 weight-5 (wt%) hydrochloric acid (9 mL) was added and the mixture was stirred for 1 h at room temperature before it was added to ice water.

4,8-Bis[5'-(2''-phenylethyl)thiophene-2'-yl]benzo[1,2-*b*:4,5-*b*']dithiophene (**M27**). Synthesis was carried out after the general procedure. The water phase was then extracted three times with CF and the combined organic phases were dried over $MgSO_4$. Filtration and removal of the solvent under reduced pressure yielded the crude product. Purification by column chromatography using a gradient of petroleum ether and CF afforded a yellow solid (249 mg, 44%). ^{1}H NMR ($CDCl_3$, 500 MHz) δ (ppm): 3.11 (t, *J* = 8.0 Hz, 4H), 3.25 (t, *J* = 8.0 Hz, 4H), 6.91 (d, *J* = 3.4 Hz, 2H), 7.23–7.35 (m, 10H), 7.29 (d, *J* = 3.4 Hz, 2H), 7.46 (d, *J* = 5.7 Hz, 2H), 7.63 (d, *J* = 5.7 Hz, 2H). ^{13}C NMR ($CDCl_3$, 126 MHz) δ

(ppm): 32.4, 38.1, 123.5, 124.2, 124.9, 126.4, 127.7, 128.0, 128.6, 128.7, 136.7, 137.5, 139.2, 141.2, 145.9.

2,2'-(Benzo[1,2-*b*:4,5-*b*']dithiophene-4,8-diyl)bis(thiophene-5,2-diyl)bis(ethan-1-ol) (**M28**). Synthesis was carried out after the general procedure. The water phase was extracted three times with diethyl ether and the resulting organic fraction was dried over $MgSO_4$. Filteration and removal of the solvent under reduced pressure yielded the crude product. Purification by column chromatography (silica gel) using an eluent mixture of ethyl acetate and hexane (1/1) revealed a product mixture (the desired alcohol and the methyl ester analogue). During the workup of **M28**, the acetic ester was partly formed while using ethyl acetate as a solvent. The product mixture was dissolved in THF (20 mL), NaOH solution (2.5 M in H_2O; 10 mL) was added and stirred overnight. The organic phase was washed twice with water, then dried over $MgSO_4$ and the solvent was removed under reduced pressure. Purification by column chromatography using an eluent mixture of ethyl acetate and hexane (4/1) afforded a brown solid of the **M28** (204 mg, 46%). ^{1}H NMR (DMSO-d_6, 400 MHz) δ (ppm): 3.05 (t, *J* = 6.5 Hz, 4H), 3.73 (td, *J* = 6.4 Hz, *J* = 3.7 Hz, 4H), 4.92 (t, *J* = 3.7 Hz, 2H), 7.08 (d, *J* = 3.5 Hz, 2H), 7.38 (d, *J* = 3.5 Hz, 2H), 7.60 (d, *J* = 5.7 Hz, 2H), 7.85 (d, *J* = 5.7 Hz, 2H). ^{13}C NMR (DMSO-d_6, 101 MHz) δ (ppm): 33.3, 61.7, 122.9, 123.4, 125.9, 128.1, 129.4, 135.9, 136.4, 138.2, 143.6.

{4,8-Bis[5'-(2''-phenylethyl)thiophen-2'-yl]benzo[1,2-*b*:4,5-*b*']dithiophene-2,6-diyl}bis(trimethylstannane) (**BDT-Ph**). The bis-stannylation was performed according to the general procedure. **M27** (225 mg, 0.40 mmol) in THF (10 mL), BuLi in hexane (0.64 mL, 1.60 mmol) and Me_3SnCl in hexane (2.0 mL, 2.0 mmol). Recrystallization from hexane yielded dark yellow crystals (193 mg, 54%). ^{1}H NMR ($CDCl_3$, 500 MHz) δ (ppm): 0.43 (s, 18H), 3.13 (t, *J* = 8.0 Hz, 4H), 3.27 (t, *J* = 8.0 Hz, 4H), 6.93 (d, *J* = 3.5 Hz, 2H), 7.23–7.35 (m, 10H), 7.31 (d, *J* = 3.5 Hz, 2H), 7.67 (s, 2H). ^{13}C NMR ($CDCl_3$, 126 MHz) δ (ppm): -8.1, 32.4, 38.1, 122.5, 124.9, 126.3, 127.8, 128.6, 128.7, 131.2, 137.5, 138.3, 141.3, 142.6, 143.5, 145.5.

2,2'-{[2,6-bis(trimethylstannyl)benzo[1,2-*b*:4,5-*b*']dithiophene-4,8-diyl]bis(thiophene-5,2-diyl)}bis(ethan-1-ol) (**BDT-OH**). The bis-stannylation was performed according to the general procedure. **M28** (199 mg, 0.45 mmol) in THF (15 mL), BuLi in hexane (1.26 mL, 3.15 mmol) and Me_3SnCl in hexane (3.6 mL, 3.6 mmol). A green solid precipitated after addition of BuLi. Therefore, the reaction temperature was raised right away and stirred for 3h at room temperature. Purification of the crude product was done by recycling SEC, yielding pure **BDT-OH** (95 mg, 27%). ^{1}H NMR (DMSO-d_6, 400 MHz) δ (ppm): 0.40 (s, 18H), 1.70 (t, *J* = 6.1 Hz, 2H), 3.21 (t, *J* = 6.1 Hz, 4H), 3.99 (q, *J* = 6.1 Hz, 4H), 7.04 (d, *J* = 3.5 Hz, 2H), 7.36 (d, *J* = 3.5 Hz 2H), 7.66 (s, 2H). ^{13}C NMR (DMSO-d_6, 75 MHz) δ (ppm): -8.1, 33.8, 63.5, 122.3, 126.1, 128.2, 131.1, 137.5, 139.2, 141.8, 142.8, 143.4.

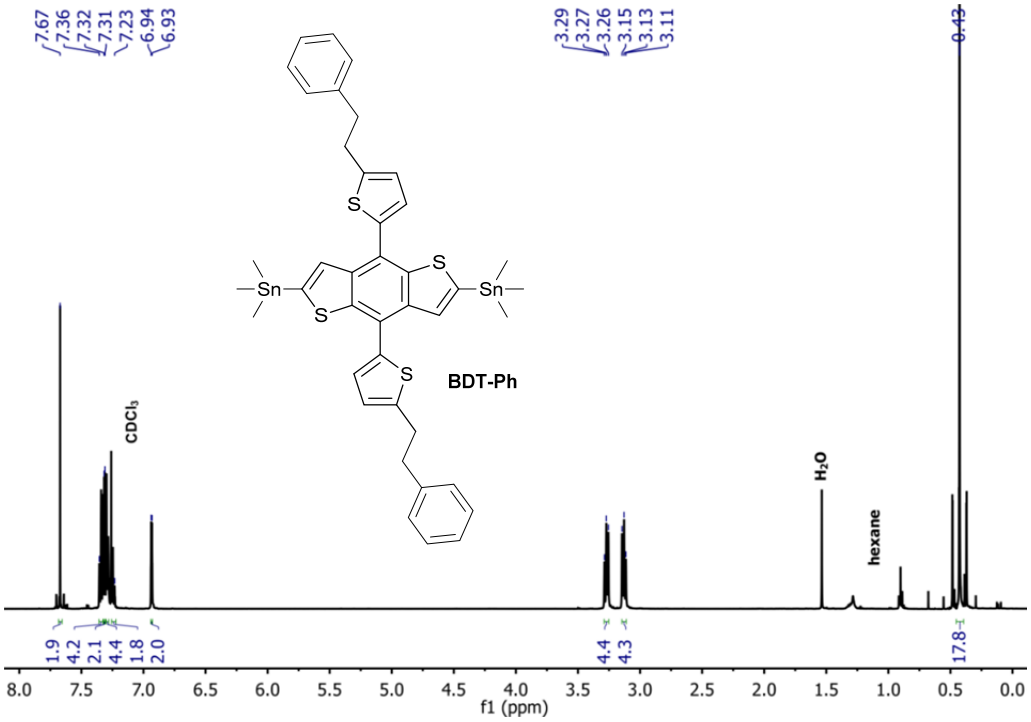

Figure A.17. *^{1}H NMR spectrum of compound **BDT-Ph** in $CDCl_3$.* Reprinted from [53] with permission from Wiley-VCH Verlag GmbH & Co. KGaA, Weinheim ©2015.

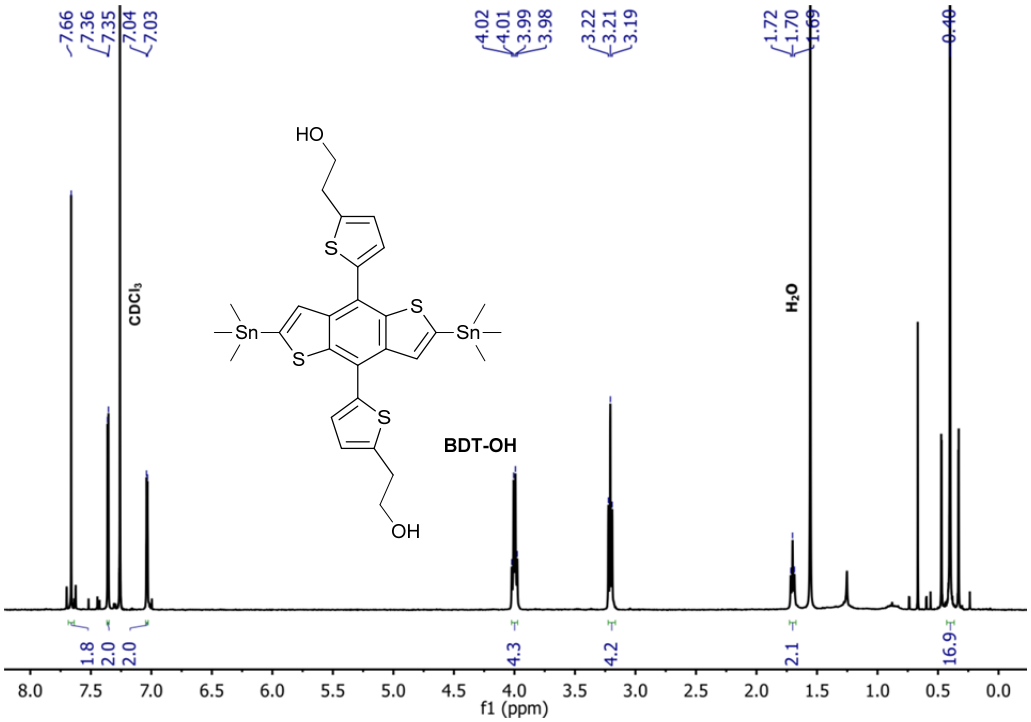

Figure A.18. *^{1}H NMR spectrum of compound **BDT-OH** in $CDCl_3$.* Reprinted from [53] with permission from Wiley-VCH Verlag GmbH & Co. KGaA, Weinheim ©2015.

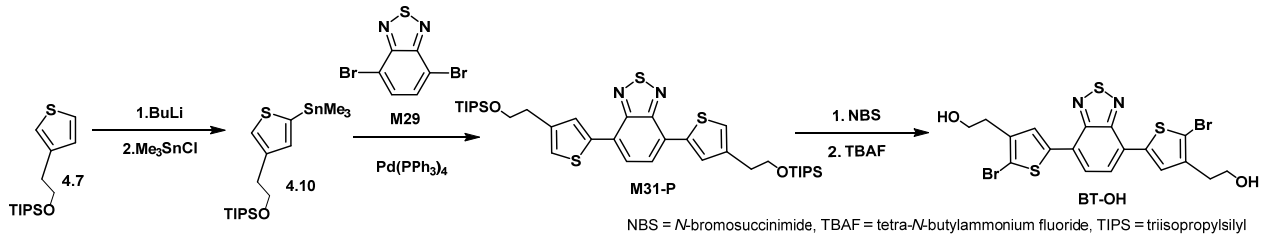

***Scheme A.13**. Synthesis, di-bromination and deprotection of **M31** based monomer.*

Triisopropyl{2-[2'-(trimethylstannyl)thiophen-3'-yl]ethoxy}silane (**4.10**). The mono-stannylation was performed according to the general procedure. **4.7** (1.0 g, 3.5 mmol) in THF (20 mL), BuLi in hexane (1.4 mL, 3.5 mmol) and Me_3SnCl in hexane (4.6 mL, 4.6 mmol): 1.27 g of a light brown liquid with impurities (stannylation in 5-position) was obtained (2.8 mmol, 80%). It was preceded further with a crude product as it was easier to perform purification of the product in the following step. ^{1}H NMR ($CDCl_3$, 400 MHz) δ (ppm): 0.34 (s, 9H), 1.03–1.05 (m, 21H), 2.91 (t, *J* = 7.0 Hz, 2H), 3.89 (t, *J* = 7.0 Hz, 2H), 7.07 (s, 1H), 7.28 (s, 1H).

Protected 2,2'-(benzo[*c*][1,2,5]thiadiazole-4,7-diylbis(thiophene-5,3-diyl))bis(ethan-1-ol) (**M31-P**)**.** A general Stille cross-coupling reaction was performed [16]. **4.10** (402.6 mg, 0.90 mmol), **M29** (88.2 mg, 0.30 mmol) and in this case tetrakis(triphenylphosphine) palladium(0) (17.3 mg, 0.03 mmol) were dissolved in dry toluene (5 mL) and dry DMF (0.5 mL). After removing the solvent from the product solution, a red solid was obtained (202.5 mg, 96%). ^{1}H NMR ($CDCl_3$, 400 MHz) δ (ppm): 1.06–1.08 (m, 42H), 2.95 (t, *J* = 6.7 Hz, 4H), 3.97 (t, *J* = 6.7 Hz, 4H), 7.14 (d, *J* = 1.2 Hz, 2H), 7.83 (s, 2H), 8.03 (d, *J* = 1.2 Hz, 2H). ^{13}C NMR ($CDCl_3$, 126 MHz) δ (ppm): 12.2, 18.2, 34.5, 64.1, 123.1, 125.6, 126.2, 129.6, 139.1, 140.9, 152.8.

Brominated 2,2'-(benzo[*c*][1,2,5]thiadiazole-4,7-diylbis(thiophene-5,3-diyl))bis(ethan-1-ol) **BT-OH**. NBS (41.0 mg, 0.24 mmol) was added to a solution of **M31-P** (80.7 mg, 0.12 mmol) in THF (15 mL). A general NBS-di-bromination was performed. Without further purification of the crude di-brominated product, tetrabutylammonium fluoride (TBAF) (0.40 g, 1.5 mmol) was added to the solution and the mixture was stirred for 1.5 h. The organic phase was washed twice with water and dried over $MgSO_4$. After filtration and removal of the solvent under reduced pressure, the brown solid was purified using column chromatography with an eluent gradient of dichloromethane and methanol. Further purification was performed by recrystallization from acetone, affording a red solid (29.2 mg, 44%). ^{1}H NMR ($CDCl_3$, 400 MHz) δ (ppm): 2.77 (t, *J* = 7.0 Hz, 4H), 3.67 (td, *J* = 7.0 Hz, 5.3 Hz, 4H), 4.83 (t, *J* = 5.3 Hz, 2H), 7.98 (s, 2H), 8.12 (s, 2H). ^{13}C NMR ($CDCl_3$, 126 MHz) δ (ppm): 32.9, 60.2, 112.2, 124.2, 125.1, 128.3, 137.6, 140.0, 151.2.

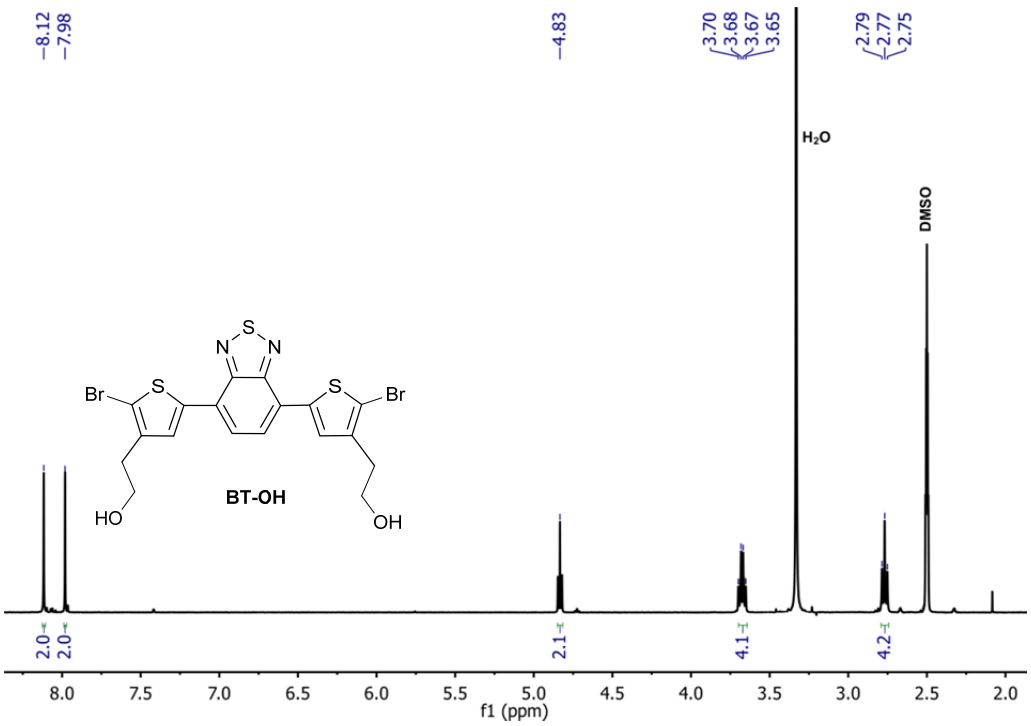

***Figure A.19**. [1]H NMR spectrum of compound **BT-OH** in DMSO-d_6.* Reprinted from [53] with permission from Wiley-VCH Verlag GmbH & Co. KGaA, Weinheim ©2015.

Polymer Synthesis

Standard Stille cross-coupling polymerization

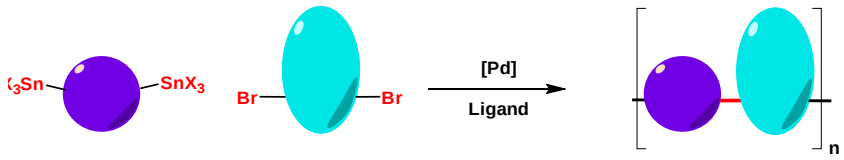

***Scheme A.14**. Schematic drawing of the Stille cross-coupling polymerization.*

In a general procedure for the polymerization [54] 1 eq. of brominated A_M and 1 eq. of stannylated donor monomer were dissolved in anhydrous toluene (70 mg monomer mL^{-1}) in a 8 mL vial. Then, 0.03 eq. of tris(dibenzylideneacetone)dipalladium(0) ($Pd_2(dba)_3$) and 0.09-0.18 eq. of tris(o-tolyl)phosphine ($P(o\text{-}tol)_3$) were added before the mixture was heated for at least 20 h at 110°C. The raw polymer solution was precipitated into methanol and the solid polymer was filtrated before a Soxhlet extraction was performed with methanol and n-hexane (optional were CH_2Cl_2 and CF). The leftover polymers were dissolved in hot CF or CB and precipitated into methanol, filtrated and dried under vacuum.

Polymers from Chapter 2

The polymers prepared by combinatorial pairing of **M1**-**M13** with **M14**-**M22** including **P1**-**P9** were mostly prepared by standard Stille cross-coupling polymerizations. As the polymerization was not part of this work, it is therefore not described further.

Polymers from Chapter 3

The polymers were prepared by Stille cross coupling polymerization:

Poly{[thiophene]-alt-[4,7-bis(4-(2-hexyldecyl)thiophen-2-yl)benzo[*c*][1,2,5] thiadiazole]} (**P14**) was received as a dark solid from the CF phase (54% yield) M_n = 21.4 kDa, Đ = 1.6. (^{1}H NMR in Appendix B Figure B.3.1).

Poly{[3,4-di(2-hexyldecyloxy)thiophene]-alt-[4,7-di(thiophene-2-yl)benzo[*c*][1,2,5]thiadiazole]} (**P15**) was received as a dark solid from the CF phase (98% yield). Polymer aggregated, no M_n/Đ was detected. (^{1}H NMR in Appendix B Figure B.3.1).

Poly{[2,2'-bithiophene]-alt-[4,7-bis(4-(2-hexyldecyl)thiophen-2-yl)benzo[*c*][1,2,5] thiadiazole]} (**P16**) was received as a dark solid from the CF phase (92% yield) M_n = 24.9 kDa, Đ = 1.8. (^{1}H NMR in Appendix B Figure B.3.1).

Poly{[4,7-bis(4-(2-hexyldecyl)thiophen-2-yl)benzo[*c*][1,2,5]thiadiazole]-alt-[4,7-di(thiophene-2-yl)benzo[*c*] [1,2,5]thiadiazole]} (**P17**) was received as a dark solid from the CB phase (48% yield). Polymer was insuficient soluble in CB, no M_n/Đ was detected. (^{1}H NMR in Appendix B Figure B.3.1).

Poly{[4,7-di(thiophene-2-yl)benzo[*c*][1,2,5]thiadiazole]-alt-[4,7-bis(4'-(2-octyldodecyl)-3-(2-hexyldecyl)-[2,2'-bithiophen]-5-yl)benzo[*c*][1,2,5]thiadiazole]} (**P18**) was received as a dark solid from the hexane phase (89% yield) M_n = 43.7 kDa, Đ = 1.9. (^{1}H NMR in Appendix B Figure B.3.1).

Poly{[3,4-di(2-hexyldecyloxy)thiophene]-alt-[4,7-di([2,2'-bithiophen]-5-yl)benzo[*c*][1,2,5]thiadiazole]} (**P19**) was received as a dark solid from the CF phase (9% yield) Polymer aggregated, no M_n/Đ was detected. (^{1}H NMR in Appendix B Figure B.3.1).

Poly{[3,4-di(2-hexyldecyloxy)thiophene]-alt-[4,7-bis(3'-(2-hexyldecyl)-[2,2'-bithiophen]-5-yl)benzo[*c*][1,2,5] thiadiazole]} (**P20**) was received as a dark solid from the CF phase (6% yield). No M_n/Đ was detected due to a low value. (^{1}H NMR in Appendix B Figure B.3.1).

Poly{[2,2'-bithiophene]-alt-[4,7-bis(4'-(2-octyldodecyl)-3-(2-hexyldecyl)-[2,2'-bithiophen]-5-yl)benzo[*c*] [1,2,5]thiadiazole]} (**P21**) was received as a dark solid from the CF phase (84% yield) M_n = 42.1 kDa, Đ = 1.8. (^{1}H NMR in Appendix B Figure B.3.1).

Polymers from Chapter 4

The polymers were prepared by Stille cross coupling polymerization:

Poly{[2,5-bis(2-hexyldecyloxy) phenylene]-alt-[4,7-di(thiophene-2-yl)benzo[*c*][1,2,5]thiadiazole]} (**P2**) was received as a blue solid (96% yield). M_n = 42 kDa, Đ = 1.9. (^{1}H NMR in Appendix B Figure B.4.1)

Poly{2,2'-[5,5'-(2,5-bis(2-hexyldecyloxy)-1,4-phenylene)dithiophene]-alt-[2,5-bis(4-hexyl thiophen-2-yl)thiazolo[5,4-*d*]thiazole]} (**P8**) was received as a red solid (79% yield). M_n = 44 kDa, Đ = 1.9. No NMR spectrum was detected due to a low solubility.

Poly{4,8-bis[5'-(2"-hexyldecyl)-thiophen-2'-yl]benzo[1,2-*b*:4,5-*b*']dithiophene-alt-4,7-bis(4'-hexylthiophene 2'-yl)benzo[*c*][1,2,5] thiadiazole} (**P24**) was received as a dark solid (81% yield) M_n = 22 kDa, Đ = 3.9. (^{1}H NMR in Appendix B Figure B.4.1)

The BT based statistical copolymers **P25a,b** were received as blue solids (^{1}H NMR in Appendix B Figure B.4.1). **P25a** (98% yield) M_n = 39 kDa, Đ = 2.1. **P25b** (97% yield) M_n = 43 kDa, Đ = 2.1.

The TzTz based statistical copolymers **P26a,b** were received as red solids. **P26a** (95% yield). M_n = 30 kDa, Đ = 3.1. **P4b** (89% yield) M_n = 78 kDa, Đ = 1.5.

Polymers with 2-phenylethyl modified donor side chains (**P27a,b**) were received as dark solid (^{1}H NMR in Appendix B Figure B.4.1). (**P27a**) (89% yield) M_n = 19 kDa, Đ = 4.1. (**P27b**) (88% yield) M_n = 18 kDa, Đ = 3.7.

Polymers with 2-hydroxyethyl modified donor side chains (**P28a,b**) were received as dark solid (^{1}H NMR in Appendix B Figure B.4.1). (**P28a**) (92% yield) M_n = 23 kDa, Đ = 4.5. (**P28b**) (95% yield) M_n = 25 kDa, Đ = 7.9.

Polymers with 2-hydroxyethyl modified A_M side chains (**P29a,b**) were received as dark solid (^{1}H NMR in Appendix B Figure B.4.1). (**P29a**) (88% yield) M_n = 16 kDa, Đ = 3.8. (**P29b**) (92% yield) M_n = 13 kDa, Đ = 3.2.

Polymer Solar Cell Preparation

Roll coated polymer solar cells

The RC PSCs had a general structure of PET/Silver grid/PEDOT-PSS/ZnO/ polymer:$PC_{61}BM$/PEDOT-PSS/Silver grid. The polymer and $PC_{61}BM$ were dissolved in solvent (CF, CB, ODCB or a mixture) (40 mg mL^{-1}, with a polymer/$PC_{61}BM$ ratio of 1:1, 1:1.5 or 1:2(wt/wt %)) and stirred at 50-100°C for 1 h to overnight. The solution was slot-die coated (Figure A.4 left) with a mini roll-coater [55] on a *flextrode* substrate at 60-80 °C similar as described in literature [56] using different flow rates for the solution or a different speed of the roll to vary the thickness of the active layer (~350-600 nm). The active layer was dewetted with 1-buthanol (Figure A.6 middle left) to prepare it for coating of the next layer. The PEDOT:PSS was slot-die coated on top

the active layer (Figure A.4 middle right) and dried for 20-30 min; the back Ag electrode was then flexographically printed on top of the PEDOT-PSS layer (Figure A.4 right), both as described in literature [56]. The foil was removed from the roll and the PSCs were annealed in a hot air oven at 80-120 ^{o}C for 5- 10 min [57,58]. At least five perfect looking cells of the sample were cut out from the foil and measured to obtain the average PCE. 3-5 PSCs per coating batch (except for the PSCs from Chapter 2) were encapsulated between two glass slides using UV-curable adhesive (Figure A.5). The adhesive was activated for a few minutes using a solar simulator. The exact area (~1 cm^2) of all cells was determined using LBIC (Figure A.5, yellow image). Prior to the testing of the devices the cells were switched [59]. The RC PSCs were tested under AM 1.5 (1000 W/m^2) conditions. *J-V* curves were recorded to determine the PV parameters (V_{OC}, J_{SC}, FF and PCE).

Spin coated polymer solar cells

The SC PSCs had a traditional architecture consisting of glass/ITO/PEDOT:PSS/polymer:$PC_{61}BM$/ Ca/Al. Prior to the solar cell processing, the ITO were thoroughly cleaned using soap, demineralized water, acetone, isopropanol and UV/O_3 treatment. PEDOT:PSS was thereafter deposited at a thickness of ~30 nm, then annealing at 130 °C for 15 minutes was applied to remove any residual water. Further processing was carried out in a nitrogen containing glovebox (O_2/H_2O < 1 ppm), starting with the deposition of the active layer by SC. The blend solutions had a total concentration of 15-50 mg mL^{-1} with different polymer:$PC_{61}BM$ ratios (1:1.5 and 1:2 (wt/wt%)) were prepared using different processing solvents (CF, ODCB/CB mixture and ODCB). The devices were finished off by vacuum deposition of the top electrodes (Ca and Al) with layer thicknesses of 30 and 80 nm, respectively. The SC device performance measurements were done using the Newport class A solar simulator.

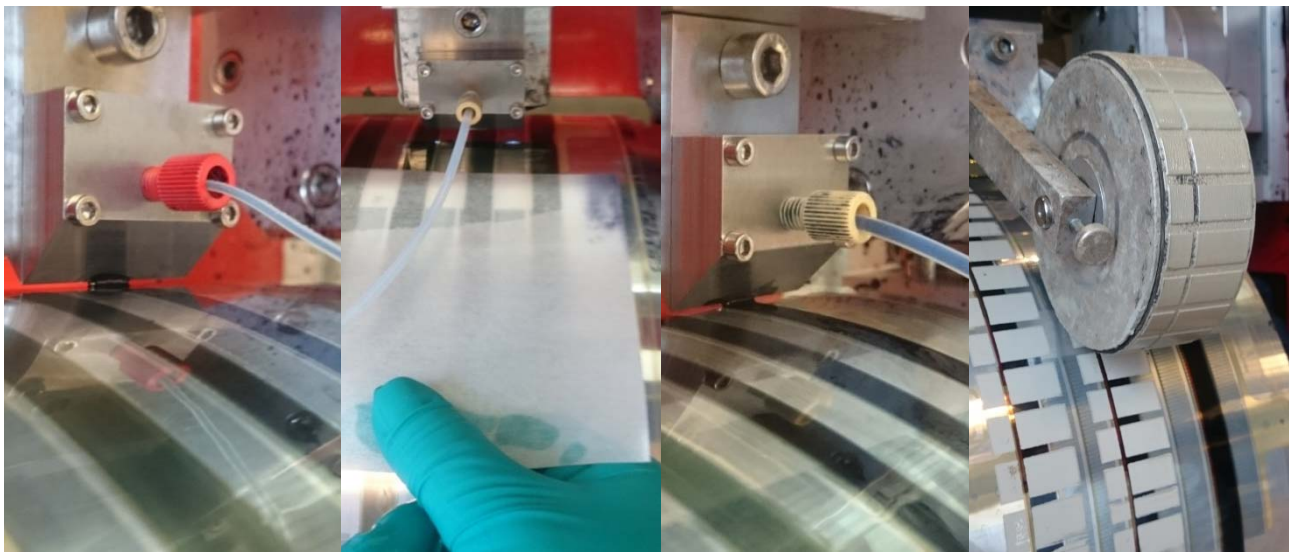

Figure A.20*. Slot-die coating of the active layer (left), dewetting of the active layer (middle, left), slot-die coating of the PEDOT-PSS (middle, right) and flexographic printing of the back electrode (right).*

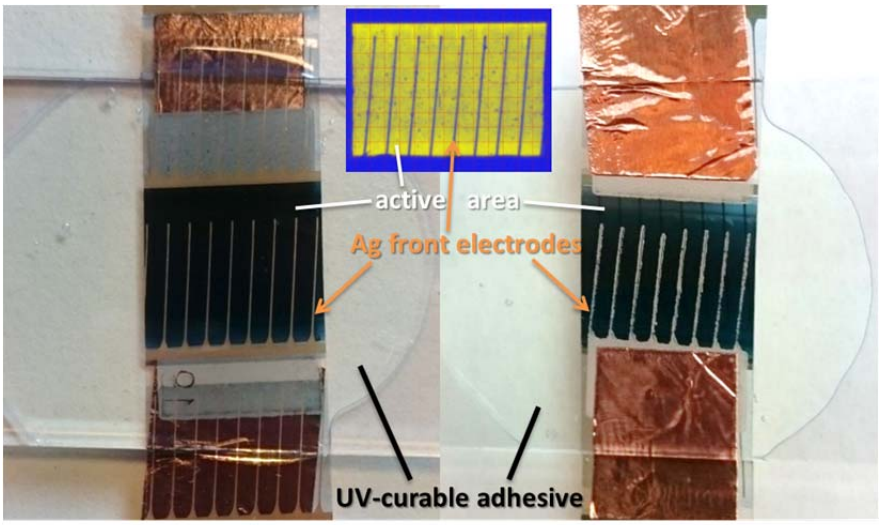

***Figure A.21**. Photographs of the front (left) and back side (right) of an encapsulated RC PSC including UV-curable adhesive and LBIC image (yellow top) of a PSC. (Distance between the electrode fingers is 1 mm).*

References

1. Hösel, M.; Søndergaard, R. R.; Jørgensen, M.; Krebs, F. C. Fast Inline Roll-to-Roll Printing for Indium-Tin-Oxide-Free Polymer Solar Cells Using Automatic Registration. *Energy Technol.* **2013**, *1*, 102–107.

2. Bundgaard, E.; Krebs, F. C. Low-Band-Gap Conjugated Polymers Based on Thiophene , Benzothiadiazole , and Benzobis (thiadiazole). *Macromolecules* **2006**, *39*, 2823–2831.

3. Gevorgyan, S. A.; Krebs, F. C. Bulk Heterojunctions Based on Native Polythiophene. *Chem. Mater.* **2008**, *20*, 4386–4390.

4. Bundgaard, E.; Hagemann, O.; Bjerring, M.; Nielsen, N. C.; Andreasen, J. W.; Andreasen, B.; Krebs, F. C. Removal of Solubilizing Side Chains at Low Temperature: A New Route to Native Poly(thiophene). *Macromolecules* **2012**, *45*, 3644–3646.

5. Bard, A. J.; Faulkner, L. R. *Electrochemical Methods: Fundamentals and Applications*; Harris, D., Ed.; 2nd ed.; John Wiley & Sons, Inc.: New York, USA, 2012.

6. Trasatti, S. The Absolute Electrode Potential: an Explanatory Note. *Pure Appl. Chem.* **1986**, *58*, 955–966.

7. Danley, R. L.; Caulfield, P. A.; Aubuchon, S. R. Rapid-Scanning Differential Scanning Calorimeter. *Am. Lab.* **2008**, *40*, 9–11.

8. Wouters, S.; Demir, F.; Beenaerts, L.; Van Assche, G. Calibration and performance of a fast-scanning DSC—Project RHC. *Thermochim. Acta* **2012**, *530*, 64–72.

9. Tromholt, T.; Madsen, M. V.; Carlé, J. E.; Helgesen, M.; Krebs, F. C. Photochemical stability of conjugated polymers, electron acceptors and blends for polymer solar cells resolved in terms of film thickness and absorbance. *J. Mater. Chem.* **2012**, *22*, 7592–7601.

10. Krebs, F. C.; Søndergaard, R.; Jørgensen, M. Printed metal back electrodes for R2R fabricated polymer solar cells studied using the LBIC technique. *Sol. Energy Mater. Sol. Cells* **2011**, *95*, 1348–1353.

11. Reese, M. O.; Gevorgyan, S. A.; Jørgensen, M.; Bundgaard, E.; Kurtz, S. R.; Ginley, D. S.; Olson, D. C.; Lloyd, M. T.; Morvillo, P.; Katz, E. A.; Elschner, A.; Haillant, O.; Currier, T. R.; Shrotriya, V.; Hermenau, M.; Riede, M.; Kirov, K. R.; Trimmel, G.; Rath, T.; Inganäs, O.; Zhang, F.; Andersson, M.; Tvingstedt, K.; Lira-Cantu, M.; Laird, D.; McGuiness, C.; Gowrisanker, S.; Pannone, M.; Xiao, M.; Hauch, J.; Steim, R.; Delongchamp, D. M.; Rösch, R.; Hoppe, H.; Espinosa, N.; Urbina, A.; Yaman-Uzunoglu, G.; Bonekamp, J.-B.; van Breemen, A. J. J. M.; Girotto, C.; Voroshazi, E.; Krebs, F. C. Consensus stability testing protocols for organic photovoltaic materials and devices. *Sol. Energy Mater. Sol. Cells* **2011**, *95*, 1253–1267.

12. Liang, F.; Lu, J.; Ding, J.; Movileanu, R.; Tao, Y. Design and synthesis of alternating regioregular oligothiophenes/ benzothiadiazole copolymers for organic solar cells. *Macromolecules* **2009**, *42*, 6107–6114.

13. Hu, H.; Jiang, K.; Yang, G.; Liu, J.; Li, Z.; Lin, H.; Liu, Y.; Zhao, J.; Zhang, J.; Huang, F.; Qu, Y.; Yan, H. Terthiophene-Based D-A Polymer with an Asymmetric Arrangement of Alkyl Chains That Enables Efficient Polymer Solar Cells. *J. Am. Chem. Soc.* **2015**, *137*, 14149–14157.

14. Livi, F.; Zawacka, N. K.; Angmo, D.; Jørgensen, M.; Krebs, F. C.; Bundgaard, E. Influence of Side Chain Position on the Electrical Properties of Organic Solar Cells Based on Dithienylbenzothiadiazole- alt -phenylene Conjugated Polymers. *Macromolecules* **2015**, *48*, 3481–3492.

15. Huo, L.; Zhang, S.; Guo, X.; Xu, F.; Li, Y.; Hou, J. Replacing alkoxy groups with alkylthienyl groups: a feasible approach to improve the properties of photovoltaic polymers. *Angew. Chemie Int. Ed.* **2011**, *50*, 9697–9702.

16. Hou, Q.; Zhou, Q.; Zhang, Y.; Yang, W.; Yang, R.; Cao, Y. Synthesis and electroluminescent properties of high-efficiency saturated red emitter based on copolymers from fluorene and 4,7-Di(4-hexylthien-2-yl)-2,1, 3-benzothiadiazole. *Macromolecules* **2004**, *37*, 6299–6305.

17. Van Pham, C.; Mark Jr., H. B.; Zimmer, H. A Convenient Synthesis of 3-Alkylthiophenes Synthetic. *Synth. Commun.* **1986**, *16*, 689–696.

18. Carlé, J. E.; Andreasen, J. W.; Jørgensen, M.; Krebs, F. C. Low band gap polymers based on 1,4-dialkoxybenzene, thiophene, bithiophene donors and the benzothiadiazole acceptor. *Sol. Energy Mater. Sol. Cells* **2010**, *94*, 774–780.

19. Huo, L.; Zhang, S.; Guo, X.; Xu, F.; Li, Y.; Hou, J. Replacing Alkoxy Groups with Alkylthienyl Groups: A Feasible Approach To Improve the Properties of Photovoltaic Polymers. *Angew. Chemie Int. Ed.* **2011**, *50*, 9697–9702.

20. Hou, J.; Chen, H.-Y.; Zhang, S.; Yang, Y. Synthesis and Photovoltaic Properties of Two Benzo[1,2- b :3,4- b′]dithiophene-Based Conjugated Polymers. *J. Phys. Chem. C* **2009**, *113*, 21202–21207.

21. Blouin, N.; Michaud, a.; Leclerc, M. A Low-Bandgap Poly(2,7-Carbazole) Derivative for Use in High-Performance Solar Cells. *Adv. Mater.* **2007**, *19*, 2295–2300.

22. Eggert Carlé, J.; Wenzel Andreasen, J.; Jørgensen, M.; Christian Krebs, F. Low band gap polymers based on 1,4-dialkoxybenzene, thiophene, bithiophene donors and the benzothiadiazole acceptor. *Sol. Energy Mater. Sol. Cells* **2010**, *94*, 774–780.

23. Arroyave, F. A.; Richard, C. A.; Reynolds, J. R. Efficient Synthesis of (BDTD) and Its Chemical Transformations into Precursors for π‐Conjugated Materials. *Org. Lett.* **2012**, *14*, 6138–6141.

24. Pilgram, K.; Zupan, M.; Skiles, R. Bromination of 2,1,3-benzothiadiazoles. *Heterocycl. Chem.* **1970**, *7*, 629–633.

25. Osaka, I.; Sauvé, G.; Zhang, R.; Kowalewski, T.; McCullough, R. D. Novel Thiophene-Thiazolothiazole Copolymers for Organic Field-Effect Transistors. *Adv. Mater.* **2007**, *19*, 4160–4165.

26. Hou, Q.; Xu, Y.; Yang, W.; Yuan, M.; Peng, J.; Cao, Y. Novel red-emitting fluorene-based copolymers. *J. Mater. Chem.* **2002**, *12*, 2887–2892.

27. Yue, W.; Zhao, Y.; Song, D.; Tian, H.; Xie, Z.; Yan, D.; Geng, Y.; Wang, F. Poly(oligothiophene-alt-benzothiadiazole)s: Tuning the structures of oligothiophene units toward high-mobility “black” conjugated polymers. *Macromolecules* **2009**, *42*, 6510–6518.

28. Helgesen, M.; Gevorgyan, S. a.; Krebs, F. C.; Janssen, R. a. J. Substituted 2,1,3-Benzothiadiazole- And Thiophene-Based Polymers for Solar Cells − Introducing a New Thermocleavable Precursor. *Chem. Mater.* **2009**, *21*, 4669–4675.

29. Yamamoto, T.; Lee, B.-L.; Kokubo, H.; Kishida, H.; Hirota, K.; Wakabayashi, T.; Okamoto, H. Synthesis of a New Thiophene/Quinoxaline CT-Type Copolymer with High Solubility and Its Basic Optical Properties. *Macromol. Rapid Commun.* **2003**, *24*, 440–443.

30. Gadisa, a.; Mammo, W.; Andersson, L. M.; Admassie, S.; Zhang, F.; Andersson, M. R.; Inganäs, O. A New Donor–Acceptor–Donor Polyfluorene Copolymer with Balanced Electron and Hole Mobility. *Adv. Funct. Mater.* **2007**, *17*, 3836–3842.

31. Helgesen, M.; Carlé, J. E.; Krebs, F. C. Slot-Die Coating of a High Performance Copolymer in a Readily Scalable Roll Process for Polymer Solar Cells. *Adv. Energy Mater.* **2013**, *3*, 1664–1669.

32. Sun, X. X.; Lou, Y. Z.; Chen, Q. Q.; Li, L.; Zhuang, X. X.; Li, Y. C. Synthsis of [1,2,5]thiadiazolo[3,4-C]pyridine: A Novel Analogue to BT. *Adv. Mater. Res.* **2011**, *335–336*, 90–95.

33. Liang, Y.; Feng, D.; Wu, Y.; Tsai, S.-T.; Li, G.; Ray, C.; Yu, L. Highly efficient solar cell polymers developed via fine-tuning of structural and electronic properties. *J. Am. Chem. Soc.* **2009**, *131*, 7792–7799.

34. Nielsen, C. B.; Bjørnholm, T. New regiosymmetrical dioxopyrrolo- and dihydropyrrolo-functionalized polythiophenes. *Org. Lett.* **2004**, *6*, 3381–3384.

35. Bürgi, L.; Turbiez, M.; Pfeiffer, R.; Bienewald, F.; Kirner, H.-J.; Winnewisser, C. High-Mobility Ambipolar Near-Infrared Light-Emitting Polymer Field-Effect Transistors. *Adv. Mater.* **2008**, *20*, 2217–2224.

36. Zhang, Y.; Chien, S.-C.; Chen, K.-S.; Yip, H.-L.; Sun, Y.; Davies, J. a; Chen, F.-C.; Jen, A. K.-Y. Increased open circuit voltage in fluorinated benzothiadiazole-based alternating conjugated polymers. *Chem. Commun.* **2011**, *47*, 11026–11028.

37. Cho, N.; Song, K.; Lee, J. K.; Ko, J. Facile synthesis of fluorine-substituted benzothiadiazole-based organic semiconductors and their use in solution-processed small-molecule organic solar cells. *Chem. Eur. J.* **2012**, *18*, 11433–11439.

38. Xiao, L.; Liu, B.; Chen, X.; Li, Y.; Tang, W.; Zou, Y. Fluorine substituted benzothiazole-based low bandgap polymers for photovoltaic applications. *RSC Adv.* **2013**, *3*, 11869–11876.

39. Blouin, N.; Michaud, A.; Gendron, D.; Wakim, S.; Blair, E.; Neagu-plesu, R.; Bellete, M.; Durocher, G.; Tao, Y.; Leclerc, M. Toward a Rational Design of Poly (2,7-Carbazole) Derivatives for Solar Cells. *J. Am. Chem. Soc.* **2008**, *6*, 732–742.

40. Liu, X.; Kim, Y. J.; Kim, M. J.; Park, C. E.; Kim, Y. H. A unique concept of copolymer composed of main chain donor and side chain acceptor for promising bulk heterojunction solar cells. *Synth. Met.* **2015**, *205*, 195–200.

41. Guo, X.; Ortiz, R. P.; Zheng, Y.; Hu, Y.; Noh, Y. Y.; Baeg, K. J.; Facchetti, A.; Marks, T. J. Bithiophene-imide-based polymeric semiconductors for field-effect transistors: Synthesis, structure-property correlations, charge carrier polarity, and device stability. *J. Am. Chem. Soc.* **2011**, *133*, 1405–1418.

42. Seitz, D. E.; Lee, S.; Hanson, R. N.; Bottaro, J. C. Synthesis and Reactivity of the 2,5- Bis(Trimethylstannyl) Derivatives of Thiophene and Furan. *Synth. Commun.* **1983**, *13*, 121–128.

43. Hoffmann, K. J.; Carlsen, P. H. J. Study of an Efficient and Selective Bromination Reaction of Substituted Thiophenes. *Synth. Commun.* **1999**, *29*, 1607–1610.

44. Neo, W. T.; Ong, K. H.; Lin, T. T.; Chua, S.-J.; Xu, J. Effects of fluorination on the electrochromic performance of benzothiadiazole-based donor–acceptor copolymers. *J. Mater. Chem. C* **2015**, *3*, 5589–5597.

45. Kim, Y. J.; Kim, H. N.; Hwang, M. C.; Kim, Y. H.; Park, C. E. A weak donor/strong acceptor alternating copolymer for efficient bulk heterojunction solar cells. *Synth. Met.* **2014**, *198*, 93–100.

46. Carlé, J. E.; Jørgensen, M.; Krebs, F. C. Polymers for organic photovoltaics based on 1,5-bis(2-hexyldecyloxy)-naphthalene, thiophene, and benzothiadiazole. *J. Photonics Energy* **2011**, *1*, 011111 (1-10).

47. Helgesen, M.; Carlé, J. E.; Krebs, F. C. Slot-Die Coating of a High Performance Copolymer in a Readily Scalable Roll Process for Polymer Solar Cells. *Adv. Energy Mater.* **2013**, *3*, 1664–1669.

48. Collins, K. D.; Rühling, A.; Lied, F.; Glorius, F. Rapid assessment of protecting-group stability by using a robustness screen. *Chem. Eur. J.* **2014**, *20*, 3800–3805.

49. Dhayalan, V.; Alcañiz, F.; Werner, V.; Karaghiosoff, K.; Knochel, P. Preparation of a New Spirobi[thieno[2,3-c]pyran] and Its Selective Mono- and Dimetalation: Application for the Preparation of Soluble Conjugated Oligothiophenes and Pyrene Derivatives. *Synthesis (Stuttg).* **2015**, *47*, 3972–3982.

50. Wang, N.; Chen, Z.; Wei, W.; Jiang, Z. Fluorinated Benzothiadiazole Based Conjugated Polymers for High-Performance Polymer Solar Cells without Any Processing Additives or Post Treatments Fluorinated Benzothiadiazole Based Conjugated Polymers for High-Performance Polymer Solar Cells without Any. *J. Am. Chem. Soc.* **2013**, *135*, 17060–17068.

51. Vandenbergh, J.; Conings, B.; Bertho, S.; Kesters, J.; Spoltore, D.; Esiner, S.; Zhao, J.; Van Assche, G.; Wienk, M. M.; Maes, W.; Lutsen, L.; Van Mele, B.; Janssen, R. A. J.; Manca, J.; Vanderzande, D. J. M. Thermal Stability of Poly[2-methoxy-5-(2'-phenylethoxy)-1,4-phenylenevinylene] (MPE-PPV): Fullerene Bulk Heterojunction Solar Cells. *Macromolecules* **2011**, *44*, 8470–8478.

52. Ellinger, S.; Ziener, U.; Thewalt, U.; Landfester, K.; Möller, M. Synthesis and self-organization of α,ω-substituted oligothiophenes with long, branched alkyl substituents. *Chem. Mater.* **2007**, *19*, 1070–1075.

53. Heckler, I. M.; Kesters, J.; Defour, M.; Penxten, H.; Van Mele, B.; Maes, W.; Bundgaard, E. A stability study of polymer solar cells using conjugated polymers with di ff erent donor or acceptor side chain patterns. *J. Mater. Chem. A Mater. energy Sustain.* **2016**, *4*, 16677–16689.

54. Carlé, J. E.; Helgesen, M.; Zawacka, N. K.; Madsen, M. V.; Bundgaard, E.; Krebs, F. C. A comparative study of fluorine

substituents for enhanced stability of flexible and ITO-free high-performance polymer solar cells. *J. Polym. Sci. Part B Polym. Phys.* **2014**, *52*, 893–899.

55. Dam, H. F.; Krebs, F. C. Simple roll coater with variable coating and temperature control for printed polymer solar cells. *Sol. Energy Mater. Sol. Cells* **2012**, *97*, 191–196.

56. Carlé, J. E.; Andersen, T. R.; Helgesen, M.; Bundgaard, E.; Jørgensen, M.; Krebs, F. C. A laboratory scale approach to polymer solar cells using one coating/printing machine, flexible substrates, no ITO, no vacuum and no spincoating. *Sol. Energy Mater. Sol. Cells* **2013**, *108*, 126–128.

57. Helgesen, M.; Bjerring, M.; Nielsen, N. C.; Krebs, F. C. Influence of the Annealing Temperature on the Photovoltaic Performance and Film Morphology Applying Novel Thermocleavable Materials. *Chem. Mater.* **2010**, *22*, 5617–5624.

58. Helgesen, M.; Carlé, J. E.; Andreasen, B.; Hösel, M.; Norrman, K.; Søndergaard, R.; Krebs, F. C. Rapid flash annealing of thermally reactive copolymers in a roll-to-roll process for polymer solar cells. *Polym. Chem.* **2012**, *3*, 2649–2655.

59. Larsen-Olsen, T. T.; Søndergaard, R. R.; Norrman, K.; Jørgensen, M.; Krebs, F. C. All printed transparent electrodes through an electrical switching mechanism: A convincing alternative to indium-tin-oxide, silver and vacuum. *Energy Environ. Sci.* **2012**, *5*, 9467–9471.

Appendix B:

Additional Data

Chapter 3

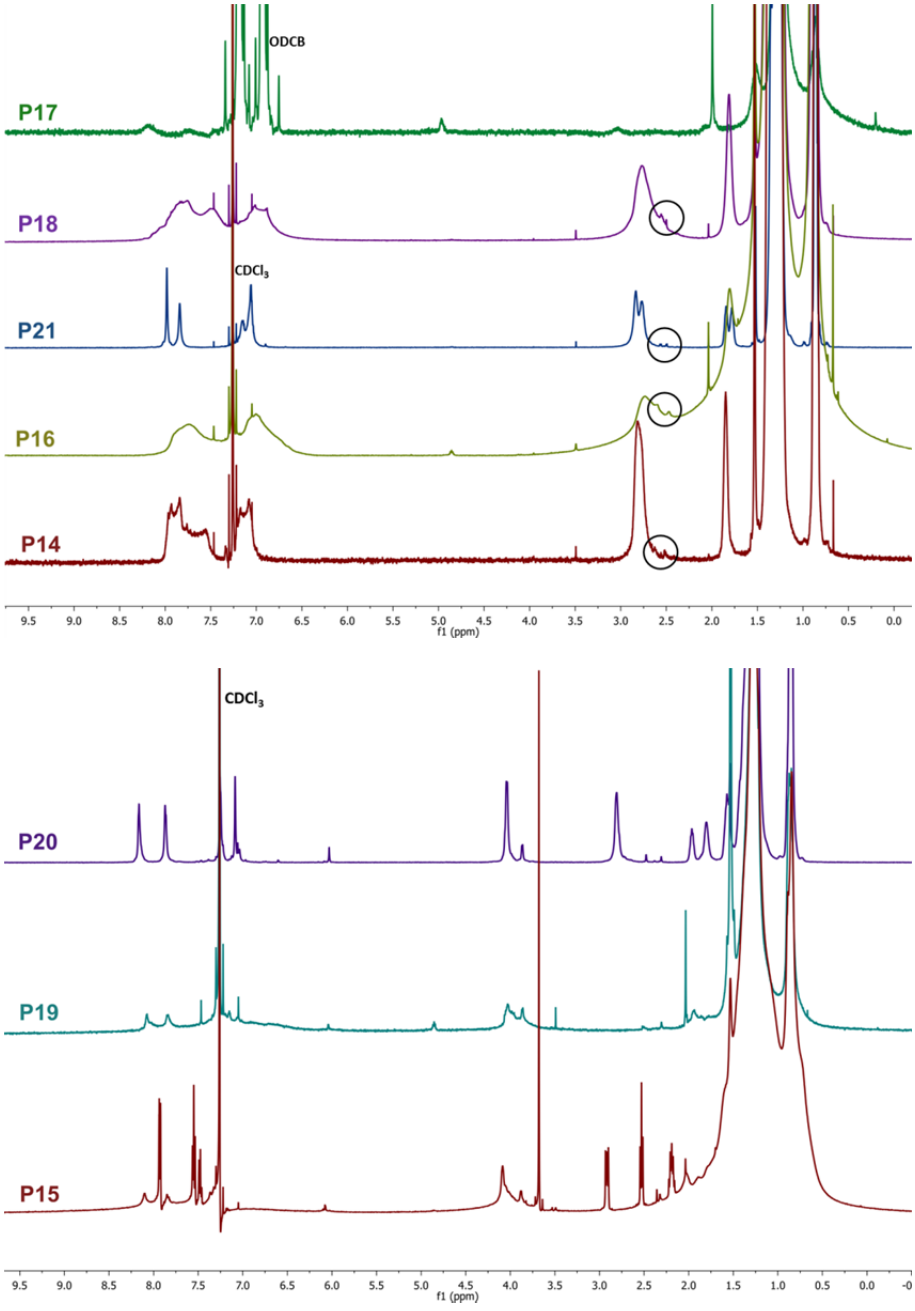

Figure B.3.1 *^{1}H NMR spectrum of polymer **P14-P22** in $CDCl_3$ or ODCB-d_6 (with high (top) and low (bottom) molecular weight). The end groups of some polymers are circled.*

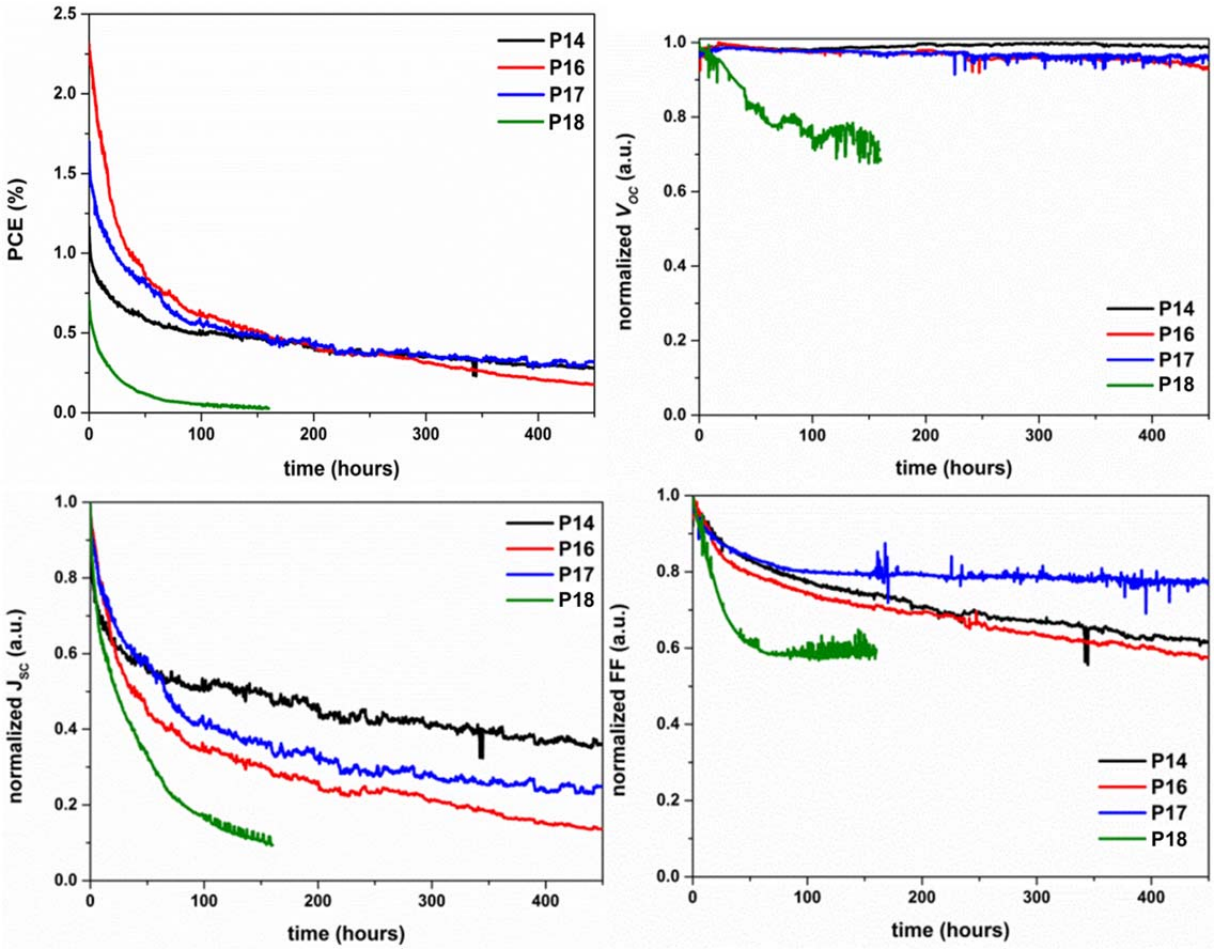

***Figure B.3.2**. Stability tests under solar irradiance of the PSCs showing the normalized V_{OC} (left), J_{SC} (middle) and FF (right).*

Chapter 4

The following spectra (Figure B.4.1-A.4.7) are adapted from *Bundgaard et al. Materials (Basel)., 2016, **9**, 181* under the Creative Commons Attribution License; by MDPI or from *Bundgaard et al. Adv. Energy Mater., 2015, **4**, 16677* with permission from Wiley-VCH Verlag GmbH & Co. KGaA, Weinheim ©2015.

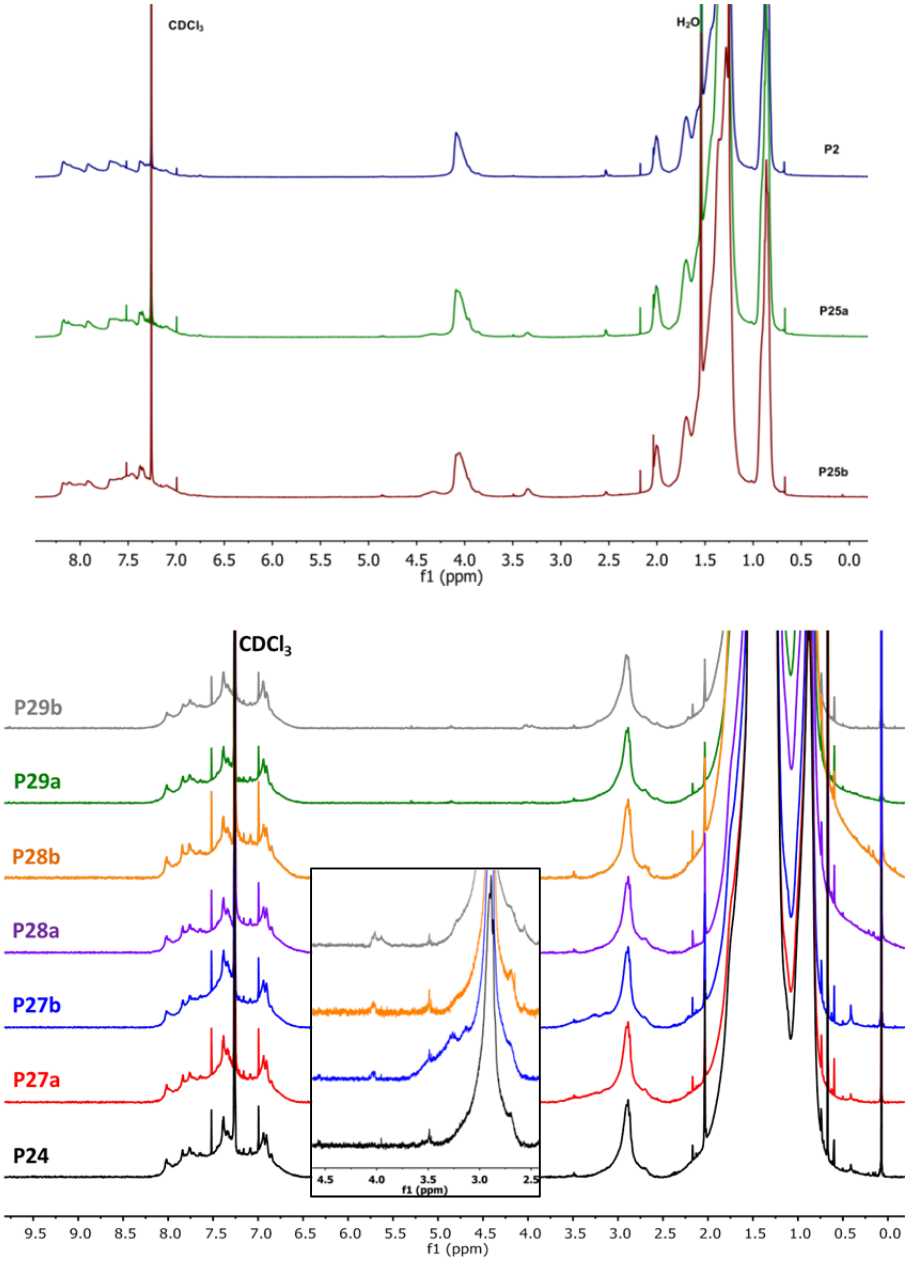

Figure B.4.1. *^{1}H NMR spectra of **P2** and **P25a,b** (top) and **P24** and **P27–P29** (bottom) in $CDCl_3$.*

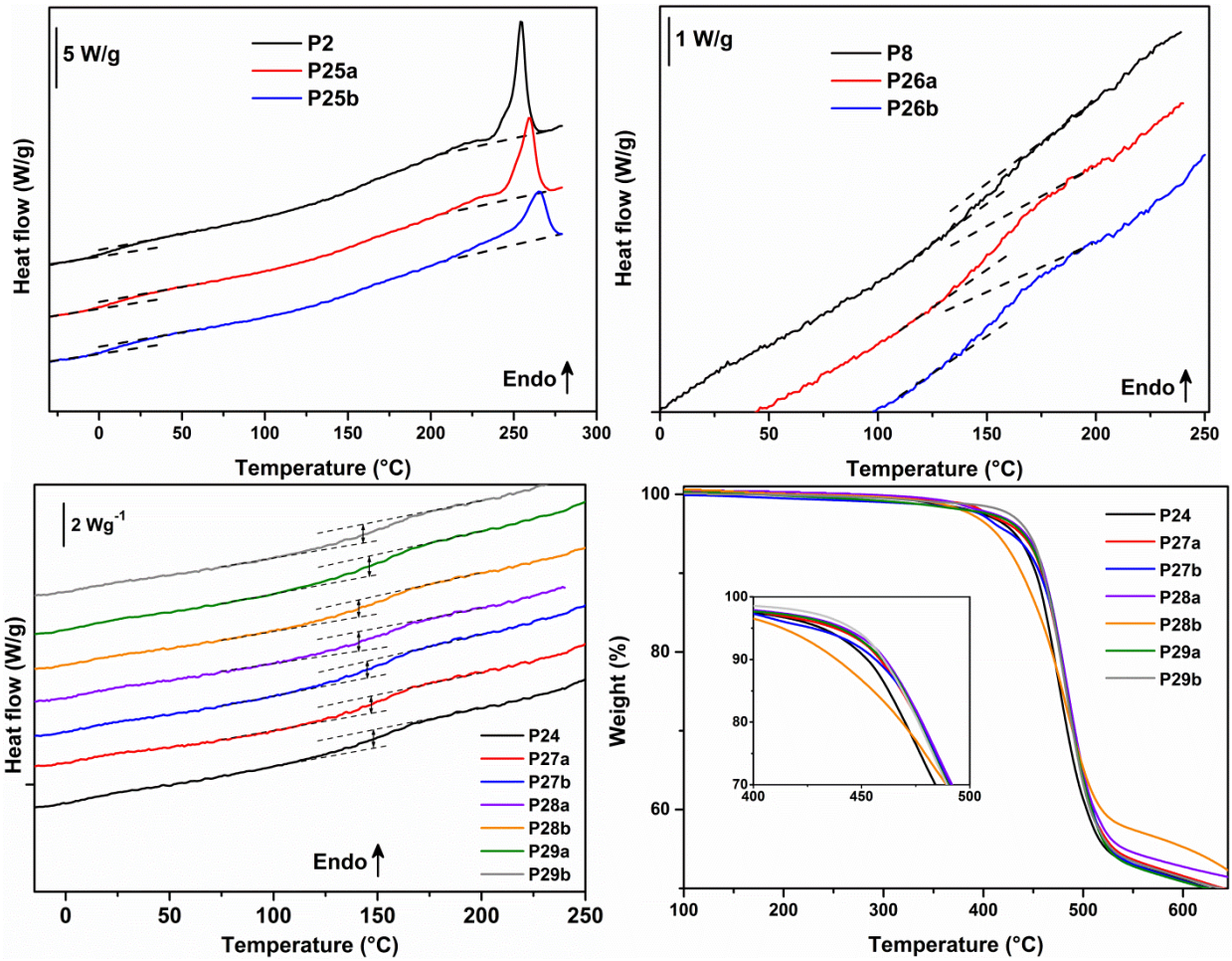

Figure B.4.2. *RHC thermograms for the BT (top, left), TzTz (top, right) and BDT (bottom, left) based polymers (curves shifted vertically for clarity); TGA profiles for polymers* ***P24*** *and* ***P27–P29*** *(bottom, right).*

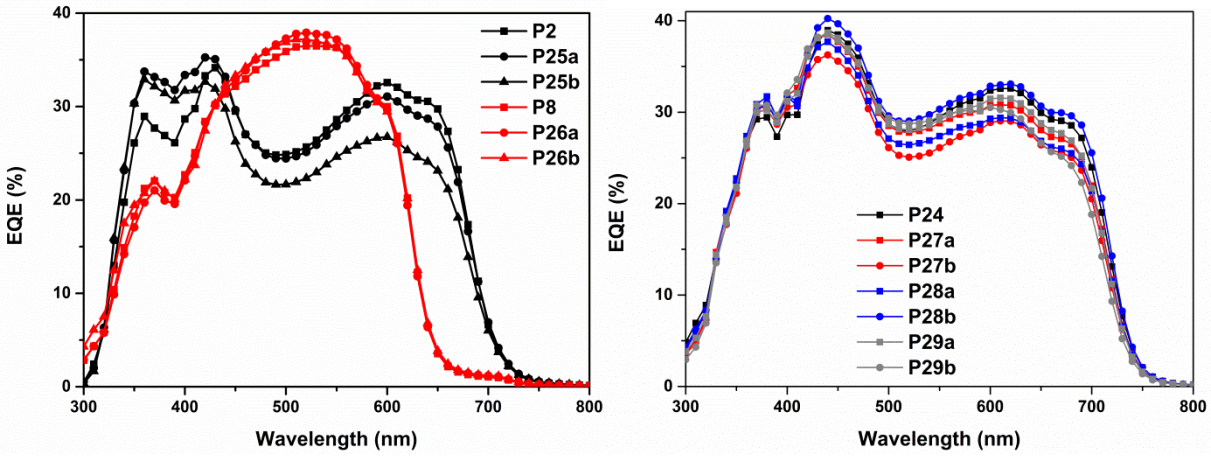

Figure B.4.3. *EQE spectra of the best PSCs prepared via RC of the BT and TzTz (left) and the BDT based polymer (right).*

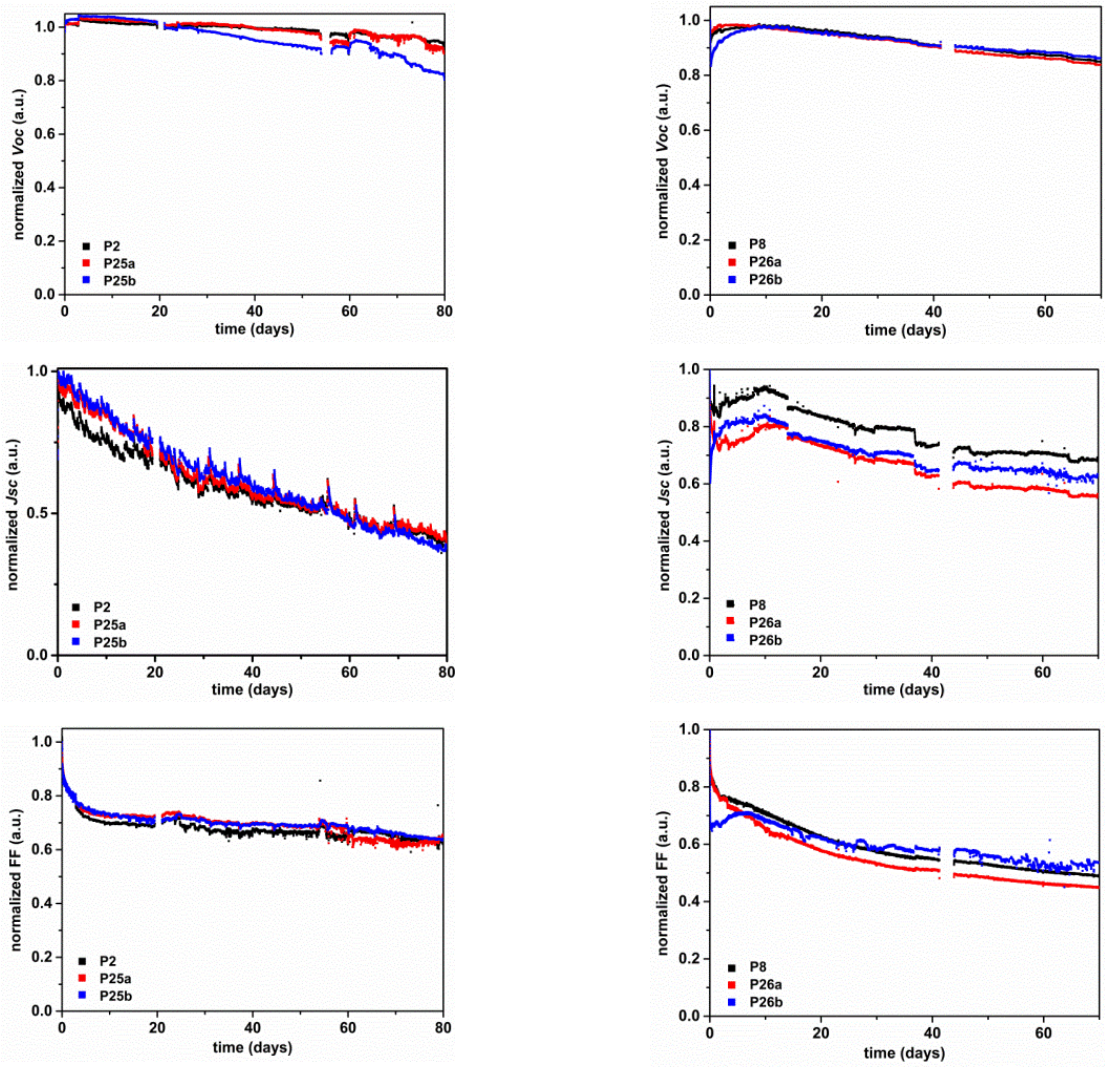

Figure B.4.4. *Average lifetime measurements (ISOS-L-1) for the RC devices using the BT (left) and TzTz (right) based polymer series showing the normalized V_{OC} (top), J_{SC} (middle) and FF (bottom) trends.*

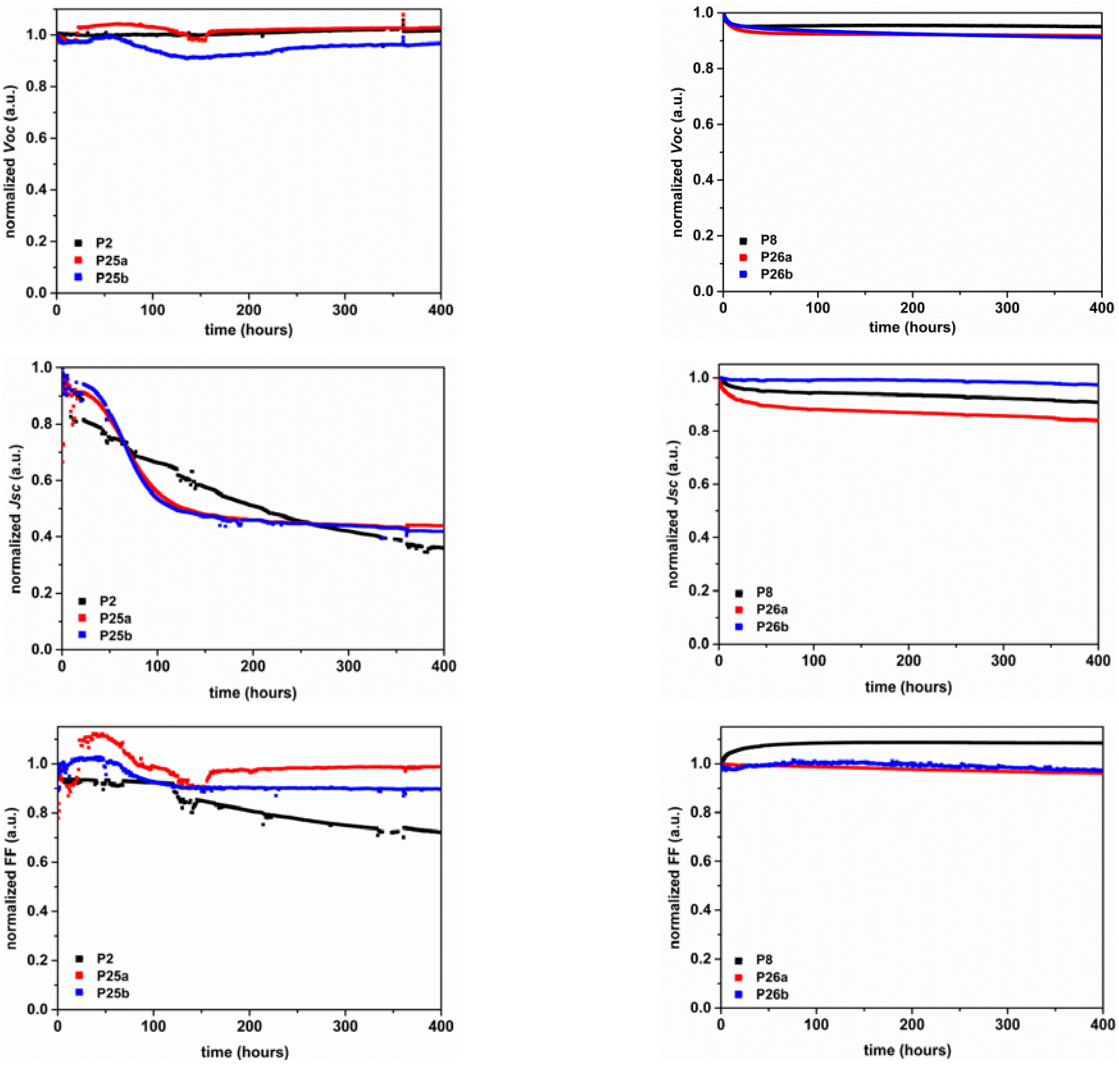

Figure B.4.5. *Thermal degradation tests (ISOS-D-2) of the SC devices using the BT (left) and TzTz (right) based polymer series showing the normalized V_{OC} (top), J_{SC} (middle) and FF (bottom) trends.*

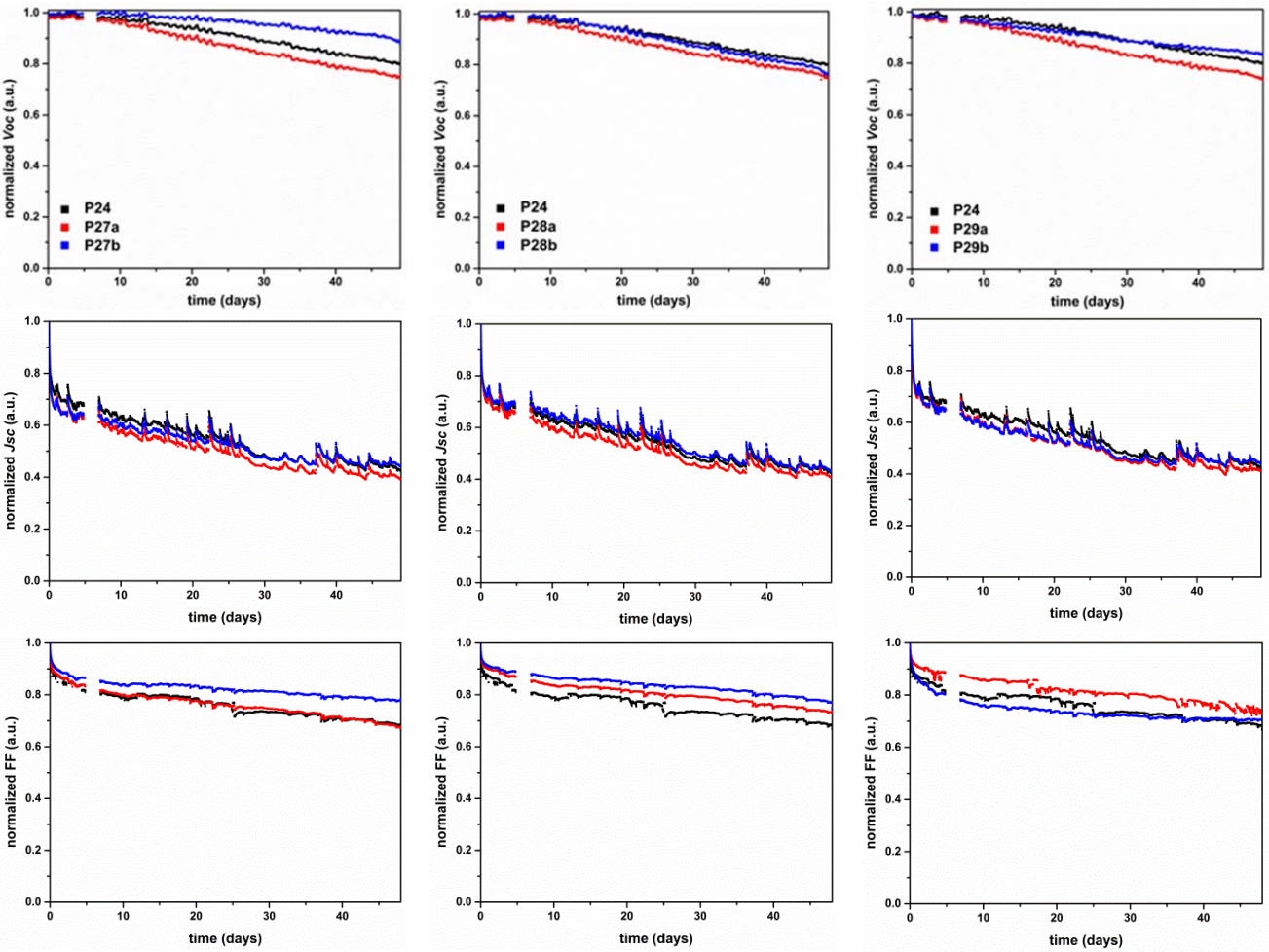

Figure B.4.6. *Average lifetime measurements (ISOS-L-1) for the RC devices based on* ***P27a,b*** *(left),* ***P28a,b*** *(middle) and* ***P29a,b*** *(right) in comparison to* ***P24*** *under constant sun irradiance (AM 1.5) in terms of normalized V_{OC} (top), J_{SC} (middle) and FF(bottom).*

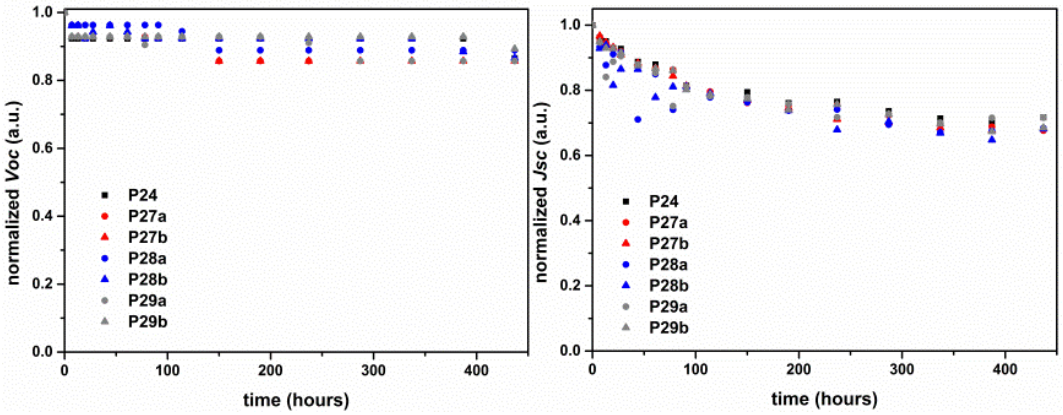

Figure B.4.7. *Thermal degradation tests (ISOS-D-2) of the SC devices using the BDT based polymer series showing the normalized V_{OC} (left) and J_{SC} (right) trends.*

Chapter 5

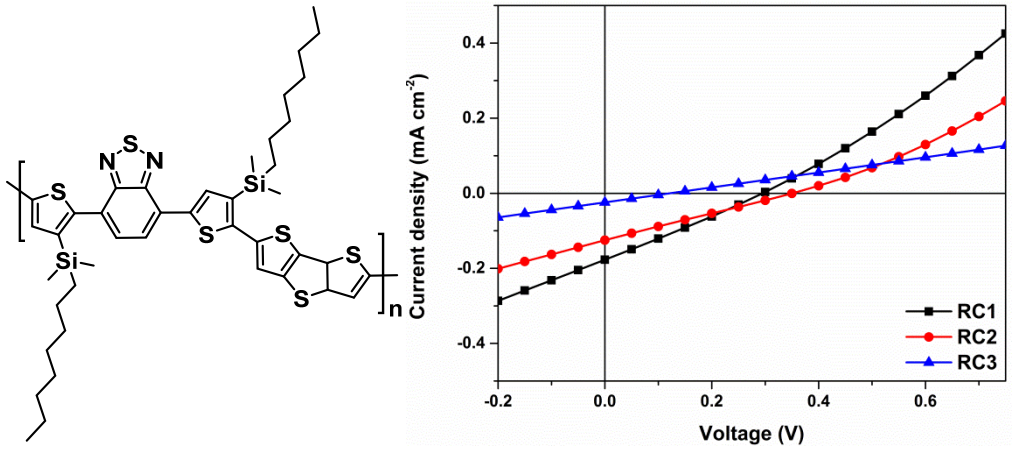

Figure B.5.1. *Structure of the acid cleavable polymer (left) and J-V characteristics of the PSCs(right).*

An acid cleavable polymer (Figure B.5.1 left) and $PC_{61}BM$ (1:2-ratio) were dissolved in CF. To 1.0 mL of the polymer blend 0.5 mL (0.2 M) trifluoroacidic acid was added. After stirring for 30 min at 50°C the solution changed colour from green to dark purple and turned viscous. The solution was coated thereafter twice at 60°C onto a layer of PEDOT:PSS on a plastic substrate with a total layer thickness of ~500-600 nm. The coating solution had a concentration of 20 mg mL^{-1} of the polymer and $PC_{61}BM$. After coating of the active similar to the polymers from Chapter 2, the substrate was heated at 80°C for 1-3h to remove residual trifluoroacidic acid.

For RC 2: The active layer was wetted twice with hexane/2% triethylamine to remove the leftover side chains and acid and again with pure hexane.

For RC 3: The active layer was wetted with trifluoroacitic acid in *n*-buthanol (1:4 volume-%).

Hereafter a layer of ZnO in isopropanol was coated at 60°C on top of the active yielding a thickness of ~90 nm. Finally another layer of PEDOT:PSS and the silver top electrode were coated. The PSCs were measured under AM1.5 (1000 W m^{-2}). All devices failed almost completely. (Table B.5.1, Figure B.5.1 right)

Table B.5.1*. J-V characteristics*[a] *(V_{OC}, J_{SC}, FF and PCE) for the PSCs based on the cleaved polymer.*

Polymer	PCE (%)	V_{OC} (V)	J_{sc} (mA m^{-2})	FF (%)
RC1[a]	0.020	0.29	0.18	26.3
RC2[b]	0.016	0.35	0.13	24.7
RC3[c]	0.001	0.12	0.02	24.9

[a] The roll-coating was performed without additional removal step of the side chains/acid, [b] After coating of the active layer, it was wetted twice with hexane/2% triethylamine, then hexane, [c] After coating of the active layer, it was wetted with tricluoroacitic acid in buthanol.

Appendix C:

Publications and Personal Contribution

Publications

E. Bundgaard, F. Livi, O. Hagemann, J. E. Carlé, M. Helgesen, I. M. Heckler, N. K. Zawacka, D. Angmo, T. T. Larsen-Olsen, G. A. dos Reis Benatto, B. Roth, M. V. Madsen, M. R. Andersson, M. Jørgensen, R. R. Søndergaard, and F. C. Krebs, *Matrix Organization and Merit Factor Evaluation as a Method to Address the Challenge of Finding a Polymer Material for Roll Coated Polymer Solar Cells*, *Adv. Energy Mater.*, **2015**, *5*, 1402186 (1–16). The article is attached as Appendix C.1 with permission from Wiley-VCH Verlag GmbH & Co. KGaA, Weinheim ©2015. The original article can be found under doi:10.1002/aenm.201402186. My contributions in this work were:

- Preparation of the polymer solar cells and testing under a solar simulator
- Literature research for all monomer synthesis and all polymers applied in polymer solar cells

J. Toušek, J. Toušková, J. Ludvík, A. Liška, Z. Remeš, O. Kylián, J. Kousal, R. Chomutová, I. M. Heckler, E. Bundgaard, and F. C. Krebs, *Comparison of the electron work function, hole concentration and exciton diffusion length for P3HT and PT prepared by thermal or acid cleavage*, *Solid. State. Electron.*, **2016**, *116*, 111–118. The article is attached as Appendix C.2 with permission from Elsevier ©2016. The original article can be found under doi:10.1016/j.sse.2015.11.002. My contributions in this work were:

- Spin coating of the polymers on a glass substrate
- UV-vis and IR measurements

I. M. Heckler, J. Kesters, M. Defour, M. Madsen, H. Penxten, J. D'Haen, B. Van Mele, W. Maes, and E. Bundgaard, *The Influence of Conjugated Polymer Side Chain Manipulation on the Efficiency and Stability of Polymer Solar Cells*, *Materials (Basel).*, **2016**, *9*, 181 (1–18). The article is attached as Appendix C.3 under the Creative Commons Attribution License; by MDPI. The original article can be found under doi: 10.3390/ma9030181 (open access). My contributions in this work were:

- Article writing
- Synthesis of the polymers, characterization with UV-vis and NMR
- Preparation and characterization of the roll-coated polymer solar cells
- Lifetime testing of the roll coated polymer solar cells

I. M. Heckler, J. Kesters, M. Defour, H. Penxten, B. Van Mele, W. Maes, and E. Bundgaard, *A stability study of polymer solar cells using conjugated polymers with different donor or acceptor side chain patterns*, *J. Mater. Chem. A.*, **2016**, *4*, 16677–16689. The article is attached as Appendix C.4 and was reproduced with permission from The Royal Society of Chemistry ©2016. The original article can be found under doi**:** 10.1039/C6TA07244E. My contributions in this work were:

- Article writing
- Synthesis of the polymers, characterization with UV-vis, NMR and photodegradation
- Preparation and characterization of the roll-coated polymer solar cells
- Lifetime testing of the roll coated polymer solar cells

S. A. Gevorgyan, I. M. Heckler, E. Bundgaard, M. Corazza, M. Hösel, R. R. Søndergaard, G. A. dos Reis Benatto, M. Jørgensen and F. C. Krebs, *Improving, characterizing and predicting the lifetime of organic photovoltaics, J. Phys. D: Appl. Phys.*, **2017**, *50,* 103001. The article is attached as Appendix C.5 and was reproduced with permission from ©IOP Publishing. All rights reserved. The original article can be found under DOI: 10.1088/1361-6463/50/10/103001. My contributions in this work were:

- Writing one chapter about polymer stability.

I. M. Heckler and E. Bundgaard, **2017**, in progress. My contributions in this work were:

- Article writing
- Synthesis of the polymers, characterization with UV-vis and NMR
- Preparation and characterization of the roll-coated polymer solar cells
- Lifetime testing of the roll coated polymer solar cells

Conferences: oral presentations

I. M. Heckler, J. Kesters, W. Maes, and E. Bundgaard, *The influence of side chain manipulation of conjugated polymers on the stability of polymer solar cells,* International Conference on Hybrid and Organic Photovoltaics (HOPV16), June **2016**, Swansea, United Kindom.

I. M. Heckler, J. Kesters, W. Maes, and E. Bundgaard, *A stability study of manipulated conjugated polymers in polymer solar cells*, Global Organic Photovoltaic Conference (eGOPV 2016), September **2016**, e-conference, https://www.youtube.com/watch?v=CPvI4KX5HkQ&feature=youtu.be.

I. M. Heckler and E. Bundgaard, *Polymer Materials for Solar Cells: Optimization and Stability Strategy*, DTU Energy's annual PhD symposium 2016, November **2016**, Lyngby, Denmark.

Conferences and Summer school: poster presentations

The conference posters are attached as Appendix C.6.

I. M. Heckler and E. Bundgaard, *Improvement of the stability of polymers for organic solar cells by different strategies*, International Summer School on Organic Photovoltaics, September **2014**, Strasbourg, France.

I. M. Heckler and E. Bundgaard, *Improvement of the stability of polymers for organic solar cells by different strategies*, DTU Energy's annual PhD symposium 2014, November **2014**, Lyngby, Denmark.

****Best Poster Award****

I. M. Heckler and E. Bundgaard, *Polymers with improved stabilty for polymer solar cells*, 4th Zing Polymer Chemistry Conference, December **2014**, Cancun, Mexico.

I. M. Heckler, J. Kesters, W. Maes, and E. Bundgaard, *Influence of side chain substituted conjugated polymers on the stability of polymer solar cells*, DTU Energy's annual PhD symposium 2015, November **2015**, Lyngby, Denmark.

Science Dissemination

G. Benatto, L. Hildebrand Rossander, I. M. Heckler and F. C. Krebs, *Organic Solar Cells @ Roskilde Festival,* Roskilde Festival 2016, June **2016**, Roskilde, Denmark: presentation (poster and oral) of organic solar cells at a science stand of the festival.

www.MaterialsViews.com

ADVANCED ENERGY MATERIALS
www.advenergymat.de

FULL PAPER

Matrix Organization and Merit Factor Evaluation as a Method to Address the Challenge of Finding a Polymer Material for Roll Coated Polymer Solar Cells

Eva Bundgaard, Francesco Livi, Ole Hagemann, Jon E. Carlé, Martin Helgesen, Ilona M. Heckler, Natalia K. Zawacka, Dechan Angmo, Thue T. Larsen-Olsen, Gisele A. dos Reis Benatto, Bérenger Roth, Morten V. Madsen, Mats R. Andersson, Mikkel Jørgensen, Roar R. Søndergaard, and Frederik C. Krebs*

The results presented demonstrate how the screening of 104 light-absorbing low band gap polymers for suitability in roll coated polymer solar cells can be accomplished through rational synthesis according to a matrix where 8 donor and 13 acceptor units are organized in rows and columns. Synthesis of all the polymers corresponding to all combinations of donor and acceptor units is followed by characterization of all the materials with respect to molecular weight, electrochemical energy levels, band gaps, photochemical stability, carrier mobility, and photovoltaic parameters. The photovoltaic evaluation is carried out with specific reference to scalable manufacture, which includes large area (1 cm^2), stable inverted device architecture, an indium-tin-oxide-free fully printed flexible front electrode with ZnO/PEDOT:PSS (poly(3,4-ethylenedioxythiophene):polystyrene sulfonate), and a printed silver comb back electrode structure. The matrix organization enables fast identification of active layer materials according to a weighted merit factor that includes more than simply the power conversion efficiency and is used as a method to identify the lead candidates. Based on several characteristics included in the merit factor, it is found that 13 out of the 104 synthesized polymers outperformed poly(3-hexylthiophene) under the chosen processing conditions and thus can be suitable for further development.

1. Introduction

Polymer solar cells (PSCs) are seen as an important solution to the estimated increase in global energy consumption of 1 GW per day due to the low energy payback time (EPBT), the potentially high energy return factor (ERF), the small or nonexisting ecotoxicity, and the fully scalable high speed manufacture. This is mainly ascribed to the reduced amount of energy used during production and the avoidance of scarce materials, which has already resulted in an EPBT of 90 days for system-integrated PSCs[1] with the potential of reaching an EPBT of only 1 day.[2] The potentially high ERF can be achieved through increased device lifetime, higher device efficiency, and lower energy production cost.

Research into PSCs has increased exponentially over the last decade, with more than 46 500 published papers.[3] This increase is partly attributable to the fact that the polymer composition in the active layer has varied due to the use of a large number of different types of conjugated polymers. The most common factor for comparison in the PSC research field is the power conversion efficiency (PCE). In the past decade, the main focus has been on increasing the PCE, and lately efficiencies of over 10% have been reported for small area devices (mm^2 scale).[4] Much of the increase in PSC efficiency arises from an optimization of the light-absorbing conjugated polymer applied in the active layer of the device. Low band gap polymers have been developed to absorb light at wavelengths longer than 650 nm and thus have a band gap below 2 eV.[5] This is done by a very common approach where two monomers, one electron donating and one electron accepting unit, are coupled to produce a low band gap polymer with a charge transfer band at longer wavelengths (lower energy) together with π–π transitions in order to cover a larger part of the solar spectrum. In theory this will give a higher photocurrent compared to, e.g.,

Dr. E. Bundgaard, F. Livi, O. Hagemann, Dr. J. E. Carlé, Dr. M. Helgesen, I. M. Heckler, N. K. Zawacka, Dr. D. Angmo, Dr. T. T. Larsen-Olsen, G. A. dos Reis Benatto, B. Roth, Dr. M. V. Madsen, Dr. M. Jørgensen, Dr. R. R. Søndergaard, Prof. F. C. Krebs
Department of Energy Conversion and Storage
Technical University of Denmark
Frederiksborgvej 399, 4000 Roskilde, Denmark
E-mail: evbu@dtu.dk

Prof. M. R. Andersson
Ian Wark Research Institute
University of South Australia
Mawson Lakes, South Australia 5059, Australia

Prof. M. R. Andersson
Department of Chemical and Biological Engineering/Polymer Technology
Chalmers University of Technology
41296 Göteborg, Sweden

DOI: 10.1002/aenm.201402186

poly(3-hexylthiophene) (P3HT), which has a band gap of 2 eV, due to an absorption profile that is better matched with the solar spectrum. Thus, a potentially higher PCE of the PSC can be reached, given that the energy level alignment with the acceptor in the active layer is optimal.[5] For large-area PSC modules, the reported PCE values are significantly lower (2%–3%)[4] and studies by Jørgensen et al.[6] clearly demonstrate this. Thus, the 10% efficiency can be viewed as somewhat misleading for several reasons. First of all, interlaboratory measures of efficiency are not necessarily comparable, which has led to a practice of sending the hero devices to be certified at certain trusted laboratories. The same principle has been applied in so-called round robin studies,[7,8] where the same devices were tested at several laboratories with considerable variation as a result. Another important issue is that an overwhelming majority (95%) of the devices is made with glass substrates, often using indium-tin-oxide (ITO) as the transparent electrode and with a diminutive active area. Any real-world application would probably use flexible plastic substrates, no scarce materials (e.g., indium), roll-to-roll (R2R) fabrication, and considerably larger devices as convincingly demonstrated in the first polymer solar park.[1] However, less interest has been devoted to these types of devices, even though all indications show that the PCEs obtained in the former laboratory-scale devices cannot be transferred to larger R2R-fabricated devices.[9] The transfer of any successful PSC from small scale to large scale in a R2R setting requires ambient atmosphere, flexible substrates, freedom from indium and vacuum, and, to complicate matters even further, potentially opens up for a myriad of film forming techniques and inks. Such a transfer, however, has been simplified by the development of the mini roll coater, which applies processing conditions similar to large-scale R2R, but in smaller scale (100×1 cm^2).[9] It is essential to note the vast number of choices which can influence the performance of a PSC based on a given active material, and to realize the impossibility of testing all factors for all active polymer materials. Instead, focus should be on settings that are realistic in the context of production and end application. For all the above reasons, the countless scientific studies obtained thus far will only offer a partial answer to the question of whether a given conjugated polymer is suitable for R2R-processed PSCs.

Our main interests lie in developing PSCs to the level of larger-scale fabrication, and we therefore needed a more rational approach. This was in part inspired by how pharmaceutical companies use screening studies to find lead compounds that can later be optimized both with respect to detailed structure and application. They start by building a large library of compounds, which is tested using fairly simple procedures. This gives insights into which chemical structures perform best and should be further elaborated. Even though several thousand different polymer materials have been applied as light-absorbing polymer material in the active layer, to our knowledge such a systematic screening has only been carried out in one instance in the field of PSC using ink jet printing. However, this screening was restricted to two different polymers and two different fullerenes.[10] Moreover, while many polymer materials have been compared in reviews,[11–13] one must keep in mind that laboratories using different methods (spin speed, light source) will generate different PCE measurements of the same polymer as demonstrated in round robin studies.[7,8] This makes a review based on a comparison of different polymers measured at different laboratories less reliable. In the present study we have utilized a screening strategy comprising the selection of 8 donor and 13 acceptor monomers which give a total of 104 polymers after the combinatorial pairing. This constituted the library that formed the basis for the screening of the photovoltaic properties of roll-coated PSCs and other properties. Our work demonstrates the challenges associated with the design of polymer materials for scaled PSCs, which include a multitude of materials and processing parameters and progress significantly beyond simple criteria such as evaluation according to PCE alone. We conclude on the effort needed for identification of new lead candidates[14,15] and estimate that only a few percent of all newly reported polymers qualify for further development. We expect that only a small fraction of these will qualify for scaled manufacture of PSCs.

2. Results and Discussion

Table 1 offers a comprehensive overview of all the data collected for the 104 possible polymers based on 13 acceptor monomers (left column) and 8 donor monomers (top row). Each cell in the table represents a unique polymer and contains 8 entries: optical band gap (eV), highest occupied molecular orbital/lowest unoccupied molecular orbital (HOMO/LUMO) energies, hole mobility, average PCE and standard deviation together with the highest open circuit voltage (V_{OC}) obtained, PCE values from the literature, photochemical stability, and finally the number of synthetic steps.

2.1. Data Handling

Computer programs and databases were developed in order to handle the enormous amount of data which was produced upon characterization of the 104 polymer materials. For each polymer, 12 different PSC types were prepared (based on 2 different solvents in 2 different polymer/[60]PCBM (phenyl-C_{61}-butyric acid-methyl-ester) ratios coated with 3 different thicknesses). About 50 devices were made for each of these 12 combinations, for which at least 5 of the samples were measured to give the average PCE. This adds up to some 5340 *I–V* curves measured in total. Each experiment had its own folder and the IV measurement program was set to save the data in the corresponding folder based on the solvent/ratio/thickness combination. On our internal webpage we added a data analysis program, which gave an overview of the data collected during the characterizations. This allowed us to keep track of the progress and gave a clear overview of which polymers performed best. The following measured data were also saved in the database: UV–vis (2 absorption curves for each polymer in solution and as film), square wave voltammetry (SWV; 4 curves for each polymer, i.e., 2 forward and 2 reverse), hole mobility (2 *I–V* curves in the dark for 2 different active layer thickness), absorption curves used to determine photochemical stability (12 absorption curves are measured per hour, the total number

Table 1. Combination sheet for donors and acceptors in the screening. The dotted lines on the monomer unit indicate where the units are coupled together by a C–C bond. The values listed are: 1) The optical band gap in eV estimated from the absorption spectrum. 2) The value of the highest occupied molecular orbital (HOMO) measured by square wave voltammetry (SWV) and the lowest unoccupied molecular orbital (LUMO) estimated from the electrochemical HOMO and the optical band gap, both in eV. 3) Size exclusion chromatography (SEC) traces, which were calculated on the basis of polystyrene standards. The average number molecular weight, M_n (g mol^{-1}) and polydispersity (PD) are indicated. 4) The hole mobility measured on a pure polymer film (ITO/PEDOT:PSS/polymer/Al). For P3HT the hole mobility was found to be 1.26E-07 m^2 V^{-1} s (270 nm) and 8.02E-8 m^2 V^{-1} s (300 nm). The reported values are for an annealed film. An (x) indicates a value for a sample which has not been annealed. 5) The average and standard deviation (calculated from the 10 best performing devices) PCE from the PSC devices prepared by roll coating together with the V_{OC}. The value in () is the highest measured PCE. 6) Values of the reported PCE are listed for reference. Unless stated differently, here the devices were prepared by spin coating on a glass/ITO substrate, using thermal evaporation under vacuum for the back electrode with a normal device geometry and $PC_{60}BM$ as acceptor. 7) The photochemical stability measured on the pure polymers. It is listed in the table as [% h^{-1}] ± standard deviation (absorption maximum). Notice that since the degradation rate is in % h^{-1}, lower values indicate more stable polymers. The degradation rate is 4% h^{-1} for P3HT and 1% h^{-1} for P3HT/[60]PCBM. 8) The number of synthetic steps for the polymer, indicated by #, starting from simple cheap and commercially available molecules, such as 3-bromothiophene or benzothiadiazole. For experimental details and all measured data, please use the links provided in the Supporting Information.

1. E_g [eV]									
2. HOMO/LUMO level [eV]									
3. Mn [g mol^{-1}]; PD									
4. Hole mobility [cm2 V^{-1} s]									
5. PCE% average ± std (highest); Voc [V]									
6. PCE [in %] reported in literature [reference]									
7. Photochemical stability [% h^{-1}]									
8.#synthetic steps									
	1. 1.47	1. 1.35	NA	D5 R=$C_{12}H_{25}$	NA	1. 1.73	D8 R=$C_{12}H_{25}$	1. 1.69	
	2. −5.00/−3.53	2. −5.06/−3.71	6. 1.71 (HD on D3)[19,20]	1. 1.79	6. No reference	2. −5.07/−3.332	1. 1.89	2. −5.43/−3.71	
	3. 96 000; 9.9	3. 2 370 000; 4.4	8. #9	2. −5.50/−3.71	8. #11	3. 13 000; 2.1	2. −5.39/−3.50	3. 6900; 1.4	
	4. 3.96E-07	4. 8.35E-09		3. 9300; 2.2		4. 6.62E-07	3. 4700; 1.7	4. 1.93E-08	
	5. 1.30 ± 0.04 (1.37); 0.57	5. 0.37 ± 0.04 (0.45); 0.71		4. 2.92E-08		5. 2.0 ± 0.1 (2.21); 0.76	4. NA	5. 0.03 ± 0.07 (0.06); 0.57	
	6. 5.6 ($PC_{70}BM$)[16,17]	6. 2.54 (D2 has 2 thiophenes)[18]		5. 0.02 ± 0 (0.02); 0.79		6. 2.2[22–24]	5. NA	6. No reference	
	7. 1.11 ± 0.10 (0.31)	7. 0.25 ± 0.03 (0.36)		6. No PCE[21]		7. 1.48 ± 0.16 (0.44)	6. 1.23[21,25]	7. 7.22 ± 0.3 (0.26)	
	8. #11	8. #9		7. 2.46 ± 0.15 (0.62)		8. #6	7. 30.88 ± 2.61 (0.25)	8. #8	
				8. #5			8. #8		

Continued

ADVANCED ENERGY MATERIALS
www.advenergymat.de

Materials Views
www.MaterialsViews.com

Table 1. Continued

	A2 R=$C_{12}H_{25}$; D1 R=hexyl	A2 R=$C_{12}H_{25}$	A2 R=$C_{12}H_{25}$	A2 R=$C_{12}H_{25}$; D5 R=H	A2 R=H	A2 R=$C_{12}H_{25}$	A2 and D8 R=$C_{12}H_{25}$	A2 R=$C_{12}H_{25}$
	1. 1.52	1. 1.61	1. 1.69	1. 1.58	1. 1.88	1. 1.65	1. 2.05	1. 1.64
	2. –5.03/–3.51	2. –4.95/–3.30	2. –5.06/–3.37	2. –4.92/–3.34	2. –5.51/–3.63	2. –5.07/–3.42	2. –5.17/–3.12	2. –5.24/–3.62
	3. 9500; 2.0	3. 12 400; 11.4	3. 90 000; 4.5	3. 540 000; 4.2	3. 1860; 2.9	3. 7500; 3.2	3. 8600; 1.5	3. 9400; 1.8
	4. 4.28E-08	4. 3.98E-08	4. 9.75E-10	4. 9.87E-09	4. 3.81E-09	4. 1.48E-07	4. 2.16E-08	4. 1.2E-08
	5. 0.44 ± 0.03 (0.48); 0.54 6. 2.95 (A2 R=H, PC71BM	5. 1.02 ± 0.14 (1.3); 0.63	5. 0.5 ± 0.06 (0.61); 0.62	5. 0.07 ± 0 (0.08); 0.50	5. NA	5. 1.24 ± 0.1 (1.38); 0.65	5. NA	5. NA
	7. 16.9 ± 0.5 (0.15)	7. 0.54 ± 0.04 (0.24)	7. 1.17 ± 0.09 (0.26)	7. 0.45 ± 0.05 (0.44)	7. 8.51 ± 0.95 (0.27)	7. 0.83 ± 0.07 (0.60)	7. 20.22 ± 3.05 (0.52)	7. 5.67 ± 0.29 (0.21)
	8. #14	8. #12	8. #12	8. #8	8. # 14	8. #9	8. #11	8. #11
	1. 1.70	Gel	1. 1.83	D5 R=H	1. 1.99	1. 1.83	D8 R=$C_{12}H_{25}$	1. 1.84
	2. NA	2. –5.10/–3.49	2. –5.15/–3.32	1. 1.67	2. –5.41/–3.42	2. –4.98/–3.15	1. 1.74	2. –5.30/–3.46
	3. 50 000; 10.8	3. 2 300 000; 6.7	3. 16 000; 3.5	2. –4.98/–3.31	3. 3800; 3.1	3. 24 000; 2.7	2. –4.92/–3.18	3. 19 000; 2.1
	4. NA	6. 4.76[37]	4. 1.99E-07	3. 7300; 1.9	4. 2.11E-07	4. 4.52E-07	3. 2200; 3.1	4. 5.58E-07
	5. 0.21 ± 0.05 (0.32); 0.68	8. #15	5. 0.55 ± 0.07 (0.69); 0.68	4. NA	5. 0.19 ± 0.16 (0.21); 0.69	5. 0.35 ± 0.04 (0.43); 0.69	4. 2.11E-07	5. 0.23 ± 0.04 (0.31); 0.71
	6. 1.99[27]		6. 4.02 ($PC_{71}BM$)[38]	5. 0.49 ± 0.06 (0.59); 0.58	6. 5.4 (A3 OC_8H_{17}, D6 N-C_8H_{17}, $PC_{71}BM$)[40,41]	6. No reference	5. 0.22 ± 0.05 (0.32); 0.64	6. No reference
	7. 12.0 ± 1.1 (0.13)		7. 1.55 ± 0.04 (0.64)	6. 1.78[39]	7. 5.52 ± 0.34 (0.38)	7. 2.23 ± 0.02 (0.69)	6. No reference	7. 5.08 ± 0.12 (0.49)
	8. #17		8. #15	7. NA	8. #17	8. #12	7. 7.35 ± 0.59 (0.35)	8. #14
					8. #11		8. #14	

Continued

Table 1. Continued

A4

	1. 1.70	1. 1.66	1. 1.82	D5 R=H	NA	1. 1.89	D8 R=$C_{12}H_{25}$	1. 1.96
	2. –5.16/–3.46	2. –5.25/–3.59	2. –5.19/–3.39	1. 1.73	6. No reference	2. –5.24/–3.35	NA	2. –5.50/–3.54
	3. 15 000; 2.1	3. 22 000; 9.1	3. 8000; 6.1	2. –5.28/–3.55	8. #15	3. 6400; 2.1	6. No reference	3. 7000; 1.5
	4. 2.07E-08	4. Unstable	4. Unstable	3. 29 000; 9.2		4. 1.66E-07	8. #12	5. NA
	5. 0.05 ± 0.01 (0.07); 0.66	5. 0.17 ± 0.01 (0.2); 0.80	5. 0.03 ± 3.34 (0.03); 0.59	4. 4.58E-10		5. NA		6. No reference
	6. No PCE[42]	6. No reference	6. No reference	5. 0.49 ± 0.07 (0.68); 0.94		6. 2.82 ($PC_{71}BM$)[44]		7. 5.81 ± 0.53 (0.17)
	7. 22.31 ± 0.72 (0.35)	7. 3.10 ± 0.24 (0.66)	7. 6.85 ± 0.20 (0.39)	6. 6.0 ($PC_{71}BM$)[43]		7. 18.1 ± 0.45 (0.1)		8. #12
	8. #15	8. #13	8. #13	7. 1.51 ± 0.11 (0.25)		8. #10		
				8. #9				

A5

	1. 1.64	1. 1.73	1. 1.59	D5 R=$C_{12}H_{25}$	1. 1.92	1. 1.66	D8 R=$C_{12}H_{25}$	1. 1.82
	2. –5.03/–3.39	2. –4.90/–3.17	2. –5.01/–3.47	1. 1.66	2. –5.29/–3.37	2. –5.06/–3.34	1. 1.70	2. –5.35/–3.53
	3. 18000; 3.0	3. 100700; 3.1	3. 50 000; 1.3	2. –5.03/–3.37	3. 11 000;26.7	3. 34 000; 3.4	2. –5.17/–3.32	3. 138 000; 8.0
	4. NA	4. 1.20E-08	4. Gel	3. 119 000; 16.6	4. 2.72E-09	4. 2.40E-09	3. 261 000; 7.6	4. 2.00E-10
	5. 0.29 ± 0 (0.29); 0.66	5. 1.37 ± 0.07 (1.48); 0.65	5. 1.09 ± 0.03 (1.13); 0.64	4. 6.24E-10	5. 0.1 ± 0 (0.1); 0.8	5. 0.57 ± 0.06 (0.65); 0.65	4. 6.90E-07	5. NA
	6. 2.15 (A5, R in para, $PC_{71}BM$)[45]	6. No reference	6. 1.68 (A5, R in para, $PC_{71}BM$)[45]	5. 0.18 ± 0.3 (0.21); 0.62	6. 2.04 (inverted, $PC_{71}BM$)[34,46]	6. No reference	5. 0.06 ± 0.05 (0.1); 0.62	6. No reference
	7. 8.84 ± 0.21 (0.23)	7. 0.33 ± 0.01 (0.40)	7. 5.71 ± 0.81 (0.10)	6. No reference	7. 1.85 ± 0.01 (0.83)	7. 1.01 ± 0.08 (0.31)	6. No reference	7. 2.01 ± 0.08 (0.37)
	8. #15	8. #15	8. #15	7. 0.56 ± 0.06 (0.80)	8. #17	8. #12	7. 3.09 ± 0.06 (0.25)	8. #14
				8. #11			8. #14	

Continued

ADVANCED ENERGY MATERIALS
www.advenergymat.de

Materials Views
www.MaterialsViews.com

Table 1. Continued

	1. 1.77	1. 1.95	1. 1.94	D5 R=H	NA	1. 1.92	D8 R=$C_{12}H_{25}$	1. 1.95
	2. –5.13/–3.36	2. –5.23/–3.28	2. –5.21/–3.27	1. 1.81	6. 2.04 ($PC_{71}BM$, A6 hexyl, inverted)[46]	2. –5.00/–3.08	NA (not soluble)	2. –5.28/–3.34
	3. 9600; 2.0	3. 11000; 2.2	3. 4600; 1.9	2. –5.15/–3.30	8. #11	3. 15 000; 1.6	6. No reference	3. 21 600; 2.7
	4. 1.40E-08	4. 3.28E-10	4. 4.15E-08	3. 1800; 1.4		4. 7.60E-08	8. #8	4. Gel
	5. 1.03 ± 0.1 (1.14); 0.7	5. 0.85 ± 0.1 (1.05); 0.77	5. 0.61 ± 0.07 (0.72); 0.66	4. 3.20E-09		5. 0.30 ± 0.07 (0.45); 0.58		5. 0.71 ± 0.07 (0.87); 0.79
	6. 5.59 ($PC_{71}BM$, A6 hexyl)[47]	6. 5.22 (A6 H, $PC_{71}BM$)[48]	6. 2.60 ($PC_{71}BM$)[49]	5. NA		6. No reference		6. 3.0 (A6 hexyl)[50]
	7. 10.8 ± 0. 5 (0.17)	7. 1.03 ± 0.05 (0.61)	7. 0.81 ± 0.07 (0.82)	6. No reference		7. 3.58 ± 0.47 (0.32)		7. 2.32 ± 0.21 (0.49)
	8. #11	8. #9	8. #9	7. 1.85 ± 0.18 (0.57) 8. #5		8. #6		8. #8
A6								
	1. 1.35	1. 1.61	1.1.59	D5 R=$C_{12}H_{25}$	NA	1. 1.55	D8 R=$C_{12}H_{25}$	1. 1.87 (solution dewets on glass)
	2. –5.23/–3.88	2. –5.31/–3.70	2. –5.33/–3.74	1. 1.81	6. No reference	2. –5.26/–3.71	NA	2. –5.75/–3.88
	3. 2600; 1.6	3. 3200;3.5	3. 1200; 2.0	2. –5.62/–3.81	8. #11	3. 1200; 3.3	6. No reference	3. (225; 5.5)
	4. 5.78E-08	4. 5.06E-10	4. 3.12 E-09	3. 1100; 1.6		4. 1.48E-09	8. #8	4. NA
	5. 0.02 ± 0.01 (0.03); 0.57	5. NA	5. NA	4. NA		5. 0.03 ± 0.93 (0.05); 0.47		5. NA
	6. No reference	6. 1.96 ($PC_{71}BM$)[51]	6. No reference	5. NA		6. No reference		6. No reference
	7. 0.60 ± 0.04 (0.33)	7. 0.46 ± 0.04 (0.26)	7. 0.31 ± 0.07 (0.19)	6. No reference		7. 1.30 ± 0.10 (0.28)		7. NA
	8. #11	8. #9	8. #9	7. NA 8. #5		8. #6		8. #8
A7								
	1. 1.36	1. 1.35	1. 1.36	D5 R=$C_{12}H_{25}$	NA	1. 1.56	D8 R=$C_{12}H_{25}$	1. 1.54
	2. –5.01/–3.64	2. –5.21/–3.85	2. –5.09/–3.73	1. 1.27	6. No reference	2. –5.04/–3.48	1. 1.57	2. –5.46/–3.92
	3. 16000; 2.0	3. 14000; 2.4	3. 14 000; 2.2	2. –5.11/–3.83	8. #15	3. 6100; 2.6	2. –5.06/–3.49	3. 1200; 4.8
	4. 7.65E-07	4. 1.72E-08	4. 2.00E-08	3. 5000; 1.4		4. 1.15E-07	3. 3700; 2.2	4. 7.82E-09
	5. 0.2 ± 0.03 (0.26); 0.51	5. 0.57 ± 0.06 (0.69); 0.69	5. 0.12 ± 0.02 (0.14); 0.57	4. 2.01E-07		5. 0.04 ± 0.02 (0.07); 0.63	4. 1.23E-08	5. 0.01 ± 0.01 (0.01); 0.56
	6. 6.0 ($PC_{71}BM$, A8 C_8H_{17})[52]	6. 9.0[53–55]	6. 7.4 ($PC_{71}BM$)[56]	5. 0.04 ± 0.02 (0.08); 0.82		6. No reference	5. NA	6. No reference
	7. 0.62 ± 0.04 (1.06)	7. 1.27 ± 0.15 (0.48)	7. 0.8 ± 0.04 (0.34)	6. No reference		7. 5.17 ± 0.71 (0.33)	6. No reference	7. 12.4 ± 1.5 (0.18)
	8. #15	8. #15	8. #13	7. 7.62 ± 0.51 (0.18) 8. #9		8. #10	7. 3.67 ± 0.26 (0.24) 8. #12	8. #12
A8								

Continued

Table 1. Continued

	1. 1.73	1. 1.86	1. 1.86	D5 R=H	NA	1. 2.08 (solution dewets on glass)	D8 R=$C_{12}H_{25}$	1. 2.06 (solution dewets on glass)
	2. –5.37/–3.65	2. –5.43/–3.56	2. –5.35/–3.49	1. 2.07 (solution dewets on glass)	6. No PCE[64]	2. –5.41/–3.33	1. 1.79	2. –5.76/–3.70
	3. 9500;2.8	3. 11000; 3.6	3. 41 000;14.5	2. –5.53/–3.46	8. #12	3. 7200; 1.7	2. –5.28/–3.48	3. (425; 5.9)
	4. 5.53E-08	4. 7.42E-08	4. 3.40E-09	3. 39 000; 1.5		4. 7.20E-08	3. 3500; 1.3 (not all in solution)	4. NA
	5. 0.23 ± 0.06 (0.38); 0.8	5. 0.67 ± 0.03 (0.74); 0.94	5. 0.47 ± 0.08 (0.64); 0.81	4. 3.90E-09		5. NA	4. 1.80E-11	5. NA
	6. 7.3 ($PC_{71}BM$)[57]	6. 6.17[18,58,59]	6. 6.8[60–62]	5. NA		6. No reference	5. NA	6. No reference
	7. 6.56±0.79 (0.5)	7. 0.56±0.05 (0.37)	7. 0.54 ± 0.03 (0.64)	6. 0.75 (A9 $C_{12}H_{25}$, D5 H)[63]		7. NA	6. 5.1 (A9 $C_{12}H_{25}$)[65,66]	7. NA
	8. #12	8. #10	8. #10	7. 0.63 ± 0.05 (0.26) 8. #6		8. #7	7. 0.37 ± 0.02 (0.27) 8. #9	8. #9
A9								
	1. 1.30	1. 1.35	1. 1.36	D5 R=H	1. 1.71	1. 1.38	D8 R=$C_{12}H_{25}$	1. 1.52
	2. –5.13/–3.83	2. –5.24/–3.89	2. –5.26/–3.90	1. 1.30	2. –5.27/–3.56	2. –5.07/–3.69	1. 1.34	2. –5.34/–3.84
	3. 21000; 2.5	3. 103000; 3.3	3. 68 000; 3.3	2. –5.15/–3.85	3. 6700; 3.5	3. 34 000; 4.2	2. –5.06/–3.72	3. 2300; 5.4
	4. 7.60E-08	4. 5.20E-09	4. 5.80E-09	3. 233 000; 8.0	4. 9.70E-09	4. 1.73E-06	3. 1200; 2.8	4. 1.80E-09
	5. NA	5. 0.04±0.47 (0.07); 0.58	5. NA	4. 2.08E-06	5. NA	5. NA	4. 1.68E-10	5. NA
	6. 2.10 ($PC_{71}BM$)[67]	6. 6.60 ($PC_{71}BM$)[59,68,69]	6. 2.83 ($PC_{71}BM$)[67,69][	5. NA	6. 2.26 (D6 R=N–$CH(C_{10}H_{21})_2$)[71,72]	6. No reference	5. NA	6. No PCE[74]
	7. 1.71 ± 0.03 (0.76)	7. 2.46 ± 0.05 (1.14)	7. 1.12 ± 0.04 (1.47)	6. 4.7 (D5 R=H, $PC_{71}BM$)[70]	7. 22.5 ± 0.94 (0.43)	7. 4.42 ± 0.18 (0.82)	6. 3.2 (different side chains)[73]	7. 15.4 ± 0.4 (0.37)
	8. #10	8. #8	8. #8	7. 0.86 ± 0.08 (0.89) 8. #4	8. #10	8. #5	7. 18.8 ± 0.6 (0.4) 8. #7	8. #7
A10								

Continued

ADVANCED ENERGY MATERIALS
www.advenergymat.de

Materials Views
www.MaterialsViews.com

Table 1. Continued

A12	1. 1.50	1. 1.69	NA	D5 R=$C_{12}H_{25}$	NA	1. 1.71	D8 R=$C_{12}H_{25}$	1. 1.67
	2. –5.12/–3.62	2. –5.16/–3.47	6. No reference	1. 1.96	6. No reference	2. –5.09/–3.38	1. 2.09	2. –5.57/–3.90
	3. 6800; 1.9	3. 313000; 10.8	8. #9	2. –5.76/–3.80	8. #11	3. 5600; 2.1	2. –5.67/–3.57	3. 37000; 2.3
	4. 3.75E-07	4. 3.13E-08		3. 13 000; 3.1		4. 1.77E-07	3. 5300; 2.0	4. 9.25E-10
	5. 1.22 ± 0.03 (1.25); 0.67	5. 0.16 ± 0.02 (0.19); 0.74		4. Unstable		5. 0.85 ± 1.09 (0.89); 0.70	4. 1.43E-08	5. 0.25 ± 0.02 (0.28); 0.77
	6. No reference	6. No reference		5. NA		6. 5.02 ($PC_{71}BM$)[36]	5. 0.01 ± 0.01 (0.03); 0.40	6. No reference
	7. 0.52 ± 0.02 (0.61)	7. 0.13 ± 0.01 (0.27)		6. No reference		7. 0.63 ± 0.06 (0.37)	6. No reference	7. 32.3 ± 5.1 (0.15)
	8. #11	8. #9		7. 11.5 ± 0.5 (0.35) 8. #5		8. #6	7. 1.84 ± 0.24 (0.31) 8. #8	8. #8
A13	A13 R= $C_{12}H_{25}$	A13 R=$C_{12}H_{25}$	A13 R=$C_{12}H_{25}$	A13 R=$C_{12}H_{25}$; D5 R=H	A13 R=$C_{12}H_{25}$	A13 R=$C_{12}H_{25}$	A13 R=$C_{12}H_{25}$; D8 R=HD	A13 R=$C_{12}H_{25}$
	1. 1.50	1. 1.65	1. 1.59	1. 1.52	1. 1.72	1. 1.58	1. 1.58	1. 1.53
	2. –5.08/–3.58	2. –5.09/–3.44	2. –5.09/–3.50	2. –4.95/–3.43	2. –5.37/–3.65	2. –4.91/–3.33	2. –5.18/–3.60	2. –5.23/–3.70
	3. 12000; 7.5	3. 80000; 18.2	3. 66 000; 9.0	3. 512 000; 5.3	3. 3200; 2.2	3. 10 000; 2.1	3. 2100; 1.9	3. 12 000; 76.7
	4. 1.96E-08	4. 2.12E-08	4. 9.85E-07	4. NA	4. 3.12E-08	4. 6.80E-08	4. 5.76E-08	4. 3.71E-08
	5. 0.53 ± 0.11 (0.67); 0.65	5. NA	5. NA	5. NA	5. 0.01 ± 0 (0.01); 0.50	5. NA	5. NA	5. NA
	6. No reference	6. 6.21 (A13 R=C_8H_{17}, D2 $C_{12}H_{25}$, $PC_{71}BM$)[75]	6. No reference	6. No reference	6. No reference	6. No reference	6. No reference	6. No reference
	7. 2.76 ± 0.12 (0.47)	7. 0.42 ± 0.03 (0.23)	7. 0.86 ± 0.09 (0.24)	7. NA	7. 0.46 ± 0.04 (0.36)	7. 0.92 ± 0.06 (0.35)	7. 1.94 ± 0.08 (0.26)	7. 2.27 ± 0.1 (0.19)
	8. #14	8. #12	8. #12	8. #8	8. #14	8. #9	8. #11	8. #11
A14	A14 R = $C_{12}H_{25}$	A14 R=$C_{12}H_{25}$	A14 R=$C_{12}H_{25}$	A14 R=$C_{12}H_{25}$; D5 R=H	A14 R=$C_{12}H_{25}$	A14 R=$C_{12}H_{25}$	A14 R=$C_{12}H_{25}$; D8 R=$C_{12}H_{25}$	A14 R=$C_{12}H_{25}$
	1. 1.37	1. 1.47	NA	1. 1.33	NA	1. 1.46	1. 1.49	1. 1.52
	2. –5.14/–3.77	2. –5.05/–3.58	6. 1.34 (A14 R=hexyl)[77]	2. –4.92/–3.59	6. 0.7 (A14 R=H)[35]	2. –5.04/–3.58	2. –5.31/–3.82	2. –5.33/–3.81
	3. 9800; 1.7	3. 4600; 4.1	8. #12	3. 28 000; 11.1	8. #14	3. 19 000; 2.6	3. 19 000; 2.5	3. 1600; 1.9
	4. 6.07E-08	4. 8.94E-08		4. Dewetting		4. 1.43E-09	4. 1.81E-08	4. 5.03E-09 (x)
	5. 0.21 ± 0.06 (0.31); 0.59	5. 0.35±0.03 (0.40); 0.60		5. 0.02 ± 0.01 (0.03); 0.41		5. 0.19 ± 0.02 (0.21); 0.54	5. 0.02 ± 0 (0.02); 0.70	5. 0.06 ± 0 (0.06); 0.45
	6. No reference	6. 4.84 (inverted, A14 R=EH)[63,76]		6. No reference		6. No reference	6. No reference	6. No reference
	7. 1.01 ± 0.02 (0.37)	7. 0.20 ± 0.01 (0.46)		7. 0.38 ± 0.09 (0.42)		7. 1.9 ± 0.2 (0.33)	7. 1.55 ± 0.07 (0.24)	7. 2.76 ± 0.42 (0.25)
	8. #14	8. #12		8. #8		8. #9	8. #11	8. #11

Table 2. Manpower and materials consumption.

Manpower	Man months	Materials consumption (PSC)	Amount
Polymer synthesis	8	[60]PCBM	9.7 g
UV-vis, SEC, CV, mobility, stability	4	PEDOT:PSS	2 L
Program development	1	Silver ink	1 kg
Data analysis	6	Solvents	1.3 L
Paper writing	2	Foil	200 m^2
Sum	26		

depends on the lifetime of the polymer), and size exclusion chromatography (SEC; 1 curve per polymer).

2.2. Manpower and Consumption of Material

A large amount of resources, both in terms of manpower and materials, has been expended in the project as listed in **Table 2**.

2.3. Number of Synthetic Steps (Entry 8)

The embedded energy in a PSC is the amount of energy which has been put into the production of the final device, and here the light-absorbing polymer material is responsible for a large part of that energy, which scales with the number of synthetic steps.[78] Once a high-performing polymer material has been discovered, its application in large-scale R2R processes is the next step and thus large amounts are needed. In order to achieve a low embedded energy in the polymer, the number of synthetic steps has to be as low as possible and the synthetic procedure optimized to give a high yield. The purification (preferably by recrystallization and/or distillation procedures) should be facile and the starting materials have a low cost.[15] To exemplify this we show the synthetic routes for A8D2 (13 steps, best reported efficiency 9.0%[55] and for P3HT (3 steps, best reported efficiency 6%)[79] in **Scheme 1**. A much higher embedded energy (and cost) for A8D2 compared to P3HT[80] is clearly indicated.

The polymers in Table 1 were synthesized by Stille or Suzuki cross coupling polymerizations. The number of synthetic steps from starting materials such as thiophene or benzothiadiazole is shown for each polymer.[15]

2.4. Synthesis and SEC (Entry 3)

The monomer units were chosen on the basis of high efficiencies reported in the literature and on the complexity of the synthetic route. For example, as A11 (see **Figure 1**) we chose an acceptor monomer, such as naphtha-dithiadiazole, which has been reported to give efficiencies up to 6%.[82–84] However, the synthesis is highly complicated using tetrasulfurtetranitride (S_4N_4), which is a shock-sensitive compound, and 1,5-dibromo-2,6-dihydroxynaphthalene as starting materials. Even though the latter was claimed to be commercially available, it was not possible to purchase the final monomer compound. Consequently, in the end it was not chosen as one of the acceptors for the study. As another example, our choice for donor unit D4 (see Figure 1) was the benzo[2,1-b;3,4-b′]dithiophene with 2-hexyl-decyl as side chains, which has shown PCEs of 4.5%.[67,85] However, the synthesis was insufficient in large scale and the subsequent purification too challenging to ensure a pure monomer. The side chains were chosen for each monomer to ensure a good solubility of all the resulting polymer materials, even though for some structures a shorter side chain, e.g., hexyl, would have been sufficient. All polymers were prepared by a Stille cross coupling polymerization of a di-stannyl and a di-bromo derivative of the donor and acceptor units, respectively, using a palladium catalyst. The exception was polymers based on D6, which were prepared by a Suzuki cross coupling.

Not all 104 polymers could be successfully synthesized due to low reactivity, or steric hindrance, which is indicated by a NA in the table. The polymers that were successfully synthesized were analysed by SEC (see the Supporting Information), and large variations in the molecular weight (M_n) were found. The low molecular weight polymers are mainly attributed to steric hindrance from side chains, (e.g., A4D8), to a low reactivity of the donor as in the case of D6, and to poor solubility leading to precipitation of oligomers. Finally, some monomers, such as D7, which cannot be purified by recrystallization, may contain minor impurities, which could complicate the polymerization reaction.

2.5. UV–Vis and Optical Band Gap (Entry 1)

The optical band gaps of the polymers were estimated from the onset of the UV–vis absorption spectra (see the Supporting Information) and were within the range of 2.09 to 1.27 eV with only four polymers having a band gap above 2 eV. This corresponds well with the aim of preparing low band gap polymers based on a donor/acceptor approach. The acceptors A8 and A10 produced the polymers with the lowest band gaps.

2.6. Electrochemical Measurements and Energy Levels (Entry 2)

The HOMO levels were estimated from the onset of the SWV curves using ferrocene as reference (see the Supporting Information) and calculated according to literature procedures.[86–88] The LUMO levels were calculated from the optical band gap and the HOMO level (see the Supporting Information). The HOMO level of P3HT was found to be −4.9 eV, which is somewhat higher compared to the literature value (−5.20 eV).[89] The LUMO level of [60]PCBM was found to be −3.85 eV, which is a little lower than the literature value (−3.75 eV).[90] The HOMO level of the polymer has an effect on the V_{OC}, since it is generally proportional to the difference between the HOMO of the donor polymer and the LUMO of the acceptor [60]PCBM. Thus, lowering the HOMO of the polymer will increase the maximum V_{OC}.[91] This should be considered in view of the fact that lowering the HOMO of the polymer will increase the band gap and thereby potentially also decrease the current. Several polymers, for instance A4D5, A8D5, and

ADVANCED ENERGY MATERIALS
www.advenergymat.de

Materials Views
www.MaterialsViews.com

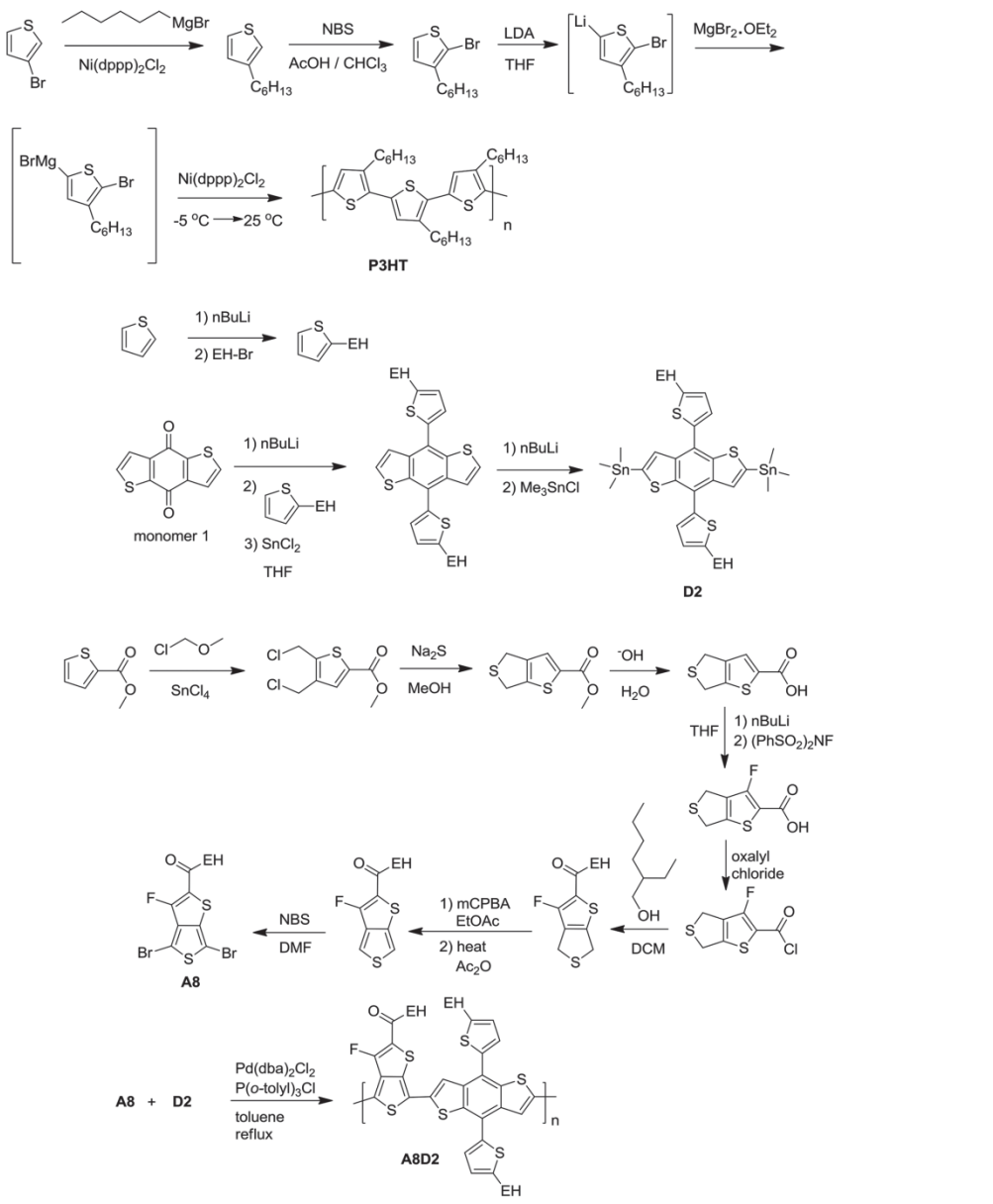

Scheme 1. Comparison of the synthetic routes of P3HT[81] (top) and the high performing polymer A8D2[55] (bottom). Monomer 1 is now commercially available in large quantities; it was, however, originally synthesized in two steps from 3-thiophenecarbonyl chloride.

A9D2, showed a very high V_{OC} compared to P3HT, which is a consequence of a low HOMO level. Unfortunately, the current density for these polymers in PSC devices was much lower than for P3HT, and the resulting PCE is therefore also lower (see **Table 3**). The current can be optimized for instance by varying the ratio between polymer and [60]PCBM. Thus, a high V_{OC} is especially important if one would like to use the polymer material in tandem solar cells.[92]

2.7. Hole Mobility (Entry 4)

The hole mobility was measured in the dark on a polymer film sandwiched between an ITO electrode, poly(3,4-ethylenedioxythiophene) polystyrene sulfonate (PEDOT:PSS), and an evaporated Al electrode (see the Supporting Information). The hole mobility is highly dependent on the solvent from which the analysed film is spin coated. The values

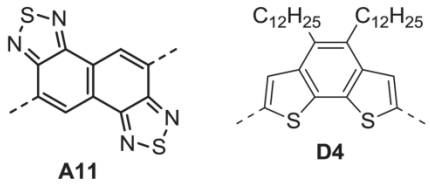

Figure 1. Structures of A11 and D4, which were eliminated from the matrix due to difficulties in the synthesis.

reported here were measured on films prepared from chlorobenzene and were found to be subject to some variation. The hole mobility of P3HT was measured at 1.26×10^{-3} cm^2 V^{-1} s^{-1} for a 270 nm thick film, which is in good agreement with the literature values (1×10^{-3}–6×10^{-3} cm^2 V^{-1} s^{-1}).[93] Several polymers, for instance A3D7, A5D8, and A8D1, showed a higher hole mobility than P3HT, but this did not result in a higher PCE (see Table 1), which could be due to poor morphology or insufficient thickness of the active layer film.

2.8. Photochemical Stability (Entry 7)

The photochemical stability of the polymer films was measured as described in the literature by means of an automatic set up that measured the absorption as a function of time at AM1.5 (1000 W m^{-2}).[94] The stability was found to be highest for polymers with the benzothiadiazole-like acceptor unit (A1, A2, A5, A7, A12, A13, and A14) and the donor unit thiophene (D5 and D8), dithienosilole (D1), and a combination of thiophene and benzene (D3 and D7). This is in good agreement with the literature, where the benzothiadiazole, dithienosilole, and thiophene units are reported to be among the most photochemically stable monomer units.[95]

2.9. Roll-Coated Polymer Solar Cells (Entry 5)

The polymers were employed in fully roll-coated and printed PSC devices using Flextrode substrate[96,97] on a mini roll coater as described earlier.[9,98,99] Several parameters can be studied during such a screening, e.g., solvent, annealing, ratio between polymer and [60]PCBM, film thickness, and coating temperature. All these parameters influence the photovoltaic response of the PSC. However, evaluating all parameters would be impossible within a reasonable timescale, and it would certainly not be possible to do it in this study which included 104 polymers. Consequently, we chose to vary only a subset of the parameters during the screening. The parameters we chose to study included: (1) the ratio between the polymer and [60]PCBM (1:1 or 1:2), (2) the solvent from which the polymer/[60]PCBM mixture is coated (chloroform or o-dichlorobenzene), and (3) the thickness of the coated active layer (thin, medium, and thick, which corresponds to a wet thickness of around 10, 12, and 15 µm, and a dry thickness of around 315, 400, and 475 nm, respectively). The active layer was thick compared to spin coated films (100 nm) to avoid electrical shorts from the less smooth films.[100] The coating temperature was kept constant at 70 °C, which may have affected the morphology of the active layer. However, the choice of a high and low boiling solvent will also affect the different morphologies which can be obtained from a given polymer. The photovoltaic responses are presented as the average efficiency plus/minus the standard deviation together with the maximum recorded PCE and V_{OC}. Many of the polymers failed to generate working devices despite the variations tested. This was due to coating defects such as dewetting, insufficient solubility, destruction of the devices during switching,[97] and electrical shorts due to defects.

2.10. PCE Values from the Literature (Entry 6)

All monomers and some of the polymer materials have been reported in the literature. The values from these studies are listed for reference in Table 1. The PCE values are reported for small spin coated devices with a normal geometry, prepared with an ITO electrode and thermally evaporated electrodes under vacuum, rather than for roll coated devices with a larger area. Also, the devices made for this study were not optimized

Table 3. The maximum PCE for roll-coated devices relative to the PCE of P3HT/PCBM roll-coated devices. The colors indicate: bold: polymer performs better than P3HT, grey: roughly the same performance as P3HT, and plain text: poorer performance than P3HT. NA indicates a failure (please refer to Table S2, Supporting Information, for the specific type of failure).

	D1	D2	D3	D5	D6	D7	D8	D9
A1	0.9	0.3	NA	NA	NA	**1.4**	NA	NA
A2	0.3	0.8	0.4	0.3	NA	0.9	NA	NA
A3	0.2	NA	0.4	0.4	0.1	0.3	0.2	0.2
A4	NA	0.1	NA	0.4	NA	NA	NA	NA
A5	0,2	0.9	0.7	0.1	0.1	0.4	0.1	NA
A6	0.7	0.7	0.5	NA	NA	0.2	NA	0.6
A7	NA	NA	NA	NA	NA	NA	NA	NA
A8	0.2	0.4	0.1	0.1	NA	NA	NA	NA
A9	0.2	0.5	0.4	NA	NA	NA	NA	NA
A10	NA	NA	NA	NA	NA	NA	NA	NA
A12	0.8	0.1	NA	NA	NA	0.6	NA	0.2
A13	0.4	NA	NA	NA	NA	NA	NA	NA
A14	0.2	0.3	NA	NA	NA	0.1	NA	NA

for maximum performance, but rather prepared using the exact same procedures to make comparison possible.

2.11. Comparison of the Polymers

The PCE of the polymers relative to P3HT:PCBM (Table 3) shows that only one polymer (A1D7) generates devices with a better PCE. Only 8 polymers performed similarly to P3HT:PCBM and the rest much more poorly, which is indicated by the low value, or simply by NA in the table. Failure could have occurred for the following reasons: (1) problems in the synthesis, (2) insolubility, (3) dewetting of the active layer on the Flextrode substrate or dewetting of the PEDOT:PSS layer on top of the active layer, (4) no switching of the device, or (5) a shunted device, which is described in more details below. This result indicates the significant challenge in finding polymers that are suitable for R2R-fabricated PSC devices. As seen in Table 1, many of the polymers that failed have been shown to perform excellently in spin-coated devices, however, as described above it is not possible to compare these results with the results of this screening. The 9 polymers that performed on par or better than P3HT:PCBM, based on the PCE alone, are considered promising candidates for further optimization. These are based on the donors D1, D2, D7 and the acceptors A1, A2, A5, A6, and A12.

Although most reports in the literature focus on the PCE, other parameters are also important. We have combined all these factors in a merit factor (χ) defined as

$$\chi = \frac{\text{PCE} \times \text{stability} \times V_{OC} \times \text{band gap}}{\text{number of synthetic steps}} \quad (1)$$

$$\chi_{rel} = \chi / \chi_{P3HT:PCBM} \quad (2)$$

The photochemical stability of polymers used in PSCs varies greatly as shown in previous studies[95] and must be taken into consideration in the selection of an active material. In the merit factor, it is the degradation rate of the polymer normalized to the degradation rate of P3HT at equal absorption value (see the Supporting Information). It is desirable to have a high V_{OC}, and it is therefore incorporated into the merit factor. The band gap (in nm) of the polymer determines how much of the solar spectrum is utilized and gives a theoretical upper limit for the current output of the device. The voltage and band gap are included in order to indentify the polymers which could give high PCE, i.e., a high voltage and/or an absorption to longer wavelengths theorectically gives a higher PCE. Finally, we also consider the number of synthetic steps needed to prepare the polymer, since this obviously has a great impact on the embedded energy and therefore also on the cost. Instead of looking at the merit factor for each polymer we introduce the relative merit factor. The relative merit factor (χ_{rel}) of the polymers is a simplified measure of an overall score against the standard P3HT:PCBM active layer combination and is seen in Table 4. This ranks 13 out of the 104 polymers as better or equal to the standard, which makes them candidates for future development. This demonstrates that the success rate is quite low and that the requirements for roll and R2R fabrication seems to be much higher than for spin coating (which cannot be scaled to industrial applications).

Figure 2 provides an overview of the V_{OC}, the HOMO energy levels, and the optical band gap (E_g). It is clear that when preparing 104 different polymer materials, smooth and continuous variation in the different properties can be achieved. This highlights the strength of the synthetic organic chemistry approach to materials, since almost any number can be matched within a large range through the synthetic approach. We observed V_{OC} values within the range of 0.4 to 0.8 V, HOMO energy level within the range of −4.9 to −5.8 eV, and the band gap within the range of 2.1 to 1.3 eV. The relation between the HOMO and V_{OC} is known to be $V_{OC} = \text{HOMO}_{polymer} - \text{LUMO}_{acceptor} - 0.3$ V[101] and we found that to some extend the polymers in this screening follow this trend though with a little higher loss in the device of 0.6 V (see Figure S1, the Supporting Information).

Table 4. The relative merit factor χ_{rel}. The colors indicate: bold: polymer performs better than P3HT, grey: roughly the same performance as P3HT, and plain text: poorer performance than P3HT. A minimum 70% yield for each step is assumed. Thus, the yield is not taken into account for the synthetic steps. NA indicates a failure (please refer to Table S2, Supporting Information, for the specific type of failure).

	D1	D2	D3	D5	D6	D7	D8	D9
A1	1.4	**3.0**	NA	NA	NA	**2.7**	NA	NA
A2	NA	**3.1**	0.6	1.0	NA	1.2	NA	NA
A3	NA	NA	0.2	NA	NA	0.1	NA	NA
A4	NA	NA	NA	1.0	NA	NA	NA	NA
A5	NA	**2.9**	0.4	0.2	NA	0.7	NA	NA
A6	0.2	0.8	0.5	NA	NA	0.1	NA	0.4
A7	0.1	NA	NA	NA	NA	0.1	NA	NA
A8	0.1	0.5	0.2	NA	NA	NA	NA	NA
A9	NA	1.9	0.9	NA	NA	NA	NA	NA
A10	NA	NA	NA	NA	NA	NA	NA	NA
A12	1.8	**2.6**	NA	NA	NA	**2.7**	NA	NA
A13	0.2	NA	NA	NA	NA	NA	NA	NA
A14	0.3	1.6	NA	0.1	NA	0.1	NA	NA

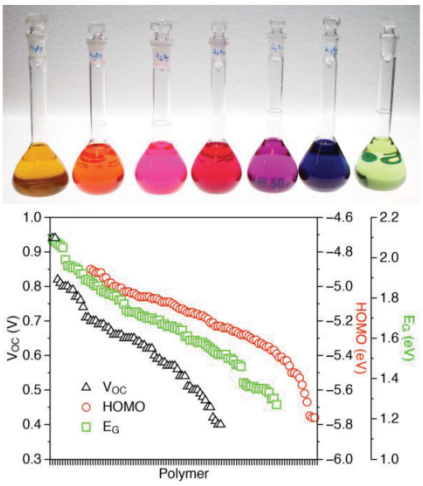

Figure 2. Top: Illustration of the different polymer solutions with the different color/absorbance achieved by coupling the different donor and acceptors in the screening. Bottom: Illustration of the accessible ranges for V_{OC}, E_g, and HOMO levels as a function of polymer number arranged according to the numerical data value (which is different for each property) to show the smooth variation that can be attained. For a complete list of polymers with numerical data, see Table S1, Supporting Information.

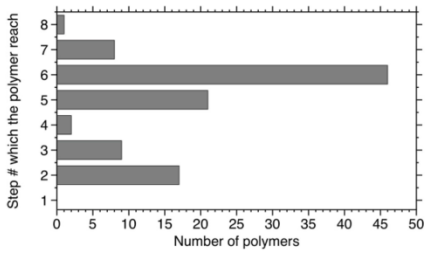

Figure 3. Illustration of the number of polymers that failed at a given step in the serieal value chain for the process that comprises steps: 1 = design, 2 = synthesis, 3 = characterization, 4 = ink, 5 = coating, 6 = device, 7 = performance (PCE), 8 = PCE better than P3HT.

The enormous spans of V_{OC}, HOMO, and band gap can be efficiently explored in final devices where overall performance for instance depends on band gaps being of a particular value (i.e., in tandem devices), or where energy levels need a certain value (i.e., with specific electrode materials).

3. Future and Outlook

It is clear from this study that a large research effort is required for the successful development of a material that meets all the requirements of roll coating/printing besides reaching the customary high efficiency target. The method presented here shows the magnitude of the task, but also how to rationally address the challenge and as such represent the first stage of the search. As we have demonstrated, there are a number of steps in the highly linear approach from synthesis through materials characterisation, processing and devices studies. As illustrated in **Figure 3**, the outcome for any of the materials may stop at any of these stations along the path. The entries in Figure 3 represent the following steps where failure may occur: 1) design, 2) synthesis, 3) characterization, 4) ink, 5) coating, 6) device, 7) PCE, and 8) PCE better than P3HT. As can be seen, failure at steps 1 to 4 account for 28 of the polymers. These failed mainly due to steric hindrance, low molecular weight, or insolubility. A solution could be to re-synthesize them with other side chains to enhance solubility, lower steric hindrance, and increase the molecular weight. Failure at step 5 accounts for 20 of the polymers. Failure mainly occurred due to dewetting of the active layer, which could be solved by using a different device structure, e.g., using a different substrate, or by enhancing the adhesion of the polymer to the Flextrode substrate. Failure at step 6 accounts for almost half of the polymers. In some instances, it represents mechanisms, such as electronic shorts in the device during swithcing, which can be solved by increasing the thickness of the active layer, or insufficient switching, which can be solved by using a different device structure which does not need switching. However, in most cases (see Table 3), it represents a very low PCE. There are several posibilities to overcome this. For example, if the V_{OC} is low, another acceptor than [60]PCBM can be used. Similarly, if the I_{SC} is low, the ratio of the polymer and [60]PCBM can be optimized. For some materials, the hurdles may be overcome and the potential realized through suitable modification, but it is clear that the earlier in the process a material fails, the greater the effort needed to overcome the problem.

To progress from the results of this work, the most suitable candidates (see **Figure 4**) should be further explored through side chain engineering, processing optimisation, and device architecture studies. Of course, it is not impossible that this approach will miss the ultimate material for PSCs, but it is highly unlikely. The majority of materials that have been successful in the past already shows potential in an unrefined form, and this potential has been further explored in subsequent studies. This study should thus be seen as a mining effort for raw candidate materials that, when further refined, can be expected to deliver with respect to performance at all levels (efficiency, physical properties, operational stability, cost, and processability).

4. Conclusion

This screening of 104 light-absorbing polymers for PSCs has illustrated the massive challenge of discovering materials which can offer high efficiency, high stability, and compatibility with large-scale R2R processing. The challenge for the polymer materials has been shown to lie not only in the polymer backbone, but also in the side chains, more specifically where the side chains are attached, and in the size and nature of the side chain. The donor–acceptor approach has pointed out a number of units worthy of further study. A further study will include side chain variations, the morphology of the active layer, the stability of the device, new device structures like tandem architectures, where polymer materials with high

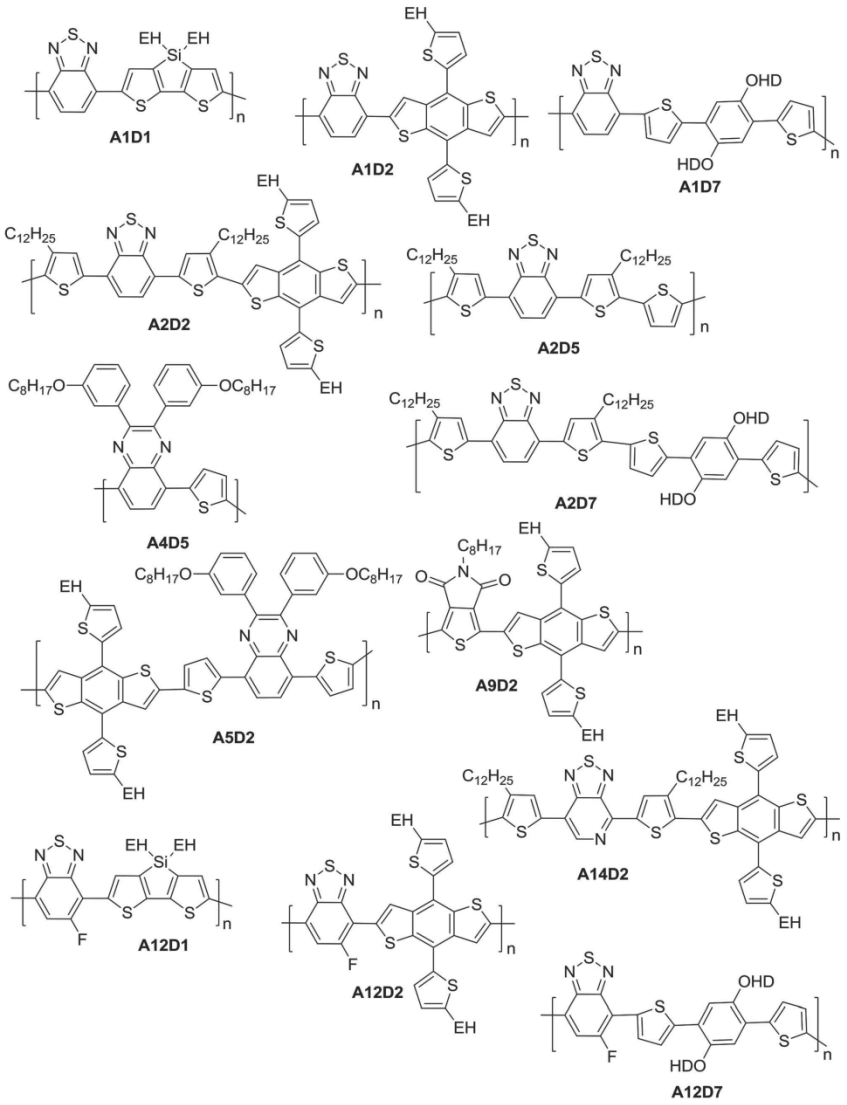

Figure 4. The 13 polymer backbones which were found to be suited for roll-coated PSCs in this screening. Side chains' length and position will be studied in future experiments.

V_{OC} are of great interest, and finally devices optimized through the use of other PEDOT:PSS types. The present study has shown that 13 polymers out of 104 (corresponding to 12.5% of the polymers) are performing better than the prototypical reference material P3HT and are therefore suitable for further development.

Supporting Information

Supporting Information is available from the Wiley Online Library or from the author.

Acknowledgements

The authors extend a special thanks to Michael Corazza, Henrik F. Dam, Thomas R. Andersen, Markus Hösel, and Hanne P. Andersen for contribution to the discussions, illustrations, and proof-reading of the manuscript, respectively. This work was supported by the Villum Foundation's Young Investigator Programme (2nd round, project: Materials for Energy Production). Partial financial support was also received from the Eurotech Universities Alliance project "Interface science for photovoltaic (ISPV)," the EUIndian framework of the "Largecells" project that received funding from the European Commission's Seventh Framework Programme (FP7/2007–2013. Grant No. 261936), the European Commission as part of the Framework 7 ICT 2009 collaborative project ROTROT (Grant No. 288565), Energinet.

dk (Project No. 10728), the EUDP (j.no. 64012-0202), and the Danish National Research Foundation in the project "Danish Chinese Center for organic based solar cells with morphological control."

Received: December 3, 2014
Revised: January 9, 2015
Published online: February 19, 2015

[1] F. C. Krebs, N. Espinosa, M. Hösel, R. R. Søndergaard, M. Jørgensen, *Adv. Mater.* **2014**, *26*, 29.
[2] N. Espinosa, M. Hösel, D. Angmo, F. C. Krebs, *Energy Environ. Sci.* **2012**, *5*, 5117.
[3] Web of Science search: "polymer solar cells" "organic solar cells" "organic photovoltaics," **October 2014.**
[4] M. A. Green, K. Emery, Y. Hishikawa, W. Warta, E. D. Dunlop, *Prog. Photovoltaics Res. Appl.* **2014**, *22*, 1.
[5] E. Bundgaard, F. Krebs, *Sol. Energy Mater. Sol. Cells* **2007**, *91*, 954.
[6] M. Jørgensen, J. E. Carlé, R. R. Søndergaard, M. Lauritzen, N. A. Dagnæs-Hansen, S. L. Byskov, T. R. Andersen, T. T. Larsen-Olsen, A. P. L. Böttiger, B. Andreasen, L. Fu, L. Zuo, Y. Liu, E. Bundgaard, X. Zhan, H. Chen, F. C. Krebs, *Sol. Energy Mater. Sol. Cells* **2013**, *119*, 84.
[7] T. T. Larsen-Olsen, F. Machui, B. Lechene, S. Berny, D. Angmo, R. Søndergaard, N. Blouin, W. Mitchell, S. Tierney, T. Cull, P. Tiwana, F. Meyer, M. Carrasco-Orozco, A. Scheel, W. Lövenich, R. de Bettignies, C. J. Brabec, F. C. Krebs, *Adv. Energy Mater.* **2012**, *2*, 1091.
[8] S. A. Gevorgyan, O. Zubillaga, J. M. V. de Seoane, M. Machado, E. A. Parlak, N. Tore, E. Voroshazi, T. aernouts, H. Müllejans, G. Bardizza, N. Taylor, W. Verhees, J. M. Kroon, P. Morvillo, C. Minarini, F. Roca, F. A. Castro, S. Cros, B. Lechêne, J. F. Trigo, C. Guillén, J. Herrero, B. Zimmermann, S. B. Sapkota, C. Veit, U. Würfel, P. S. Tuladhar, J. R. Durrant, S. Winter, S. Rousu, M. Välimaki, V. Hinrichs, S. R. Cowan, D. C. Olson, P. Sommer-Larsen, F. C. Krebs, *Renew. Energy* **2014**, *63*, 376.
[9] J. E. Carlé, T. R. Andersen, M. Helgesen, E. Bundgaard, M. Jørgensen, F. C. Krebs, *Sol. Energy Mater. Sol. Cells* **2013**, *108*, 126.
[10] A. Teichler, R. Eckardt, S. Hoeppener, C. Friebe, J. Perelaer, A. Senes, M. Morana, C. J. Brabec, U. S. Schubert, *Adv. Energy Mater.* **2011**, *1*, 105.
[11] A. Facchetti, *Chem. Mater.* **2011**, *23*, 733.
[12] L. Bian, E. Zhu, J. Tang, W. Tang, F. Zhang, *Prog. Polym. Sci.* **2012**, *37*, 1292.
[13] H. Zhou, L. Yang, W. You, *Macromolecules* **2012**, *45*, 607.
[14] R. Po, M. Maggini, N. Camaioni, *J. Phys. Chem. C* **2010**, *114*, 695.
[15] G. Marzano, C. V. Ciasca, F. Babudri, G. Bianchi, A. Pellegrino, R. Po, G. M. Farinola, *Eur. J. Org. Chem.* **2014**, *2014*, 6583.
[16] J. Hou, H. Y. Chen, S. Zhang, G. Li, Y. Yang, *J. Am. Chem. Soc.* **2008**, *130*, 16144.
[17] H. Y. Chen, J. Hou, A. E. Hayden, H. Yang, K. N. Houk, Y. Yang, *Adv. Mater.* **2010**, *22*, 371.
[18] R. S. Kularatne, P. Sista, H. Q. Nguyen, M. P. Bhatt, M. C. Biewer, M. C. Stefan, *Macromolecules* **2012**, *45*, 7855.
[19] Y. Huang, F. Liu, X. Guo, W. Zhang, Y. Gu, J. Zhang, C. C. Han, T. P. Russell, J. Hou, *Adv. Energy Mater.* **2013**, *3*, 930.
[20] J. Hou, M.-H. Park, S. Zhang, Y. Yao, L. M. Chen, J.-H. Li, Y. Yang, *Macromolecules* **2008**, *41*, 6012.
[21] E. Bundgaard, F. C. Krebs, *Macromolecules* **2006**, *39*, 2823.
[22] J. E. Carlé, J. W. Andreasen, M. Jørgensen, F. C. Krebs, *Sol. Energy Mater. Sol. Cells* **2010**, *94*, 774.
[23] C. Liu, J. Tsai, W. Lee, W. Chen, S. A. Jenekhe, *Macromolecules* **2008**, *41*, 6952.
[24] T. L. Nguyen, H. Choi, S. J. Ko, M. A. Uddin, B. Walker, S. Yum, J. E. Jeong, M. H. Yun, T. Shin, S. Hwang, J. Y. Kim, H. Y. Woo, *Energy Environ. Sci.* **2014**, *7*, 3040.
[25] W. Yue, Y. Zhao, H. Tian, D. Song, Z. Xie, D. Yan, Y. Geng, F. Wang, *Macromolecules* **2009**, *42*, 6510.
[26] L. Huo, H.-Y. Chen, J. Hou, T. L. Chen, Y. Yang, *Chem. Commun.* **2009**, 5570.
[27] M. Helgesen, T. J. Sørensen, M. Manceau, F. C. Krebs, *Polym. Chem.* **2011**, *2*, 1355.
[28] L. Huo, J. Hou, S. Zhang, H. Y. Chen, Y. Yang, *Angew. Chem. Int. Ed.* **2010**, *49*, 1500.
[29] F. Wu, D. Zha, L. Chen, Y. Chen, *J. Polym. Sci. Part A Polym. Chem.* **2013**, *51*, 1506.
[30] X. Guo, M. Zhang, L. Huo, F. Xu, Y. Wu, J. Hou, *J. Mater. Chem.* **2012**, *22*, 21024.
[31] E. Zhou, J. Cong, K. Hashimoto, K. Tajima, *Macromolecules* **2013**, *46*, 763.
[32] B. Qu, H. Yang, D. Tian, H. Liu, Z. Cong, C. Gao, Z. Chen, L. Xiao, Z. Gao, W. Wei, Q. Gong, *Synth. Met.* **2012**, *162*, 2020.
[33] J. Hou, H. Y. Chen, S. Zhang, Y. Yang, *J. Phys. Chem. C* **2009**, *113*, 21202.
[34] N. Blouin, A. Michaud, D. Gendron, S. Wakim, E. Blair, R. Neagu-Plesu, M. Belletête, G. Durocher, Y. Tao, M. Leclerc, *J. Am. Chem. Soc.* **2008**, *130*, 732.
[35] A. Operamolla, S. Colella, R. Musio, A. Loiudice, O. H. Omar, G. Melcarne, M. Mazzeo, G. Gigli, G. M. Farinola, F. Babudri, *Sol. Energy Mater. Sol. Cells* **2011**, *95*, 3490.
[36] K. H. Ong, S. L. Lim, H. S. Tan, H. K. Wong, J. Li, Z. Ma, L. C. H. Moh, S. H. Lim, J. C. De Mello, Z. K. Chen, *Adv. Mater.* **2011**, *23*, 1409.
[37] B. Liu, X. Chen, Y. He, Y. Li, X. Xu, L. Xiao, L. Li, Y. Zou, *J. Mater. Chem. A* **2013**, *1*, 570.
[38] P. Ding, C. C. Chu, B. Liu, B. Peng, Y. Zou, Y. He, K. Zhou, C. S. Hsu, *Macromol. Chem. Phys.* **2010**, *211*, 2555.
[39] M. Helgesen, S. A. Gevorgyan, F. C. Krebs, R. A. J. Janssen, *Chem. Mater.* **2009**, *21*, 4669.
[40] R. Qin, W. Li, C. Li, C. Du, C. Veit, H. F. Schleiermacher, M. Andersson, Z. Bo, Z. Liu, O. Inganäs, U. Wuerfel, F. Zhang, *J. Am. Chem. Soc.* **2009**, *131*, 14612.
[41] A. A. B. Alghamdi, D. C. Watters, H. Yi, S. Al-Faifi, M. S. Almeataq, D. Coles, J. Kingsley, D. G. Lidzey, A. Iraqi, *J. Mater. Chem. A* **2013**, *1*, 5165.
[42] C. Gao, W. Wang, H. Wu, H. Liu, Y. Mi, Z. An, J. Liu, *CN102816305A* **2012**.
[43] E. Wang, L. Hou, Z. Wang, S. Hellström, F. Zhang, O. Inganäs, M. R. Andersson, *Adv. Mater.* **2010**, *22*, 5240.
[44] L. J. Lindgren, F. Zhang, M. Andersson, S. Barrau, S. Hellström, W. Mammo, E. Perzon, O. Inganäs, M. R. Andersson, *Chem. Mater.* **2009**, *21*, 3491.
[45] C. Bathula, C. E. Song, W. H. Lee, J. Lee, S. Badgujar, R. Koti, I. N. Kang, W. S. Shin, T. Ahn, J. C. Lee, S.-J. Moon, S. K. Lee, *Thin Solid Films* **2013**, *537*, 231.
[46] H. Il Kim, J. M. Cho, W. S. Shin, S. K. Lee, J. C. Lee, S. J. Moon, J. H. Kim, *J. Korean Phys. Soc.* **2012**, *60*, 2034.
[47] M. Zhang, X. Guo, Y. Li, *Adv. Energy Mater.* **2011**, *1*, 557.
[48] L. Huo, X. Guo, S. Zhang, Y. Li, J. Hou, *Macromolecules* **2011**, *44*, 4035.
[49] M. Yang, B. Peng, B. Liu, Y. Zou, K. Zhou, Y. He, C. Pan, Y. Li, *J. Phys. Chem. C* **2010**, *114*, 17989.
[50] J. E. Carlé, M. Helgesen, M. V. Madsen, E. Bundgaard, F. C. Krebs, *J. Mater. Chem. C* **2014**, *2*, 1290.
[51] H. R. Tseng, G. C. Bayan, L. Ying, B. B. Y. Hsu, W. Wen, *WO 2012/174561A2*, **2012**.

[52] S. Akiyama, M. Okabe, M. Furuya, *JP 2012233072 A* **2012**.
[53] S. Zhang, L. Ye, W. Zhao, D. Liu, H. Yao, J. Hou, *Macromolecules* **2014**, *47*, 4653.
[54] S.-H. Liao, H. J. Jhuo, Y. S. Cheng, S. A. Chen, *Adv. Mater.* **2013**, *25*, 4766.
[55] L. Yu, Y. Liang, F. He, *WO 2013/116643 A1* **2013**.
[56] Y. Liang, Z. Xu, J. Xia, S. T. Tsai, Y. Wu, G. Li, C. Ray, L. Yu, *Adv. Mater.* **2010**, *22*, E135.
[57] T. Chu, J. Lu, S. Beaupré, Y. Zhang, J. R. Pouliot, S. Wakim, J. Zhou, M. Leclerc, Z. Li, J. Ding, Y. Tao, *J. Am. Chem. Soc.* **2011**, *133*, 4250.
[58] J. Yuan, Z. Zhai, H. Dong, J. Li, Z. Jiang, Y. Li, W. Ma, *Adv. Funct. Mater.* **2013**, *23*, 885.
[59] T. E. Kang, H.-H. Cho, H. J. Kim, W. Lee, H. Kang, B. J. Kim, *Macromolecules* **2013**, *46*, 6806.
[60] C. Piliego, T. W. Holcombe, J. D. Douglas, C. H. Woo, P. M. Beaujuge, J. M. J. Fréchet, *J. Am. Chem. Soc.* **2010**, *132*, 7595.
[61] Y. Zou, A. Najari, P. Berrouard, S. Beaupré, R. B. Aïch, Y. Tao, M. Leclerc, *J. Am. Chem. Soc.* **2010**, *132*, 5330.
[62] Y. Zhang, S. K. Hau, H. L. Yip, Y. Sun, O. Acton, A. K. Y. Jen, *Chem. Mater.* **2010**, *22*, 2696.
[63] T. Umeyama, M. Oodoi, O. Yoshikawa, T. Sagawa, S. Yoshikawa, D. Evgenia, N. Tezuka, Y. Matano, K. Stranius, N. V. Tkachencko, H. Lemmetyinen, H. Imahori, *J. Mater. Chem.* **2011**, *21*, 12454.
[64] M. Leclerc, P. Berrouard, *WO 2013/056355 A1* **2013**.
[65] C. M. Liu, M. S. Su, J. M. Jiang, Y. W. Su, C. J. Su, C. Y. Chen, C. S. Tsao, K. H. Wei, *ACS Appl. Mater. Interfaces* **2013**, *5*, 5413.
[66] M. C. Yuan, M. Y. Chiu, S. P. Liu, C. M. Chen, K. H. Wei, *Macromolecules* **2010**, *43*, 6936.
[67] L. Huo, J. Hou, H. Y. Chen, S. Zhang, Y. Jiang, T. L. Chen, Y. Yang, *Macromolecules* **2009**, *42*, 6564.
[68] L. Dou, J. Gao, E. Richard, J. You, C. C. Chen, K. C. Cha, Y. He, G. Li, Y. Yang, *J. Am. Chem. Soc.* **2012**, *134*, 10071.
[69] S. Zhang, L. Ye, Q. Wang, Z. Li, X. Guo, L. Huo, H. Fan, J. Hou, *J. Phys. Chem. C* **2013**, *117*, 9550.
[70] J. C. Bijlevelt, A. P. Zoombelt, S. G. J. Mathijssen, M. M. Wienk, M. Turbiez, D. M. de Leeuw, A. J. Janssen, *J. Am. Chem. Soc.* **2009**, *131*, 16616.
[71] E. Zhou, S. Yamakawa, K. Tajima, C. Yang, K. Hashimoto, *Chem. Mater.* **2009**, *21*, 4055.
[72] Z. Yingping, D. Gendron, R. B. Aïch, A. Najari, Y. Tao, M. Leclerc, *Macromolecules* **2009**, *42*, 2891.
[73] M. M. Wienk, M. Turbiez, J. Gilot, R. A. J. Janssen, *Adv. Mater.* **2008**, *20*, 2556.
[74] M. Düggeli, O. F. Aebischer, P. Hayoz, M. Rodona Turon, M. Turbiez, J.-C. Flores, H. J. Kirner, P. Murrer, N. Chebotareva, T. Schäfer, *WO 2010/136353A1* **2010**.
[75] Q. Peng, X. Liu, D. Su, G. Fu, J. Xu, L. Dai, *Adv. Mater.* **2011**, *23*, 4554.
[76] J. Yuan, X. Huang, H. Dong, J. Lu, T. Yang, Y. Li, A. Gallagher, W. Ma, *Org. Electron.* **2013**, *14*, 635.
[77] H. Kang, B. Zhao, Z. Cao, J. Zhong, H. Li, Y. Pei, P. Shen, S. Tan, *Eur. Polym. J.* **2013**, *49*, 2738.
[78] N. Espinosa, R. Garcia-Valverde, A. Urbina, F. Lenzmann, M. Manceau, D. Angmo, F. C. Krebs, *Sol. Energy Mater. Sol. Cells* **2012**, *97*, 3.
[79] G. Zhao, Y. He, Y. Li, *Adv. Mater.* **2010**, *22*, 4355.
[80] T. P. Osedach, T. L. Andrew, V. Bulović, *Energy Environ. Sci.* **2013**, *6*, 711.
[81] R. D. Mccullough, S. P. Williams, S. Tristram-Nagle, M. Jayaraman, *Synth. Met.* **1995**, *69*, 279.
[82] M. Wang, X. Hu, L. Liu, C. Duan, P. Liu, L. Ying, F. Huang, Y. Cao, *Macromolecules* **2013**, *46*, 3950.
[83] I. Osaka, M. Shimawaki, H. Mori, I. Doi, E. Miyazaki, T. Koganezawa, K. Takimiya, *J. Am. Chem. Soc.* **2012**, *134*, 3498.
[84] M. Wang, X. Hu, P. Liu, W. Li, X. Gong, F. Huang, Y. Cao, *J. Am. Chem. Soc.* **2011**, *133*, 9638.
[85] M. Yuan, A. H. Rice, C. K. Luscombe, *J. Pol. Sci. A: Pol. Chem.* **2011**, *49*, 701.
[86] A. J. Bard, L. R. Faulkner, *Electrochemical Methods: Fundamentals and Applications*, 2nd ed., Wiley, New York **2001**.
[87] C. M. Cardona, W. Li, A. E. Kaifer, D. Stockdale, G. C. Bazan, *Adv. Mater.* **2011**, *23*, 2367.
[88] V. V Pavlishchuk, A. W. Addison, *Inorganica Chim. Acta* **2000**, *298*, 97.
[89] M. Al-Ibrahim, *Sol. Energy Mater. Sol. Cells* **2004**, *85*, 13.
[90] C. J. Brabec, N. S. Sariciftci, J. C. Hummelen, *Adv. Funct. Mater.* **2001**, *11*, 15.
[91] M. C. Scharber, D. Wuhlbacher, M. Koppe, P. Denk, C. Waldauf, A. J. Heeger, C. L. Brabec, *Adv. Mater.* **2006**, *18*, 789.
[92] G. Dennler, M. C. Scharber, T. Ameri, P. Denk, K. Forberich, C. Waldauf, C. J. Brabec, *Adv. Mater.* **2008**, *20*, 579.
[93] D. M. DeLongchamp, B. M. Vogel, Y. Jung, M. C. Gurau, C. A. Richter, O. A. Kirillov, J. Obrzut, D. A. Fischer, S. Sambasivan, L. J. Richter, E. K. Lin, *Chem. Mater.* **2005**, *17*, 5610.
[94] T. Tromholt, M. V. Madsen, J. E. Carlé, M. Helgesen, F. C. Krebs, *J. Mater. Chem.* **2012**, *22*, 7592.
[95] M. Manceau, E. Bundgaard, J. E. Carlé, O. Hagemann, M. Helgesen, R. Søndergaard, M. Jørgensen, F. C. Krebs, *J. Mater. Chem.* **2011**, *21*, 4132.
[96] M. Hösel, R. R. Søndergaard, M. Jørgensen, F. C. Krebs, *Energy Technol.* **2013**, *1*, 102.
[97] T. T. Larsen-Olsen, R. R. Søndergaard, K. Norrman, M. Jørgensen, F. C. Krebs, *Energy Environ. Sci.* **2012**, *5*, 9467.
[98] T. R. Andersen, H. F. Dam, B. Andreasen, M. Hösel, M. V. Madsen, S. A. Gevorgyan, R. R. Søndergaard, M. Jørgensen, *Sol. Energy Mater. Sol. Cells* **2014**, *120*, 735.
[99] D. Angmo, H. F. Dam, T. R. Andersen, N. K. Zawacka, M. V. Madsen, J. Stubager, F. Livi, R. Gupta, M. Helgesen, J. E. Carlé, T. T. Larsen-Olsen, G. U. Kulkarni, E. Bundgaard, F. C. Krebs, *Energy Tech.* **2014**, *2*, 651.
[100] F. C. Krebs, *Sol. Energy Mater. Sol. Cells* **2009**, *93*, 394.
[101] M. C. Scharber, D. Mühlbacher, M. Koppe, P. Denk, C. Waldauf, A. J. Heeger, C. J. Brabec, *Adv. Mater.* **2006**, *18*, 789.

Solid-State Electronics 116 (2016) 111–118

Contents lists available at ScienceDirect

Solid-State Electronics

journal homepage: www.elsevier.com/locate/sse

Comparison of the electron work function, hole concentration and exciton diffusion length for P3HT and PT prepared by thermal or acid cleavage

J. Toušek [a,*], J. Toušková [a], J. Ludvík [b], A. Liška [b,e], Z. Remeš [c], O. Kylián [a], J. Kousal [a], R. Chomutová [a], I.M. Heckler [d], E. Bundgaard [d], F.C. Krebs [d]

[a] Charles University in Prague, Faculty of Mathematics and Physics, V Holesovickach 2, 182 00 Prague 8, Czech Republic
[b] J. Heyrovsky Institute of Physical Chemistry of the Academy of Sciences, Dolejskova 2155/3, 182 23 Prague 8, Czech Republic
[c] Institute of Physics of the Academy of Sciences, Cukrovarnicka 10, 162 53 Prague 6, Czech Republic
[d] Technical University of Denmark, Department for Energy Conversion and Storage, Frederiksborgvej 399, DK-4000 Roskilde, Denmark
[e] Charles University in Prague, Faculty of Science, Albertov 6, 128 43 Prague 2, Czech Republic

ARTICLE INFO

Article history:
Received 31 March 2015
Received in revised form 11 September 2015
Accepted 2 November 2015
Available online 21 November 2015

Keywords:
Polythiophene
Hole concentration
Energy level diagram
Exciton diffusion length
Morphology

ABSTRACT

The electron work function, hole concentration and diffusion length were compared for poly(3-hexylthiophene) polymer (P3HT) that is commonly used for construction of solar cells, and two types of native polythiophene (PT) samples which are prospective candidates for this purpose. The polythiophene samples were prepared from 2 different precursors by thermal or chemical treatment at room temperature. Cyclic voltammetry and work function measurements were used for estimating the concentration of holes. The measured data were evaluated assuming the validity of band theory based on the tight-binding model. Published data on the valence bandwidth were used for calculating the value of the overlap integral which is related to the hole effective mass. Energy band diagrams were constructed for all 3 materials. Finally, the exciton diffusion length, which is a critical parameter for the application of conjugated polymer materials in solar cells, was measured by a modified surface photovoltage method. The approach allowed us to identify the differences in the material properties related to the processing method. Morphology of the samples determined by AFM was another tool showing these differences. It is stated that a native polythiophene prepared by treatment with acids is a prospective material for solar cells and shows a similar quality as that produced by a thermal process.

1. Introduction

Polythiophenes and conjugated copolymers employing thiophene are among the most frequently used semiconducting organic materials in the field of organic electronics. The solubility of polythiophenes functionalized with solubilizing side chains enables formation of active layers with application in the areas of light-emitting diodes [1], organic solar cells [2], and organic field-effect transistors [3]. The most studied polythiophene is poly(3-hexyl-thiophene) (**P3HT**), see scheme in Fig. 1, in which hexyl side chains ensure solubility. However, removal of the side chain has been demonstrated to increase the operational stability of organic solar cells based on polythiophenes [4]. Besides the increased stability upon removal of side chains it also enables coating of the active layer from solution and, after film formation, a specific treatment can remove the side chains. This results in active layers comprising insoluble polythiophene (PT), see scheme in Fig. 1. This permits subsequent coating by other coatinglayers while avoiding the risk for damaging the already coated layer. This is particularly relevant for multilayer structures such as tandem solar cells that may comprise many layers.

Insoluble PT can be prepared using poly-(3-(2-methylhexyloxy carbonyl)dithiophene) (**P3MHOCT**) as a precursor where the side chains are removed by thermal treatment at 300 °C [5]. The product of this side chain removal is denoted **PT1.** This method can induce defects and undesirable side reactions. The polydimethyl octylsilyl terthiophene (**PDMOST**) was then developed as a precursor whose side chains are removed without heating but through treatment with acids [6]. The product of this side chain removal is denoted **PT2**. This method of preparation may, however, also affect the properties of deposited coatings. In this study we

* Corresponding author. Tel.: +420 22191 2263.
E-mail address: jiri.tousek@mff.cuni.cz (J. Toušek).

http://dx.doi.org/10.1016/j.sse.2015.11.002
0038-1101/

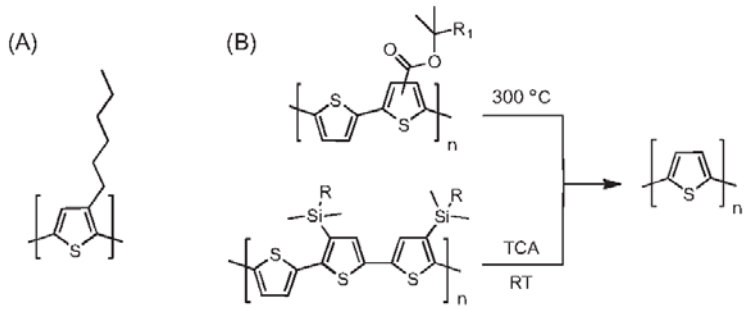

Fig. 1. Scheme of traditional soluble **P3HT** shown in (A) and the two reactions leading to native polythiophene shown in (B) as **PT1** from the thermal cleaving at 300 °C (top) and **PT2** prepared by trichloroacetic acid (TCA) cleavage (below).

therefore carried out optical, photoelectrical and electrical measurements to compare the 3 above-mentioned materials.

The band theory based on the tight-binding model [7] was used to find the charge transport parameters in the investigated materials. An important feature of the band model is that electrons are delocalized. Thiophenes are denoted as low band – gap polymers due to a high degree of delocalization of the π-electrons [8]. The band model is meaningful if the width of the band is sufficiently large. The width of the valence band where transport of holes takes place (p-type semiconductor is considered) reflects the degree of overlap of the atomic orbitals. If the overlap is weak, the band is narrow and the macroscopic parameters such as e.g. charge carrier mobility are low. The influence of the chemical and structural defects in the tight binding model was included by introducing potential wells with random depths [7]. If the spread of well depths is comparable with the bandwidth, the total wavefunction is a sum of local functions with random phases and the charges are localized. The disorder lowers electrical conductivity and mobility.

The band theory was also applied to semiconductors with localized states in the band gap; the conduction is realized by charges elevated from trap states to delocalized levels in bands where the charges move freely [9,10]. The validity of relations for band dispersion (Appendix A) in the tight binding model assumes insignificant effect of defects. The defects would negatively influence the properties of the polythiophene material. But especially, very high electrical conductivity (1000 S/cm) was measured for regioregular P3HT [11] and the mobility of about 0.1 $cm^2/V\,s$ and about 10^{-4} $cm^2/V\,s$ was published in regioregular P3HT depending on the direction of the charge transport [12,13]. Yamamoto [14] stated that π-conjugated regioregular polythiophenes with long side chains show a strong tendency to self-assembly and form π – stacked structure leading to high conductivity and mobility. Hence, the morphology of polythiophene layers is very probably the main factor influencing their behavior.

Starting from the calculated values of the valence energy bandwidth, the hole effective mass can be determined from the relation (1) [7]

$$m^* = \frac{\hbar^2}{2\beta a^2} \tag{1}$$

where the overlap integral β is equal to 1/4 of the bandwidth and a is the lattice constant (See Appendix A). The value of the bandwidth in polythiophenes was theoretically estimated and ranged from 2.2 eV to 3.2 eV [15–17]; 2.44 eV was published recently [16] while $a = 0.771$ nm was reported in Ref. [18]. The knowledge of the hole effective mass enables the calculation of the effective density of states in the valence band

$$N_V = 2\left(\frac{2\pi m^* kT}{h^2}\right)^{3/2} \tag{2}$$

where T is the temperature and the other symbols have the usual meaning. The effective density of states appears in the relation for the concentration of free holes, which is $p = N_V \exp(-(E_F - E_V)/kT)$ for the nondegenerate case, E_F is the Fermi level and E_V is the top of the valence band.

In this paper we use the band model to evaluate the hole concentration and the exciton diffusion length and give a complete energy level diagram of the **P3HT** and the polythiophene samples (**PT1** and **PT2**) prepared from two different precursors by thermal or acid treatment.

2. Experimental

The samples were prepared by the spin coating of solution of active layers (P3HT, P3MHOCT or PDMOST) on ITO/glass substrates as described in [5,6]. The thermal treatment at 300 °C to eliminate side groups leads to insoluble polythiophene (**PT1**) as it is described in a previous paper [19] where the process of the successive removal of the groups is presented in detail on the basis of thermogravimetric data. The thermal behavior linked mainly to the ester functionality was confirmed by NMR analysis. The insoluble polythiophene **PT2** was prepared from the coating solution of PDMOST precursor mixed with trichloroacetic acid. This room-temperature process of cleavage of the side groups is described in Ref. [6].

Morphology of the samples was evaluated by atomic force microscopy (AFM). AFM measurements were performed in the semi-contact mode using NSC-17 silicon cantilevers (Schaefer Technologie, GmbH) by means of Quesant Q-scope atomic force microscope (scan rate 2 Hz, resolution 512 × 512 points).

FT-IR measurements were performed on a Perkin Elmer Spectrum One FT-IR Spectrometer.

Optical transmittivity and reflectivity were determined on a dual beam spectrometer based on a monochromator equipped with gratings optimized for ultraviolet (blazed at 300 nm) and visible-near infrared regions (blazed at 750 nm). A Xe lamp served as the light source and two UV-enhanced Si photodiodes as detectors, covering the spectral range from 200 to 1100 nm. This method was applied to the P3HT material.

The photothermal deflection spectroscopy (PDS) was used for evaluating the optical absorptance of insoluble **PT1** and **PT2** samples. The PDS represents a direct and elegant way to obtain the optical absorption coefficients and avoids the evaluation of the transmittance spectra. The sample was immersed in a transparent liquid (Florinert FC72) and periodically illuminated by the light

from the monochromator. Besides, He–Ne laser was used as a probe beam source. The relative absorptance spectra are detected by a position detector monitoring the laser beam parallel to the sample surface. The absorbed heat in the sample generates periodical thermal waves in the liquid surrounding the sample, causing the periodical deflection of the laser beam. The amplitude of the deflection normalized on black sample spectra gives the optical absorption of the sample. The optical absorption coefficients are calculated at each wavelength using the absorptance spectrum.

Electrochemical experiments were performed at room temperature in acetonitrile/toluene mixture 1:1, where 0.1 M tetraethyl- or tetrabutylammonium hexafluorophosphate was used as supporting electrolyte. The aprotic solution was degassed with argon before and during all experiments. A 10 ml two-compartment electrochemical cell was used together with a three-electrode system. The sample was attached as a working electrode; the reference electrode was a SCE (Saturated Calomel Electrode) with a double salt bridge for prevention of mixing the aqueous and aprotic solvents. A platinum foil placed parallel to the working electrode was used as the auxiliary electrode. Cyclic voltammetry was used as the main electrochemical experimental method with a scan rate of 100 mV/s. The measurements were carried out starting from 0 V (vs. SCE) followed by the positive scan up to +2.0 V and then back to 0 V. A PGSTAT 101 (Autolab) potentiostat controlled by NOVA software was used for all experiments. Ferrocene was added to the solution during measurements of P3HT as a voltage standard with an oxidation potential of 0.38 V.

Measurement of the work function of the studied materials was performed by the Kelvin probe. In principle, it is a vibrating capacitor with a reference gold electrode deposited on a glass plate. The polymer layer deposited on ITO/glass served as a second electrode. The gold electrode is located just above the surface of the sample. Voltage is created between the two electrodes due to a difference in the work functions. When the gold electrode vibrates, alternating voltage appears in the external detection circuit. The signal is amplified by narrow band pass amplifier, which is used as a null detector.

Current and voltage gold electrodes were evaporated and arranged on the top of the layers deposited on glass substrate for the conductivity measurement in the regime of an alternating current. A narrow band amplifier was applied with Keithley 616 electrometer as an impedance transformer.

The measurement was performed at several frequencies to enable approximation of the conductivity to zero frequency.

As the exciton diffusion length is an important parameter influencing the solar cell efficiency, the surface photovoltage (SPV) measurement was used for its extraction. The arrangement of the experiment is shown in Fig. 2. The electric field necessary for formation of the SPV was created in the space charge region (SCR) at the (Al or C)/polymer interface, while ITO served as an ohmic contact to the polymer. The photovoltage was measured using illumination from the substrate. The photogenerated excitons diffuse to the SCR, where dissociation takes place. The SPV spectra were acquired using low frequency chopped light from the monochromator. The intensity of the light was checked by the TS100 thermopile and the SPV signal was recalculated for constant photon flux density impinging on the sample. Optical measurements yielded the optical absorption coefficients needed for the SPV measurement evaluation. The transparency of the ITO layer was taken into account. More information concerning the SPV experiment can be found in Refs. [20,21].

The small signal condition was respected so that Eq. (3) for the photovoltage V was fulfilled.

$$V \sim J = J_b + J_s \tag{3}$$

The current density J is a sum of the diffusion current density (J_b) caused by excitons generated in the bulk and the drift current density (J_s) originating from excitons generated in the SCR. The calculations of J_b and J_s are shown in Appendix B.

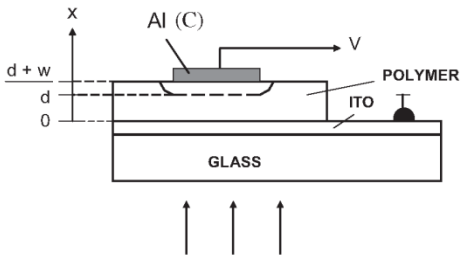

Fig. 2. Arrangement for the SPV measurements. The voltage is measured between the top Al or C rectifying electrode and the ITO bottom layer. The light is chopped to generate alternating voltage (w is the thickness of the space charge region, d is the thickness of the bulk).

3. Results and discussion

The first studied parameter of the films prepared on glass/ITO substrate was their morphology. Figs. 3–5 show examples of 10 μm × 10 μm AFM scans of all three types of polythiophene films. The samples differ in their surface roughness. The highest value of root-mean-square (RMS) roughness was observed for

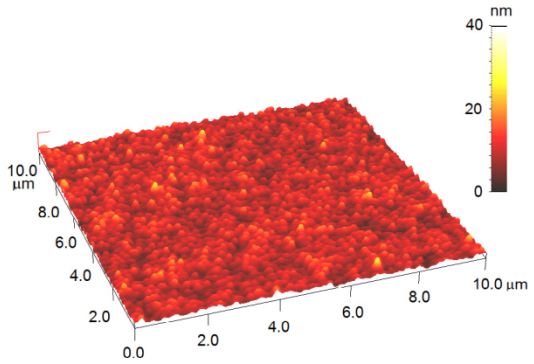

Fig. 3. AFM image of **PT1** layers. Roughness of the surface: RMS ~3.0 nm.

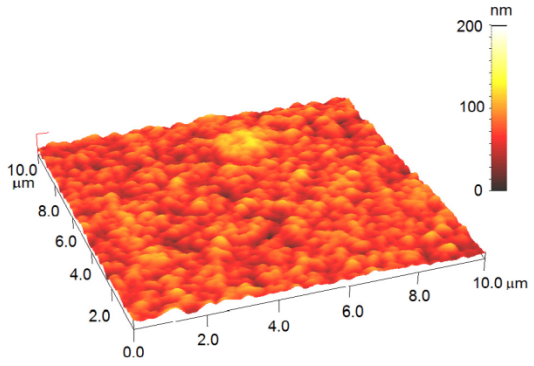

Fig. 4. AFM image of **PT2** layers. Roughness of the surface: RMS ~15 nm.

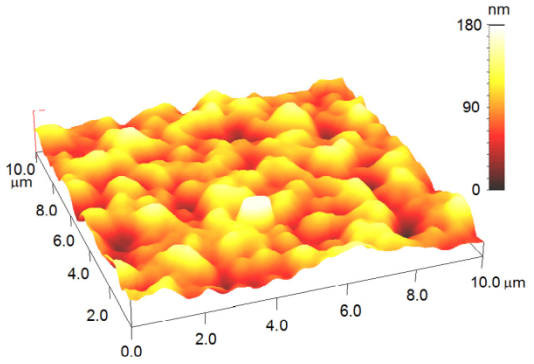

Fig. 5. AFM image of **P3HT** layers. Roughness of the surface: RMS ~26 nm.

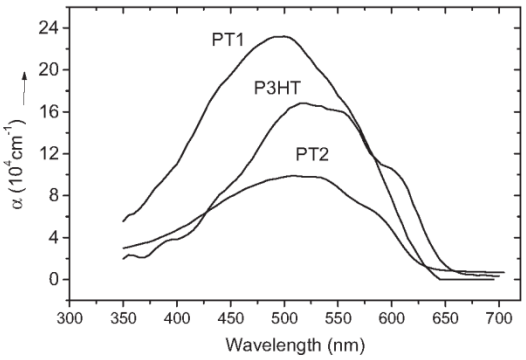

Fig. 7. Absorption spectra of **PT1**, **PT2** and **P3HT** polymers.

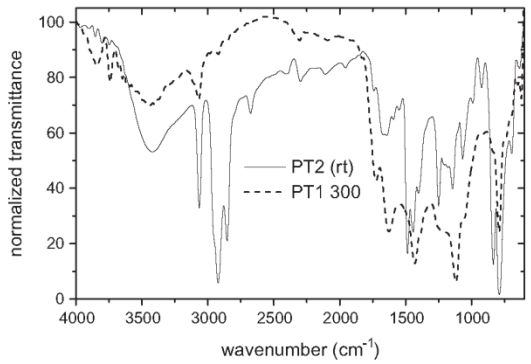

Fig. 6. FT-IR spectra of **PT1** and **PT2** polythiophenes.

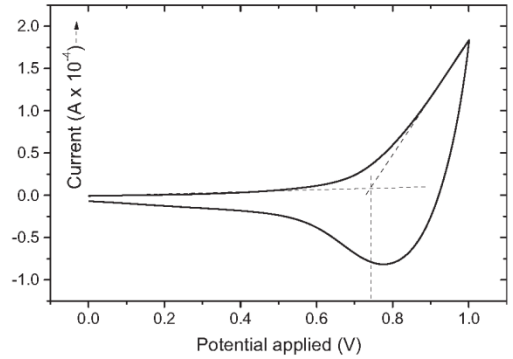

Fig. 8. Cyclic voltammogram of polythiophene **PT1** on ITO/glass substrate.

P3HT (26 nm), followed by **PT2** (15 nm) and, finally, the lowest surface roughness was observed for **PT1** films (3 nm). In spite of these differences, all films were sufficiently smooth for optical, electrical and photoelectrical measurements.

Fig. 6 shows the infrared spectra of **PT1** and **PT2**. After treatment of **PDMOST** with acid an intensive broad band for Si–OH around 3500–3000 cm^{-1} appears in **PT2** spectrum. The characteristic bands for the C–H stretching vibration of the CH_2 chain are seen at 3000–2800 cm^{-1}, because of a residual side chain in the film. However, these C–H stretching vibrations of the CH_2 chain disappear in the FT-IR spectrum during the formation of **PT1**. The characteristic absorption bands for ester moieties appeared before cleavage at 1705 cm^{-1} for the C=O and at 1307 cm^{-1} for the C—O vibration decrease in their intensity within heating of the film at 300 °C. During the thermal treatment an intensive broad band around 3500–3000 cm^{-1} appeared due to the formation of carboxylic acid.

Absorption coefficients (Fig. 7) were obtained from the optical measurements. The maximum of the absorption spectrum was about 2×10^5 cm^{-1} for **PT1** and **P3HT** and 9×10^4 cm^{-1} for **PT2**. The optical absorption spectra were used to determine the optical band gap by plotting $(\alpha h\nu)^2$ versus $h\nu$ (not shown). The band gaps of **PT1**, **PT2** and **P3HT** samples were 2.06 ± 0.01 eV, 2.02 ± 0.01 eV and 2.02 ± 0.01 eV, respectively. The optical band gap of **P3HT** is in a good agreement with previously published values that indicated **P3HT** optical band gap to be in the range of 1.9–2.0 eV [22].

Figs. 8–10 show the positive branch of the Cyclic voltammetry diagrams. The onset potentials of the p-doping are determined by the intersection of the two tangents drawn in the place where

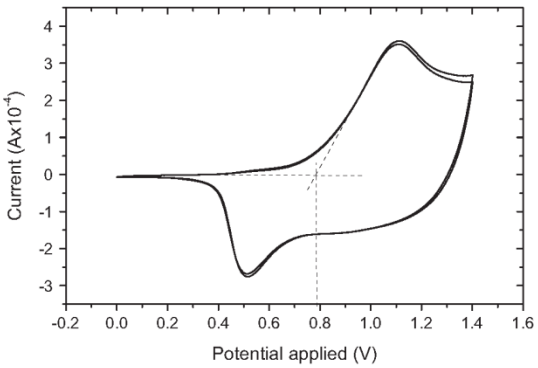

Fig. 9. Cyclic voltammogram of polythiophene **PT2** on ITO/glass substrate.

the anodic current begins to rise. The Φ potentials were (0.74 ± 0.02) V, (0.79 ± 0.02) V and (0.74 ± 0.02) V for **PT1**, **PT2** and **P3HT**, respectively. For p-type conducting polymers, the solid state ionization potential is equal to the electrochemical potential at which the polymer can be oxidized plus 4.4 V (if measured versus SCE) [23]. The HOMO energy level of **PT**1, **PT2** and **P3HT** was, consequently, calculated according to Eq. (4), where e is the charge of an electron [23,24].

$$E_{\mathrm{HOMO}}\,(\mathrm{eV}) = -e(\Phi + 4.4\,\mathrm{V}) \tag{4}$$

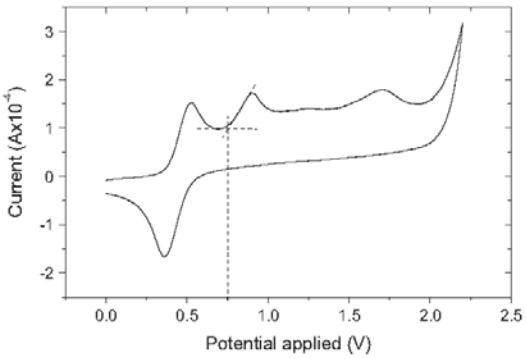

Fig. 10. Cyclic voltammogram of polythiophene **P3HT** on ITO/glass substrate. The first reversible couple of peaks belongs to ferrocene which was used in the solution as internal standard for calibration.

This gives the HOMO levels in **PT1**, **PT2** and **P3HT** of (−5.14 ± 0.02) eV, (−5.19 ± 0.02) eV and (−5.14 ± 0.02) eV, respectively. The HOMO of **P3HT** agrees well with the values in the literature [25–27]. The voltammograms of samples in the form of thin layers deposited on ITO/glass substrates were acquired at room temperature in the electrochemical cell.

The **PT1**, **PT2** and **P3HT** polymers are insoluble in the acetonitrile/toluene electrolyte. The oxidation takes place on the layer surface. On being oxidized, the layer of the polymers was in all cases slowly dissolved and only 2–3 repeated scans were therefore possible. This fact indicates that the process is irreversible since the dissolved oxidized form (probably non-stable radical cations) is not re-deposited. Nevertheless, from the shape of the curves of **PT1** and **PT2** it is evident that the dissolved oxidized intermediates are reducible. In the case of P3HT, the expected reduction response of the intermediate might be covered by the reduction peak of ferrocene.

The surface potential measurements using the Kelvin probe were employed in order to find the electron work function in the polymers. The Kelvin probe measures the difference of the work functions of the polymers and the known work function of gold [28]. The work function measured on several samples was found to be (4.98 ± 0.05) eV, (5.07 ± 0.05) eV and (5.27 ± 0.05) eV for **PT1**, **PT2** and **P3HT**, respectively.

Table 1
Optical band gap, HOMO level, work function, hole concentration and electrical conductivity for **PT1**, **PT2** and **P3HT** as obtained from absorption spectra, cyclic voltammetry, the Kelvin probe and conductivity measurements. The hole concentration is calculated according to the relations in Appendix C.

Sample	Band gap (eV)	HOMO level (eV)	Work function (eV)	Concentration (cm^{-3})	Conductivity $\Omega^{-1} cm^{-1}$
PT1	2.06	−5.14	4.98	1.8×10^{15}	17×10^{-5}
PT2	2.02	−5.19	5.07	8.3×10^{15}	2.7×10^{-5}
P3HT	2.02	−5.14	5.27	6.2×10^{18}	1.8×10^{-5}

The results of optical, voltammetry and work function measurements (Table 1) were used to construct energy level diagrams shown in Fig. 11. The HOMO levels in the three types of polythiophenes were found from the measurement of voltammetry using Eq. (4). The LUMO level was calculated by addition of the HOMO level obtained electrochemically to the optical band gap, as described in the literature [29]. Average values of the optical band gaps 2.06 eV, 2.02 eV and 2.02 eV for **PT1**, **PT2** and **P3HT**, respectively were used in Fig. 11. Using 2.5 eV as the value for the width of the valence band, we calculated the hole effective mass $m^* = 0.11$ from Eq. (1) and effective density of states in the valence band $N_V = 8.3 \times 10^{17}\ cm^{-3}$ according to Eq. (2). The value of the hole effective mass is well comparable with the value 0.14 presented in Ref. [30] for the hole transport along the chains. The HOMO level positions together with the value of the work function determine the Fermi level which allows calculating the concentration of holes in the valence band. Relation (C1) in Appendix C was used in the case of **PT1** and **PT2**. In contrast, **P3HT** shows the Fermi level shifted into the valence band and the concentration of holes had to be calculated in approximation (C2) for degenerated case. The effect is probably caused by p-doping due to the presence of oxygen in air [31,32]. In Ref. [5] it has been mentioned that the side chains make **P3HT** material soft and allow for diffusion of small molecules. Another transport parameter that we have measured was the electrical conductivity of the samples. **PT1** polymer shows about one order of magnitude higher conductivity compared with **PT2** and **P3HT**. It can be the result of a better organization of the structure after the thermal treatment during the removal of the side chains.

A novel approach to the surface photovoltage (SPV) method [33] was used to determine the exciton diffusion length. Figs. 12–14 show the theoretical and experimental SPV spectra of the **PT1**, **PT2** and **P3HT** samples illuminated from the substrate side. Fitting theoretical curves calculated according to Appendix B to the experiment gives, among others, the thickness of the bulk (d), thickness of the SCR (w) and diffusion length (L). The total thickness ($d + w$) of each polymer layer obtained from SPV is compared with the respected value (h) from ellipsometry measurement.

Diffusion length of 5 nm in **P3HT** is low and is similar to that given in Ref. [34], i.e. 3.5 nm. The higher diffusion lengths in **PT1** and **PT2** may be caused by higher lifetime of excitons because of the lower concentration of equilibrium carriers in the native polythiophenes (see Table 1).

The samples **PT1** and **P3HT** show a minimum at wavelengths where the absorption spectra reach a maximum (see Fig. 7). It follows from the fact that the SPV signal depends on the x/L ratio, where x is the distance between the point where the exciton is generated and the boundary of the space charge region where the dissociation takes place. As follows from the arrangement of

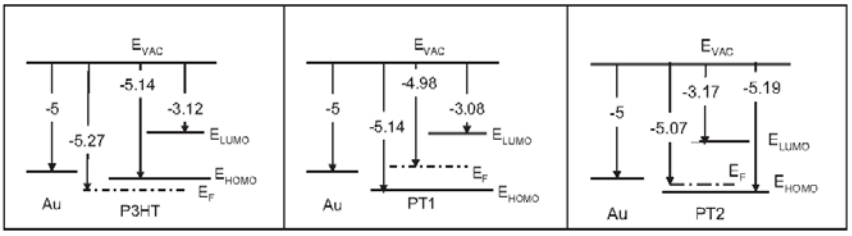

Fig. 11. Energy level diagram of the **P3HT**, **PT1**, **PT2** samples evaluated from the voltammetry, the Kelvin probe and optical measurements.

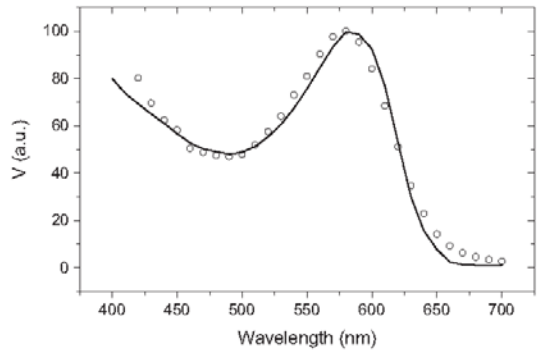

Fig. 12. Normalized PV spectra of **PT1** sample. Full line – theory fitted to the experimental points with the parameters: $w = 4$ nm, $d = 100$ nm, $L = 9$ nm, $h = 107$ nm.

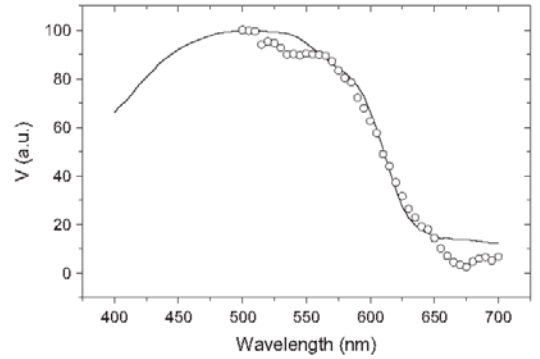

Fig. 13. Normalized PV spectra of **PT2** sample. Full line – theory fitted to the experimental points with the parameters: $w = 85$ nm, $d = 55$ nm, $L = 13$ nm, $h = 140$ nm.

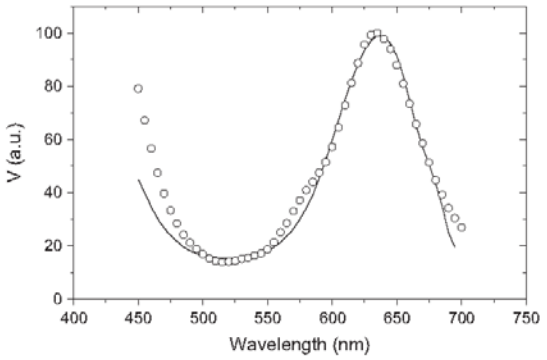

Fig. 14. Normalized PV spectra of **P3HT** polymer. Full line – theory fitted to the experimental points with the parameters: $w = 35$ nm, $d = 240$ nm, $L = 5$ nm, $h = 290$ nm.

the experiment (Fig. 2), the higher the absorption the longer the distance. At maximum absorption the losses of excitons are the highest because at relatively short diffusion length the excitons have to pass a large path to attain the space charge region. On the other hand, the **PT2** spectrum shows a tendency to reach a maximum at the wavelength corresponding to the maximum of absorption, because the losses of excitons during diffusion are not substantial when diffusion length is comparable with the thickness of the bulk.

4. Conclusion

Polythiophenes prepared from two different precursors which were thermally cleaved (samples **PT1**) or cleaved at room temperature using acid (samples **PT2**) and **P3HT** were studied. Measurement of the voltammetry and the work function together with the optical absorption allowed construction of the energy level diagrams. It was found that the Fermi level for **PT1** and **PT2** is inside the band gap near the HOMO level while for **P3HT** it is localized in the valence band, which is probably caused by the presence of oxygen. The band theory based on the tight-binding model was used to find some charge transport parameters in the investigated materials. Using the published value of the width of the valence band, effective density of states $N_V = 8.3 \times 10^{17}$ cm^{-3} was calculated which enabled us to obtain the hole concentration. The concentrations in the samples **PT1** and **PT2** are comparable, ranging from 1.8×10^{15} cm^{-3} to 8.3×10^{15} cm^{-3}, whereas three orders of magnitude higher concentration is obtained for **P3HT**, which corresponds well with the location of the Fermi level.

Comparison of **PT1** and **PT2** native polymers shows a similar morphology if they are deposited on glass/ITO conductive substrate. The hole concentrations do not differ much and the exciton diffusion length is slightly higher in **PT2** than in **PT1**. One order of magnitude higher electrical conductivity was found for **PT1** as compared with **PT2** and **P3HT.** The diffusion lengths in both these materials significantly exceed that in **P3HT** probably due to a much lower concentration of the charge carriers in the native polythiophenes. The optical absorption spectra of the materials are in approximately the same region and absorption coefficients of **PT2** are only a little lower than those of **PT1**. Relaying on these results, we can conclude that both **PT1** and **PT2** could be processed into functional solar cells. An important consequence is the possibility of preparation of native polythiophenes with similar properties regardless of whether the side chains are removed with heating or through treatment with acids. This fact appears prospective, especially for preparation of tandem solar cells.

Acknowledgements

This work has been supported by the Villum Foundation's Young Investigator Programme (2nd round, project: *Materials for Energy Production*) and by the Danish Ministry of Science, Innovation and Higher Education under a Sapere Aude Top Scientist Grant (No. DFF – 1335-00037A) and an Elite Scientist Grant (No. 11-116028). The authors acknowledge the support of the Czech Science Foundation project GA14-05053S.

Appendix A

Application of the tight-binding model results in the valence band dispersion in the form given by relation [7]

$$E(k) = E_0 - \alpha + 2\beta\cos(ka) \tag{A1}$$

where E_0 is energy of an isolated atom, k is in the interval $0 \leqslant k \leqslant \pi/a$, a is the lattice constant and α is

$$\alpha = -\int_{-\infty}^{+\infty} \varphi_0^*(x) W(x) \varphi_0(x) dx \tag{A2}$$

φ_0, φ_0^* are the wave functions of an isolated atom, the potential $W(x)$ is a measure of the inter-site interaction. Symbol β characterizes overlap of wave functions of electrons from the neighboring atoms

$$\beta = -\int_{-\infty}^{+\infty} \varphi_0^*(x \pm a) W(x) \varphi_0(x) dx \tag{A3}$$

For this model close to $k = 0$, expanding *cos (ka)* in Eq. (A1) and neglecting terms beyond $(ka)^2$, gives

$$m^* = \frac{\hbar^2}{2\beta a^2} \tag{A4}$$

The value of the effective mass depends on the degree of overlap of the conducting electron orbitals and, in principle, it plays the main role in the effective density of states.

Appendix B

A novel approach to the surface photovoltage (SPV) method [33] was used to determine the exciton diffusion length.

Assuming multiple reflections and neglecting interference effects we obtain for the current caused by excitons diffusing in the bulk and dissociated at the bulk – SCR interface ($x = d$):

$$\begin{aligned} j_b &= eD d\Delta n(x)/dx|_{x\ d} \\ &= -a_1 \alpha L/(1 \\ &\quad - \alpha^2 L^2)\left\{\frac{[(1-S)\exp(-d/L) - (1+S)\exp(d/L)]\exp(-\alpha d) + 2(\alpha L + S)}{(1+S)\exp(d/L) + (1-S)\exp(-d/L)} - \alpha L \exp(-\alpha d)\right\} \\ &\quad + a_2 \exp(-\alpha w)\alpha L/(1 \\ &\quad - \alpha^2 L^2)\left\{\frac{(1+S)\exp(d/L) - (1-S)\exp(-d/L) + 2(\alpha L - S)\exp(-\alpha d)}{(1+S)\exp(d/L) + (1-S)\exp(-d/L)} - \alpha L\right\} \end{aligned} \tag{B1}$$

where

$$a_1 = eI_0(1 - R_1)/(1 - R_1 R_2 \exp(-2\alpha h)) \text{ and}$$
$$a_2 = eI_0(1 - R_1)R_2 \exp(-\alpha h)/(1 - R_1 R_2 \exp(-2\alpha h))$$

e is the charge of electron, $\Delta n(x)$ is the concentration of excitons at the depth x, D is the exciton diffusion coefficient, α is the absorption coefficient, L is the exciton diffusion length, I_0 is the photon flux density impinging on the polymer layer, R_1 and R_2 are the reflectance from the illuminated and the bottom surfaces, respectively; d is the thickness of the bulk, w is the thickness of the SCR, h represents the total thickness of the layer: $h = d + w$ and S is the dimensionless surface recombination velocity ($S \equiv sL/D$), where s is the surface recombination velocity at the illuminated surface.

Contribution from the space charge region:

To obtain current from a thin space charge region ($\alpha w < 1$) the charge of electrons and holes generated in the SCR must be multiplied by a factor $G \in <0, 1>$. In this way the losses by recombination or incomplete dissociation in the SCR can be included. The current density J_s from SCR is obtained by integration of the charge photogeneration rate over thickness w.

$$\begin{aligned} J_s &= a_1 G \exp(-\alpha d)\int_0^w \alpha \exp(-\alpha x)dx + a_2 G \int_0^w \alpha \exp(-\alpha x)dx \\ &= a_1 G \exp(-\alpha d)(1 - \exp(-\alpha w)) + a_2 G(1 - \exp(-\alpha w)) \end{aligned} \tag{B2}$$

The terms in J_b and J_s, which are multiplied by a_1, represent the SPV signal generated by photons spreading in the direction of the impinging light; those multiplied by a_2 come from the reflected photons. As shown in Ref. [33], the currents J_b and J_s are independent even in the case of recombination in SCR and, consequently, total photocurrent density J is equal to the sum of (B1) and (B2)

$$J = J_b + J_s \tag{B3}$$

Appendix C

For the non-degeneration case the hole concentration p is given by a simple relation:

$$p = N_V \exp(-(E_F - E_V)/kT) \tag{C1}$$

In the case of degeneration the hole concentration was calculated according to the approximation [35] ($\eta = E_F/kT$):

$$p = \frac{2}{\sqrt{\pi}} N_V \frac{2}{3}\eta^{1.5}\left(1 + \frac{\pi^2}{8\eta^2}\right). \tag{C2}$$

References

[1] Perepichka IF, Perepichka DF, Meng H, Wudl F. Light-emitting polythiophenes. Adv Mater 2005;17:2281–305.
[2] Wang H-J, Chen Ch-P, Jeng R-J. Polythiophenes comprising conjugated pendants for solar cells: a review. Materials 2014;7:2411–39.
[3] Katz HE, Dodabalapur A, Bao Z. Oligo-and polythiophene field effect transistors. In: Fichou D, editor. Handbook of oligo-and polythiopnenes. New York: Wiley Publishing; 2008. p. 459–86.
[4] Krebs FC, Spanggaard H. Significant improvement of polymer solar cell stability. Chem Mater 2005;17:5235–7.
[5] Gevorgyan SA, Krebs FC. Bulk heterojunctions based on native polythiophene. Chem Mater 2008;20:4386–90.
[6] Bundgaard E, Hagemann O, Bjerring M, Nielsen NCh, Andreasen JW, Andreasen B, et al. Removal of solubilizing side chains at low temperature: a new route to native polythiophene. Macromolecules 2012;45:3644–6.
[7] Blythe T, Bloor D. Electrical properties of polymers. 2nd ed. Cambridge: Cambridge University Press; 2005.
[8] Chen M, Perzon E, Andersson MR, Marcinkevicius S, Jonsson SKM, Fahlman M, et al. 1 micron wavelength photo- and electroluminescence from a conjugated polymer. Appl Phys Lett 2004;84:3570–2.
[9] Gregg BA. Coulomb forces in excitonic solar cells. In: Sun SS, Sariciftci NS, editors. Organic photovoltaics. New York: CRS Press Taylor & Francis; 2005. p. 139–61.
[10] Jain SC, Willander M, Kumar V. Conducting organic materials and devices. In: Willeke GP, Weber ER, editors. Semiconductors and semimetals. Amsterdam: Elsevier Academic Press; 2007. p. 32–61.
[11] Bundgaard E, Krebs FC. Low band gap polymers for organic photovoltaics. Sol Energy Mater Solar Cells 2007;91:954–85.
[12] Coakley KM, Srinivasan BS, Ziebarth JM, Goh Ch, Liu Y, McGehee MD. Enhanced hole mobility in regioregular polythiophene infiltrated in straight nanopores. Adv Funct Mater 2005;15:1927–32.
[13] Choulis SA, Kim Y, Nelson J, Bradley DDC, Giles M, Shkunov M, et al. High ambipolar and balanced carrier mobility in regioregular poly (3-hexylthiophene). Appl Phys Lett 2004;85:3890–2.
[14] Yamamoto T. Molecular assembly and properties of polythiophenes. NPG Asia Mater 2010;2:54–60.
[15] Taliani C, Zamboni R, Danieli R, Ostoja P, Porzio W, Lazzaroni R, et al. Influence of molecular architecture on electronic and transport properties in sulfur-containing heterocyclic conducting polymers. Phys Scr 1989;40:781–5.
[16] Hutchison GR, Zhao Y-J, Delley B, Freeman AJ, Ratner MA, Marks TJ. Electronic structure of conducting polymers: limitation of oligomer extrapolation approximations and effects of heteroatoms. Phys Rev B 2003;68 (035204):1–13.
[17] Jones D, Guerra M, Favaretto L, Modelli A, Fabrizio M, Distefano G. Determination of the electronic structure of thiophene oligomers and extrapolation to polythiophene. J Phys Chem 1990;94:5761–6.
[18] Bruckner S, Porzio W. The structure of neutral polythiophene. An application of the Rietveld method. Die Makromol Chem 1988;189:961–7.
[19] Bjerring M, Sogaard Nielsen J, Nielsen NChr, Krebs FC. Polythiophene by solution processing. Macromoleculs 2007;40:6012–3.
[20] Toušek J, Toušková J, Remeš Z, Čermák J, Kousal J, Kuřitka I. Exciton diffusion length and concentration of holes in MEH-PPV polymer using the surface voltage and surface photovoltage methods. Chem Phys Lett 2012;552:49–52.
[21] Toušek J, Toušková J, Remeš Z, Kousal J, Gevorgyan SA, Krebs FC. Exciton diffusion length in some thermocleavable polythiophenes by the surface photovoltage method. Synth Metals 2011;161:2727–31.
[22] Shrotriya V, Ouyang J, Tseng RJ, Li G, Yang Y. Absorption spectra modification in poly(3-hexylthiophene): methanofullerene blend thin films. Chem Phys Lett 2005;411:138–43.
[23] de Leeuw DM, Simenon MMJ, Brown AR, Einerhand REF. Stability of n-type doped conducting polymers and consequences for polymeric microelectronic devices. Synt Metals 1997;87:53–9.
[24] Brédas JL, Silbey R, Boudreux DS, Chance RR. Chain-length dependence of electronic and electrochemical properties of conjugated systems: polyacetilen, polyphenolene, polythiophene, and polypyrrole. J Am Chem Soc 1983;105:6555–9.
[25] Wu J, Yue G, Xiao Y, Lin J, Huang M, Lan Z, et al. Homo P3HT: an ultraviolet responsive hybrid solar cell based on titania/poly(3-hexylthiophene). Sci Rep 2013;3:1283. http://dx.doi.org/10.1038/srep01283.
[26] Hu X-L, Zuo L-J, Nan Y-X, Helgesen M, Hagemann O, Bundgaard E, et al. Fine tuning the HOMO energy levels of polythieno [3,4-b]thiophene derivatives by incorporation of thiophene-3,4-dicarboxylate moiety for photovoltaic applications. Synt Metals 2012;162:2005–9.

[27] Al-Ibrahim M, Roth HK, Zhokhavets U, Gobsch G, Sensfuss S. Flexible large area polymer solar cells based on poly(3-hexylthiophene)/fullerene. Sol Energy Mat Sol Cells 2005;85:13–20.
[28] Rezek B, Čermák J, Kromka A, Ledinský M, Kočka J. Photovoltage effects in polypyllore-diamant nanosystem. Diam Relat Mater 2009;18:249–52.
[29] Carlé JE, Helgesen M, Zawacka NK, Madsen MV, Bundgaard E, Krebs FC. A comparative study of fluorine substituents for enhanced stability of flexible and ITO-free high-performance polymer solar cells. J Polym Sci, Part B: Polym Phys 2014;52:893–9.
[30] Northrup JE. Atomic and electronic structure of polymer organic semiconductors: P3HT, PQT, and PBTTT. Phys Rev B 2007;76:245202-1–2-6.
[31] Hintz H, Peisert H, Egelhaaf H-J, Chasse T. Reversible and irreversible light-induced p-dopping of P3HT by oxygen studied by photoelectron spectroscopy (XPS/UPS). J Phys Chem C 2011;115:13373–6.
[32] Cook S, Furube A, Katoh R. Matter of minutes degradation of poly(3-hexylthiophene) under illumination in air. J Mater Chem 2012;22:4282–9.
[33] Toušek J, Toušková J. The role of the space charge region in surface photovoltaic effect. J Appl Phys 2014;116:083708-1–8-8.
[34] Deibel C, Mack D, Gorenflot J, Scholl A, Krause S, Reinert F, et al. Energetics of excited states in the conjugated polymer poly (3-hexylthiophene). Phys Rev B 2010;81:085202-1–2-5.
[35] Blackemore JS. Semiconductor statistics. Oxford: Pergamon Press; 1962.

materials

MDPI

Article

The Influence of Conjugated Polymer Side Chain Manipulation on the Efficiency and Stability of Polymer Solar Cells

Ilona M. Heckler [1], Jurgen Kesters [2], Maxime Defour [3], Morten V. Madsen [1], Huguette Penxten [2], Jan D'Haen [2], Bruno Van Mele [3], Wouter Maes [2] and Eva Bundgaard [1,*]

1 Department of Energy Conversion and Storage, Technical University of Denmark (DTU), Frederiksborgvej 399, Roskilde 4000, Denmark; ilhe@dtu.dk (I.M.H.); mves@dtu.dk (M.V.M.)
2 Institute for Materials Research (IMO-IMOMEC), Hasselt University, Agoralaan 1-Building D, Diepenbeek 3590, Belgium; jurgen.kesters@uhasselt.be (J.K.); huguette.penxten@uhasselt.be (H.P.) jan.dhaen@uhasselt.be (J.D.H.); wouter.maes@uhasselt.be (W.M.)
3 Physical Chemistry and Polymer Science (FYSC), Vrije Universiteit Brussel (VUB), Pleinlaan 2, Brussels 1050, Belgium; mdefour@vub.ac.be (M.D.); bvmele@vub.ac.be (B.V.M.)
* Correspondence: evbu@dtu.dk; Tel.: +45-46-77-54-98

Academic Editor: Jennifer A. Irvin
Received: 15 December 2015; Accepted: 2 March 2016; Published: 9 March 2016

Abstract: The stability of polymer solar cells (PSCs) can be influenced by the introduction of particular moieties on the conjugated polymer side chains. In this study, two series of donor-acceptor copolymers, based on bis(thienyl)dialkoxybenzene donor and benzo[*c*][1,2,5]thiadiazole (BT) or thiazolo[5,4-*d*]thiazole (TzTz) acceptor units, were selected toward effective device scalability by roll-coating. The influence of the partial exchange (5% or 10%) of the solubilizing 2-hexyldecyloxy by alternative 2-phenylethoxy groups on efficiency and stability was investigated. With an increasing 2-phenylethoxy ratio, a decrease in solar cell efficiency was observed for the BT-based series, whereas the efficiencies for the devices based on the TzTz polymers remained approximately the same. The photochemical degradation rate for PSCs based on the TzTz polymers decreased with an increasing 2-phenylethoxy ratio. Lifetime studies under constant sun irradiance showed a diminishing initial degradation rate for the BT-based devices upon including the alternative side chains, whereas the (more stable) TzTz-based devices degraded at a faster rate from the start of the experiment upon partly exchanging the side chains. No clear trends in the degradation behavior, linked to the copolymer structural changes, could be established at this point, evidencing the complex interplay of events determining PSCs' lifetime.

Keywords: conjugated polymers; side chain variation; organic photovoltaics; roll-coating; photochemical and thermal stability

1. Introduction

Polymer solar cells (PSCs) have emerged as strong competitors in the field of renewable energy over the past two decades. Dedicated studies have highlighted their potential and wide applicability due to a myriad of inherent appealing features (low weight, flexibility, semi-transparency, color-tunability, *etc.*) [1–5]. Judicious efforts on chemical engineering of the polymer (electron donor) materials, optimization of the solar cell architecture and the acquisition of additional fundamental insights on device operation have driven the power conversion efficiencies (PCEs) of this technology to levels approaching and even surpassing the 10% threshold [6–8]. On the downside, some of the highly advanced conjugated polymers, such as PTB7-Th (poly{4,8-bis[5-(2-ethylhexyl)thiophen-2-yl]benzo[1,2-*b*:4,5-*b*′]dithiophene-2,6-diyl-*alt*-3-fluoro-2-[(2-ethylhexyl)carbonyl]thieno[3,4-*b*]thiophene-4,6-diyl};

Figure 1), require rigorous processing procedures (inert atmosphere, high temperature, *etc.*) and have so far only been successful on small laboratory-scale spin-coated (SC) devices [9]. However, for PSCs to become economically viable, large-scale production techniques (such as roll-coating (RC)) are mandatory [10,11]. RC processing has been applied for several years within the group at the Technical University of Denmark, but a recent screening of a myriad of polymers demonstrated only a few suitable candidates for large-scale (RC) device fabrication [12]. As an example, PTB7-Th, very promising in SC devices with PCEs up to 10% [13], did not allow for a proper translation to RC processing and only granted a PCE of 0.2% [12]. On the other hand, with respect to large-scale device fabrication, poly{[2,5-bis(2-hexyldecyloxy)phenylene]-*alt*-[4,7-di(thiophen-2-yl)benzo[*c*][1,2,5]thiadiazole]} **P1** and poly{2,2′-[5,5′-(2,5-bis(2-hexyldecyloxy)-1,4-phenylene)dithiophene]-*alt*-[2,5-bis(4-hexylthiophen-2-yl)thiazolo[5,4-*d*]thiazole]} **P2** (Figure 1) have been identified as suitable donor polymers for RC-processed organic photovoltaics (OPV) [12,14]. The moderate efficiency of the PSCs based on the **P2**-(**12**) polymer, containing the bis(thienyl)di(2-hexyldecyloxy)benzene donor part [12], could be improved using a hexyl side chain on the dithienylthiazolo[5,4-*d*]thiazole group (instead of dodecyl) [15]. In previous work on **P1**, the impact of the nature (alkyl/alkoxy) and positioning of the appended side chains on the electrical properties was demonstrated, especially with regards to the absorption profile, device performance and stability [16].

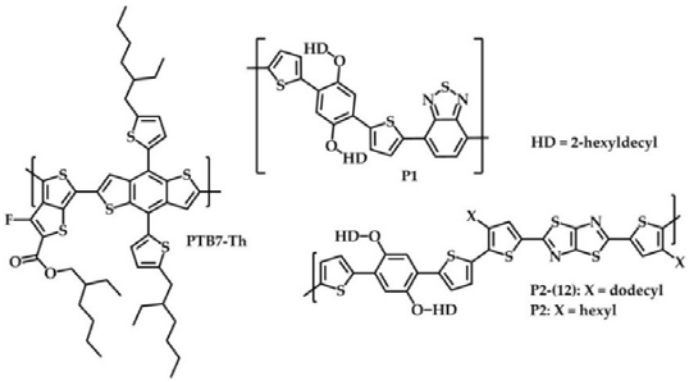

Figure 1. Chemical structures of a few low bandgap copolymer organic photovoltaics (OPV) reference materials [14–16]. PTB7-th, poly{4,8-*bis*[5-(2-ethylhexyl)thiophen-2-yl]benzo[1,2-*b*:4,5-*b*′]dithiophene-2,6-diyl-*alt*-3-fluoro-2-[(2-ethylhexyl)carbonyl]thieno[3,4-*b*]thiophene-4,6-diyl}.

Since the introduction of the bulk heterojunction concept, in which the electron donating (polymer or small molecule) and electron accepting (often (methano)fullerene) components are intimately intermixed at the nanoscale within the photoactive layer, the morphology formation and evolution of the photoactive blend, processed from organic solvents, has been a fascinating and highly important topic in the field. It has been well described that the appended side chains on conjugated polymers have a large impact on both material solubility and blend formation [17,18]. On the other hand, over time, phase separation of the blend components can occur, especially upon the application of (external) stress (heat, light, *etc.*) [19]. The use of nucleation agents [20], non-crystallizing polymer-fullerene blends [20,21], crosslinkable functional moieties [22] and post-deposition removal of the side chains [23,24] has been proposed as potential routes to circumvent these issues and increase the lifetime of the solar cell devices fabricated from these materials. Recently, it was also shown that decreasing the side chain density of a 4*H*-cyclopenta[2,1-*b*:3,4-*b*′]dithiophene (CPDT)-based low bandgap copolymer afforded a synergetic enhancement of solar cell performance and thermal stability [25]. In addition, past efforts have indicated that full displacement of the dimethyloctyloxy side chains on MDMO-PPV (poly[2-methoxy-5-(3′,7′-dimethyloctyloxy)-1,4-phenylenevinylene])

to 2-phenylethoxy (EtPh) moieties resulted in a significant enhancement of the glass transition temperature (T_g; from 45–111 °C) and, therefore, the thermal stability of the resulting PSCs, attributed to a reduced phase separation tendency of the active layer components [26]. A similar active layer stabilizing effect was obtained upon incorporation of small amounts (5%–10%) of alcohol or ester functionalities on the side chains of P3HT or PCPDTBT copolymers [27,28].

In this work, the aforementioned strategies were translated onto two promising RC processable conjugated polymers (**P1** and **P2**; Figure 1), on which the appended solubilizing 2-hexyldecyloxy (HD) side chains were partially exchanged by EtPh groups, in an attempt to elevate the T_g and, thereby, the (thermal) stability of the resulting photovoltaic devices. The influence of this side chain variation on the photovoltaic performance, as well as the thermal and photochemical stability (and thus, the lifetime) of the resulting solar cell devices was investigated.

2. Results and Discussion

2.1. *Synthesis and Material Characterization*

In this study, six low bandgap copolymers were synthesized based on thiophene (T), phenylene (P), benzo[*c*][1,2,5]thiadiazole (BT) and thiazolo[5,4-*d*]thiazole (TzTz) building blocks (Figures 1 and 2). **P1** and **P2**, bearing HD side chains on the P unit, were reported previously [12,29]. **P3a** and **P3b** were derived from **P1** and were prepared with partial substitution (5% and 10%, respectively [30]) of the HD by EtPh side chains. In the same way, **P4a** and **P4b** have the same backbone as **P2**, but also with partially-substituted side chains (5% and 10%, respectively).

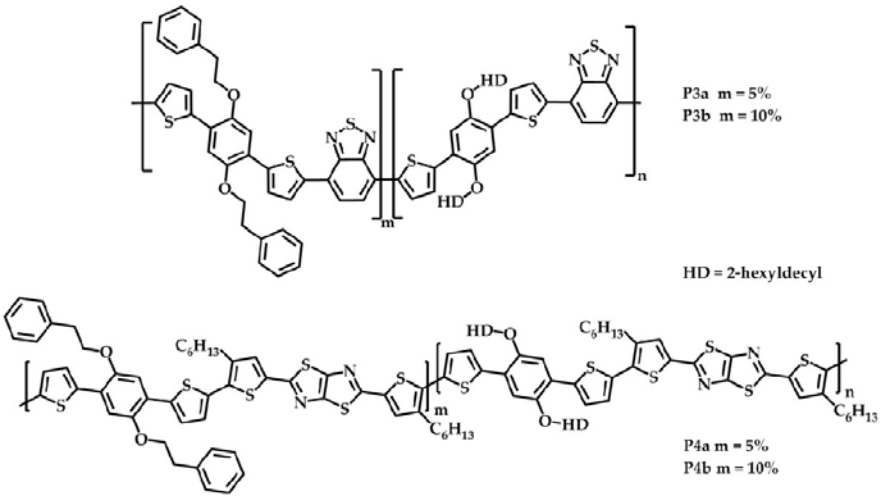

Figure 2. Chemical structures of the investigated statistical copolymers **P3a,b** and **P4a,b**.

The required distannylated monomers $\mathbf{5_{HD}}$ and $\mathbf{5_{EtPh}}$ for the envisaged Stille polycondensation were synthesized according to a procedure consisting of four steps starting from hydroquinone (Scheme 1) [16]. However, since the first two steps toward $\mathbf{5_{EtPh}}$, *i.e.*, bromination and alkylation of hydroquinone, resulted in a mixture of the di-alkylated (32%) and mono-alkylated (25%) product in rather low yields under the standard conditions used for the HD analogue, an alternative Williamson ether reaction was applied [26]. As such, 47% of the di-alkylated (and 29% of the mono-alkylated) product could be obtained. Thereafter, a Stille cross-coupling reaction with 2-(trimethylstannyl)thiophene and final stannylation of the obtained product afforded monomer $\mathbf{5_{EtPh}}$.

Standard Stille cross-coupling polymerization of monomers $\mathbf{5_{HD}}$ and $\mathbf{5_{EtPh}}$ with dibromo-BT yielded BT-based polymers **P1**, **P3a** and **P3b** (Figure 2). Whereas **P1** contains only one type of (HD) side chains, the synthesis of **P3a** and **P3b** was directed toward producing random copolymers with 5% and 10% of $\mathbf{5_{EtPh}}$ units. Correspondingly, the dibrominated 2,5-dithienyl-TzTz monomer (synthesized using a literature procedure [31]) yielded polymer **P2** and copolymers **P4a** and **P4b** with 5% and 10% of $\mathbf{5_{EtPh}}$, respectively (Figure 2). Complete substitution of the HD side chains (100% of $\mathbf{5_{EtPh}}$) was only attempted for the BT-based backbone. However, the obtained polymer could not be analyzed due to a lack of solubility.

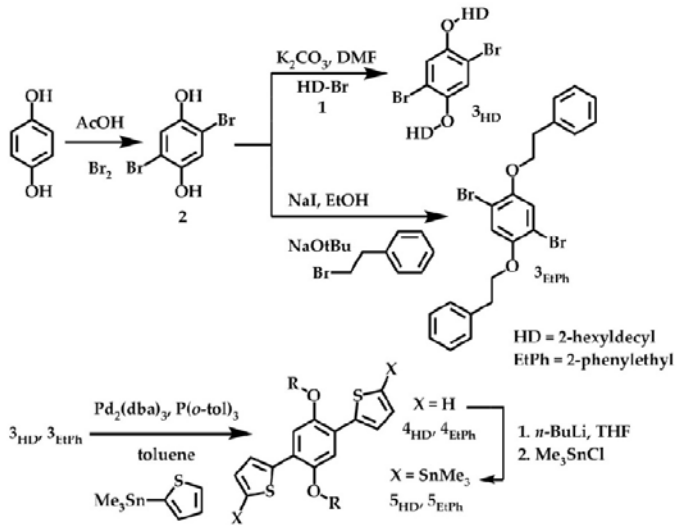

Scheme 1. Synthetic routes for the monomers $\mathbf{5_{HD}}$ and $\mathbf{5_{EtPh}}$.

The synthesized polymers were characterized with standard techniques. ^{1}H NMR spectra of the BT-based polymers were recorded in chloroform-d_1 (Figure S1a–c). No well-resolved spectra could be obtained for the TzTz-based polymers due to their low solubility in chloroform-d_1 and chlorobenzene-d_5. The spectra of **P3a** and **P3b** showed two small signals at ~4.33 and 3.34 ppm for the two CH_2 groups of the EtPh side chains. Integration of the signals at 3.34 ppm and the signals for the O–CH_2 groups of the HD side chains at 4.08 ppm afforded monomer ratios of 4.9/95.0 for **P3a** and 9.4/90.0 for **P3b**, close to the monomer feed ratio. This shows that incorporation of the EtPh side chains was successful for both polymers. The molar masses of the polymers were determined by size exclusion chromatography (SEC), affording number-average molar masses (M_n) of approximately 30–40 kDa (Table 1). In the UV-VIS spectra of the BT-based polymers in chloroform (CF) (Figure 3a), the absorption maximum (λ_{max}), as well as the onset slightly shifted to lower wavelength with an increasing amount of EtPh substituents. In contrast, minor differences were seen in the UV-VIS spectra of the polymer films (Figure 3a). The optical bandgap of all BT-based polymers is 1.73 eV. The electrochemical bandgap, as determined by cyclic voltammetry (CV), decreased slightly upon elevating the amount of EtPh groups due to a minor increase of the highest occupied molecular orbital (HOMO) level (Table 1). On the other hand, the UV-VIS spectra of **P2**, **P4a** and **P4b** in chlorobenzene (CB) (Figure 3b) showed a shift toward a higher wavelength upon increasing the EtPh ratio, with additional formation of a shoulder at the low energy end. The absorption onset for the **P4** polymers was around 640 nm, whereas for **P2**, this appeared at 580 nm. The UV-VIS spectra of the polymer films, however, once again showed minor differences (Figure 3b). The optical bandgap for the three

TzTz-based polymers is 1.91 eV. For this polymer series, there is also no significant difference in the electrochemical bandgap (values of ~2.22 eV).

Table 1. Molecular, optical and electrochemical properties of the synthesized polymers.

Polymer	EtPh [1]	M_n [2]	PDI [2]	λ_{onset} [3] Solution	λ_{onset} [3] Film	ΔE_{op} [3]	ΔE_{ec} [4]	HOMO [4]	LUMO [4]	R_d [5]
P1	0%	42	1.9	669	713	1.73	2.07	−5.37	−3.30	1.66
P3a	5%	39	2.1	656	715	1.73	2.03	−5.34	−3.31	1.63
P3b	10%	43	2.1	645	717	1.73	1.99	−5.31	−3.32	1.69
P2	0%	44	1.9	580	650	1.91	2.24	−5.24	−3.01	2.82
P4a	5%	30	3.1	640	647	1.91	2.21	−5.20	−2.99	2.60
P4b	10%	78	1.5	640	646	1.91	2.22	−5.21	−2.99	2.13

[1] Percentage of EtPh side chains in the polymer; [2] number-average molar mass (in kDa) and polydispersity index (PDI) determined by size exclusion chromatography in chlorobenzene at 60 °C against polystyrene standards; [3] in nm (λ_{onset}) and in eV (ΔE_{op}) (determined by UV-VIS spectroscopy); [4] in eV (determined by cyclic voltammetry); [5] R_d = degradation rate (%/h) calculated from photochemical stability measurements of the pure polymer films.

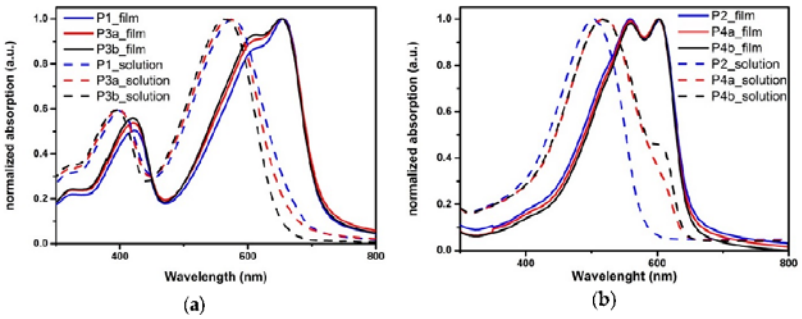

Figure 3. Normalized UV-VIS absorption spectra for the benzo[*c*][1,2,5]thiadiazole (BT)- (**a**) and thiazolo[5,4-*d*]thiazole (TzTz)- (**b**) based polymer series.

2.2. *Polymer Solar Cells*

To investigate the influence of the partially-exchanged side chains on the photovoltaic performance and long-term PSC stability, both RC and SC bulk heterojunction solar cell devices were fabricated. The solar cell architecture for the RC devices consisted of PET/silver grid/PEDOT-PSS/ZnO/polymer:phenyl-C_{61}-butyric acid methyl ester ($PC_{61}BM$)/PEDOT-PSS/silver grid, with device areas of ~1 cm^2 [12]. For the SC devices, the traditional device architecture glass/ITO/PEDOT-PSS/polymer:$PC_{61}BM$/Ca/Al was applied, with an active device area of 3 mm^2.

The photoactive layers of the RC devices prepared from **P1**, **P3a** and **P3b**, with a polymer to $PC_{61}BM$ ratio of 1:2 (wt %/wt %), were procured using *ortho*-dichlorobenzene (ODCB) as the processing solvent with a total concentration of 40 mg/mL, according to a previously-optimized procedure [12]. The coating was applied in air at 80 °C, and the photoactive layer thickness varied between 360, 450 and 540 nm. The PSCs were encapsulated between glass slides. As summarized in Table 2 and Figure S2a, **P1** granted a maximum PCE of 3.05% at an optimal layer thickness of 450 nm. For **P3a** and **P3b**, the highest PCEs were procured from active layer thicknesses of 360 nm, with performances of 2.65% and 2.17%, respectively. A slight decrease in the PCE could hence be observed upon increasing the amount of EtPh side chains, attributable to small reductions in open-circuit voltage (*Voc*) and mainly short-circuit current density (*Jsc*) (Table 2).

In a similar fashion, the photoactive layers for the SC devices based on **P1**, **P3a** and **P3b** were obtained from a 40-mg/mL solution in ODCB with a polymer to $PC_{61}BM$ ratio of 1:1.5 (wt %/wt %). In this way, PCEs of ~4% could be achieved (Table 2, Figure S2b). Once again, a small decrease in averaged PCE, *Voc* and *Jsc* could be observed upon increasing the amount of EtPh groups.

The PSCs made from the TzTz-based polymers showed less of a difference in the performance between the RC- and SC-processed solar cells (Table 2, Figure S2). The best results (maximum PCE of 2.73%) (Table 2, Figure S2a) for the RC-processed devices employing **P2** were achieved using a solvent mixture of ODCB and CB (4:1), a 1:1.5 (wt %/wt %; 40 mg/mL) ratio of **P2**:$PC_{61}BM$ and a layer thickness of 400 nm. These conditions were then also applied to **P4a** and **P4b** PSCs, yielding PCEs in the same range (2.72% and 2.76%, respectively).

The SC devices were also fabricated from ODCB:CB (4:1) as the processing solvent in a 1:1.5 (wt/wt%) ratio with a total concentration of 40 mg/mL for **P2** and **P4a** and 50 mg/mL for **P4b**. The elevated concentration for **P4b** was employed to warrant an optimal layer thickness. Upon insertion of the EtPh side chain moieties, a small increase in performance could be observed (Table 2, Figure S2b). The best device based on polymer **P4b** afforded a PCE of 3.21%. The *Voc* decreases within the series (which can tentatively be attributed to the lack of individual optimization). However, an improvement in *Jsc* can be seen by the partial exchange of the side chains (8.57 and 8.15 A/cm^2 for **P4a** and **P4b**, respectively).

Table 2. Current-voltage (*IV*) parameters [1] (*Voc*, *Jsc*, fill factor (FF) and power conversion efficiency (PCE)) for the polymer:phenyl-C_{61}-butyric acid methyl ester ($PC_{61}BM$) RC and SC solar cells based on **P1**, **P2**, **P3a**, **P3b**, **P4a** and **P4b**.

Polymer	Method [2]	*Voc* (V)	*Jsc* (mA/cm^2)	FF	PCE (Best) (%)
P1	RC [3]	0.75	7.83	0.47	2.81 (3.05)
	SC [4]	0.74	10.38	0.56	4.31 (4.42)
P3a	RC [3]	0.74	6.52	0.52	2.51 (2.65)
	SC [4]	0.72	10.22	0.56	4.15 (4.54)
P3b	RC [3]	0.73	5.76	0.50	2.10 (2.17)
	SC [4]	0.71	9.41	0.55	3.68 (4.09)
P2	RC [5]	0.69	6.69	0.61	2.67 (2.73)
	SC [6]	0.72	6.60	0.58	2.76 (2.92)
P4a	RC [5]	0.68	6.95	0.59	2.59 (2.72)
	SC [6]	0.65	8.57	0.55	3.06 (3.06)
P4b	RC [5]	0.69	7.00	0.60	2.66 (2.76)
	SC [6]	0.61	8.15	0.63	3.13 (3.21)

[1] *IV* parameters are averaged over 5 devices for RC and 2–8 devices for SC; [2] RC: roll-coating in air with an inverted device geometry of ~1 cm^2 (PET substrate/Ag grid/PEDOT-PSS/ZnO/polymer:$PC_{61}BM$/PEDOT-PSS/Ag grid); SC: spin-coating under inert atmosphere with a device geometry of 3 mm^2 (glass/ITO/PEDOT-PSS/polymer:$PC_{61}BM$/Ca/Al); [3] RC of polymer:$PC_{61}BM$ blends in a 1:2 ratio processed from *ortho*-dichlorobenzene (ODCB), with a layer thickness of 450 nm for **P1** and 360 nm for **P3a** and **P3b**; [4] SC of polymer:$PC_{61}BM$ blends in a 1:1.5 ratio processed from ODCB; [5] RC of polymer:$PC_{61}BM$ blends in a 1:1.5 ratio processed from ODCB/CB = 4/1, with a layer thickness of 400 nm; [6] SC of polymer:$PC_{61}BM$ blends in a 1:1.5 ratio processed from ODCB/CB = 4/1.

A general comparison of the different devices prepared shows, that the RC ones expectedly afforded lower efficiencies than the corresponding SC devices. This was, however, much more pronounced for the BT-based polymer series (1%–2%) as compared to the TzTz-based polymer series (0.1%–0.4%). The exchange of the side chain has a negative effect on the PCE of the BT-based PSCs, whereas the effect was neutral (RC) or even positive (SC) for the TzTz-based series.

The external quantum efficiency (EQE) spectra (Figure S3) for the BT-based RC PSCs showed a local maximum around 600 nm, with decreasing intensities for the different polymer solar cell devices with increasing amount of EtPh groups. On the other hand, there are no distinct differences in the curve progression and maximum EQE values (~37% at 520 nm) for the TzTz-based RC PSCs.

2.3. Stability Analysis

2.3.1. Material Stability

The thermal properties of the polymers were analyzed by rapid-heat cool calorimetry (RHC) (Figure S4). RHC was chosen above regular differential scanning calorimetry (DSC) because of its

increased sensitivity to thermal transitions as a result of the fast scanning rates and the low sample amounts required [32,33]. Nevertheless, it has barely been applied for low bandgap copolymers [19,25,28] to date. RHC analysis showed a semicrystalline character for the BT polymer group (Figure S4a). Whereas **P1** shows a sharp melting peak at 254 °C, partial exchange of the HD side chains with EtPh groups shifted the peak to higher temperatures (260 °C for **P3a** and 265 °C for **P3b**), but with similar melting enthalpy (11.5 J/g for **P3a** and **P3b** and 12.0 J/g for **P1**). The crystalline nature might be slightly suppressed due to the random incorporation of the thiophene-phenyl-thiophene units. While the melting peak temperature increases with an increased incorporation of the EtPh groups, the melting trajectory is broadened. A lower temperature shoulder seems more prominent for higher EtPh content. The Tg of these semicrystalline polymers could, however, not be detected in a reliable manner. In contrast, the thermograms for the TzTz polymer group show no melting peaks (in a temperature range of up to 300 °C), and these polymers seem completely amorphous. In this case, a Tg could be detected, increasing slightly between 148 and 156 °C with the amount of incorporated EtPh groups (Figure S4b). Both the melting peak temperature of the BT polymer group and the glass transition of the TzTz polymer group show a similar trend and are slightly increased with higher EtPh content.

To investigate the photochemical stability of the pristine polymer materials, the UV-VIS absorption of the polymer films as a function of time was assessed at Air Mass (AM) 1.5 (1000 W/m^2) conditions in an automatic set up (as described in the literature [34]). Upon prolonged exposure, the absorption of all polymers diminished strongly (with a slight blue shift; Figure S5), also clearly visible by a loss in film color during the experiment. From the normalized absorption degradation curves (Figure 4a,d), the degradation rates could be determined (see Table 1). The BT-based polymers exhibited degradation rates of approximately 1.66%/h, whereas the degradation rates for the TzTz-based polymers improved from 2.82%–2.13%/h with increasing amounts of EtPh side chains. The absorption of **P1**, **P3a** and **P3b** was almost completely gone after 60 h of light exposure. **P2** showed no absorption any more after 30 h, and **P4a** and **P4b** required 40 h of light exposure to show complete degradation. For **P2**, the photochemical stability improved in comparison to the previously reported **P2-12** (3.58%/h) [12]. Thus, manipulation of the side chain pattern to incorporate 10% of EtPh units does afford a further improved photochemical stability for the TzTz polymer series.

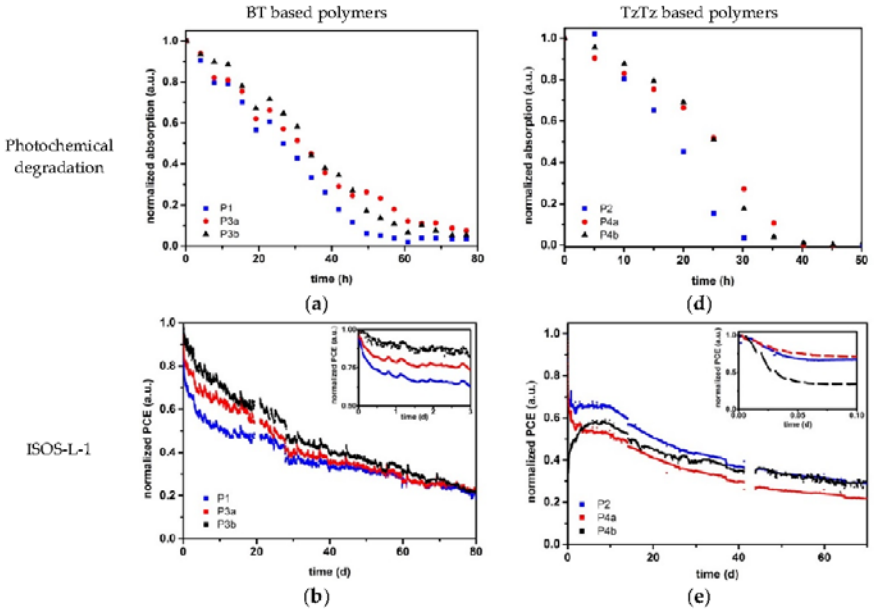

Figure 4. *Cont.*

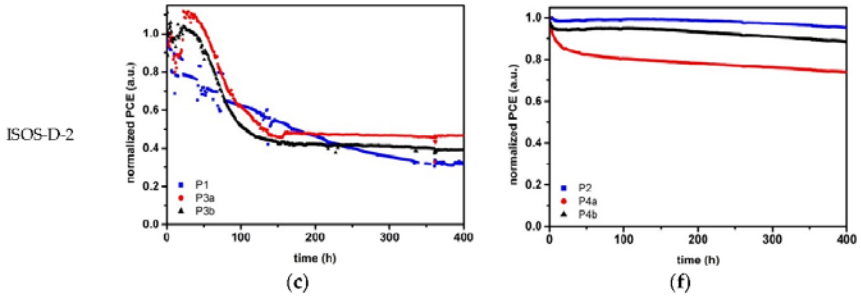

Figure 4. Maximum values of the normalized UV-VIS absorption of the polymer films as a function of time during sun irradiance (**a**,**d**), average lifetime measurements (ISOS-L-1 [35]) of the polymer solar cells (PSCs) normalized in terms of PCE (**b**,**e**) and the thermal degradation test (ISOS-D-2 [35]) of the PSCs normalized in terms of PCE (**c**,**f**) for the BT- (**a**–**c**) and TzTz- (**d**–**f**) based polymer series.

2.3.2. Device Stability

For the RC-fabricated PSCs, the photochemical stability was investigated by a lifetime study under ISOS-L-1 standards [35] using at least three to five PSCs with layer thicknesses affording the best efficiencies. All cells were subdued to AM 1.5 (1000 W/m^2) conditions for at least 70 days (1700 h). All RC devices were handled (coated, encapsulated) in the same way, such that a similar effect of UV light can be expected [36], and only relative values are reported. Initially, *IV* curves were measured every minute, with larger intervals of 10 and 30 min at longer timescales. The averages of the PV parameters over time were taken from the normalized values of each cell. Cell failures (when a cell broke down, but recovered to the initial value again) or measurement failures (when an error occurred in the system) were left out of the presented data. The results for the BT-based PSCs are shown in Figure 4b (PCE) and Figure S6a–c (*Voc*, *Jsc*, fill factor (FF)), whereas the averaged curves of the TzTz-based PSCs are shown in Figure 4e (PCE) and Figure S6d–f (*Voc*, *Jsc*, FF).

In the first phase (0–5 h) of the lifetime study, the PCE decreased quickly for all cells (Figure 4b,e), which is often referred to as the "burn-in" phase [35]. For the BT series, this burn-in was found to be more apparent for **P1** than for **P3a** and **P3b**. The EtPh side chains hence seem to have a beneficial influence on the initial degradation of the cells. As a general comparison point, the initial PCE was reduced to 80% of its initial value after 5, 29 and 111 h for **P1**, **P3a** and **P3b**, respectively. Afterwards, the PCE of all three PSCs decreased in a linear manner. However, the slope for **P3b** is larger than for **P3a** and **P1**. As such, the PCE of all BT-based devices decreased to ~25% of its initial value after 70 days. Even though the PSCs with a (higher) content of EtPh side chains are more stable in the burn-in phase, this effect was counteracted in the second phase of the lifetime testing. The *Voc*'s of **P1** and **P3a** have a similar stability, but the *Voc* of **P3b** started to degrade faster after ~20 days (Figure S6a). The change in *Jsc* is similar to the PCE decay. **P1** decreased faster in the burn-in phase, whereas **P3a** and **P3b** decreased at approximately the same rate (Figure S6b). The FF decreased in a similar manner for all three polymers (Figure S6c).

The lifetime behavior of the TzTz-based PSCs showed a different trend in the PV parameters (Figure 4e and Figure S6d–f). The efficiency of the solar cells incorporating polymers **P2** and **P4a** reduced rapidly to ~65% and ~70%, respectively, during the first 2 h (~0.1 day), whereas the performance of the devices based on **P4b** took a steep decay to ~35% during this rapid burn-in phase [35]. Hereafter, the PCE of the devices based on **P2** and **P4a** stayed rather constant until Day 10. In contrast, the PCE of the PSCs containing **P4b** remarkably recovered to ~60% again during this time. This constant process/recovery could be a result of slow photo-annealing [37] overlapping with the standard degradation. For **P2** and **P4b**, the increase in efficiency over the first 10 days seems to be higher than the decrease via degradation. After that, the PCEs of all three PSCs decreased continuously.

However, the slope for **P4b** was somewhat smaller than for **P4a** and **P2**. As such, the PCE of **P4a** decreased to ~20%, whereas **P4b** and **P2** decreased to ~30% of their initial value after 70 days. For the PSCs based on TzTz, the influence of the EtPh side chains seems to be more effective in the second stage of the degradation. The behavior of the *Voc* was the same for all three PSC types, whereas the *Jsc* and FF developed similar to the PCE (but less distinct). In general, the disappearance of the absorption of the pure polymer films (Figure 4a,d and Figure S5), combined with the photochemical degradation of the corresponding solar cells (toward similar relative values for all polymers; Figure 4b,e), seems to point to a common photo-degradation pathway for both material series. Rivaton *et al.* have proposed a photochemical degradation route in which the alkoxy side chains on the phenyl building block in MDMO-PPV are cleaved off via photolysis [38]. Since the degradation profiles observed here look very similar and the same type of alkoxy side chains are employed, we can assume a similar behavior for this polymer series, practically independent of the presence of the phenyl end groups.

The thermal stability of the OPV devices was also investigated, more specifically for the SC PSCs in a nitrogen-containing glovebox at 85 °C using a dedicated degradation chamber according to the ISOS-D-2 protocol [35]. For the solar cells employing **P3a** and **P3b**, an initial (thermal annealing) phase in which the PCE increased slightly could be observed, followed by a rapid decrease to ~50% and ~40% of the initial value, respectively (Figure 4c). Afterwards, the performance of these two materials stayed constant for the next 250 h. In comparison, the degradation of the devices based on **P1** occurred in a more linear manner. Similar to the two analogous statistical copolymers, the degradation levels out after a certain time (350 h for **P1**), at which ~30% of the initial PCE was retained (Figure 4c). The *Jsc* followed a similar trend as the PCE, whereas the *Voc* remained rather constant (Figure S7). These studies clearly show that the incorporation of EtPh side chains has a positive effect on the stability of the PSCs based on the BT polymer series in the beginning of the tests. However, for a longer term, it is clear that other degradation processes counteract this.

For the devices based on TzTz copolymers **P4a** and **P4b**, an initial burn-in phase was observed in which the PCE decreased to 85 and 95%, respectively, followed by a slow linear decay of up to another 10% over 350 h. In contrast, PSCs based on **P2** showed a remarkably high thermal stability over the entire time scale, with a retained efficiency of up to 95% of the initial value after 400 h of thermal stress (Figure 4f). The drop in *Jsc* (Figure S7e) of **P2** is balanced out by the rise in FF (Figure S7f). It must be noted, however, that the *Jsc* drop is more present for **P2** than for **P4b** (Figure S7e), but this is not reflected in the PCE due to the rise in FF for **P2**.

To gain more insight into the effect of the exchanged side chains on the thermal stability, non-encapsulated RC PSCs were heated at 85 °C for four and seven days, respectively, and optical microscope images were taken at different time intervals (Figures 5 and 6). For the BT-based PSCs, the images show no clear differences or distinct features within the first 5 h of heating. After 24 h, however, the formation of particles in the photoactive layer becomes apparent, and after four days, all films show a rather strong phase separation, which can be connected with the degradation during the long time exposure to thermal stress (Figure 4c). To further assess the thermal stability, in particular with respect to the changes in the morphology of the photoactive layer, transmission electron microscopy (TEM) measurements were performed on the active layers of **P1**, **P3a** and **P3b** taken from the SC PSCs before and after the application of the thermal stress of 85 °C for 400 h (Figure S8). Initially, the photoactive layer blends showed no remarkable features. After the application of the thermal stress, however, large phase-separated domains were formed. Unfortunately, this could not directly be related to T_g (as these could not be observed for the BT polymer series). The formation of fullerene crystals is most likely responsible for the loss in *Jsc* (and PCE), as observed before [39].

The optical microscope images taken from the photoactive layer blends employing **P2**, **P4a** and **P4b** (Figure 6) show no particular features after inducing a thermal stress of 85 °C for seven days. This result is in good correlation with the minor efficiency loss during the thermal stress test on the SC PSCs (Figure 4f). As expected, since the T_g's of these polymers are well above the degradation temperature (85 °C), the blend components remain intermixed (no phase separation), resulting in a higher thermal

stability across this series. Because of the minor rise in T_g upon implementation of the low ratio of EtPh side chains, no noticeable difference can be seen within the series (in contrast to the previous work in which 100% of the dimethyloctyloxy side chains of MDMO-PPV were exchanged) [26].

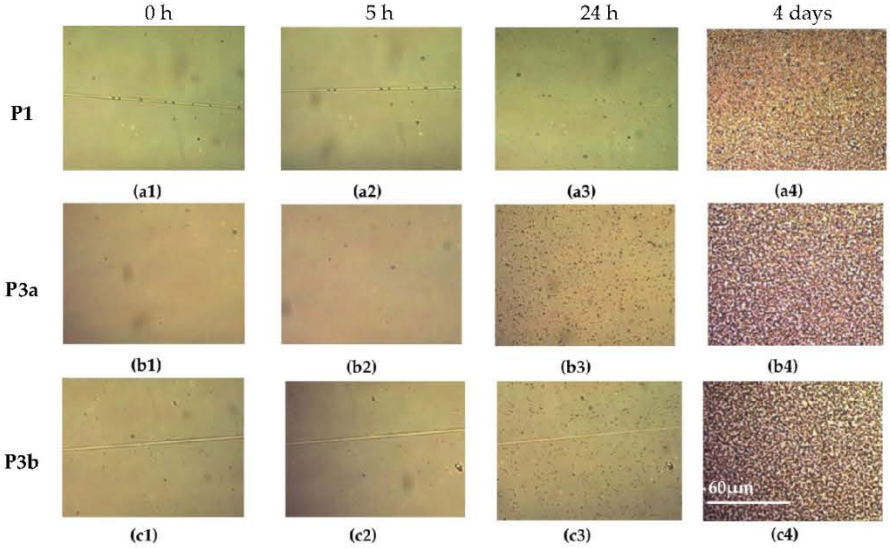

Figure 5. Optical microscope images (50× magnification) of the active layers of RC PSCs based on **P1** (**a**), **P3a** (**b**) and **P3b** (**c**) after exposure to 85 °C for 0 h (1), 5 h (2), 24 h (3) and four days (4).

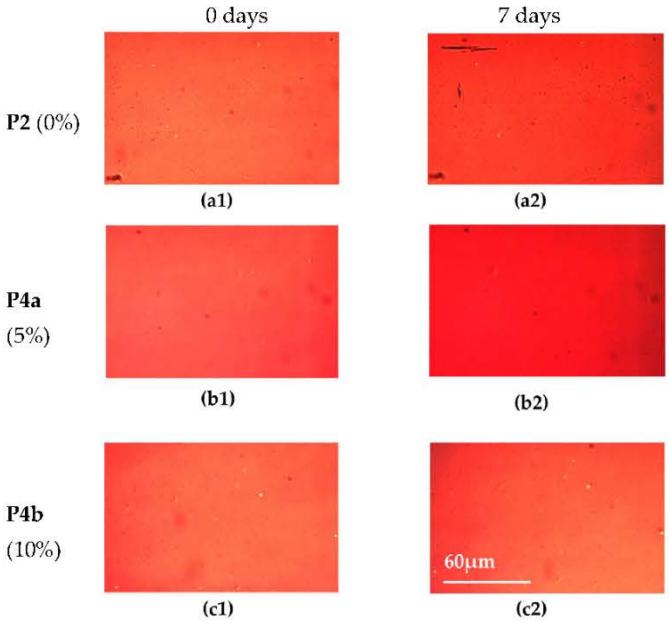

Figure 6. Optical microscope images (with 50× magnification) of the active layers of RC PSCs based on **P2** (**a**), **P4a** (**b**) and **P4b** (**c**) after exposure to 85 °C for zero days (1) and seven days (2).

Summarizing, the ISOS-L-1 lifetime study of the RC devices showed an improved stability for the PSCs based on the BT polymers with EtPh groups within the first 20 days of the study, whereas the devices based on the EtPh-decorated TzTz-based polymers had an improved stability during the last 50 days of the study. The ISOS-D-2 thermal degradation study of the SC devices employing the BT-based polymers with EtPh groups showed a rapid decrease in solar cell performance during the first part of the study, followed by a stable PCE at ~40% of the initial value, whereas the PCE of P1 continued decreasing. For the TzTz-based polymer series, the PSCs based on P2 showed a small loss (up to 5%) of the initial PCE, whereas the decrease of the PSCs based on the EtPh derivatives was higher (up to 25% for **P4a**). The comparison between the two different polymer backbones makes it clear that the exchange of some of the HD side chains by EtPh groups has a notably different influence on the PV parameters of the resulting PSCs. The lifetime measurements showed opposite effects for the two different polymer backbones with different HD/EtPh ratios. In general, the differences are quite remarkable for a maximum of 10% exchanged side chains. Unfortunately, no general trends, clear design rules nor significantly improved stabilities were realized at this stage, in contrast to previous work. Nevertheless, the results do show that side chain engineering is a powerful approach to optimize PSC efficiency, as well as stability, and provide the impetus for further research efforts.

3. Experimental Section

3.1. Material and Methods

Unless stated otherwise, all reagents and solvents were obtained from Sigma-Aldrich (St. Louis, MO, USA) and used without further purification. $PC_{61}BM$ (phenyl-C_{61}-butyric acid methyl ester) (PV-A600) was purchased from Merck Chemicals (RC) and Sollenne (SC), while PEDOT:PSS (poly(3,4-ethylenedioxythiophene):poly(styrenesulfonic acid)) (Orgacon EL-P 5010) was obtained from Agfa (RC) or Heraeus Clevios (SC). Thermally-curable Ag (PV-410) was received from DuPont, and UV-curable adhesive (DELO, Katiobond LP 655) was from DELO. Ca and Al were acquired from Alpha Aesar and Kurt J. Lesker, respectively.

NMR spectra were recorded in $CDCl_3$ on a 500-MHz Bruker spectrometer (Bruker Corporation, Billerica, MA, USA) and a 300-MHz Varian Inova-300 spectrometer (Varian Inc., Palo Alto, CA, USA).

Analytical size exclusion chromatography (SEC) was performed using a Spectra Series P100 (Agilent, Santa Clara, UT, USA) pump equipped with two mixed-B columns (10 µm, 2 cm × 30 cm, Polymer Laboratories, Varian Inc., Palo Alto, CA, USA) and an Agilent 1100 DAD UV detector (Agilent, Santa Clara, UT, USA). Chlorobenzene was used as the eluent at a flow rate of 1.0 mL· min^{-1} and a temperature of 60 °C. Molar masses were determined with UV detection at λ_{max} of the polymer and relative to polystyrene standards.

UV-VIS spectra were recorded on a UV-3600 spectrophotometer (Schimadzu Scientific Instruments, Columbia, PA, USA) or Cary 5000 UV-VIS-NIR spectrophotometer (Agilent Technologies, Victoria, Australia). The spectra were obtained from chloroform (BT-based polymers) or chlorobenzene (TzTz-based polymers) solutions and spin-coated films on glass or quartz slides. Films were spin-coated from solutions with a concentration of ~10 mg/mL. Diluted solutions (~0.01 mg/mL) were used for the solution UV-VIS measurements.

Electrochemical measurements were performed with an Autolab PGSTAT 30 potentiostat/galvanostat (Eco Chemie, Utrecht, The Netherlands) using a three-electrode microcell with a platinum working electrode, a platinum counter electrode and an $Ag/AgNO_3$ reference electrode (silver wire dipped in a solution of 0.01 M $AgNO_3$ and 0.1 M NBu_4PF_6 in anhydrous MeCN). The reference electrode was calibrated against ferrocene/ferrocenium. Anhydrous MeCN containing 0.1 M NBu_4PF_6 was used as the electrolyte and was degassed with argon prior to each measurement. To prevent air from entering the system, the experiments were carried out under a curtain of argon. The polymer samples were dissolved in chloroform. The working electrode was dipped into the polymer solution and dried at room temperature before the measurement. Cyclic voltammograms were recorded at a

scan rate of 100 $mV \cdot s^{-1}$. The HOMO-LUMO energy levels of the products were estimated using the obtained CV data. For the conversion of V to eV, the onset potentials of the first oxidation/reduction peaks were used and referenced to ferrocene/ferrocenium, which has an ionization potential of −4.98 eV *vs.* vacuum. This correction factor is based on a value of 0.31 eV for Fc/Fc^+ *vs.* SCE [40] and a value of 4.68 eV for SCE *vs.* vacuum [41]: $E_{HOMO/LUMO}\,(eV) = -4.98 - E^{Ag/AgNO3}_{onset\ ox/red}\ (V) + -E^{Ag/AgNO3}_{onset\ ox/red}\ (V)$. The accuracy of measuring redox potentials by CV is about 0.01–0.02 V. Reproducibility can be less, because the potentials do depend on concentration and temperature.

Differential scanning calorimetry (DSC) was performed on a Rapid-Heating-Cooling (RHC) instrument (TA Instruments, New Castle, PA, USA) using a liquid nitrogen cooling system and purging with helium (12 $mL \cdot min^{-1}$). The RHC cell is heated by four quartz halogen lamps. The samples (~0.25 mg) were enclosed in dedicated aluminum crucibles and lids.

The photochemical stability of the polymer films prepared by SC (for the UV-VIS measurements) was analyzed using a dedicated setup described before [34].

The PSC area was studied using a light beam induced current (LBIC) technique described in the literature [42].

An Axioskop from Zeiss (Oberkochen, Germany) was used for optical microscopy.

The external quantum efficiency (EQE) measurements were carried out using a system from PV Measurements, Inc. (Boulders, CO, USA) at 10-nm intervals between 300 and 800 nm. A calibrated Si cell was used before the experiment as a reference.

Transmission electron microscopy (TEM) measurements were performed on a FEI Tecnai Spirit (Eindhoven, The Netherlands)using an accelerating voltage of 120 kV. TEM samples were prepared from pristine devices or from the devices utilized in the automated degradation chamber. By washing away the PEDOT:PSS layer with water, freestanding films were obtained.

ISOS-L-1 lifetime tests were performed using a solar simulator with AM 1.5 (1000 W/m^2) conditions. The IV-curve tracing of the PSCs was performed using an automated acquisition setup with a Keithley 2400 SMU (Keithley Instruments, Eindhoven, The Netherlands).

ISOS-D-2 degradation tests were performed on solar cells positioned in an automated degradation chamber in nitrogen atmosphere (glovebox) with a constant temperature of 85 °C. During an initial phase, the *IV*-characteristics were measured every 30 min and at a later stage every hour, using a White 5500 K LED (LED Engin, San José, USA) from which a maximum illumination intensity of 0.53 sun could be obtained.

3.2. Monomer Synthesis

2-Hexyldecylbromide (**1**), 2,5-dibromobenzene-1,4-diol (**2**), 1,4-dibromo-2,5-bis(2-hexyldecyl oxy) benzene ($\mathbf{3_{HD}}$), 2,2′-[2,5-bis(2-hexyldecyloxy)-1,4-phenylene]dithiophene ($\mathbf{4_{HD}}$), {[2,5-bis(2-hexyldecyloxy)-1,4-phenylene]bis(thiophene-5,2-diyl)}bis(trimethylstannane) ($\mathbf{5_{HD}}$) and 2,5-bis(5-bromo-4-hexylthiophene-2-yl)thiazolo[5,4-*d*]thiazole were synthesized according to various literature procedures [14,16,29,31].

3.2.1. {[(2,5-Dibromo-1,4-phenylene)bis(oxy)]bis(ethane-2,1-diyl)}dibenzene ($\mathbf{3_{EtPh}}$)

$\mathbf{3_{EtPh}}$ was synthesized using a similar reaction as reported in the literature [26]. Compound **2** (10.0 g, 37.3 mmol) and potassium tert-butanolate (10.0 g, 89.5 mmol) were dissolved in absolute ethanol (20 mL), and the solution was degassed for 20 min. First, 2-phenylethyl bromide (11.5 mL, 82.1 mmol) was added dropwise to this solution and then sodium iodide (0.31 g, 2.1 mmol) all at once, followed by heating under reflux overnight. After cooling down, the organic solvent was removed, and water was added to dissolve the inorganic salts. The water phase was extracted three times with dichloromethane, followed by drying with $MgSO_4$, filtration and removal of the organic solvent under reduced pressure. In the end, 8.42 g of $\mathbf{3_{EtPh}}$ were obtained as a white powder by recrystallization from ethanol (yield: 47%). ^1H NMR ($CDCl_3$, 500 MHz) δ: 3.13 (*t*, *J* = 7.0 Hz, 4H), 4.83 (*t*, *J* = 7.0 Hz, 4H), 7.06 (s, 2H), 7.32–7.34 (m 10H). ^{13}C NMR ($CDCl_3$, 125 MHz) δ: 35.9, 71.1, 111.3, 118.6, 126.8, 128.6, 129.3, 138.0, 150.1.

3.2.2. 2,2′-(2,5-Diphenethoxy-1,4-phenylene)dithiophene ($\mathbf{4_{EtPh}}$)

A general Stille cross-coupling reaction was performed according to the procedure reported for $\mathbf{4_{HD}}$ [29]. Recrystallization from chloroform and methanol yielded a yellow solid (yield: 74%). ^{1}H NMR ($CDCl_3$, 500 MHz) δ: 3.23 (*t*, *J* = 7.2 Hz, 4H), 4.30 (*t*, *J* = 7.2 Hz, 4H), 7.06 (dd, *J* = 5.1, 3.7 Hz, 2H), 7.22 (s, 2H), 7.32–7.33 (m, 12H), 7.43 (dd, *J* = 3.7, 1.2 Hz, 2H). ^{13}C NMR ($CDCl_3$, 125 MHz) δ: 36.1, 70.8, 113.5, 123.4, 125.7, 125.8, 126.7, 127.0, 128.7, 129.2, 138.3, 139.1, 149.4.

3.2.3. [(2,5-Diphenethoxy-1,4-phenylene)bis(thiophene-5,2-diyl)]bis(trimethylstannane) ($\mathbf{5_{EtPh}}$)

A general method was applied for the distannylation of $\mathbf{4_{EtPh}}$ [16]. A yellow solid was obtained, which was washed three times with methanol (yield: 73%). ^{1}H NMR ($CDCl_3$, 500 MHz) δ: 0.41 (s, 12H), 3.23 (*t*, *J* = 7.2 Hz, 4H), 4.31 (*t*, *J* = 7.2 Hz, 4H), 7.15 (d, *J* = 3.5 Hz, 2H), 7.22 (s, 2H), 7.33–7.34 (m, 10H), 7.56 (d, *J* = 3.5 Hz, 2H). ^{13}C NMR ($CDCl_3$, 125 MHz) δ: −8.1, 36.2, 70.6, 113.6, 123.3, 126.7, 127.1, 128.7, 129.2, 129.3, 135.4, 138.1, 138.4, 145.2, 149.2.

3.3. Polymer Synthesis

3.3.1. General Procedure for the Stille Cross-Coupling Polymerization

4,7-Dibromobenzo[c][1,2,5]thiadiazole or 2,5-bis(5-bromo-4-hexylthiophene-2-yl)thiazolo[5,4-*d*] thiazole were polymerized in a standard procedure with different ratios of $\mathbf{5_{HD}}$ and $\mathbf{5_{EtPh}}$ (0/5%/10%), resulting in polymers **P1**, **P2**, **P3a**, **P3b**, **P4a** and **P4b**. The monomers were dissolved in anhydrous toluene (70 mg monomer/mL). Then, 0.03 equivalents (eq.) of tris(dibenzylideneacetone)dipalladium(0) and 0.09–0.18 eq of tris(o-tolyl)phosphine were added before the mixture was refluxed for at least 20 h. The raw polymer solution was worked up by the precipitation in methanol. The solids were filtrated, and Soxhlet extraction was performed with methanol and n-hexane. The leftover polymers were dissolved in hot CF and precipitated into methanol, filtrated and dried under vacuum. The polymers were characterized by ^{1}H NMR, SEC and UV-VIS.

3.3.2. Poly{[2,5-bis(2-hexyldecyloxy)phenylene]-*alt*-[4,7-di(thiophene-2-yl)benzo[*c*][1,2,5]thiadiazole]} (**P1**)

Blue solid. 96% yield. Mn = 42 kDa, polydispersity index (PDI) = 1.9. ^{1}H NMR ($CDCl_3$, 300 MHz) δ: 0.85–0.97 (m, 12H), 1.25–1.54 (m, 44H), 1.70 (br, 4H), 2.01 (br, 2H), 4.08 (br, 4H), 7.10–8.19 (m, 8H).

3.3.3. Poly{2,2′-[5,5′-(2,5-bis(2-hexyldecyloxy)-1,4-phenylene)dithiophene]-*alt*-[2,5-bis(4-hexyl thiophen-2-yl)thiazolo[5,4-*d*]thiazole]} (**P2**)

Blue solid. 79% yield. Mn = 44 kDa, PDI = 1.9.

3.3.4. BT-Based Statistical Copolymers

P3a: Blue solid. 98% yield. Mn = 39 kDa, PDI = 2.1. ^{1}H NMR ($CDCl_3$, 300 MHz) δ: 0.85–0.97 (m, 12H), 1.25–1.54 (m, 44H), 1.75 (br, 4H), 2.01 (br, 2H), 3.35 (br, 5% 4H), 4.08 (br, 4H), 4.33 (br, 5% 4H), 7.10–8.18 (m, 8H).

P3b: Blue solid. 97% yield. Mn = 43 kDa, PDI = 2.1. ^{1}H NMR ($CDCl_3$, 300 MHz) δ: 0.85–0.97 (m, 12H), 1.25–1.54 (m, 44H), 1.70 (br, 4H), 2.01 (br, 2H), 3.34 (br, 10% 4H), 4.05 (br, 4H), 4.33 (br, 10% 4H), 7.10–8.19 (m, 8H).

3.3.5. TzTz-Based Statistical Copolymers

P4a. Blue solid. 95% yield. Mn = 30 kDa, PDI = 3.1.

P4b. Blue solid. 89% yield. Mn = 78 kDa, PDI = 1.5.

3.4. Device Preparation and Testing

The RC PSCs, with a general structure PET/silver grid/PEDOT-PSS/ZnO/polymer:PC_{61}BM/PEDOT-PSS/silver grid, were produced on Flextrode substrates (PET/Silver grid/PEDOT-PSS/ZnO) [43,44] using a laboratory roll coater at ambient conditions [45,46].

The active layers based on **P1**, **P3a** and **P3b** were coated at 80 °C with a total concentration of 40 mg/mL with a polymer:$PC_{61}BM$ ratio of 1:2 (wt/wt%) using ODCB as the processing solvent [12]. The thickness of the active layer was varied (360, 450 and 540 nm). The photoactive layers based on **P2**, **P4a** and **P4b** were coated from a solvent mixture ODCB:CB (4:1) with a polymer to $PC_{61}BM$ ratio of 1:1.5 (wt %/wt %) and a layer thickness of 400 nm at 80 °C. Approximately five PSCs per coating batch were encapsulated between two glass slides using UV-curable adhesive. The adhesive was activated for a few minutes using a solar simulator. The exact area (~1 cm^2) of all cells was determined using LBIC [29]. The RC PSCs were tested under AM 1.5 (1000 W/m^2) conditions. *IV*-curves were recorded to determine the PV parameters (open-circuit voltage (*Voc*), short-circuit current density (*Jsc*), fill factor (FF) and PCE). For the RC thermal stability tests, two non-encapsulated RC PSCs were heated on a hot plate at 85 °C, and the active layer morphology was probed at regular intervals using an optical microscope.

For the spin-coated devices, the traditional solar cell architecture consisting of glass/ITO/PEDOT:PSS/polymer:$PC_{61}BM$/Ca/Al was employed. Prior to processing, the indium tin oxide (ITO, Kintec, 100 nm, 20 Ohm/sq) -coated glass substrates were thoroughly cleaned using soap, demineralized water, acetone, isopropanol and a UV/O_3 treatment. PEDOT:PSS was subsequently deposited at a thickness of ~30 nm, and annealing at 130 °C for 15 min was applied to remove any residual water. Further processing was carried out in a nitrogen-containing glovebox (O_2/H_2O < 1 ppm), starting with the deposition of the photoactive layer by spin-coating. For **P1**, **P3a** and **P3b**, blend solutions with a total concentration of 40 mg/mL with a polymer:$PC_{61}BM$ ratio of 1:1.5 (wt %/wt %) were prepared using ODCB as the processing solvent. For **P2**, **P4a** and **P4b**, the processing solvent was switched to ODCB:CB (4:1). The polymer:$PC_{61}BM$ ratio was retained at 1:1.5 (wt %/wt %), similar to the BT series, and total concentrations of 40 mg/mL for **P2** and **P4a** and 50 mg/mL for **P4b** were employed. Finally, the devices were finished off by vacuum deposition of the top electrodes, Ca and Al, with layer thicknesses of 30 and 80 nm, respectively. The SC device performance measurements were done using a Newport Class A solar simulator (Model 91195A), calibrated with a silicon solar cell to give an AM 1.5 spectrum.

4. Conclusions

Four new donor-acceptor-type low bandgap copolymers were successfully synthesized by manipulation of the side chains of two copolymers (**P1** and **P2**) based on benzo[*c*][1,2,5]thiadiazole (BT) and thiazolo[5,4-*d*]thiazole (TzTz) acceptor units, respectively. The initial goal of this work was to elevate the T_g of these two polymer series upon exchanging a small amount (5%–10%) of 2-hexyldecyloxy by 2-phenylethoxy (EtPh) side chains and thereby increasing the (thermal) stability of the resulting PSCs, as successfully demonstrated in past research efforts [26–28]. As such, partial exchange (5% or 10%) of the solubilizing 2-hexyldecyloxy side chains on the bis(thienyl) dialkoxybenzene donor parts by EtPh substituents was successfully performed. Unfortunately, due to the (semi)crystalline nature of the BT-based polymers, no distinct T_g could be observed, and given the small amount of functional moieties, the T_g of the TzTz-based polymer series only elevated slightly. The polymers were applied in polymer solar cells (PSCs) via roll-coating (RC) and spin-coating (SC) protocols. The power conversion efficiencies (PCEs) of the small-scale SC devices were higher than those for the RC devices for both polymer series, although the difference was noticeably smaller for the TzTz series. The BT-based RC devices showed a reduction in PCE with increasing amount of EtPh groups (3.05% down to 2.17%), whereas the devices based on TzTz had similar PCE values (~2.7%) for the entire series. In comparison, the SC devices showed a small (average) PCE reduction with increasing amount of EtPh side chains for both polymer groups.

The photochemical degradation rates for the BT-based polymers were similar (~1.6%/h), whereas the rate for the TzTz-based polymers decreased from 2.8 down to 2.1%/h with an increasing amount of EtPh groups. The lifetime study (up to 80 days) of the RC devices under constant sun irradiation demonstrated an improved stability in the first phase of the study (up to 20 days) for the BT-based

PSCs containing a higher amount of EtPh side chains, whereas for the TzTz-based devices, the stability improved in the last stage of the study (after 20 days). Since both polymer series exhibited a similar behavior under illumination (discoloration of the films, comparable residual relative PCEs after degradation, *etc.*), it is likely that these polymers follow a similar degradation pathway in which the alkoxy side chains are cleaved off via a photolysis mechanism [37], thereby making obsolete any influence of the side chain manipulation.

Thermal stability studies (400 h at 85 °C) of the SC devices using the BT-based polymers with manipulated side chains (**P3a** and **P3b**) showed a rapid loss in the first stage, followed by a stable regime (of ~40% of the initial PCE), whereas the PCE of the reference polymer **P1** continued decreasing. PSC devices prepared from the TzTz-based reference polymer **P2** showed a minor loss (5% of the initial PCE) during the thermal stress study, whereas the loss for the PSCs based on the polymers with manipulated side chains (**P4a** and **P4b**) was higher (up to 25% for **P4a**). For the (semicrystalline) BT-based polymer series, phase separation and fullerene crystallization were identified as the main malefactors resulting in a loss in *Jsc*, and hence, PCE. For the TzTz polymers, distinct T_g's well above the degradation temperature (85 °C) were determined, thereby reducing the phase separation tendency upon applying thermal stress. Due to the low EtPh incorporation ratio, only a slight elevation of the T_g could be achieved, limiting the effect on the thermal stability.

In conclusion, the application of altered side chain patterns on different polymer backbones, as a potential route to enhance solar cell stability, demonstrated varying results on PSC performance, as well as on the lifetime and thermal stability. However, no conclusive positive results were achieved at this stage. It hence remains difficult to generalize observations made for specific conjugated polymer derivatives (and the resulting devices) toward the whole range of materials currently investigated in the field. Future work will encompass further studies on different types and ratios of side chains and their effect on different polymer backbones in our pursuit to find a correlation between side chain structure, polymer backbone structure and device stability. Degradation of the organic/metal electrode interfaces will be investigated in more detail, as well.

Supplementary Materials: The following are available online at www.mdpi.com/1996-1944/9/3/181/s1. Figure S1a, ^{1}H NMR spectrum of polymer **P1** in $CDCl_3$, Figure S1b: ^{1}H NMR spectrum of polymer **P3a** (5% EtPh) in $CDCl_3$, Figure S1c: ^{1}H NMR spectrum of polymer **P3b** (10% EtPh) in $CDCl_3$, Figure S2: *IV*-curves for the best PSCs made via RC and SC using the BT- and TzTz-based polymer series, Figure S3: External quantum efficiency (EQE) spectra for the PSCs made via RC using the BT- and TzTz-based polymer series, Figure S4: Rapid-heat cool calorimetry (RHC) thermograms for the BT- and the TzTz-based polymers, Figure S5: Evolution of the UV-VIS absorption profiles during the photochemical stability tests, Figure S6: Average lifetime measurements for the RC devices using the BT- and TzTz-based polymer series showing the normalized *Voc*, *Jsc* and FF trends, Figure S7: Thermal degradation tests of the SC devices using the BT- and TzTz-based polymer series showing the normalized *Voc*, *Jsc* and FF trends, Figure S8: TEM images of the active layers of SC PSCs based on **P1**, **P3a** and **P3b** before and after exposure to 85 °C for 400 h.

Acknowledgments: This work has been supported by the Villum Foundation's Young Investigator Program (second round; project: Materials for Energy Production). The work was partly done during an external research stay of Ilona Heckler at Hasselt University in the group of Wouter Maes. The Hasselt University co-authors acknowledge the support by the IAP (Interuniversity Attraction Poles) 7/05 project FS2 (Functional Supramolecular Systems), granted by the Science Policy Office of the Belgian Federal Government (BELSPO), and the Research Foundation—Flanders (Fonds voor Wetenschappelijk Onderzoek-Vlaanderen) (Projects G.0415.14N, G.0B67.15N and M.ERA-NET Project RADESOL).

Author Contributions: Ilona Heckler synthesized the materials. Ilona Heckler, Maxime Defour, Bruno Van Mele, Morten Madsen and Huguette Penxten analyzed the materials. Ilona Heckler and Jurgen Kesters applied the materials in solar cells and analyzed these. Jan D'Haen performed the TEM measurements and analysis. Ilona Heckler, Jurgen Kesters, Wouter Maes and Eva Bundgaard wrote the paper.

Conflicts of Interest: The authors declare no conflict of interest.

References

1. Günes, S.; Neugebauer, H.; Sariciftci, N.S. Conjugated polymer-based organic solar cells. *Chem. Rev.* **2007**, *107*, 1324–1338. [CrossRef] [PubMed]

2. Brabec, C.J.; Gowrisanker, S.; Halls, J.J.M.; Laird, D.; Jia, S.; Williams, S.P. Polymer-fullerene bulk-heterojunction solar cells. *Adv. Mater.* **2010**, *22*, 3839–3856. [CrossRef] [PubMed]
3. Su, Y.-W.; Lan, S.-C.; Wei, K.-H. Organic photovoltaics. *Mater. Today* **2012**, *15*, 554–562. [CrossRef]
4. Cao, W.; Xue, J. Recent progress in organic photovoltaics: Device architecture and optical design. *Energy Environ. Sci.* **2014**, *7*, 2123–2144. [CrossRef]
5. Mazzio, K.A.; Luscombe, C.K. The future of organic photovoltaics. *Chem. Soc. Rev.* **2015**, *44*, 78–90. [CrossRef] [PubMed]
6. Liu, Y.; Zhao, J.; Li, Z.; Mu, C.; Ma, W.; Hu, H.; Jiang, K.; Lin, H.; Ade, H.; Yan, H. Aggregation and morphology control enables multiple cases of high-efficiency polymer solar cells. *Nat. Commun.* **2014**, *5*. [CrossRef] [PubMed]
7. Subbiah, J.; Purushothaman, B.; Chen, M.; Qin, T.; Gao, M.; Vak, D.; Scholes, F.H.; Chen, X.; Watkins, S.E.; Wilson, G.J.; *et al.* Organic solar cells using a high-molecular-weight benzodithiophene-benzothiadiazole copolymer with an efficiency of 9.4%. *Adv. Mater.* **2015**, *27*, 702–705. [CrossRef] [PubMed]
8. Yue, W.; Ashraf, R.S.; Nielsen, C.B.; Collado-Fregoso, E.; Niazi, M.R.; Yousaf, S.A.; Kirkus, M.; Chen, H.-Y.; Amassian, A.; Durrant, J.R.; *et al.* A Thieno[3,2-b][1]benzothiophene isoindigo building block for additive- and annealing-free high-performance polymer solar cells. *Adv. Mater.* **2015**, *27*, 4702–4707. [CrossRef] [PubMed]
9. Liao, S.-H.; Jhuo, H.-J.; Cheng, Y.-S.; Chen, S.-A. Fullerene derivative-doped zinc oxide nanofilm as the cathode of inverted polymer solar cells with low-bandgap polymer (PTB7-Th) for high performance. *Adv. Mater.* **2013**, *25*, 4766–4771. [CrossRef] [PubMed]
10. Brabec, C.J. Organic photovoltaics: Technology and market. *Sol. Energy Mater. Sol. Cells* **2004**, *83*, 273–292. [CrossRef]
11. Burgues-Ceballos, I.; Stella, M.; Lacharmoise, P.; Martinez-Ferrero, E. Towards industrialization of polymer solar cells: Material processing for upscaling. *J. Mater. Chem. A* **2014**, *2*, 17711–17722. [CrossRef]
12. Bundgaard, E.; Livi, F.; Hagemann, O.; Carlé, J.E.; Helgesen, M.; Heckler, I.M.; Zawacka, N.K.; Angmo, D.; Larsen-Olsen, T.T.; dos Reis Benatto, G.A.; *et al.* Matrix organization and merit factor evaluation as a method to address the challenge of finding a polymer material for roll coated polymer solar cells. *Adv. Energy Mater.* **2015**, *5*, 1402186. [CrossRef]
13. He, Z.; Xiao, B.; Liu, F.; Wu, H.; Yang, Y.; Xiao, S.; Wang, C.; Russell, T.P.; Cao, Y. Single-junction polymer solar cells with high efficiency and photovoltage. *Nat. Photonics* **2015**, *9*, 174–179. [CrossRef]
14. Carlé, J.E.; Jørgensen, M.; Krebs, F.C. Polymers for organic photovoltaics based on 1,5-*bis*(2-hexyldecyloxy)-naphthalene, thiophene, and benzothiadiazole. *J. Photonics Energy* **2011**, *1*. [CrossRef]
15. Helgesen, M.; Carlé, J.E.; dos Reis Benatto, G.A.; Søndergaard, R.R.; Jørgensen, M.; Bundgaard, E.; Krebs, F.C. Making ends meet: Flow synthesis as the answer to reproducible high-performance conjugated polymers on the scale that roll-to-roll processing demands. *Adv. Energy Mater.* **2015**, *5*. [CrossRef]
16. Livi, F.; Zawacka, N.K.; Angmo, D.; Jørgensen, M.; Krebs, F.C.; Bundgaard, E. Influence of side chain position on the electrical properties of organic solar cells based on dithienylbenzothiadiazole- alt -phenylene conjugated polymers. *Macromolecules* **2015**, *48*, 3481–3492. [CrossRef]
17. Yang, L.; Zhou, H.; You, W. Quantitatively analyzing the influence of side chains on photovoltaic properties of polymer-fullerene solar cells. *J. Phys. Chem. C* **2010**, *114*, 16793–16800. [CrossRef]
18. Nguyen, T.L.; Song, S.; Ko, S.; Choi, H.; Jeong, J.; Kim, T.; Hwang, S.; Kim, J.Y.; Woo, H.Y. Benzodithiophene-thiophene-based photovoltaic polymers with different side-chains. *J. Polym. Sci. A Polym. Chem.* **2015**, *53*, 854–862. [CrossRef]
19. Cardinaletti, I.; Kesters, J.; Bertho, S.; Conings, B.; Piersimoni, F.; D'Haen, J.; Lutsen, L.; Nesladek, M.; van Mele, B.; van Assche, G.; *et al.* Toward bulk heterojunction polymer solar cells with thermally stable active layer morphology. *J. Photonics Energy* **2014**, *4*. [CrossRef]
20. Lindqvist, C.; Bergqvist, J.; Feng, C.-C.; Gustafsson, S.; Bäcke, O.; Treat, N.D.; Bounioux, C.; Henriksson, P.; Kroon, R.; Wang, E.; *et al.* Fullerene nucleating agents: a route towards thermally stable photovoltaic blends. *Adv. Energy Mater.* **2014**, *4*. [CrossRef]
21. Lindqvist, C.; Bergqvist, J.; Bäcke, O.; Gustafsson, S.; Wang, E.; Olsson, E.; Inganäs, O.; Andersson, M.R.; Müller, C. Fullerene mixtures enhance the thermal stability of a non-crystalline polymer solar cell blend. *Appl. Phys. Lett.* **2014**, *104*. [CrossRef]

22. Rumer, J.W.; McCulloch, I. Organic photovoltaics: Crosslinking for optimal morphology and stability. *Mater. Today* **2015**, *18*, 425–435. [CrossRef]
23. Gevorgyan, S.A.; Krebs, F.C. Bulk heterojunctions based on native polythiophene. *Chem. Mater.* **2008**, *20*, 4386–4390. [CrossRef]
24. Bundgaard, E.; Hagemann, O.; Bjerring, M.; Nielsen, N.C.; Andreasen, J.W.; Andreasen, B.; Krebs, F.C. Removal of solubilizing side chains at low temperature: A new route to native poly(thiophene). *Macromolecules* **2012**, *45*, 3644–3646. [CrossRef]
25. Verstappen, P.; Kesters, J.; D'Olieslaeger, L.; Drijkoningen, J.; Cardinaletti, I.; Vangerven, T.; Bruijnaers, B.J.; Willems, R.E.M.; D'Haen, J.; Manca, J.V.; *et al.* Simultaneous Enhancement of Solar Cell Efficiency and Stability by Reducing the Side Chain Density on Fluorinated PCPDTQx Copolymers. *Macromolecules* **2015**, *48*, 3873–3882. [CrossRef]
26. Vandenbergh, J.; Conings, B.; Bertho, S.; Kesters, J.; Spoltore, D.; Esiner, S.; Zhao, J.; van Assche, G.; Wienk, M.M.; Maes, W.; *et al.* Thermal stability of poly[2-methoxy-5-(2′-phenylethoxy)-1,4-phenylenevinylene] (MPE-PPV): Fullerene bulk heterojunction solar cells. *Macromolecules* **2011**, *44*, 8470–8478. [CrossRef]
27. Kesters, J.; Kudret, S.; Bertho, S.; van den Brande, N.; Defour, M.; van Mele, B.; Penxten, H.; Lutsen, L.; Manca, J.; Vanderzande, D.; *et al.* Enhanced intrinsic stability of the bulk heterojunction active layer blend of polymer solar cells by varying the polymer side chain pattern. *Org. Electron.* **2014**, *15*, 549–562. [CrossRef]
28. Kesters, J.; Verstappen, P.; Raymakers, J.; Vanormelingen, W.; Drijkoningen, J.; D'Haen, J.; Manca, J.; Lutsen, L.; Vanderzande, D.; Maes, W. Enhanced organic solar cell stability by polymer (PCPDTBT) side chain functionalization. *Chem. Mater.* **2015**, *27*, 1332–1341. [CrossRef]
29. Carlé, J.E.; Andreasen, J.W.; Jørgensen, M.; Krebs, F.C. Low band gap polymers based on 1,4-dialkoxybenzene, thiophene, bithiophene donors and the benzothiadiazole acceptor. *Sol. Energy Mater. Sol. Cells* **2010**, *94*, 774–780. [CrossRef]
30. Campo, B.J.; Bevk, D.; Kesters, J.; Gilot, J.; Bolink, H.J.; Zhao, J.; Bolsée, J.-C.; Oosterbaan, W.D.; Bertho, S.; D'Haen, J.; *et al.* Ester-functionalized poly(3-alkylthiophene) copolymers: Synthesis, physicochemical characterization and performance in bulk heterojunction organic solar cells. *Org. Electron.* **2013**, *14*, 523–534. [CrossRef]
31. Helgesen, M.; Carlé, J.E.; Krebs, F.C. Slot-die coating of a high performance copolymer in a readily scalable roll process for polymer solar cells. *Adv. Energy Mater.* **2013**, *3*, 1664–1669. [CrossRef]
32. Danley, R.L.; Caulfield, P.A.; Aubuchon, S.R. A rapid-scanning differential scanning calorimeter. *Am. Lab.* **2008**, *40*, 9–11.
33. Ghoos, T.; van Den Brande, N.; Defour, M.; Brassinne, J.; Fustin, C.A.; Gohy, J.F.; Hoeppener, S.; Schubert, U.S.; Vanormelingen, W.; Lutsen, L.; *et al.* Amphiphilic N-methylimidazole-functionalized diblock copolythiophenes. *Eur. Polym. J.* **2014**, *53*, 206–214. [CrossRef]
34. Tromholt, T.; Madsen, M.V.; Carlé, J.E.; Helgesen, M.; Krebs, F.C. Photochemical stability of conjugated polymers, electron acceptors and blends for polymer solar cells resolved in terms of film thickness and absorbance. *J. Mater. Chem.* **2012**, *22*, 7592–7601. [CrossRef]
35. Reese, M.O.; Gevorgyan, S.A.; Jørgensen, M.; Bundgaard, E.; Kurtz, S.R.; Ginley, D.S.; Olson, D.C.; Lloyd, M.T.; Morvillo, P.; Katz, E.A.; *et al.* Consensus stability testing protocols for organic photovoltaic materials and devices. *Sol. Energy Mater. Sol. Cells* **2011**, *95*, 1253–1267. [CrossRef]
36. Jeong, J.; Seo, J.; Nam, S.; Han, H.; Kim, H.; Anthopoulos, T.D.; Bradley, D.D.C.; Kim, Y. Significant stability enhancement in high-efficiency Polymer:Fullerene bulk heterojunction solar cells by blocking ultraviolet photons from solar light. *Adv. Sci.* **2015**. [CrossRef]
37. Lilliedal, M.R.; Medford, A.J.; Madsen, M.V.; Norrman, K.; Krebs, F.C. The effect of post-processing treatments on inflection points in currentvoltage curves of roll-to-roll processed polymer photovoltaics. *Sol. Energy Mater. Sol. Cells* **2010**, *94*, 2018–2031. [CrossRef]
38. Rivaton, A.; Chambon, S.; Manceau, M.; Gardette, J.L.; Lemaître, N.; Guillerez, S. Light-induced degradation of the active layer of polymer-based solar cells. *Polym. Degrad. Stab.* **2010**, *95*, 278–284. [CrossRef]
39. Bertho, S.; Haeldermans, I.; Swinnen, A.; Moons, W.; Martens, T.; Lutsen, L.; Vanderzande, D.; Manca, J.; Senes, A.; Bonfiglio, A. Influence of thermal ageing on the stability of polymer bulk heterojunction solar cells. *Sol. Energy Mater. Sol. Cells* **2007**, *91*, 385–389. [CrossRef]
40. Bard, A.; Faulkner, L. *Electrochemical Methods: Fundamentals and Applications*, 2nd ed.; Wiley: New York, NY, USA, 2012.

41. Trasatti, S. The absolute electrode potential: An explanatory note. *Pure Appl. Chem.* **1986**, *58*, 955–966. [CrossRef]
42. Krebs, F.C.; Søndergaard, R.; Jørgensen, M. Printed metal back electrodes for R2R fabricated polymer solar cells studied using the LBIC technique. *Sol. Energy Mater. Sol. Cells* **2011**, *95*, 1348–1353. [CrossRef]
43. Hösel, M.; Søndergaard, R.R.; Jørgensen, M.; Krebs, F.C. Fast Inline roll-to-roll printing for Indium-Tin-Oxide-free polymer solar cells using automatic registration. *Energy Technol.* **2013**, *1*, 102–107. [CrossRef]
44. Larsen-Olsen, T.T.; Søndergaard, R.R.; Norrman, K.; Jørgensen, M.; Krebs, F.C. All printed transparent electrodes through an electrical switching mechanism: A convincing alternative to indium-tin-oxide, silver and vacuum. *Energy Environ. Sci.* **2012**, *5*, 9467–9471. [CrossRef]
45. Dam, H.F.; Krebs, F.C. Simple roll coater with variable coating and temperature control for printed polymer solar cells. *Sol. Energy Mater. Sol. Cells* **2012**, *97*, 191–196. [CrossRef]
46. Carlé, J.E.; Andersen, T.R.; Helgesen, M.; Bundgaard, E.; Jørgensen, M.; Krebs, F.C. A laboratory scale approach to polymer solar cells using one coating/printing machine, flexible substrates, no ITO, no vacuum and no spincoating. *Sol. Energy Mater. Sol. Cells* **2013**, *108*, 126–128. [CrossRef]

Journal of Materials Chemistry A

PAPER

View Article Online
View Journal | View Issue

Cite this: *J. Mater. Chem. A*, 2016, **4**, 16677

A stability study of polymer solar cells using conjugated polymers with different donor or acceptor side chain patterns†

Ilona M. Heckler,[a] Jurgen Kesters,[b] Maxime Defour,[c] Huguette Penxten,[b] Bruno Van Mele,[c] Wouter Maes[b] and Eva Bundgaard*[a]

Received 23rd August 2016
Accepted 25th September 2016

DOI: 10.1039/c6ta07244e

www.rsc.org/MaterialsA

Improvement of the power conversion efficiency and long term stability remains to be of crucial importance for the further development of polymer solar cells (PSCs). Herein, a donor–acceptor copolymer based on 4,8-di(thiophene-2′-yl)benzo[1,2-*b*:4,5-*b*′]dithiophene (DTBDT) and 4,7-di(thiophene-2′-yl)benzo[*c*][1,2,5]thiadiazole (DTBT), specifically selected because of its suitability for roll-coating in the ambient environment, is investigated in terms of operational stability *via* partial exchange (5 or 10%) of the alkyl side chain on either the donor or the acceptor monomer with a 2-hydroxyethyl or 2-phenylethyl group. It is shown that the exchange of the hexyl chain on the DTBT moiety has a negative impact on the stability of the polymer as well as on the performance of the resulting PSCs. On the other hand, partial exchange of the 2-hexyldecyl side chain of the BDT unit by a 2-hydroxyethyl group results in an improved photochemical stability of the polymer film and a higher efficiency of 5.6% for the spin-coated PSC. The stability of roll-coated devices also slightly increases with the incorporation of 10% of either the 2-hydroxyethyl or 2-phenylethyl side chain.

1. Introduction

Advanced conjugated polymers have been extensively studied for polymer solar cells (PSCs) over the past two decades, illustrating the remarkable potential of this technology for large scale photovoltaic applications by taking into account their specific advantages (printable, flexible, light weight, and so on).[1–5] Most research efforts have focused on improving the power conversion efficiency (PCE) and currently reported record values exceed 11%.[6] However, the scalability, while retaining the high efficiency, of these small active area (*e.g.* 5.9 mm^2) PSCs remains to be a challenging task.[7]

The common method for preparing high efficiency PSCs is bulk heterojunction (BHJ), in which most often a fullerene derivative (like [6,6]-phenyl-C_{61}-butyric acid methyl ester ($PC_{61}BM$)) functions as an electron acceptor and an organic light absorbing low bandgap conjugated polymer acts as an electron donor in a blended, interpenetrating solid-state mixture forming the photoactive layer (PAL).[8] The specific structure of the organic photoactive layer, however, has some implications for the stability of the resulting PSCs. For example, the polymer (alkyl) side chains, present to allow processing from solution, can induce multiple degradation pathways, triggered by thermal stress, light exposure and/or oxygen.[9–13] Moreover, phase separation of the electron donor and acceptor component within the PAL has been identified as one of the main problems in BHJ PSCs. To resolve this issue, efforts have been made to 'freeze' the morphology of the PAL, *e.g.* by cross-linking the polymers or fullerene derivatives,[14] or the implementation of additives to improve the blend stability.[15] Alternatively, side chain removal strategies on the deposited PAL films have been reported.[16–20] Krebs *et al.* reported the removal of alkyl ester side chains upon applying a thermal treatment at 300 °C, resulting in an insoluble polymer and a more stable PAL.[16] However, at the required temperature, this approach can hardly be translated to the roll-coating (RC) production of solar cells on plastic foils.[17] Another strategy employs chemical diversification of the side chains of the light absorbing polymers. Such a diversification was already used in a study by Friend *et al.*[21] in 1999 resulting in an enhanced photo- and thermal stability, respectively, of a phenyl substituted poly (*p*-phenylene vinylene) (PPV). This concept was then adopted in this study to improve the photo- and thermal stability. Maes *et al.* showed that a reduction of the side chain density in a polymer based on 4*H*-cyclopenta[2,1-*b*:3,4-*b*′]dithiophene (CPDT) and quinoxaline leads to a PSC with increased PCE as

[a]*Technical University of Denmark, Department of Energy Conversion and Storage, Frederiksborgvej 399, 4000 Roskilde, Denmark. E-mail: evbu@dtu.dk*

[b]*Hasselt University, Institute for Materials Research (IMO-IMOMEC), Design & Synthesis of Organic Semiconductors (DSOS), Agoralaan 1 – Building D, 3590 Diepenbeek, Belgium. E-mail: wouter.maes@uhasselt.be*

[c]*Physical Chemistry and Polymer Science (FYSC), Vrije Universiteit Brussels (VUB), Pleinlaan 2, 1050 Brussels, Belgium. E-mail: bvmele@vub.ac.be*

† Electronic supplementary information (ESI) available: Additional information of the synthesized compounds, polymer characterization, device preparation and characterization, and stability testing. See DOI: 10.1039/c6ta07244e

well as enhanced device stability when exposed to thermal stress.[22] Functionalization of the polymer side chains can also be used to engineer the glass transition temperature (T_g) of a polymer. This approach was used by the same group on a PPV derivative by incorporation of a 2-phenylethyl (EtPh) side chain to stiffen the structure.[23] The concept of side chain functionalization was also applied successfully on polythiophenes[24–27] and advanced donor–acceptor conjugated polymers.[28] The incorporation of alcohol or ester groups as part of the side chains generally resulted in an enhanced thermal stability. A previous study by Peng *et al.* shows that engineering of the side chains (branching and dimensionality) tuned the thermal stability.[29] Furthermore, Tierney *et al.*[30] reported on the impact of different types of side chains (linear alkyl, alkoxy, thienyl-alkyl) on the (photochemical) stability and $PC_{61}BM$ diffusion of benzo[1,2-*b*:4,5-*b*′]dithiophene (BDT) and diketopyrrolopyrrole based PSCs. They observed that the solar cell stability decreases in the order of linear alkyl > no > alkoxy > thienyl-alkyl side chains on the BDT unit, directly linked to an elevated rate of $PC_{61}BM$ diffusion due to the dependence on the rotational freedom and steric hindrance induced by the type of side chain.[30] On the level of fullerenes, the $PC_{61}BM$ dimerization, involving a [2 + 2] photo-cycloaddition during light exposure in the absence of oxygen, has been reported as a stabilizing mechanism for PSCs.[31–33] For different types of fullerenes (C_{60}, $PC_{61}BM$ and bis-$PC_{61}BM$), it was shown that with an increasing amount of ester groups, the stability increases due to an increased steric hindrance.[31] In a previous work,[34] we investigated the introduction of the 2-phenylethyl group on advanced low bandgap polymers. Introduction of this side chain on two different backbones (based on benzo[*c*][1,2,5]thiadiazole (BT) and thiazolo[5,4-*d*]thiazole (TzTz), respectively), using different amounts of EtPh (5 or 10%, respectively), did not lead to a clear enhancement of the stability and thus improvement of the lifetime of the final PSCs.[34] In the present study, we focus on the influence of the position of the functional side chain, *i.e.* either on the donor or the acceptor part of the polymer, on the performance and stability of PSCs based on the donor–acceptor copolymer **P1** (Fig. 1). This backbone was chosen as a lead candidate (with 2-ethylhexyl and dodecyl side chains (**P1-(EH)**, Fig. 1)[35]) from a large screening of polymers suitable for PSC production *via* the roll-coating technique. As the choice of the position, nature and length of the side chains has an important influence on the performance of the PSCs,[36] **P1**, with 2-hexyldecyl and hexyl side chains (Fig. 1), was chosen as the starting point for this study, with efficiencies around 3.7% for RC devices.[37]

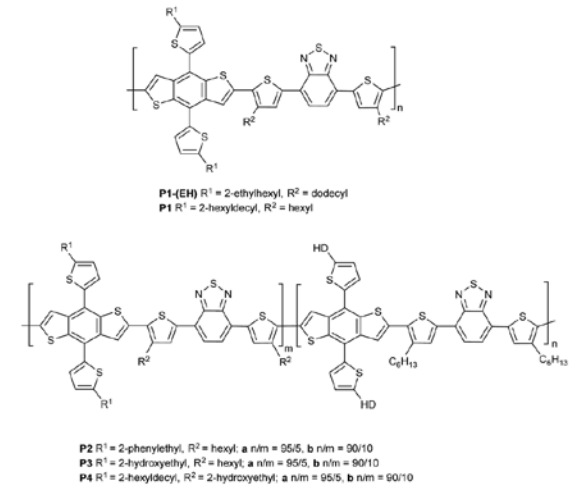

Fig. 1 Chemical structure of polymer **P1** suitable for roll-coating and the investigated polymers **P2a**, **P2b**, **P3a**, **P3b**, **P4a** and **P4b**.

2. Experimental

2.1 Materials

All reagents, chemicals and solvents were obtained from Sigma-Aldrich and used as received. $PC_{61}BM$ (PV-A600) was purchased from Merck Chemicals (RC) and Solenne (spin-coating (SC)), $PC_{71}BM$ from Solenne, poly(3,4-ethylenedioxythiophene):polystyrene sulfonate (PEDOT:PSS) (Orgacon EL-P 5010) from Agfa (RC) and Heraeus Clevios (SC), thermally curable Ag (PV-410) from DuPont, and UV-curable adhesive (Katiobond LP 655) from DELO. Ca and Al were acquired from Alpha Aesar and K. J. Lesker, respectively.

2.2 Monomer synthesis

The synthetic routes for the preparation of the monomers are shown in Scheme 1 and S1.† Triisopropyl[2-(thiophen-2′-yl)ethoxy]silane (**1c**), **BDT-HD** (>99% purity), triisopropyl[2-(thiophen-3′-yl)ethoxy]silane (**3b**) and **BT-hex** (>99% purity) were synthesized according to literature procedures with minor modifications.[38–42]

Preparative (recycling) size exclusion chromatography (recycling SEC) was performed on a JAI LC-9110 NEXT system equipped with JAIGEL 1H, 2H and 3H columns (eluent $CHCl_3$, flow rate 3.5 mL min^{-1}).

^1H and ^{13}C NMR spectra (see ESI†) were recorded in $CDCl_3$ or DMSO-d_6 on a 500 MHz (Bruker) or a 400 MHz (Varian Inova 400) spectrometer.

High-performance liquid chromatography equipped with an evaporative light scattering detector (HPLC/ELSD) was measured to detect the purity of the final monomers prior to polymerization. The analysis was carried out on an e2695 water Alliance system equipped with a 2998 PDA detector and an Agilent Technologies 1260 infinity ELSD. The column was a symmetry C18 3.5 μm, 4.6 mm × 75 mm, solvent A was 0.1% TFA in water and solvent B was 0.1% TFA in acetonitrile; the flow rate was 1 mL min^{-1}.

2-(2′-Phenylethyl)thiophene (1b). Synthesis according to the procedure for **1a**.[43] Thiophene (1.6 mL, 20 mmol) was dissolved in dry THF (20 mL). *n*-Butyl lithium (*n*-BuLi) (6.8 mL, 2.5 M in hexane, 17 mmol) was added dropwise at 0 °C. At room temperature, 2-phenylethyl bromide (2.9 mL, 21 mmol) was added in one go. The reaction mixture was then heated under reflux for 4 h. The crude product was purified by column

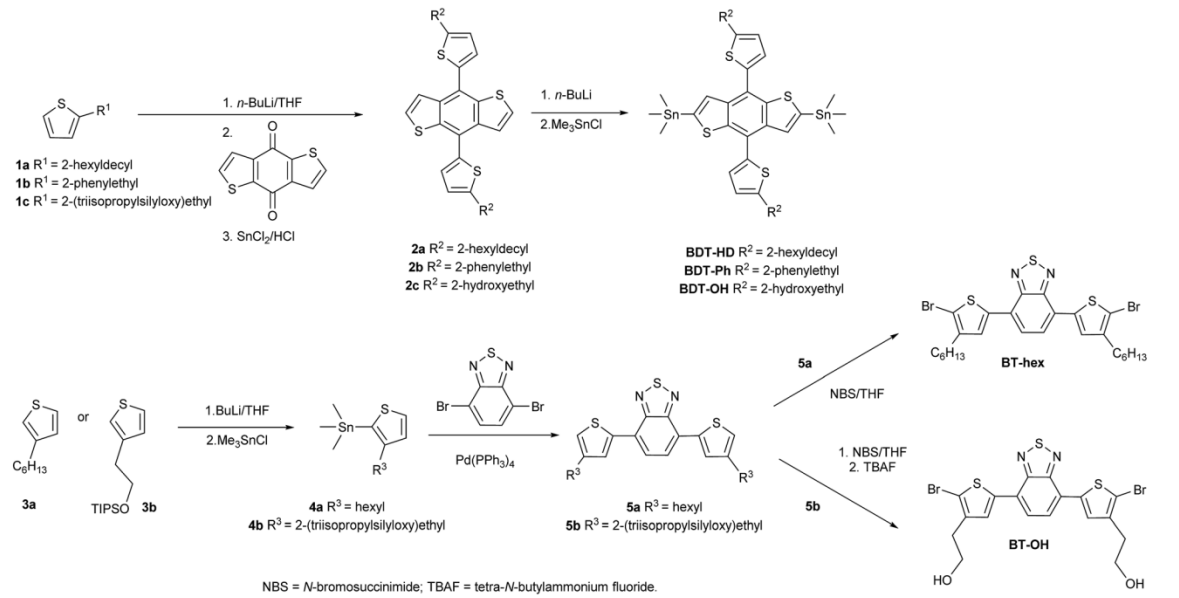

Scheme 1 Synthetic routes yielding the BDT and BT based donor and acceptor monomers.

chromatography (silica gel) using hexane as an eluent, affording a transparent liquid (1.2 g, 30%). ^{1}H NMR ($CDCl_3$, 500 MHz) δ (ppm): 3.00 (t, J = 8.0 Hz, 2H), 3.15 (t, J = 8.0 Hz, 2H), 6.78 (dd, J = 3.4 Hz, 1.1 Hz, 1H), 6.92 (dd, J = 5.1 Hz, 3.4 Hz, 1H), 7.10 (dd, J = 5.1 Hz, 1.1 Hz, 1H), 7.20–7.32 (m, 5H). ^{13}C NMR ($CDCl_3$, 126 MHz) δ (ppm): 31.9, 38.1, 123.1, 124.4, 126.2, 126.7, 128.3, 128.4, 141.2, 144.5.

General procedure for the synthesis of the benzodithiophene based compounds (2b, 2c).[39] *n*-BuLi (1.2 mL, 3.0 mmol, 2.5 M in hexane) was added dropwise at 0 °C to a solution of **1b** (565 mg, 3.0 mmol) or **1c** (797 mg, 2.8 mmol) in dry THF (20 mL). After the change from a colourless to a darker solution, the mixture was heated for 2 h at 50 °C before adding benzo[1,2-*b*:4,5-*b*′]dithiophene-4,8-dione (220 mg, 1.0 mmol), and the mixture was again heated for another hour. Then, $SnCl_2$ (1.5 g, 8.0 mmol) in 12 wt% hydrochloric acid (9 mL) was added and the mixture was stirred for 1 h at room temperature before it was finally added to ice water.

4,8-Bis[5′-(2″-phenylethyl)thiophene-2′-yl]benzo[1,2-*b*:4,5-*b*′] dithiophene (2b). The water phase was extracted three times with chloroform and the resulting organic phase was dried over $MgSO_4$. Filtration and removal of the solvent yielded the crude product. Purification by column chromatography (silica gel) using a gradient of petroleum ether and chloroform afforded a yellow solid (249 mg, 44%). ^{1}H NMR ($CDCl_3$, 500 MHz) δ (ppm): 3.11 (t, J = 8.0 Hz, 4H), 3.25 (t, J = 8.0 Hz, 4H), 6.91 (d, J = 3.4 Hz, 2H), 7.23–7.35 (m, 10H), 7.29 (d, J = 3.4 Hz, 2H), 7.46 (d, J = 5.7 Hz, 2H), 7.63 (d, J = 5.7 Hz, 2H). ^{13}C NMR ($CDCl_3$, 126 MHz) δ (ppm): 32.4, 38.1, 123.5, 124.2, 124.9, 126.4, 127.7, 128.0, 128.6, 128.7, 136.7, 137.5, 139.2, 141.2, 145.9.

2,2′-(Benzo[1,2-*b*:4,5-*b*′]dithiophene-4,8-diyl)bis(thiophene-5,2-diyl)bis(ethan-1-ol) (2c). The water phase was extracted three times with diethyl ether and the combined organic fractions were dried over $MgSO_4$, filtered and removal of the solvent yielded the crude product. Purification by column chromatography (silica gel) using an eluent mixture of ethyl acetate and hexane (1/1) revealed a product mixture (the desired alcohol and the methyl ester analogue).[44] This product mixture was again dissolved in THF (20 mL), NaOH solution (2.5 M in H_2O; 10 mL) was added and the mixture was stirred overnight. The organic phase was washed twice with water, dried over $MgSO_4$ and the solvent was removed under reduced pressure. Purification by column chromatography (silica gel) using an eluent mixture of ethyl acetate and hexane (4/1) afforded a brown solid of the pure compound **2c** (204 mg, 46%). ^{1}H NMR (DMSO-d_6, 400 MHz) δ (ppm): 3.05 (t, J = 6.5 Hz, 4H), 3.73 (td, J = 6.4 Hz, J = 3.7 Hz, 4H), 4.92 (t, J = 3.7 Hz, 2H), 7.08 (d, J = 3.5 Hz, 2H), 7.38 (d, J = 3.5 Hz, 2H), 7.60 (d, J = 5.7 Hz, 2H), 7.85 (d, J = 5.7 Hz, 2H). ^{13}C NMR (DMSO-d_6, 101 MHz) δ (ppm): 33.3, 61.7, 122.9, 123.4, 125.9, 128.1, 129.4, 135.9, 136.4, 138.2, 143.6.

General procedure for the stannylation reactions.[39,42] To a solution of the non-stannylated compound (**2b, c** or **3b**) in dry THF, *n*-BuLi (2.5 M in hexane) was added at −78 °C and the solution was stirred for 1 h. The temperature was slowly increased to room temperature and the solution was stirred for 20 min to 1 h. Afterwards, the reaction mixture was cooled down to −78 °C again and Me_3SnCl (1.0 M in hexane) was added. After the removal of the cooling bath, the mixture was stirred for another 2 h. Water was added, the phases were separated and the organic phase was washed multiple times with water, dried over $MgSO_4$, filtered, and the solvent was removed under reduced pressure.

{4,8-Bis[5′-(2″-phenylethyl)thiophen-2′-yl]benzo[1,2-*b*:4,5-*b*′] dithiophene-2,6-diyl}bis(trimethylstannane) (BDT-Ph).

Compound **2b** (225 mg, 0.40 mmol) in THF (10 mL), *n*-BuLi in hexane (0.64 mL, 1.60 mmol) and Me_3SnCl in hexane (2.0 mL, 2.0 mmol). Recrystallization from hexane yielded dark yellow crystals (193 mg, 54%, >99% purity). ^{1}H NMR ($CDCl_3$, 500 MHz) δ (ppm): 0.43 (s, 18H), 3.13 (t, J = 8.0 Hz, 4H), 3.27 (t, J = 8.0 Hz, 4H), 6.93 (d, J = 3.5 Hz, 2H), 7.23–7.35 (m, 10H), 7.31 (d, J = 3.5 Hz, 2H), 7.67 (s, 2H). ^{13}C NMR ($CDCl_3$, 126 MHz) δ (ppm): −8.1, 32.4, 38.1, 122.5, 124.9, 126.3, 127.8, 128.6, 128.7, 131.2, 137.5, 138.3, 141.3, 142.6, 143.5, 145.5.

2,2′-{[2,6-bis(trimethylstannyl)benzo[1,2-*b*:4,5-*b*′]dithiophene-4,8-diyl]bis(thiophene-5,2-diyl)}bis(ethan-1-ol) (BDT-OH). Compound **2c** (199 mg, 0.45 mmol) in THF (15 mL), *n*-BuLi in hexane (1.26 mL, 3.15 mmol) and Me_3SnCl in hexane (3.6 mL, 3.6 mmol). A green solid precipitated after the addition of *n*-BuLi, so the temperature was increased right away and the mixture was stirred for 3 h. Purification of the crude product was done by recycling SEC, yielding pure **BDT-OH** (95 mg, 27%, >99% purity). ^{1}H NMR (DMSO-d_6, 400 MHz) δ (ppm): 0.40 (s, 18H), 1.70 (t, J = 6.1 Hz, 2H), 3.21 (t, J = 6.1 Hz, 4H), 3.99 (q, J = 6.1 Hz, 4H), 7.04 (d, J = 3.5 Hz, 2H), 7.36 (d, J = 3.5 Hz, 2H), 7.66 (s, 2H). ^{13}C NMR (DMSO-d_6, 75 MHz) δ (ppm): −8.1, 33.8, 63.5, 122.3, 126.1, 128.2, 131.1, 137.5, 139.2, 141.8, 142.8, 143.4.

Triisopropyl{2-[2′-(trimethylstannyl)thiophen-3′-yl]ethoxy}silane (4b). Compound **3b** (1.0 g, 3.5 mmol) in THF (20 mL), *n*-BuLi in hexane (1.4 mL, 3.5 mmol) and Me_3SnCl in hexane (4.6 mL, 4.6 mmol): 1.27 g of a light brown liquid with impurities (stannylation in 5-position) was obtained (2.8 mmol, 80%). ^{1}H NMR ($CDCl_3$, 400 MHz) δ (ppm): 0.34 (s, 9H), 1.03–1.05 (m, 21H), 2.91 (t, J = 7.0 Hz, 2H), 3.89 (t, J = 7.0 Hz, 2H), 7.07 (s, 1H), 7.28 (s, 1H).

Stille cross-coupling reaction yielding compound 5b.[42] Compound **4b** (402.6 mg, 0.90 mmol), 4,7-dibromobenzo[*c*][1,2,5]thiadiazole (88.2 mg, 0.30 mmol) and tetrakis(triphenylphosphine)palladium(0) (17.3 mg, 0.03 mmol) were dissolved in dry toluene (5 mL) and dry DMF (0.5 mL). The reaction mixture was heated at reflux under an inert atmosphere overnight. The crude product was filtered over silica gel. After removing the solvent, a red solid was obtained (202.5 mg, 96%). ^{1}H NMR ($CDCl_3$, 400 MHz) δ (ppm): 1.06–1.08 (m, 42H), 2.95 (t, J = 6.7 Hz, 4H), 3.97 (t, J = 6.7 Hz, 4H), 7.14 (d, J = 1.2 Hz, 2H), 7.83 (s, 2H), 8.03 (d, J = 1.2 Hz, 2H). ^{13}C NMR ($CDCl_3$, 126 MHz) δ (ppm): 12.2, 18.2, 34.5, 64.1, 123.1, 125.6, 126.2, 129.6, 139.1, 140.9, 152.8.

Bromination and deprotection yielding compound BT-OH. *N*-Bromosuccinimide (NBS) (41.0 mg, 0.24 mmol) was added to a solution of compound **5b** (80.7 mg, 0.12 mmol) in THF (15 mL). The mixture was stirred at room temperature for 3 h. Without further purification, tetrabutylammonium fluoride (TBAF) (0.40 g, 1.5 mmol) was added to the solution and the mixture was stirred for another 1.5 h. The organic phase was then washed two times with water and dried over $MgSO_4$. After filtration and removal of the solvent, the brown solid was purified using column chromatography (silica gel) with an eluent gradient of dichloromethane and methanol. The product was purified further by recrystallization from acetone, affording a red solid (29.2 mg, 44%, 99% purity). ^{1}H NMR ($CDCl_3$, 400 MHz) δ (ppm): 2.77 (t, J = 7.0 Hz, 4H), 3.67 (td, J = 7.0 Hz, 5.3 Hz, 4H), 4.83 (t, J = 5.3 Hz, 2H), 7.98 (s, 2H), 8.12 (s, 2H). ^{13}C NMR ($CDCl_3$, 126 MHz) δ (ppm): 32.9, 60.2, 112.2, 124.2, 125.1, 128.3, 137.6, 140.0, 151.2.

2.3 Polymer synthesis and characterization

General procedure for the Stille cross-coupling polymerization.[37] The benzothiadiazole based monomer **BT-hex** was polymerized following a standard procedure with different ratios of **BDT-HD**, **BDT-Ph** and **BDT-OH** (Table 1), resulting in **P1**, **P2a,b** and **P3a,b**. Polymers **P4a,b** were synthesized *via* polymerization of **BDT-HD** with different ratios of **BT-hex** and **BT-OH**. The monomers were dissolved in anhydrous toluene (70 mg mL^{-1}). Tris(dibenzylideneacetone)dipalladium(0) (0.03 equiv.) and tris(*o*-tolyl)phosphine (0.09 equiv.) were then added to the vials before the mixtures were refluxed for at least 20 h. The mixtures were then precipitated into methanol. The solids were filtered and Soxhlet extractions were performed with methanol and hexane. The leftover polymers were dissolved in hot chloroform and finally precipitated once again in methanol, filtered and dried under vacuum. The final polymers were characterized by SEC, ^{1}H NMR and UV-vis spectroscopy.

- Poly{4,8-bis[5′-(2′′-hexyldecyl)-thiophen-2′-yl]benzo[1,2-*b*:4,5-*b*′]dithiophene-*alt*-4,7-bis(4′-hexylthiophene-2′-yl)benzo[*c*][1,2,5]thiadiazole} (**P1**).
- Polymers with 2-phenylethyl modified donor side chains (**P2a,b**).
- Polymers with 2-hydroxyethyl modified donor side chains (**P3a,b**).
- Polymers with 2-hydroxyethyl modified acceptor side chains (**P4a,b**).

Polymer characterization. Analytical size exclusion chromatography was performed using a Spectra Series P100 (Spectra Physics) pump equipped with two mixed-B columns (10 μm, 2 cm × 30 cm, Polymer Laboratories) and an Agilent 1100 DAD UV detector at 60 °C. Chlorobenzene was used as the eluent at a flow rate of 1.0 mL min^{-1}. The molecular weights were determined with UV detection at λ_{max} of the polymer and relative to polystyrene standards.

UV-vis spectra were recorded on an Agilent Technologies Cary 5000 UV-vis-NIR spectrophotometer. The spectra were obtained from chloroform solutions and spin-coated films on quartz slides.

Electrochemical experiments were performed with an Autolab PGSTAT30 potentiostat from Metrohm using the GPES software (version 4.9). The measurements were carried out in a three electrode one compartment microcell at room temperature using a platinum wire working electrode, a platinum wire counter electrode, a $Ag/AgNO_3$ reference electrode (0.01 M $AgNO_3$) and 0.1 M NBu_4PF_6 in anhydrous acetonitrile as the electrolyte. A constant flow of argon allows purging and blanketing of the electrolyte prior to and during analysis. For solid state voltammetry of films, samples were dissolved in chloroform. This solution was applied on the working electrode and dried at room temperature in air. Cyclic voltammograms were recorded at a scan rate of 100 mV s^{-1}. The HOMO–LUMO energy levels of the products were estimated using the onset potential of the first oxidation-reduction peak in the obtained CV curve. Cyclic

Table 1 Molecular, optical and electrochemical properties of the synthesized polymers

Polymer	Side group[a]	M_n[b]	$Đ$[b]	$\lambda_{onset,solution}$[c]	$\lambda_{onset,film}$[c]	ΔE_{op}[c]	ΔE_{ec}[d]	HOMO[d]	LUMO[d]
P1	—	22.5	3.9	736	747	1.66	1.85	−5.28	−3.43
P2a	5% D-EtPh	19.3	4.1	736	751	1.65	1.88	−5.27	−3.39
P2b	10% D-EtPh	18.3	3.7	736	750	1.66	1.87	−5.27	−3.40
P3a	5% D-EtOH	23.1	4.5	737	753	1.65	1.87	−5.26	−3.39
P3b	10% D-EtOH	25.4	7.9	738	748	1.66	1.82	−5.20	−3.38
P4a	5% A-EtOH	16.2	3.8	736	747	1.66	1.92	−5.29	−3.37
P4b	10% A-EtOH	13.3	3.2	735	744	1.66	1.90	−5.28	−3.38

[a] Percentage of exchanged side chains (2-phenylethyl (EtPh) or 2-hydroxyethyl (EtOH) on the donor (D) or acceptor (A) moiety). [b] M_n (in kDa) and dispersity ($Đ$) determined by SEC in chlorobenzene at 60 °C. [c] λ_{onset} (in nm) and ΔE_{op} (optical bandgap, in eV) determined by UV-vis spectroscopy. [d] ΔE_{ec} (electrochemical bandgap), HOMO and LUMO (in eV) determined by cyclic voltammetry.

voltammograms are not background corrected and characteristic potential values are mean values over several experiments. All potentials are rescaled to ferrocene which is used as an external standard. For the conversion of potentials (V) obtained from the electrochemical measurements to molecular orbital energies (eV), we scale the formal potential of the Fc/Fc^+ redox couple to the vacuum level with a value of −4.98 eV, considering that 0.0 V on the ferrocene scale corresponds to 0.31 V *versus* SCE[45] (0.55 V *versus* NHE) and that 0.0 V *versus* NHE[46] is equivalent to −4.44 eV.

$$E_{HOMO/LUMO}\,(eV) = -4.98 - E_{onset\ vs.\ Ag/AgNO_3}\,(V) + E_{onset\ vs.\ Ag/AgNO_3}\,(Fc/Fc^+)\,(V).$$

Alternatively, the LUMO energy levels were calculated as the difference between the HOMO energy and the optical bandgap. To estimate the optical bandgap, the wavelength at the intersection of the tangent line drawn at the low energy side of the absorption spectrum with the x-axis was used in the equation E_g (eV) = 1240/wavelength (nm). The accuracy of measuring redox potentials by CV is about 0.01–0.02 V. Reproducibility can be less because the potentials do not depend on concentration and temperature.

Differential scanning calorimetry was performed on a prototype TA Instruments Rapid Heat Cool calorimeter (RHC) using a liquid nitrogen cooling system and purged with helium (12 mL min^{-1}). The RHC cell is heated by four quartz halogen lamps. The samples (~0.250 mg) were enclosed in dedicated non-hermetical aluminium crucibles.[47,48]

The photochemical stability of the polymer films prepared by SC on glass slides was analysed using a setup described in the literature.[49]

2.4 Device preparation and characterization

For the SC devices, the traditional solar cell architecture consisting of glass/ITO/PEDOT:PSS/polymer:$PC_{61}BM$/Ca/Al was employed. Prior to processing, the indium tin oxide (ITO, Kintec, 100 nm, 20 Ohm sq.$^{-1}$) coated glass substrates were thoroughly cleaned using soap, demineralized water, acetone, isopropanol and a UV/O_3 treatment. PEDOT:PSS was subsequently deposited at a thickness of ~30 nm and annealed at 130 °C for 15 minutes to remove any residual water. Further processing was carried out in a nitrogen containing glovebox (O_2/H_2O < 1 ppm), starting with the deposition of the PAL layer by spin-coating. For **P1**, **P2a,b**, **P3a,b** and **P4a,b**, blend solutions with a total concentration of 15 mg mL^{-1} with a polymer : $PC_{61}BM$ ratio of 1 : 2 (wt/wt%) were prepared using chloroform (CF) as the processing solvent. A lower total concentration was chosen in comparison to the RC devices to compensate for the faster evaporation rate of CF, yielding a device thickness of around 110 nm. Finally, the devices were finished off by vacuum deposition of the top electrodes, Ca and Al, with layer thicknesses of 30 and 80 nm, respectively. The SC solar cell performance measurements were carried out using a Newport class A solar simulator (model 91195A), calibrated with a silicon solar cell to give an Air Mass (AM) 1.5G spectrum. Stability tests according to ISOS-D-2 standards (under thermal stress) were performed on a hotplate (280 × 200 mm, type PZ28-2ET, Harry Gestigkeit GmbH, with a PR5 programmer controller) in a nitrogen atmosphere at a constant temperature of 85 °C. The current–voltage (I–V) characteristics were measured manually at specific time intervals using a Newport class A solar simulator (model 91195A), calibrated with a silicon solar cell to give an AM 1.5G spectrum.

The RC PSCs, with a typical architecture of PET/Ag grid/PEDOT:PSS/ZnO/polymer:$PC_{61}BM$/PEDOT:PSS/Ag grid, were produced on a flextrode substrate (produced in house: PET/Ag grid/PEDOT:PSS/ZnO)[50,51] using a laboratory roll coater under ambient conditions.[52,53] During the optimization of the RC process for **P1**, the temperature (60, 70 and 80 °C), the solvent (ODCB, CF, CB/3% CN and ODCB/CB = 4/1), the polymer : $PC_{61}BM$ ratio (1 : 1, 1 : 1.5 and 1 : 2 (wt/wt%)) and the elevated layer thickness (390 and 450 nm; to avoid the formation of pinholes during processing) were varied. The material concentration was kept at 40 mg mL^{-1}. PSCs with PALs based on **P2a,b** were coated from ODCB/CB = 4/1, whereas the active layers based on **P3a,b** and **P4a,b** were coated from ODCB/CB = 3/2. Five PSCs per coating were encapsulated between two glass slides using a UV-curable adhesive. The adhesive was activated for a few minutes using a solar simulator. The exact area of all cells was determined using a Light Beam Induced Current (LBIC) technique described in the literature.[54] The RC PSCs were tested under a solar simulator (AM 1.5). I–V curves were recorded to determine the photovoltaic parameters (open-circuit voltage (V_{oc}), short-circuit current density (J_{sc}), fill factor (FF) and PCE). External quantum efficiency (EQE) measurements

were carried out using a system from PV Measurements Inc. at 10 nm intervals between 300 and 800 nm. A calibrated Si cell was used before the experiment as a reference. Stability tests of the PSCs according to ISOS-L-1 standards (under solar irradiation) were performed using a solar simulator with AM 1.5 (1000 W m $^{-2}$). The *I–V* curve tracing of the PSCs was performed using an automated acquisition setup with a Keithley 2400 SMU.

3. Results and discussion

3.1 Synthesis and characterization

Material synthesis. In this study, seven low bandgap copolymers (Fig. 1) based on 4,8-di(thiophene-2′-yl)benzo[1,2-*b*:4,5-*b*′]dithiophene (DTBDT, donor) and 4,7-di(thiophene-2′-yl) benzo[*c*][1,2,5]thiadiazole (DTBT, acceptor) building blocks were synthesized (Scheme 1).[37] **P1** was presented previously bearing a 2-hexyldecyl (HD) and a hexyl side chain on the donor and acceptor moieties, respectively,[37] whereas for **P2a,b**, the HD side chain was partially (5 or 10%) exchanged by 2-phenylethyl (EtPh) groups, and for **P3a,b** by 2-hydroxyethyl (EtOH) groups. For **P4a,b**, the hexyl side chain on the acceptor part was partially (5 or 10%) substituted by EtOH groups.

The required monomers for the polymerizations were synthesized according to the procedures shown in Scheme 1 and S1.† The donor monomer **BDT-HD** was synthesized *via* a standard three-step protocol[39,43] starting from thiophene and benzo[1,2-*b*:4,5-*b*′]dithiophene-4,8-dione (BDT-dione). After alkylation of thiophene in the 2-position (**1a**), the molecule was lithiated with *n*-BuLi at the 5-position, before it was reacted with BDT-dione. Reduction with tin(II) chloride ($SnCl_2$) in the hydrochloric acid environment finally yielded **DTBDT 2a**. Stannylation of **2a** using *n*-BuLi and Me_3SnCl afforded **BDT-HD**. The donor monomer **BDT-Ph** was synthesized in a similar manner. **BDT-OH** was also synthesized using the same reaction conditions, but 2-(thiophen-2′-yl)ethanol was used as the starting material. The alcohol group was first protected with a triisopropylsilyl (TIPS) unit (**1c**). During the third step of the coupling procedure with the BDT-dione, the reduction of the molecule with $SnCl_2$, the TIPS group was removed by the reducing agent, directly yielding the desired alcohol **2c**.[44] Stannylation of the obtained product was performed according to the procedure for **BDT-HD**. However, a larger excess (7 equiv.) of *n*-BuLi was used to obtain a fully lithiated compound.

The acceptor monomer **BT-hex** was synthesized *via* a standard four-step procedure from 3-bromothiophene and 4,7-dibromobenzo[*c*][1,2,5]thiadiazole (BT-diBr).[42] After alkylation of thiophene in the 3-position (yielding **3a**), it was stannylated further in the 2-position (**4a**) before reacting with BT-diBr. Bromination with NBS then yielded **BT-hex**. **BT-OH** was synthesized using similar steps. However, 2-(thiophen-3′-yl) ethanol was used as a starting material. It was again first protected with a TIPS group (**3b**). Stannylation of **3b** and subsequent coupling with BT-diBr yielded compound **5b**. After bromination of **5b** with NBS, the alcohol was directly deprotected with TBAF yielding monomer **BT-OH**.

Standard Stille cross-coupling polymerization of the monomers based on BT and BDT yielded **P1**, **P2a,b**, **P3a,b** and **P4a,b** (Fig. 1). While **P1** was obtained as a standard alternating copolymer (based on **BDT-HD** and **BT-hex**), the synthesis of **P2a,b** and **P3a,b** targeted statistical copolymers with the same backbone, but with partial exchange of the (HD) side chains on the donor moiety using 5 or 10% of **BDT-Ph** and **BDT-OH**, respectively. Copolymers **P4a** and **P4b** were synthesized using 5 or 10% of **BT-OH** instead of the regular DTBT acceptor monomer (**BT-hex**).

Polymer characterization. The synthesized polymers were characterized using standard techniques. ^{1}H NMR spectra of the polymers were recorded in deuterated chloroform (Fig. S1.16†). The spectra of the polymers show the main signals of the polymer backbone as well as of the HD solubilizing side chain. The polymers **P2a–P4b** show small signals of the ethyl groups of the exchanged side chains (not always clearly visible due to overlapping with the α-CH_2 signals of the HD side chains).

The molecular weights (M_n) were measured by SEC to be between 15 and 25 kDa (Table 1).

The optical properties were determined by UV-vis spectroscopy. The absorption spectra of all polymers in chloroform solution (Fig. 2a) showed minor differences. For the entire polymer series, the absorption onset can be found around 736 nm (Table 1). In the wavelength range of the absorption maximum (around 670 nm), the UV-vis curve for **P2a,b**, **P3a** and **P4a,b** flattens out slightly. Only **P3b** has a similar curve progression as the parent copolymer **P1**. The absorption spectra of the polymer films (Fig. 2b) show two maxima between 600 and 700 nm, with onset wavelengths varying slightly (in the range of 10 nm, Table 1). However, the maximum around 700 nm is most defined for **P1**, whereas for the altered copolymers, the intensities are more equivalent or even a more elevated maximum around 630 nm is observed. The optical bandgaps were all estimated at approximately 1.66 eV.

Cyclic voltammetry (CV) was performed to estimate the HOMO and LUMO energy levels of the polymers (Table 1). The electrochemical bandgap was calculated to be 1.85 eV for **P1**. Alteration of the side chains resulted in slightly increased values for the bandgap (*e.g.* 1.90 eV for **P4a,b**), with the exception of **P3b**, showing a lower bandgap of 1.82 eV. **P3b** has the highest HOMO level of −5.20 eV. The HOMO levels of the other copolymers are similar to the value obtained for the parent copolymer **P1** (around −5.28 eV). The LUMO levels of the modified polymers increased slightly relative to **P1**. A comparison between the different side chain modifications on the acceptor and donor moieties shows that the HOMO shifts to a lower value for the acceptor modification.

Thermogravimetric analysis (TGA) (Fig. S2†) showed different thermal stabilities for the polymers with and without manipulated side chains. The decomposition of all copolymers starts around 400 °C. The small temperature differences between all samples could be due to the different side chains or slightly different molecular weights. The thermal properties of the polymers were finally also investigated by rapid-heat cooling calorimetry (RHC) (Fig. S3†). This method was chosen instead

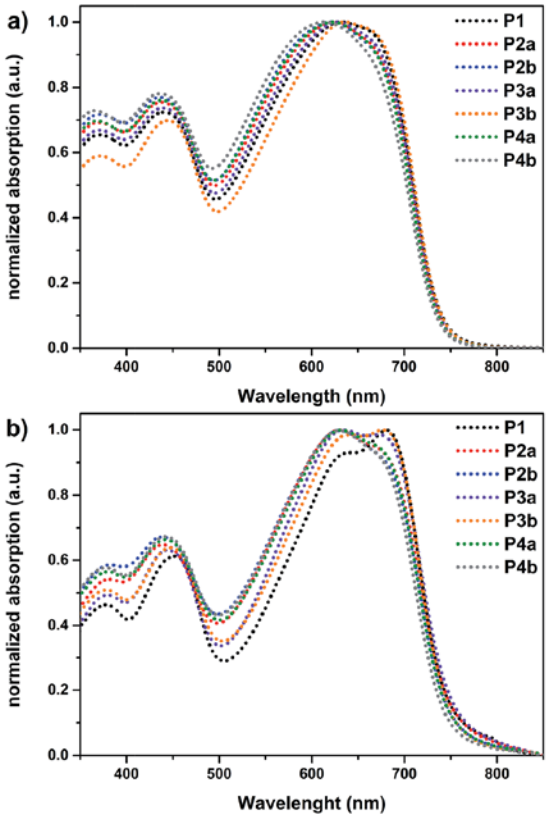

Fig. 2 Normalized UV-vis absorption spectra of the polymer solutions in chloroform (a) and the polymer films on quartz (b).

of regular differential scanning calorimetry due to the low sample amounts required and the increased sensitivity to thermal transitions (*e.g.* T_g).[47,55] RHC analysis reveals that all materials are amorphous. A broad T_g is detectable for all polymers in the range of 135 to 150 °C.

3.2 Photovoltaic properties

The novel polymers were applied in BHJ PSCs *via* both RC and SC techniques. The influence of the two different side chains (EtOH and EtPh) as well as the influence of the side chain modification on either the acceptor or donor moiety (using EtOH) was investigated in terms of photovoltaic performance and stability (under solar irradiance and thermal stress). The SC devices had a traditional architecture glass/ITO/PEDOT:PSS/polymer:$PC_{61}BM$/Ca/Al with a PAL area of 3 mm^2. The PSC architecture for the RC devices consisted of PET/Ag grid/PEDOT:PSS/ZnO/polymer:$PC_{61}BM$/PEDOT:PSS/Ag grid, with device areas of ~1 cm^2.[35]

For the SC BHJ PSCs, a small solvent screening (*ortho*-dichlorobenzene (ODCB) and CF) was performed (Table S1†) for **P1**, based on the conditions used for the RC processing of the PSCs made from **P1-(EH)**.[35] CF was determined to be the most optimal solvent, with a polymer : $PC_{61}BM$ ratio of 1 : 2 and a total concentration of 15 mg mL^{-1}, warranting layer thicknesses of around 110 nm. The reduced blend concentration was chosen due to the more rapid evaporation of CF in comparison with ODCB. The use of [6,6]-phenyl-C_{71}-butyric acid methyl ester did not increase the performance of the produced PSCs.

The RC process of the PSCs based on **P1** was additionally optimized by a variation in the temperature (60, 70 and 80 °C), solvent (ODCB, CF, chlorobenzene (CB)/3% 2-chloronaphthalene (CN) and ODCB/CB = 4/1), polymer : $PC_{61}BM$ ratio (1 : 1, 1 : 1.5 and 1 : 2) and PAL thickness (390 and 450 nm). The results (Table S2†) revealed the highest values for the photovoltaic parameters when utilizing a polymer : $PC_{61}BM$ ratio of 1 : 2 (40 mg mL^{-1}) and coating from ODCB/CB (4/1) at 80 °C with a PAL thickness of 450 nm. For consistency, these parameters were maintained for the RC processing of the copolymer PSCs (**P2a,b**, **P3a**, **P4a**). Since the properties of the photoactive films produced from the **P3** and **P4** analogues were rather poor in comparison to the **P1** film (Table S3†), the cosolvent ratio changed to ODCB/CB = 3/2 to obtain improved film morphology and performance characteristics (Table S4†).

The solar cell characteristics are summarized in Table 2 and Fig. S4.† The SC devices were found to be better than the RC PSCs, in terms of V_{oc} (~0.75 *vs.* ~0.72 V) J_{sc} (~10 *vs.* ~8 mA cm^{-2}) and FF (~0.67 *vs.* ~0.60). As such, PCEs of around 4–5% could be achieved for the SC devices (Table 2). The devices based on the reference material **P1** exerted an averaged PCE of 4.50%. A slight elevation of the performance could be achieved for copolymer **P3a** (4.89%), whereas **P4b** showed a lower performance, with averaged PCE values of 4.34%. The solar cell characteristics for the RC devices revealed an averaged PCE of 3.43% for **P1**, and the partial side chain substitutions have negligible effects on the performance. A strong reduction in PCE was, similar to the SC processing, obtained for **P4b**, demonstrating a PCE of 3.04%. Overall, the J_{sc} and V_{oc} are similar for the entire (co)polymer series, and the slight variation in performance can be traced back to (rather) small differences in FF (0.60 for **P1** *vs.* ~0.55 for **P4a** and **P4b**). The external quantum efficiency (EQE) spectra of the PSCs (with highest efficiency) do not show any particular features and only minor vertical shifts can be observed (Fig. S5†).

In general, both the RC and SC device series demonstrate a (small) negative influence of the modification of the acceptor side chain on the performance of the resulting PSCs, especially when increasing the modification ratio (as observed in the case of **P4b**).

On the other hand, functionalization of the side chains on the donor moiety can result in slight improvements in PCE, although in this case observed only within the SC device series.

3.3 Stability testing

Thermal stability study of the solar cells. The thermal stability of the SC solar cells was investigated according to ISOS-D-2 [56] standard conditions by placing the devices on a hotplate at 85 °C in a nitrogen atmosphere and measuring the *I–V* characteristics on a regular timescale. As illustrated by the relative PCE decays in Fig. 3a (absolute PCEs in Fig. S6a†), all

Table 2 Photochemical degradation rate (R_d) of the polymer films and I–V parameters[a] (V_{oc}, J_{sc}, FF and PCE) for the polymer : $PC_{61}BM$ solar cells based on **P1**, **P2a,b**, **P3a,b** and **P4a,b**

Polymer	R_d[b] (relative to **P1**)	Method[c]	V_{oc} [V]	J_{sc} [mA cm^{-2}]	FF	PCE (best) [%]
P1	1.15 ± 0.07 (1.00)	SC[d]	0.75	9.74	0.61	4.50 (5.27)
		RC[e]	0.73	7.79	0.60	3.43 (3.60)
P2a	1.17 ± 0.10 (1.02)	SC[d]	0.76	9.79	0.62	4.58 (4.73)
		RC[e]	0.73	7.73	0.59	3.35 (3.47)
P2b	1.16 ± 0.02 (1.01)	SC[d]	0.76	9.23	0.61	4.31 (4.49)
		RC[e]	0.73	7.79	0.57	3.25 (3.43)
P3a	1.04 ± 0.08 (0.91)	SC[d]	0.76	10.80	0.60	4.89 (5.55)
		RC[f]	0.72	7.63	0.58	3.17 (3.38)
P3b	0.83 ± 0.09 (0.72)	SC[d]	0.72	10.48	0.67	5.03 (5.33)
		RC[f]	0.71	7.76	0.60	3.27 (3.54)
P4a	1.14 ± 0.11 (0.99)	SC[d]	0.76	9.93	0.60	4.50 (4.74)
		RC[f]	0.72	7.99	0.55	3.16 (3.42)
P4b	1.46 ± 0.09 (1.27)	SC[d]	0.76	9.30	0.61	4.34 (4.54)
		RC[f]	0.73	7.76	0.54	3.04 (3.16)

[a] I–V parameters averaged over 5 devices for RC and 4–8 devices for SC. [b] Photochemical degradation rate in %/hour. [c] SC: spin-coating under an inert atmosphere with a normal device geometry (glass/ITO/PEDOT:PSS/polymer:$PC_{61}BM$/Ca/Al) for 3 mm^2 active area. RC: roll-coating in air at 80 °C, 1 : 2 ratio for polymer : $PC_{61}BM$, an active layer thickness of 450 nm and an inverted device geometry for ~1 cm^2 (PET substrate/Ag-grid/PEDOT:PSS/ZnO/polymer:$PC_{61}BM$/PEDOT:PSS/Ag-grid). [d] 1 : 2 ratio processed from CF. [e] Processed from ODCB/CB = 4/1. [f] Processed from ODCB/CB = 3/2.

solar cell devices behave similarly for the duration of the heat treatment (450 h), with PCEs decreasing to 60–70% of their initial values.

Deconvolution into the separate I–V parameters shows only a minor decay in relative V_{oc} (to 85–90%) (Fig. S6b†). Similarly, the J_{sc} also stays relatively stable over the entire experiment, with values approximating 70% after 450 h (Fig. S6c†). The main differences in relative PCE among the different PSCs originate from differences in FF behaviour (Fig. S6d†), for which small morphological rearrangements or minor electrode improvements induce a slight improvement at the start of the experiment. A similar degradation curvature for all PAL materials can partially be rationalized by the chosen degradation temperature (85 °C), which is far below the T_g of all copolymers (135 to 150 °C), as such that the crystallization and phase separation of $PC_{61}BM$, a known thermal degradation pathway,[23,25] will not readily occur.

Photochemical stability study of the (co)polymers. The photochemical stability of the (co)polymer materials was investigated by measuring their absorption in a thin film under illumination at AM 1.5 (1000 W m^{-2}) using an automated setup as described in the literature.[49] The polymer films, spin coated on glass substrates, were directly exposed to solar irradiation. The degradation rates (Table 2) could be determined from the corresponding absorption (maximum) decay curves (Fig. 3b). **P1**, **P2a,b** and **P4a** degraded with a similar rate (~1.15%/hour), whereas the degradation rate for **P4b** increased to 1.46%/hour. However, the manipulation of the side chain on the donor part of the polymers using EtOH resulted in both cases in a slightly higher stability. While **P3a** had a degradation rate of 1.04%/hour, it decreased even further to 0.83%/hour for **P3b**. Detailed analysis of the curve slope reveals that the improved stability is already visible after ~10 hours, whereas the slope for **P4b** starts to decrease at a stronger rate around this time. All samples were fully bleached at the end of the stability test. No absorption could be detected anymore after ~23 hours for **P4b**, 27–31 hours for **P1**, **P2a,b**, **P3a** and **P4a**, and ~37 hours for **P3b**.

The incorporation of the different side chains on different positions of the (co)polymers thus clearly results in different photochemical stabilities of the polymers. Incorporation of the EtPh side chains shows no noteworthy effect on the photochemical stability, with degradation curves following a very similar pathway as the reference material **P1**. Substitution of 5% of the side chains by EtOH moieties on the acceptor building block also reveals no added value. In fact, a negative trend could be observed with 10% incorporation of the EtOH group for **P4b**. However, incorporation of the EtOH side chain onto the donor moiety revealed a slower photochemical degradation, most pronounced in the case of 10% substitution. In this case, the new side chain is not directly attached on the conjugated polymer backbone, but on the thiophene side chain of the BDT building block.

Any chemical reaction within the active layer can contribute to the degradation of the active layer. Multiple degradation mechanisms for polymers in PSCs subdued to solar irradiance in an ambient (oxygen) environment have been described in the literature. Light as a main trigger for the degradation of conjugated polymers has been shown to result in photobleaching (disruption of conjugation), photooxidation (disruption of the conjugation/side chain removal), free radical attack/photolysis (chain scission/cross linking/side chain removal) and photodoping (weakly bound donor–acceptor charge transfer complex, reversible).[57] In 1993 Abdou and Holdcroft demonstrated the formation of singlet oxygen by photobleaching, which then reacts with the thiophene in the polymer backbone through a Diels–Alder addition, leading to the disruption of the π-conjugation. In a second and third process, a free radical pathway occurs, resulting in either chain scission or cleavage of the side chain.[58] Photooxidation of conjugated polymers grants oxygen-containing polymers with ruptures of

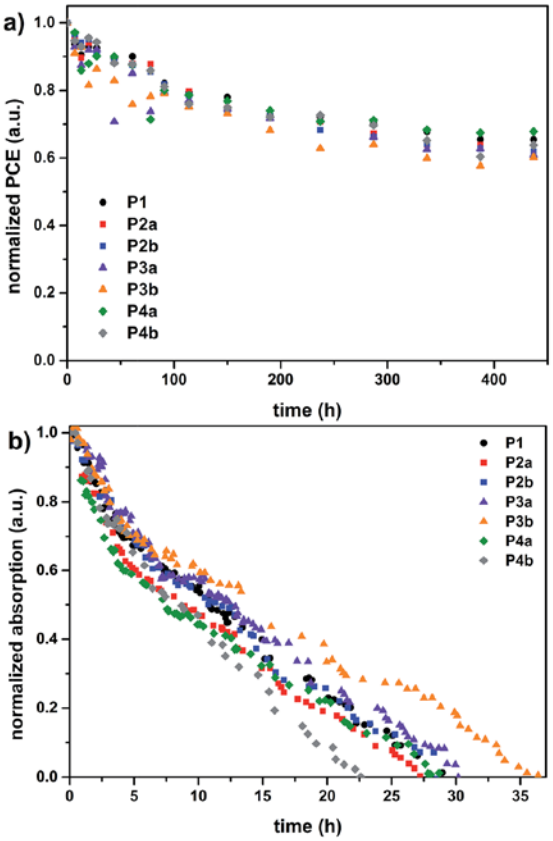

Fig. 3 (a) Stability measurements of SC PSCs based on **P1**–**P4b** under thermal stress (85 °C) in terms of the averaged PCE. (b) Normalized UV-vis absorption maximum evolution of the polymer films under constant sun irradiance (AM 1.5).

the aromatic system and formation of a R–SO_x species at the thiophene part.[59] Radical oxidation of the hexyl side chain on P3HT and subsequent stepwise oxidation of the sulfur atom of thiophene have been shown to lead to the loss of the π-conjugation and therefore results in bleaching of the polymer material.[60] Since for **P4a** and **P4b** the EtOH side chain is anchored onto the thiophene rings of the acceptor unit, part of the π-conjugated backbone, this degradation pathway may induce a more rapid degradation in comparison with the other (co)polymers. However, it is difficult to specify clearly the degradation mechanisms occurring within these polymer series, especially for **P3b** and **P4b**, respectively, addressing how the incorporation of different side chains influenced these degradation mechanisms.

In addition, reversible p-doping of the polymer by oxygen can take place. Slow physical adsorption of oxygen on the polymer chain forms a weak charge-transfer complex and this process is accelerated by light exposure.[57] Different studies show that the PV performance of conjugated polymers is dependent on the molecular weight.[61–63] Photoinduced oxidation, chain scission and opening of the π-conjugated system can result in a variation of the polymer chain length and therefore affects the optical and photovoltaic properties of the degraded polymers.[64] In conclusion, all described mechanisms may occur in the polymer films during exposure to light, but it was not specifically investigated as how the polymers degrade under this external stress.

Photostability study of the solar cells. The RC PSCs were then analysed in ISOS-L-1 [56] lifetime tests, in which three cells of each polymer were subdued to AM 1.5 (1000 W m^{-2}) illumination for 50 days. At the start of the measurements, *I*–*V* curves were recorded every couple of minutes, and this was prolonged to 30 minutes at later timescales. The averaged and absolute PV parameters of the three cells were plotted against time (Fig. 4 and S7†). During the initial phase (0–5 hours/"burn-in" phase[56]) of the lifetime study, the PCE decreased relatively fast for all cells, from >3% to <2.5% for **P1**, **P2a,b**, **P3a,b** and **P4a**, except for the cells from **P4b**, which decreased from a PCE of 2.7% to ~2.0% (Fig. S7a†). In normalized terms (Fig. 4a), analysis of the device data after 5 hours for the reference material **P1** revealed a decay to 70% of the initial value, whereas the devices based on copolymers **P3a,b** and **P4a,b** retained a relative performance of between 72% and 74% for the 5% and 10% functionalization, respectively. Copolymers **P2a** and **P2b** demonstrated relative PCEs of 65 and 70%, respectively, after 5 hours (Fig. 4a), retaining the trend within the side chain ratio, but performing worse than the reference material. After 5 days under constant sun irradiation, the PSCs based on **P1** and **P3b** showed a PCE of ~1.9%, while the efficiency of the devices based on **P4b** decreased to 1.4%. The PSCs based on **P3b** still demonstrated a PCE of 60% of the initial value, while the solar cells made from **P2a** and **P4b** decreased more strongly (to 50% of the initial PCE). The relative efficiencies for the PSCs based on **P1**, **P2b**, **P3a** and **P4a** were in between these two values (~55% of the initial value).

During the final stage of the measurements, the efficiencies decreased in a quite linear manner with different slopes for the different polymers. After 50 days under constant sun irradiation, the PSCs based on **P3b** and **P4b** performed at 24% and 26% of their initial PCE, respectively, while the efficiency of the devices made from **P1**, **P2a**, **P3a** and **P4a** decreased to ~22% of the initial value. The efficiency of the PSCs based on **P2b** decreased the least, to 30% of the initial value.

From the photostability measurements on RC devices, it can thus be concluded that 5% exchange of the side chains by functional moieties does not result in improved device stabilities. The substitution of 10% (**P2b**, **P3b** and **P4b**) of the side chains does result in a small increase of the stability of the PSCs, measurable for both side chains studied here and applied in different positions.

The other *I*–*V* characteristics (V_{oc}, J_{sc}, FF) showed a similar trend. The negative influence (with respect to PCE) of the substituted EtOH side chain on the acceptor part in **P4b** is also reflected in a faster decrease of the J_{sc} and FF during the first stage. This decrease could not be compensated during the progression of the experiment. Surprisingly, the PSCs based on this polymer retained a higher V_{oc}, even after solar irradiation for 50 days. On the other hand, the beneficial influence of the

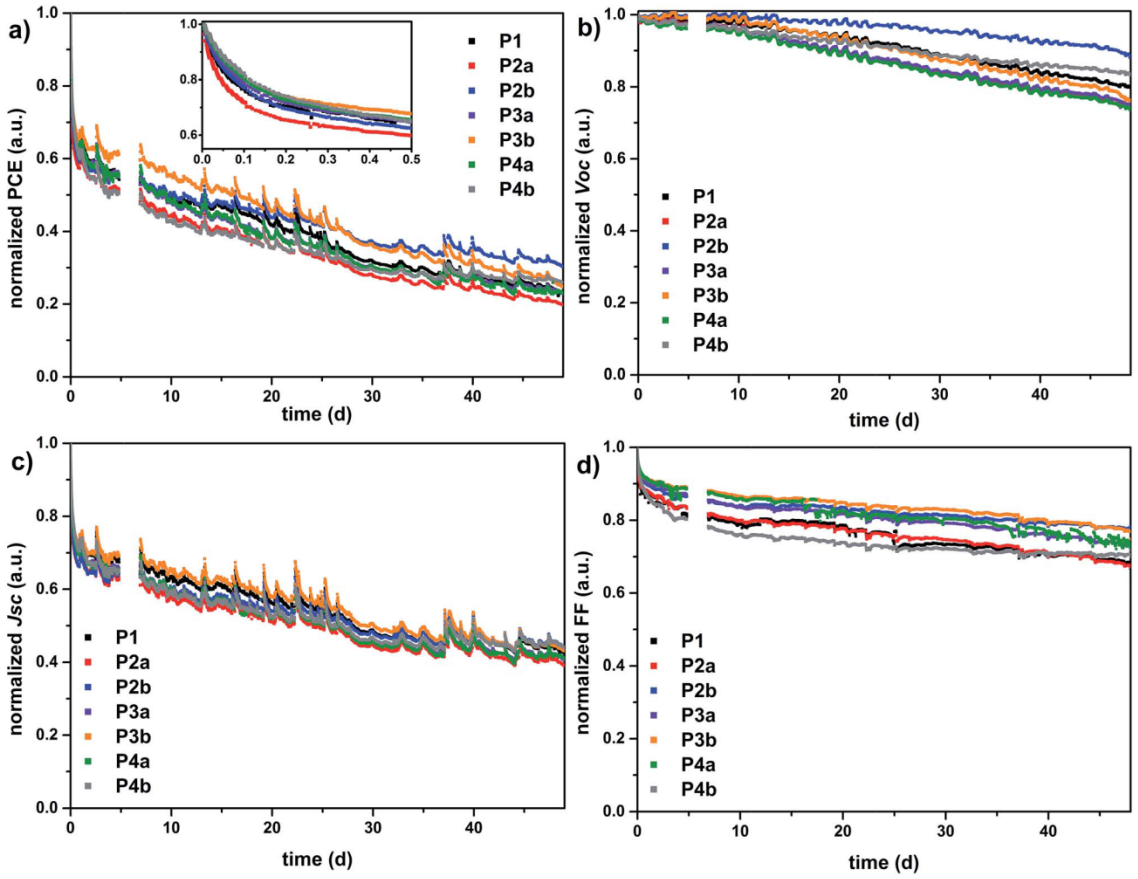

Fig. 4 Stability measurements of RC PSCs based on **P1–P4b** under constant sun irradiance (AM 1.5) according to ISOS L-1 standards in terms of normalized PCE (a), V_{oc} (b), J_{sc} (c) and FF (d) (no data could be gathered between 5 and 7 days due to a software error).

EtPh side chain in **P2b** is seen for all three characteristics during the stability test. These PSCs have the highest retained values for V_{oc}, J_{sc} and FF (0.62 V, 3.5 mA cm^{-2} and 45%). The reference polymer device parameters are in the centre span. The FF of **P3b** is also more stable than the FF of the reference **P1** device (75% of the initial value).

Discussion on the stability results. The influence of the introduction of stabilizing side chains was studied by Friend *et al.*[21] and Vanderzande *et al.*,[23] previously and adopted herein to improve the photo- and thermal stability. In particular, the influence on the thermal stability and phase separation of the active layer was part of the beginning of the study, as the (photochemical) stability of a polymer:fullerene BHJ can also be governed by PCBM crystallization and dimerization.[31–33] The PCBM dimerization is probably also part of the rather complicated degradation pathway occurring here, but is not specifically investigated in this study. Due to undetectable T_g and no difference within the thermal degradation test (first section in 3.3) of the PSCs, the stability discussion in this study moves from an influence on the thermal to an influence on the photochemical stability of the polymer and PSC, respectively. So the thermal stability and the related PCBM crystallization was not explored further in this study.

It has been shown before, that the polymer structure (nature of the backbone, amount and length of the side chains) can influence the (photochemical) stability of the polymers and thus of the resulting polymer solar cells.[29,65–67] Manceau *et al.* showed that different donor or acceptor groups within the backbone structure changes the photochemical stability of the resulting polymer. As a result they proposed some general rules for the structure-stability ranking of donor–acceptor polymers for PSCs.[10] Very recently, the group of Andersson reported a copolymer series combining a quinoxaline acceptor unit with differently substituted BDT or unsubstituted thienothiophene units, investigating the effect of structural modifications on the polymer film and the corresponding PSC stability.[67] Similar to our observations, their results demonstrate a different trend among the photochemical stability of the neat polymer films and the corresponding solar cells.[67] In the current contribution, comparison of the photostability analysis of the PSCs reveals that the location of the functional side chains, either on the donor or acceptor building block, influences the stability of the

resulting materials and devices. For both light-induced degradation tests, **P4b**, with exchanged side chains on the acceptor part, shows the most rapid degradation. On the other hand, when applying the same strategy on the BDT donor building block (**P2b** and **P3b**, bearing EtPh and EtOH, respectively), slight improvements in stability can be noted. On the material level, EtOH incorporation already granted more stable materials at 5% incorporation ratio, whereas 10% was required on the device level. Even though 10% EtPh incorporation showed a minor effect on the photochemical degradation, improved solar cell stability could be achieved. The thermal degradation of the SC PSCs proceeded similar for all devices containing different polymers.

4. Conclusions

In this work, a reference donor–acceptor polymer **P1** based on benzo[1,2-*b*:4,5-*b*′]dithiophene (BDT) and dithienylbenzo[*c*][1,2,5]thiadiazole (DTBT) was successfully adapted through partial exchange (5 or 10%) of the solubilizing side chains (hexyldecyl (HD) on the donor or hexyl on the acceptor part), as a means to investigate to which extent the functionalized side chains can lead to improved polymer solar cell stability. The incorporation of the functional moieties 2-phenylethyl (EtPh) and 2-hydroxyethyl (EtOH) resulted in statistical copolymers **P2a** (5% EtPh for HD), **P2b** (10% EtPh for HD), **P3a** (5% EtOH for HD), **P3b** (10% EtOH for HD), **P4a** (5% EtOH for hexyl) and **P4b** (10% EtOH for hexyl).

All polymers were investigated in bulk heterojunction solar cells, prepared by both spin-coating and roll-coating, with maximum PCEs up to 5.0% and 3.4%, respectively. For roll-coating, the best performance was obtained from PSCs based on **P1**, whereas **P3b** was found to be superior in performance when the photoactive layer was spin-coated. The photovoltaic efficiency suffered the most upon substitution of the side chain pattern on the acceptor unit (**P4a,b**).

Degradation tests (thermal and photochemical) were performed on the PSCs. When treated at 85 °C for 450 hours, the spin-coated PSCs based on all (co)polymers showed very similar features, without distinguishable differences. Since this standardized degradation temperature lies far below the T_g of the polymers, no phase separation/crystallization of the $PC_{61}BM$ acceptor is to be expected.

Photochemical stability measurements on both roll-coated devices and (co)polymer films also revealed small fluctuations. For all copolymers, 5% side chain substitution has barely any impact. Furthermore, incorporation of 10% of the EtOH side chain on the acceptor moiety (**P4b**) resulted in a more rapid deterioration of the material. However, in comparison with the reference material **P1**, an improvement of the stability of the PSCs could be obtained when incorporating 10% of EtPh or EtOH on the side chains of the donor building block (**P2b**, **P3b**).

These results show that 10% side chain substitution can already slightly improve the stability of the polymer films and the resulting PSCs. Thus, it is clearly shown that the variation of side chains, especially at different positions (acceptor or donor unit of the polymer), has an influence on the stability. To find the ideal side chains and positions for polymers suitable for roll coating, it is necessary to perform some further screening.

Acknowledgements

This work has been supported by the Villum Foundation's Young Investigator Programme (2nd round, project: Materials for Energy Production). The work was partly carried out by an external research stay of I. Heckler at Hasselt University in the group of Prof. W. Maes. The Hasselt University co-authors acknowledge the financial support by the Science Policy Office of the Belgian Federal Government (BELSPO; IAP 7/05 project 'Functional Supramolecular Systems'), The Hasselt University and VUB co-authors are also grateful for financial support by the Research Program of the Research Foundation-Flanders (FWO) (project G.0415.14N). TA Instruments is acknowledged for the RHC equipment. P. C. Johansen from the Department of Chemistry at the Technical University of Denmark is acknowledged for HPLC/ELSD measurements.

References

1 S. Günes, H. Neugebauer and N. S. Sariciftci, *Chem. Rev.*, 2007, **107**, 1324–1338.
2 C. J. Brabec, S. Gowrisanker, J. J. M. Halls, D. Laird, S. Jia and S. P. Williams, *Adv. Mater.*, 2010, **22**, 3839–3856.
3 Y.-W. Su, S.-C. Lan and K.-H. Wei, *Mater. Today*, 2012, **15**, 554–562.
4 W. Cao and J. Xue, *Energy Environ. Sci.*, 2014, **7**, 2123–2144.
5 K. A. Mazzio and C. K. Luscombe, *Chem. Soc. Rev.*, 2015, **44**, 78–90.
6 J. Zhao, Y. Li, G. Yang, K. Jiang, H. Lin, H. Ade, W. Ma and H. Yan, *Nat. Energy*, 2016, **1**, 15027.
7 Y. Liu, J. Zhao, Z. Li, C. Mu, W. Ma, H. Hu, K. Jiang, H. Lin, H. Ade and H. Yan, *Nat. Commun.*, 2014, **5**, 5293.
8 R. S. Kularatne, H. D. Magurudeniya, P. Sista, M. C. Biewer and M. C. Stefan, *J. Polym. Sci., Part A: Polym. Chem.*, 2013, **51**, 743–768.
9 M. Manceau, A. Rivaton, J. L. Gardette, S. Guillerez and N. Lemaître, *Polym. Degrad. Stab.*, 2009, **94**, 898–907.
10 M. Manceau, E. Bundgaard, J. E. Carlé, O. Hagemann, M. Helgesen, R. Søndergaard, M. Jørgensen and F. C. Krebs, *J. Mater. Chem.*, 2011, **21**, 4132–4141.
11 M. O. Reese, A. M. Nardes, B. L. Rupert, R. E. Larsen, D. C. Olson, M. T. Lloyd, S. E. Shaheen, D. S. Ginley, G. Rumbles and N. Kopidakis, *Adv. Funct. Mater.*, 2010, **20**, 3476–3483.
12 H. Hintz, H.-J. Egelhaaf, L. Lüer, J. Hauch, H. Peisert and T. Chassé, *Chem. Mater.*, 2011, **23**, 145–154.
13 A. Tournebize, J.-L. Gardette, C. Taviot-Guého, D. Bégué, M. A. Arnaud, C. Dagron-Lartigau, H. Medlej, R. C. Hiorns, S. Beaupré, M. Leclerc and A. Rivaton, *Polym. Degrad. Stab.*, 2015, **112**, 175–184.
14 J. W. Rumer and I. McCulloch, *Mater. Today*, 2015, **18**, 425–435.
15 V. Turkovic, S. Engmann, N. Tsierkezos, H. Hoppe, U. Ritter and G. Gobsch, *ACS Appl. Mater. Interfaces*, 2016, **122**, 255.

16 M. Helgesen, M. V. Madsen, B. Andreasen, T. Tromholt, J. W. Andreasen and F. C. Krebs, *Polym. Chem.*, 2011, **2**, 2536–2542.
17 M. Helgesen, J. E. Carlé, B. Andreasen, M. Hösel, K. Norrman, R. Søndergaard and F. C. Krebs, *Polym. Chem.*, 2012, **3**, 2649–2655.
18 E. Bundgaard, O. Hagemann, M. Bjerring, N. C. Nielsen, J. W. Andreasen, B. Andreasen and F. C. Krebs, *Macromolecules*, 2012, **45**, 3644–3646.
19 E. Bundgaard, M. Helgesen, J. E. Carlé, F. C. Krebs and M. Jørgensen, *Macromol. Chem. Phys.*, 2013, **214**, 1546–1558.
20 S. A. Gevorgyan and F. C. Krebs, *Chem. Mater.*, 2008, **20**, 4386–4390.
21 A. T. H. Koch, N. T. Harrison, N. Haylett, R. Daik, W. J. Feast and R. H. Friend, *Synth. Met.*, 1999, **100**, 113–122.
22 P. Verstappen, J. Kesters, L. D'Olieslaeger, J. Drijkoningen, I. Cardinaletti, T. Vangerven, B. J. Bruijnaers, R. E. M. Willems, J. D'Haen, J. V. Manca, L. Lutsen, D. J. M. Vanderzande and W. Maes, *Macromolecules*, 2015, **48**, 3873–3882.
23 J. Vandenbergh, B. Conings, S. Bertho, J. Kesters, D. Spoltore, S. Esiner, J. Zhao, G. Van Assche, M. M. Wienk, W. Maes, L. Lutsen, B. Van Mele, R. A. J. Janssen, J. Manca and D. J. M. Vanderzande, *Macromolecules*, 2011, **44**, 8470–8478.
24 J. Kesters, S. Kudret, S. Bertho, N. Van den Brande, M. Defour, B. Van Mele, H. Penxten, L. Lutsen, J. Manca, D. Vanderzande and W. Maes, *Org. Electron.*, 2014, **15**, 549–562.
25 I. Cardinaletti, J. Kesters, S. Bertho, B. Conings, F. Piersimoni, J. D'Haen, L. Lutsen, M. Nesladek, B. Van Mele, G. Van Assche, K. Vandewal, A. Salleo, D. Vanderzande, W. Maes and J. V. Manca, *J. Photonics Energy*, 2014, **4**, 040997.
26 S. Bertho, B. Campo, F. Piersimoni, D. Spoltore, J. D'Haen, L. Lutsen, W. Maes, D. Vanderzande and J. Manca, *Sol. Energy Mater. Sol. Cells*, 2013, **110**, 69–76.
27 B. J. Campo, D. Bevk, J. Kesters, J. Gilot, H. J. Bolink, J. Zhao, J.-C. Bolsée, W. D. Oosterbaan, S. Bertho, J. D'Haen, J. Manca, L. Lutsen, G. Van Assche, W. Maes, R. A. J. Janssen and D. Vanderzande, *Org. Electron.*, 2013, **14**, 523–534.
28 J. Kesters, P. Verstappen, J. Raymakers, W. Vanormelingen, J. Drijkoningen, J. D'Haen, J. Manca, L. Lutsen, D. Vanderzande and W. Maes, *Chem. Mater.*, 2015, **27**, 1332–1341.
29 X. Xu, Y. Wu, J. Fang, Z. Li, Z. Wang, Y. Li and Q. Peng, *Chem.–Eur. J.*, 2014, **20**, 13259–13271.
30 G. E. Morse, A. Tournebize, A. Rivaton, T. Chassé, C. Taviot-Gueho, N. Blouin, O. R. Lozman and S. Tierney, *Phys. Chem. Chem. Phys.*, 2015, **17**, 11884–11897.
31 A. Distler, T. Sauermann, H. J. Egelhaaf, S. Rodman, D. Waller, K. S. Cheon, M. Lee and D. M. Guldi, *Adv. Energy Mater.*, 2014, **4**, 1300693.
32 T. Heumueller, W. R. Mateker, A. Distler, U. F. Fritze, R. Cheacharoen, W. H. Nguyen, M. Biele, M. Salvador, M. von Delius, H.-J. Egelhaaf, M. D. McGehee and C. J. Brabec, *Energy Environ. Sci.*, 2016, **9**, 247–256.
33 F. Piersimoni, G. Degutis, S. Bertho, K. Vandewal, D. Spoltore, T. Vangerven, J. Drijkoningen, M. K. Van Bael, A. Hardy, J. D'Haen, W. Maes, D. Vanderzande, M. Nesladek and J. Manca, *J. Polym. Sci., Part B: Polym. Phys.*, 2013, **51**, 1209–1214.
34 I. Heckler, J. Kesters, M. Defour, M. Madsen, H. Penxten, J. D'Haen, B. Van Mele, W. Maes and E. Bundgaard, *Materials*, 2016, **9**, 181.
35 E. Bundgaard, F. Livi, O. Hagemann, J. E. Carlé, M. Helgesen, I. M. Heckler, N. K. Zawacka, D. Angmo, T. T. Larsen-Olsen, G. A. dos Reis Benatto, B. Roth, M. V. Madsen, M. R. Andersson, M. Jørgensen, R. R. Søndergaard and F. C. Krebs, *Adv. Energy Mater.*, 2015, **5**, 1402186.
36 F. Livi, N. K. Zawacka, D. Angmo, M. Jørgensen, F. C. Krebs and E. Bundgaard, *Macromolecules*, 2015, **48**, 3481–3492.
37 J. E. Carlé, M. Helgesen, N. K. Zawacka, M. V. Madsen, E. Bundgaard and F. C. Krebs, *J. Polym. Sci., Part B: Polym. Phys.*, 2014, **52**, 893–899.
38 K. D. Collins, A. Rühling, F. Lied and F. Glorius, *Chem.–Eur. J.*, 2014, **20**, 3800–3805.
39 L. Huo, S. Zhang, X. Guo, F. Xu, Y. Li and J. Hou, *Angew. Chem., Int. Ed.*, 2011, **50**, 9697–9702.
40 V. Dhayalan, F. Alcañiz, V. Werner, K. Karaghiosoff and P. Knochel, *Synthesis*, 2015, **47**, 3972–3982.
41 N. Wang, Z. Chen, W. Wei and Z. Jiang, *J. Am. Chem. Soc.*, 2013, **135**, 17060–17068.
42 Q. Hou, Q. Zhou, Y. Zhang, W. Yang, R. Yang and Y. Cao, *Macromolecules*, 2004, **37**, 6299–6305.
43 S. Ellinger, U. Ziener, U. Thewalt, K. Landfester and M. Möller, *Chem. Mater.*, 2007, **19**, 1070–1075.
44 During one of the workup steps of **2c**, the acetic ester was partly formed while using ethyl acetate as a solvent. The product mixture (alcohol and ester) was saponified using a sodium hydroxide solution, before continuing the synthesis.
45 A. J. Bard and L. R. Faulkner, *Electrochemical Methods: Fundamentals and Applications*, John Wiley & Sons, Inc., New York, USA, 2nd edn, 2012.
46 S. Trasatti, *Pure Appl. Chem.*, 1986, **58**, 955–966.
47 R. L. Danley, P. A. Caulfield and S. R. Aubuchon, *Am. Lab.*, 2008, **40**, 9–11.
48 S. Wouters, F. Demir, L. Beenaerts and G. Van Assche, *Thermochim. Acta*, 2012, **530**, 64–72.
49 T. Tromholt, M. V. Madsen, J. E. Carlé, M. Helgesen and F. C. Krebs, *J. Mater. Chem.*, 2012, **22**, 7592–7601.
50 M. Hösel, R. R. Søndergaard, M. Jørgensen and F. C. Krebs, *Energy Technol.*, 2013, **1**, 102–107.
51 T. T. Larsen-Olsen, R. R. Søndergaard, K. Norrman, M. Jørgensen and F. C. Krebs, *Energy Environ. Sci.*, 2012, **5**, 9467–9471.
52 H. F. Dam and F. C. Krebs, *Sol. Energy Mater. Sol. Cells*, 2012, **97**, 191–196.
53 J. E. Carlé, T. R. Andersen, M. Helgesen, E. Bundgaard, M. Jørgensen and F. C. Krebs, *Sol. Energy Mater. Sol. Cells*, 2013, **108**, 126–128.

54 F. C. Krebs, R. Søndergaard and M. Jørgensen, *Sol. Energy Mater. Sol. Cells*, 2011, **95**, 1348–1353.
55 T. Ghoos, N. Van Den Brande, M. Defour, J. Brassinne, C.-A. Fustin, J.-F. Gohy, S. Hoeppener, U. S. Schubert, W. Vanormelingen, L. Lutsen, D. J. Vanderzande, B. Van Mele and W. Maes, *Eur. Polym. J.*, 2014, **53**, 206–214.
56 M. O. Reese, S. A. Gevorgyan, M. Jørgensen, E. Bundgaard, S. R. Kurtz, D. S. Ginley, D. C. Olson, M. T. Lloyd, P. Morvillo, E. A. Katz, A. Elschner, O. Haillant, T. R. Currier, V. Shrotriya, M. Hermenau, M. Riede, K. R. Kirov, G. Trimmel, T. Rath, O. Inganäs, F. Zhang, M. Andersson, K. Tvingstedt, M. Lira-Cantu, D. Laird, C. McGuiness, S. Gowrisanker, M. Pannone, M. Xiao, J. Hauch, R. Steim, D. M. Delongchamp, R. Rösch, H. Hoppe, N. Espinosa, A. Urbina, G. Yaman-Uzunoglu, J.-B. Bonekamp, A. J. J. M. van Breemen, C. Girotto, E. Voroshazi and F. C. Krebs, *Sol. Energy Mater. Sol. Cells*, 2011, **95**, 1253–1267.
57 N. Grossiord, J. M. Kroon, R. Andriessen and P. W. M. Blom, *Org. Electron.*, 2012, **13**, 432–456.
58 A. Abdou and S. Holdcroft, *Macromolecules*, 1993, **26**, 2954–2962.
59 J. Kettle, H. Waters, Z. Ding, M. Horie and G. C. Smith, *Sol. Energy Mater. Sol. Cells*, 2015, **141**, 139–147.
60 F. C. Krebs, *Stability and Degradation of Organic and Polymer Solar Cells*, John Wiley & Sons, Ltd, West Sussex, United Kingdom, 1st edn, 2012.
61 C. Müller, E. Wang, L. M. Andersson, K. Tvingstedt, Y. Zhou, M. R. Andersson and O. Inganäs, *Adv. Funct. Mater.*, 2010, **20**, 2124–2131.
62 D. J. D. Moet, M. Lenes, J. D. Kotlarski, S. C. Veenstra, J. Sweelssen, M. M. Koetse, B. de Boer and P. W. M. Blom, *Org. Electron.*, 2009, **10**, 1275–1281.
63 T. Vangerven, P. Verstappen, J. Drijkoningen, W. Dierckx, S. Himmelberger, A. Salleo, D. Vanderzande, W. Maes and J. V. Manca, *Chem. Mater.*, 2015, **27**, 3726–3732.
64 A. Rivaton, A. Tournebize, J. Gaume, P.-O. Bussière, J.-L. Gardette and S. Therias, *Polym. Int.*, 2014, **63**, 1335–1345.
65 S. Chambon, A. Rivaton, J. L. Gardette and M. Firon, *Sol. Energy Mater. Sol. Cells*, 2007, **91**, 394–398.
66 M. Manceau, S. Chambon, A. Rivaton, J. L. Gardette, S. Guillerez and N. Lematre, *Sol. Energy Mater. Sol. Cells*, 2010, **94**, 1572–1577.
67 D. Gedefaw, M. Tessarolo, M. Prosa, M. Bolognesi, P. Henriksson, W. Zhuang, M. Seri, M. Muccini and M. R. Andersson, *Sol. Energy Mater. Sol. Cells*, 2016, **144**, 150–158.

IOP Publishing Journal of Physics D: Applied Physics

J. Phys. D: Appl. Phys. **50** (2017) 103001 (35pp) doi:10.1088/1361-6463/50/10/103001

Topical Review

Improving, characterizing and predicting the lifetime of organic photovoltaics

Suren A Gevorgyan, Ilona Maria Heckler, Eva Bundgaard, Michael Corazza, Markus Hösel, Roar R Søndergaard, Gisele Alves dos Reis Benatto, Mikkel Jørgensen and Frederik C Krebs

Department of Energy Conversion and Storage, Technical University of Denmark, Frederiksborgvej 399, 4000-Roskilde, Denmark

E-mail: surg@dtu.dk

Received 22 December 2015, revised 26 October 2016
Accepted for publication 8 November 2016
Published 7 February 2017

Abstract

This review summarizes the recent progress in the stability and lifetime of organic photovoltaics (OPVs). In particular, recently proposed solutions to failure mechanisms in different layers of the device stack are discussed comprising both structural and chemical modifications. Upscaling is additionally discussed from the perspective of stability presenting the challenges associated with device packaging and edge protection. An important part of device stability studies is the characterization, and this review provides a short overview of the most advanced techniques for stability characterization reported recently. Lifetime testing and determination is another challenge in the field of organic solar cells and the final sections of this review discuss the testing protocols as well as the generic marker for device lifetime and the methodology for comparing all the lifetime landmarks in one common diagram. These tools were used to determine the baselines for OPV lifetime tested under different ageing conditions. Finally, the current status of lifetime for organic solar cells is presented and predictions are made for progress in the near future.

Keywords: organic photovoltaics, lifetime, stability, degradation, lifetime testing, advanced characterization

(Some figures may appear in colour only in the online journal)

1. Introduction

Emerging thin film solar cell technologies, such as organic solar cells, perovskites and others alike, have a strong potential for producing very cheap energy, which is one of the key motivations for the research in these fields and it is believed that successful commercialization of the products based on such technologies may revolutionize the energy sector. One of the key criteria for commercialization of these technologies however is the achievement of the necessary level of durability and lifetime for a given application. The lifetime of the aforementioned technologies today is still not sufficient for most of energy production applications and therefore a significant effort is necessary to improve device stability in order to bring them into the market. Among these technologies some of the most prominent ones are organic photovoltaics (OPVs) and hybrid technologies, such as perovskite and dye synthesized solar cells. While this review will primarily focus on stability of OPVs and in particular polymer solar cells (PSC), many of the discussed challenges and their solutions are also applicable to the other technologies due to vivid similarities in device architectures [1].

Organic solar cells tend to lose their initial performance with time, which is due to failing of either one or several components (materials) in the device. It all comes down to two types of modifications that cause the failure of a material:

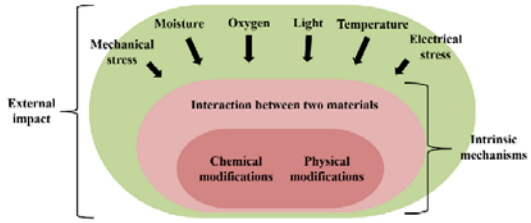

Figure 1. Diagram of the internal ageing mechanisms inside the devices and the external impact from environment is presented. The internal mechanisms are associated with the chemical and structural modifications of the materials caused by the interaction between two materials inside the device. External impact is associated with oxygen, moisture, light and electrical and mechanical stresses.

chemical and physical modifications, as will be shown further in the text. Chemical modifications are associated with alterations in the chemical structure of the molecules in the material due to reaction with another material or substance, such as breaking of the polymer bonds due to oxidation processes [2]. Physical changes are associated with structural modifications in the material structure, where the material may for example transform from crystalline into a less favorable amorphous structure with poorer electron transport properties or in the case of commonly used donor/acceptor mixture in the device, the reorganization of the mixture may lead to less favorable phase separation due to clustering of the individual components [3]. Such modifications may be caused by internal and/or external factors, as is depicted in figure 1. Internal factors are associated with reaction between two materials or substances inside the device, such as the reaction between the electrode and the active mixture in the device, or the influence of additives on the active mixture morphology etc [4]. External factors may accelerate internal processes i.e. an elevated temperature facilitate the morphological reorganization of the active mixture [5]. Elevated temperature may also grant access to new harmful processes, such as diffusion of moisture inside the device or increased corrosion rates for the metal electrodes [6]. The main external factors that are well known to deteriorate device performance are oxygen, moisture, light, temperature, mechanical and electrical stresses, and the reader is referred to a number of reviews that have discussed each mechanism in detail for each factor influencing device stability [7–13]. This review will instead focus on proposed solutions for the different failure mechanisms that have been reported recently.

The review provides a complete overview of solutions for the entire chain of stability issues ranging from material chemistry and device architecture to upscaling and characterization and complements these with an overview of the current status of OPV lifetime and predictions for the future. The review is split into several parts. In section 2 general overview of the architectural challenges of OPV devices is presented. In sections 3–5 the different layers of traditional architecture of OPV device are discussed in terms of stability by covering chemical, physical and architectural issues. This is then followed by discussions of upscaling and packaging in section 6. The final sections cover the advanced characterization of stability and measuring of the lifetime, present the status of the OPV lifetime today and make predictions for the near future.

2. Device architecture

One of the common ways of improving the stability is optimization of device architecture. The latter constitutes improved combinations, thicknesses and order of layers in the device, protected device terminals, improved packaging with appropriate edge sealing and other similar solutions. As of today the market for OPVs has not been completely defined yet and thus, there are still no existing standards for the final product architecture of these devices, which leaves a broad space for making variations in architectural modification of OPVs. However, the challenge with certain architectural modifications is that, although, these lead to lifetime improvement, such modifications may be in opposition to the envisioned architecture of an OPV end product and therefore, their usefulness may be a subject of dispute. Several examples are discussed in this section.

The use of a thick layer or even a multilayer of top evaporated electrodes has been frequently reported to significantly improve the stability of OPVs (see e.g. [14, 15]). While the method has shown orders of magnitude improvements in the stability of unencapsulated devices [16], this has primarily been demonstrated by comparing lab scale devices with a glass substrate on one side protecting the device and the top electrode on the other. Since the thick glass substrates comprise an impervious barrier with zero transmission rate for air and moisture diffusion, the top part of the device including the top electrode obviously becomes the only path for the diffusion of environmental agents and will therefore be the defining factor for the device stability. Therefore, changing the thickness of the top electrode can have a major impact on the stability of such a non-symmetric device. Similarly, changing the material of the electrode can also drastically affect the device stability, such as for example when switching from the aluminum (Al) used in normal structure devices to silver (Ag) used in inverted structures [17, 18]. In a traditionally envisioned structure of a large scale processed flexible OPV device the stack of the layers is sandwiched between two barriers with one side serving as the substrate, which allows one to avoid the additional layer of a costly substrate [19, 20]. Alternatively, a cheap polyethylene terephthalate (PET) with no barrier properties is often used as an extra substrate for the convenience of processing. In such configurations, the front transparent electrode will be equally vulnerable to environmental impact and therefore, the above suggested architectural modifications of the back electrode or the layer sequence may become useless in this case. Moreover, the non-transparent electrode on the back of the device is easier to substitute with a cheap flexible solid metal foil, while finding a cost efficient flexible transparent electrode with strong resistivity towards environmental impact for the front side of the device may be much more challenging.

Another questionable architectural modification is associated with sample dimensions. Often, laboratory scale

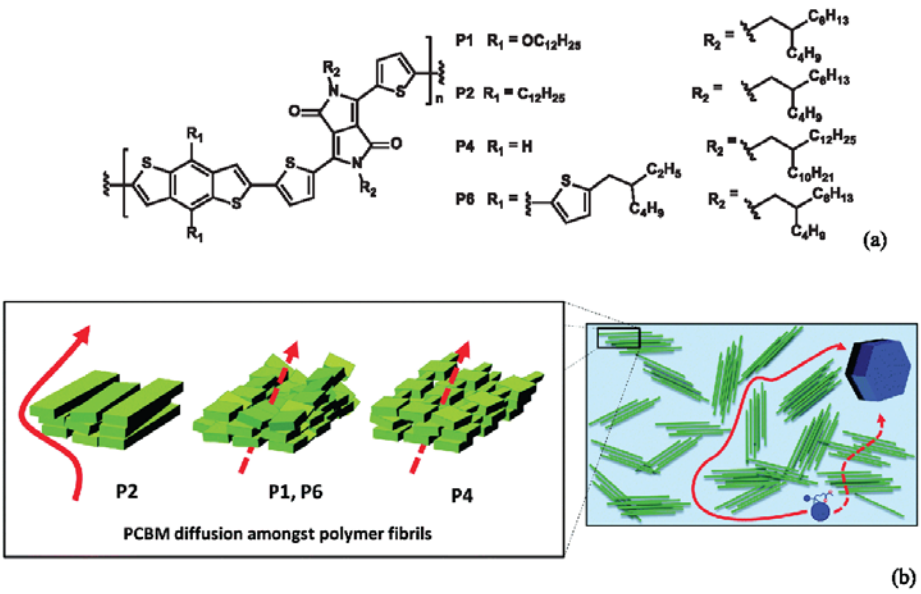

Figure 2. Illustration of different polymer (a) aggregate formations based on side chain distribution and rotation ((b), left). In a BHJ material these aggregates regulate the transport of PCBM which can either pass around the aggregates or through them ((b), right). Reprinted with permission from [27]. Copyright 2015 Royal Society of Chemistry.

samples of 1 cm^2 and smaller, packaged in much larger barrier materials are used for stability measurements. While these are useful for comparing the stability of the particular samples with other samples of similar nature, due to the edge diffusion effects the obtained stability data cannot be utilized for assessing the potential of the technology in terms of lifetime, since the actual end products (in forms of modules and panels) will not have the same dimensional ratio between the device and packaging and may therefore be prone to stronger edge effects.

One of the most important assets of OPVs is the potentially low cost of the technology, and while new materials or material modifications are often reported, which significantly improve the stability of OPV devices, in most cases it remains unclear whether such materials are cheap or can be made cheaply available eventually, as a majority of the reports do not discuss this subject.

It is therefore recommended to always bear in mind the eventual product design and competitiveness while carrying out any architectural modifications for improving the device performance.

3. Photoactive layer

This section discusses the recent achievements related to the improvement of the stability of the active layer by chemical or physical modifications. While section 3.1 covers the chemical solutions used for improving the material properties, section 3.2 addresses the effects related to structural alterations and the external impact.

3.1. Recent chemical advances

In recent years many articles and reviews have addressed the stability of polymer solar cells (PSCs) with a specific focus on the chemical manipulation of the materials used in PSCs to improve the thermal and morphological stability for a longer lifetime of the PSCs [9, 10, 21–24]. Different pathways of degradation make it necessary to be creative in terms of material manipulation which can lead to their stabilization. In this section recent chemical improvements are shown for improving the stability of the photoactive layer (PAL) against both intrinsic and extrinsic ageing mechanisms. The section is divided into three parts, one discussing new approaches to improve the stability of the PSCs by chemical diversification of the side chains, the other considering the backbone alterations of the light absorbing polymers and the third part discussing the acceptor materials.

3.1.1. Chemical diversification of the side chain of the light absorbing polymer. As the side chains in organic materials represent a weak point in the light absorbing layer, several new approaches have been presented recently that address this issue. Peng *et al* [25] investigated the influence of the branching (linear or branched) and dimensionality (alkoxy or thienyl) of the side chains of a polymer based on benzodithiophene (BDT) and monofluorinated quinoxaline (Qx) on its thermal stability. The 2D conjugated structures were shown to increase the thermal stability of the polymer. An increased degree of branching induces higher lamellar-like ordering of the polymer, leading to a more stable PAL. However the research was performed on the pure polymer and not on a polymer:PCBM blend nor

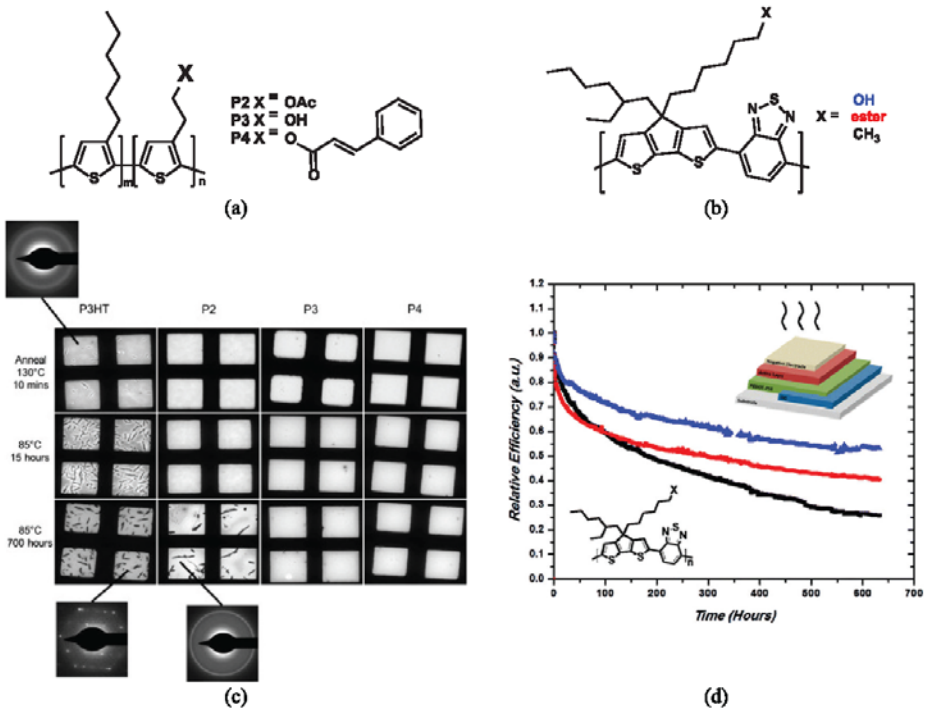

Figure 3. Molecular structure of modified a polythiophene (a) and a CPDTBT based polymer (b), TEM and SAED images of PT based:PCBM blends (1:1) degraded at 85 °C (c) [32] and the thermal degradation of the efficiency of PSCs based on CPDTBT polymers with different side groups stored in nitrogen at 85 °C (d). (c) Reprinted with permission from [32]. Copyright 2014 Elsevier. (d) Reprinted with permission from [34]. Copyright 2014 American Chemical Society.

on a PSC [25]. Similarly, Tournebize *et al* reported a study on poly[(benzo[1,2-b:4,5-b]dithiophene)-alt-(thieno[3,4-c] pyrrole-4,6-dione)] (PBDTTPD) and while comparing the photostability of this polymer with traditional polymers discovered that PBDTTPD significantly outperformed the others [26]. The reason was ascribed to the fact that the alkoxy side-chains on BDT subunits mitigate the photodegradation of the whole polymer. Tierney *et al* [27] investigated the impact of different types of side chains on the (photochemical) stability of BDT-diketopyrrolopyrrole (DPP) based PSCs (figure 2). The stability of the bulk heterojunction (BHJ) is controlled by two different processes: the PCBM crystallization and dimerization, which means that the stability depends on the rate of crystallization. The authors claimed that this could be influenced by the type of side chains; whereas the stability decreases from linear alkyl side chain > no side chains > alkoxy side chains > branched side chains. The branched side chains cause steric hindrance in solid films, locking the polymer chain in place and reducing the paths in the 3D space for the fullerene diffusion. An increase of the steric hindrance as well as the rotational freedom can be seen for the alkoxy and thienylethylhexyl side chains. However, polymer with linear side chains are the most stable ones due to an even distribution of the chains along the backbone and dense packed polymer aggregates, where no PCBM molecule can migrate through (figure 2), leading to a low diffusion rate for the series due to thermal instability of the polymer:PCBM BHJ [27]. Not only the type of side chain but also the different length of the conjugated side chains is directly influencing the thermal and morphological stability of the devices. The study by Yang *et al* [28] deals with the use of different amounts of thiophenes in the side chain of BDT. The alkyl-thienothiophene substituted polymer with the longest side chain revealed the optimal morphology and best thermal stability in comparison to alkoxy and alkyl-thiophene substituted polymers.

Maes *et al* [29] reduced the side chain density in a polymer based on cyclopentadithiophene (CPDT) and Qx leading to a PSC with increased efficiency and device stability under continuous thermal stress. This tuning of the side chain pattern led to an optimized morphology of the PAL [29].

The immutability of the morphology of the BHJ to have an optimal function of the solar cell is one of the main focuses of the chemical diversification of light absorbing polymers. Instability of the BHJ morphology is often a result of prolonged thermal annealing leading to a phase separation/demixing of the polymer and PCBM (crystallization of the PCBM). One approach would be to do a side chain functionalization/modification to yield a polymer with higher glass transition temperature (T_g). This has already been done in 2011 by Vanderzande *et al* [30] on a polyphenylvinylene (PPV) derivative using a phenylethoxy side chain. Recently this concept was adopted (also from the same group) [31] and applied to various more promising (advanced conjugated) polymers for PSCs. The usage of alcohol or ester (and cinnamoyl) groups as part

of the side chains of polythiophene (figure 3(a)) [21, 31–33] or a polymer based on CPDT and benzothiadiazole (BT) (figure 3(b)) [34] resulted in a higher T_g and thus an enhanced thermal stability (figure 3(a)). In the case of polythiophene (PT) the specific functional moieties were introduced in a small ratio (10%) into a random poly(3-alkylthiophene) improving the thermal stability significantly through a decay in demixing of the PAL [21, 31–33]. The phase separation and morphology development are shown in the images of transmission electron microscopy (TEM) and selected-area electron diffraction (SAED) patterns (figure 3(c)) [32]. In the case of the CPDT based polymer the specific functional groups are incorporated into the whole polymer. These results show an absence of phase separation and crystallization as well as an enhancement in the long-term stability of the solar cell parameters, as shown in figure 3(d) for samples stored in nitrogen at 85 °C temperature [34]. However, the adoption of this concept on advanced conjugated polymers (like polymers based on BT or thiazolothiazole) using the phenethyl group to partially exchange the solubility side chain, did not lead to a clear enhancement of the stability of the BHJ PSCs [35]. This means that this approach cannot be applied to all suitable advanced conjugated backbones for PSCs.

In another approach the alcohol moieties were used to crosslink with another molecule. Shiao *et al* described a series of maleimide-thiophene copolymers containing partial 2-hydroxyethyl or 6-hydroxyhexyl units, which were cross-linked with 3,3′-dimethoxy-4,4′-biphenylene diisocyanate (DMBPI) leading to an increased thermal stability [36].

3.1.2. Chemical diversification of the light absorbing polymer backbone. The structure of the polymer backbone can also have an influence on the stability of the PSCs. However, this influence is not as drastic as it is for the side chains. It is already well known that the stability depends on the monomer units. For example a polymer containing fluorene is less stable than a polymer containing BDT as the donor unit [24, 37]. Gedefaw *et al* studied a series of p-type copolymers, which combined a fluorinated quinoxaline (FQ) acceptor unit either with a differently substituted BDT or an unsubstituted thieno[3,2-b]thiophene (TT) and showed their effect on both film and device stability [38]. In particular, the authors demonstrated that while in the form of pristine films the polymer with TT showed the best photostability, in the form of devices the polymers with BDT led to the most stable devices retaining 85% of the performance after 72h of light exposure. In another study dithienobenzodithiophene (DTBDT) donor was fused with 2-ethyl-1-(thieno [3,4-b] thiophen-2-yl) hexan-1-one (TTEH) or 6-octyl-5H-thieno [3′,4′:4,5] thieno [2,3-c] pyrrole-5,7 (6H)-dione (DTPD) acceptor units and the stability was investigated. Due to its flat structure pDTBDT-TTEH formed a crystalline structure, while pDTBDT-DTPD had a highly twisted structure resulting in very amorphous structure and therefore, the former significantly outperformed the latter in terms of shelf life highlighting the importance of the morphology in the stability [39]. Hou *et al* [40] showed that there is also an influence of the chemical structure of the backbone units. A polymer which contains two fused thiophenes is

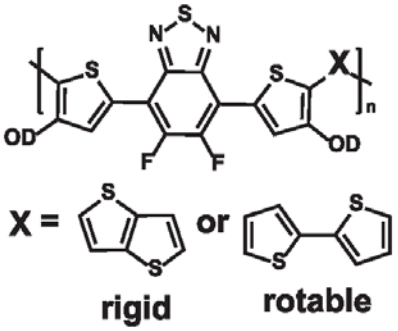

Scheme 1. Polymers with different backbone structures.

theoretically more thermodynamically stable, than a polymer with two non-fused thiophenes (scheme 1). The more rigid and stable backbone confirmation is more stable thermodynamically. The thermal properties (melting and crystallization temperatures) are also higher.

Further, direct substituents on the monomer units can influence the stability of the polymers. In another study Carlé *et al* [41] showed that with an increasing number of fluorine substituents on a BT unit in two different polymer groups, the photochemical stability of the polymers were clearly enhanced. As a result the incorporation of fluorine substituents in the polymer backbone has a positive effect on the stability of the solar cell devices. Similar results were shown by Livi *et al* (figure 4) and Li *et al* demonstrating clear enhancement of the efficiency and stability of such PSCs (figure 4) [42, 43].

Other ways to stabilize the intrinsic stability of the donor have been the use of polythiophene block copolymers selectively functionalized with isoorotic acid moieties and a diaminopyridine tethered fullerene derivative (PCBP), which showed strong complexation through hydrogen bonding. A solar cell was fabricated by Li *et al* employing the polythiophene block copolymers with issoorotic acid moieties and by varying the amount of PCBP and PCBM. The authors found that such complementary hydrogen bonding not only led to improved device stability, but also to tunable and long-range ordered morphologies by adjusting the amount and nature of fullerene derivatives [44].

3.1.3. Chemical diversification of the acceptor molecules in the photoactive layer. In the processing of the PAL in the solar cells specific solvent additives are often used to influence the morphology of the PAL and thus the efficiency of the PSCs. This principle is similar to adding or (partially) exchanging (10–15%) the PCBM with small molecules to influence (the morphology and thus) the stability of the PAL. In the approach of Chuang *et al* [45], a cross-linkable open-cage fullerene (scheme 2(a)) was partially incorporated into the PAL. The cross-linking can be induced via heat treatment of the styryl moiety resulting in a longer lifetime of the correspondent PSCs under thermal stress. Cross-linkable azido C60-fullerene derivatives were also used in poly(3-hexylthiophene) P3HT and PCBM mixture based solar cells to drastically suppress the formation of PCBM crystals in the BHJ and macro-phase separation, leading to a very stable morphology [46].

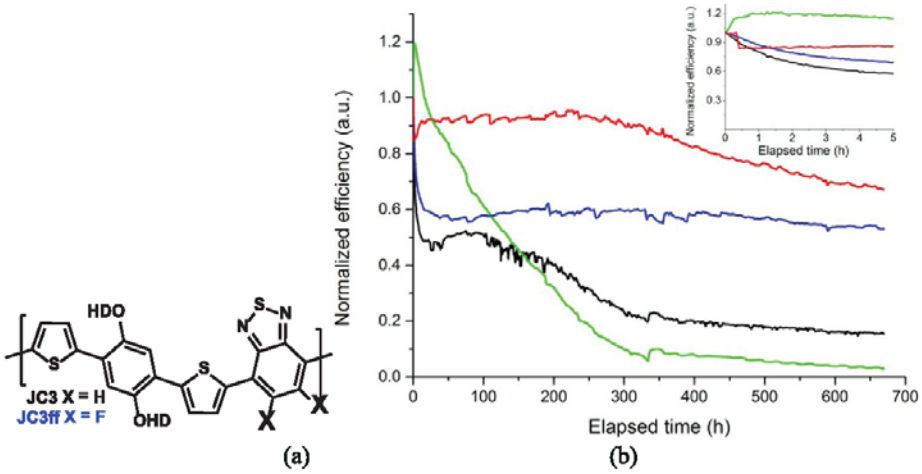

Figure 4. Lifetime studies of JC3 (black in (a) and (b)), JC3ff (blue in (a) and (b)) and poly(3-hexylthiophene) P3HT (green in (b)). (Red curve in (b) is beyond the scope of this review). The encapsulated samples were exposed to 1.2 Sun light illumination at 130 °C temperature. Reprinted with permission from [43]. Copyright 2015 American Chemical Society.

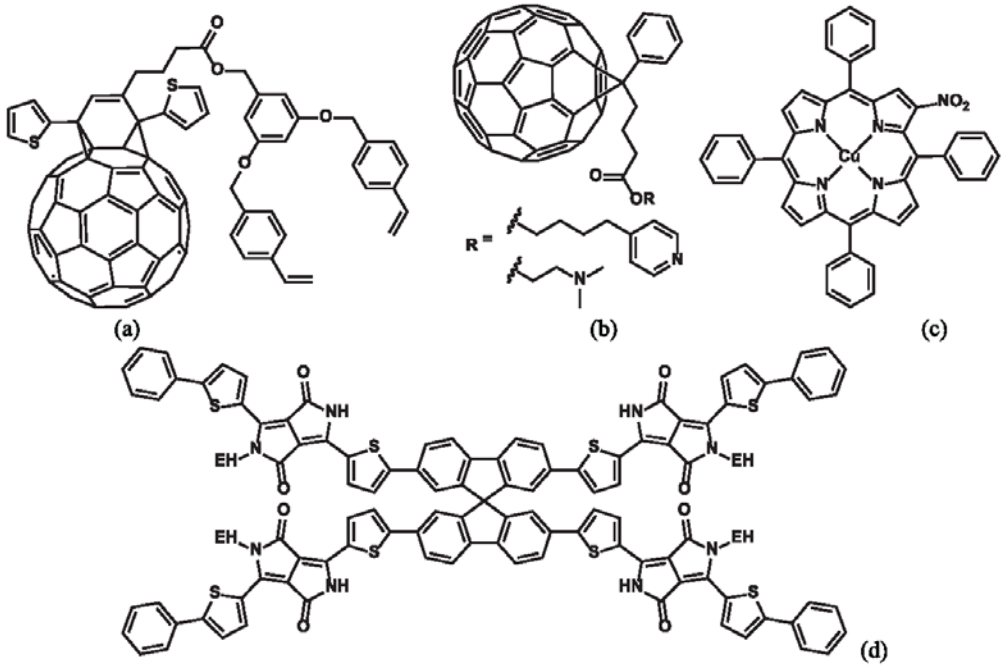

Scheme 2. Small molecule additives to the PAL (cross-linkable open cage fullerene [45] (a), and PCBM derivatives [47] (b) and porphyrin compound [48] (c) and PCBM replacement (spirobifluorene [49] (d)) to improve the stability of the PSC.

Andersson *et al* [47] modified fullerenes with pyridine and amine groups, respectively (scheme 2(b)). Partial incorporation of these fullerene derivatives into the PAL blend of a thiophene-Qx donor polymer:PCBM shows a significant increase in the thermal stability of the BHJ nanostructure, where the fullerene crystallization is hindered at the annealing temperature. In addition, these materials can also be used as self-assembling interlayers on the indium tin oxide surface.

Another strategy to prevent fullerene aggregation is to stabilize the PAL via incorporation of a porphyrin compound. This addition does not only stabilize the morphology of the polymer:PCBM film, but depresses the PCBM crystallization.

After discovering that these compounds are sufficient for PSC stability [50], Yang *et al* [48] performed a small screening of different porphyrin compounds including different metals (Cu, Zn, Ni, non-metallized) or different substituents (NO_2, C_4F_6Cl, non-substituent) to see the influence on self-aggregation and photo-thermal stability. The PSC (P3HT:PCBM), which was doped with 8 wt% of the most promising porphyrin compound (scheme 2(c)), showed the smallest decrease in efficiency preserving 83% of initial photoconversion efficiency (PCE) after 48 h at 130 °C in comparison to the pristine devices, which retained 28.4% after 3 h at 130 °C [48]. Liao *et al* developed a [6,6] phenyl-C 61 butyric acid pentafluorophenyl ester ($PC_{61}BP^F$) used together with PCBM. Such a mixture is responsible for creating a supramolecular attraction between the pentafluorophenyl group of $PC_{61}BP^F$ and the C60 cores of $PC_{61}BP^F$/PCBM, which can prevent the $PC_{61}BP^F$/PCBM materials from severe aggregation [51]. By doping only 8.3 wt% ($PC_{61}BP^F$), in a P3HT:PCBM device, a PCE of 3.68% was reached after 25 h of heating at 150 °C, preserving 95% of its original value. In sharp contrast, the PCE of the device that used a traditional P3HT:PCBM blend decayed drastically. Such an approach was effective also with a low band-gap polymer such as PDTBCDTBT, which is based on dithienobenzo-carbazole (DTBC).

To prevent fullerene crystallization in the PAL, the PCBM can be replaced by a fullerene free material. After a decade of slow progress, non-fullerene acceptors are now undergoing rapid development and are emerging as a focus area in the field of organic semiconductors [52]. The novel non-fullerene electron acceptor spirobifluorene with four diketopyrrolopyrrole endcapped with a benzene ($SF(DPPB)_4$) (scheme 2(d)) was designed to suppress strong intermolecular aggregation. Excellent thermal stability was shown upon thermal treatment of the P3HT:$SF(DPPB)_4$ PSC at 150 °C for 3 h. Its efficiency remained unchanged, whereas the efficiency of the fullerene based PSC dropped significantly [49]. In another study, as an acceptor {[N,N0-bis(2-octyldodecyl)-naphthalene-1,4,5,8-bis(dicarboxi-mide)-2,6-diyl]-alt-5,50-(2,20-bithiophene)} (P(NDI2OD-T2)) was used and as a donor 7,70-(4,4-bis(2-ethylhexyl)-4H-silolo [3,2-b:4,5-b0]dithiophene-2,6-diyl) bis(6-fluoro-4-(50-hexyl-[2,20-bithiophen]-5-yl)benzo[c] [1,2,5]-thiadiazole), p-DTS ($FBTTh_2)_2$ was used, which led to a device exhibiting excellent thermal stability in air without encapsulation preserving 70% of its initial performance after heating at 180 °C for 20 h (see a comparison with other polymers in figure 5) [5].

Chen *et al* [53] used ter(ethylene oxide) (TEO) functionalization to manipulate the polymer donor (P-BDTT-TT-TEO) and fullerene acceptor (PCB-TEO) [53]. The TEO side chains induce more ordered molecular packing leading to a well-defined morphology and enhanced stability of the PAL. PCB-TEO is an effective compatibilizer located at the interface of the acceptor and donor to strengthen and manipulate the interaction between PCBM and PBDTT-TT-TEO (figure 6(I)). Direct blending of the TEO manipulated acceptor and the donor results in poor performance. Therefore, an appropriate amount (5%) of PCB-TEO was incorporated in the PAL blend. Thermal stability in inert atmosphere of the

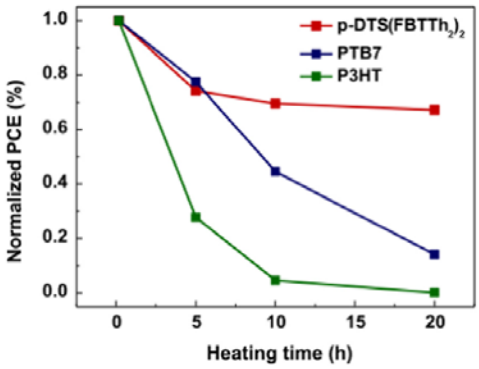

Figure 5. Degradation curves of unencapsulated devices with different polymers coupled with the acceptor P(NDI2OD-T2) tested in air. The heating temperature was 180 °C and was applied before the deposition of the front electrode. Reprinted with permission from [5]. Copyright 2015 Elsevier.

different PSCs (figure 6(II)) and films (figure 6(III)) showed increased stability with the incorporation of TEO in acceptor or acceptor and donor. This approach is very promising in terms of thermally stable devices with well-defined and stable morphology [53].

Table 1 outlines the improvements discussed above. It is difficult to pinpoint the best solutions among the reported data, since the conducted tests and samples vary greatly and therefore, are incomparable. The comparability for the general lifetime of OPV devices was addressed in 2011 by developing ISOS testing guidelines, which will be discussed in section 7. It would however be relevant in addition to ISOS guidelines to develop common testing procedure for determining film photostability. This would allow for the easy comparison and determination of the reported chemical modifications of the films that lead to the best photostability.

3.2. Structural properties and external impact

This section addresses the studies related to the structural and morphological aspects of PAL stability and is split into three parts. The first part primarily deals with structural and morphological modifications within the active mixture and the effect of the third components. Such changes often originate from the properties of the materials and are not linked to external impact. The discussion in the second part is oriented more towards the impact of the external agents on the PAL and presents certain solutions for making the PAL more resistive towards such agents. The final part addresses the mechanical properties of the PAL.

3.2.1. Intrinsic stability: additives and ternary blends. In a bulk heterojunction of polymer solar cell an optimal interpenetrating network of donor and acceptor is a key for optimal performance. However, the morphology of such a network often is not stable and may deteriorate after certain period of operation or storage resulting in device performance decay. It is therefore vital to develop methods for stabilizing the

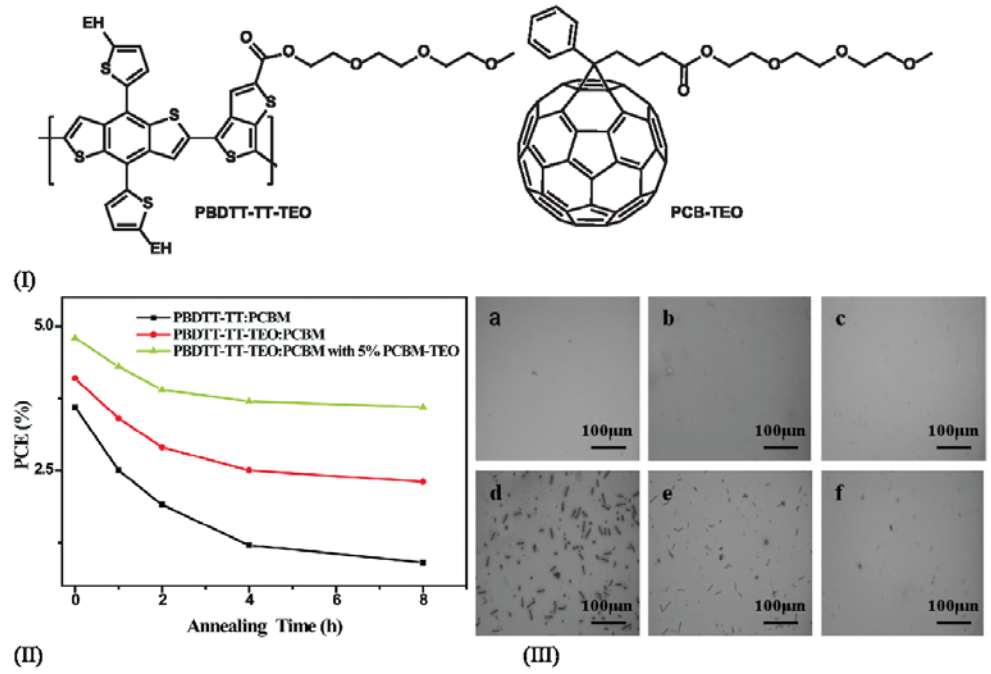

Figure 6. (I) Illustration of the TEO modified polymer and fullerene derivative (PBDTT-TT-TEO and PCE-TEO), (II) lifetime of PSCs based on these materials in terms of their PCE under 150 °C and inert atmosphere and (III) optical micrographs of films based on PBDTT-TT:PCBM (a and d), PBDTT-TT-TEO:PCBM ((b) and (e)) and PBDTT-TT-TEO:PCBM:PCB-TEO ((c) and (f)) before ((a)–(c)) and after ((d)–(f)) annealing at 150 °C for 8 h. The dark areas correspond to PCBM crystals. Reprinted with permission from [53]. Copyright 2014 Royal Society of Chemistry.

morphology of the mixture in order to preserve the optimal performance for extended period of time. As was discussed in section 3.2 optimizing the side chains is one way to improve the morphological stability of the film. On the other hand, solvent vapor annealing was also found to have a strong influence on both efficiency and stability, by altering the blend morphology [54]. However, while the additive can improve the PCE, it often impacts the stability negatively. For example, when 1,8-diiodoctane (DIO) was used as a solvent additive in active mixture of poly[[4,8-bis [(2-ethylhexyl) oxy]benzo[1,2-b:4,5-b′] dithiophene-2,6-diyl] [3-fluoro-2-[(2-ethylhexyl) carbonyl] thieno[3,4-b] thiophenediyl]] (PTB7) and PCBM [55] or poly[2,6-(4,4-bis-(2-ethylhexyl)-4H-cyclopenta [2,1-b;3,4-b′]dithiophene)-alt-4,7(2,1,3-benzothiadiazole)] (PCPDTBT) and PCBM [56], it significantly improved the efficiency of the devices, but reduced the stability bringing the samples to the same level of PCE after prolonged exposure to air for 300 h. Meanwhile in another study, Huang *et al* reported that using the poor anti-solvent isopropanol (IPA) during the spin coating of poly[4,8-bis(5-(2-ethylhexyl)thiophen-2-yl) benzo[1,2-b;4,5-b′] dithiophene-2,6-diyl-alt-(4-(2-ethylhexyl)-3-fluorothieno[3,4-b] thiophene-)-2-carboxylate-2-6-diyl)] PBDTTT-EFT (also known as PCE10) and $PCBM_{[70]}$ helped remove the residual DIO and led to an improved photochemical stability [57]. Kettle *et al* instead looked at alternative additives while studying PCPDTBT polymer, which would be less harmful for stability and proposed less volatile napthalene-based additives, such as 1-bromo-naphthalene (BrN) or 1-chloro-naphthalene (ClN) for improving PAL performance [58]. The authors demonstrated that, although these additives increased the surface roughness of the active films resulting in somewhat reduced PCE, the stability was improved by a factor of 3. The improvement was ascribed to reduced morphological changes and reduced oxidation of the thiphene ring. It was also possible to employ additives that promoted a cross-link. Khiev *et al* effectively improved the thermal stability by using a poly(3-hexylthiophene) (P3HT) end-capped with anthracene (P3HT-A) in a blend with PCBM, treaded with UV light. It was proposed that the P3HT-A chain reacts with PCBM fullerene via a [2 + 2] cyclo-addition to stabilize the blend. When comparing the UV-cured device with the device without UV treatment, only the latter presented large fullerene crystallization after thermal ageing [59]. Therefore, efforts were made on stabilizing the donor and/or the acceptor, as they both had a major role in the stabilization process.

Another example of intrinsic instabilities in photoactive material has been reported recently by Bracher *et al* [60]. The authors studied the effect of the residual palladium catalyst left inside the material from the synthesis of poly[*N*-9′′-heptadecanyl-2,7-carbazole-alt-5,5-(4′,7′-di-2-thienyl-2′,1′,3′-benzothiadiazole)] (PCDTBT) on the efficiency and stability of the devices based on this material and revealed that palladium self-assembles into nanoparticles, which initiate the growth of

Table 1. Overview of all chemical diversifications in this review.

Affected molecule[a]	Affected unit[b]	Comparison/ realization[c]	Chemical diversification	Effect on stability/morphology	Ref
Diversification in donor/polymer					
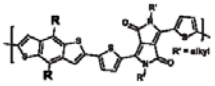	Side chain	Dimension	**R** = no/**linear**/branched/ alkoxy/alkyl-thiophene	Even distribution (=linear alkyl chain) → reduces the PCBM diffusion rate → more stable polymer solar cell	[27]
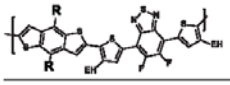	Side chain	Dimension	**R** = alkoxy/ alkyl-thiophene/ **alkyl-thienothiophene**	Increasing number of thiophene → improved morphological/thermal stability	[28]
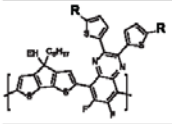	Side chain	Reduction	copolymer with **R** = EH and **R** = **H**	Partly removal of the side chains → enhances the thermal stability → more fine intermixed blends	[29]
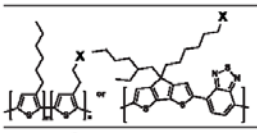	Side chain	Doping/ exchange	**X** = ester or **alcohol** group	(Partly) incorporation → increase of the glass transition temperature → enhances thermal and morphological stability	[21, 31–34]
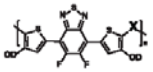	Back-bone	Fused/ non-fused	**X** = bisthiophene or **thienothiophene**	Fused thiophenes: more rigid backbone/ stable confirmation → higher melting and crystallization temperatures → stronger interchain interaction.	[40]
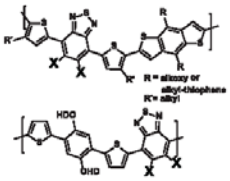	Back-bone	Doping	**X** = hydrogene or **fluorine**	Fluorination of benzothiadiazole → better photochemical stability of the polymer → slower decay rate of the PSC device	[41, 43]
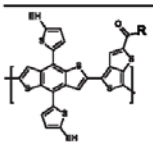	Side chain	Exchange	**R** = **ter(ethylene oxide)**	Functionalized copolymer (and fullerene acceptor) → changes morphology → manipulates miscibility between polymer and fullerene → more thermally stable PSCs.	[53]
Diversification in acceptor/PCBM (see scheme 2 and figure 6)					
PCBM	Side chain	Doping	Cross-linkable group	Addition of crosslinkable fullerene → reduce the PCBM phase aggregation rate → highly stable PSCs.	[45]
PCBM	Side chain	Doping	Pyridine or amine groups	Addition of functionalized fullerene → hinders the PCBM crystallization → increased thermal stability	[47]
PCBM	Molecule	Doping	Porphyrin	Addition of porphyrin → supramolecular interactions → depresses PCBM crystallization (decreased T_m and increased T_c) → stabilized morphology.	[48, 50]
PCBM	Molecule	Exchange	Spirobifluorene	Non-fullerene electron acceptor → suppressed intermolecular aggregation → improved thermal stability.	[49]
PCBM	Side chain	Doping	Ter(ethylene oxide)	See the entry in row 7 above, in this table (side chain, exchange)[d]	[53]

[a] Chemical structures: EH = 2-ethylhexyl, OD = 2-octyldodecyl, PCBM = phenyl-fullerene (C61 or C71)-butyric acid methyl ester, P3HT = poly(3-hexylthiophene), PEDOT:PSS = poly(3,4-ethylenedioxythiophene)-poly(styrenesulfonate);
[b] part of the molecule is which is affected by the chemical diversification,
[c] comparison or realization which affected the molecule part,
[d] effect is only described with the manipulation of both polymer and PCBM.

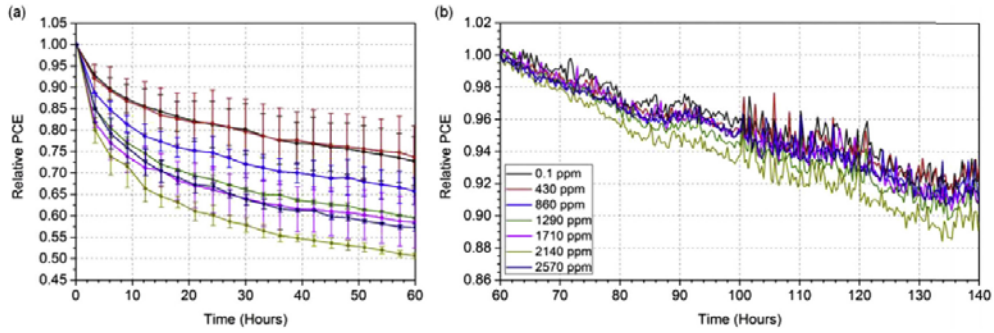

Figure 7. The ageing of encapsulated samples with various concentrations of palladium as a function of exposure to light in air. Reprinted with permission from [60]. Copyright 2015 Elsevier.

large aggregates inside the polymer. The authors used photocurrent mapping to demonstrate that such aggregates result in shunts in the device which reduces the photocurrent and contributes in the rapid initial burn-in of the device performance (see figure 7) during light soaking in air.

A relatively new branch of organic solar cells (OSCs) consist of PAL with a third component besides the donor and acceptor (organic or inorganic, semiconductor or insulator). Cheng *et al* presented a broad review of different third components that have been used in OPVs and argued that the use of such an extra component allowed for broader and stronger absorption, more efficient charge transport pathways, better charge extraction at the electrodes and improved stability [61]. The reason for the better stability was attributed to the fact that fullerene tends to aggregate into big clusters after some time or after thermal treatment, which deteriorates the morphology of the active layer and reduces the PCE drastically. The use of a third component can suppress aggregation of PCBM by means of solidifying the morphology of the active layer as a cross-linker, or freezing the scale of phase separation via some special intermolecular interactions. For example, PTB7:$PCBM_{[60]}$ degraded by more than 80% after 16 h of exposure to thermal heating at 150 °C, while the same device with the third component of 2 wt% bis-azide cross-linker 4,4′-bis(azidomethyl)-1,1′-biphenyl (BABP) degraded only by 20% after the same thermal exposure [61, 62]. Another way to increase both performance and stability is to incorporate Ag and Al nanoparticles (NPs) into the active layer [63, 64]. In poly(p-phenylene-ethynylene)-alt-poly(p-phenylene-vinylene):phenyl-C61- butyric acid methyl ester (AnE-PVstat:PCBM)-based bulk heterojunction solar cells, by incorporating Ag NPs of 6 nm in diameter in the PAL, the PCE was increased from 2.46% to 3.10%. Moreover the devices were tested under indoor solar simulator, showing a threefold improvement in stability with the Ag NPs [64].

3.2.2. Resistance against extrinsic impact. It is well established that agents, such as oxygen and water combined with light, significantly affect the stability of polymer solar cells, and resistance towards these agents is described here as extrinsic stability. The morphology of the active layer not only influences the intrinsic, but also the extrinsic stability. One of the recent works demonstrated for instance how the more crystalline and denser materials showed improved stability towards light exposure compared to more amorphous materials [65]. In particular, when crystalline and amorphous materials were compared, only the amorphous materials showed a significant decrease of open circuit voltage (V_{OC}) after ageing [66]. This was explained by the energy state disorder caused by light induced traps. In amorphous materials, the energy state disorder has a significant influence on V_{OC}, while in the crystalline materials since the charge carrier density is higher several times such a disorder does not play a major role [67]. Oxygen is known to cause drastic degradation, especially in combination with light [68]. The use of single-crystalline P3HT nanofibril with tightly packed π–π bonding was found to effectively reduce the permeation of oxygen, which led to an improved stability compared to standard P3HT. In particular, after 30 d of constant sunlight illumination, the standard P3HT lost 80% of its initial performance, while the nanofibril one only 20% [69].

Using hindered phenols as additives, substantial improvement of the stability was achieved for samples exposed to 1000 W m^{-2} constant illumination under ambient condition. In particular, the use of octadecyl 3-(3,5- di-tert-butyl-4-hydroxyphenyl)propionate in P3HT:PCBM solar cells led to increased power by a factor of 3, compared to the reference device without the stabilizing additive. Turkovic *et al* suggested the hydrogen donation mechanism in combination with the radical scavenging properties of the propionate type hindered phenols was responsible for the significant reduction of radicals within the photoactive layer, which could in turn stabilize the performance by decreasing the exciton recombination [70].

A common issue for OPVs is the quick drop in performance experienced during the initial stage of ageing, which is called 'burn-in'. Voroshazi *et al* suggested that burn-in depends on the external impact and in particular is light dependent [71]. By altering the thickness or the acceptor in the bulk of active mixture they found that upon continuous illumination of P3HT:$PCBM_{[60]}$ cells, the burn-in, which was mostly caused by the drop in the short circuit current density (J_{SC}), was due to the ageing of the active bulk, while in PCDTBT:$PCBM_{[70]}$ the drop in the efficiency mostly originated from the drop

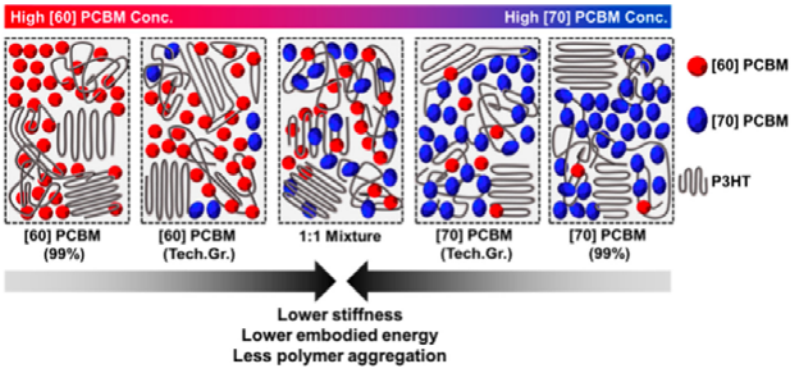

Figure 8. Schematic summary of the effect of mixed grades of methanofullerenes on the mechanical properties of P3HT:methanofullerene blends. Reprinted with permission from [76]. Copyright 2015 American Chemical Society.

in the fill factor (FF) due to the blend/anode interface degradation. The authors suggested that a stable device without burn-in is possible by accurately engineering the employed materials. Meanwhile, Kong *et al* by selectively extracting the trap-free high molecular weight components in PCDTBT showed that it is possible to reduce the burn-in loss and the resulted optimized device showed burn-in free behavior with 40% increased performance [72].

3.2.3. Mechanical stability. In recent years, the interest in studying and solving issues related to the mechanical stability of OSC is rapidly growing, since roll-to-roll (R2R) printed flexible devices are often subjected to high mechanical stress during processing and handling, which may impair device stability. Kim *et al* studied the mechanical stability of the photoactive layer of OPVs and proposed a method for improving the mechanical and thermal stability of PAL by adding the novel compatibilizer poly(3-hexylthiophene)-graft-poly(2-vinylpyridine) (P3HT-g-P2VP) in the active blend of P3HT and fullerene derivative [73]. This led to a better interface between P3HT and the fullerene derivative, which improved both thermal stability and as a result, the cell having 5% P3HT-g-P2VP, lost less than 10% of its initial performance after 72 h of thermal ageing at 150 °C compared to almost full degradation of the reference device without the compatibilizer. Moreover, while studying the mechanical properties the authors recorded around a 20% increase in the fracture energy in the blend, indicating a much more mechanically stable device.

Corazza *et al* studied the effect of external stresses, such as heat, UV light or humidity exposure on the mechanical properties of different layer in the device [74]. It was found that the combination of humidity and annealing (45% RH and 85 °C) caused the growth of macrostructures in the active layer exposed directly to these conditions resulted in the development of a weak layer within the bulk leading to a mechanically unstable layer. Interestingly, when UV light exposure was added to the experiment, the mechanical deterioration of the PAL by the external stresses was reduced. This was ascribed to the fact that the UV light may have dried the samples and therefore protected it from the impact of humidity. The authors suggested that optimized treatment of the device with different external stressors may eventually lead to a more stable device. In another study, Kim *et al* substituted fullerene with poly[[N,N′-bis(2-hexyldecyl)-naphthalene-1,4,5,8-bis(dicarboximide)-2,6-diyl]-alt-5,5′-thiophene] P(NDI2HD-T), which not only improved the efficiency, but also significantly enhanced the strength and flexibility of the PAL, with an improvements of 60 and 470 times, respectively in elongation at break and toughness [75]. Such an improvement originated from the fact that the polymer based acceptor is intrinsically more ductile and is therefore better able to entangle with the polymer chains of the donor. Savagatrup *et al* studied the different mixtures of fullerenes $PCBM_{[70]}$ and $PCBM_{[60]}$ in varying rations in the active blend with P3HT polymer and analyzed the effect of the different ratios on the mechanical stability of the blend [76]. The studies revealed that the films of pure $PCBM_{[70]}$ had approximately five times higher mechanical compliance (robustness, flexibility and stretchability) than films of pure $PCBM_{[60]}$. It was also found that BHJ films comprising technical grades (with purity of ⩾90%) of $PCBM_{[60]}$ or $PCBM_{[70]}$ were approximately two to four times more compliant compared to 99% purity. This proved that that technical grade not only lowers the cost of manufacturing, but may simultaneously increase the mechanical stability of the film and the device. The smallest range of stretchability was found for BHJs with 99% $PCBM_{[60]}$ (fracture at 3.5% strain), while the greatest was found for technical grade $PCBM_{[70]}$ (11.5% strain) (see figure 8). The same authors proposed in another article a rational way of designing molecularly stretchable electronics, in order to ideally allow a chemist to synthesize a material that could exhibit both the mechanical and electronic properties required for a particular application [77]. The idea was to design materials that allowed for the best compromise of compliance and charge mobility. For example, poly(3-heptylthiophene) (P3HpT) which combines low-T_g amorphous domains, but well-ordered crystalline domains, is reported to be the most efficient and most elastic material considered in the study.

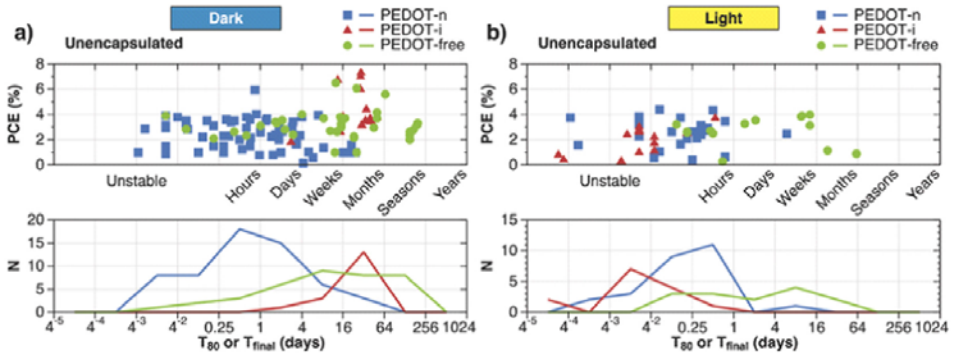

Figure 9. Distribution of lifetimes for unencapsulated samples grouped into three categories: samples with PEDOT:PSS between the anode and the PAL in the normal architecture (blue squares), between the PAL and anode in the inverted architecture (red triangles) and PEDOT:PSS free samples (green circles). Plots are grouped according to dark (a) and illumination (b) tests. Each data point corresponds to one aged sample reported in the literature. The upper plots show the initial performance against lifetime (the scale is expressed in logarithmic scale with base 4 and is associated with common time units). The bottom plots show the distribution of the data in a histogram format, where the *y*-axis represents the number of the reported data points. Reprinted with permission from [16]. Copyright 2016 Wiley.

Bruner *et al* studied the effect of the molecular weight (M_w) of P3HT on the temperature dependent decohesion behavior of the BHJ of P3HT:PCBM in inert atmosphere [78]. The authors discovered that the de-cohesion readily occurs within the BHJ layer at loads well below the fracture resistance. It was also observed that in the P3HT with higher M_w, the decohesion threshold became higher, indicating that larger domains of entangled and bridged P3HT limited crack propagation. Dupont *et al* studied normal and inverted structure devices and found that the interface P3HT:PCBM/PEDOT:PSS (where PEDOT:PSS stands for poly(3,4-ethylenedioxythiophene)-poly(styrenesulfonate)) is the weakest in inverted structures with the configuration: Ag/PEDOT:PSS/P3HT:PCBM/ZnO_x/ITO (where ITO is indium tin oxide), while in the case of a normal geometry device with configuration: Al/Ca/P3HT:PCBM/PEDOT:PSS/ITO, the fracture occurred within the bulk of P3HT:PCBM [79]. This was explained by the formation of a strong $P3HT^+$:PSS^- interface for the normal device due to P3HT-rich regions gradually diffusing towards the PEDOT:PSS interface. This effect is reduced in inverted structure due to the different device configuration. For the inverted geometry, several techniques were proposed for improving the mechanical properties: (1) surface activation of the underlying layer by means of O_2 plasma treatment with the addition of a few percent of CF_4 could provide extra reactivity to the surface. (2) Solvation could soften the surface of the polymer layer and therefore increase the degree of intermixing between the two polymer layers. (3) Microgels, such as poly(allylamine hydrochloride) and dextran (PAH-D), could be used as an adhesive interlayer [79].

4. Intermediate layers

The layers that are typically placed between the active absorbing layer and the electrodes are often referred to as intermediate or buffer layers or depending on whether they are positioned adjacent to a cathode or anode they are called electron or hole transport layers, respectively. The main functions of the intermediate layers in terms of electric properties are better alignment of the work functions of the electrodes with the energy levels of active mixture and selectively conducting either the positive or negative carriers through the layer while blocking the opposite carriers. Such properties help to drastically reduce the recombination mechanisms in the carrier transport and improve device efficiency. In terms of processing, the intermediate layers can both smooth out the rough surface of the front electrode and protect the active layer from the direct deposition of the back electrode, since both often result in shunts. Intermediate layers play a crucial role also in terms of device lifetime and depending on the type of materials can significantly improve or deteriorate device stability. This section discusses the recent discoveries associated with the intermediate layers and their impact on the device stability.

4.1. Hole transport layer

Hole transport layer (HTL) is the buffer layer between the anode and active layer and has the role of transporting the positive carriers and blocking the negative carriers. The most commonly reported HTL is poly(3,4-ethylenedioxythiophene) polystyrene sulfonate (PEDOT:PSS). The effect of PEDOT:PSS on the stability of devices has been debated for several years already and it remains unclear as to which extent PEDOT:PSS limits the device stability. The hygroscopic nature of aqueous solution of PEDOT:PSS results in a rapid uptake of water, which leads to loss of conductivity of the HTL itself [80] and corrosion of other materials in the device [81]. In particular, if the PEDOT:PSS layer is used in combination with transparent electrode indium tin oxide (ITO), the acidic PSS starts etching the ITO [82–84]. UV light sensitivity of PEDOT:PSS has also been claimed to result in conductivity loss of the material [85]. Nevertheless, there have also been instances where PEDOT:PSS was shown not to have an effect on device stability [86] or even to slow down the ageing compared to other

HTLs [87, 88]. A recent study addressed this controversy by analyzing a large number of articles with lifetime data reported in the literature and constructing comparative plots of the lifetimes for samples with and without PEDOT:PSS [16]. In this study the lifetime and initial PCE values were determined from the reported ageing curves and collected in one plot. In figure 9 the upper plots represent the so-called o-diagram, which depicts the initial performance (*Y*-axes) of the sample against the lifetime (*X*-axes) and the time is expressed in logarithmic scale with base 4, which allows associating the time blocks with the common time units. The detailed description of the o-diagram can be found in section 7.2.3. The lower plots show the distributions of the corresponding numbers of data per time blocks. The study demonstrated that indeed most of the reported PEDOT:PSS based unencapsulated devices (blue squares) show inferior stability compared to PEDOT:PSS free devices (green circles), when tested in the dark or under light exposure. The only exception was PEDOT:PSS used in combination with a Ag electrode in an inverted structure tested in the dark (red triangles), where the shelf-life of these samples was similar to the PEDOT-free samples. The results indicated that PEDOT:PSS based devices with normal structure are particularly susceptible to ageing in the dark, which is possibly due to the direct contact of PEDOT:PSS and ITO and the presence of an Al electrode, which is sensitive to humidity. The fact that inverted devices with PEDOT:PSS show comparable stability only in dark conditions, but degrade rapidly under light, confirms that PEDOT:PSS is sensitive to light exposure. In the same study, the encapsulated samples (not shown in the plots) revealed similar lifetimes independent of the presence of PEDOT:PSS and ageing conditions, which suggests that the encapsulation sufficiently protected the samples from humidity, minimizing the effect of the structural differences of the device on stability.

Additional proof of this is the recent study by Kumar *et al*, where the authors compared the stability of normal devices with PEDOT:PSS or MoO_x under different environmental conditions and showed that while some differences were observed for unencapsulated samples under different conditions, these were diminished, when the samples were encapsulated [89]. Unfortunately, the tests were interrupted after 400 h and therefore, for the encapsulated samples the rates of ageing in the stabilized phases were not possible to determine, making it difficult to understand if a difference would eventually appear during longer test periods. At this point it is important to stress therefore that conducting the ageing for a sufficiently long period is vital for extracting reliable data. For example, as Voroshazi *et al* suggested longer term tests may reveal secondary effects that shorter term studies do not uncover [88]. In their long term shelf-life studies the authors demonstrate, that the inverted structures, where PEDOT:PSS or MoO_x was used in combination with a Ag electrode, showed similar ageing in the first 1000 h of storage, but significantly faster ageing was recorded for MoO_x devices at a later stage (see figure 10). The results corroborate well with the figure 9 data and statement that in inverted structures PEDOT:PSS does not impose a limitation on device shelf-life at least on a scale of a few years.

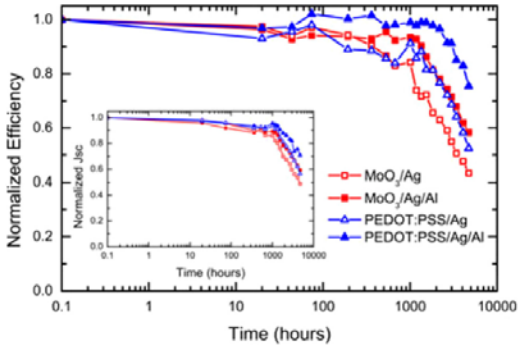

Figure 10. Normalized device efficiency as a function of air exposure time for inverted unencapsulated cells with various HTL/anode combinations. The values are averages over 12 cells. Inset: normalized J_{SC} as a function of air exposure time for the same devices. Reprinted with permission from [88]. Copyright 2014 IEEE.

The study recently published by Glen *et al*, showed instead the superior performance of MoO_x devices compared to PEDOT:PSS in normal structure devices tested in the dark, demonstrating that in normal structures PEDOT:PSS is rather problematic, which again well corroborates with figure 9 and the statement that PEDOT:PSS is problematic in normal structures [90].

In a different study Bovill *et al* conducted comparative light exposure studies of normal structure devices utilizing three different HTLs, such as PEDOT:PSS, MoO_x and V_2O_5 and PCDTBT as active material [87]. The study revealed a superior stability performance of PEDOT:PSS based devices compared to the other two and the reason was claimed to be the fact that PCDTBT is less sensitive towards humidity and therefore the hygroscopic nature of PEDOT:PSS did not do much harm to the device. However, the studied samples were encapsulated in glass and obviously the water content inside the device was already limited in the first place and it is highly likely that this was the reason that the hydrophilicity of PEDOT:PSS was not problematic for this short term (600 h) study. Greenbank *et al* conducted thermal stress tests of inverted structure devices in the dark to explore the stability properties of PEDOT:PSS, MoO_x and WO_x as HTLs and in combination with Al or Ag [91]. The experiments were conducted in a glove box (N_2 atmosphere) in the dark at a temperature of 85 °C, although they were wrongly referred to as ISOS-D-2 tests according to common ISOS test guidelines (the latter mainly assumes tests in the air, as will be discussed in section 7.2.1 and tests in inert atmosphere do not qualify as ISOS tests). One of the important revelations was that when PEDOT:PSS was paired with Al, the device showed very fast ageing compared to the one paired with Ag, which suggests that the combination of PEDOT:PSS and Al is rather harmful for device stability. For samples with a Ag electrode PEDOT:PSS showed a slightly slower ageing rate compared to the two metal oxides.

Alteration of the composition of PEDOT:PSS for improving device stability is another approach that has recently been addressed in the literature a number of times. As an

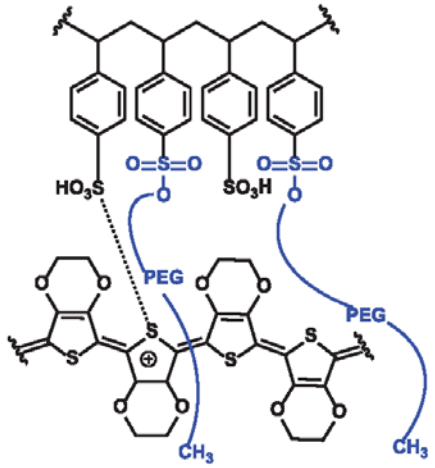

Figure 11. Schematic description of the PEDOT:PSS-g-PEGME graft copolymer. Reprinted with permission from [94]. Copyright 2015 Elsevier.

example Savva *et al* studied different compositions of PEDOT:PSS, where after comparative studies it was shown that the PEDOT:PSS PH derivative treated with Zonyl:Dynol produced the most stable interfaces and thus, led to the most stable devices [92]. Lee *et al* mixed PEDOT:PSS with MoO_x, and succeeded in demonstrating a reduced water transmission rate and therefore improved stability of devices stored in the dark, although the measurements were again not sufficiently long and lacked sufficient data to make certain conclusions [93]. A different way of PEDOT modification was proposed by Lee *et al* that constituted condensation reaction of the PEDOT:PSS with poly(ethylene glycol) methyl ester (PEGME) (figure 11) [94]. This resulted in significantly slowed uptake of water by the PEDOT:PSS and reduced the In diffusion from ITO into PEDOT:PSS, which enhanced the stability of the resulting PSCs shown by an increase in the half-life by up to 3.5 times for the device consisting of a 1:1 weight ratio of PSS-PEGME in comparison to a pristine layer.

Doping of PEDOT:PSS with amphiphilic perfluorosulfonic copolymer (Nafion) was proposed as an alternative method for improving performance and stability. The highly hydrophilic $-SO_3H$ groups of the Nafion interacts with the PSS, while the highly hydrophobic fluorocarbon backbone prefers interaction with PEDOT. The consequence is the enhanced conductivity and increased surface roughness of the doped layer. The stable Nafion skeleton stabilizes the PEDOT:PSS film, due to its excellent thermal and mechanical stability. The compensation of the decohesion of the PEDOT:PSS layer leads to the improved efficiency and long-term stability of the PSCs as was shown for encapsulated samples during dark storage (figure 12) [95].

Some alternative HTL concepts have also been reported recently; for example, Yuan *et al* suggested using bismuth selenide (L-Bi_2Se_3) as HTL [96]. Although the superiority of the novel HTL over well-known MoO_x in terms of PCE was only minor and in terms of stability there was no sufficient data to reliably determine the ageing rate difference, it may be worth investigating L-Bi_2Se_3 further to reveal the true potential of the material. Another method was proposed by Kim *et al*, where microwave-reduced graphene oxide was utilized as HTL and when compared to PEDOT:PSS a major improvement in stability in the dark was demonstrated [97]. Unfortunately, no information was provided for the performance of the devices under light in order to truly estimate the potential of this approach.

Shi *et al* [98] modified P3HT with triethylene glycol (TEG) to receive the conjugated diblock copolymer poly(3-hexylthiophene)-b-poly(3-triethylene glycol thiophene) (P3HT-b-P3TEGT) (figure 13(a)). The incorporation of this copolymer into the PAL forms a self-assembled anode buffer layer through spontaneous migration towards the PAL surface. Upon chelation of the lithium ions of the TEG side chains, the buffer layer can form an interfacial modification and ohmic contact between the Ag electrode and the PAL, through a reduction in the contact resistance and an increase in the electrical conduction. The lifetime of PSCs containing PEDOT:PSS as HTL (ITO/ZnO_x/P3HT:PCBM/PEDOT:PSS/Ag) in comparison to PSCs containing P3HT-b-P3TEGT and P3HT-b-P3TEGT:Li^+, respectively, as an anode buffer layer (ITO/ZnO_x/P3HT:PCBM:P3HT-b-P3TEGT(:Li^+)/Ag) was investigated by the group (figure 13(b)), showing an enhancement of the unencapsulated device stability in air. The formation of an anode interfacial layer led to preferred BHJ morphology with improved transport of holes and electrons to the anode and cathode, respectively [98].

4.2. Electron transport layer

The electron transport layer (ETL) is the intermediate layer adjacent to the cathode and has the role of transporting electrons and blocking the holes. Similar to HTL, ETL can have a major impact on the stability of the device and many reports have addressed this earlier [11, 13]. This section will primarily focus on recent developments related to ETL stability.

The most commonly used ETL for OPVs is ZnO_x. Its easy processing and good electron transport properties make ZnO_x one of the best candidates for inverted structure solar cells. MacLeod *et al* investigated the effect of ZnO_x processed from different precursors on the stability of devices [99]. In particular, ZnO_x processed from a diethylzinc (deZn) precursor appeared to be more stable than the one processed from zinc acetate (ZnAc). Moreover, the modification of both types with dipolar phosphonic acid (PA), which is known to change the work function, resulted in the alteration of both PCE and stability behavior. Although PA treatment resulted in the improvement of stability for ZnAc based devices and somewhat stronger burn-in for deZn based devices, the overall ageing rate of the stabilized phase of the curves appeared to improve for both types of devices when the samples were exposed to light in air while maintaining a low temperature via active cooling (see figure 14). Nevertheless, the measurements were interrupted before clear patterns of stabilized ageing rates could be identified and therefore, firm conclusions cannot be made at this point.

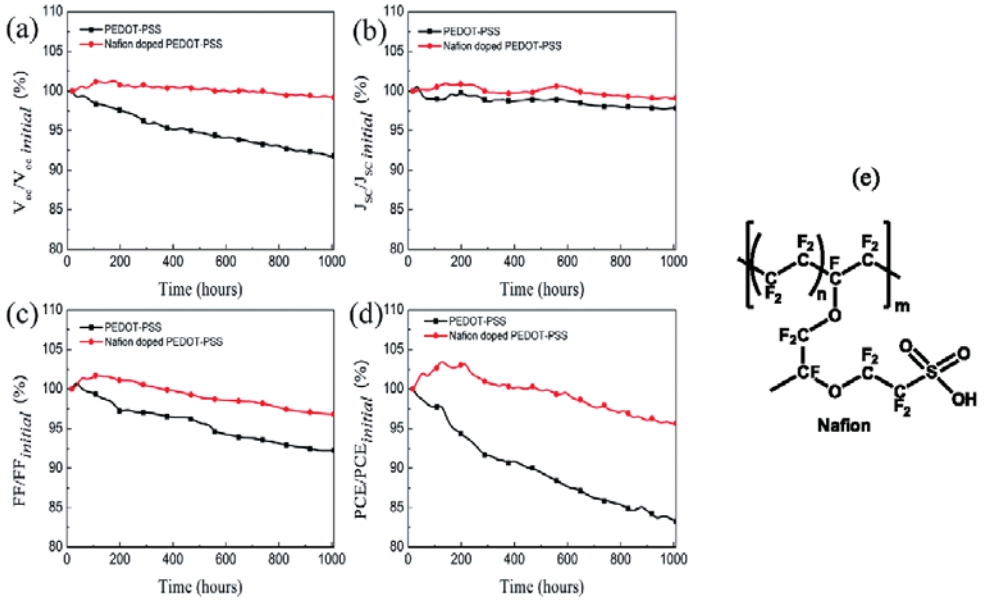

Figure 12. Lifetime V_{OC} (a), J_{SC} (b), FF (c) and PCE (d) of encapsulated devices based on PEDOT:PSS or Nafion (e) doped PEDOT:PSS (1:2). The devices where stored in the dark under ambient conditions. Reprinted with permission from [95]. Copyright 2015 Royal Society of Chemistry.

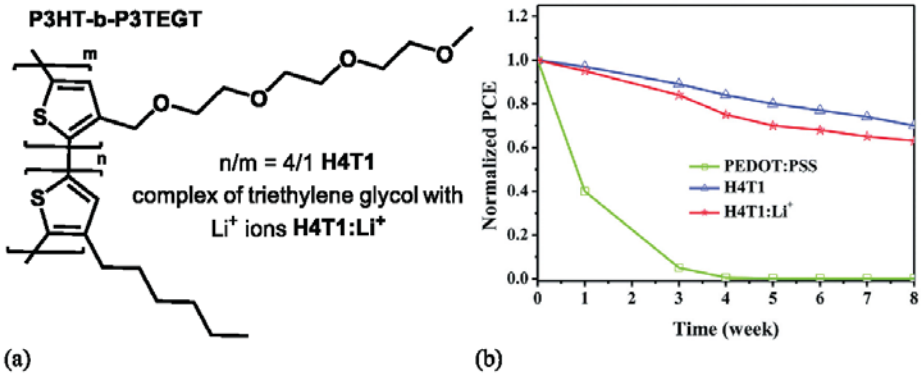

Figure 13. Chemical structure of P3HT-b-P3TEGT (a) and its influence on the lifetime of a PSC (b). The unencapsulated PSC devices were stored in air under ambient conditions. Reprinted with permission from [98]. Copyright 2014 Royal Society of Chemistry.

Doping of ZnO_x with aluminum has been reported to improve the conductivity of the film increasing device PCE [100]. Chen *et al* investigated the stability of inverted structure devices utilizing aluminum doped ZnO_x and demonstrated that the samples could retain up to 86% of initial performance after 900 h of dark storage in air [101]. Unfortunately, there was no direct comparison with non-doped ZnO_x presented in the study and therefore, it was unclear whether the doping improved the stability. Meanwhile Kam *et al* thermally deposited a thin layer of Al on top of a ZnO_x layer and showed that this eliminated the rapid drop of open circuit voltage (burn-in) observed in the standard devices during exposure to UV light. Based on the UV and UV-free exposure tests and ultraviolet photoelectron spectroscopy (UPS) analyses the authors concluded that the reason for the V_{OC} drop was the reduction of the barrier height of the films and as a consequence, the hole blocking properties, which was compensated by the insertion of a thin aluminum layer [102]. Bai *et al* instead suggested applying ethanedithiol (EDT) treatment to passivate the surface of the solution processed ZnO_x film, which led to increased PCE and somewhat increased stability [103].

Additionally, there have been a number of attempts to substitute ZnO_x with novel materials. In particular, George *et al* presented a number of polymer based intermediate layers, which were utilized in inverted devices as ETLs, and although no gain was achieved in terms of PCE, the devices with novel

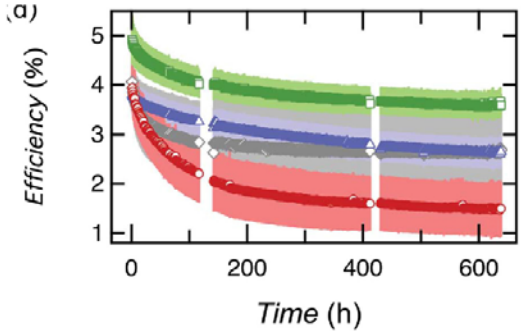

Figure 14. PCE ageing of unencapsulated devices with ZnAc (red circles), deZn (blue triangles), PA-modified ZnAc (green squares), and PA-modified deZn (gray diamonds) electrodes. The samples were exposed to sulfur plasma lamp with intensity close to 0.8 sun. The sample temperature was kept close to 25 °C via active cooling. Tests were conducted in air. Bars indicated ±1 standard deviation of the mean. Reprinted with permission from [99]. Copyright 2015 Royal Society of Chemistry.

ETLs showed stability as good as titanium oxide (TiO_x) based devices and offered novel easy processable materials for ETL [104]. As another alternative for ETL Weerasinghe *et al* recently reported roll-to-roll coated and printed OPV modules with polyethylenimine-ethoxylate (PEIE) utilized as ETL [105]. The authors claimed that the novel ETL increased the module PCE by 20% compared to traditional ZnO_x ETL, although no comparative data was presented. Authors additionally claimed that PEIE did not impair device stability and robustness, although again comparative data with other materials was not provided. The important advantage of PEIE was that it could be obtained by simple dilution and did not require steps, such as sol-gel synthesis. In another study Raïssi *et al* employed copper phthalocyanine-3,4′,4″,4‴ tetra-sulfonated acid tetrasodium salt (TS-CuPc) as ETL in an inverted OPV device with an active layer of P3HT:PCBM and a combination of MoO_x/Ag acting as the anode [106]. Solution processed TS-CuPc led to stable (unencapsulated) devices showing no degradation after 140 d of storage in air in the dark (figure 15).

Wang *et al* compared a range of different ETL materials in a traditional normal structure OPV configuration based on a P3HT:PCBM active layer [107]. In particular, lithium fluoride (LiF), sodium chloride (NaCl), NaCl/Mg combination, tris-(8-hydroxy-quinoline) aluminum (Alq3), bathocuproine (BCP) and 1,3,5-tris (2-*N*-phenylbenzimidazolyl) benzene (TPBI) were tested in encapsulated devices stored in the dark in inert atmosphere for 350 h. Except for LiF, NaCl and NaCl/Mg the samples of the remaining three ETLs rapidly degraded demonstrating that the ETL can indeed have a drastic effect on the intrinsic stability of OPVs. Chen *et al* [108] synthesized a fluorine-based organic small molecule electrolyte (SME) with different conjugated backbones (scheme 3) and used it to substitute ZnO_x. An enhanced efficiency (26% improvement) in comparison to ZnO_x could be achieved. The authors additionally claimed that the stability of the device can be improved by SMEs as buffer layer, although no comparative data was presented to prove that [108].

5. Electrodes

5.1. Non-transparent electrode

The most commonly used non-transparent electrodes are Al for a normal structure and Ag or gold (Au) for inverted structures. Al is very reactive towards water and in the previous section examples have already been discussed showing that the combination of hydrophilic PEDOT:PSS and Al is detrimental for the devices tested in an environment with presence of humidity, while Ag based devices remained stable in the same environment [90, 91]. Han *et al* found that replacing the Al electrode (100 nm) in normal geometry organic solar cells with an Al/Cu bilayer (25 nm Al and 80 nm Cu) drastically improves the device's lifetime when tested under highly damp conditions (90% RH and 27 °C), making it comparable to the inverted OSCs. They attributed this to the lower water vapor transmission rate (WVTR) of the Al/Cu bilayer compared to the single Al layer [6]. Glen *et al* studied the dependence of device stability on the grain size of an Al top electrode and revealed that the electrodes with larger grain sizes showed slightly better stability compared to smaller grain sizes [109]. In the case of PEDOT:PSS free devices Yeom *et al* compared the stability of devices with Al, Ag or Au as the back electrode during storage in the dark without any external protection [110]. The samples were based on PTB7:$PCBM_{[70]}$ blended with ZnO_x and MoO_x as intermediate layers. Al based devices showed much faster ageing confirming that even without PEDOT:PSS Al still acts as a bottleneck in an environment with the presence of humidity.

A different study by Voroshazi *et al* showed that the combination of a MoO_x/Ag/Al multilayer electrode can also be a source of instabilities. In particular the advanced characterization showed that during light exposure due to heating Al tends to migrate through Ag and possibly react with MoO_x by creating an oxide layer at the interface. Due to such interfacial alterations the reflection of the light inside the device is changed resulting in up to a 20% drop in short circuit current [111]. An example of multilayer protective top electrode layer was presented also by Romero-Gomez *et al*, who used MgF_2/MoO_x as the top electrode [112]. The use of this layer resulted in a many-fold improvement in device stability, when tested in the dark.

5.2. Transparent electrodes

The most commonly used transparent electrode in OPVs is ITO due to its good conductivity and high transparency. However, ITO is well known to be brittle and although flexible ITO substrates have been demonstrated, these typically tend to break and rapidly lose conductivity upon multiple bending [113]. Additionally ITO is expensive to process and therefore, solar cells produced with ITO will inevitably have a higher energy payback time (EPBT) [114, 115]. ITO is also harmful to device stability and this is particularly evident when it is used in combination with PEDOT:PSS [116], as has also been discussed earlier in this review. One of the recent studies by Kettle *et al* confirms the migration of indium (In) and tin (Sn)

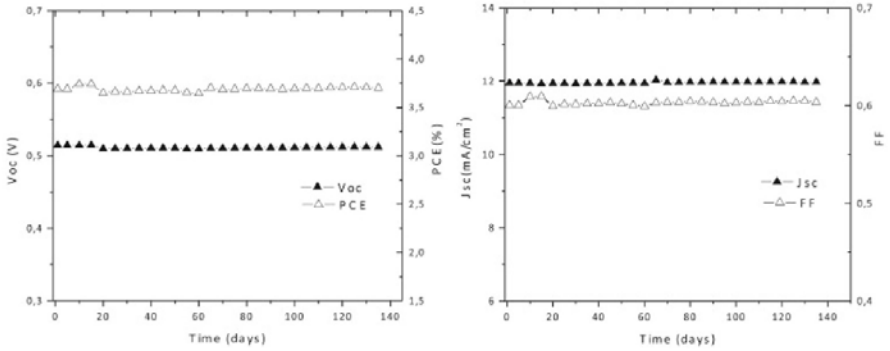

Figure 15. Studies of all parameters of ITO/TS-CuPc/P3HT-PCBM/MoO3/Ag devices over the time stored in air without encapsulation. Reprinted with permission from [106]. Copyright 2016 Elsevier.

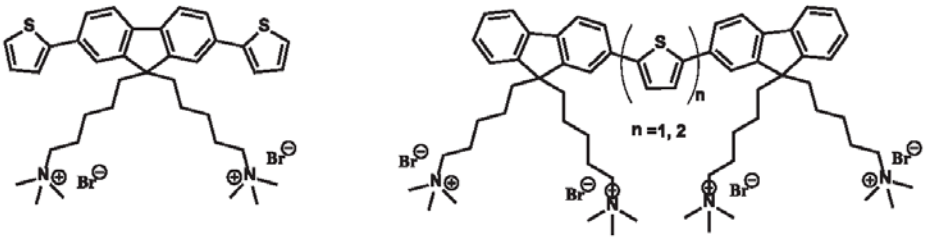

Scheme 3. Fluorene based small molecule electrolyte as cathode interfacial layer in PSCs.

through the entire device, which is a result of the etching of ITO by PEDOT:PSS [56]. Therefore, the research in recent years has been largely focused on replacing ITO with alternative types of electrodes.

Replacement of ITO with aluminum doped zinc oxide (AZO) was proposed by Chen *et al*, an approach that has already been discussed in the section 4.2. In particular, the use of AZO combined with 1 nm Ca as a transparent cathode in inverted structure devices was proven to provide comparable PCE with a reference ITO based device and slightly increased air stability in the dark [117]. Wang *et al* used the multi-structure $ZnO_x/AgO_x/ZnO_x$ (ZAOZ) as a transparent conductive electrode (TCE) [118]. Such an electrode deposited on PET provided an average transmittance of 91%, and a sheet resistance of 20 Ω sq^{-1}. The device with configuration TCE/PTB7-F20:$PCBM_{[70]}$/PEDOT:PSS/Ag showed only a 10% drop in PCE after a bending radius of 1 mm, whereas the ITO device PCE dropped by approximately 60%. Another sandwiched electrode consisting of nickel oxide (NiO)/Ag/NiO (known as NAN) having high transmittance of ~82% combined with a low sheet resistance of 7.6 $\Omega \cdot sq^{-1}$ was proposed by Xue *et al* [119]. This electrode also improved the flexibility of the devices and was shown to preserve carrier transport properties and carrier density after storage at elevated temperature and humidity conditions for 1 d or a prolonged 1 year shelf life, as can be seen in figure 16.

The replacement of ITO with highly conductive PEDOT:PSS or a combination of PEDOT:PSS and for example a Ag grid has been widely utilized already for a number of years. Here we propose the recent advances related to these configurations. Fan *et al* replaced ITO with PEDOT:PSS, which was treated with methanol and methanesulfonic acid (MSA) in order to improve its conductivity up to 3560 S cm^{-1} [120]. With such a layer normal structure organic solar cell Ca/Al/P3HT:PCBM/PEDOT:PSS (buffer)/PEDOT:PSS (electrode)/PET achieved a PCE of 3.92% (compared to 4.30% for the standard ITO electrode). Using PEDOT:PSS instead of ITO guaranteed good mechanical flexibility, with more than 80% of the initial PCE maintained after bending 100 times with a bending radius of 14 mm in ambient atmosphere. Skorenko *et al* [121] and Li *et al* [122] independently studied PEDOT produced via vapor phase polymerization (VPP) as an alternative for ITO replacement. The high electric conductivity and high resistance towards mechanical stress (bending and stretching) was shown for VPP-PEDOT. Li *et al* in particular combined VPP-PEDOT with Ag grid to produce devices and showed significantly improved device stability for the sample based on the alternative electrode in comparison to the traditional Ag grid/PEDOT:PSS(PH1000) electrode configuration [122].

Silver nanowires (AgNW) have been extensively used as an ITO replacement and a number of recent publications discuss the clear advantage in mechanical flexibility of the samples with AgNW [123–129]. Nevertheless, in most cases the device stability in terms of air exposure does not show any improvement. Only when Lee *et al* studied the hybrid combination of AgNW and graphene, where the transparent electrode was developed by dry-transferring a chemical vapor deposition-grown monolayer graphene onto an AgNW, the authors succeeded in showing a slight improvement in stability of devices

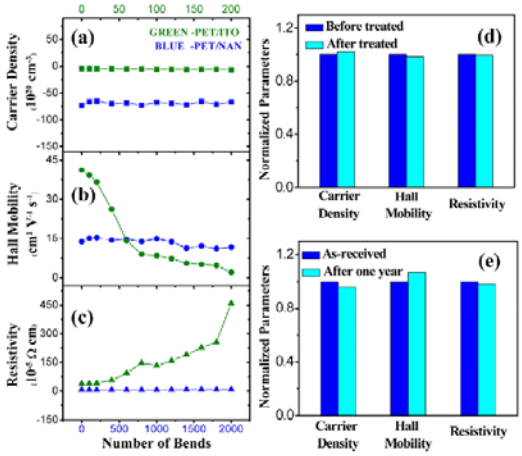

Figure 16. (a) Carrier density, (b) Hall mobility, and (c) resistivity of the PET/ITO and PET/NAN flexible electrodes after repeated bending. The green curves are for the PET/ITO (top *x*-axis) electrode, and the blue curves are for the PET/NAN (bottom *x*-axis) electrode. The bending angle was about 90°. (d) Carrier density, Hall mobility, and resistivity before and after the NAN electrode was stored at a constant temperature of 60 °C and relative humidity of 90% for 24 h. (e) Normalized changes in carrier density, Hall mobility and resistivity of the NAN electrode before and after it was preserved in air for 1 year. Reprinted with permission from [119]. Copyright 2014 American Chemical Society.

with the hybrid configuration compared to a single AgNW [130]. A Ag nanomesh was fabricated on a flexible substrate by another group using nano-imprint lithography (NIL) [131]. The Ag nanomesh transparent conductive electrode exhibited high transmittance of >88% and low sheet resistance of 15 Ω sq^{-1}, as well as good mechanical flexibility. The stability of the device Ag nanomesh/ZnO_x/PTB7:$PCBM_{[70]}$/PEDOT:PSS/Ag stored in air under ambient conditions, was comparable to the ITO based device.

6. Upscaling and packaging

So far, the majority of reported OSC and PSC are typically fabricated on small glass sheets using spin coating methods and active cell sizes below 1 cm^2 [132]. Even though such cells can show record efficiencies beyond 10% [133–135], they are often measured under inert atmosphere and lack appropriate encapsulation or have glass lids attached using epoxy glue. Although, devices produced with such methods and architectures show the potential of the technology in terms of PCE, they are far from the envisioned commercial OPV products. For demonstrating the true potential of an OPV as a product it is vital to utilize and develop processing techniques that will enable large-scale cost-efficient fabrication and architectures that will allow achieving long-term stability under real world conditions. The latter in particular has to be compatible with large-scale processing.

The ideal large-scale fabrication methods for polymer based organic solar cells are solution-based R2R printing and coating methods such as flexo printing, inkjet printing, spray coating, slot-die coating, gravure printing, screen printing and eventually laser scribing [136, 137]. These methods enable the fabrication of modules with sizes up to 100 m in length [138, 139] and even modules with up to 14 layers in a tandem configuration [140]. Other studies deliver freely shaped solar cells [141] or devices with a very high geometrical fill factor [142–145]. Small-molecule based organic solar cells can be manufactured on an industrial scale using R2R vacuum deposition tools and laser processing [146]. Most reports on upscaled organic solar cells however concentrate on the manufacture of devices, but neglect the importance of similar sized encapsulation procedures, which are important for making the solar cells stable against environmental impact. The post processing and integration into to the intended application is for a large majority completely neglected which is a testimony to the rather unevolved technological level of OPV.

Rigid glass panels are the best known barriers where solar cells can be sandwiched in between two panels [147]. Solar cells need to be placed some centimeter away from the edges to avoid edge ingress and adhesives with low WVTR and low intrinsic water levels need to be selected to improve lifetime. These large-area glass-glass encapsulations are typically used in building integrated photovoltaic (BIPV) products, such as glass facades [148]. The fabrication of third generation photovoltaics directly on glass and additional glass encapsulation is a procedure commonly used for large area dye sensitized solar cells or in the future possibly for perovskite based technologies. The typical sealing method is based on heat fusing or laser assisted glass frit sealing [149–151]. The freedom in 3D shape is limited and the natural flexibility of foil based solar cells is sacrificed. Although ultrathin flexible glass as a substrate and barrier is starting to gain attraction especially in the field of organic light emitting diodes (OLEDs), the utilization for OPVs is currently limited [152].

The best flexible candidates for environmental protection are the foil-based barrier films ranging from food barriers to multilayer ultra-barrier films with WVTR reaching up to 10^{-6} g/m²/d. The barrier films are either commercially available from a variety of manufacturers (price is highly dependent on barrier performance) or manufactured in research laboratories using solution coating, vacuum deposition, sputtering or atomic layer deposition (ALD) of metal oxides and polymer interlayers [153–156].

The rolls of flexible barrier films can easily be integrated in roll-to-roll and roll-to-batch production lines of OPVs and the solar cells can either be processed directly onto the barrier substrate [157] (in some cases with additional corona pretreatment) with subsequent encapsulation using an additional barrier film for the opposite side, or if the substrate does not possess barrier properties, then the complete device with substrate is sandwiched between two barrier foils. Various adhesive methods exist for making the barrier foil stick to the substrate [158] and many hundreds of meters can be continuously laminated [138, 139] or for architectural purposes processed in batches [142] in a R2R process. The earliest R2R produced organic solar cells used *pressure sensitive adhesives* (PSA). PSAs are applied to the barrier foil as a separate step, and this barrier laminate (containing pressure sensitive

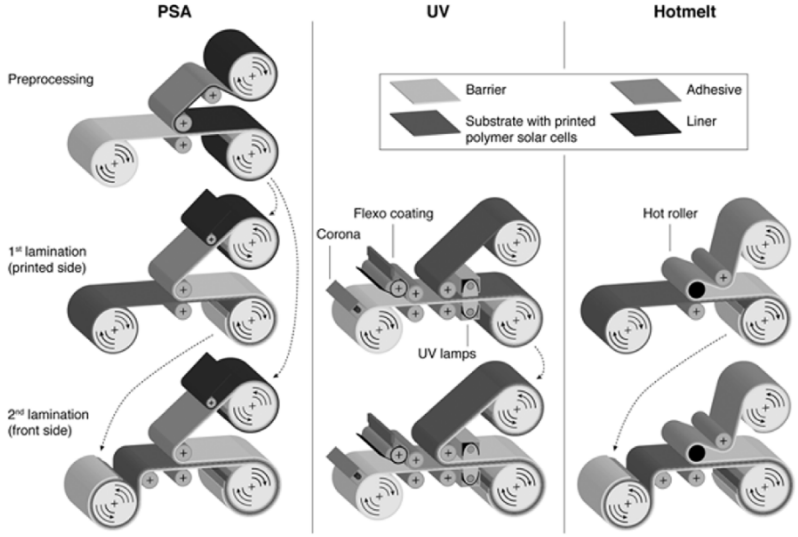

Figure 17. Process workflow for the R2R encapsulation of flexible OPV modules. Reproduced with permission from [158]. Copyright 2013 Wiley.

glue on one side—similar to ordinary Scotch tape) is then laminated onto the substrate carrying the device [159, 160]. Thus, PSA lamination requires several preprocessing steps to prepare the laminate and it produces waste in the form of release-liner (coated paper or polymer film) in the same length as the barrier film. In contrast, *hotmelt* and *UV-curable* adhesives are directly applied onto the foil and used to attach the barrier film on the printed solar cells [158] (see figure 17). In the case of hotmelt lamination, when the laminate is brought together with the substrate in a hot nip, the adhesive becomes momentarily liquid which allows contact between the substrate and barrier before the adhesive hardens upon cooling. For *UV curing* adhesive lamination UV curable adhesive is applied between the substrate and the barrier followed by exposure to UV-light in order to cure the adhesive. In both lamination processes the glues are fluid while entering the nip rollers and cooled or light activated after passing the nip. The fluid phase avoids the inclusion of tiny air bubbles that often occur with PSAs. Overall, according to Hösel *et al* [158], the UV-curable adhesive leads to the highest stability of the three (UV > hotmelt > PSA sequence for better stability). The authors additionally conclude that the UV-adhesive makes a very efficient edge sealing. It should be noted here that UV-curable adhesive systems are typically based on epoxies or isocyanates, which can cause serious allergies and permanent skin damage for humans (see figure 18).

In another study, stability tests over more than 900 h under illumination showed that single-sided lamination with UV-curable adhesive achieves better stability than double-side PSA lamination [161]. Long-term outdoor tests in Africa of double-sided encapsulated large-area modules with hotmelt office lamination pouches proved the functionality of hotmelt as a glue, but failed due to the poor quality of the plastic film. Strong UV-radiation made the lamination pouch brittle and

Figure 18. Permanent skin damage as a result of exposure to UV-curing epoxy resins. Great care must be exercised in the laboratory and when scaling up.

led to bleaching and delamination at the edges of the modules. This proves that barrier films need to be resistant against environmental impacts over the expected lifetime of the solar cells. More details can be found elsewhere on the descriptions of the different lamination process [162] and flexible barrier film preparation and properties [163].

Weerasinghe *et al* recently showed that PSA barriers may contain significant amounts of moisture after prolonged storage of the foil before device manufacturing and can therefore affect the device stability, when used for packaging [164]. The authors showed that the stability of the encapsulated devices could be significantly increased by simply pre-outgassing the PSA barrier in a vacuum oven before encapsulation.

Edge sealing of continuously coated and cut solar cell modules was found to be highly important for the lifetime and stability of large-scale OPVs [105, 165, 166] and perovskite solar cells [167]. In particular, when Weerasinghe *et al* described 'hand lamination' of small R2R processed solar cell

modules either by PSA lamination or by hotmelt (ethylene-vinyl acetate (EVA) adhesive) combined with barrier gasket applied along the perimeter of the OPV device, they showed an improved stability in both cases stressing the importance of the edge sealing [105, 166]. It should be mentioned here that no reference studies were presented using only the hotmelt, so it is difficult to evaluate how much the increased stability can be ascribed to the introduction of the extra edge sealing gasket and how much can be ascribed to the EVA hotmelt adhesive. Nevertheless, water and oxygen ingress from the side is a critical factor that has been addressed earlier and proved the necessity of large protective rims around OPVs [168]. Additionally, the electrical terminals of the modules can be the first direct entry point between the encapsulation layers for diffusions of the ambient agents. It has been shown in long term outdoor studies up to 10 000 h that water ingress through the contact points can lead to destructive degradation of parts of the solar cell next to the contacts [169], thus appropriate protection of the electrode is also an important necessity.

Other failures that have been shown in upscaled solar cells with flexible encapsulation are typically associated with delamination of the encapsulant, bubble formation and bleaching from the edges, if not properly sealed [170, 171]. Major destructive behavior was also observed in very large organic solar cell modules (100 m $\times$ 0.3 m) with high open circuit voltages of 10 kV, initiated possibly by pinholes, delamination, shunts and water ingress [172]. The defective area formed hotspots that tend to form arcs and slowly melted the lamination foil until inflammation. The problems could be solved by cut-replace repair procedures that enabled modules with 150 W_{peak} after more than 4300 h outdoors. The initial performance was well beyond 200 W_{peak} for one module under 1 sun illumination and after the initial burn-in the module demonstrated around 400 d of lifetime calculated for the stabilized performance [16].

Meanwhile, a recent study by Nehm *et al* on the barrier properties of flexible PET substrates with an added zinc-tin-oxide (ZTO) barrier showed an important link between device temperature and the performance of the barrier. In particular the authors showed that the WVTR of the barrier not only has a linear relationship with humidity, but also a linear logarithmic relationship with the reciprocal temperature ($1/T$) [173]. The study, which was based on calcium tests, also showed a clear dependency on whether the interface of Ca tester was with the barrier film from the ZTO side or the PET side. Such dependence was ascribed to interface diffusion processes. This shows that barrier properties are not easily determined simply by a given WVTR, but that consideration of factors such as climate and device interfaces have to be taken into account.

7. Stability and lifetime characterization

An important element when aiming at improving OPV stability is the proper testing and characterization of the failure mechanisms, as well as correct stability rating of the photovoltaic performance. It is vital to be able to record and understand the mechanisms that cause the ageing of OPVs in order to protect the devices against these mechanisms. It is also important to be able to rate the stability of the samples in order to both enable easy comparison of the different device stabilities produced by different laboratories and establish the progress of lifetime improvements. This section will first discuss the recent reports on various advanced characterization techniques that were utilized for the characterization of failure mechanisms. This will then be followed by a discussion of the ISOS test guidelines that have commonly been used in the OPV field in recent years. Recently proposed methods for identifying a generic marker of lifetime and comparing the lifetimes of various devices via a so-called o-diagram are also discussed.

7.1. Advanced characterization of stability

Many different techniques have been employed for studying stability of organic solar cells, which range from simple IV-testing to advanced photo-electrical characterization, transient measurements and scanning microscopy. Such tools allow locating and recording specific ageing mechanisms and therefore, help in eliminating them. This section outlines a number of advanced characterization techniques that have been employed recently for studying device ageing.

Impedance spectroscopy has proven to be a rather useful technique for studying the electric properties of individual layers and complete OPV devices. As an example Lin *et al* has recently demonstrated the use of impedance spectroscopy for analyzing the stability behavior of individual layers in the traditional OPV device during the ageing process [174]. In particular using voltage–current IV and impedance spectroscopy IS measurements it was demonstrated that there is significant capacitance increase at the PEDOT:PSS/ITO interface, which indicated the increased amount of charge traps. This and the increased resistance at the PEDOT:PSS/active layer interface were claimed to be the main reasons for the initial rapid degradation (burn-in) of the device. Guerrero *et al* combined absorbance measurements, capacitance–voltage (C–V) and impedance spectroscopy in order to investigate the ageing mechanism of P3HT:PCBM based devices stored for 1 year in the dark in a glovebox [175]. Based on such optical and electrical characterizations the authors concluded that the main ageing mechanism was the development of localized charge transfer complexes ($P3HT^{\bullet+}$–$PCBM^{\bullet-}$), which not only reduced the photocurrent due to the reduction of the light absorption properties, but also reduced the voltage, since the formation of such complexes led to the creation of electronic defect states, which affected the hole Fermi level resulting in a decrease of V_{OC}. Karuthedath *et al* used instead microsecond and femtosecond laser pulses to study the charge transients of P3HT:PCBM and Si-PCPDTBT:PCBM films and devices and determined that during the photoageing of the active mixtures the charge generation was intact, but the charge recombination was strongly reduced, which as a consequence reduced the charge mobility [176]. Table 2 below summarizes the list of other recently reported advanced characterizations of ageing mechanisms including the ones discussed above. For other reported techniques the reader should refer to earlier published reviews [7, 8]

Table 2. List of various advanced characterization techniques reported in recent years and the short descriptions of the sample types and the ageing mechanisms discovered with the use of these techniques.

Characterization tools	Tested sample	Observations	Ref.
• Impedance spectroscopy	ITO/PEDOT:PSS (interface) PEDOT:PSS/P3HT:PCBM (interface)	Increased amount of charge traps Increased resistance	[174]
• Impedance spectroscopy	ITO/ZnO_x/PTB7:$PCBM_{[70]}$/MoO_x/Ag (bulk and interfaces)	Charge accumulation at the electrodes	[177]
• Impedance spectroscopy • Absorbance measurement • Capacitance–voltage (C–V)	ITO/ZnO_x/P3HT:PCBM/MoO_x/Ag (bulk and interfaces)	Development of localized charge transfer complexes ($P3HT^{\bullet+}$–$PCBM^{\bullet-}$) as main ageing mechanism	[175]
• Transient measurements with femtosecond laser	P3HT:PCBM Si-PCPDTBT:PCBM (bulk)	Charge generation is intact during photo-oxidation, but charge recombination is strongly reduced indicating reduced charge mobility	[176]
• Atomic force microscopy (AFM) • X-ray photoelectron spectroscopy (XPS) • UV–visible spectroscopy • Infrared spectroscopy (IR) • Time-of-flight secondary ion mass spectrometry (TOF:SIMS)	Si-PCPDTBT film surface Si-PCPDTBT film bulk	Rapid surface oxidation accompanied with loss of carbon and sulfur and swelling of the film, followed by gradual oxidation of the bulk and shrinking of the film. Oxidation of Si bridging atom is the first step in the photo-oxidation process of the film.	[178]
• Damp-heat test • X-ray photoelectron spectroscopy • Scanning electron microscopy • Energy-dispersive x-ray analysis	ITO/ZnO_x/active layer/PEDOT:PP/Ag	Migration of Ag atoms causing creation of shunts was observed. ZnO_x etching by PEDOT:PSS was also suggested.	[179]
•Capacitance–temperature measurement • Confocal scanning microscopy	ITO/PEDOT:PSS/Active layer/ZnO_x/Ag	Threshold temperature T_{max}, at which the morphology becomes thermally unstable, is determined and allows determining thermal stability of materials and devices.	[180]
• Intensity-resolved EQE	Ag/PEDOT:PSS/P3HT:PCBM/LiF:Al	EQE shape dependence on light intensity reveals generation of traps in PCBM	[181]

7.2. Lifetime measurements and reporting

7.2.1. Before and after ISOS standards. One of the main milestones in the lifetime testing of organic photovoltaics was the establishment of ISOS guidelines, which were published in 2011 based on the consensus of the discussion and conclusions reached during the first 3 years of the International Summit on OPV Stability (ISOS) [182]. The guidelines offer instructions on how to perform a stability test of OPVs and similar technologies under different conditions, such as dark tests (shelf life), outdoor tests, indoor weathering and thermal cycling tests. Table 3 shows a short summary of the tests. One of the earlier interlaboratory studies demonstrated how different environmental conditions, such as relative humidity, temperature, light intensity or spectrum drastically affect the outcome of the stability test of an OPV device [183]. Therefore the purpose of the ISOS guidelines was to help researchers in different laboratories harmonize testing procedures by choosing common testing conditions. To achieve this, the guidelines in particular recommend a number of important limitations, some of which are:

- Only light sources that resemble AM1.5G well must be used in indoor weathering tests. The light sources with poor performance in the UV range, such as classical sulfur plasma lamps or light emitting diodes with limited wavelength range do not qualify for ISOS tests.
- Specific sample temperatures or relative humidity of the environment must be used during certain indoor tests, as is specified in table 3

Since, however the level of equipment at different laboratories varies significantly, the guidelines addressed this by offering three levels of testing varying in the complexity of the procedure and equipment requirements that can suit both advanced accredited test laboratories and research laboratories with limited equipment. Obviously, the higher the level of tests chosen, the better accuracy of the tests can be achieved.

One of the recent studies demonstrated how following the ISOS guidelines can improve the reproducibility of the test results. In particular, identical samples were distributed among seven laboratories in different countries and tests were conducted according to ISOS-D-2 (high temperature storage) and ISOS-D-3 (damp heat) tests [184]. Figure 19 shows good overlap among the curves of the samples tested at different laboratories. As a comparison, in similar interlaboratory studies conducted before ISOS, where the laboratories did not follow common protocol the ageing rates of the dark tests varied by an order of magnitude due to different temperature and humidity conditions used during the tests [183]. The recent analyses of the literature related to OPV stability demonstrated how the publication of ISOS guidelines affected the reported lifetime data. In particular, all the reported stability data and test

Table 3. Overview of different types of ISOS test protocols. Reproduced with permission from [182].

Three levels						
Basic (level 1):	'Hand held' measurements using the simplest equipment and few conditions.					
Intermediate (level 2):	Fixed conditions and protocols suited for most labs.					
Advanced (level 3):	Standardized tests applied in certified labs. Extended range of parameters to monitor etc.					
Test type	Dark			Outdoor		
Test ID	ISOS-D-1 shelf	ISOS-D-2 high temp. storage	ISOS-D-3 damp heat	ISOS-O-1 outdoor	ISOS-O-2 outdoor	ISOS-O-3 outdoor
Light source	None	None	None	Sunlight	Sunlight	Sunlight
Temp.[a]	Ambient	65 °C/85 °C	65 °C/85 °C	Ambient	Ambient	Ambient
Relative humidity (RH)[a]	Ambient	Ambient (low)	85%	Ambient	Ambient	Ambient
Environment[a]	Ambient	Oven	Env. chamber	Outdoor	Outdoor	Outdoor
Characterization light source	Solar simulator or sunlight	Solar simulator	Solar simulator	Solar simulator	Sunlight	Sunlight and solar simulator
Load[b]	Open circuit	Open circuit	Open circuit	MPP or open circuit	MPP or open circuit	MPP
Test type	Laboratory weathering testing			Thermal cycling		
Test ID	ISOS-L-1 laboratory weathering	ISOS-L-2 laboratory weathering	ISOS-L-3 laboratory weathering	ISOS-T-1 thermal cycling	ISOS-T-2 thermal cycling	ISOS-T-3 thermal cycling
Light source	Simulator	Simulator	Simulator	None	None	None
Temp.[a]	Ambient	65 °C/85 °C	65 °C/85 °C	Between room temp. and 65 °C/85 °C	Between room temp. and 65 °C/85 °C	−40 °C to +85 °C
Relative humidity (RH)[a]	Ambient	Ambient	Near 50%	Ambient	Ambient	Near 55 %
Environment/setup	Light only	Light and temp.	Light, temp., RH	Hot plate/oven	Oven/env. chamb.	Env. chamb.
Characterization light source	Solar simulator	Solar simulator	Solar simulator	Solar simulator or sunlight	Solar simulator	Solar simulator
Load[b]	MPP or open circuit	MPP or open circuit	MPP	Open circuit	Open circuit	Open circuit

Note: [a]The ambient conditions are defined as 23 °C/50 % RH in general, and 27 °C/65 % RH accepted in tropical countries according to ISO291 (2008): Plastics—Standard atmospheres for conditioning and testing.
[b] Open circuit refers to a simply disconnected device or device connected to a source meter set to 0 current.

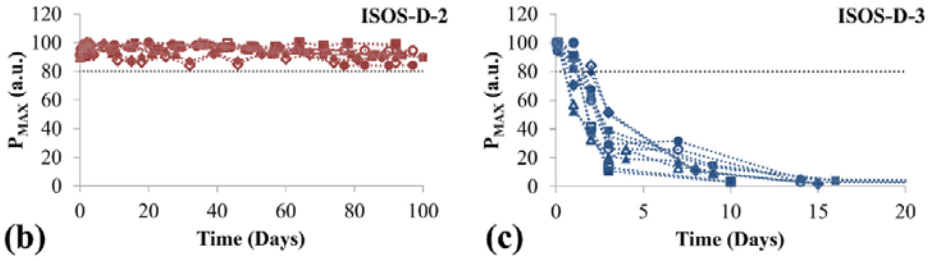

Figure 19. Testing of R2R manufactured and packaged flexible OPV modules under ISOS-D-2 (b) and ISOS-D-3 (c) test conditions in different laboratories. The plots represent the maximum power against the time. Reprinted with permission from [184]. Copyright 2014 Elsevier.

conditions were categorized according to whether the conditions were compatible with ISOS guidelines or not. The compatibility was determined by if the test conditions sufficed the important ISOS criteria, such as device temperature, light source type etc. The reports were grouped into these published before year 2012 and from year 2012 (since ISOS guidelines were published right before 2012). Figure 20 shows the ratio of the number of compatible and non-compatible stability data reported before and from the year 2012. From the plot it is clear that while the ISOS compatible data was around 40% before 2012, it reached 60% for articles published from year 2012. 25% of the articles published from year 2012 explicitly cite ISOS protocols. The majority of non-compatible data are the tests conducted in inert atmosphere or with light sources with a poor UV component, although some publications erroneously regard these conditions as part of ISOS test guidelines.

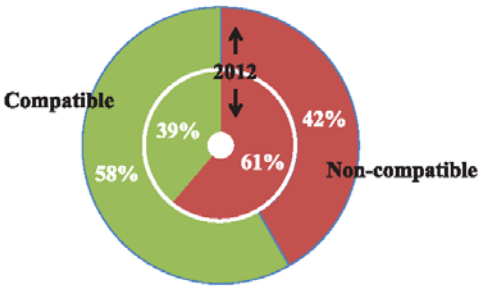

Figure 20. Shows the percent of ISOS compatible (green) and non-compatible (red) stability data reported in literature published before (inner circle) and from (outer circle) year 2012.

It is therefore important to clarify here that any ISOS testing procedure is intended for tests in air and any tests in inert atmosphere cannot be qualified as ISOS protocols. Similarly, ISOS guidelines emphasize the importance of the use of light sources with an appropriate UV component, since it is the UV part of the light that causes the main damage to the cell.

It should be stressed that tests in inert atmosphere can merely be used for comparing two different samples in the same test conditions, but do not give a true insight into the device stability potential in a real environment and cannot be utilized for comparative studies with other reports. Therefore researchers are highly encouraged to refer instead to ISOS guidelines for evaluating the stability of their devices, if the purpose is eventually to truly assess the stability in real environment. It is also important to add that the low UV light or low intensity light soaking tests can be rather useful for imitating operation in indoor environments and unfortunately at this stage ISOS testing categories do not cover such tests. An extension of the ISOS guidelines in this direction would therefore be a useful effort and should be addressed by the ISOS community.

Table 4 lists a number of recent publications that used ISOS guidelines to conduct lifetime measurements of OPV samples. The tests range from simple shelf life to sophisticated thermal cycling tests.

7.2.2. Lifetime marker. Operational lifetime in the PV field is commonly referred to the time when the sample degrades by 20% from initial performance, marked as T_{80}. However, due to the varying shapes of ageing curves for OPV devices, such a simple definition may not be sufficient for truly representing the device stability. Therefore, apart from the guidelines for conducting lifetime tests the ISOS protocols also suggest the method for reporting the lifetime [182]. Figure 21 depicts a typical ageing curve of an OPV and presents the parameters that describe the lifetime. In particular, ISOS suggests using two lifetime values to describe the ageing:

- T_{80} which is the time when the sample degrades by 20% from the initial value E_0 (E is the parameter describing the sample performance, such as for example PCE)
- T_{S80} which is the time when the sample degrades by 20% from arbitrarily defined E_S second starting value defined by the user and is calculated from the corresponding second starting time value T_S

E_S, T_S typically describe the point where the curve enters into a more stabilized phase, as can be seen in figure 21 and T_{S80} will correspondingly describe the lifetime for the more stabilized performance of the device, while T_{80} describes the initial typically more rapid ageing, often called 'burn-in'. It must be noted also that it is important to report also the E_0 and E_S values together with the lifetime values, as often the device performance stabilizes only after fully degrading and therefore, E_0 and E_S will allow distinguishing among well performing and degraded samples. Table 5 shows the list of all the ageing parameters defined by ISOS and their description.

Although the representation of the lifetime via two parts of the curve gives a better insight into the device ageing, the E_S, T_S values randomly defined by the user may lead to ambiguity and may jeopardize the comparability of the data reported by different groups. Roesch *et al* addressed this by proposing a method for mathematically determining the point T_S [188]. In particular, the approach is based on the assumption that the degradation curve can be approximated using the biexponential function shown in (1):

$$\eta(t) \approx A \cdot e^{-\frac{t}{\tau_1}} + B \cdot e^{-\frac{t}{\tau_2}} \tag{1}$$

where the first term describes the fast decay and the second term the stabilized section of the curve. τ_1 and τ_2 are the respective time constants of the exponential decays and can be determined by fitting the model to the real curves. The authors suggest that the burn-in stage comes to its end when the first term in the equation reaches 1% of its initial performance. In other words, T_S can be determined by the equation (2):

$$A \cdot e^{-\frac{T_S}{\tau_1}} = 0.01 \cdot A \rightarrow T_S = -\tau_1 \cdot \ln 0.01 \tag{2}$$

Finally, the authors suggest using as a representative of lifetime a special figure of merit, the 'lifetime energy yield' (LEY) to describe the energy produced by the device throughout its lifetime: LEY of the solar cells can be calculated by integrating the fitted double exponential function over the operational lifetime of the device until T_{S80} as defined in equation (3*a*) and shown in figure 22:

$$\mathrm{LEY} = \int_{t=0}^{T_{S80}} \eta(t)\mathrm{d}t \cdot 1\,\mathrm{kW\,m^{-2}} \tag{3a}$$

The proposed method of determining T_S however relies on the fitting of the curves with a double exponential, which imposes a limitation on the types of ageing curves the method can be applied to.

A slightly modified approach is therefore proposed here for determining T_S value. We first of all suggest defining LEY′ as the lifetime energy yield determined by setting the integral boundaries from T_S (instead of T_0) to T_{S80} (equation (3*b*)) and generalizing $\eta(t)$ as any function that fits the best for the particular curve, including linear function:

$$\mathrm{LEY}' = \int_{T_S}^{T_{S80}} \eta(t)\mathrm{d}t \cdot 1\,\mathrm{kW/m^{-2}} \tag{3b}$$

As a next step T_S is chosen such that it gives the largest possible LEY′. Geometrically speaking this will be proportional to simply maximizing the product $E_S * T_{S80}$ calculated from the

Table 4. Presents the list of ISOS protocols used in the recent publications. The table also provides the types of the test samples and the observations made during the studies.

Test condition	Tested sample	Observations	Ref.
• ISOS-O-1	Ag-grid/PEDOT:PSS/ZnO_x/ P3HT:PCBM/PEDOT:PSS/Ag-grid packaged in PET/SiOx barrier material	OPV was compared to Si performance in outdoor conditions for 4 months. At reduced light intensities OPV performance was reduced due to the lack of light doping. Positive temperature coefficient was identified for OPVs	[171]
• ISOS-D-1 • ISOS-O-1 • ISOS-L-1	ITO/PEDOT:PSS or MoO_x/ P3HT:ICBA/Ca/Al	MoO_x based samples outperform PEDOT:PSS samples in dark and outdoor conditions, but similar PCE ageing is recorded for indoor light soaking tests (see section 4.1)	[89]
• ISOS-O-2 • ISOS-L-2	Eight different device structures	Unprotected terminals of the devices were the main bottlenecks for stability	[185]
• ISOS-D-2 • ISOS-O-3	Ag-grid/PEDOT:PSS/ZnO_x/ P3HT:PCBM/PEDOT:PSS/Ag-grid packaged in PET/SiOx barrier material	Demonstration of 2 years stability	[186]
• ISOS-T-3	ITO/ZnO_x/P3HT:PCB/PEDOT:PSS/Ag	Thermal cycling of 200 times does not affect device performance. Adhesion between active layer and PEDOT:PSS is strengthened due to the elevated temperature of the test	[187]

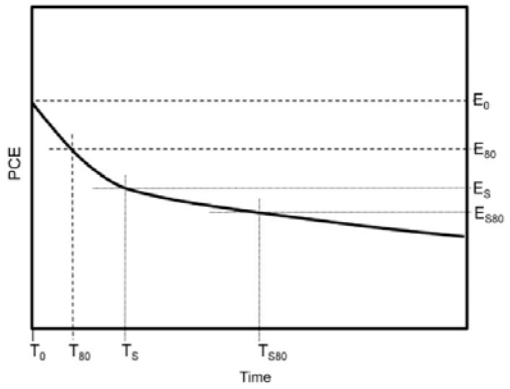

Figure 21. Example of a degradation curve with the stability markers. Reprinted with permission from [182]. Copyright 2011 Elsevier.

fitted function $\eta(t)$. Figure 23(b) shows an example of the product $E_S * T_{S80}$ as a function of T_S, calculated from the curves reported in figure 23(a) by using a linear fitting function. For the curve '3' in figure 23(a) the section with the initial increase in performance, which is typically associated with device preconditioning, is simply neglected and the starting point T_0 is moved to the time where the curve reaches its maximum. From figure 23(b) it is obvious that apart from curve '1' all the others curves show maximum energy at E_0 value, which means that these samples either never entered into a more stabilized phase or degraded before reasonable stabilization could be achieved. In this case the maximum lifetime energy yield is determined by setting $T_S = T_0$ and the pair E_0 and T_{80} and LEY (calculated from T_0 to T_{80}) will represent the device lifetime. Meanwhile, for curve '1' in figure 23(b) there is a certain point after T_0, where the maximum lifetime energy yield is achieved and this point will define the T_S. The lifetime will then be represented by the pair E_S and T_{S80} and LEY_S (calculated from T_S to T_{S80}). The method allows generically determining T_S without limiting the function $\eta(t)$ to a single type and therefore, addressing various shapes of ageing curves.

Table 5. The list of the parameters describing the lifetime according to the ISOS guidelines.

Parameter	Description
E_0, T_0	E_0 is the initial performance measured at time $T_0 = 0$,
E_S, T_S	E_S is the performance measured at time T_S, arbitrarily defined by the user
E_{80}, T_{80}	T_{80} is the lifetime calculated from T_0 that defines the time when the sample reaches $E_{80} = 0.8 * E_0$ performance
E_{S80}, T_{S80}	T_{S80} is the lifetime calculated from T_S that defines the time when the sample reaches $E_{S80} = 0.8 * E_S$ performance

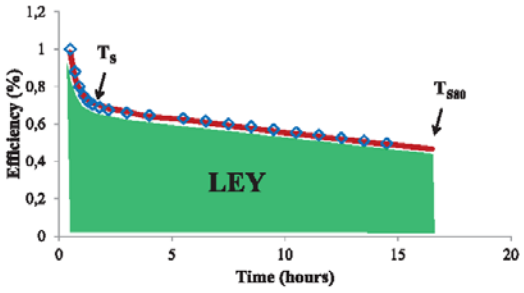

Figure 22. Example degradation curve with parameters calculated from a double exponential fit, marked: burn-in time T_S, operational lifetime T_{S80} and lifetime energy yield (LEY).

Based on the discussions above we offer the following summary of the steps to determine and report the lifetime of an OPV:

1. Conduct the ageing tests of the sample according to ISOS guideline and construct the ageing curve.
2. Calculate the product $E_S * T_{S80}$ as a function of T_S using the most suitable function for the ageing curve and determine the point where the product $E_S * T_{S80}$ is maximum and define that point as T_S.

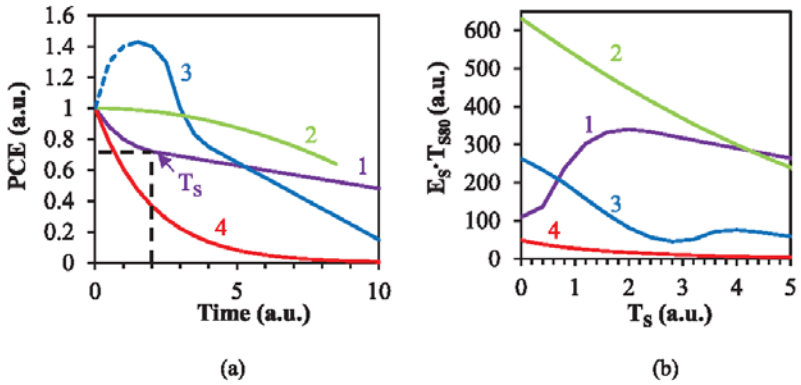

Figure 23. (a) Ageing curves of different shapes taken from real measurements and (b) the product E_S * T_{S80} as a function of T_S, calculated for the corresponding curves in (a).

3. Calculate LEY using the equation (3*b*) with boundaries of the integral set from T_S to T_{S80}.
4. Report E_S, T_{S80} and LEY.

It is our belief that the proposed methodology will allow one to generically determine the lifetime for any shape of curves and will enable fair comparison of lifetime among research groups.

It is important to note here that extrapolation of the measured lifetime data that never reached T_{80} value was not discussed here, as this is a complex process that can be a source of large errors and therefore, requires a separate investigation. It is obvious however, that if the sample stability extends beyond a few years, extrapolation can be very useful for estimating the lifetime and this must be done with extra care and only for data with a reasonable density of measurements. Even in this case however it is important to bear in mind that often secondary effects may accelerate the ageing of a sample at a later stage and therefore any extrapolated data can only be used as an indication rather than proof of a device lifetime.

7.2.3. Lifetime comparison: o-diagram and baselines. One of the efficient ways for comparing the lifetime of different devices is plotting their initial performance E_0 versus the lifetime T_{80}. However, since the reported OPV lifetime often varies from minutes up to years, the time scale should then be used in logarithmic format for easier presentation. In our earlier publication we suggested a logarithmic scale with base 4 for the time parameter T, which allowed splitting the time axes into time blocks, which could be associated with common time units such as hours, days, weeks etc. The plot was named o-diagram (o stands for OPV) and was utilized in a number of our studies for comparing the lifetime of different devices [184, 189, 190] and was also discussed earlier in this review in section 4.1. Figure 24 shows an example of the o-diagrams, which were used to compare the stability of a large number of samples tested under different ISOS test conditions. In figure 6 diagrams are presented each corresponding to one ISOS test distinguished by colors. Each diagram has *y*-axes representing PCE and *x*-axes representing the lifetime.

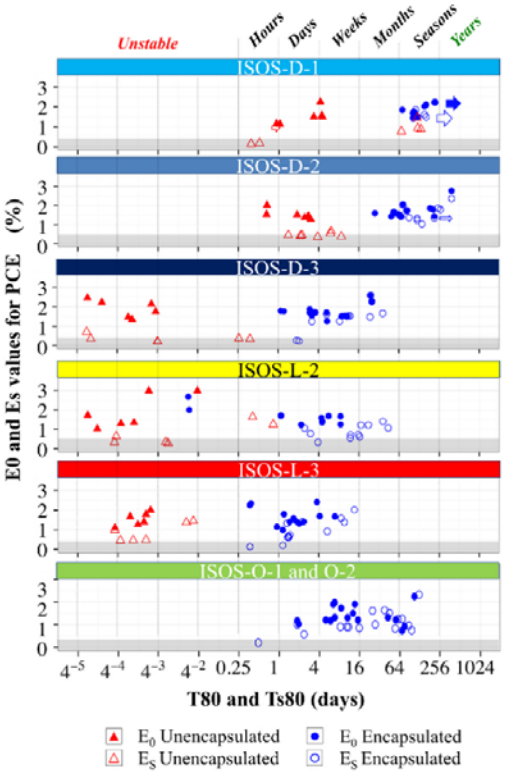

Figure 24. The o-diagram presents the E_0, T_{80} (solid markers) and E_S, T_{S80} (open markers) values for all the tested samples under different ISOS test conditions (the conditions of the tests are reported in the literature [182]). The blue circles and the red triangles represent correspondingly the devices with and without encapsulation. The grey zone marks the area where the devices are considered fully degraded (below 30% of initial performance). The arrow shows the data that represents T_{final} (the time of the last measurement) instead of T_{80}, which can be much higher. Reprinted with permission from [190]. Copyright 2015 Elsevier.

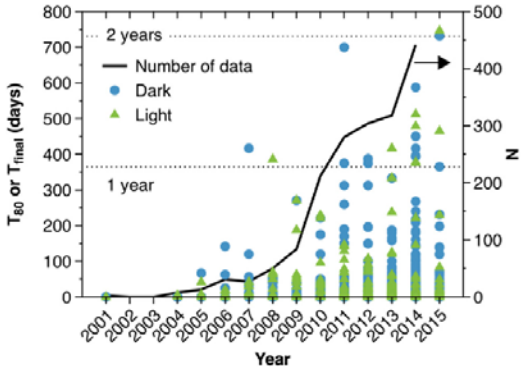

Figure 25. Lifetime of both encapsulated and unencapsulated device extracted from literature versus the year of publication. Blue circles and green triangles represent the data measured in the dark and under light, respectively. The black solid line shows the number of reports per year. Reprinted with permission from [191]. Copyright 2016 Wiley.

The *x*-axes are presented in logarithmic scale with base 4 expressed in days, shown at the bottom, which are split into time blocks associated with the common time units shown on the top. The blue and red labels represent the lifetime of the samples with and without encapsulation. The figure demonstrates how the samples tested under different conditions cluster in certain time blocks and therefore their lifetime can be categorized according to the common time units, such as for example samples tested under ISOS-D-1 (shelf life) and ISOS-D-2 (high temperature storage) conditions last mostly for couple of seasons, while under the harsh tests of ISOS-L-3 (indoor weathering under elevated temperatures and humidity) only days and weeks. In this study the o-diagram was used to gauge and compare the lifetime of the same samples tested under different ISOS test conditions. Similarly, in another two studies the same approach was used to categorize the lifetime of all the devices that have been reported in the literature so far, which allowed us to identify certain trends in the OPV lifetime, determining the best reported lifetime and establishing a baseline for OPV lifetime [16, 191]. The latter studies are discussed in detail in the next section.

8. Current status and predictions of OPV lifetime

Recently two studies were reported, based on the meta-analyzes of OPV lifetime data reported in literature. The first one presented the analyses of all the articles reporting lifetime data of OPVs published before mid-2013 [16] and the second one analyzed the remaining articles until mid-2015 [191]. The idea was to identify the pair of E_0 and T_{80} parameters for each ageing curve and to combine these in the o-diagram for comparative analyses. Section 4.1 has already discussed an example of the use of this data for comparing samples with and without PEDOT:PSS in terms of lifetime.

A number of lessons were learned from these studies. In particular, figure 25 shows the lifetime values extracted from literature data distributed versus the years of publications. The blue circles and green triangles represent both encapsulated and unencapsulated samples tested in the dark and under light, respectively. The black solid line shows the number of data points per year. The figure demonstrates how both the number of reports and the lifetime are rapidly increasing. This shows that the lifetime issue has become one of the most important and urgent challenges of OPV field and therefore, significant improvements can be seen in the past several years with reported lifetime values crossing the 2 years threshold.

More importantly, the studies allowed determining the typical OPV performance under specific test conditions [191]. All the literature data were split into four categories: Group 1 and 2—unencapsulated samples tested under light and in the dark, respectively, group 3 and 4—encapsulated samples tested under light and dark respectively. Group 3 additionally was split into three categories—samples tested (a) under light sources with spectrum close to AM1.5G, (b) outdoors and (c) under light sources with poor UV content or low intensity. The groups were additionally associated with but not limited to the corresponding ISOS guidelines marked in the legends of the plots. The distributions of the lifetime data in the time blocks (same scale as in o-diagram) were then constructed and are presented in figure 26. The *y*-axis represent the number of data points and *x*-axis the time. The blocks marked with red show the median and the green show the maximum number of samples with the corresponding lifetime values reported for each test condition. The table on the right lower corner lists all the median and maximum values for the different categories. For the unencapsulated samples tested in the dark (right upper corner) two distinct picks are identified, where the picks with lower and higher lifetime values correspond to the normal and inverted structures, respectively. These distributions are named as baselines for OPV lifetime and are suggested to be used in the following way:

For any newly developed (OPV) solar cell:

- If the achieved lifetime is beyond the median, then the sample has an improved stability.
- If the achieved lifetime is in the maximum region or beyond, then the sample has an outstanding or record lifetime, respectively.

The reason the category 3 was split according to the light source type was because the light source can have a significant impact on device lifetime, as was discussed in the ISOS guidelines.

From the figure it is additionally evident that while there is only little difference in stability for samples with and without encapsulation when tested in the dark (especially for inverted structures), significant difference is observed for indoor light tests, where unencapsulated samples last mostly only couple of hours and reach several 100 h when encapsulated. Nevertheless, the comparison is very generic and the ration may differ significantly from one type of devices or test conditions to another. Larger amount of data is therefore needed for more accurate comparison.

The literature data analyses also allowed us to construct the diagram of the best reported lifetimes of devices per year, which is shown in figure 27. Four trends are shown for

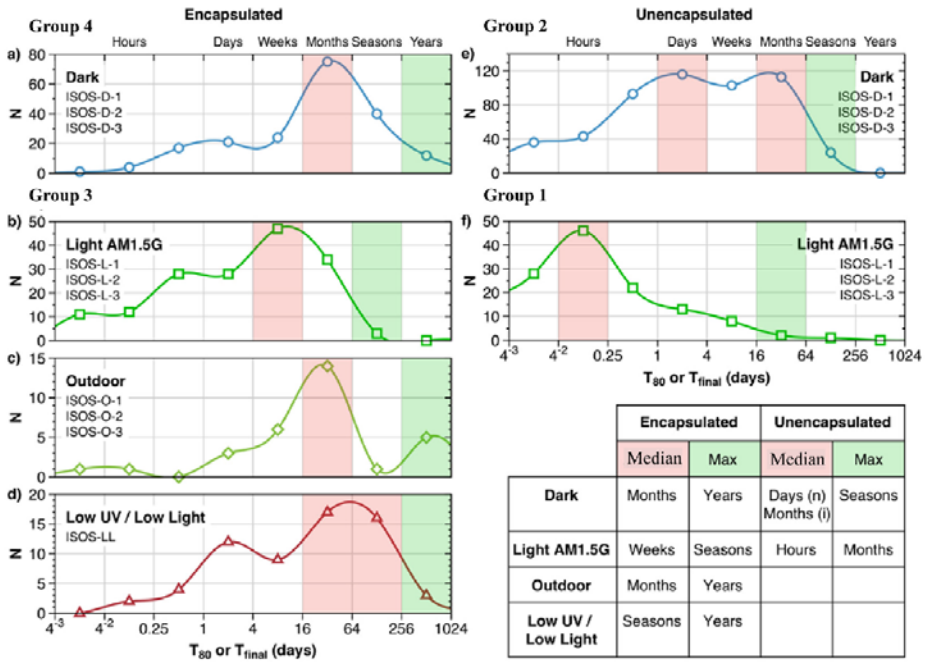

	Encapsulated		Unencapsulated	
	Median	Max	Median	Max
Dark	Months	Years	Days (n) Months (i)	Seasons
Light AM1.5G	Weeks	Seasons	Hours	Months
Outdoor	Months	Years		
Low UV / Low Light	Seasons	Years		

Figure 26. Baselines of the lifetime of OPVs tested under different ageing conditions for encapsulated (left plots) and unencapsulated (right plots) samples. The plots represent the number of data points distributed among the time blocks corresponding to the logarithmic scale with base 4 (similar to o-diagram). The scale is associated with the common time units shown on the top *x*-axis of each plot. The median and maximum lifetime values for each distribution are highlighted with red and green bands and are listed in the table on the right lower corner. For unencapsulated samples tested in the dark two distinct peaks, i.e. two median values corresponding to days and months, are associated with the normal and inverted structures. The test conditions are associated with, but not limited to the ISOS test conditions. Reprinted with permission from [191]. Copyright 2016 Wiley.

samples tested, respectively, in the dark, under low UV light, in outdoor conditions and indoor under a light source with spectrum close to AM1.5G. The diagram was reported in the earlier publication [191] and is now updated with the latest achievement of 4 years (1463 d) of shelf life for flexible R2R processed and packaged OPV modules manufactured at the Technical University of Denmark. The 4 years measurements are presented in figure 28 and are a continuation of an earlier reported study, where over 2 years of lifetime was reported for R2R coated modules by Krebs *et al* [186]. The details of the modules and the measurements can be found in the aforementioned publication.

The diagram of the best lifetimes also highlights the fact that the lifetime of OPVs experienced rapid improvements in recent years and 2 years has already been achieved for outdoor tests and 4 years for shelf life.

Today at least one important question still remains: how to predict the lifetime of an OPV device based on accelerated tests? Methods for accurate prediction are necessary, since the lifetime of OPVs is gradually improving and the testing period becomes impractical for rapid scientific progress. While an answer to this question has not been given yet, steps are being taken towards addressing this issue. In particular, based on the collected literature data presented above a database was established, which is hosted online at the address http://plasticphotovoltaics.com/lifetime-predictor.html. The data is freely accessible to the public and a user-friendly interface has been developed that allows analyzing the data by applying specific filters. The page also allows uploading any new data. The purpose of the online data is to gradually expand the lifetime database of OPVs and create sufficient data that will allow developing more accurate baselines particularly for ISOS tests and eventually establishing prediction tools for devices with prolonged lifetimes.

Meanwhile, based on the data presented above and the fact that in last 2 years the lifetime of OPVs was reported to improve from 1 year to 2–4 years, it is fair to assume that already today there are samples under testing that will last up to 3–4 years under light and much longer in the dark and if the same progress continues, by 2020 samples will be produced that will last more than 7–8 years. Moreover, if we employ novel measures, such as LEY discussed in section 7.2.2 and instead of the T_{80} threshold use perhaps another metric to define the usable lifetime span that is more true to when an OPV technology becomes unfit for use (e.g. T_{50}), it would appear 7–15 years is within reach in the near future, if not already here. Therefore, with the given very low embedded energy in the production it is highly likely that within the next few years the energy produced by stable OPVs will reach a cost level that will compete even with fossil fuels [215].

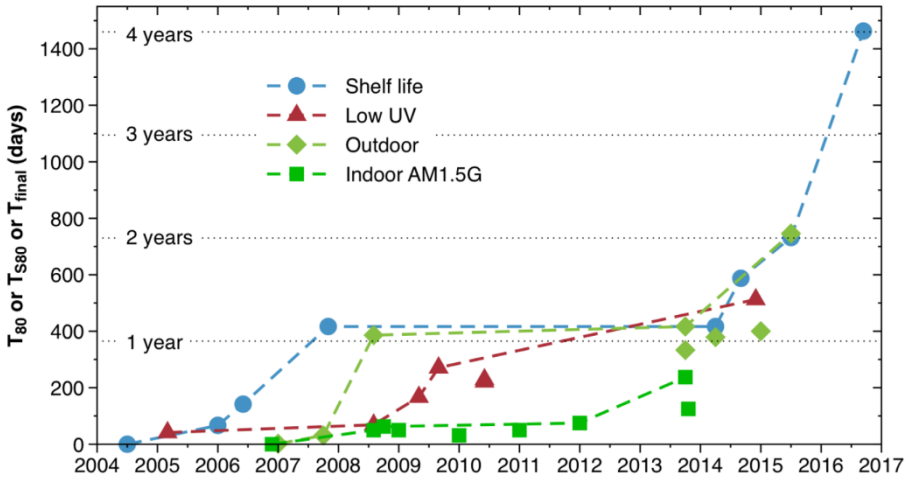

Indoor AM1.5G			Shelf life			Outdoor			Low UV		
PCE (%)	Lifetime (d)	Ref.	PCE (%)	Lifetime (d)	Ref.	PCE (%)	Lifetime (d)	Ref.	PCE (%)	Lifetime (d)	Ref.
1.08	0.083	[80]	0.8	0.042	[192]	0.0024	2	[193]	2.5	42	[194]
NA	50	[195]	0.035	67	[196]	4.2	31	[197]	4.1	69	[198]
NA	63	[199]	0.16	142	[200]	NA	386	[195]	2.32	167	[201]
1.09	50	[202]	2.8	417	[203]	1.43	417	[169]	5.9	271	[204]
3.54	31	[205]	1.27	417	[206]	1.43	333	[169]	2.7	229	[207]
NA	50	[208]	6.05	587.5	[72]	NA	379	[206]	6.07	221	[209]
2.1	75	[210]	1.06	732	[186]	1.42	400	[211]	2.7	513	[212]
3.42	125	[213]	1.06	1463	Continuation of [186]	1.11	746	[186]			
2.59	238	[214]									

Figure 27. Best lifetime values for different test conditions reported for each year. The table below shows the corresponding initial efficiencies and references. Some of the data points have been defined by the last measurement T_{final} of the experiment, since the 20% ageing threshold was not reached during the test. The dashed lines connect the data points to highlight the evolvement of record values. The horizontal dotted lines mark the 1 and 2 year values.

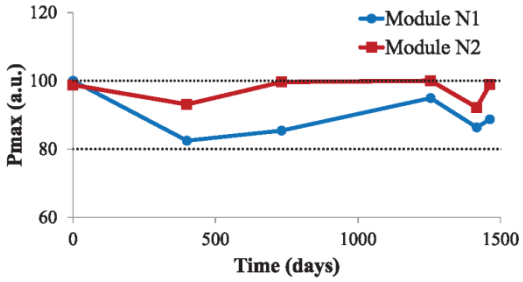

Figure 28. Shelf life of flexible R2R processed, ITO-free, encapsulated OPV modules manufactured at the Technical University of Denmark in 2012. The normalized values of maximum power P_{max} versus the time is presented. The two curves correspond to two identical modules stored in the dark in air.

9. Conclusions

In conclusion, the review discussed the stability of organic solar cells by addressing the entire chain of challenges ranging from physical and chemical modifications on the atomic level to device upscaling and packaging and lifetime characterization. The importance of maintaining the compatibility of devices with final product design, while developing architectural solutions for device stabilization, was stressed. The ageing mechanisms in different layers of the devices were discussed and an overview of recently proposed solutions was presented. This included the overview of recent advances in chemical modifications of the active layer via side chain modifications, diversification of the back bones and improvement of the acceptor materials. The latter involved cross linking of fullerenes or the use of fullerene free materials. The pros and cons of additives were discussed in terms of the morphological stability of the films, as well as the inclusion of the third component in the active mixture. The mechanical stability of the layers and interfaces was additionally discussed, which has gained increased attention in recent years. In particular, it was demonstrated that certain compatibilizers or a set of external stresses could improve the cohesion of certain layers in the device. Molecular weight or donor: acceptor rations were additional parameters affecting the mechanical stability of the layers. Device upscaling and packaging were addressed as

well, and the importance of appropriate edge sealing was highlighted and supported with some examples. Characterization of device stability and lifetime were discussed, which included the overview of the recently reported advanced characterization techniques that were used for studying the ageing mechanism. A summary of the ISOS guidelines for testing device lifetime was presented and accomplished by presentation of a generic marker for lifetime determination for any shape of ageing curves and the lifetime energy yield as an additional marker for lifetime rating. The lifetime comparison of the different reports via an o-diagram was discussed as well. The review was concluded by presenting the status of OPV lifetime today and predicting its progress in the near future. In particular, today up to 4 years of stability has been reported and if the same progress continues, by 2020 samples with a lifetime up to 7–8 years will likely be achieved. Moreover, if different and perhaps more suitable metrics are defined that will better reflect the usefulness of OPV in operation for certain applications, such as for example the energy produced by the samples until T_{50} lifetime, up to 15 years stability can be envisaged for OPVs in the near future.

Acknowledgment

IMH and EB acknowledge Villum Foundation (Yong Investigator programme, 'Materials for energy production') for supporting this work.

References

[1] Djurišić A B, Liu F, Ng A M C, Dong Q, Wong M K, Ng A and Surya C 2016 Stability issues of the next generation solar cells *Phys. Status Solidi* **10** 281–99
[2] Manceau M, Rivaton A, Gardette J L, Guillerez S and Lemaître N 2009 The mechanism of photo- and thermooxidation of poly(3-hexylthiophene) (P3HT) reconsidered *Polym. Degrad. Stab.* **94** 898–907
[3] Turkovic V, Engmann S, Gobsch G and Hoppe H 2012 Methods in determination of morphological degradation of polymer:fullerene solar cells *Synth. Met.* **161** 2534–9
[4] Waters H, Bristow N, Moudam O, Chang S W, Su C J, Wu W R, Jeng U S, Horie M and Kettle J 2014 Effect of processing additive 1,8-octanedithiol on the lifetime of PCPDTBT based organic photovoltaics *Org. Electron. Phys. Mater. Appl.* **15** 2433–8
[5] Kim Y J, Chung D S and Park C E 2015 Highly thermally stable non-fullerene organic solar cells: p-DTS(FBTTh2)2:P(NDI2OD-T2) bulk heterojunction *Nano Energy* **15** 343–52
[6] Han D, Lee H, Jeong S, Lee J, Lee J-Y and Yoo S 2015 Stability enhancement of normal-geometry organic solar cells in a highly damp condition: a study on the effect of top electrodes *Org. Electron.* **25** 31–6
[7] Jørgensen M, Norrman K and Krebs F C 2008 Stability/degradation of polymer solar cells *Sol. Energy Mater. Sol. Cells* **92** 686–714
[8] Grossiord N, Kroon J M, Andriessen R and Blom P W M 2012 Degradation mechanisms in organic photovoltaic devices *Org. Electron.* **13** 432–56
[9] Jørgensen M, Norrman K, Gevorgyan S A, Tromholt T, Andreasen B and Krebs F C 2012 Stability of polymer solar cells *Adv. Mater.* **24** 580–612
[10] Lee J U, Jung J W, Jo J W and Jo W H 2012 Degradation and stability of polymer-based solar cells *J. Mater. Chem.* **22** 24265–83
[11] Cao H, He W, Mao Y, Lin X, Ishikawa K, Dickerson J H and Hess W P 2014 Recent progress in degradation and stabilization of organic solar cells *J. Power Sources* **264** 168–83
[12] Giannouli M, Drakonakis V M, Savva A, Eleftheriou P, Florides G and Choulis S A 2015 Methods for improving the lifetime performance of organic photovoltaics with low-costing encapsulation *ChemPhysChem* **16** 1134–54
[13] Cheng P and Zhan X 2016 Stability of organic solar cells: challenges and strategies *Chem. Soc. Rev.* **45** 2544–82
[14] Lloyd M T, Olson D C, Berry J, Kopidakis N, Reese M O, Steirer K X and Ginley D S 2010 Enhanced lifetime in unencapsulated organic photovoltaics with air stable electrodes *35th IEEE Photovoltaic Specialists Conf.* (IEEE) pp 001060–3
[15] Voroshazi E, Cardinaletti I, Uytterhoeven G, Hadipour A, Rand B P and Aernouts T 2013 Role of electron and hole collecting buffer layers on the stability of inverted polymer: fullerene photovoltaic devices *IEEE 39th Photovoltaic Specialists Conf. (PVSC)* (IEEE) pp 3212–5
[16] Gevorgyan S A, Madsen M V, Roth B, Corazza M, Hösel M, Søndergaard R R, Jørgensen M and Krebs F C 2016 Lifetime of organic photovoltaics: status and predictions *Adv. Energy Mater.* **6** 1–17
[17] Drakonakis V M, Savva A, Kokonou M and Choulis S A 2014 Investigating electrodes degradation in organic photovoltaics through reverse engineering under accelerated humidity lifetime conditions *Sol. Energy Mater. Sol. Cells* **130** 544–50
[18] Züfle S, Neukom M T, Altazin S, Zinggeler M, Chrapa M, Offermans T and Ruhstaller B 2015 An effective area approach to model lateral degradation in organic solar cells *Adv. Energy Mater.* **5** 1500835
[19] Krebs F C, Hoesel M, Corazza M, Roth B, Madsen M V, Gevorgyan S A, Sondergaard R R, Karg D and Jorgensen M 2013 Freely available OPV-the fast way to progress *Energy Technol.* **1** 378–81
[20] Espinosa N, Hösel M, Jørgensen M and Krebs F C 2014 Large scale deployment of polymer solar cells on land, on sea and in the air *Energy Environ. Sci.* **7** 855
[21] Cardinaletti I *et al* 2014 Toward bulk heterojunction polymer solar cells with thermally stable active layer morphology *J. Photonics Energy* **4** 040997
[22] Rumer J W and McCulloch I 2015 Organic photovoltaics: crosslinking for optimal morphology and stability *Mater. Today* **18** 425–35
[23] Lu L, Zheng T, Wu Q, Schneider A M, Zhao D and Yu L 2015 Recent advances in bulk heterojunction polymer solar cells *Chem. Rev.* **115** 12666–731
[24] Bundgaard E, Helgesen M, Carlé J E, Krebs F C and Jørgensen M 2013 Advanced functional polymers for increasing the stability of organic photovoltaics *Macromol. Chem. Phys.* **214** 1546–58
[25] Xu X, Wu Y, Fang J, Li Z, Wang Z, Li Y and Peng Q 2014 Side-chain engineering of benzodithiophene-fluorinated quinoxaline low-band-gap co-polymers for high-performance polymer solar cells *Chem. Eur. J.* **20** 13259–71
[26] Tournebize A *et al* 2015 Is there a photostable conjugated polymer for efficient solar cells? *Polym. Degrad. Stab.* **112** 175–84
[27] Morse G E, Tournebize A, Rivaton A, Chassé T, Taviot-Gueho C, Blouin N, Lozman O R and Tierney S 2015 The effect of polymer solubilizing side-chains on solar cell stability *Phys. Chem. Chem. Phys.* **17** 11884–97

[28] Li Z, Wu F, Lv H, Yang D, Chen Z, Zhao X and Yang X 2015 Side-chain engineering for enhancing the thermal stability of polymer solar cells *Adv. Mater.* **27** 6999–7003

[29] Verstappen P *et al* 2015 Simultaneous enhancement of solar cell efficiency and stability by reducing the side chain density on fluorinated PCPDTQ$_x$ copolymers *Macromolecules* **48** 3873–82

[30] Vandenbergh J *et al* 2011 Thermal stability of poly[2-methoxy-5-(2′-phenylethoxy)-1,4-phenylenevinylene] (MPE-PPV): fullerene bulk heterojunction solar cells *Macromolecules* **44** 8470–8

[31] Campo B J *et al* 2013 Ester-functionalized poly(3-alkylthiophene) copolymers: Synthesis, physicochemical characterization and performance in bulk heterojunction organic solar cells *Org. Electron.* **14** 523–34

[32] Kesters J *et al* 2014 Enhanced intrinsic stability of the bulk heterojunction active layer blend of polymer solar cells by varying the polymer side chain pattern *Org. Electron. Phys. Mater. Appl.* **15** 549–62

[33] Bertho S, Campo B, Piersimoni F, Spoltore D, D'Haen J, Lutsen L, Maes W, Vanderzande D and Manca J 2013 Improved thermal stability of bulk heterojunctions based on side-chain functionalized poly(3-alkylthiophene) copolymers and PCBM *Sol. Energy Mater. Sol. Cells* **110** 69–76

[34] Kesters J, Verstappen P, Raymakers J, Vanormelingen W, Drijkoningen J, D'Haen J, Manca J, Lutsen L, Vanderzande D and Maes W 2015 Enhanced organic solar cell stability by polymer (PCPDTBT) side chain functionalization *Chem. Mater.* **27** 1332–41

[35] Heckler I, Kesters J, Defour M, Madsen M, Penxten H, D'Haen J, Van Mele B, Maes W and Bundgaard E 2016 The influence of conjugated polymer side chain manipulation on the efficiency and stability of polymer solar cells *Materials* **9** 181

[36] Lee R-H, Chen W-Y and Shiau S-Y 2013 Synthesis and photovoltaic properties of a series of bulk heterojunction solar cells based on interchain-linked conjugated polymers *Polym. J.* **45** 744–57

[37] Manceau M, Bundgaard E, Carlé J E, Hagemann O, Helgesen M, Søndergaard R, Jørgensen M and Krebs F C 2011 Photochemical stability of π-conjugated polymers for polymer solar cells: a rule of thumb *J. Mater. Chem.* **21** 4132

[38] Gedefaw D, Tessarolo M, Prosa M, Bolognesi M, Henriksson P, Zhuang W, Seri M, Muccini M and Andersson M R 2016 Induced photodegradation of quinoxaline based copolymers for photovoltaic applications *Sol. Energy Mater. Sol. Cells* **144** 150–8

[39] Shin N, Yun H-J, Yoon Y, Son H J, Ju S-Y, Kwon S-K, Kim B and Kim Y-H 2015 Highly stable polymer solar cells based on poly(dithienobenzodithiophene-co-thienothiophene) *Macromolecules* **48** 3890–9

[40] Zhang S, Yang B, Liu D, Zhang H, Zhao W, Wang Q, He C and Hou J 2016 Correlations among chemical structure, backbone conformation, and morphology in two highly efficient photovoltaic polymer materials *Macromolecules* **49** 120–6

[41] Carlé J E, Helgesen M, Zawacka N K, Madsen M V, Bundgaard E and Krebs F C 2014 A comparative study of fluorine substituents for enhanced stability of flexible and ITO-free high-performance polymer solar cells *J. Polym. Sci.* B **52** 893–9

[42] Nguyen T L *et al* 2014 Semi-crystalline photovoltaic polymers with efficiency exceeding 9% in a ~300 nm thick conventional single-cell device *Energy Environ. Sci.* **7** 3040–51

[43] Livi F, Zawacka N K, Angmo D, Jørgensen M, Krebs F C and Bundgaard E 2015 Influence of side chain position on the electrical properties of organic solar cells based on dithienylbenzothiadiazole-alt-phenylene conjugated polymers *Macromolecules* **48** 3481–92

[44] Li F, Yager K G, Dawson N M, Yang J, Malloy K J and Qin Y 2013 Complementary hydrogen bonding and block copolymer self-assembly in cooperation toward stable solar cells with tunable morphologies *Macromolecules* **46** 9021–31

[45] Chen C-P, Huang C-Y and Chuang S-C 2015 Highly thermal stable and efficient organic photovoltaic cells with crosslinked networks appending open-cage fullerenes as additives *Adv. Funct. Mater.* **25** 207–13

[46] Diacon A, Derue L, Lecourtier C, Dautel O, Wantz G and Hudhomme P 2014 Cross-linkable azido C 60-fullerene derivatives for efficient thermal stabilization of polymer bulk-heterojunction solar cells *J. Mater. Chem.* C **2** 7163

[47] George Z, Xia Y, Sharma A, Lindqvist C, Andersson G G, Inganäs O, Moons E, Müller C and Andersson M R 2016 Two-in-one: cathode modification and improved solar cell blend stability through addition of modified fullerenes *J. Mater. Chem.* A **4** 2663–9

[48] Wang S, Wang M, Chen Z and Yang X 2015 Selection strategy of porphyrins for achieving thermally stable polymer solar cells *J. Mater. Chem.* A **3** 21051–9

[49] Li S, Liu W, Shi M, Mai J, Lau T-K, Wan J-H, Lu X, Li C-Z and Chen H 2016 A spirobifluorene and diketopyrrolopyrrole moieties based non-fullerene acceptor for efficient and thermally stable polymer solar cells with high open-circuit voltage *Energy Environ. Sci.* **9** 1–11

[50] Wang S, Qu Y, Li S, Ye F, Chen Z and Yang X 2015 Improved thermal stability of polymer solar cells by incorporating porphyrins *Adv. Funct. Mater.* **25** 748–57

[51] Liao M-H, Tsai C-E, Lai Y-Y, Cao F-Y, Wu J-S, Wang C-L, Hsu C-S, Liau I and Cheng Y-J 2014 Morphological stabilization by supramolecular perfluorophenyl-C 60 interactions leading to efficient and thermally stable organic photovoltaics *Adv. Funct. Mater.* **24** 1418–29

[52] Lin Y and Zhan X 2014 Non-fullerene acceptors for organic photovoltaics: an emerging horizon *Mater. Horiz.* **1** 470

[53] Chen L, Tian S and Chen Y 2014 Enhanced performance for organic bulk heterojunction solar cells by cooperative assembly of ter(ethylene oxide) pendants *Polym. Chem.* **5** 4480

[54] Wu Q, Bhattacharya M, Moore L M J and Morgan S E 2014 Air processed P3HT:PCBM photovoltaic cells: morphology correlation to annealing, degradation, and recovery *J. Polym. Sci.* B **52** 1511–20

[55] Kim W, Kim J K, Kim E, Ahn T K, Wang D H and Park J H 2015 Conflicted effects of a solvent additive on PTB7:PC 71 BM bulk heterojunction solar cells *J. Phys. Chem.* C **119** 5954–61

[56] Kettle J, Waters H, Ding Z, Horie M and Smith G C 2015 Chemical changes in PCPDTBT:PCBM solar cells using XPS and TOF-SIMS and use of inverted device structure for improving lifetime performance *Sol. Energy Mater. Sol. Cells* **141** 139–47

[57] Huang W, Gann E, Xu Z-Q, Thomsen L, Cheng Y-B and McNeill C R 2015 A facile approach to alleviate photochemical degradation in high efficiency polymer solar cells *J. Mater. Chem.* A **3** 16313–9

[58] Kettle J, Waters H, Horie M and Smith G C 2016 Alternative selection of processing additives to enhance the lifetime of OPVs *J. Phys. D: Appl. Phys.* **49** 85601

[59] Khiev S, Derue L, Ayenew G, Medlej H, Brown R, Rubatat L, Hiorns R C, Wantz G and Dagron-Lartigau C 2013 Enhanced thermal stability of organic solar cells by using photolinkable end-capped polythiophenes *Polym. Chem.* **4** 4145

[60] Bracher C, Yi H, Scarratt N W, Masters R, Pearson A J, Rodenburg C, Iraqi A and Lidzey D G 2015 The effect

of residual palladium catalyst on the performance and stability of PCDTBT:PC70BM organic solar cells *Org. Electron.* **27** 266–73
[61] Cheng P and Zhan X 2015 Versatile third components for efficient and stable organic solar cells *Mater. Horiz.* **2** 462–85
[62] Derue L *et al* 2014 Thermal stabilisation of polymer-fullerene bulk heterojunction morphology for efficient photovoltaic solar cells *Adv. Mater.* **26** 5831–8
[63] Kakavelakis G, Stratakis E and Kymakis E 2013 Aluminum nanoparticles for efficient and stable organic photovoltaics *RSC Adv.* **3** 16288
[64] Tore N, Parlak E A, Tumay T A, Kavak P, Sarıoğlan Ş, Bozar S, Günes S, Ulbricht C and Egbe D A M 2014 Improvement in photovoltaic performance of anthracene-containing PPE–PPV polymer-based bulk heterojunction solar cells with silver nanoparticles *J. Nanopart. Res.* **16** 2298
[65] Mateker W R, Heumueller T, Cheacharoen R, Sachs-Quintana I T, McGehee M D, Warnan J, Beaujuge P M, Liu X and Bazan G C 2015 Molecular packing and arrangement govern the photo-oxidative stability of organic photovoltaic materials *Chem. Mater.* **27** 6345–53
[66] Heumueller T, Mateker W R, Sachs-Quintana I T, Vandewal K, Bartelt J A, Burke T M, Ameri T, Brabec C J and McGehee M D 2014 Reducing burn-in voltage loss in polymer solar cells by increasing the polymer crystallinity *Energy Environ. Sci.* **7** 2974
[67] Heumueller T, Burke T M, Mateker W R, Sachs-Quintana I T, Vandewal K, Brabec C J and McGehee M D 2015 Disorder-induced open-circuit voltage losses in organic solar cells during photoinduced burn-in *Adv. Energy Mater.* **5** 1500111
[68] Hermenau M, Riede M, Leo K, Gevorgyan S A, Krebs F C and Norrman K 2011 Water and oxygen induced degradation of small molecule organic solar cells *Sol. Energy Mater. Sol. Cells* **95** 1268–77
[69] Oh J Y, Shin M, Lee H W, Lee Y-J, Baik H K and Jeong U 2014 Enhanced air stability of polymer solar cells with a nanofibril-based photoactive layer *ACS Appl. Mater. Interfaces* **6** 7759–65
[70] Turkovic V, Engmann S, Tsierkezos N, Hoppe H, Ritter U and Gobsch G 2014 Long-term stabilization of organic solar cells using hindered phenols as additives *ACS Appl. Mater. Interfaces* **6** 18525–37
[71] Voroshazi E, Cardinaletti I, Conard T and Rand B P 2014 Light-induced degradation of polymer: fullerene photovoltaic devices: an intrinsic or material-dependent failure mechanism? *Adv. Energy Mater.* **4** 1400848
[72] Kong J *et al* 2014 Long-term stable polymer solar cells with significantly reduced burn-in loss *Nat. Commun.* **5** 5688
[73] Kim H J, Kim J-H, Ryu J-H, Kim Y, Kang H, Lee W B, Kim T-S and Kim B J 2014 Architectural engineering of rod-coil compatibilizers for producing mechanically and thermally stable polymer solar cells *ACS Nano* **8** 10461–70
[74] Corazza M, Rolston N, Dauskardt R H, Beliatis M, Krebs F C and Gevorgyan S A 2016 Role of stress factors on the adhesion of interfaces in R2R fabricated organic photovoltaics *Adv. Energy Mater.* **6** 1501927
[75] Kim T, Kim J-H, Kang T E, Lee C, Kang H, Shin M, Wang C, Ma B, Jeong U, Kim T-S and Kim B J 2015 Flexible, highly efficient all-polymer solar cells *Nat. Commun.* **6** 8547
[76] Savagatrup S, Rodriquez D, Printz A D, Sieval A B, Hummelen J C and Lipomi D J 2015 [70]PCBM and incompletely separated grades of methanofullerenes produce bulk heterojunctions with increased robustness for ultra-flexible and stretchable electronics *Chem. Mater.* **27** 3902–11
[77] Savagatrup S, Printz A D, O'Connor T F, Zaretski A V and Lipomi D J 2014 Molecularly stretchable electronics *Chem. Mater.* **26** 3028–41
[78] Bruner C, Novoa F, Dupont S and Dauskardt R 2014 Decohesion kinetics in polymer organic solar cells *ACS Appl. Mater. Interfaces* **6** 21474–83
[79] Dupont S R, Voroshazi E, Heremans P and Dauskardt R H 2013 Adhesion properties of inverted polymer solar cells: processing and film structure parameters *Org. Electron.* **14** 1262–70
[80] Kawano K, Pacios R, Poplavskyy D, Nelson J, Bradley D D C and Durrant J R 2006 Degradation of organic solar cells due to air exposure *Sol. Energy Mater. Sol. Cells* **90** 3520–30
[81] Voroshazi E, Verreet B, Buri A, Müller R, Di Nuzzo D and Heremans P 2011 Influence of cathode oxidation via the hole extraction layer in polymer:fullerene solar cells *Org. Electron. Phys. Mater. Appl.* **12** 736–44
[82] Norrman K, Madsen M V, Gevorgyan S A and Krebs F C 2010 Degradation patterns in water and oxygen of an inverted polymer solar cell *J. Am. Chem. Soc.* **132** 16883–92
[83] Bulle-Lieuwma C W T, van Gennip W J H, van Duren J K J, Jonkheijm P, Janssen R A J and Niemantsverdriet J W 2003 Characterization of polymer solar cells by TOF-SIMS depth profiling *Appl. Surf. Sci.* **203–4** 547–50
[84] de Jong M P, Van Ijzendoorn L J and de Voigt M J A 2000 Stability of the interface between indium-tin-oxide in polymer light-emitting diodes *App. Phys. Lett.* **77** 2255–7
[85] Sapkota S B, Fischer M, Zimmermann B and Würfel U 2014 Analysis of the degradation mechanism of ITO-free organic solar cells under UV radiation *Sol. Energy Mater. Sol. Cells* **121** 43–8
[86] Lloyd M T, Olson D C, Lu P, Fang E, Moore D L, White M S, Reese M O, Ginley D S and Hsu J W P 2009 Impact of contact evolution on the shelf life of organic solar cells *J. Mater. Chem.* **19** 7638
[87] Bovill E, Scarratt N, Griffin J, Yi H, Iraqi A, Buckley A R, Kingsley J W and Lidzey D G 2015 The role of the hole-extraction layer in determining the operational stability of a polycarbazole:fullerene bulk-heterojunction photovoltaic device *Appl. Phys. Lett.* **106** 73301
[88] Voroshazi E, Cardinaletti I, Uytterhoeven G, Li S, Empl M, Aernouts T and Rand B P 2014 Role of electron-and hole-collecting buffer layers on the stability of inverted polymer: fullerene photovoltaic devices *IEEE J. Photovolt.* **4** 265–70
[89] Kumar P, Bilen C, Vaughan B, Zhou X, Dastoor P C and Belcher W J 2016 Comparing the degradation of organic photovoltaic devices under ISOS testing protocols *Sol. Energy Mater. Sol. Cells* **149** 179–86
[90] Glen T S, Scarratt N W, Yi H, Iraqi A, Wang T, Kingsley J, Buckley A R, Lidzey D G and Donald A M 2016 Dependence on material choice of degradation of organic solar cells following exposure to humid air *J. Polym. Sci.* B **54** 216–24
[91] Greenbank W, Hirsch L, Wantz G and Chambon S 2015 Interfacial thermal degradation in inverted organic solar cells *Appl. Phys. Lett.* **107** 263301
[92] Savva A, Georgiou E, Papazoglou G, Chrusou A Z, Kapnisis K and Choulis S A 2015 Photovoltaic analysis of the effects of PEDOT:PSS-additives hole selective contacts on the efficiency and lifetime performance of inverted organic solar cells *Sol. Energy Mater. Sol. Cells* **132** 507–14
[93] Lee S J, Kim B S, Kim J-Y, Yusoff A R B M and Jang J 2015 Stable organic photovoltaic with PEDOT:PSS and MoOX mixture anode interfacial layer without encapsulation *Org. Electron.* **19** 140–6

[94] Lee J J, Lee S H, Kim F S, Choi H H and Kim J H 2015 Simultaneous enhancement of the efficiency and stability of organic solar cells using PEDOT:PSS grafted with a PEGME buffer layer *Org. Electron.* **26** 191–9

[95] Hou X, Li Q, Cheng T, Yu L, Wang F, Lin J, Dai S, Li Y and Tan Z 2015 Improvement of the power conversion efficiency and long term stability of polymer solar cells by incorporation of amphiphilic Nafion doped PEDOT-PSS as a hole extraction layer *J. Mater. Chem.* A **3** 18727–34

[96] Yuan Z, Wu Z, Bai S, Cui W, Liu J, Song T and Sun B 2015 Layered bismuth selenide utilized as hole transporting layer for highly stable organic photovoltaics *Org. Electron.* **26** 327–33

[97] Kim N, Xin G, Cho S M, Pang C and Chae H 2015 Microwave-reduced graphene oxide for efficient and stable hole extraction layers of polymer solar cells *Curr. Appl. Phys.* **15** 953–7

[98] Shi Y, Tan L, Chen L and Chen Y 2014 Self-assembled buffer layer from conjugated diblock copolymers with ethyleneoxide side chains for high efficiency polymer solar cells *J. Mater. Chem.* C **0** 1–11

[99] MacLeod B A *et al* 2015 Stability of inverted organic solar cells with ZnO contact layers deposited from precursor solutions *Energy Environ. Sci.* **8** 592–601

[100] Stubhan T, Oh H, Pinna L, Krantz J, Litzov I and Brabec C J 2011 Inverted organic solar cells using a solution processed aluminum-doped zinc oxide buffer layer *Org. Electron.* **12** 1539–43

[101] Chen M-H, Kuo Y-C, Lin H-H, Chao Y-P and Wong M-S 2015 Highly stable inverted organic photovoltaics using aluminum-doped zinc oxide as electron transport layers *J. Power Sources* **275** 274–8

[102] Kam Z, Wang X, Zhang J and Wu J 2015 Elimination of burn-in open-circuit voltage degradation by ZnO surface modification in organic solar cells *ACS Appl. Mater. Interfaces* **7** 1608–15

[103] Bai S *et al* 2015 Ethanedithiol treatment of solution-processed ZnO thin films: controlling the intragap states of electron transporting interlayers for efficient and stable inverted organic photovoltaics *Adv. Energy Mater.* **5** 1401606

[104] George Z, Voroshazi E, Lindqvist C, Kroon R, Zhuang W, Wang E, Henriksson P, Hadipour A and Andersson M R 2015 Improved performance and life time of inverted organic photovoltaics by using polymer interfacial materials *Sol. Energy Mater. Sol. Cells* **133** 99–104

[105] Weerasinghe H C, Rolston N, Vak D, Scully A D and Dauskardt R H 2016 A stability study of roll-to-roll processed organic photovoltaic modules containing a polymeric electron-selective layer *Sol. Energy Mater. Sol. Cells* **152** 133–40

[106] Raïssi M, Leroy-Lhez S and Ratier B 2016 Enhanced photocurrent and stability of organic solar cells using solution-based TS-CuPc interfacial layer *Org. Electron.* **37** 183–9

[107] Wang D, Zeng W, Chen S, Su X, Wang J and Zhang H 2015 Effect of a cathode buffer layer on the stability of organic solar cells *Semicond. Sci. Technol.* **30** 85017

[108] Chen L, Liu X, Wei Y, Wu F and Chen Y 2016 Alcohol-soluble interfacial fluorenes for inverted polymer solar cells: sequence induced spatial conformation dipole moment *Phys. Chem. Chem. Phys.* **18** 2219–29

[109] Glen T S, Scarratt N W, Yi H, Iraqi A, Wang T, Kingsley J, Buckley A R, Lidzey D G and Donald A M 2015 Grain size dependence of degradation of aluminium/calcium cathodes in organic solar cells following exposure to humid air *Sol. Energy Mater. Sol. Cells* **140** 25–32

[110] Yeom H R, Heo J, Kim G-H, Ko S-J, Song S, Jo Y, Kim D S, Walker B and Kim J Y 2015 Optimal top electrodes for inverted polymer solar cells *Phys. Chem. Chem. Phys.* **17** 2152–9

[111] Voroshazi E, Uytterhoeven G, Cnops K, Conard T, Favia P, Bender H, Muller R and Cheyns D 2015 Root-cause failure analysis of photocurrent loss in polythiophene:fullerene-based inverted solar cells *ACS Appl. Mater. Interfaces* **7** 618–23

[112] Romero-Gomez P, Betancur R, Martinez-Otero A, Elias X, Mariano M, Romero B, Arredondo B, Vergaz R and Martorell J 2015 Enhanced stability in semi-transparent PTB7/PC71BM photovoltaic cells *Sol. Energy Mater. Sol. Cells* **137** 44–9

[113] Ghosh D S, Liu Q, Mantilla-Perez P, Chen T L, Mkhitaryan V, Huang M, Garner S, Martorell J and Pruneri V 2015 Highly flexible transparent electrodes containing ultrathin silver for efficient polymer solar cells *Adv. Funct. Mater.* **25** 7309–16

[114] Espinosa N, García-Valverde R, Urbina A, Lenzmann F, Manceau M, Angmo D and Krebs F C 2012 Life cycle assessment of ITO-free flexible polymer solar cells prepared by roll-to-roll coating and printing *Sol. Energy Mater. Sol. Cells* **97** 3–13

[115] Peng C, Jia Z, Bianculli D, Li T and Lou J 2011 *In situ* electro-mechanical experiments and mechanics modeling of tensile cracking in indium tin oxide thin films on polyimide substrates *J. Appl. Phys.* **109** 103530

[116] Galagan Y, Mescheloff A, Veenstra S C, Andriessen R and Katz E A 2015 Reversible degradation in ITO-containing organic photovoltaics under concentrated sunlight *Phys. Chem. Chem. Phys.* **17** 3891–7

[117] Chen D, Zhang C, Wang Z, Zhang J, Tang S, Wei W, Sun L and Hao Y 2014 High efficient ITO free inverted organic solar cells based on ultrathin Ca modified AZO cathode and their light soaking issue *Org. Electron.* **15** 3006–15

[118] Wang W *et al* 2014 Transparent ultrathin oxygen-doped silver electrodes for flexible organic solar cells *Adv. Funct. Mater.* **24** 1551–61

[119] Xue Z, Liu X, Zhang N, Chen H, Zheng X, Wang H and Guo X 2014 High-performance NiO/Ag/NiO transparent electrodes for flexible organic photovoltaic cells *ACS Appl. Mater. Interfaces* **6** 16403–8

[120] Fan X, Wang J, Wang H, Liu X and Wang H 2015 Bendable ITO-free organic solar cells with highly conductive and flexible PEDOT:PSS electrodes on plastic substrates *ACS Appl. Mater. Interfaces* **7** 16287–95

[121] Skorenko K H, Faucett A C, Liu J, Ravvin N A, Bernier W E, Mativetsky J M and Jones W E 2015 Vapor phase polymerization and mechanical testing of highly electrically conductive poly(3,4-ethylenedioxythiophene) for flexible devices *Synth. Met.* **209** 297–303

[122] Li Y *et al* 2015 Ambient stable large-area flexible organic solar cells using silver grid hybrid with vapor phase polymerized poly(3,4-ethylenedioxythiophene) cathode *Sol. Energy Mater. Sol. Cells* **143** 354–9

[123] Jin Y, Li L, Cheng Y, Kong L, Pei Q and Xiao F 2015 Cohesively enhanced conductivity and adhesion of flexible silver nanowire networks by biocompatible polymer sol–gel transition *Adv. Funct. Mater.* **25** 1581–7

[124] Lee H, Han G, Kim M, Ahn H and Lee H 2015 High mechanical and tribological stability of an elastic ultrathin overcoating layer for flexible silver nanowire films *Adv. Mater.* **27** 2252–9

[125] Song Y, Jiang Y, Shi L, Cao S, Feng X, Miao M and Fang J 2015 Solution-processed assembly of ultrathin transparent conductive cellulose nanopaper embedding AgNWs *Nanoscale* **7** 13694–701

[126] Song M, Park J H, Kim C S, Kim D-H, Kang Y-C, Jin S-H, Jin W-Y and Kang J-W 2014 Highly flexible and transparent conducting silver nanowire/ZnO composite film for organic solar cells *Nano Res.* **7** 1370–9

[127] Song M, Kim J-K, Yang S-Y and Kang J-W 2014 Solution-processed silver nanowires as a transparent conducting electrode for air-stable inverted organic solar cells *Thin Solid Films* **573** 14–7

[128] Kim Y *et al* 2015 Inverted layer-by-layer fabrication of an ultraflexible and transparent Ag nanowire/conductive polymer composite electrode for use in high-performance organic solar cells *Adv. Funct. Mater.* **25** 4580–9

[129] He X, He R, Liu A, Chen X, Zhao Z, Feng S, Chen N and Zhang M 2014 A highly conductive, flexible, transparent composite electrode based on the lamination of silver nanowires and polyvinyl alcohol *J. Mater. Chem.* C **2** 9737–45

[130] Lee D, Lee H, Ahn Y, Jeong Y, Lee D-Y and Lee Y 2013 Highly stable and flexible silver nanowire-graphene hybrid transparent conducting electrodes for emerging optoelectronic devices *Nanoscale* **5** 7750–5

[131] Song M *et al* 2015 ITO-free highly bendable and efficient organic solar cells with Ag nanomesh/ZnO hybrid electrodes *J. Mater. Chem.* A **3** 65–70

[132] Jørgensen M *et al* 2013 The state of organic solar cells—a meta analysis *Sol. Energy Mater. Sol. Cells* **119** 84–93

[133] You J, Dou L, Yoshimura K, Kato T, Ohya K, Moriarty T, Emery K, Chen C-C, Gao J, Li G and Yang Y 2013 A polymer tandem solar cell with 10.6% power conversion efficiency *Nat. Commun.* **4** 1446

[134] Zhou H, Zhang Y, Mai C-K, Collins S D, Bazan G C, Nguyen T-Q and Heeger A J 2015 Polymer homo-tandem solar cells with best efficiency of 11.3% *Adv. Mater.* **27** 1767–73

[135] Zhao J, Li Y, Yang G, Jiang K, Lin H, Ade H, Ma W and Yan H 2016 Efficient organic solar cells processed from hydrocarbon solvents *Nat. Energy* **1** 15027

[136] Søndergaard R, Hösel M, Angmo D, Larsen-Olsen T T and Krebs F C 2012 Roll-to-roll fabrication of polymer solar cells *Mater. Today* **15** 36–49

[137] Krebs F C 2009 Fabrication and processing of polymer solar cells: a review of printing and coating techniques *Sol. Energy Mater. Sol. Cells* **93** 394–412

[138] Sommer-Larsen P, Jørgensen M, Søndergaard R R, Hösel M and Krebs F C 2013 It is all in the pattern-high-efficiency power extraction from polymer solar cells through high-voltage serial connection *Energy Technol.* **1** 15–9

[139] Krebs F C, Espinosa N, Hösel M, Søndergaard R R and Jørgensen M 2014 25th anniversary article: rise to power—OPV-based solar parks *Adv. Mater.* **26** 29–39

[140] Andersen T R *et al* 2014 Scalable, ambient atmosphere roll-to-roll manufacture of encapsulated large area, flexible organic tandem solar cell modules *Energy Environ. Sci.* **7** 2925–33

[141] Eggenhuisen T M *et al* 2015 High efficiency, fully inkjet printed organic solar cells with freedom of design *J. Mater. Chem.* A **3** 7255–62

[142] Berny S *et al* 2016 Solar trees: first large-scale demonstration of fully solution coated, semitransparent, flexible organic photovoltaic modules *Adv. Sci.* **3** 1500342

[143] Galagan Y *et al* 2015 Roll-to-roll slot-die coated organic photovoltaic (OPV) modules with high geometrical fill factors *Energy Technol.* **3** 834–42

[144] Spyropoulos G D *et al* 2016 Organic and perovskite solar modules innovated by adhesive top electrode and depth-resolved laser patterning *Energy Environ. Sci.* **9** 2302–13

[145] Kubis P, Li N, Stubhan T, Machui F, Matt G J, Voigt M M and Brabec C J 2015 Patterning of organic photovoltaic modules by ultrafast laser *Prog. Photovolt. Res. Appl.* **23** 238–46

[146] Uhrich C L, Falkenberg C, Rabe J, Heimke B, Klemet M, Wilde C, Wichtendahl R and Pfeiffer M 2014 Organic solar cells: from lab to roll-to-roll production *Proc. SPIE* **9184** 918415

[147] Yan F, Noble J, Peltola J, Wicks S and Balasubramanian S 2012 Semitransparent OPV modules pass environmental chamber test requirements *Sol. Energy Mater. Sol. Cells* **114** 214–8

[148] Heliatek 2014 Heliatek announces largest BIOPV façade installation *Press Release* (www.heliatek.com/en/press/press-releases/details/heliatek-announces-largest-biopv-facade-installation)

[149] Hinsch A, Veurman W, Brandt H, Flarup Jensen K and Mastroianni S 2014 Status of dye solar cell technology as a guideline for further research *ChemPhysChem* **15** 1076–87

[150] Ribeiro F, Maçaira J, Cruz R, Gabriel J, Andrade L and Mendes A 2012 Laser assisted glass frit sealing of dye-sensitized solar cells *Sol. Energy Mater. Sol. Cells* **96** 43–9

[151] Sastrawan R *et al* 2006 A glass frit-sealed dye solar cell module with integrated series connections *Sol. Energy Mater. Sol. Cells* **90** 1680–91

[152] Formica N, Mantilla-Perez P, Ghosh D S, Janner D, Chen T L, Huang M, Garner S, Martorell J and Pruneri V 2015 An indium tin oxide-free polymer solar cell on flexible glass *ACS Appl. Mater. Interfaces* **7** 4541–8

[153] Fahlteich J, Steiner C, Top M, Wynands D, Wanski T, Mogck S, Kucukpinar E, Amberg-Schwab S, Boeffel C and Schiller N 2015 10.1: Invited paper : roll-to-roll manufacturing of functional substrates and encapsulation films for organic electronics: technologies and challenges *SID Symp. Dig. Tech. Pap.* **46** 106–10

[154] Charton C, Schiller N, Fahland M, Holländer A, Wedel A and Noller K 2006 Development of high barrier films on flexible polymer substrates *Thin Solid Films* **502** 99–103

[155] Carcia P F, McLean R S, Groner M D, Dameron A and George S M 2009 Gas diffusion ultrabarriers on polymer substrates using Al_2O_3 atomic layer deposition and SiN plasma-enhanced chemical vapor deposition *J. Appl. Phys.* **106** 23533

[156] Fahlteich J, Schönberger W, Fahland M and Schiller N 2011 Characterization of reactively sputtered permeation barrier materials on polymer substrates *Surf. Coat. Technol.* **205** S141–4

[157] Angmo D, Hösel M and Krebs F C 2012 All solution processing of ITO-free organic solar cell modules directly on barrier foil *Sol. Energy Mater. Sol. Cells* **107** 329–36

[158] Hösel M, Søndergaard R, Jørgensen M and Krebs F C 2013 Comparison of UV-curing, hotmelt, and pressure sensitive adhesive as roll-to-roll encapsulation methods for polymer solar cells *Adv. Eng. Mater.* **15** 1068–75

[159] Krebs F C, Tromholt T and Jørgensen M 2010 Upscaling of polymer solar cell fabrication using full roll-to-roll processing *Nanoscale* **2** 873–86

[160] Krebs F C, Fyenbo J and Jørgensen M 2010 Product integration of compact roll-to-roll processed polymer solar cell modules: methods and manufacture using flexographic printing, slot-die coating and rotary screen printing *J. Mater. Chem.* **20** 8994

[161] Emmott C J M, Moia D, Sandwell P, Ekins-Daukes N, Hösel M, Lukoschek L, Amarasinghe C, Krebs F C and Nelson J 2016 In-situ, long-term operational stability of organic photovoltaics for off-grid applications in Africa *Sol. Energy Mater. Sol. Cells* **149** 284–93

[162] Søndergaard R R, Hösel M and Krebs F C 2013 Roll-to-roll fabrication of large area functional organic materials *J. Polym. Sci.* B **51** 16–34

[163] Ahmad J, Bazaka K, Anderson L J, White R D and Jacob M V 2013 Materials and methods for encapsulation of OPV: a review *Renew. Sustain. Energy Rev.* **27** 104–17

[164] Weerasinghe H C, Watkins S E, Duffy N, Jones D J and Scully A D 2015 Influence of moisture out-gassing from encapsulant materials on the lifetime of organic solar cells *Sol. Energy Mater. Sol. Cells* **132** 485–91

[165] Tanenbaum D M, Dam H F, Rösch R, Jørgensen M, Hoppe H and Krebs F C 2012 Edge sealing for low cost stability enhancement of roll-to-roll processed flexible polymer solar cell modules *Sol. Energy Mater. Sol. Cells* **97** 157–63

[166] Weerasinghe H C, Vak D, Robotham B, Fell C J, Jones D and Scully A D 2016 New barrier encapsulation and lifetime assessment of printed organic photovoltaic modules *Sol. Energy Mater. Sol. Cells* **155** 108–16

[167] Weerasinghe H C, Dkhissi Y, Scully A D, Caruso R A and Cheng Y-B 2015 Encapsulation for improving the lifetime of flexible perovskite solar cells *Nano Energy* **18** 118–25

[168] Adams J *et al* 2015 Water ingress in encapsulated inverted organic solar cells: correlating infrared imaging and photovoltaic performance *Adv. Energy Mater.* **5** 1501065

[169] Gevorgyan S A *et al* 2013 Interlaboratory outdoor stability studies of flexible roll-to-roll coated organic photovoltaic modules: stability over 10 000 h *Sol. Energy Mater. Sol. Cells* **116** 187–96

[170] Loi A, Muellejans H, Sample T, Dunlop E and Bardizza G 2016 Accelerated ageing test of organic photovoltaic mini-modules: study of the electrical performances after exposure at different humidity, irradiance and temperature conditions *EU PVSEC Proc.* (www.eupvsec-proceedings.com/proceedings/dvd.html)

[171] Bristow N and Kettle J 2015 Outdoor performance of organic photovoltaics: Diurnal analysis, dependence on temperature, irradiance, and degradation *J. Renew. Sustain. Energy* **7** 13111

[172] Hösel M, Søndergaard R R, Jørgensen M and Krebs F C 2014 Failure modes and fast repair procedures in high voltage organic solar cell installations *Adv. Energy Mater.* **4** 1–7

[173] Nehm F, Dollinger F, Fahlteich J, Klumbies H, Leo K and Müller-Meskamp L 2016 Importance of interface diffusion and climate in defect dominated moisture ultrabarrier applications *ACS Appl. Mater. Interfaces* **8** 19807–12

[174] Ke L, Zhang N, Low E, Wang R, Kam Z M, Wang X, Liu B and Zhang J 2015 Organic photovoltaic initial stage degradation analysis using impedance spectroscopy *Synth. Met.* **202** 63–7

[175] Guerrero A, Heidari H, Ripolles T S, Kovalenko A, Pfannmöller M, Bals S, Kauffmann L-D, Bisquert J and Garcia-Belmonte G 2015 Shelf life degradation of bulk heterojunction solar cells: intrinsic evolution of charge transfer complex *Adv. Energy Mater.* **5** 1401997

[176] Karuthedath S, Sauermann T, Egelhaaf H-J, Wannemacher R, Brabec C J and Lüer L 2015 The effect of oxygen induced degradation on charge carrier dynamics in P3HT:PCBM and Si-PCPDTBT:PCBM thin films and solar cells *J. Mater. Chem.* A **3** 3399–408

[177] Arredondo B, Martín-López M B, Romero B, Vergaz R, Romero-Gomez P and Martorell J 2016 Monitoring degradation mechanisms in PTB7:PC71BM photovoltaic cells by means of impedance spectroscopy *Sol. Energy Mater. Sol. Cells* **144** 422–8

[178] Tournebize A, Seck M, Vincze A, Distler A, Egelhaaf H-J, Brabec C J, Rivaton A, Peisert H and Chassé T 2016 Photodegradation of Si-PCPDTBT:PCBM active layer for organic solar cells applications: A surface and bulk investigation *Sol. Energy Mater. Sol. Cells* **155** 323–30

[179] Kim S H, Son H J, Park S H, Hahn J S and Kim D H 2016 A study for degradation of flexible organic photovoltaic modules via damp-heat test: by accessing individual layers of the module *Sol. Energy Mater. Sol. Cells* **144** 187–93

[180] Tessarolo M *et al* 2015 Predicting thermal stability of organic solar cells through an easy and fast capacitance measurement *Sol. Energy Mater. Sol. Cells* **141** 240–7

[181] Katz E A, Mescheloff A, Visoly-Fisher I and Galagan Y 2016 Light intensity dependence of external quantum efficiency of fresh and degraded organic photovoltaics *Sol. Energy Mater. Sol. Cells* **144** 273–80

[182] Reese M O *et al* 2011 Consensus stability testing protocols for organic photovoltaic materials and devices *Sol. Energy Mater. Sol. Cells* **95** 1253–67

[183] Gevorgyan S A *et al* 2011 An inter-laboratory stability study of roll-to-roll coated flexible polymer solar modules *Sol. Energy Mater. Sol. Cells* **95** 1398–416

[184] Gevorgyan S A *et al* 2014 Interlaboratory indoor ageing of roll-to-roll and spin coated organic photovoltaic devices: testing the ISOS tests *Polym. Degrad. Stab.* **109** 162–70

[185] Owens C *et al* 2015 Comparative indoor and outdoor degradation of organic photovoltaic cells via inter-laboratory collaboration *Polymers* **8** 1

[186] Angmo D and Krebs F C 2015 Over 2 years of outdoor operational and storage stability of ITO-free, fully roll-to-roll fabricated polymer solar cell modules *Energy Technol.* **3** 774–83

[187] Balcaen V, Rolston N, Dupont S R, Voroshazi E and Dauskardt R H 2015 Thermal cycling effect on mechanical integrity of inverted polymer solar cells *Sol. Energy Mater. Sol. Cells* **143** 418–23

[188] Roesch R, Faber T, von Hauff E, Brown T M, Lira-Cantu M and Hoppe H 2015 Procedures and practices for evaluating thin-film solar cell stability *Adv. Energy Mater.* **5** 1501407

[189] Corazza M, Krebs F C and Gevorgyan S A 2014 Predicting, categorizing and intercomparing the lifetime of OPVs for different ageing tests *Sol. Energy Mater. Sol. Cells* **130** 99–106

[190] Corazza M, Krebs F C and Gevorgyan S A 2015 Lifetime of organic photovoltaics: linking outdoor and indoor tests *Sol. Energy Mater. Sol. Cells* **143** 467–72

[191] Gevorgyan S A *et al* 2016 Baselines for lifetime of organic solar cells *Adv. Energy Mater.* **6** 1600910

[192] Heutz S, Sullivan P, Sanderson B M, Schultes S M and Jones T S 2004 Influence of molecular architecture and intermixing on the photovoltaic, morphological and spectroscopic properties of CuPc-C60 heterojunctions *Sol. Energy Mater. Sol. Cells* **83** 229–45

[193] Katz E A, Gevorgyan S, Orynbayev M S and Krebs F C 2006 Out-door testing and long-term stability of plastic solar cells *Eur. Phys. J. Appl. Phys.* **36** 307–11

[194] Yang X, Loos J, Veenstra S C, Verhees W J H, Wienk M M, Kroon J M, Michels M a J and Janssen R A J 2005 Nanoscale morphology of high-performance polymer solar cells *Nano Lett.* **5** 579–83

[195] Hauch J A, Schilinsky P, Choulis S A, Childers R, Biele M and Brabec C J 2008 Flexible organic P3HT:PCBM bulk-heterojunction modules with more than 1 year outdoor lifetime *Sol. Energy Mater. Sol. Cells* **92** 727–31

[196] Dennler G, Lungenschmied C, Neugebauer H, Sariciftci N S and Labouret A 2005 Flexible, conjugated polymer-fullerene-based bulk-heterojunction solar cells: basics, encapsulation, and integration *J. Mater. Res.* **20** 3224–33

[197] Laird D W, Vaidya S, Li S, Mathai M, Woodworth B, Sheina E, Williams S and Hammond T 2007 Advances in plexcore active layer technology systems for organic photovoltaics: roof-top and accelerated lifetime analysis

of high performance organic photovoltaic cells *Proc. SPIE* **6656** 66560X
[198] Franke R, Maennig B, Petrich A and Pfeiffer M 2008 Long-term stability of tandem solar cells containing small organic molecules *Sol. Energy Mater. Sol. Cells* **92** 732–5
[199] Hauch J A, Schilinsky P, Choulis S A, Rajoelson S and Brabec C J 2008 The impact of water vapor transmission rate on the lifetime of flexible polymer solar cells *Appl. Phys. Lett.* **93** 103306
[200] Lungenschmied C, Dennler G, Czeremuzskin G, Latrèche M, Neugebauer H and Sariciftci N S 2006 Flexible encapsulation for organic solar cells *Proc. SPIE* **6197** 619712
[201] Zimmermann B, Würfel U and Niggemann M 2009 Longterm stability of efficient inverted P3HT:PCBM solar cells *Sol. Energy Mater. Sol. Cells* **93** 491–6
[202] Tipnis R, Bernkopf J, Jia S, Krieg J, Li S, Storch M and Laird D 2009 Large-area organic photovoltaic module-Fabrication and performance *Sol. Energy Mater. Sol. Cells* **93** 442–6
[203] Potscavage W J, Yoo S, Domercq B, Kim J, Holt J and Kippelen B 2007 Integrated organic photovoltaic modules *Proc. SPIE* **6656** 66560R
[204] Schwartz G, Maennig B, Uhrich C, Gnehr W, Sonntag S, Erfurth O, Wollrab E, Walzer K and Pfeiffer M 2009 Efficient and long-term stable organic vacuum deposited tandem solar cells *Proc. SPIE* **7416** 74160K
[205] Gao D, Helander M G, Wang Z B, Puzzo D P, Greiner M T and Lu Z H 2010 C60:LiF blocking layer for environmentally stable bulk heterojunction solar cells *Adv. Mater.* **22** 5404–8
[206] Angmo D, Sommeling P M, Gupta R, Hösel M, Gevorgyan S A, Kroon J M, Kulkarni G U and Krebs F C 2014 Outdoor operational stability of indium-free flexible polymer solar modules over 1 year studied in India, Holland, and Denmark *Adv. Eng. Mater.* **16** 976
[207] Hermenau M, Leo K and Riede M 2010 Comparison of different conditions for accelerated ageing of small molecule organic solar cells *Proc. SPIE* **7722** 77220K
[208] Cros S, De Bettignies R, Berson S, Bailly S, Maisse P, Lemaitre N and Guillerez S 2011 Definition of encapsulation barrier requirements: a method applied to organic solar cells *Sol. Energy Mater. Sol. Cells* **95** S65–9
[209] Uhrich C L *et al* 2010 Efficient and long-term stable organic vacuum deposited tandem solar cells *Proc. SPIE* **7722** 77220G
[210] Tanenbaum D M *et al* 2012 The ISOS-3 inter-laboratory collaboration focused on the stability of a variety of organic photovoltaic devices *RSC Adv.* **2** 882
[211] Roth B, dos Reis Benatto G A, Corazza M, Søndergaard R R, Gevorgyan S A, Jørgensen M and Krebs F C 2015 The critical choice of PEDOT:PSS additives for long term stability of roll-to-roll processed OPVs *Adv. Energy Mater.* **5** 1401912
[212] Sapkota S B, Spies A, Zimmermann B, Dürr I and Würfel U 2014 Promising long-term stability of encapsulated ITO-free bulk-heterojunction organic solar cells under different aging conditions *Sol. Energy Mater. Sol. Cells* **130** 144–50
[213] Roesch R, Eberhardt K R, Engmann S, Gobsch G and Hoppe H 2013 Polymer solar cells with enhanced lifetime by improved electrode stability and sealing *Sol. Energy Mater. Sol. Cells* **117** 59–66
[214] Karpinski A, Berson S, Terrisse H, Mancini-Le Granvalet M, Guillerez S, Brohan L and Richard-Plouet M 2013 Anatase colloidal solutions suitable for inkjet printing: Enhancing lifetime of hybrid organic solar cells *Sol. Energy Mater. Sol. Cells* **116** 27–33
[215] Mulligan C J, Bilen C, Zhou X, Belcher W J and Dastoor P C 2015 Levelised cost of electricity for organic photovoltaics *Sol. Energy Mater. Sol. Cells* **133** 26–31

The reprinted figures in this review are reprinted in this with permission from different publishers:

Figure 2: Reproduced from [1] with permission of Royal Society of Chemistry and the PCCP Owner Societies.

Figure 3: Adapted from [2] with permission from Elsevier ©2014 and reprinted with permission from [3]. ©2015, American Chemical Society.

Figure 4: Reprinted with permission from [4]. ©2015 American Chemical Society.

Figure 5: Reprinted from [5] with permission from Elsevier ©2015.

Figure 6: Reproduced from [6] with permission from The Royal Society of Chemistry ©2014.

Figure 7: Reprinted from [7] under the Creative Commons Attribution License. The article can be found under doi.org/10.1016/j.orgel.2015.10.001.

Figure 8: Reprinted with permission from [8]. ©2015 American Chemical Society.

Figure 9: Reprinted from [9] with permission from Wiley-VCH Verlag GmbH & Co. KGaA, Weinheim. ©2015.

Figure 10: Reprinted from [10]. © 2013, IEEE.

Figure 11: Adapted from [11] with permission from Elsevier ©2015.

Figure 12: Reproduced from [12] with permission from The Royal Society of Chemistry ©2015.

Figure 13: Reproduced from [13] with permission from The Royal Society of Chemistry ©2014.

Figure 14: Reproduced from [14] with permission from The Royal Society of Chemistry ©2014.

Figure 15: Reprinted from [15] with permission from Elsevier ©2016.

Figure 16: Reprinted with permission from[16]. ©2015 American Chemical Society.

Figure 17: Reprinted from [17] with permission from Wiley-VCH Verlag GmbH & Co. KGaA, Weinheim. ©2013.

Figure 19: Reprinted from [18] with permission from Elsevier ©2014.

Table 3 and Figure 21: Reprinted from [19] with permission from Elsevier ©2013.

Figure 22: Reprinted from [20] with permission from Wiley-VCH Verlag GmbH & Co. KGaA, Weinheim. ©2015.

Figure 24: Reprinted from [21] with permission from Elsevier ©2013.

Figure 25-27: Reprinted from[22] with permission from Wiley-VCH Verlag GmbH & Co. KGaA, Weinheim. ©2016.

References

1. Morse, G. E.; Tournebize, A.; Rivaton, A.; Chassé, T.; Taviot-Gueho, C.; Blouin, N.; Lozman, O. R.; Tierney, S. The effect of polymer solubilizing side-chains on solar cell stability. *Phys. Chem. Chem. Phys.* **2015**, *17*, 11884–11897.

2. Kesters, J.; Kudret, S.; Bertho, S.; Van den Brande, N.; Defour, M.; Van Mele, B.; Penxten, H.; Lutsen, L.; Manca, J.; Vanderzande, D.; Maes, W. Enhanced intrinsic stability of the bulk heterojunction active layer blend of polymer solar cells by varying the polymer side chain pattern. *Org. Electron.* **2014**, *15*, 549–562.

3. Kesters, J.; Verstappen, P.; Raymakers, J.; Vanormelingen, W.; Drijkoningen, J.; D'Haen, J.; Manca, J.; Lutsen, L.; Vanderzande, D.; Maes, W. Enhanced Organic Solar Cell Stability by Polymer (PCPDTBT) Side Chain Functionalization. *Chem. Mater.* **2015**, *27*, 1332–1341.

4. Livi, F.; Zawacka, N. K.; Angmo, D.; Jørgensen, M.; Krebs, F. C.; Bundgaard, E. Influence of Side Chain Position on the Electrical Properties of Organic Solar Cells Based on Dithienylbenzothiadiazole- alt -phenylene Conjugated Polymers. *Macromolecules* **2015**, *48*, 3481–3492.

5. Kim, Y. J.; Chung, D. S.; Park, C. E. Highly thermally stable non-fullerene organic solar cells: p-DTS(FBTTh2)2:P(NDI2OD-T2) bulk heterojunction. *Nano Energy* **2015**, *15*, 343–352.

6. Chen, L.; Tian, S.; Chen, Y. Enhanced performance for organic bulk heterojunction solar cells by cooperative assembly of ter(ethylene oxide) pendants. *Polym. Chem.* **2014**, *5*, 4480.

7. Bracher, C.; Yi, H.; Scarratt, N. W.; Masters, R.; Pearson, A. J.; Rodenburg, C.; Iraqi, A.; Lidzey, D. G. The effect of residual palladium catalyst on the performance and stability of PCDTBT : PC 70 BM organic solar cells. *Org. Electron.* **2015**, *27*, 266–273.

8. Savagatrup, S.; Rodriquez, D.; Printz, A. D.; Sieval, A. B.; Hummelen, J. C.; Lipomi, D. J. PCBM and Incompletely

Separated Grades of Methanofullerenes Produce Bulk Heterojunctions with Increased Robustness for Ultra-Flexible and Stretchable Electronics. *Chem. Mater.* **2015**, *27*, 3902–3911.

9. Gevorgyan, S. A.; Madsen, M. V.; Roth, B.; Corazza, M.; Hösel, M.; Søndergaard, R. R.; Jørgensen, M.; Krebs, F. C. Lifetime of Organic Photovoltaics: Status and Predictions. *Adv. Energy Mater.* **2015**, 1–17.

10. Voroshazi, E.; Cardinaletti, I.; Uytterhoeven, G.; Hadipour, A.; Rand, B. P.; Aernouts, T. Role of electron and hole collecting buffer layers on the stability of inverted polymer: Fullerene photovoltaic devices. *2013 IEEE 39th Photovolt. Spec. Conf.* **2013**, *4*, 3212–3215.

11. Lee, J. J.; Lee, S. H.; Kim, F. S.; Choi, H. H.; Kim, J. H. Simultaneous enhancement of the efficiency and stability of organic solar cells using PEDOT:PSS grafted with a PEGME buffer layer. *Org. Electron. physics, Mater. Appl.* **2015**, *26*, 191–199.

12. Hou, X.; Li, Q.; Cheng, T.; Yu, L.; Wang, F.; Lin, J.; Dai, S.; Li, Y.; Tan, Z. Improvement of the power conversion efficiency and long term stability of polymer solar cells by incorporation of amphiphilic Nafion doped PEDOT-PSS as a hole extraction layer. *J. Mater. Chem. A* **2015**, *3*, 18727–18734.

13. Shi, Y.; Tan, L.; Chen, L.; Chen, Y. Self-assembled buffer layer from conjugated diblock copolymers with ethyleneoxide side chains for high efficiency polymer solar cells. *J. Mater. Chem. C* **2014**, *2*, 8054–8064.

14. MacLeod, B. A.; Tremolet de Villers, B. J.; Schulz, P.; Ndione, P. F.; Kim, H.; Giordano, A. J.; Zhu, K.; Marder, S. R.; Graham, S.; Berry, J. J.; Kahn, A.; Olson, D. C. Stability of inverted organic solar cells with ZnO contact layers deposited from precursor solutions. *Energy Environ. Sci.* **2015**, *8*, 592–601.

15. Raïssi, M.; Leroy-Lhez, S.; Ratier, B. Enhanced photocurrent and stability of organic solar cells using solution-based TS-CuPc interfacial layer. *Org. Electron.* **2016**, *37*, 183–189.

16. Xue, Z.; Liu, X.; Zhang, N.; Chen, H.; Zheng, X.; Wang, H.; Guo, X. High-Performance NiO/Ag/NiO Transparent Electrodes for Flexible Organic Photovoltaic Cells. *ACS Appl. Mater. Interfaces* **2014**, *6*, 16403–16408.

17. Hösel, M.; Søndergaard, R. R.; Jørgensen, M.; Krebs, F. C. Comparison of UV-curing, hotmelt, and pressure sensitive adhesive as roll-to-roll encapsulation methods for polymer solar cells. *Adv. Eng. Mater.* **2013**, *15*, 1068–1075.

18. Gevorgyan, S. A.; Corazza, M.; Madsen, M. V.; Bardizza, G.; Pozza, A.; Müllejans, H.; Blakesley, J. C.; Dibb, G. F. A.; Castro, F. A.; Trigo, J. F.; Guillén, C. M.; Herrero, J. R.; Morvillo, P.; Maglione, M. G.; Minarini, C.; Roca, F.; Cros, S.; Seraine, C.; Law, C. H.; Tuladhar, P. S.; Durrant, J. R.; Krebs, F. C. Interlaboratory indoor ageing of roll-to-roll and spin coated organic photovoltaic devices: Testing the ISOS tests. *Polym. Degrad. Stab.* **2014**, *109*, 162–170.

19. Reese, M. O.; Gevorgyan, S. A.; Jørgensen, M.; Bundgaard, E.; Kurtz, S. R.; Ginley, D. S.; Olson, D. C.; Lloyd, M. T.; Morvillo, P.; Katz, E. A.; Elschner, A.; Haillant, O.; Currier, T. R.; Shrotriya, V.; Hermenau, M.; Riede, M.; Kirov, K. R.; Trimmel, G.; Rath, T.; Inganäs, O.; Zhang, F.; Andersson, M.; Tvingstedt, K.; Lira-Cantu, M.; Laird, D.; McGuiness, C.; Gowrisanker, S.; Pannone, M.; Xiao, M.; Hauch, J.; Steim, R.; Delongchamp, D. M.; Rösch, R.; Hoppe, H.; Espinosa, N.; Urbina, A.; Yaman-Uzunoglu, G.; Bonekamp, J.-B.; van Breemen, A. J. J. M.; Girotto, C.; Voroshazi, E.; Krebs, F. C. Consensus stability testing protocols for organic photovoltaic materials and devices. *Sol. Energy Mater. Sol. Cells* **2011**, *95*, 1253–1267.

20. Roesch, R.; Faber, T.; Von Hauff, E.; Brown, T. M.; Lira-Cantu, M.; Hoppe, H. Procedures and practices for evaluating thin-film solar cell stability. *Adv. Energy Mater.* **2015**, *5*, 1–24.

21. Corazza, M.; Krebs, F. C.; Gevorgyan, S. A. Lifetime of organic photovoltaics: Linking outdoor and indoor tests. *Sol. Energy Mater. Sol. Cells* **2015**, *143*, 467–472.

22. Gevorgyan, S. A.; Espinosa, N.; Ciammaruchi, L.; Roth, B.; Livi, F.; Tsopanidis, S.; Z??fle, S.; Queir??s, S.; Gregori, A.; Benatto, G. A. dos R.; Corazza, M.; Madsen, M. V.; H??sel, M.; Beliatis, M. J.; Larsen-Olsen, T. T.; Pastorelli, F.; Castro, A.; Mingorance, A.; Lenzi, V.; Fluhr, D.; Roesch, R.; Maria Duarte Ramos, M.; Savva, A.; Hoppe, H.; Marques, L. S. A.; Burgu??s, I.; Georgiou, E.; Serrano-Luj??n, L.; Krebs, F. C. Baselines for Lifetime of Organic Solar Cells. *Adv. Energy Mater.* **2016**, *6*, 1600910 (1-9).

DTU Energy Conversion
Department of Energy Conversion and Storage

Improvement of the stability of polymers for organic solar cells by different strategies

Ilona M. Heckler and Eva Bundgaard

Department of Energy Conversion and Storage, Technical University of Denmark, Frederiksborgvej 399, DK-4000 Roskilde, Denmark. ilhe@dtu.dk.

Abstract

Conjugated polymers are applied as donor materials in the active layer of polymer solar cells (PSCs). For a long lifetime of the PSCs the stability of the polymer layer is an important factor and researchers are now focusing more and more on this area. The side chains on polymers ensure a high solubility in organic solvents, however, they are not needed after film formation, but can affect the properties of the active layer in the PSCs by for instance introducing a poor morphological stability. The stability can be improved by eg. cross-linking of the side chain, introduction of a stabilizing group or simply by removing the side chains.

Introduction

Conjugated polymers like poly(3-hexylthiphene) (P3HT) are investigated intensively in terms of efficiency and stability as donor material in the active layer of polymer solar cells (PSCs). For a long lifetime of PSCs, the stability of the polymer layer is a very important factor. There are several different strategies to improve the morphological stability of PSCs which include:

- Addition of a stabilizing group on the side chain like in P[3HT-co-3(PAOE)T][2] (figure 1) which have an improved stability compared to pure P3HT.
- Cross-linking of functionalized side chains on the polymer gives an insoluble network which stabilizes the morphology and thus increase the stability of the PSCs. One example is the usage of an azide group as in P3HT-N5.[3] (figure 1).
- Removal of the side chains after film formation in a thermal or acidic step results in the highly stable and insoluble polymer like polythiophene (PT).

Here we present recent results from the studies of side chain removal.

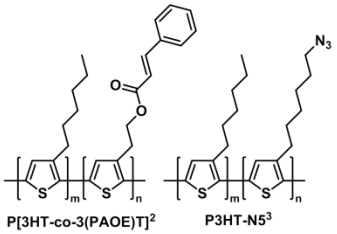

Figure 1: Polythiophene with functionalized side chains to improve the stability of PSCs.

Removal of the polymer side chains

Two approaches[4,5] to remove the side chains of the polymer (see figure 2) lead to a stable and insoluble polymer film.

- The use of thermo-cleavable side chains result in the stable polymer PT1[4] (figure 2). Complete cleavage of the polymer (P3MHOCT) occurs around 300°C yielding pure PT.
- The use of acid-cleavable side chains result in the insoluble poymer PT2[5] (figure 2).

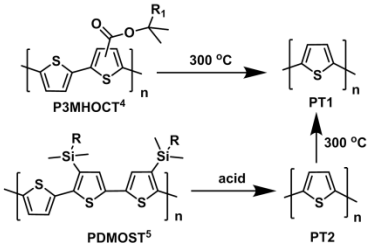

Figure 2: Polythiophene (PT) with a thermo- and acid-cleavable side chain yielding pure PT.[4,5,6]

Comparison of the cleaved polythiophene

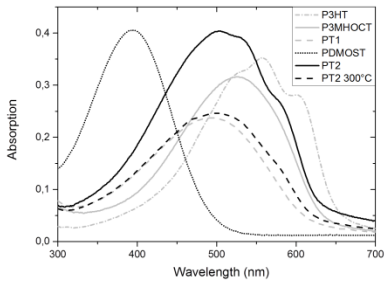

Figure 3: Uv-vis absorption of cleavable polymer film in different stages.

Recent studies[6] of PT1 and PT2 showed that the eg. hole mobility of the two were not identical. Based on uv-vis measurements (figure 3 and 4) it was found that the morphology of the two was not identical. Heating of PT2 to 300°C changes the uv-vis absorption spectrum to be similar to PT1.

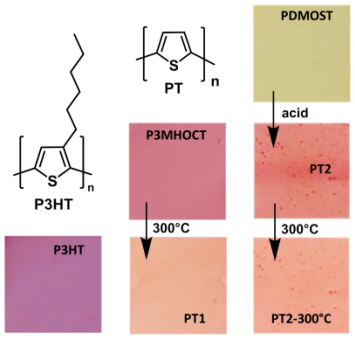

Figure 4: Section of the cleavable polymer film in different stages.

Conclusion

The morphological stability of conjugated polymers like polythiophene derivatives can be improved by removal of side chains via thermo- or acid-cleavage resulting in highly stable and insoluble polymers. However, comparison of the two PT polymers reveal different morphologies. The difference can be overcome by thermal treatment of the acid cleaved polymer at 300°C.

Acknowledgments

The authors thank the Villum Fundation young investigator programme (*materials for energy production*) for financial support.

References

1. S. Berthoa, G. Janssen, T. J. Cleij, B. Conings, W.Moons, A. Gadisa, J. D'Haen, E. Goovaerts, L. Lutsen, J. Manca, D. Vanderzande, *Sol. Energy Mater. Sol. Cells*, **2008**, *92*, 753.
2. S. Bertho, B. Campo, F. Biersimoni, D. Spoltore, J. D'Haen, L. Lutsen, W. Maes, D. Vanderzande and J. Manca, *Sol. Energy Mater. Sol. Cells*, **2013**, *110*, 69.
3. C.-Y. Nam, Y. Auinn, Y. S. Park, H. Hlaing, X. Lu, B. M. Ocko, C. T. Black and R. B. Grubbs, *Macromolecules*, **2012**, *45*, 2338.
4. S. A. Gevorgyan and F. C. Krebs, *Chem. Mater.*, **2008**, *20*, 4386. F. C. Krebs and H. Spanggaard, *Chem. Mater.*, **2005**, *17*, 5235.
5. E. Bundgaard, O. Hagemann, M. Bjerring, N. C. Nielsen, J. W. Andreasen, B. Andreasen and F. C. Krebs, *Macromolecules*, **2012**, *45*, 3644.
6. J.Toušek, J.Toušková, J.Ludvík, A.Liška, Z.Remeš, J.Kousal , I. M. Heckler, E. Bundgaard, F. C. Krebs, *Synthetic Metals*, **2014**, submitted.

DTU Energy
Department of Energy Conversion and Storage

Polymers with improved stability for polymer solar cells

Ilona M. Heckler and Eva Bundgaard

Department of Energy Conversion and Storage, Technical University of Denmark, Frederiksborgvej 399, DK-4000 Roskilde, Denmark. ilhe@dtu.dk.

Introduction

Low band gap polymers are investigated intensively in terms of efficiency and stability as donor material in the active layer of polymer solar cells (PSCs). For a long lifetime of the PSCs, the stability of the polymer layer is a very important factor and can be influenced by the introduction of stabilizing side chains. This principle was shown by Vanderzande *et. al.*[1,2] on different examples (see figure 1) for an improvement of the thermal stability.

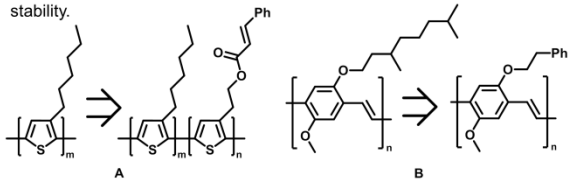

Figure 1: A) 3-hexylthiophene replaced by a random copolymer of 3-hexylthiophene and 3-cinnamoyl thiophene.[1] B) Polyphenylvinylene (PPV) derivative replaced by another PPV with stabilizing side chains.[2]

Monomer Synthesis

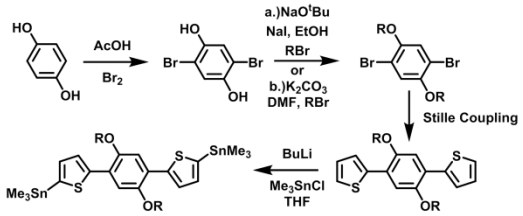

Figure 2: Four synthetic steps[2,3] resulting in two different stannylated monomer. R= phenylethyl (a.) or 2-hexyldecyl (b.)

Polymer Synthesis

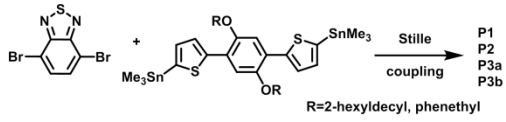

Figure 3: Stille coupling polymerization[3] of the stannylated monomer(s) with 4,7-dibromobenzo[c][1,2,5]thiadiazole.

Table 1: Molecular weight of the polymers[a].

Polymer	Mn (g/mol)	Mw (g/mol)	PDI	Polymer	Mn (g/mol)	Mw (g/mol)	PDI
P1	nd	nd	nd	**P3a**	7900	22100	2.8
P2[b]	-	-	-	**P3b**	12200	27300	2.2

[a]Molecular weight measured by SEC against PS standard. [b]Polymer insoluble in common organic solvents.

Results

Four different polymers has been synthesized (see figure 4). Two of the polymers (**P1** and **P2**) are the homo-copolymers, while the other two are co-copolymers with an incorporation of the monomer with the phenylethyl group of 5% (**P3a**) or 10% (**P3b**). The hexyl-decyl side chain ensures a high solubility.

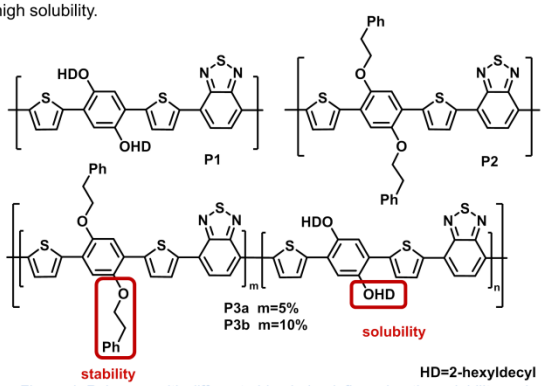

Figure 4: Polymers with different side chains influencing the solubility and stability

The polymers were applied in the active layer of PSC. The cells were tested in terms of efficiency and lifetime (table 2). Insolubility of **P2** led to no results.

Table 2: Application of the polymers in solar cells[a].

Polymer	PCE (%)[b]	Voc (V)[b]	Isc (mA/cm^2)[b]	FF (%)[b]	T_{80} (h)[c]
P1	2,39	0,75	-5,02	57,6	4,0
P2[d]	-	-	-	-	-
P3a	2,38	0,71	-7,22	51,3	10,5
P3b	2,45	0,74	-5,48	46,5	7,7

[a]solar cells produced in a roll process with inverted device geometry: PET substrate/ Ag-grid/ PEDOT- PSS/ ZnO/ polymer : [60]PCBM/ PEDOT-PSS/ Ag-grid. [b]Maximal solar cell device characterization: PCE=power conversion efficiency, Voc=open circuit voltage, Isc= short circuit current, FF=fill factor. [c]Lifetime test ISOS-L-1 according to Krebs et al.[4], T_{80}= period of time when device has decayed 20% from initial PCE. [d]Polymer insoluble in common organic solvents.

Conclusion

Polymers with a side chain variation could be successfully synthesized and applied in polymer solar cells. The lifetime test shows a small improvement in the stability. However further studies of the polymers in terms of photochemical and thermal stability will be needed.

Acknowledgments

The authors thank the Villum Fundation Young Investigator Programme (*Materials for Energy Production*) for financial support.

References

1. S. Bertho, B. Campo, F. Piersimoni, D. Spoltore, J. D'Haen, L. Lutsen, W. Maes, D. Vanderzande and J. Manca, *Sol. Energy Mater. Sol. Cells*, **2013**, *110*, 69.
2. J. Vandenbergh, B. Conings, S. Berthoa, J. Kesters, D. Spoltore, S. Esiner, J. Zhao, G. Van Assche, M. M. Wienk, W. Maes, L. Lutsen, B. Van Mele, R. A. J. Janssen, J. Manca, D. J. M. Vanderzande *Macromolecules*, **2011**, *44*, 8470.
3. E. Bundgaard *et al., Advanced Energy Materials*, **2014**, submitted.
4. F. C. Krebs *et al., Sol. Energy Mater. Sol. Cells*, **2011**, *95*, 1253.

DTU Energy
Department of Energy Conversion and Storage

Influence of side chain substituted conjugated polymers on the stability of polymer solar cells

Ilona M. Heckler*, Jurgen Kesters§, Wouter Maes§ and Eva Bundgaard*

**Department of Energy Conversion and Storage, Technical University of Denmark, ilhe@dtu.dk.*
§ Institute for Materials Research, Design & Synthesis of Organic Semiconductors, Hasselt University, Belgium.

Introduction

Highly advanced conjugated polymers are studied intensively in the field of polymer solar cells (PSC). The stability has been investigated via several synthetic routes:

- removal of the side chain [1]
- cross linking of functionalized side chains [2]
- **introduction of stabilizing side chains** [3]

A recent screening[4] of a myriad of polymers in PSC demonstrated a few suitable candidates for large scale production. In this study we focus on the stability of two of the candidate backbones (Figure 1: **P1** and **P2**).

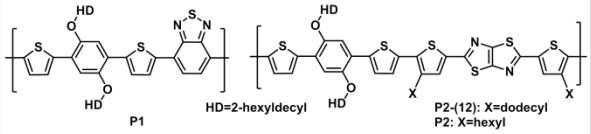

Figure 1: Suitable polymers for large scale production

Polymer characterization and testing

P1 (BT based) and **P2** (TzTz based), which are applicable in roll coated solar cells, were manipulated by the introduction of the stabilizing side chain 2-phenethyl (EtPh). To ensure solubility of the polymers, 5 and 10 %, respectively, of the side chains were exchanged. Stille coupling polymerization yielded **P3a**, **P3b**, **P4a** and **P4b**.

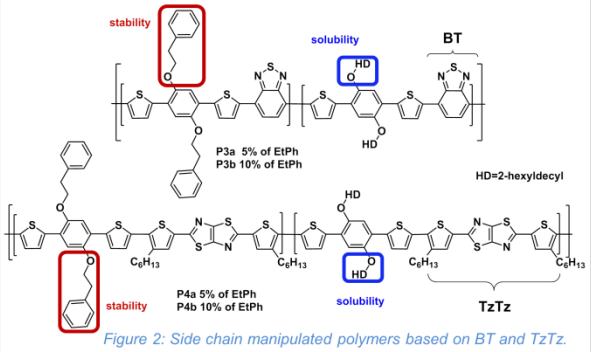

Figure 2: Side chain manipulated polymers based on BT and TzTz.

Table 1: Polymer characterization and application in PSC.

Polymer	M_n [a]	Đ [a]	R_d [b]	PCE (best) [b]	*Voc* [b]	*Jsc* [b]	FF [b]
P1	42	1.9	1.66	2.81 (3.05)	0.75	7.33	0.51
P3a	39	2.1	1.63	2.51 (2.65)	0.74	6.52	0.52
P3b	43	2.1	1.69	2.09 (2.16)	0.73	5.97	0.50
P2	42	1.9	2.82	2.67 (2.73)	0.69	6.69	0.61
P4a	30	3.1	2.60	2.59 (2.72)	0.68	6.95	0.59
P4b	43	2.1	2.13	2.66 (2.76)	0.69	7.00	0.60

[a] M_n (molecular weight in kDa) and Đ (dispersity) were measured by size exclusion chromatography in chlorobenzene at 60°C. [b] R_d (degradation rate in %/h) calculated from photochemical stability measurements. [c] *IV*-characteristics (PCE= power conversion efficiency in %; Voc=open circuite current in V; Jsc= short circuit current in mA; FF=fill factor) of polymer solar cells with an inverted geometry: PET substrate/Ag-grid/PEDOT-PSS/ZnO/ polymer:PCBM/PEDOT-PSS/Ag-grid.

Stability Study

The PSCs were tested under sun irradiance (Figure 3a and 3d) and thermal stress (Figure 3b and 3e). The pure polymer films were also exposed to sun light while UV-Vis absorption was measured (Figure 3c and 3f).

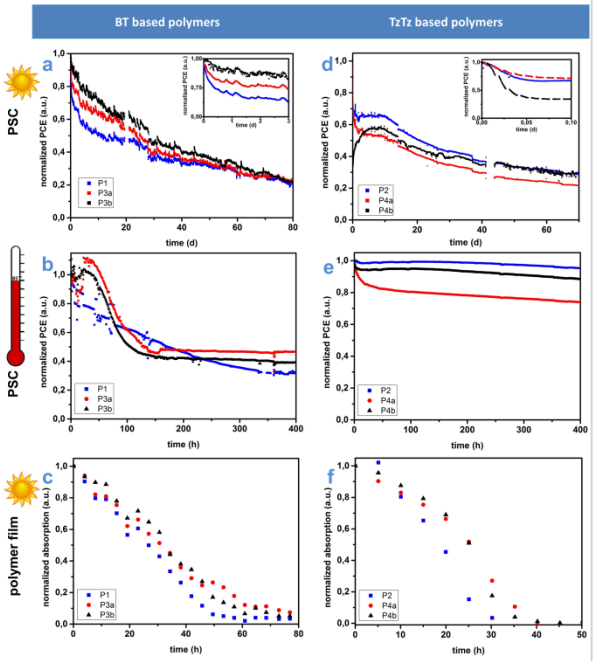

Figure 3: Normalized PCE values of the PSCs under sun irradiance (a, d); Normalized PCE values of the PSCs (prepared via spin coating) under thermal stress (85°C) (b, e) and normalized UV-Vis absorption values of the polymer film under sun irradiance (c, f).

Conclusion

- **BT** based series: decrease in efficiency of the PSCs with incorporated side chains; influence of sun irradiance on the PSC was improved in the beginning of the experiment; thermal stress degraded all PSC, but the manipulated polymers were more stable.
- **TzTz** based series: similar efficiencies; higher stability for the manipulated polymer film, whereas the tests of the PSC showed similar or higher degradation for manipulated polymers

Acknowledgments

The authors thank the Villum Fundation Young Investigator Programme (*Materials for Energy Production*) for financial support. I.H. thanks W. Maes for the opportunity to do her research stay in his group.

References

1. (a) S. A. Gevorgyan and F. C. Krebs, *Chem. Mater.*, **2008**, *20*, 4386–4390. (b) E. Bundgaard, O. Hagemann, M. Bjerring, N. C. Nielsen, J. W. Andreasen, B. Andreasen, and F. C. Krebs, *Macromolecules*, **2012**, *45*, 3644–3646.
2. C. Nam, Y. Qin, Y. Park, H. Hlaing, X. Lu, B. M. Ocko, C. T. Black, and R. B. Grubbs, *Macromolecules*, **2012**, *45*, 2338–2347.
3. J. Vandenbergh, B. Conings, S. Bertho, J. Kesters, D. Spoltore, S. Esiner, J. Zhao, G. Van Assche, M. M. Wienk, W. Maes, L. Lutsen, B. Van Mele, R. A. J. Janssen, J. Manca, and D. J. M. Vanderzande, *Macromolecules*, **2011**, *44*, 8470–8478.
4. E. Bundgaard, F. Livi, O. Hagemann, J. E. Carlé, M. Helgesen, I. M. Heckler, N. K. Zawacka, D. Angmo, T. T. Larsen-Olsen, G. A. dos Reis Benatto, B. Roth, M. V. Madsen, M. R. Andersson, M. Jørgensen, R. R. Søndergaard, and F. C. Krebs, *Adv. Energy Mater.*, **2015**, *5*, 1402186(1–16).